THE ORIGIN OF ULTRAPOTASSIC IGNEOUS ROCKS

by

Francis
Stephen F.Foley

B.Sc. (Southampton)
M.Sc. (Memorial University of Newfoundland)

Submitted in fulfilment of the requirements
for the degree of
Doctor of Philosophy

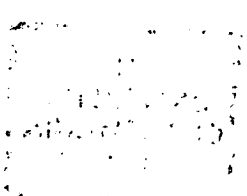

University of Tasmania
Hobart
August 1986

This thesis embodies the major results of my research in the Geology Department, University of Tasmania between 1982 and 1986. It consists of five major articles and two minor articles [included as appendices] which have been prepared for publication in the following international journals or conference proceedings:

	Part	Status
Earth Sci Rev	I	in press
Tschermaks Min Petr Mitt	II	published
Contrib Mineral Petrol	III	published
Contrib Mineral Petrol	IV	in press
Proc Fourth Internat Kim Conf	V	submitted
Geochim Cosmochim Acta	App.III	in prep.
American Mineralogist	App.IV	published

These have been modifed only slightly for inclusion in this thesis to avoid excessive repetition.

Many of these papers have co-authors as listed in the table of contents. For the articles included as major parts, the work is predominantly my own: the contributions of co-authors are indicated in the acknowledgements [pages vi-vii].

The thesis contains no material which has been accepted or submitted for the award of any other degree or diploma in any university and, to the best of my knowledge and belief, contains no copy or paraphrase of material previously published or written by another person, except where due reference is made.

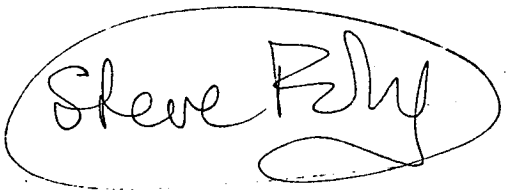

Stephen F. Foley
University of Tasmania
August 1986

THESIS CONTENTS

Acknowledgements

I am greatly indebted to many people for discussions, instruction in techniques, and provision of information during the research for, and production of this thesis. The following deserve special acknowledgement:

- Prof. David Green, my supervisor, for his advice and guidance at all stages. His unusually rapid comprehension and assessment of new results and ideas led to many suggestions which have improved interpretation and experimental design.
- Wayne Taylor, for assistance with computing, instruction in the use and interpretation of FTIR, groundwork in the development of the capsule-piercing technique for mass spectrometry, development of the thermodynamic model presented in Part IV, and many useful discussions.
- Giampiero Venturelli [Parma, Italy], for his collaboration in producing a more thorough database of ultrapotassic rocks than would otherwise have been achieved, and for discussions, criticisms and clarifications of the resulting review. Lorenzo Toscani [Parma, Italy] also assisted in database compilation.
- Lynton Jaques [Canberra, Australia] for many comments on parts of the thesis in its early stages, and for provision of large amounts of material prior to publication. His great knowledge of the West Kimberley lamproites constantly led to refinement of the aims and interpretations of my experimental program, and contributed directly in estimation of the olivine lamproite composition used in Part V, and in the study of the Al-spinels (Appendix 4).
- Keith Harris, for the manufacture of many experimental parts, for his expertise in glasswork, and for valuable discussions on experimental design and interpretation.
- Wieślaw Jablonski, Ron Berry and Ross Lincolne for maintaining a functional microprobe, including battling with a reluctant integrated wavelength/energy dispersive system.
- Noel Davies, for essential assistance in operation of the mass spectrometer and FTIR spectrometer.
- David Ellis [now A.N.U., Canberra], for his boundless enthusiasm for study of the Gaussberg rock in the early part of my research, and for advice and discussions on phase theory and the manipulation of multidimensional projections.
- Scott Kuehner, whose past experience with ultrapotassic rocks was invaluable in the formulation of many interpretations in this thesis.

- Tony Crawford, for discussions and unpublished information about the Spanish lamproites, and for many opinions, often unsolicited, about igneous geochemistry.
- Graeme Wheller, for his efforts in computer programming which made the production of Part I much easier, and for discussions about Indonesian volcanic rocks.
- Many colleagues in the Geology Department at Tasmania who have assisted at different stages with a variety of tasks or have helped with clarifications through discussion: John Adam, Steve Eggins, Trevor Falloon, Ramsay Ford, Klaus Nickel, Nic Odling, Neil Ortez, Ewan Reid, Bob Tingey, Rick Varne, Margaret Wallace and Jan van Moort.
- Various correspondents who have generously supplied material before publication or samples for analytical or comparative study; John Sheraton, Barbara Scott-Smith, Alan Edgar, Steve Bergman, Dave Nelson, Peter Nixon and Roger Mitchell.
- Visitors to Tasmania who have given valued opinions and advice; Alok Gupta, Kurt Mengel, Alan Thompson and Trevor Green.
- Other members of the Geology Department, who made for a happy and stimulating work environment.
- Many members of the Athletic Association of Tasmania for many enjoyable, relaxing hours spent at various athletics meets in Tasmania and Melbourne, and my non-geological flatmates Cameron Beech, Francis Tumeo, Veddy Ndyetabura, Godwin Agwunobi, Mike Lindfield and Chris Gelber, who stimulated much activity of the mind in non-geological spheres.

LIST OF TABLES

LIST OF FIGURES

ABSTRACT

This thesis consists of a review of ultrapotassic igneous rock occurrences and three experimental programs designed to examine the petrogenesis of the lamproites.

A definition for ultrapotassic rocks is introduced using the whole-rock chemical screens $K_2O>3$ wt%, MgO>3 wt% and $K_2O/Na_2O>2$. Three major end-member groups are recognised; Group I (lamproites) are characterised by low CaO, Al_2O_3 and Na_2O, high K_2O/Al_2O_3 and Mg-number, and extremely high incompatible element contents; Group II have low SiO_2 and high CaO, and lower incompatible elements than group I although they have high relatively Sr; Group III rocks occur in orogenic areas and have high CaO and Al_2O_3, and low TiO_2, Nb and Ba typical of island arc rocks. Primary magmas for all three groups probably originate by partial melting of mantle material enriched in incompatible elements. The chemical signatures of the groups indicate differences in (i) source composition prior to enrichment, (ii) the chemical nature of the enriching agent, and (iii) pressure-temperature conditions of melting.

The liquidus mineralogy of a pristine, primary leucite lamproite from Gaussberg, Antarctica, was studied at 1 atm with controlled fO_2. Oxygen fugacity at the time of crystallisation of the Gaussberg rock is shown by ferric value $[100Fe^{3+}/(Fe^{3+}+Fe^{2+})]$ of spinel, Fe_2O_3 content of leucite and Mg-number of olivine, to have been just below NNO. Application of the spinel ferric value calibration to other lamproites indicates that they began to crystallise at fO_2 ranging from MW to above NNO. The ferric value of spinel is very sensitive to changes in oxygen fugacity, and may prove useful as a 'diamond survivability indicator': diamonds are unlikely to survive in the more oxidised lamproite magmas.

The effect of fluorine, an important constituent of ultrapotassic rocks, on phase relationships in the kalsilite-forsterite-quartz system was studied at 28kbar. Fluorphlogopite is found to be stable to 300°C higher than hydroxyphlogopite, and the peritectic point PHL+EN+FO+L, which can be used to model melting of a mica-harzburgite mantle, lies at an equally magnesian composition. Fluorine acts as a melt polymerising agent as shown by the expansion of the enstatite phase volume relative to forsterite and by FTIR spectroscopic studies. Fluorine forms bonds with network modifying cations and removes $KAlO_2$ groups from the aluminosilicate network, causing an increase in Si/(Si+Al) in the network. However, in the presence of water fluorine will appear to depolymerise

melts due to the action of OH released by HF dissolution; the viscosity will be lowered by fluorine in either case due to the formation of fluoride complexes.

A model is developed for the origin of lamproitic magmas by partial melting of a mica-harzburgite mantle in a reduced environment in the presence of fluorine. Lamproites typically carry depleted mantle nodules and have H_2O-and F-rich, but CO_2-poor compositions. Primary lamproite magmas appear to range in silica content from around 40 wt% (olivine lamproites) to at least 52 wt% (leucite lamproites). In a reduced mantle (fO_2 ~IW to IW+2 log units) CH_4 will be the dominant carbon species in fluids, and CO_2 will be very rare even in a carbon-rich environment. CH_4 also acts as a depolymeriser, so that production of silicic melts will be optimised in a reduced, fluorine-rich mantle. Olivine lamproites may be produced by melting of a similar composition at higher pressures. Calculations show that oxidation from the proposed reduced conditions at source to observed surface oxidation states can be achieved by dissociation of only ~0.1 wt% H_2O driven by diffusive loss of H_2.

Silica-poor rocks of Group II may originate in an oxidised environment with abundant CO_2 but little H_2O. Fluorine will maintain a large phase field for mica in these conditions so that initial melts will be magnesian and strongly silica-undersaturated.

A technique is developed for liquidus experiments at high pressures in the presence of reduced H_2O>CH_4 fluids. Two lamproite compositions were studied by this technique to test the hypothesis outlined above. The olivine lamproite has olivine as the liquidus phase at all pressures studied (up to 40 kbar), but the increasing stability of orthopyroxene+ mica with pressure indicates that there may be a OL+OPX+PHL point at the liquidus between 45 and 55 kbar. This is consistent with the occurrence of diamonds in olivine lamproites. The leucite lamproite has liquidus fields for olivine, mica and orthopyroxene with increasing pressure, but has no point where the three coexist. These phase relationships can be interpreted to fit the mica-harzburgite melting model (with melting at ~20 kbar) if minor olivine fractionation occurs at high pressures, or possibly if the water content of the source differs from that of the experiments. Thus, pressure variation may be the principal control of lamproite chemistry.

Several experiments with variable CH_4/H_2O or H_2O/CO_2 fluids enable comparison of melting behaviour at varying fO_2. At very low fO_2, melting temperatures are increased due to lowered water activity, but mica stability is increased due to its higher F/OH.

PART I

THE ULTRAPOTASSIC ROCKS : CHARACTERISTICS, CLASSIFICATION, AND CONSTRAINTS FOR PETROGENETIC MODELS

'A little boy goes into a grocer's shop with a penny in his hand and asks: "Could I have a penny's worth of mixed sweets?" The grocer takes two sweets and hands them to the boy saying: "Here you have two sweets. You can do the mixing yourself."'

Niels Bohr
quoted by Heisenberg [1958]

1.1 INTRODUCTION

The terms 'ultrapotassic' and 'highly potassic' are generally used to describe rocks which have high contents of K_2O and other incompatible elements together with a high K_2O/Na_2O ratio, and yet have other features such as high Mg-number [100Mg/(Mg+Fe)], Ni and Cr which are characteristic of relatively primitive basaltic magmas. This unusual chemistry leads to the frequent occurrence of leucite and mica as phenocryst phases together with olivine.

Much has been written about ultrapotassic rock occurrences with relatively little attempt to systematically document and compare them. Early workers produced treatises on alkaline petrographic provinces in which they developed petrographically-based classifications which led to an array of rock names such as orendite, wyomingite [Cross 1897], katungite, mafurite [Holmes and Harwood 1932], cedricite and wolgidite [Wade and Prider 1940] which have little, if any, applicability to rocks outside the type area. This unwieldly nomenclature has led to a tendency to lump ultrapotassic rocks into a single group, a situation which has led to some confused petrogenetic speculation. A number of recent papers [Jaques et al. 1984a; Scott-Smith and Skinner 1984a; Mitchell 1986; Bergman 1986] propose simplifications of the nomenclature, but these still rely partly or wholly on modal mineralogy.

A large part of the nomenclature problem is due to the mineralogical diversity: the great variability in appearance and abundance of the 'definitive' minerals results in multiple names for rocks which may be very similar chemically. A petrographically-based classification is therefore less suitable for ultrapotassic rocks, and indeed other types of alkaline rocks, than for the more common, less alkaline rock groups.

The purpose of this paper is to introduce specific chemical parameters to delimit the term 'ultrapotassic', to review the available data and from it suggest a classification scheme which will be useful for petrogenetic modelling.

1.2 RATIONALE FOR CLASSIFICATIONS

Petrological studies proceed from an empirical data gathering stage to petrogenetic modelling, a process in which classification is an important intermediate stage. The structuring of the classification is important if it is to assist in petrogenetic modelling. Classifications used in petrology are of two basic types; partition classifications and resemblance classifications [cf. Körner 1966]. A partition classification attempts to define groups according to rigid rules in the manner of mathematical sets. It is the more empirical of the two types and is the basis of the petrographic classifications used for naming rocks. The applications of partition classifications in petrology tend to be more archival than heuristic because of the rigidity of the resultant boundaries. They are useful for comparative descriptions but are less useful for borderline cases which are essential to discussions of petrogenesis.

The classification developed here for ultrapotassic rocks is a resemblance classification by which rocks are grouped on the basis of similarity to standard members and dissimilarity from standard non-members. Rocks are therefore treated as transitional between end-members rather than being partitioned into small distinct groups. This is more suited to the complexity of processes which are involved in petrogenesis, the modelling of which is too inexact a science for the definite groupings produced by a partition classification. The retention of transitional types due to inexact boundaries in a heuristic classification is essential because the concepts under investigation in petrogenetic modelling are rarely independent or mutually exclusive. The

introduction of strict but arbitrary partitions produces artificial boundaries which run the risk of being carried over into petrogenetic models. The proposition of end-members is not intended to imply uniqueness of process, since each end-member will be the result of a complex interaction of physical and chemical processes. These must be considered at a later stage than classification. However, recognition of end-members should help to isolate which conditions are involved in each case.

A resemblance classification is necessarily more genetic than a partition classification in that it requires abstraction of a greater number of properties of the rocks. We group them chiefly by major element chemical characteristics, but also selectively consider geological setting, ultramafic nodule content and trace element characteristics. Because of this the resemblance classification must be more susceptible to changes, either in the data base or in its theroetical grounding, than is a petrographic partition classification. It is important to remember in using any classification that "... any decision as to which classification is best is itself a hypothesis, which subsequent investigations may lead us to reject" [Copi 1978, p.495].

1.3 ULTRAPOTASSIC ROCK DATA

Current usage of the terms 'ultrapotassic' and 'highly potassic' appears to rest on an assumed mutual understanding amongst petrologists as to which rocks are included without a widely used definition. This usage is derived from descriptions of a few classic localities such as the Roman region of Italy, the western branch of the East African rift valley, the Leucite Hills of Wyoming, and the West Kimberley area of Western Australia. In order to review occurrences of ultrapotassic rocks a definition must be adopted, and here we introduce limits based on whole-rock chemistry.

Owing to the continuous variation in oxide abundances, chemical screens are necessarily arbitrary, but are chosen to approximately coincide with general usage. The chemical screens used are:

[1] $K_2O/Na_2O > 2$: Higher values of 3 [Carmichael, Turner and Verhoogen 1974] and 2.5 [Venturelli and Di Battistini 1980] have been used previously, but the present value is chosen to include rocks from the Toro Ankole volcanic field of Uganda which are generally

treated as ultrapotassic.

[2] K_2O > 3 wt% : This avoids confusion with rocks which have a high K_2O/Na_2O ratio but only low total alkalies, and thus excludes virtually all kimberlites.

[3] MgO > 3 wt% : to restrict attention to mafic as opposed to salic rocks.

In a survey of the literature, 827 analyses of ultrapotassic rocks from 82 localities were found using these chemical screens. These are summarised in table 1 together with sources of data and ages, where available. Table 1 also lists the groupings as defined in the next section, and latitutdes and longitudes: location maps for many of these localities are given by Bergman [1986].

The choice of chemical screens allows inclusion of most major rock types generally treated in discussions of ultrapotassic rocks, but also includes many which are not. The most notable of these are ultrabasic (eg. Fen, Oka) and alkaline lamprophyres (especially minettes), and vaugnerites and durbachites which are generally treated as ferromagnesian-rich 'granitic' rocks. The presence or absence of particular minerals is not used in defining the term ultrapotassic. We do not follow the tendency of some petrologists to treat 'ultrapotassic' as being synonymous with 'leucite-bearing'. Leucite is a common mineral in many ultrapotassic rocks but is not diagnostic and also occurs in rocks with a K_2O/Na_2O ratio which may be barely greater than 1 [Duda and Schmincke 1978; Baker et al. 1964; Gupta and Yagi 1980; Holmes and Harwood 1937].

Table 2 reports available Sr, Nd, Pb and O isotope measurements for ultrapotassic rocks. Unfortunately, most of these are from samples for which major and trace element analyses are not available, so that only an approximate treatment of the isotope data is possible.

1.4 ULTRAPOTASSIC ROCK CLASSIFICATION

Ultrapotassic rocks defined by the chemical screens noted above are an exceptionally heterogeneous group with large variations in most major element oxide abundances. Four groups are outlined here of which three are apparent 'end-members' on a selection of oxide-oxide variation diagrams, and the fourth is merely a convenient transitional group.

ASIA:					
IV	Afyon, Turkey	38°N,30°E	3	9 - 15	Keller 1983; Besang et al 1977
II	Turja, Kola Peninsula, USSR	66°N,35°E	1	Caledonian	Kranck 1928; Gerasimovskiy et al 1974
II	Bergydamalakh, Anabar, USSR	67°N,110°E	1	?	Ukhanov 1963
IV	Aldan Shield, East Siberia, USSR	55°N,120°E	6	Jur - Cret	Maksimov & Ugryumov 1971
IV	Baltoro, Karakorum Himalaya	86°N,76°E	2	~3	Viterbo & Zanettin 1959; Desio 1979
II	Damodar Valley, India	22°N,87°E	4	?	Gupta et al 1983
IV	Manchuria, China	45°N,125°E	1	Quaternary	Tomita 1970
II	Boshan, China	35°N,110°E	1	?Caledonian	He Guan-Zhi 1984
IV	Tsao-hi, northern Taiwan	25°N,122°E	1	?	Chao Tsung-pu 1960
III	Segamat, Malaysia	2°N,103°E	3	?	Grubb 1965
IV	Kajan, Kalimantan, Indonesia	1°N,115°E	5	?	LaCroix 1926; Pirsson 1905; Iddings & Morley 1915
III	Muriah, Java, Indonesia	7°S,111°E	1	Quaternary	Ferrara et al 1981
III	Sangenges, Sumbawa, Indonesia	8°S,118°E	3	Quaternary	Foden, 1979
III	Batu Tara, Indonesia	8°S,123°E	21	Quaternary	Van Padang 1951; Wheller et al [1986]
III	Dezhnev, eastern Siberia, USSR	66°N,170°W	3	(107-105)	Perchuk 1965
NORTH AMERICA:					
III	Western Alaska, USA	65°N,166°W	7	107 - 105	Miller 1972
II	Batbjerg, Kangerdlugssuaq, E.Greenland	68°N,33°W	3	445	Brooks et al 1976, 1981
I	Holsteinsborg-Itivdleq, West Greenland	67°N,53oW	49	1227	Scott 1977, 1979, 1981
II	Oka, Quebec, Canada	46°N,74°W	1	117-118	Gold 1970; Eby 1984; Shafilqullah et al 1970
IV	British Columbia, Canada	49°N,117°W	2	?	Daly 1912
IV	Bearpaw Mountains, Montana, USA	48°N,109°W	2	?	Larsen 1941; Knopf 1936; Schmidt et al 1961
IV	Highwood Mountains, Montana, USA	47°N,110°W	16	?	Nash & Wilkinson 1970, 1971; Witkind 1973; Knopf 1936; Buie 1941; Burgess 1941; Larsen 1941; Pirsson 1905
I	Smoky Butte, Montana, USA	47°N,107°W	3	27	Velde 1975; Fraser et al. 1985
IV	Yellowstone-Absaroka, Mt-Wy, USA	45°N,110°W	3	~50	Joplin 1966; Nicholls & Carmichael 1969; Pirsson 1905; Chadwick 1970
IV	Black Hills, South Dakota, USA	44°N,103°W	1	?	Kirchner 1979
I	Leucite Hills, Wyoming, USA	41°N,109°W	31	1.1	Kuehner et al 1981; Cross 1896; Schultz & Cross 1912; Ogden 1979; Carmichael 1967; Johnston 1959; Smithson 1959; Yagi & Matsumoto 1966; Barton & Hamilton 1978; Barton & van Bergen 1981
I/II	Northeast Utah, USA	40°N,111°W	3	13, 38, 39	Best et al 1968
IV	Spanish Peaks, Colorado, USA	37°N,105°W	6	26-22	Johnson 1964, 1968; Stormer 1972
IV	Navajo field, Arizona-New Mexico, USA	35°N,110°W	24	31-25	Roden & Smith 1979; Ehrenberg 1982; Nicholls 1969; Roden 1981; Rogers et al 1982; Williams 1936
IV	Sierra Nevada, California, USA	37°N,119°W	9	~3.5	Dodge & Moore 1981; van Kooten 1980, 1981
I	Hills Pond, Kansas, USA	37°N,95°W	8	90	Merrill et al 1977; Zartman et al 1967; Cullers et al 1985
I	Arkansas (Prairie Creek & Magnet Cove), USA	34°N,93°W	4	106-99	Bolivar & Brookins 1979; Scott-Smith & Skinner 1984b; Gogineni et al 1978; Kemp 1891; Zartman et al 1967
AUSTRALIA:					
IV	New South Wales	32°S,147°E	22	15-10	Cundari 1973; Cundari et al 1978
I	West Kimberley, West Australia	18°S,124°E	42	25-18	Jaques et al 1984a,b; Prider 1960, 1982; Wade & Prider 1940; Nixon et al 1984; Atkinson et al 1984
I	East Kimberley, West Australia	16°S,128°E	1	Proterozoic	Atkinson et al 1984
IV	Mordor, Northern Territory	23°S,134°E	2	~1150	Langworthy & Black 1978
IV	West Tasmania	42°S,145°E	3	post-Devonian	Solomon 1964; Sutherland & Corbett 1974
ANTARCTICA:					
I	Gaussberg, Wilhelm II Land	66°S,89°E	11	0.056	Sheraton 1981; Sheraton & Cundari 1980; Tingey et al 1983
II	Beaver Lake, MacRobertson Land	71°S,71°E	2	130-110	Ravich et al 1978; Walker & Mond 1971
I	Mount Bayliss, MacRobertson Land	73°S,62°S	2	430-413	Sheraton & England 1980
I	Priestly Peak, Enderby Land	67°S,50°E	4	?	Sheraton & England 1980

Asia							
Afyon, Turkey	0.7072 [2] 0.7071-0.7073						Keller 1983
Muriah	0.7041 [2] 0.7040-0.7042	+1.2 [1]					Whitford et al 1981; Ferrara et al 1981
Sangenges	0.7053 [1]	-1.3 [1]					Whitford et al 1978; Jenner et al [unpubl.]
Batu Tara	0.7066 [2] 0.7061-0.7071	-2.5 [2] -1.2 to -3.7					Jenner et al [unpubl.]
Australia							
West Kimberley	0.7153 [8] 0.7123-0.7187	-12.6 [8] -7.4 to -15.4		15.736 [13] 15.687-15.796	17.469 [13] 17.239-17.882	38.254 [13] 37.797-38.593	McCulloch et al 1983; Nelson et al 1986
New South Wales	0.7052 [11] 0.7050-0.7056	-1.0 [11] +0.4 to -4.1	8.1 [17] 6.2-11	15.596 [11] 15.558-15.618	18.198 [11] 17.874-18.439	38.353 [11] 38.135-38.562	Taylor et al 1984; Nelson et al 1986
Mordor	(0.7158) [1]						Langworthy & Black 1978
Antarctica							
Gaussberg	0.7096 [7] 0.7092-0.7098	14.0 [7] -13.0 to -14.3	6.5 [4] 6.1-7.0	15.662 [2] 15.649-15.674	17.595 [2] 17.588-17.602	38.440 [2] 38.402-38.478	Taylor et al 1984; Collerson & McCulloch 1983
North America							
Holsteinsborg	0.7038 [1]						Scott 1981
Batbjerg	0.7046 [1]						Brooks et al 1976
Sierra Nevada	0.7063 [3] 0.7061-0.7064			15.674 [5] 15.663-15.679	18.898 [5] 18.871-18.916	38.943 [5] 38.913-38.972	Van Kooten 1981
Navajo	0.7073 [10] 0.7055-0.7119						Powell & Bell 1970; Roden 1981
Leucite Hills	OW 0.7058 [37] 0.7053-0.7078 M 0.7055 [16] 0.7054-0.7056	-15.4 [12] -13.7 to -17.0 -11.3 [7] -10.5 to-12.3	9.9 [3] 8.8-12.0 11.1 [2] 10.3-11.9				Vollmer et al 1984; Kuehner 1980;
Smoky Butte	0.7061 [6] 0.7059-0.7063	-23.9 [6] 21.7 to -26.0		15.269 [6] 15.190-15.527	16.244 [6] 16.025-16.643	36.39 [6] 36.20-36.68	Fraser et al 1985
Prairie Creek	0.7082 [2] 0.7066-0.7097						Bolivar & Brookins 1979
Highwood Mts	0.7075 [5] 0.7072-0.7081						Powell & Bell 1970

The three major groups are essentially an extension of the classification suggested by Barton [1979] but are separated here purely on a chemical basis. Some minerals such as clinopyroxene and leucite have distinctive compositions in each group, and some minerals occur exclusively in one particular group. However, mineralogy can serve only as a guide to a chemical classification and is not treated as diagnostic for two reasons: (a) heteromorphism is a major problem in alkaline rocks due to the large number of potential minerals, many of which do not occur as phenocrysts, so that occurrence of a particular mineral may be due only to conditions and degree of crystallisation; (b) presence or absence of a given mineral is a partition-type delimiter and cannot be transitional, and thus must be of secondary importance in our resemblance classification.

The major groupings are illustrated in chemical variation diagrams in figures 1 to 6. The K_2O/SiO_2 plot conventionally used to classify basaltic rock types is not used as it does not distinguish between the major types of ultrapotassic rocks. Figures 1-4 contain diagrams which are more useful as group discriminants, whereas figures 5-6 depict additional features of petrological interest. Because of the large number of analyses group IV rocks are plotted separately in figures 1 to 6 for clarity and are cross-referenced to groups I, II and III by the lines serving as approximate group delimiters. These lines are not intended as strict boundaries but merely include the majority of analyses in each group for comparison with group IV and for ease of reference. The plots in figures 1 to 6 emphasise the gradational nature of ultrapotassic rock chemistry in that even after removal of a substantial transitional group strict boundaries are, in many cases, difficult to draw.

The major element characteristics of the groups, together with other pertinent features, are outlined below. They are discussed in further detail in the section on petrogenesis.

1.4.1 MAJOR ELEMENTS:

1.4.1.1 Group I

This group is equivalent to Barton's [1979] 'Leucite Hills Type' and Sahama's 'Orenditic' class. The term lamproite [Wade and Prider 1940] was originally, and is consistently, applied to rocks of this group. Where used later in this paper, 'lamproites' will refer to rocks of Group I. Group I

rocks are best distinguished by their low contents of Al_2O_3, CaO and Na_2O (figures 1, 3 and 4). They have high K_2O/Al_2O_3, generally above 0.6, and frequently are perpotassic ($K_2O/Al_2O_3 > 1$) (figure 2). SiO_2 content is variable (36 - 60 wt %), but high K_2O/Al_2O_3 is maintained even in rocks richest in silica. The Mg-number is generally higher than in the other groups.

Group I is best separated from group III by Al_2O_3 content (particularly CaO vs Al_2O_3; figure 1) and from group II by CaO and SiO_2. The incompatible trace elements such as Ba, Rb and Zr, whilst high in all ultrapotassic rocks, are most abundant in group I. The best examples are from West Kimberley and Gaussberg, and these are preferred to the Leucite Hills as standard members because of the relatively low SiO_2, high CaO madupites of the Leucite Hills which could be considered transitional between groups I and II. Rocks from other areas such as the northwestern Alps, southeastern Spain, Koudiat-el-Anzazza (Algeria) and West Greenland have chemical characteristics which are less extreme than the group I end-members.

The chemistry of the lamproites, especially the low Al_2O_3, leads to distinctive mineral compositions such as low Al clinopyroxene, mica and amphibole [Barton 1979; Cundari and Ferguson 1982] and the occurrence of rare Al-free accessory minerals such as priderite [$(K,Ba)(Ti,Fe)_8O_{16}$], wadeite [$Zr_2K_4Si_6O_{18}$] and shcherbackovite [$(Na,K)(Ba,K)(Ti,Nb)_2Si_4O_{14}$]. For more details of lamproite mineralogy, see Mitchell [1986], Bergman [1986] and source references listed in table 1.

1.4.1.2 Group II

Members of this group are distinguished chiefly by their consistently low SiO_2 (< 46 wt %), and most of the overlap with the low-silica olivine lamproites of group I is removed by reference to the high CaO of group II (figures 1, 3 and 4). They also have low Al_2O_3 (figure 1) but, due to less extreme K_2O, have lower K_2O/Al_2O_3 (figure 2). Na_2O is also low and Mg-number is variable but mostly above 60. The rocks of this group are commonly referred to as kamafugites [Sahama 1974, Gallo et al. 1984] and are equivalent to Barton´s ´Toro-Ankole Type´. The Toro Ankole rocks are the most abundant members of this group and will serve as the standard members. Other rocks included are the Cupaello and San Venanzo occurrences in Italy, plus olivine melilitites and ultrabasic

GROUPS I, II, III

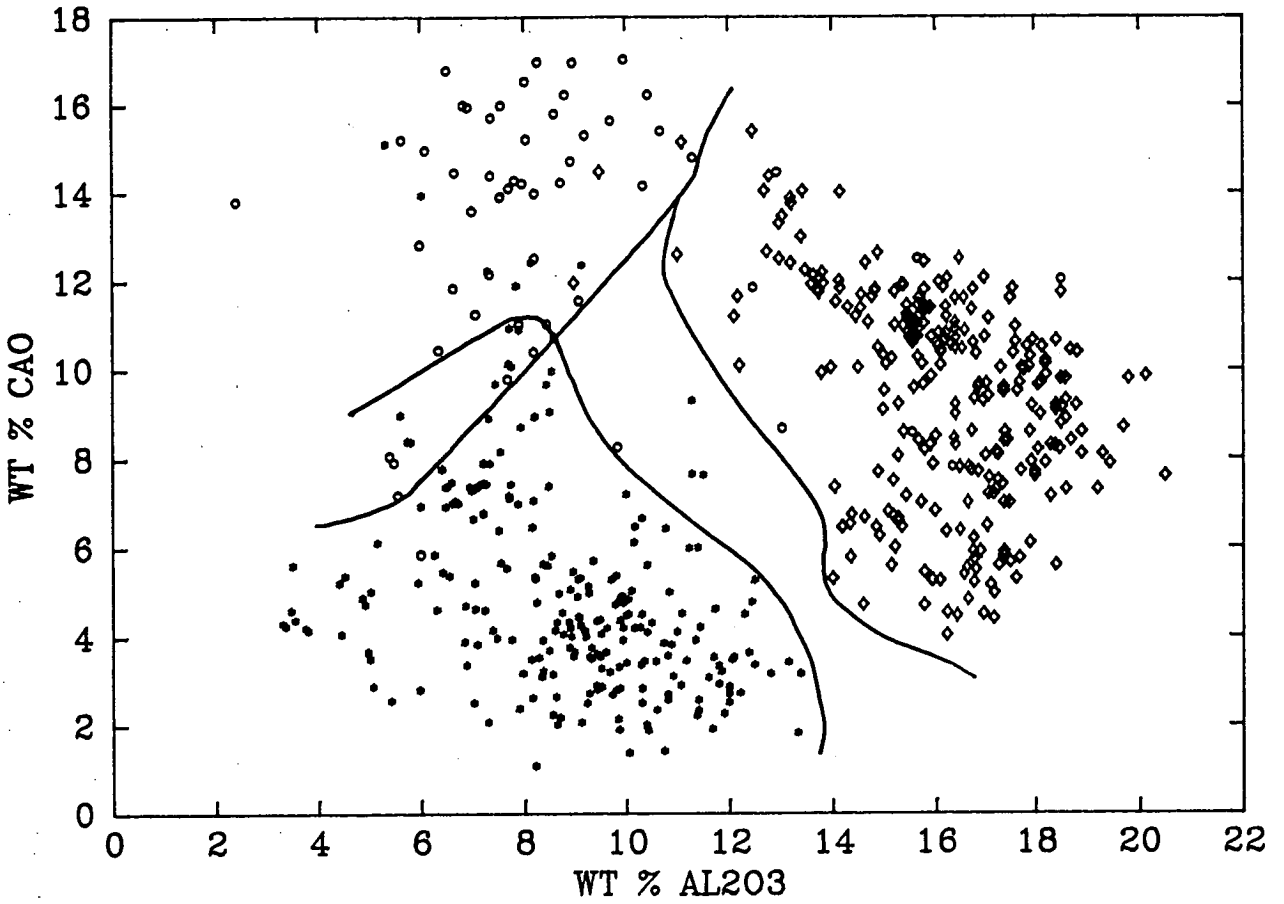

GROUP IV

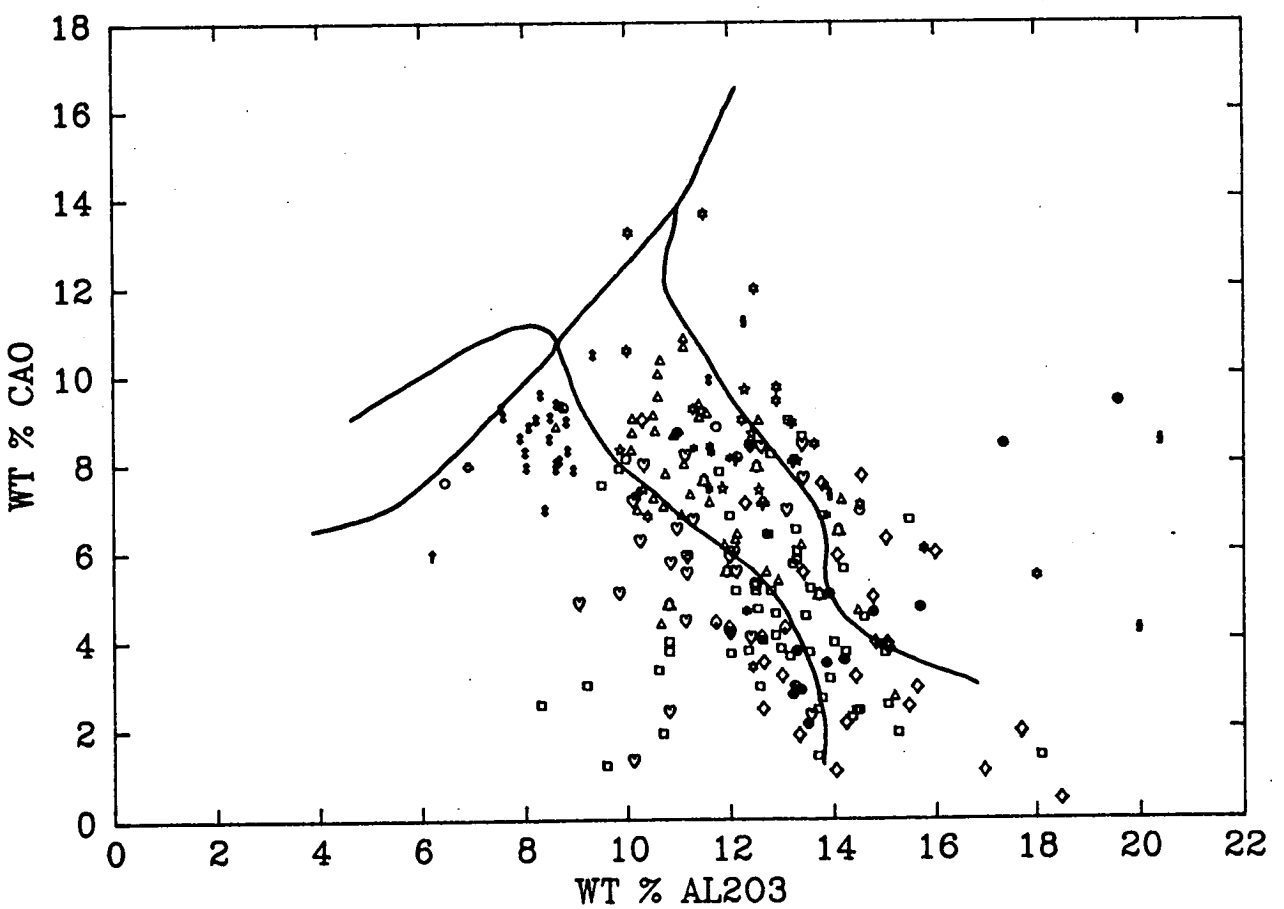

GROUPS I, II, III

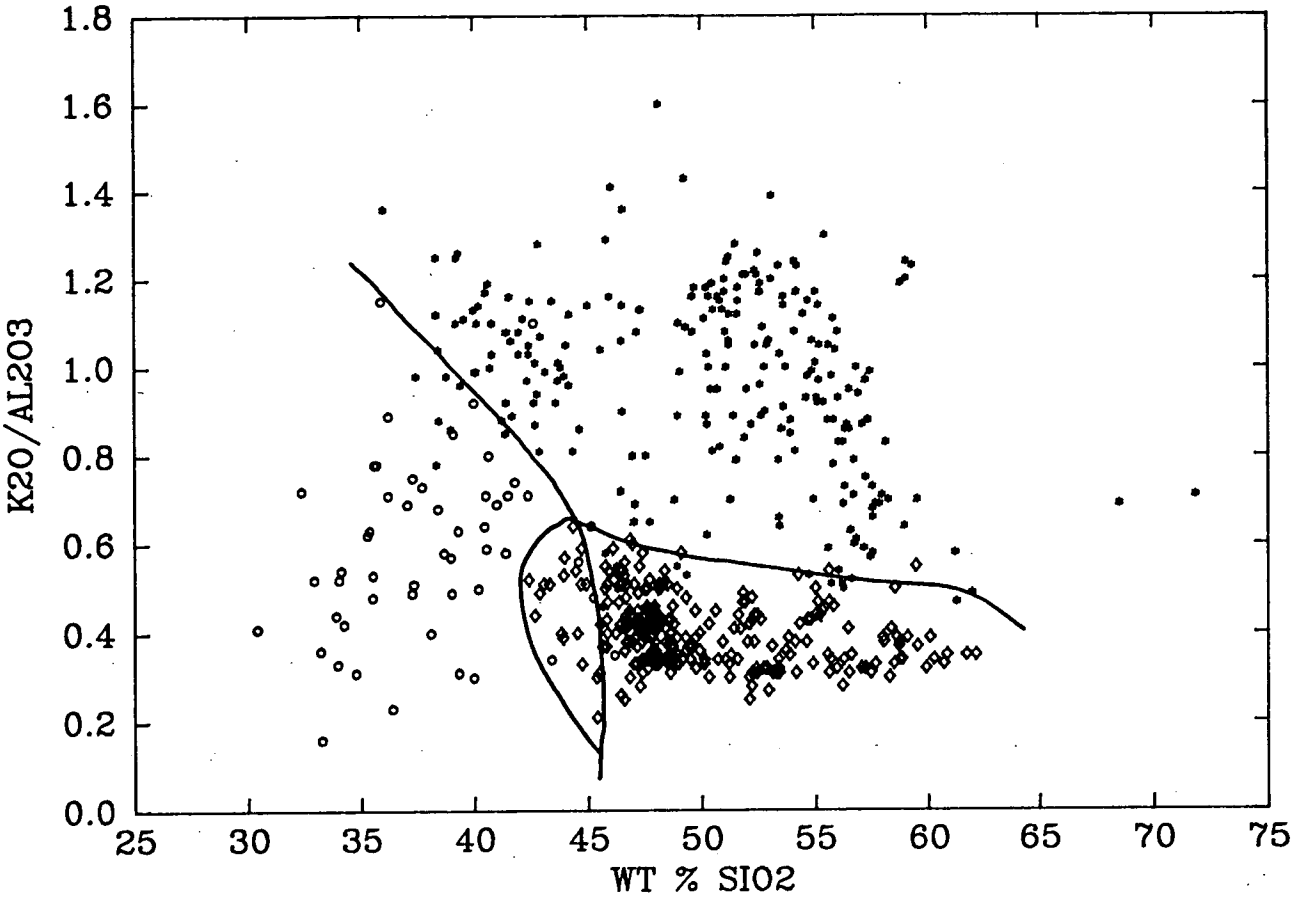

GROUP IV

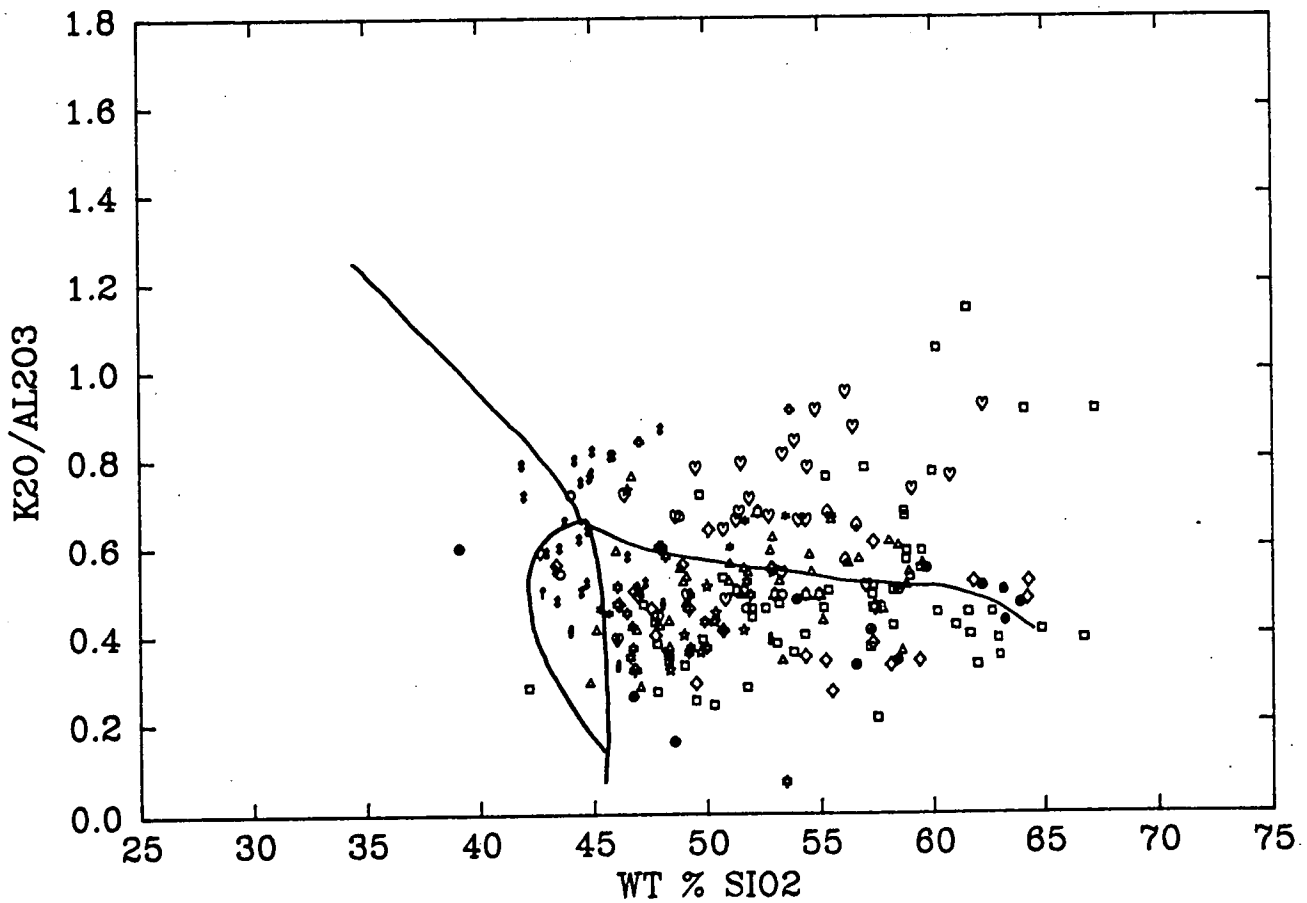

GROUPS I, II, III

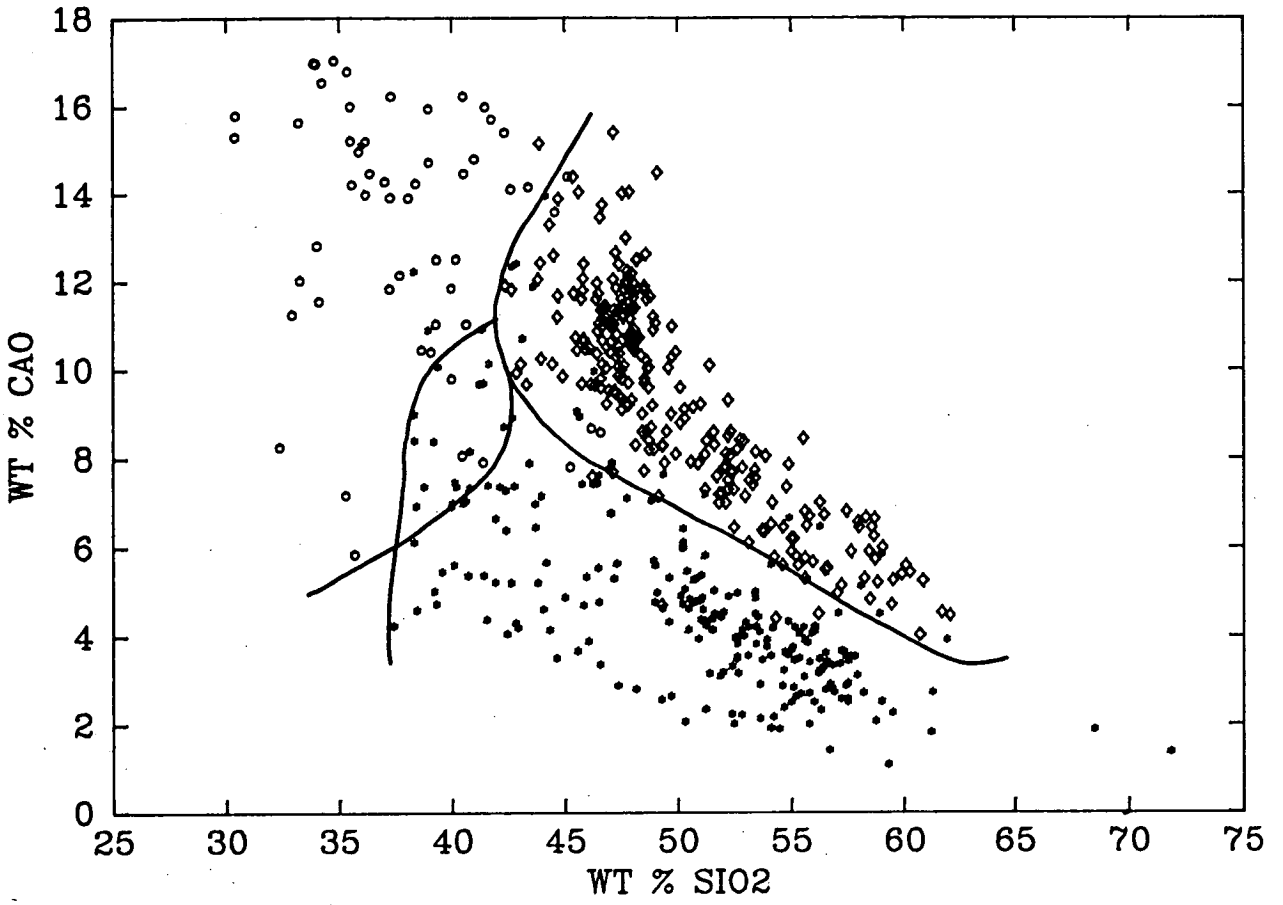

GROUP IV

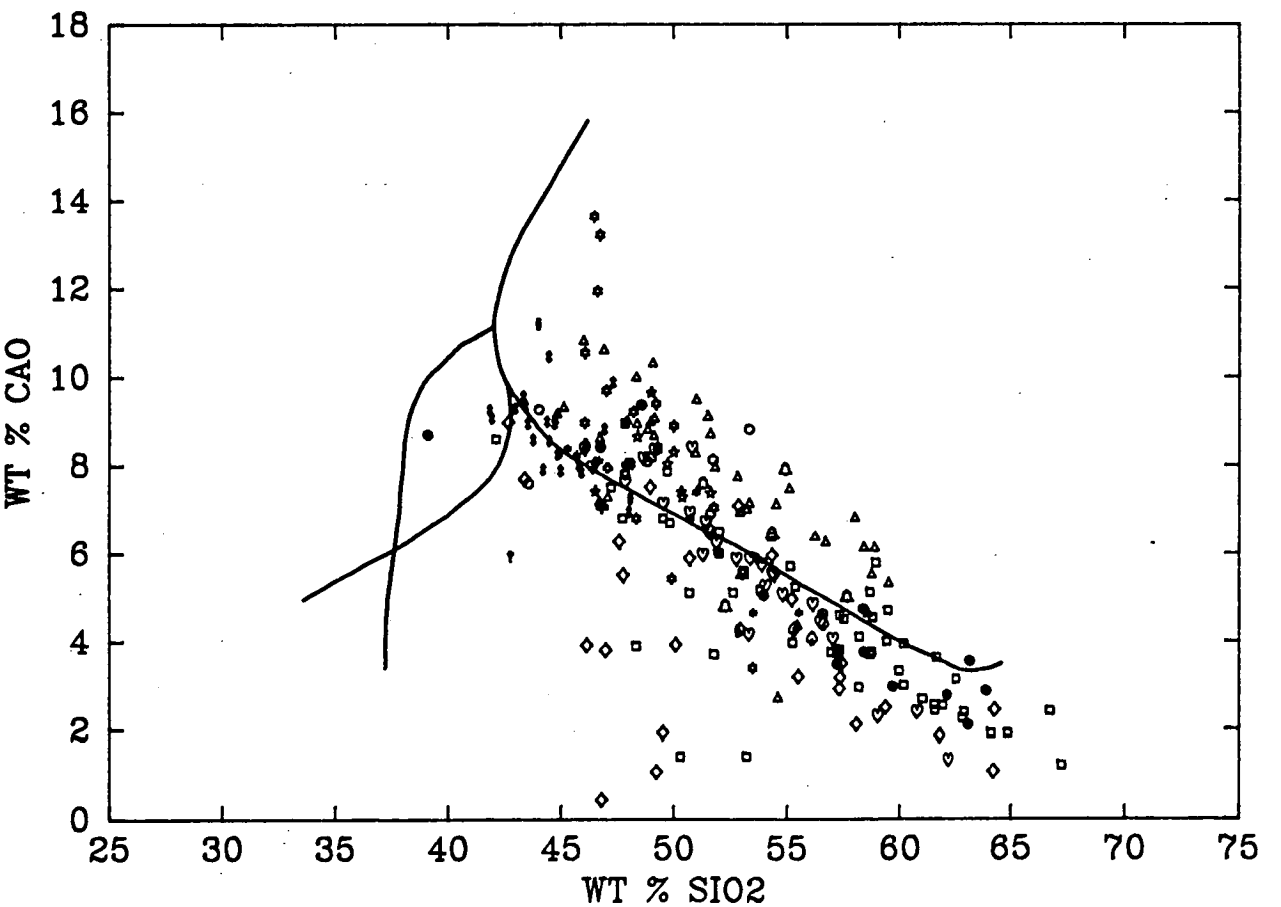

GROUPS I, II, III

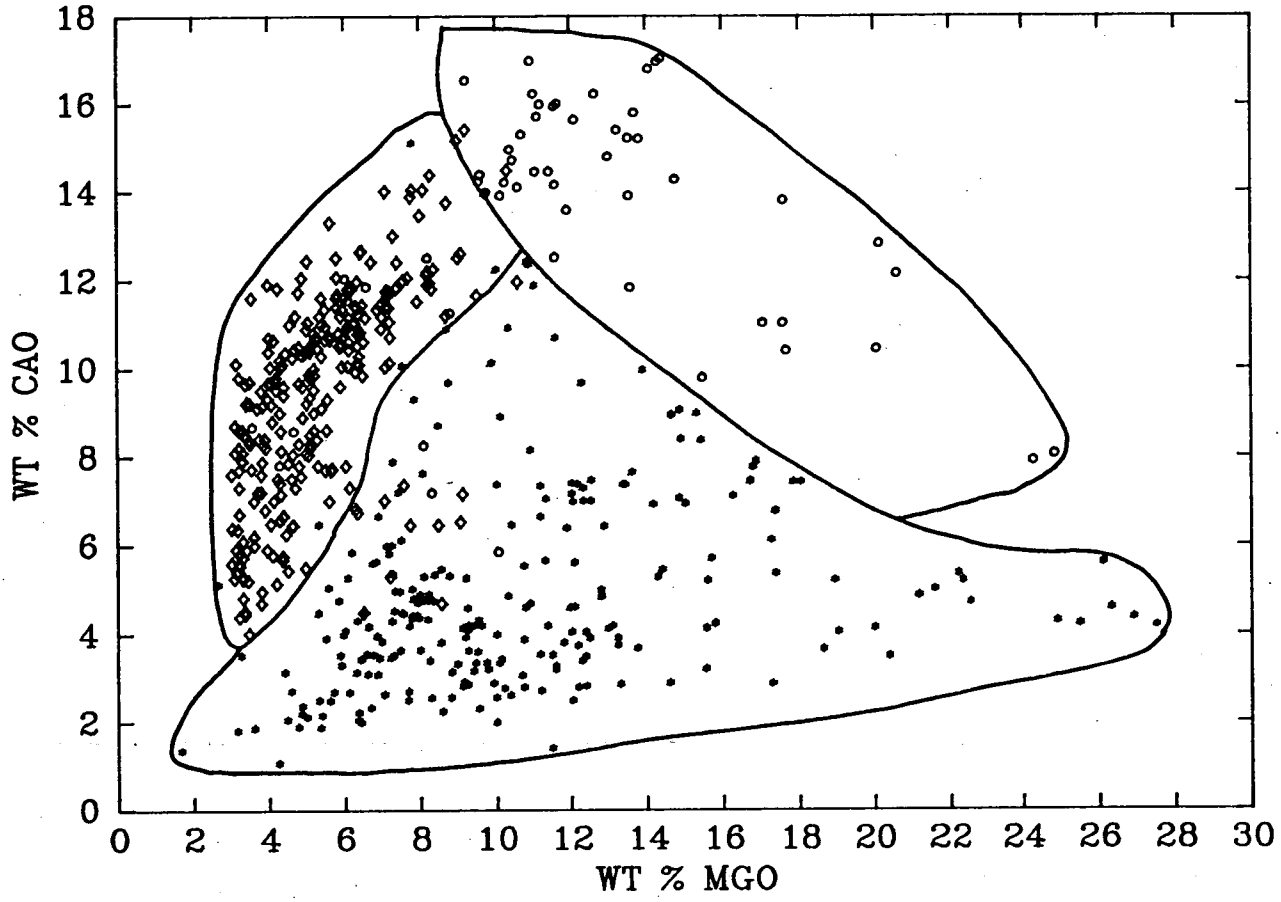

GROUP IV

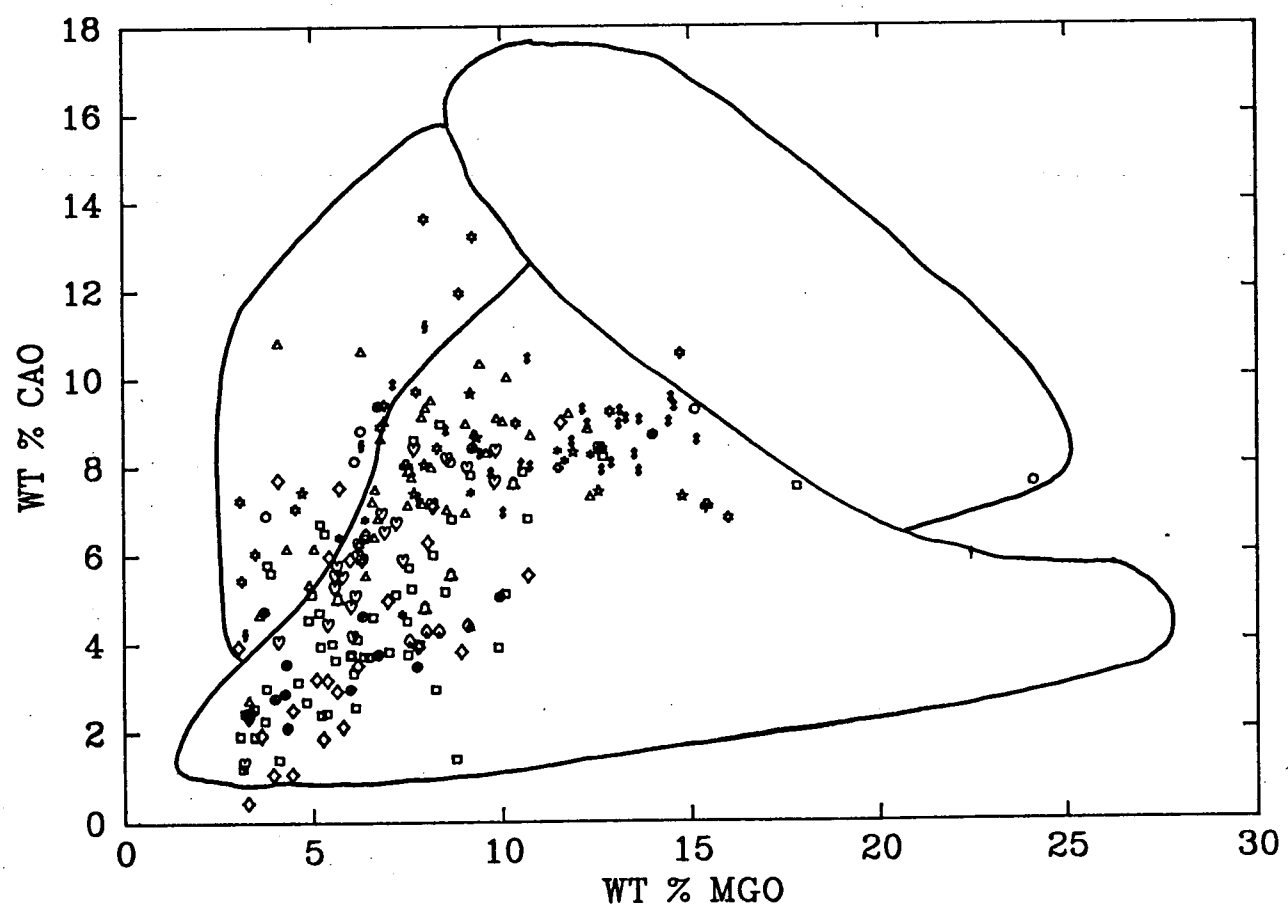

GROUPS I, II, III

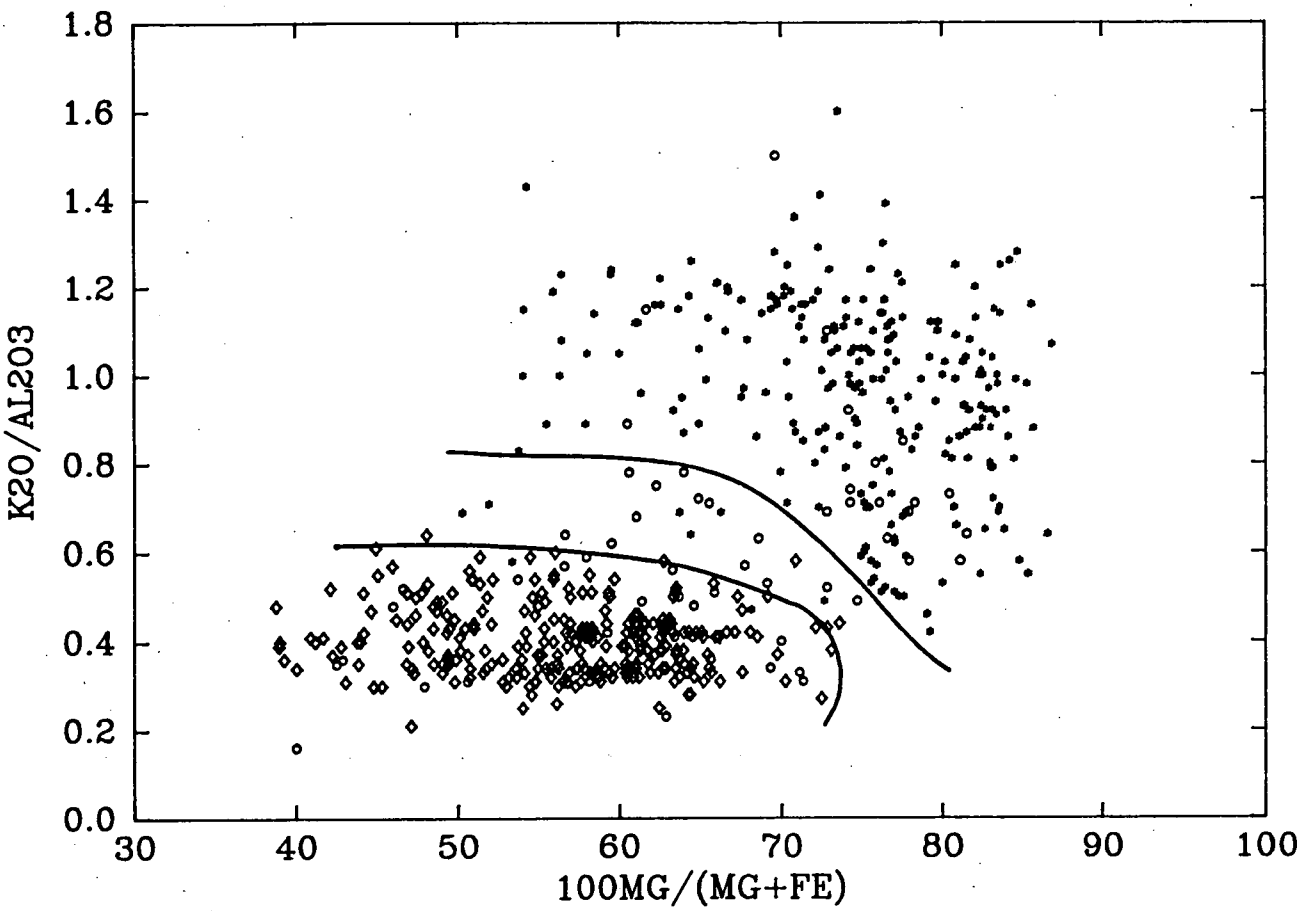

GROUP IV

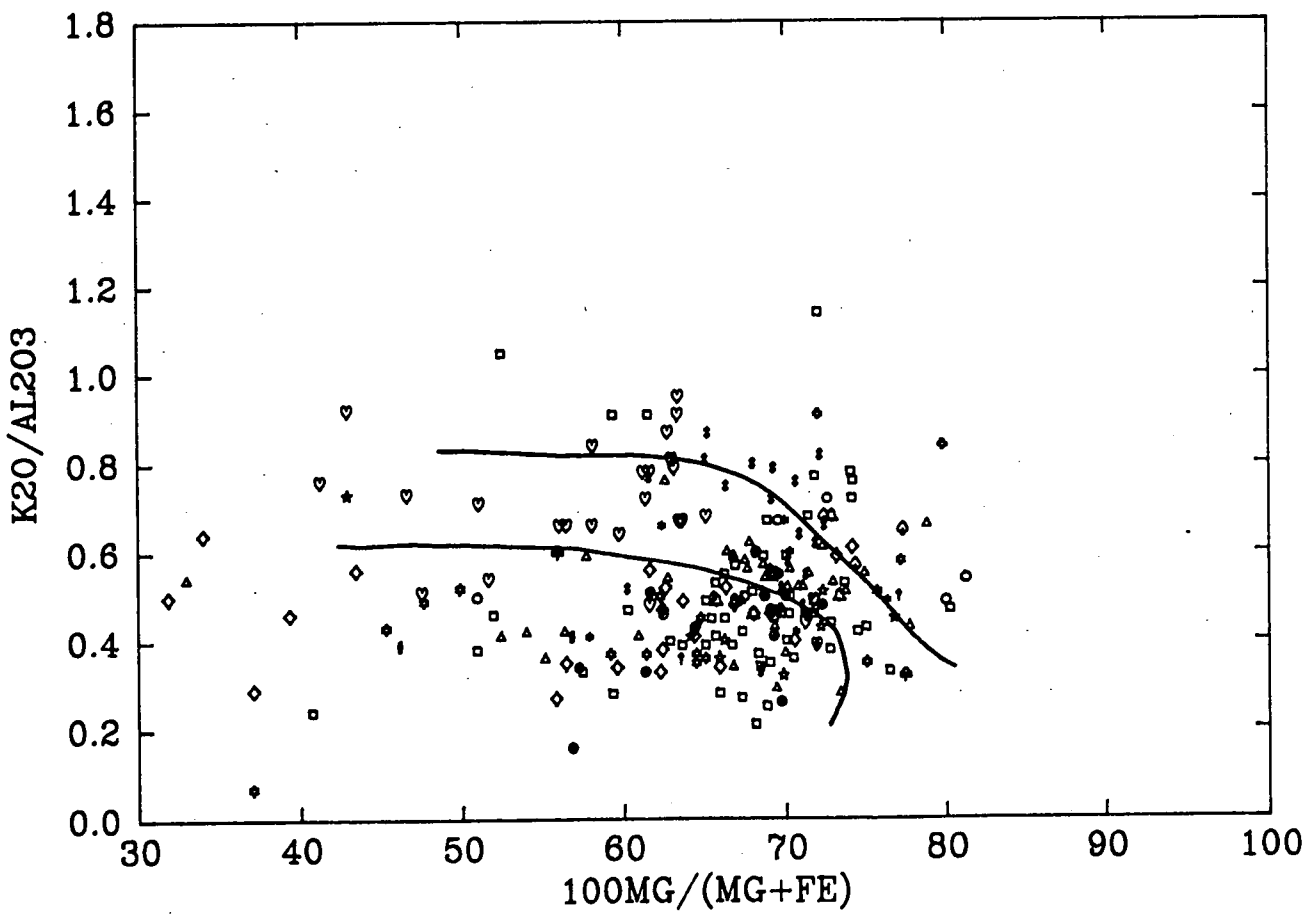

GROUPS I, II, III

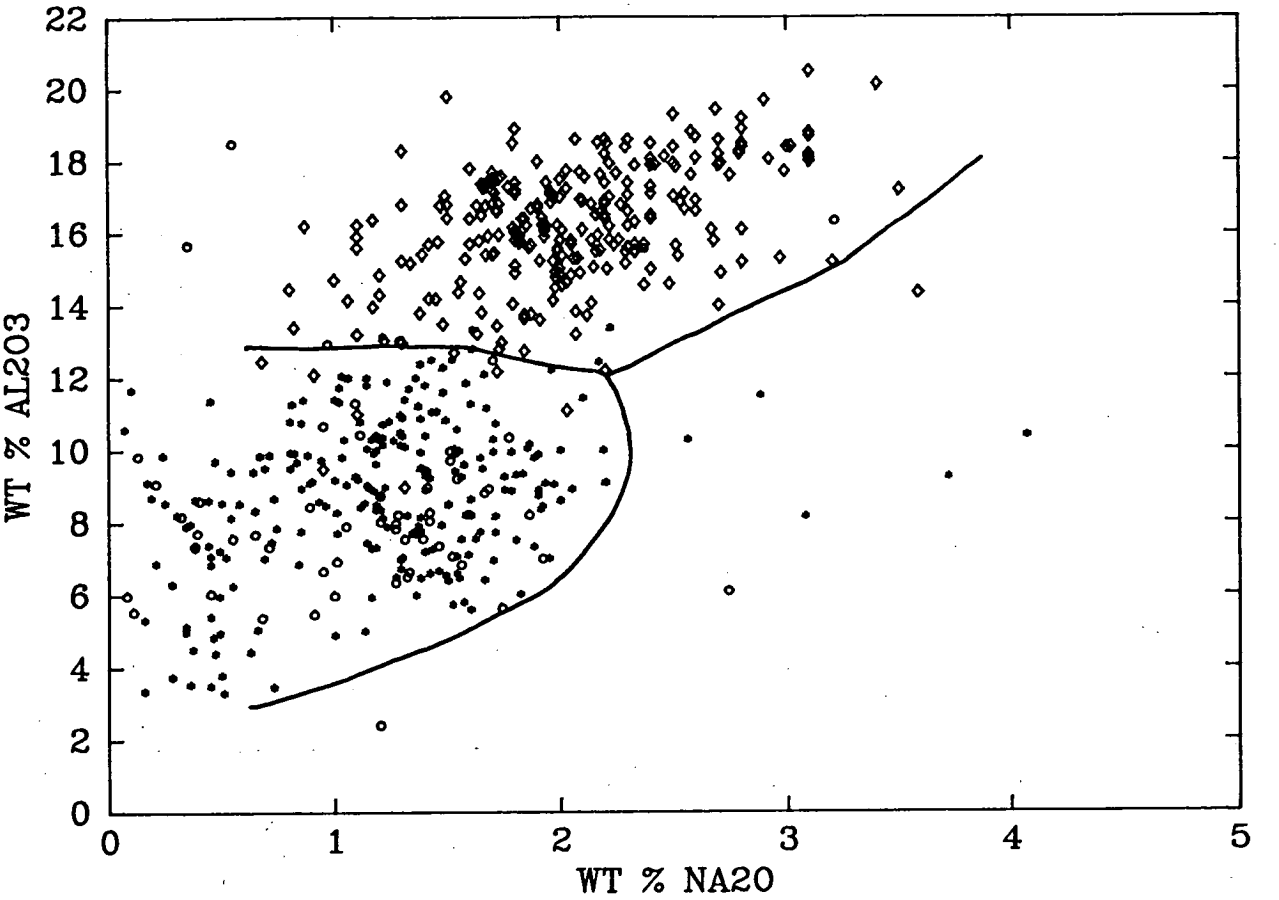

GROUP IV

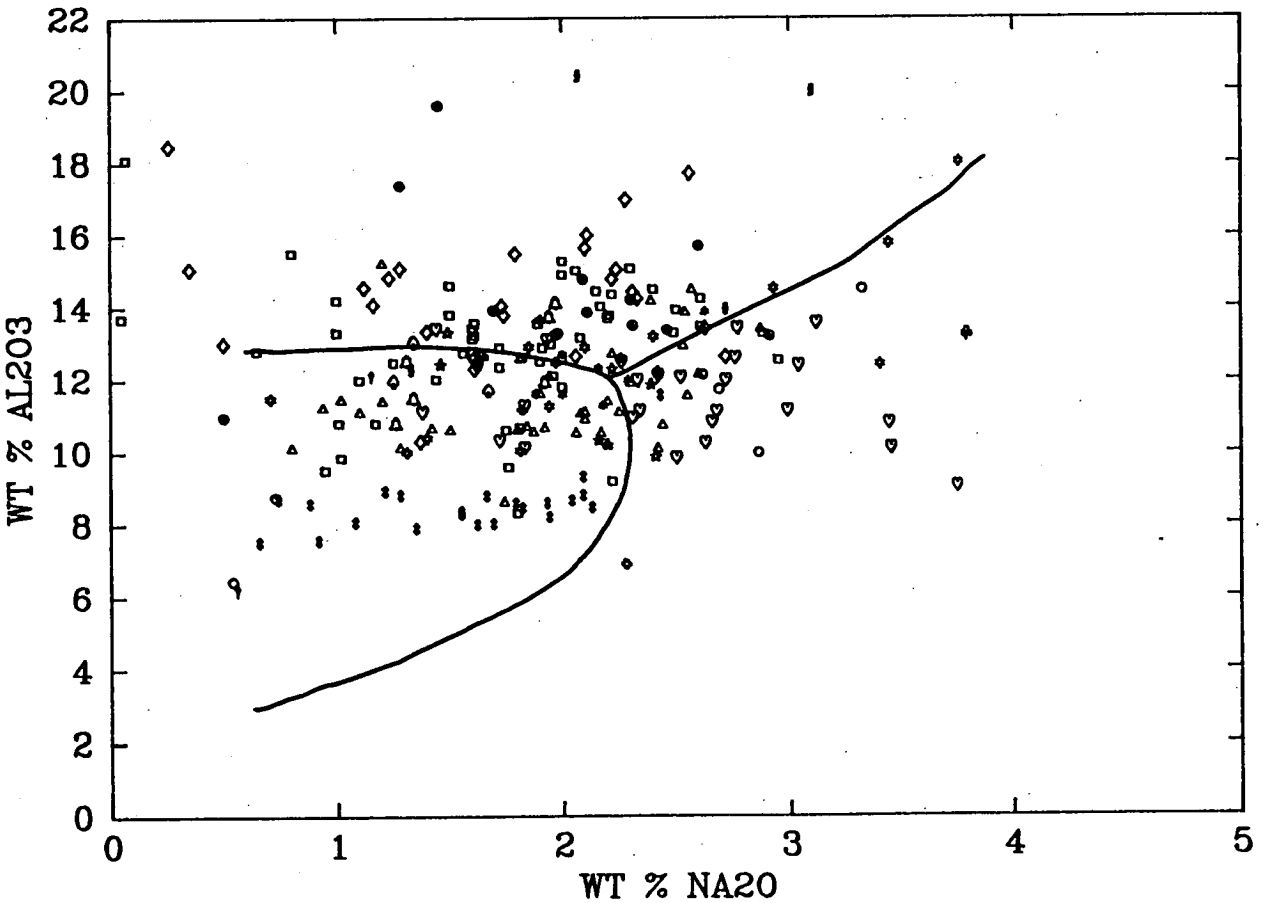

lamprophyres from a number of areas (table 1). Petrographically, group II rocks often contain melilite, perovskite and kalsilite due to the low SiO_2 contents, and groundmass carbonate frequently occurs.

1.4.1.3 Group III

This group is equivalent to Barton's "Roman Province Type", but no general rock name like lamproite or kamafugite has been applied. The principal major element characteristic of group III is their high Al_2O_3 content, which leads to low K_2O/Al_2O_3 (generally less than 0.5; figure 2) despite K_2O contents which are normally higher than group II rocks. The CaO content of the more basic group III rocks is generally intermediate between that of groups I and II, and decreases toward more differentiated rocks (figure 3). Mg-number is lower than in the other groups, being only rarely above 70 (figure 5), and rocks with extremely low silica contents (< 42 wt %) do not occur, although contents less than 50 wt % are common.

For the standard members we take the Roman Province volcanics since they form the bulk of the analyses, but there is less variation between localities in group III, so that the distinction of a specific end-member is not so important here. The Indonesian examples are also typical of group III and will be used later in petrogenetic arguments because of their simpler tectonic environment.

The high Al_2O_3 content is the principal factor in determining the mineralogy of these rocks: plagioclase is common, as is clinopyroxene which contains greater amounts of Al_2O_3 than in group I [Barton 1979; Cundari and Ferguson 1982]. Leucites characteristically have low Fe_2O_3 contents, but this may be due to the high Al_2O_3 content of the rocks rather than reflecting oxygen fugacity, since the Fe_2O_3 content depends on $K_D^{Al\text{-}Fe3+}_{lc\text{-}lq}$ [Part 2]. The high Al_2O_3 and SiO_2 together prevent crystallisation of Al-free accessories and silica-undersaturated minerals such as kalsilite, melilite, perovskite, priderite and wadeite which are characteristic of the other two groups. The rocks from the Alban Hills, central Italy, are an exception, frequently containing melilite.

1.4.1.4 Group IV

As noted above (section 2), the recognition of transitional types is a logical consequence of a resemblance classification. The choice of rocks

included in group IV is to some extent arbitrary, since the only criterion is that they have intermediate characteristics. Rocks from one locality frequently have a range in composition, and some samples fall close to one group end-member. However, other samples from the same locality are chemically very different and fall outside the 'field' for the group. Rather than separate rocks from one locality into separate groups, they are included in Group IV. Most localities included in group IV do not have any samples with characteristics close to end-members of the other groups.

Group IV rocks are generally transitional between groups I and III (figures 1 to 6) rather than between I and II or II and III. This is because rocks from end-member localities for groups I and III are relatively well separated chemically (figures 1-4) whereas transitional members between, for example, groups I and II are from suites which contain rocks strongly resembling group end-members, such as the Leucite Hills. Many group IV rocks have high Mg-number and SiO_2 less than 55 wt % (figures 1 to 5). Figure 6 indicates that many have distinct Na_2O vs Al_2O_3 characteristics which are not purely transitional.

A large part of group IV is taken up by rocks which are not usually considered at all in discussions of ultrapotassic rocks, some of which may result from very different petrogenetic processes. These are treated only briefly here as the purpose of this paper is to discuss the three very different group end-members.

1.4.2 GEOLOGICAL SETTING

This section considers the setting of ultrapotassic rocks in terms of both tectonics and associated rock types. In broad tectonic terms, group I rocks occur either in stable continental areas or in orogenic areas. Group II rocks occur dominantly in rift environments, and group III rocks occur exclusively in active orogenic zones.

The standard members of group I occur in stable continental areas and normally have no associated non-ultrapotassic rocks, except possibly kimberlites in the case of Western Australia [Atkinson et al. 1984]. Other group I rocks occur in orogenic areas and may be associated with calc-alkaline or shoshonitic rocks (eg. northwestern Alps, southeastern Spain). These non-standard suites are apparently not always directly associated with active subduction and the closure of ocean basins (Dal Piaz

et al. 1979; Venturelli et al. 1984a,b) since the magmas may be emplaced after the cessation of continental collision and subduction. The contrast between the stable continental and orogenic rocks is expressed chemically in the diagram P_2O_5/TiO_2 vs TiO_2 (figure 7). Group I rocks from stable continental areas have high TiO_2 whereas rocks from more recently tectonically active areas have lower TiO_2 and a greater spread in P_2O_5/TiO_2. The orogenic versus continental distinction is further illustrated by the group II and III rocks (figure 7b). The rocks from the northwestern Alps, southeastern Spain, Algeria and Corsica appear to form a distinct province associated with Mediterranean tectonics, and have similar P_2O_5/TiO_2 characteristics to group III lavas of the Roman province, but with slightly higher TiO_2. The Pendennis minette, which also falls into the low TiO_2 region, is associated with group IV rocks from Jersey and Devonshire with Hercynian tectonics of the English Channel area. The dividing line in figure 7a between non-orogenic and orogenic areas is quite sharp at around 2 wt % TiO_2, with rocks from continental North America grouped closely at 1.7 to 2.8 wt % TiO_2.

The region indicated for group II in figure 7b is dominantly due to the Toro Ankole volcanics of the East African rift which form the bulk of the analyses. The Toro Ankole volcanics are part of an extensive suite of alkaline rocks in the western branch of the rift valley [Pouclet 1980a,b; Pouclet et al. 1984]. Associated rocks include alkali basalts and nephelinites which have progressively higher K_2O/Na_2O and total alkalies and lower silica northwards [Pouclet et al. 1984] towards the Toro Ankole volcanic field where ultrapotassic rocks occur together with carbonatites [Von Knorring and Du Bois 1961; Nixon and Hornung 1973].

Group II also includes a number of ultrabasic lamprophyres and olivine melilitites which plot amongst the Toro Ankole rocks in figure 7b, and are also associated with rifts. The Oka, Fen and Aland Islands lamprophyres form part of a widespread province of rift-associated rocks throughout the North Atlantic region approximately 500 my old [Doig 1970]. The remaining association of group II rocks is between olivine melilitites and kimberlites in South Africa [McIver 1981] and on the Anabar Shield where the two rock types occur together in the same igneous body [Ukhanov 1963]. A kimberlite from the Kimberley area of South Africa qualifies as ultrapotassic [Dawson 1972], and has group II characteristics. Some Arkansas ultrapotassic rocks falling in between

GROUP 1

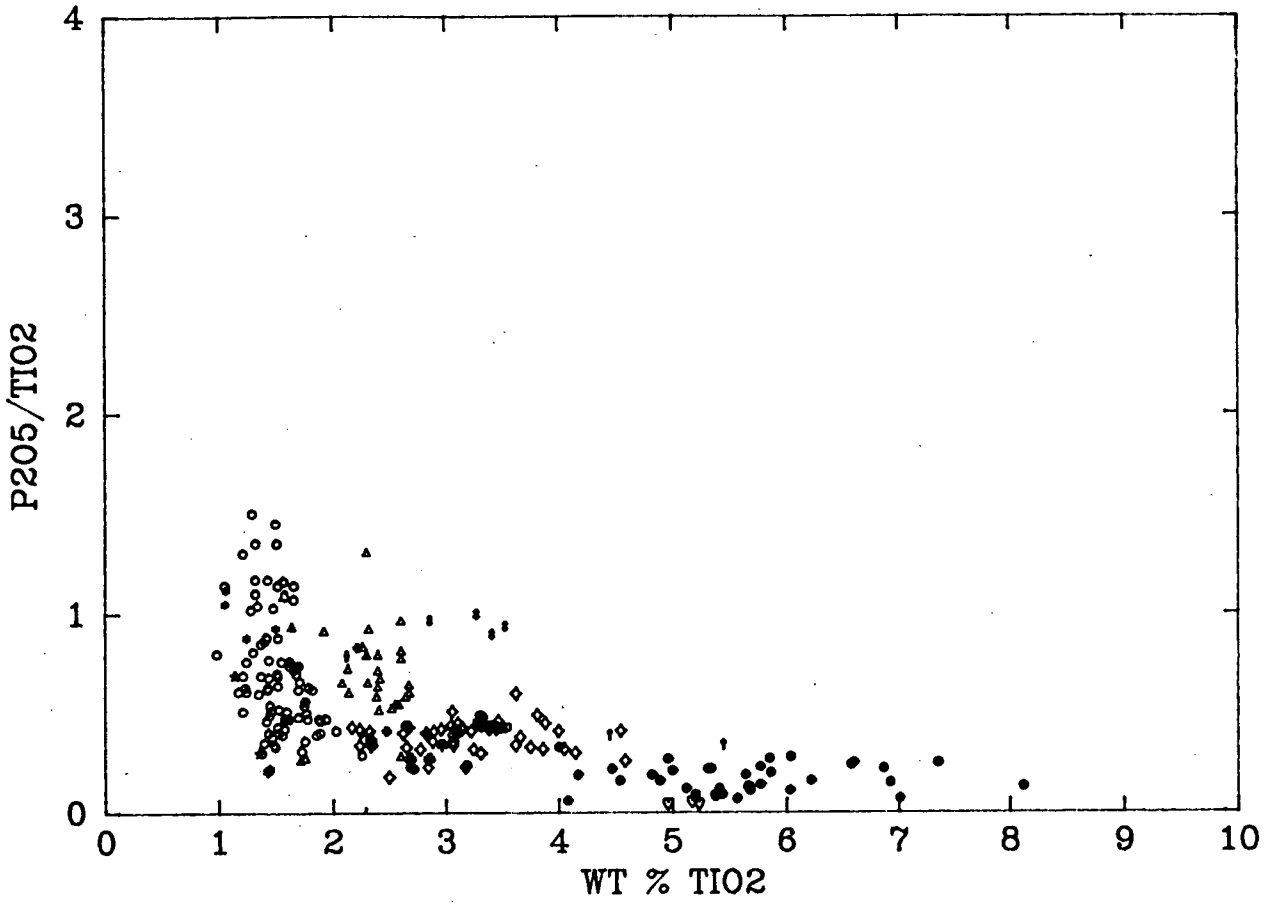

GROUPS 2 & 3

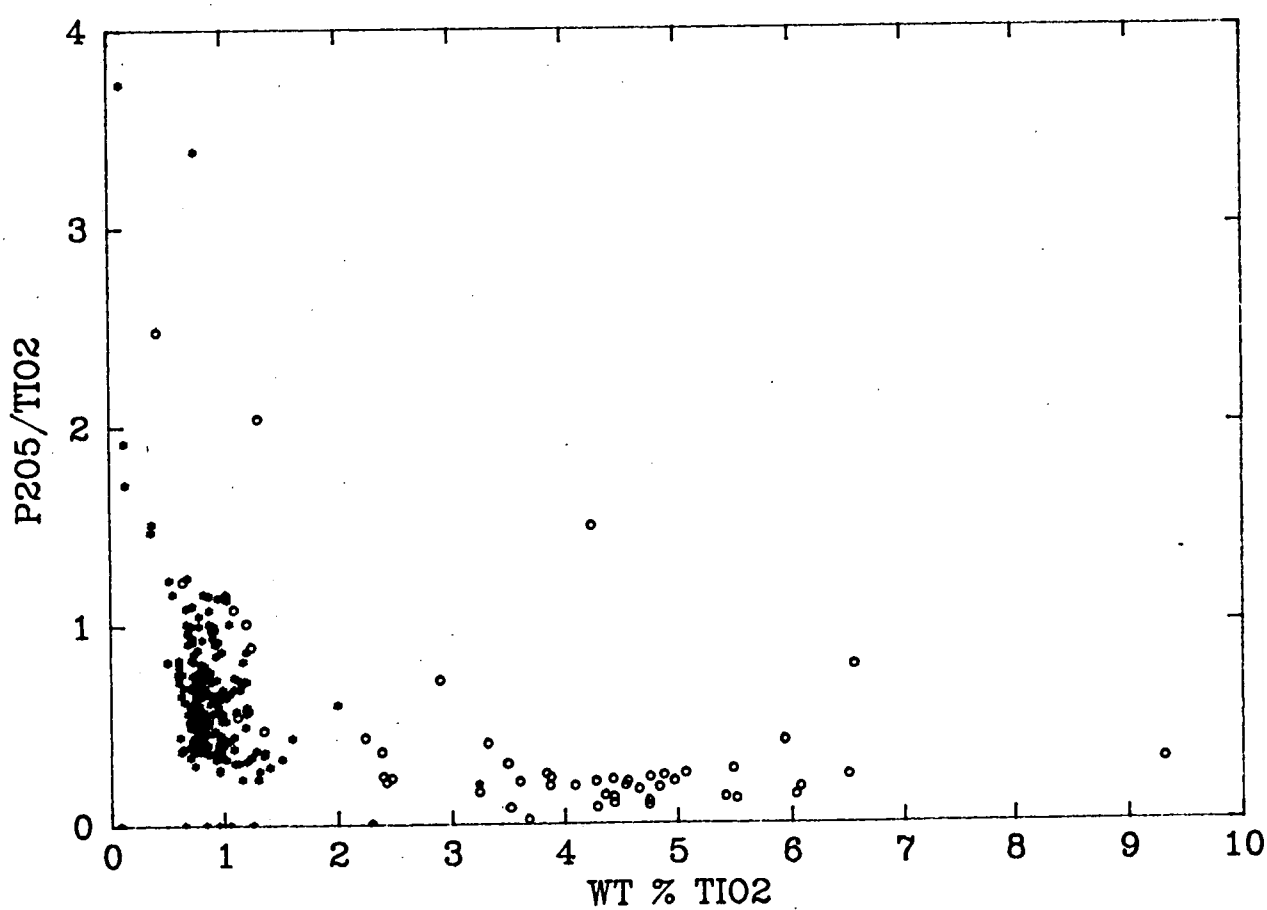

groups I and II may be transitional in nature between ultrapotassic rocks and kimberlites [Scott-Smith and Skinner 1984b].

The scatter amongst group II to high P_2O_5/TiO_2 values at high TiO_2 is due to the Damodar Valley glimmerites [Gupta et al. 1983] which have unusual mica-carbonate-apatite mineralogy and may not represent primary mantle-derived liquids. The Italian kamafugites of San Venanzo and Cupaello plot in a similar position to Roman region lavas in figure 7b.

Group III rocks form the alkaline end-member of orogenic island arc volcanics in Indonesia and Italy, and also occur behind the Aleutian Arc. In Indonesia, where the occurrences are better documented than the Aleutians and the tectonic setting is simpler than Italy, they are associated with a chemically continuous series with increasing K_2O from arc tholeiites, through shoshonites to leucitites [Wheller et al. 1986]. This series includes members which are leucite-bearing but do not meet the chemical definition of ultrapotassic rocks used in this paper. Similar leucite-bearing rocks occur in other orogenic areas with no ultrapotassic representatives eg. Utsuryo Island, Korea [Harumoto 1970; Nelson et al. 1986].

1.4.3 ULTRAMAFIC NODULES

Ultrapotassic rocks commonly contain sedimentary xenoliths as well as high grade metamorphic rocks of presumed lower crustal origin. Ultramafic nodules of accidental or cognate origin are rarer, and where present are usually subordinate to crustal xenoliths. The ultramafic nodule occurrences are summarised in table 3 from which it can be seen that nodule mineralogy is variable, with each ultrapotassic group having characteristic types. The most notable feature for ultrapotassic rock genesis is the rarity of garnet- and spinel-lherzolites which are common in many less potassic alkaline rocks. [Green 1970; Frey and Green 1974; Menzies 1983; Harte 1983].

Nodules from group I rocks are mostly peridotitic, but lherzolitic types are subordinate to garnet- and clinopyroxene-poor varieties believed to indicate depletion by loss of a basaltic melt component [Green and Ringwood 1963, 1967a]. Clinopyroxene- and mica- rich nodules are mostly considered to be products of magma crystallisation at high pressures.

TABLE 3: Ultramafic xenoliths occurrences in ultrapotassic rocks.

REGION	XENOLITH TYPES	REFERENCES
Group I:		
West Kimberley	Dunite > dps-chr-Harzburgite, Cr-dps, Cr-spn, pyrope xcts	Jaques et al 1984a; Wade & Prider 1940
Gaussberg	Spn-Lherzolite, cognate cpx-ol-lc, dps-chr-Harzburgite	Reinisch 1912; Sheraton & Cundari 1980; Collerson & McCulloch 1983; Vyalov & Sobolev 1959
Leucite Hills	Dunite, mica-ol-Pyroxenite (often cpx- or mica- rich)	Carmichael 1967; Barton & van Bergen 1981
Prairie Creek	Mica rich, k-richterite-bearing Peridotite	Mitchell & Lewis 1983
West Greenland	Dunite > Lherzolite, Websterite, Harzburgite	Scott 1981
Southeast Spain	Dunite, spn-peridotite	Borley 1967; Venturelli et al 1984b; Nixon et al 1984
Group II:		
Western branch, East African Rift	'Olivine-biotite-pyroxene series' Bt-Pyroxenite, glimmerite, Dunite, with cpx, bt, sph, ilm/Ti-mt,prv, melanite (occasionally Ne)	Holmes 1937, 1942; Combe & Holmes 1945; Holmes & Harwood 1932, 1937; Lloyd & Bailey 1975; Lloyd 1981
Bergydamalakh	mica-Peridotite	Ukhanov 1963
Beaver Lake	Spn-Lherzolite > spn-Harzburgite, Wehrlite, rare dunites, (no garnet)	Grikurov et al 1980; Ravich et al 1978
Fen	Spn-Lherzolite, Harzburgite, carbonatite	Griffin 1973
Group III:		
Italian Roman Province	Pyroxenite, Bt-Pyroxenite, ol-pyroxenite (occasionally carbonate-bearing), Bt-gabbro	Fornaseri et al 1963; Cundari & LeMaitre 1970; Fornaseri & Turi 1969; Appleton 1972; Giannetti 1982; Cundari 1982; Belkin et al 1985;
Group IV:		
Sierra Nevada	Pyroxenite & Peridotite with variable amount of phlogopite	Van Kooten 1980
Navajo	Lherzolite, Websterite, rarer eclogite, humite-bearing and carbonate-bearing types	Roden & Smith 1979; Smith 1979; Ehrenberg 1979, 1982
Channel Isles	Bt-Pyroxenite, glimmerite	Rock 1984

Nodules from group II rocks from the African rift valley have a predominance of clinopyroxene and mica (the 'olivine-bioitite-pyroxene' series of Holmes and Harwood 1937). Reaction textures indicate that these mineralogies result from replacement of pre-existing minerals, which may have been more normal mantle peridotite minerals [Lloyd and Bailey 1975]. Orthopyroxene and garnet have not yet been recorded in nodules from the Toro Ankole volcanic field, and a substantial proportion of the olivine is frequently also replaced by reactions forming mica and clinopyroxene [Lloyd 1981, 1984]. Nodules in group II rocks from other areas may also have mica-rich assemblages, but also contain olivine-orthopyroxene-rich types. Many of these host rocks are chemically similar to ultrabasic lamprophyres which contain a similar range of nodules [Nixon and Boyd 1979; Rock 1986].

Ultramafic nodules in group III rocks are documented only from the Roman province, specifically the Alban Hills, Roccamonfina and Somma-Vesuvius. They are dominated by clinopyroxene-rich rocks which are generally agreed to be cognate [Cundari 1982; Giannetti 1982], but the pressure of crystallisation and degree of crustal interaction are still debated [see discussion of Varekamp 1983; Hermes and Cornell 1983]. Belkin et al. [1985] have suggested depths of origin up to 13km from inclusion barometry.

Nodule occurrences in group IV rocks are little known except for the well-studied Navajo volcanic field rocks. This field is notable for the unique occurrence of humite group minerals in the nodules. In most cases, the lack of information about nodules may be due to the rocks being poorly described, but in others the absence of apparently mantle-derived rocks may be significant, eg. the durbachites of Czechoslovakia have none despite a wide range of lower crustal xenoliths [Holub 1977].

1.4.4 TRACE ELEMENTS

This compilation includes a standard set of 13 trace elements; Ba, Rb, Sr, Zr, Nb, Y, La, Ce, Nd, Sc, V, Ni and Cr. Discussion concentrates on the incompatible trace elements because these show significant variations in behaviour from the compatible trace elements (Sc, V, Ni, Cr) which follow the behaviour of most of the major elements. Spidergrams are chosen as the best method of displaying incompatible element variations [cf. Thompson et al. 1983]; the ranges of these both

within and between groups are plotted in figures 8 to 10 using the normalising values given by Thompson [1982]. A major difficulty in compiling trace element data is the paucity of exhaustive trace element studies, so that a compilation even for rocks from one locality frequently necessitates combination of analyses from different samples.

In figures 8 and 9, the ranges for standard group I and group II rocks are separated from the ranges for the groups as a whole to demonstrate the specific characteristics of some non-standard members. The trace element patterns must, in detail, be affected by crystal fractionation, but data from the West Kimberley suite indicates that this is less than the variations between groups. Discussion of the patterns of individual non-standard localities is generally beyond the scope of this review, but will be considered where major deviations from group averages occur.

The general pattern of incompatible element abundances for ultrapotassic rocks is one of extreme enrichment, which increases towards the left of the spidergram, relative to the more abundant less alkaline rock types, referenced by MORB in figures 8 to 10. The order of elements in figures 8 to 10 is arbitrarily chosen to fit a descending order for MORB values from right to left, which is an approximate measure of increasing incompatibility. The MORB values plotted are from Sun [1980], but the difference between these and other MORB values is insignificant in terms of the enrichments seen here.

Group I rocks show the highest overall abundances, with the West Kimberley and Gaussberg rocks (the standard members) generally occupying the highest part of the range, particularly for Ba, Rb, K, Nb and La (figure 8). At the right hand side of the diagram, Zr and Ti are generally higher than in other groups but are variable within group I. Sr and Y are relatively depleted: Sr produces a noticeable negative spike in the pattern and is less enriched, having abundances similar to group III rocks. Yttrium, however, is distinctly lower than in other groups, particularly for West Kimberley and Gaussberg, and is frequently also depleted with respect to MORB.

In the West Kimberley suite, which contains rocks ranging in SiO_2 from 36 to 60 wt %, the only notable differences in the spidergrams

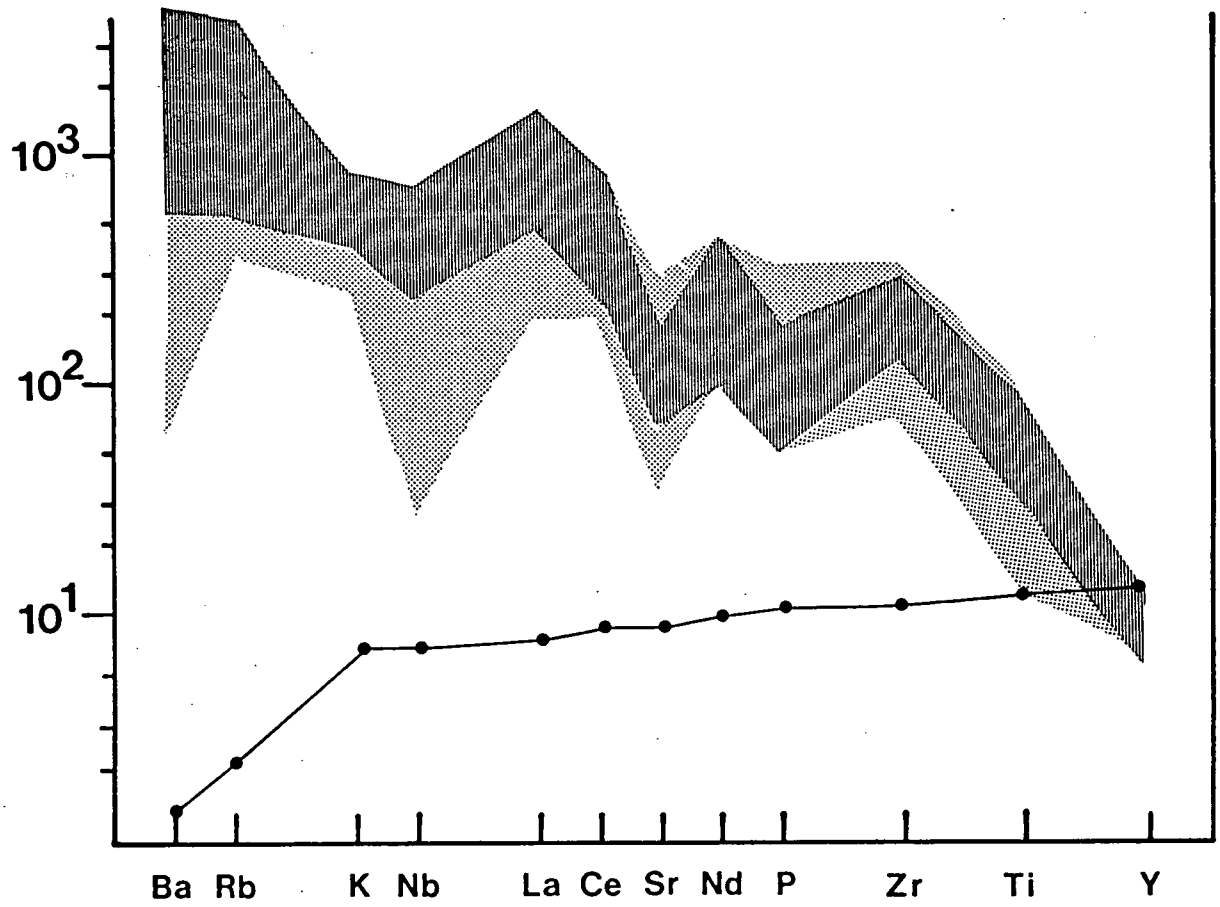

Figure 8

Spidergram showing the range in incompatible element abundances for Group I with the range for standard members (West Kimberley and Gaussberg) indicated by darker shading. The solid line depicts MORB values of Sun [1980]. X-axis is sample/chondrite, using the normalising factors given by Thompson [1982].

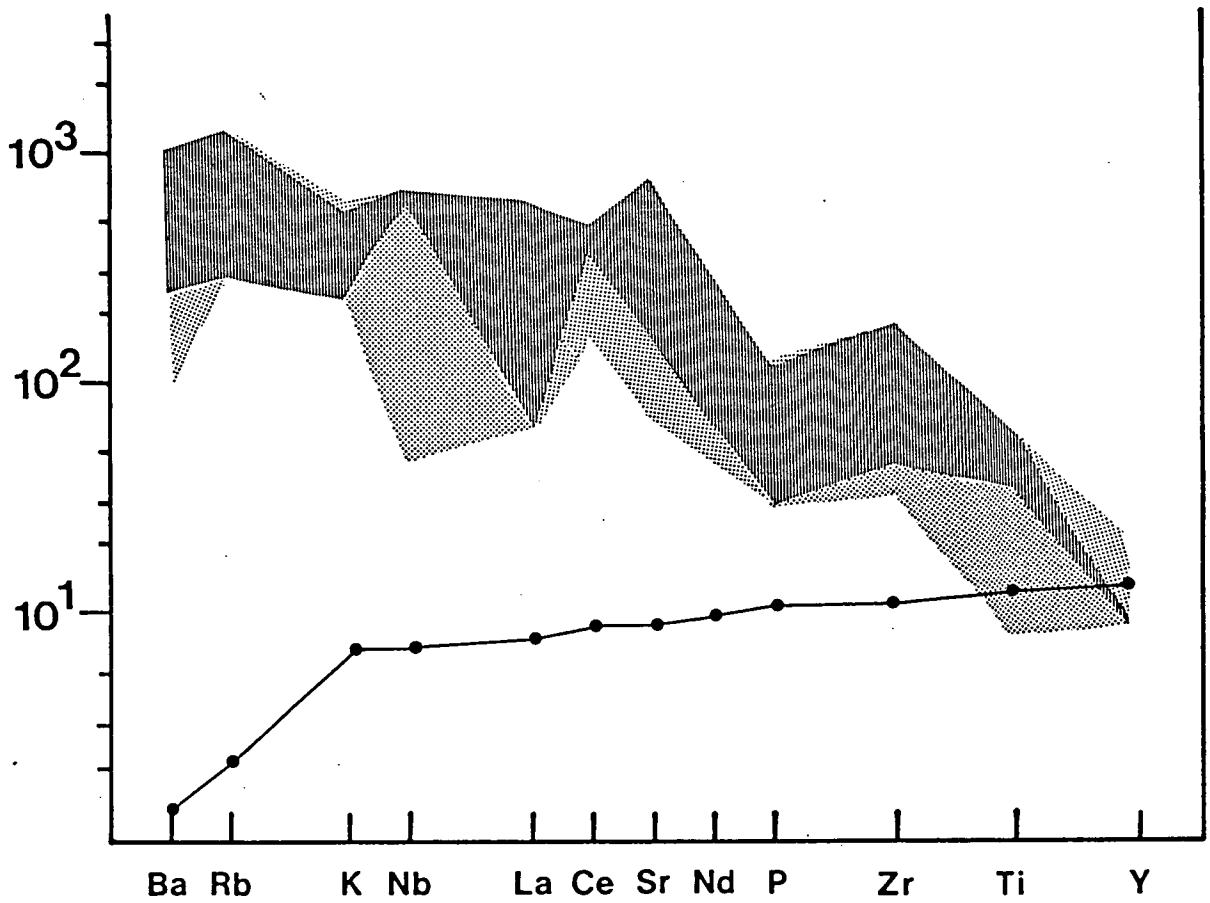

Figure 9

Spidergram showing the range for group II with standard members (Toro Ankole) in dark shading. Some constrictions in the pattern for Toro Ankole probably reflect scarcity of data. The solid line depicts MORB values of Sun [1980].

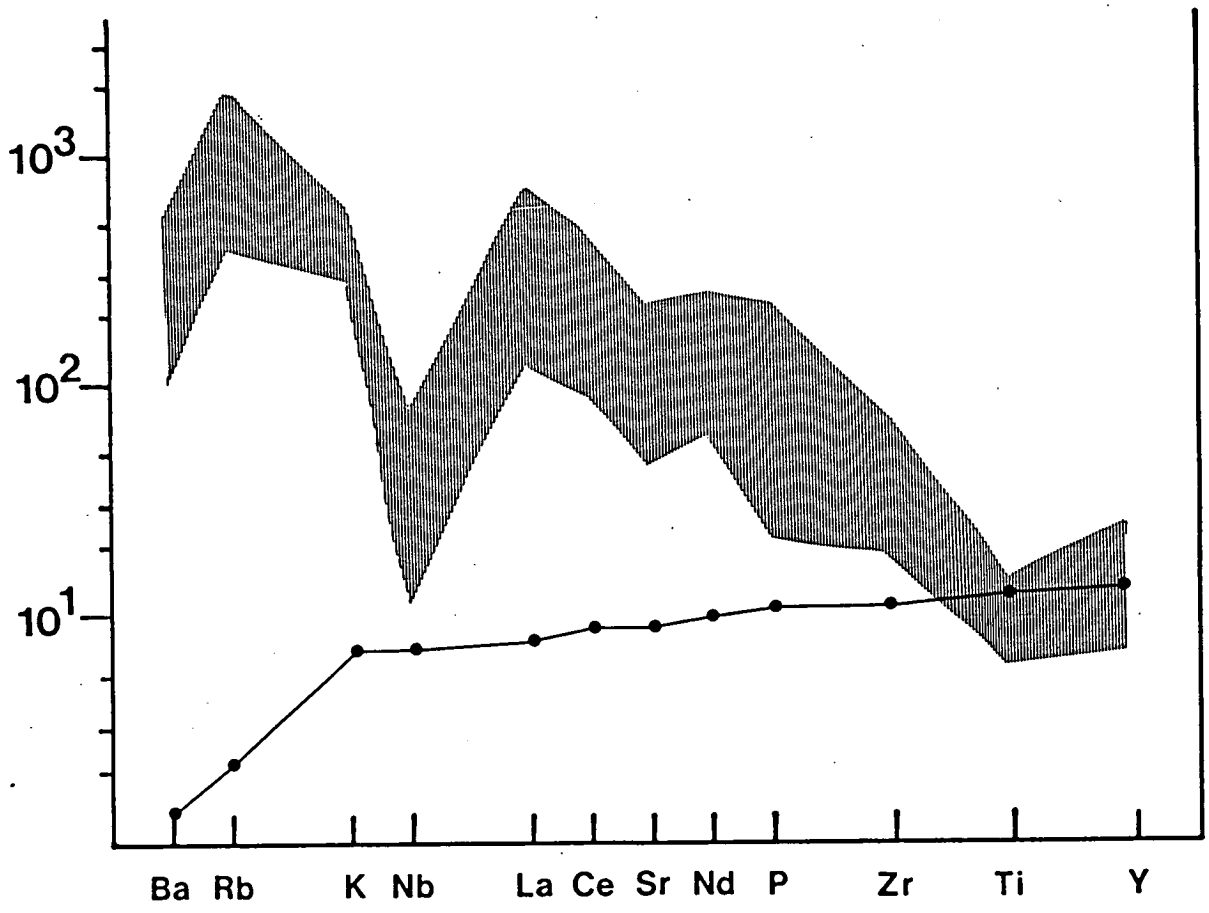

Figure 10

Spidergram showing the range of incompatible elements in group III rocks. Note the negative spikes at Ba, Nb and Ti. The solid line depicts MORB values of Sun [1980].

between the low silica olivine lamproites and the higher silica leucite lamproites are in K, Nb, Nd, Zr and Ti. For olivine lamproites the K*/Nb* ratio is less than 1 (where * = chondrite-normalised), which is a feature also seen in Prairie Creek lamproites and most members of group II, all of which have low SiO_2 contents. The olivine lamproites also have lower Zr and Ti than the leucite lamproites. The rare-earth element (REE) patterns are apparently similar; the patterns produced by Nixon et al. [1984] and Jaques et al. [1984a] disagree as to whether the olivine- or leucite-lamproites are the more LREE-enriched. An approximate series of enrichment can be drawn for standard group I rocks as follows

Ba,Rb > La > K > Ce > Nb > Nd > Zr > Sr,P > Ti > Y

Non-standard group I rocks typically have less extreme enrichment, particularly in elements at the far left of the diagram (figure 8). In some localities, particularly southeastern Spain and the northwestern Alps (referred to here as Mediterranean-type), they have marked negative spikes in the spidergram for Nb, Ti and Ba. This is similar to the pattern seen in group III rocks (figure 10). On most major element diagrams (figures 1 to 6) rocks from these localitites are offset towards Group III from standard group I. These Mediterranean-type features appear to be a further indicator of tectonic environment, as they are from orogenic areas and also have similar P_2O_5/TiO_2 vs TiO_2 (figure 7) to group III rocks. Note that these negative spikes, especially Nb, are not so marked as in group III rocks. However, the REE patterns are distinct: both group III and standard group I rocks have steep LREE-enriched patterns with a uniform slope (apart from the Eu anomaly of group III), whereas the Mediterranean-type group I have a curved LREE pattern due to lower La and higher Ce and Nd than in West Kimberley and Gaussberg (figure 11). The average La/Nd for Spanish lamproites is 0.61 as against 1.67 for West Kimberley and Gaussberg.

It is interesting to note that REE data for the Leucite Hills [Kay and Gast 1973] and Priestly Peak [new data: see appendix 2] give slightly curved patterns. It has been suggested that the Leucite Hills magmatism may be related to a fossil subduction zone [Rowell and Edgar 1983] thus belying its apparently non-orogenic setting: this will be discussed further in the petrogenesis section. In addition to the negative spikes mentioned already, the Mediterranean-type rocks have La, Sr, Zr and Ce contents which are within the lower part of, or just below the range for

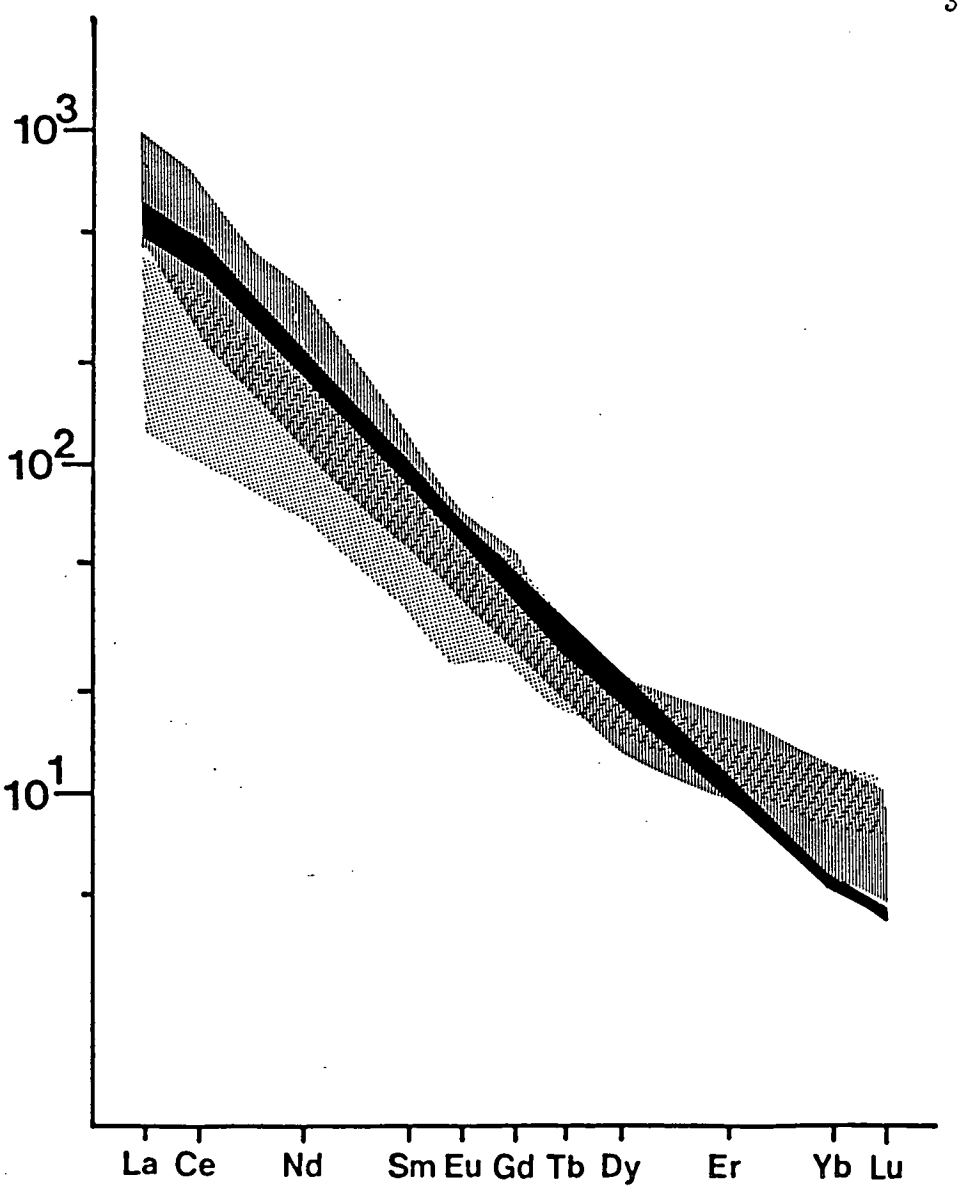

Figure 11 [a]

Rare earth element diagram of Groups I, II and III standard types. Group I in vertical shading; Group II solid; Group III in stipple.

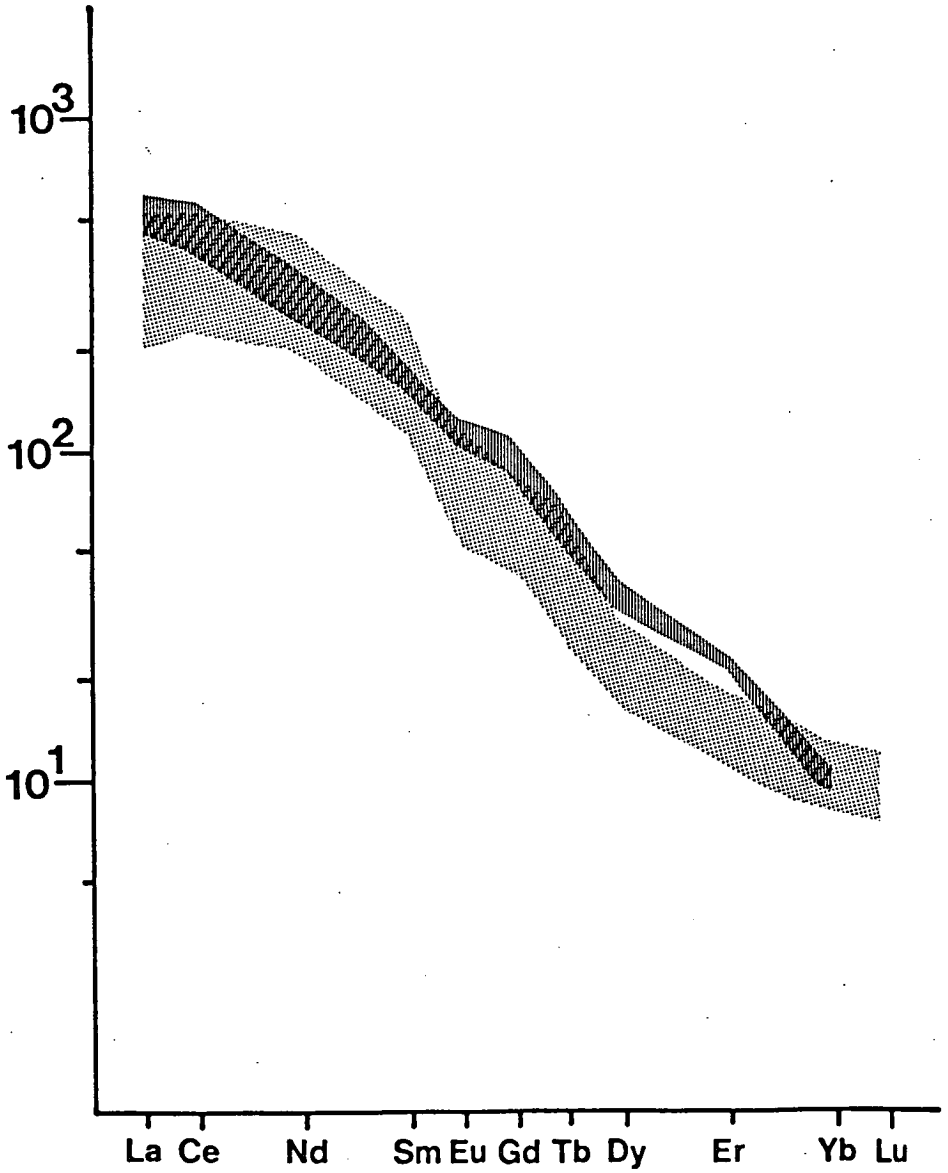

Figure 11 [b]

Rare earth element diagram of Mediterranean type Group I (Southeastern Spain & Northwestern Alps) in stipple, and Priestly Peak, Antarctica (see Appendix 2) in vertical shading.

standard group I rocks. Rb, P, K, and Nd are essentially identical, and Y tends to be slightly higher.

The Prairie Creek samples are all SiO_2-poor, and they have been suggested to be transitional between lamproites and kimberlites [Scott-Smith and Skinner 1984b]. They have a flatter spidergram pattern with values in the lower part of, but not below, the rest of the group I rocks. This pattern is similar to that seen in Group II rocks, but lacks the positive Sr spike (see below).

The group II spidergram is also split into standard and non-standard types (figure 9). The Toro Ankole volcanics make up the bulk of the analyses, but very few are complete. The apparent contractions in the ranges at Nb, Ce and Y are probably not real since they are the elements for which fewest data are available. The group II range generally overlaps the lower part of the Group I range, but values for La, P, Zr, Rb and Ce are below those for all group I rocks. Strontium is strongly enriched in group II which is the opposite pattern to group I where Sr characteristically forms a dip in the spidergram. This Sr enrichment is expressed in its promotion in the enrichment order for group II;

Rb > Ba > Sr > Nb > K,La > Ce > Zr > Nd > P,Ti > Y

The lower part of the group II range, which has depletions in Ba, Nb and to a lesser extent Ti, is entirely due to the San Venanzo and Cupaello occurrences in Italy. These are included in group II on major element chemistry, but have trace elements more characteristic of Group III or Mediterranean-type group I. They are the only group II rocks with K*/Nb* > 1.

Group III trace element patterns have very pronounced depletions in Ba, Nb and Ti and are generally less enriched in incompatible elements (figure 10). Ba, Nb, Ti and Zr never attain even the minimum value found in West Kimberley and Gaussberg. Sr forms a slight dip in the pattern, but this is less marked than in group I. The Ti 'depletion' is accentuated by Y values which are high relative to group I. Patterns for groups II and III overlap for most elements but Nb, Ti and Sr are much lower in group III, the last of these being due to high Sr in group II. Group II also tend to have higher Rb and K, and lower P. The approximate enrichment order is as follows;

Rb > K > Ba,La > Ce > Sr,Nd,P > Zr > Nb > Y > Ti

Trace element data for group IV rocks is sparser and extremely variable in character. The heterogeneous nature of the group leads to a larger range for almost all elements which includes types much less enriched in incompatible elements (especially for many minettes). Amongst the nodule-bearing localities, the Sierra Nevada rocks have unusual patterns with some elements (eg. Zr, Ti, P, Sr) within the range for group I, and yet enrichment in LREE is less than in all three major ultrapotassic rock groups. Patterns for the Navajo minettes are markedly different, with enrichments for most elements similar to group III or Mediterranean-type group I. The negative spikes for Ba, Nb and Ti are more variable than in these groups; the Ba spike is nearly as large as group III, Nb less marked, and Ti is in some cases barely depleted.

1.4.5 ISOTOPES

Studies of a number of isotopic systems for a given ultrapotassic rock are rare; there are no Pb data for group II rocks and only three group I localities have been studied thoroughly. As a result, group isotopic characteristics are difficult to delineate and those noted here may require substantial revision when more data become available. Amongst the available data given in table 2, $^{87}Sr/^{86}Sr$ are the most abundant, and these are displayed in figure 12. Their relationship to ε_{Nd}, where known, is shown in figure 13.

Group I rocks show a large variation in $^{87}Sr/^{86}Sr$ but all show strongly negative ε_{Nd}. The extension of the mantle array defined by basaltic rocks with positive ε_{Nd} is difficult to draw, but there is no doubt that lamproites range from values to the left of the array (Leucite Hills) to values far to the right. The Gaussberg and West Kimberley rocks have distinctive Pb isotopic compositions with low $^{206}Pb/^{204}Pb$ and high $^{207}Pb/^{204}Pb$ which plot to the left of the geochron. For a detailed discussion of Pb isotopes in ultrapotassic rocks, the reader is referred to the recent paper by Nelson et al. [1986], but it should be noted that their discussion includes rocks which are not ultrapotassic as defined here.

The Italian group III rocks show a trend of increasing $^{87}Sr/^{86}Sr$ (figure 12) and decreasing ε_{Nd} (figure 13) from south to north. The

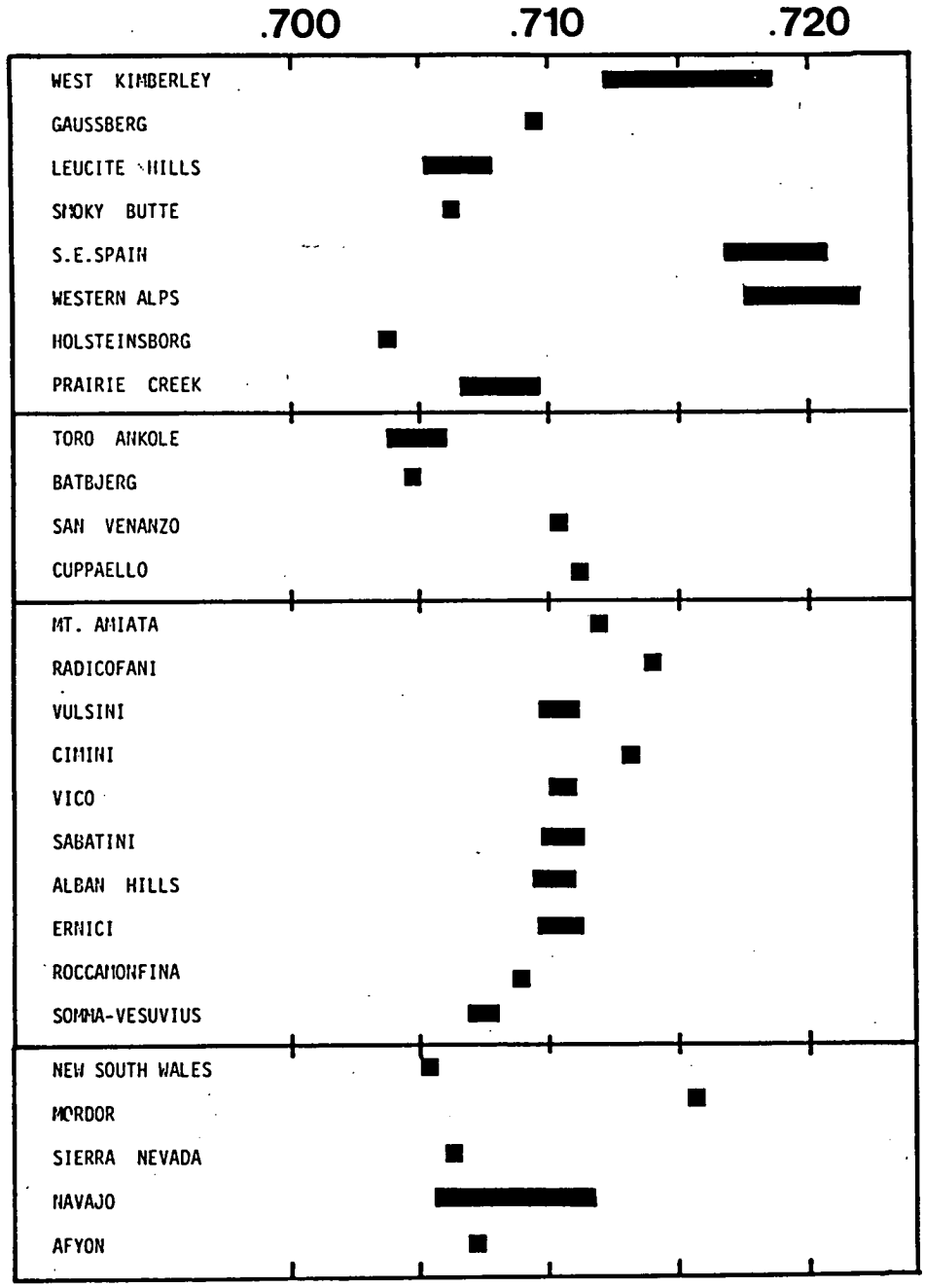

Figure 12

Sr isotope compositions and ranges for ultrapotassic rock localities. The four groups are listed in sequence. Group III is listed in geographical order from north to south.

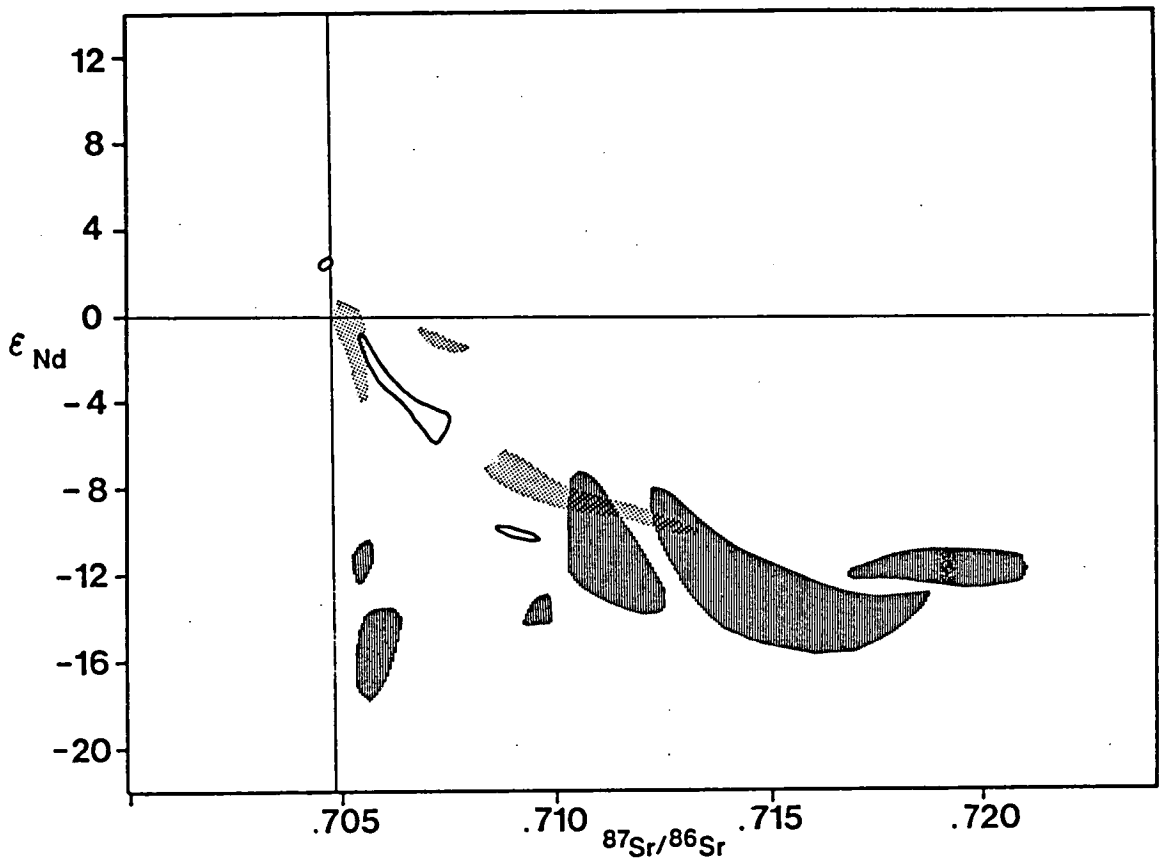

Figure 13

Nd-Sr isotopic variations in ultrapotassic rock groups. Group I in vertical shading; Group III in stipple. The solid outlines delineate compositions for rocks related to Group II ultrapotassic rocks from the Western Rift of Africa.

Spanish lamproites form an extension of this trend on figure 13 and also on the plot of each Pb isotope ratio against $^{87}Sr/^{86}Sr$ [Nelson et al. 1986]. The Western Alps rocks so far have only Sr isotopes measured, but these have high $^{87}Sr/^{86}Sr$ similar to the northern Italian group III rocks,

Group II rocks from the western rift have low $^{87}Sr/^{86}Sr$ ratios, and although ε_{Nd} are lacking, the related non-ultrapotassic rocks plotted on figure 13 indicate that western rift rocks in general may form a similar negative correlation of $^{87}Sr/^{86}Sr$ and ε_{Nd}. The San Venanzo and Cupaello rocks have similar $^{87}Sr/^{86}Sr$ to the Italian group III rocks, which is in keeping with their trace element characteristics.

Oxygen isotope measurements are available only for a limited number of Group I and Group III samples. In both cases they vary from low values close to those accepted as primary mantle values [Taylor et al. 1984] to higher values generally believed to indicate some crustal input. The average values for different localitites within groups are quite variable (table 2).

1.5 PETROGENETIC CONSTRAINTS

1.5.1 SCOPE

Many of the petrogenetic problems posed by the ultrapotassic rocks are similar to those of other alkaline rock types such as kimberlites, melilitites and non-ultrapotassic lamprophyres. These are principally the explanation of extreme incompatible element enrichments and the difficulty of deriving the rocks by partial melting of supposedly normal garnet/spinel lherzolitic mantle material. Because of these similarities, many models proposed for the genesis of ultrapotassic rocks have been generally applied to a number of alkaline rock types. As was pointed out in section 1.3, the ultrapotassic rocks are separated from other alkaline rocks by arbitrary abstraction of chemical attributes. They are, in many respects, part of a continuum of alkaline rock types which implies production of these rocks by the operation of a corresponding continuum of processes or source compositions. Bearing this in mind, much of the discussion which follows may find application amongst other groups of alkaline rocks.

This section includes discussion of the factors which discriminate between ultrapotassic and other alkaline rock groups, but concentrates on

the petrogenetic implications of the differences between ultrapotassic rock groups described in section 1.4. Petrogenetic models for specific localities must take into account many local factors in addition to the broad trends outlined in this paper. We do not consider specific localities except where they may be of general importance in petrogenetic models.

Firstly, we consider previous explanations of the extreme enrichment in incompatible elements, high K_2O and K_2O/Na_2O common to all groups, from which we conclude that pre-enrichment of the source, generally referred to as mantle metasomatism, is the most likely cause. We then explore the possible physical and chemical variations of the sources and the extent to which the chemical variations between the ultrapotassic groups may be due to conditions of melting or conditions during the process of enrichment. Models formed on the basis of the available data may be found to be inappropriate when further data become available, but from these models we can suggest methods of investigation to test the suggestions made.

1.5.2 PREVIOUS MODELS FOR THE PETROGENESIS OF ULTRAPOTASSIC ROCKS

Hypotheses previously suggested for the petrogenesis of ultrapotassic rocks explain the extreme enrichment in incompatible elements by a variety of processes including (i) high degrees of crystal fractionation from more normal basaltic melts originating by partial melting of garnet peridotite mantle, (ii) assimilation of crustal material rich in these incompatible elements, (iii) zone refining operating over a large vertical distance in the mantle, and (iv) partial melting of a pre-enriched phlogopite-bearing peridotite source. Gupta and Yagi [1980] have reviewed petrogenetic models in detail, and so only a brief exposition is given here with our reasons for preferring the last option. The processes listed above are treated in turn, and discussed further in later sections.

1.5.2.1 Crystal Fractionation

This process has been proposed most recently by O'Hara and Yoder [1967] who suggested that high pressure fractionation of clinopyroxene and garnet from a picritic magma would not only cause enrichment in incompatible elements, but also increase the K_2O/Na_2O ratio of the residual liquid due to the low K_2O/Na_2O of the crystallising phases. The picritic magma could be produced by 30-40% melting of garnet lherzolite at pressures greater than 30kb, which is more reasonable than earlier models

of fractional crystallisation from peridotitic magma which would require nearly complete melting of mantle material (see Gupta and Yagi 1980 p.217-220). However, this model can be criticised on the following grounds. (i) Interpretation of isotopic data shows that eclogite nodules in kimberlites, which were assumed by O'Hara and Yoder [1967] to be accumulates of the proposed parental picritic magmas, are not genetically related to the host kimberlite, but are older, accidental inclusions [Allsopp et al. 1969]. (ii) Enrichment in incompatible elements to the degree seen in many ultrapotassic rocks would require very high degrees of crystal fractionation (greater than 95%) and in this case more abundant examples of less extreme rock types might be expected to occur, but do not [Dawson 1971; Mitchell and Brunfelt 1975]. (iii) Such extreme degrees of fractionation should also decrease the Mg-number to well below that of primary magmas [Green 1971]. (iv) Eclogite fractionation from picritic liquids may not produce a marked increase in K_2O/Na_2O of the liquid, so that residual liquids probably resemble nephelinites [Green and Ringwood 1967a; Gupta and Yagi 1980,p.193-196; Ferguson and Cundari 1975]. It must be noted here that experimental data on liquidus mineral compositions in picrites are limited to 30kb and less. Melts produced by substantial partial melting of garnet peridotites at higher pressures will also be broadly picritic [Takahashi and Scarfe 1985], but the compositions of phases which may fractionate at these higher pressures are not yet known accurately. (v) The production of a variety of ultrapotassic rocks by extreme amounts of fractionation from similar parent magmas does not explain the observed range of isotope compositions.

Garnet and clinopyroxene fractionation is thought to occur in kimberlites where griquaite nodules result [Nixon and Boyd 1973], but it is not considered to be the principal petrogenetic process.

1.5.2.2 Involvement of crustal material

Mixing between materials of mantle and crustal origin was popular in early petrogenetic models because it explained the apparently contradictory compositional features of ultrapotassic rocks of high Mg-number, Ni and Cr contents ('mantle charcateristics'), and high Rb, Zr and Ba ('crustal characteristics'). The major flaw in these hypotheses invoking substantial assimilation eg. of limestone or granite by basalt or carbonatite, is their inability to explain more than selected groups of elemental variations. For example, the mixture of carbonatite and granite

proposed by Holmes [1950] and Higazy [1954] for group II rocks explains high abundances of most incompatible elements, but cannot explain high Ni and Cr. Hypotheses based on partial data sets are often found lacking when more complete data becomes available. Rock [1980] ably demonstrates how, by consideration of only rare earth elements, one can give the impression of a good chemical match which may not exist given a more complete data set. The existence of potassium-rich rocks with very low silica contents precludes a general origin by assimilation of silica-rich crustal material.

Reaction between crustal xenoliths and host magma is obviously present in many cases such as the leucitization of granitic xenoliths in East Africa [Holmes 1945] and assimilation of carbonates in Italy [Rittman 1933], but the widespread occurrence of ultrapotassic rocks with similar compositions but different xenolith populations argues against assimilation as a major factor in petrogenesis. Assimilation hypotheses have also been criticised because of the need for superheated parental basic magmas, since large amounts of assimilation should cause crystallisation, and thus stop the proposed mechanism short of completion.

1.5.2.3 Zone refining

Harris [1957] has advanced the zone refining mechanism as a petrological process. He envisaged initial melting of mantle material at 500-1000 km depth and gradual enrichment of incompatible elements in the rising liquid batch in accordance with their degree of incompatibility, measured by the bulk partition coefficient between melt and solid ($D^{l/s}$). The rate of this enrichment depends on D and the zone length (depth of melt zone/ depth of mantle passed through) and should exponentially approach a limit where the concentration ratio (liquid/solid) is equal to D and the concentration in crystallising phases is equal to the concentration in the surrounding mantle. Harris and Middlemost [1969] modified the hypothesis for kimberlites by allowing for further enrichment by crystal fractionation as the liquid approached subcratonic areas with low heat flow. Late stage enrichment would lead to separation of a volatile phase resulting in explosive emplacement.

The proposition of initial melting at greater than 500 km is the weakest part of the zone refining hypothesis. It makes the process independent of tectonic environment, so that its application to the

origins of kimberlites and ultrapotassic rocks which occur in particular tectonic environments becomes hard to defend. The products of zone refining should be more widespread and be found with equal abundance in oceanic areas [Dawson 1980]. One could argue that the products of zone refining are indeed common in other areas, but are manifested in alkali basalts rather than more extreme compositions in areas which do not have a low enough heat flow for Harris and Middlemost's [1969] modification of the zone refining model to operate. However, this would leave the occurrence of group III rocks in island arcs unexplained. Furthermore, if considerable fractionation is required to produce ultrapotassic rocks then zone refining becomes subordinate to fractionation with respect to the ultrapotassic rocks.

Another major assumption, recognised by Harris in his original paper, is that there will be sufficient density contrast between the melt and surrounding mantle at 500 km to allow the magma to rise. Recent estimates and measurements of silicate liquid densities at very high pressures suggest that there may be a density switchover between liquid and solids somewhere between 200 and 350 km, below which melt would sink rather than rise [Ohtani 1985; Rigden et al. 1985]. This may considerably limit the depth range over which zone refining could operate, although alkali-rich, volatile-charged melts may remain less dense than surrounding mantle to greater depths.

1.5.2.4 Partial melting of a pre-enriched mantle source

Following the development of models for the origin of basaltic magmas by partial melting of garnet peridotite mantle, trace element modelling showed that melts containing very high incompatible element contents could only originate by extremely small degrees of melting [<<1%; Gast 1968; Sun and Hanson 1975]. The apparent problem of separating such small melt fractions could be avoided if the peridotite was pre-enriched in incompatible elements by the upward movements of either volatiles [Bailey 1970] or a small melt fraction [Green 1971]. This enriched migrating fluid would be trapped by crystallisation of amphibole [Varne and Graham 1971] above depths of about 100 km [Green 1973a]and by mica at greater depths [Kushiro et al. 1967; Modreski and Boettcher 1972]. The operation of this process was supported by a series of papers describing xenoliths bearing evidence of enrichment processes and including primary hydrous minerals, i.e. minerals stable in the mantle prior to incorporation in the host

magma [eg. Dawson and Powell 1969; Erlank and Finger 1970; Varne and Graham 1971; Erlank 1973; Frey and Green 1974; Lloyd and Bailey 1975; Harte et al. 1975].

By this model, ultrapotassic rocks could originate by partial melting of mica-bearing peridotite because the higher K/Na value of mica favours production of higher K/Na melts.

More recently, isotopic studies have provided further evidence for mantle enrichment events, and a wide range in the age of the enrichment events has been inferred. In some rocks, trace element patterns show enrichment indicted by high Nd/Sm and Rb/Sr values which are not reflected by Nd and Sr isotopic compositions. This indicates that enrichment must have occurred more recently than approximately 200 my. Other rocks, including the majority of ultrapotassic rocks, have higher $^{87}Sr/^{86}Sr$ and lower $^{143}Nd/^{144}Nd$ values (figure 13) which indicate older and/or more extreme enrichment events, although the precise ages depend on the mixing models chosen [McCulloch et al. 1983; Nelson et al. 1986].

The amassed chemical, isotopic and petrological data on igneous rocks and xenoliths make partial melting models powerful and flexible. Indeed, models invoking variations in degree and type of enrichment and conditions of partial melting now suffer from a lack of specificity rather than a lack of evidence. In the following sections, we shall attempt to constrain these parameters as applied to the genesis of ultrapotassic rocks.

1.5.3 THE ORIGIN OF CHEMICAL VARIATIONS IN ULTRAPOTASSIC ROCKS

1.5.3.1. Primary magmas

In order for meaningful discussion of the effects of partial melting and mantle enrichment processes to be possible, it is necessary to decide which compositions represent the primary mantle-derived magmas which are least modified by crystal fractionation or crustal contamination. The most commonly used criteria for distinguishing primary compositions are that they should have Mg-number of around 70 or higher, have high Ni (>500ppm) and Cr (>1000ppm) contents and SiO_2 contents not greatly exceeding 50 wt% [Green 1970; Frey et al. 1978]. These values are determined by experimental data on liquids in equilibrium with peridotite of Mg-number around 90 at mantle pressures, and thus assume a peridotite mantle composition. Cr and

Ni abundances would fall rapidly if substantial crystal fractionation of ferromagnesian phases (which must be the liquidus phases for liquids in equilibrium with mantle mineral assemblages) has occurred. A further important criterion is the presence of mantle-derived ultramafic xenoliths which would be expected to be eliminated together with phenocryst phases had any substantial fractionation occurred.

The presence of modally metasomatised [Harte 1983] xenoliths in many ultrapotassic rocks means that the assumption of an olivine + orthopyroxene bearing residue to constrain liquid compositions may be inappropriate. High degrees of mantle enrichment may result in the formation of local clinopyroxene + phlogopite + garnet or spinel source rocks which have different Mg-numbers, and a different set of accessory minerals compared to 'normal' mantle material. Liquids derived from such a highly modified mantle may not be constrained by the Mg-number, Ni and Cr contents noted above. Liquid compositions will be controlled by the mineralogy of the source mantle, but experimental studies of probable modified mantle compositions are needed in order to constrain the chemical signature of primary melts. Preliminary experiments on a mica clinopyroxenite proposed as a group II source by Lloyd et al. [1985] indicate that melts from this composition may have Mg-numbers in the low sixties.

Applying these criteria to the ultrapotassic rocks, group I and II rocks commonly have mantle derived ultramafic inclusions (table 3). Their Mg-numbers are normally high and well within the range for primary magmas (figure 1). Group I rocks from the West Kimberley area range in SiO_2 content up to 60 wt%, but low Ni and Cr contents in the most silicic indicate that fractionation has occurred [Jaques et al. 1984a]. However, a wide range of primary magma compositions amongst lamproites almost certainly exists: mantle-derived xenoliths are common in olivine lamproites and occur in leucite lamproites with 51 wt % SiO_2 [Sheraton and Cundari 1980]. The Mg-numbers of these proposed primary magmas is 70 or above, and the MgO content varies from 8 wt% in leucite lamproites to well above 20 wt% in olivine lamproites.

Group II rocks from the western branch of the East African rift include a greater proportion of fractionated rocks, and petrological and statistical studies indicate that they are related to a range of primary

magmas which differ in composition both within and between volcanic fields [Pouclet 1980b; Pouclet et al. 1981; Ferguson and Cundari 1975]. The related more sodic rocks in other parts of the rift are derived from distinct primary magmas.

The majority of Group III lavas from Italy are products of crystal fractionation making recognition of primary compositions difficult and controversial. A number of candidates do have 'primary' Mg-numbers, but have relatively low Ni and Cr [Rogers et al. 1985]. The clinopyroxene-rich nodules which are abundant at some localities are thought to represent accumulated magmatic material at intermediate to high pressures [Cundari 1982; Giannetti 1982]. The presence of ultramafic xenoliths thus cannot be used as a criterion for distinguishing primary magmas. Primary magmas for Italian group III rocks are considered to be rich in CaO (13-16 wt%) with relatively low SiO_2 (46-49 wt%) and Al_2O_3 (12-13 wt%) and are ultrapotassic, even though K_2O contents are considerably higher in the more differentiated rocks [Cundari and LeMaitre 1970; Rogers et al. 1985; Holm et al. 1982]. Fractionation is dominated by clinopyroxene, as demonstrated by the trend of decreasing CaO in figure 3 and by its occurrence in cognate nodules, but minor olivine fractionation may also occur at an early stage. Indonesian group III rocks include rocks with similarly high Mg-numbers but with slightly lower CaO and higher K_2O (5-6 wt%). In both these suites, the distinctively low Ti and Nb are only slightly enriched by crystal fractionation.

The most important result of isolating possible primary magmas is that the ultrapotassic group characteristics remain distinct in the primary magmas. This means that one group cannot be a fractionation product of another, and that the variation between groups must reflect characteristics developed at source. These chemical variations could occur at any of three stages; (i) prior to mantle enrichment, (ii) during the mantle enrichment process, and (iii) during the partial melting process. These possibilities will now be considered in turn.

1.5.3.2. Mantle heterogeneity prior to enrichment

Chemical variations between non-alkaline basaltic magma types indicate that source rocks do not all conform to the plagioclase, spinel or garnet lherzolite modelled as primary mantle material [Carter 1970]. The loss of a substantial fraction of basaltic melt from a primary

lherzolite will leave a harzburgitic or dunitic residue enriched in Ni, Cr/Al and Mg-number, and depleted in incompatible elements including light rare earths (LREE). This process will melt out the garnet and clinopyroxene or Al-spinel and clinopyroxene components leading to depletions in Ca, Al and Na [Green and Ringwood 1963; Jaques and Green 1979]. These elements are crucial to the recognition of depleted sources because they leave a chemical signature which may be overprinted but not swamped during later enrichment episodes. Cr decreases in the residue during a depletion event, but behaves less incompatibly than Al, leading to increased Cr/Al in residual spinel [Kurat et al. 1980]. Remelting of depleted mantle leads to magmas which have lower Al, Ca and Na and higher Mg-number, Ni and Cr than magmas derived from more fertile sources. Examples of such magmas are the boninites or high-Mg andesites [Green 1973a; Hickey and Frey 1982].

The major element characteristics of group I ultrapotassic rocks indicate a depleted source. Group I rocks have low CaO, Al_2O_3 (figure 1) and Na_2O (figure 6) and also carry dunite and harzburgite xenoliths (table 3). Spinel-bearing lherzolite xenoliths are present, but are subordinate to more depleted types. In addition, the Sc depletion seen in group I rocks (figure 14) may also indicate depletion since this element is partitioned strongly into garnet and clinopyroxene [Irving 1978].

Group II rocks also have low Al_2O_3 and Na_2O (figure 6) suggesting a depleted source, but have high CaO (figure 1). This chemical signature has two possible origins: [i] a source depleted by melt loss but from which clinopyroxene was not completely eliminated. After later enrichment events, small degree partial melts may still be buffered at high CaO contents by the presence of clinopyroxene in the source; or [ii] depletion followed by later selective introduction of CaO by carbonate complexing either during the enriching event or during magma genesis. The association of increasing K_2O with decreasing SiO_2 and increasing carbonate in the volcanics of the western rift [Pouclet 1980b] may indicate a CO_2-rich enrichment event. The Sr-spike in the incompatible element pattern (figure 9) would also be expected in a carbonate-rich environment. Due to the extensive mineral reactions accompanying mantle metasomatism [Lloyd and Bailey 1975; Lloyd 1981], no petrographic check on the presence or degree of previous mantle depletion is possible.

If process [i] above is the correct one for group II rocks, the

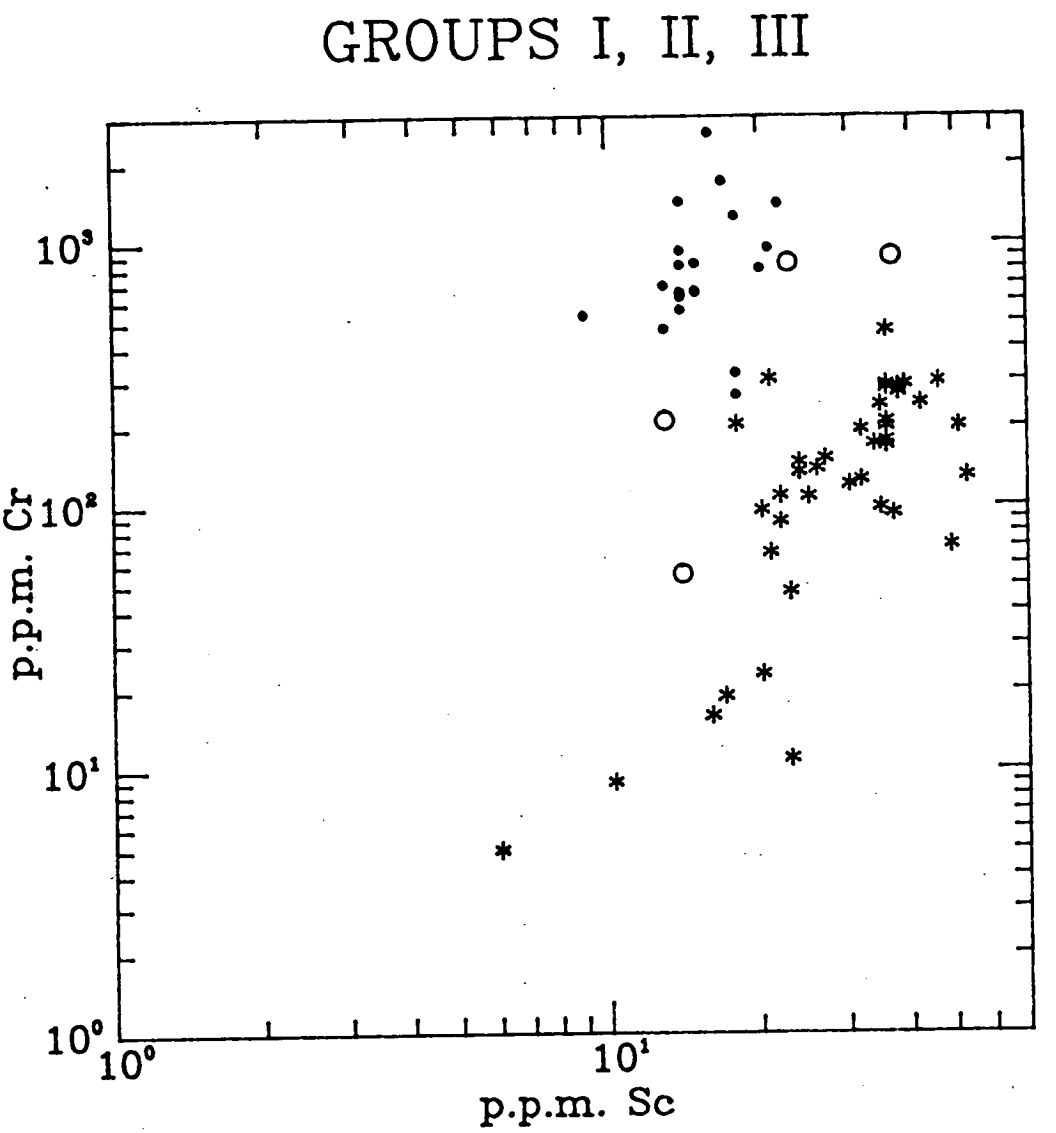

Figure 14

Sc vs Cr variation diagram. Group I = points; Group II = circles; Group III = asterisks. Group I higher Cr and lower Sc is inferred to indicate a depleted source.

degree of partial melting producing the ultrapotassic magmas would have to be small, since clinopyroxene must remain as a residual phase. The Toro Ankole ultrapotassic rocks define a rough trend with CaO decreasing with Al_2O_3; the lower CaO samples may be due to slightly higher degrees of melting where clinopyroxene has been eliminated. If the mica + clinopyroxene-rich metasomatised nodules are correctly interpreted as representative of the source of group II, then option [ii] above is the more likely because the clinopyroxene-poor lherzolite mantle which would be residual from option [i] could not result in clinopyroxene-rich rocks unless Ca was also introduced during the K-enriching event. Lloyd et al. [1985] melted a representative southwest Ugandan phlogopite clinopyroxenite nodule composition at 20-30 kbar, and suggested that metling of such a composition could give rise to Group II lavas with 20-30% melting.

A number of non-standard group II rocks such as some South African olivine melilitites (table 1; McIver 1981; McIver and Ferguson 1979) have high Al_2O_3, and plot well away from the bulk of group II analyses in figure 1 (they are within the Group III field for this diagram). Group II sources therefore may vary in their degree of depletion by earlier melting episodes.

Group III rocks show high values of CaO, Al_2O_3 and Na_2O (figures 1,6), so that there is no evidence of a substantial depletion event in their source. Rogers et al. [1985] consider that the relatively low MgO, Ni and Cr of magnesian leucitites from Italy with respect to expected values in primary magmas may indicate an olivine-poor source.

1.5.3.3 Variation at the mantle enrichment stage

Chemical variations produced at the mantle enrichment stage can be divided into two major types: those due to stability of incompatible element rich minerals in which the enriching component is trapped, and the nature, composition and origin of the enriching fluid itself. For evidence of these, we must look to the incompatible element variations (figures 8 to 10) and to petrological studies of metasomatised mantle xenoliths.

1.5.3.3.1 Stability of incompatible element-rich minerals

Mica and amphibole, particularly K-richterite, have long been recognised as important repositories in the mantle for potassium and the

related elements Rb and Ba as well as volatiles [Kushiro and Erlank 1970; Dawson 1971; Dawson and Powell 1969]. However, the spidergrams for ultrapotassic rocks indicate that all incompatible elements are enriched, which requires sites for a much greater number of elements than those contained in mica and amphibole. This is particularly true for the standard members of group I which have the greatest enrichment of elements at the left of the diagram (figure 8) and which also have patterns with nearly constant slopes.

Incompatible elements may be held in a variety of phases which have been described from metasomatised xenoliths such as crichtonite series minerals, wadeite, priderite, rutile, perovskite and ilmenite. The crichtonite series minerals are Cr-titanates which have a variety of end-members rich in K, Ba, Ca, Pb, Sr, U and REE [Haggerty 1983; Haggerty et al. 1983]. They may occur in association with Nb-Cr-rutile, Cr-Mg-ilmenite and Ca-Cr(Nb,Zr)-armalcolite [Haggerty 1983]. Of particular interest to group I ultrapotassic rocks, crichtonite stability is apparently limited to high Cr, Mg and low Fe, Al environments [Haggerty 1983] and so their stability may be promoted in lamproite source regions. The enriching fluid must be rich in Ti and the more incompatible elements, bur Cr could be provided by exchange with the wall rocks [Jones et al. 1982]. Wadeite and priderite, which occur as groundmass phases in lamproites, are also characteristic of Al-poor environments and are stable to at least 25kbar at mantle solidus temperatures [Arima and Edgar 1980; Dubeau and Edgar 1985].

Whilst these minerals appear to be likely candidates for storage of incompatible elements in the upper mantle, their applicability to ultrapotassic rock source regions is difficult to judge. The low Al_2O_3, refractory bulk composition which is required for many of them may discount their importance in group III regions. The known crichtonite-bearing mineral parageneses are estimated to have formed at 20-30kb pressure [Haggerty 1983; Jones et al. 1982]: experimental stability studies are lacking at present but experiments on the associated armalcolites suggest that this pressure range may be the high pressure limit [Lindsley et al. 1974]. Beyond these pressures, rutile, which can incorporate large amounts of Nb and Cr, may be dominant. The presence of diamonds in olivine lamproites from West Kimberley demonstrate that at least some lamproites originate at considerably greater depths. Mica and amphibole

stability is greatly increased by fluorine [Holloway and Ford 1975; Part 3] which is abundant in ultrapotassic rocks, particularly group I [Jaques et al. 1984a; Part 4], so that presence of mica well into the diamond stability field may reasonably be assumed.

The above summary demonstrates that the 'fertility' of the mantle, as well as pressure and temperature, may exert critical control on the stability of minerals containing incompatible elements brought in during mantle enrichment events. However, experimental work, coupled with studies of metasomatised nodules from lamproites, is needed to ascertain which minerals are the most likely storage sites for these incompatible elements in ultrapotassic source regions. Variation in the stabilities of these minerals may cause a zonation of incompatible elements in the mantle by differential abstraction of elements from a passing fluid phase. Melting of such a zoned mantle could then produce rocks with specific signatures on an incompatible element enriched spidergram.

1.5.3.3.2 The composition and origin of the enriching fluid

Variations in the chemistry of mantle enrichment events could be produced by differences in the composition of the enriching agent itself due either to variable solvent composition or to the nature of the solute source. Opinions differ as to whether the enriching agent is a small fraction of silicate melt [Varne and Graham 1971; Green 1971] or a fluid [Bailey 1970; Lloyd and Bailey 1975]. Alternatively, metasomatism may be caused by the release of vapour on freezing of a small, volatile-enriched melt fraction [Wyllie 1980].

Experimental studies indicate that H_2O-rich fluids carry much more solute than CO_2-rich fluids [Schneider and Eggler 1984], and that the solute is rich in normative quartz and feldspar, but poor in Ti. No experimental data are available for the case of a reduced environment, but CH_4-H_2O fluids would probably have a lower solute content since CH_4 is unlikely to dissolve much material [Taylor 1985]. Thus, it may be that a vapour undersaturated melt is the more likely transport medium for the Ti- and incompatible-element rich, but not notably Si-rich, material seen in 'metasomatised' mantle, and that metasomatism occurs when this freezes and releases vapours. The relative stability of minerals which control the composition of the C-H-O-F dominated vapour phase when the melt freezes will then determine the ability of these vapours to remove the material brought

in by the melt [Olafsson and Eggler 1983; Schneider and Eggler 1984]. A water-rich vapour could remove some of the silica introduced by a melt, leaving a low-silica, incompatible element-rich signature.

Variations in the composition of the solute source may cause different trace element signatures at a much earlier stage. Models for the origin of the enriching fluid invoke either dehydration of subducted material [Ringwood 1974; Wyllie and Sekine 1982] or degassing from an unconstrained lower mantle source [Bailey 1970; Wyllie 1980].

Subduction zone processes are most relevant in the case of Group III rocks which are from orogenic areas with subduction active beneath ultrapotassic rock localities either at present, in the case of Indonesia, or as recently as the Tertiary in the case of Italy. Models for the petrogenesis of arc volcanics generally attribute their characteristics to involvement of subducted material by dehydration reactions in the subducted slab or, at deeper levels, by partial melting of the slab. Various arc suites may result from differing degrees of involvement of subducted material in the mantle wedge above the subduction zone [Ringwood 1974; Green 1980; Gill 1981].

Of particular interest to ultrapotassic rocks are the low Ti-group element contents and high K_2O, Rb, and LREE. It is important in assessing the origin of arc ultrapotassic rock geochemical characteristics to separate the characteristics of the enriching component from those common to most non-ultrapotassic arc magmas. Wheller et al. [1986] have attempted this distinction for rocks from the Sunda-Banda Arc of Indonesia. This region is important to the present discussion in that it represents the simplest tectonic environment (an entirely oceanic subduction setting) containing group III ultrapotassic rocks, and is thus the best area in which to isolate the sources of geochemical characteristics. Within the Sunda-Banda Arc, increasing K correltes with increasing Nb and Ba, but not with Ti, which remains at very low abundances in ultrapotassic rocks [Wheller et al. 1986]. This indicates that Nb and Ba (together with K) were added to the arc source during an enrichment event, and therefore that the strong depletions in Ti, Ba and Nb characteristic of group III (figure 10) relative to other ultrapotassic rock groups have an origin independent of K-enrichment. This Ti-group depletion is a general characteristic of arc volcanics, and must result

from similar processes in both ultrapotassic and less alkaline rock types.

The elevated K_2O contents which must exist in the source to produce ultrapotassic magmas by partial melting are generally also attributed to dehydration or melting in the subducted slab. It has been argued that the most potassic arc magmas may form at greater depth than less alkaline magmas due to either [i] H_2O-rich fluids carrying K_2O in solution reacting to form mica in the overlying mantle wedge [Fyfe and McBirney 1975; Wyllie and Sekine 1982]; or [ii] the higher stability of mica relative to other common hydrous minerals causing concentration of potassium at deeper levels of the subducted slab. The latter may be an explanation of the proposed 'K-h' correlation of K_2O contents of magmas with depth to the Benioff Zone [Hatherton and Dickinson 1967; Ninkovich and Hays 1972]. Models using potassium derived from the slab require subducted sediments or basaltic oceanic crust altered by reaction with seawater, since the K_2O content of unaltered oceanic crust and the underlying oceanic lithosphere would be very low.

In the Lombok-Sumbawa sector of the Indonesian arc, the lack of a K-h correlation led Foden and Varne [1980] to propose that the high K_2O in some lavas was not derived from the slab, but from deeper levels of the mantle tapped by major cross-arc fractures or disturbed by the subducted slab. Wheller et al. [1986] consider that the weight of evidence is against a recently subducted sediment or altered oceanic crust origin for potassium in the high K_2O volcanics of the Sunda-Banda Arc, and that the K-rich component is derived from within the mantle. Their evidence includes low ^{10}Be contents, low $\delta^{18}O$ values and no deviation of Nd, Sr and Pb isotope compositions towards values typical of sedimentary material. Wheller [1986] suggested that as arcs mature, enriched areas may form beneath thickened crust due to decreased regional heat flow and continuing mantle degassing and metasomatism. These enriched areas may be disturbed either concurrently or at a later stage by the subducted slab or fluids derived from it giving rise to K-rich magmas.

The low Ti-group characteristics of arc magmas are generally also attributed to either dehydration or melting of the subducted slab. Dehydration resulting in permeation of Ti-poor, H_2O-rich fluids into the mantle wedge is unlikely to be the cause of Ti-depletion, since corresponding enrichments in Si, Al and incompatible elements, all of

which dissolve to a large extent in H_2O-rich fluids at mantle pressures [Schneider and Eggler 1984] should also be seen.

Contamination of the mantle wedge by a partial melt of subducted material at higher pressures should enrich the mantle in incompatible elements. This will include TiO_2 unless the partition coefficient for Ti between the liquid and a titanium-rich mineral increases with pressure causing saturation of the liquid in a titanate mineral at low TiO_2 contents. The effect of such residual accessory phases may only be very noticeable in spidergrams if $D_i^{ct/lq}$ differs by two orders of magnitude or more for element i between the accessory phase and coexisting silicate minerals. The effect on the spidergram will also be more apparent where only a restricted range of incompatible elements is readily accepted into the mineral. A restricted range is strong evidence for control by accessory phases, since sites in crystal lattices can be expected to be much more selective than solubilities in fluids or melts.

Green and Pearson [1986] found that the wt% TiO_2 at which titanate saturation occurs is decreased by increasing pressure, SiO_2 content, oxygen fugacity and alkali content, and by decreasing temperature. Green and Pearson [1986] argued that titanate saturation in group III source regions is unlikely, but their discussion was limited to the magma generation stage and to 30 kbar pressure. Their observations indicate that alkali-rich low-degree partial melts at very high pressures (>30 kbar) may be TiO_2-saturated, in which case melts either from the subducted slab or from deeper levels unrelated to the slab, may be Ti-poor. A plot of TiO_2 against Nb (figure 15) shows a good correlation as would be expected in some titanate minerals. This plot also demonstrates that the negative spikes for these elements in the non-standard group II pattern (figure 9) is entirely due to rocks from San Venanzo and Cupaello. There is insufficient data on phase stabilities and partition coefficients at high pressures to evaluate titanate control. For example, Varne [1985] has suggested control by perovskite, but perovskites differ greatly in Nb and REE content between different rocks due to as yet unknown variations in their conditions of origin [Boctor and Meyer 1979; Jones and Wyllie 1984; Treiman and Essene 1985]. Perovskite contains very little Ba, so that involvement of a barian titanate such as priderite may be required. The chemical signatures noted by Wheller et al. [1986] for K-enrichment and independent arc sources are both depleted in Ti, but differ in Nb and Ba,

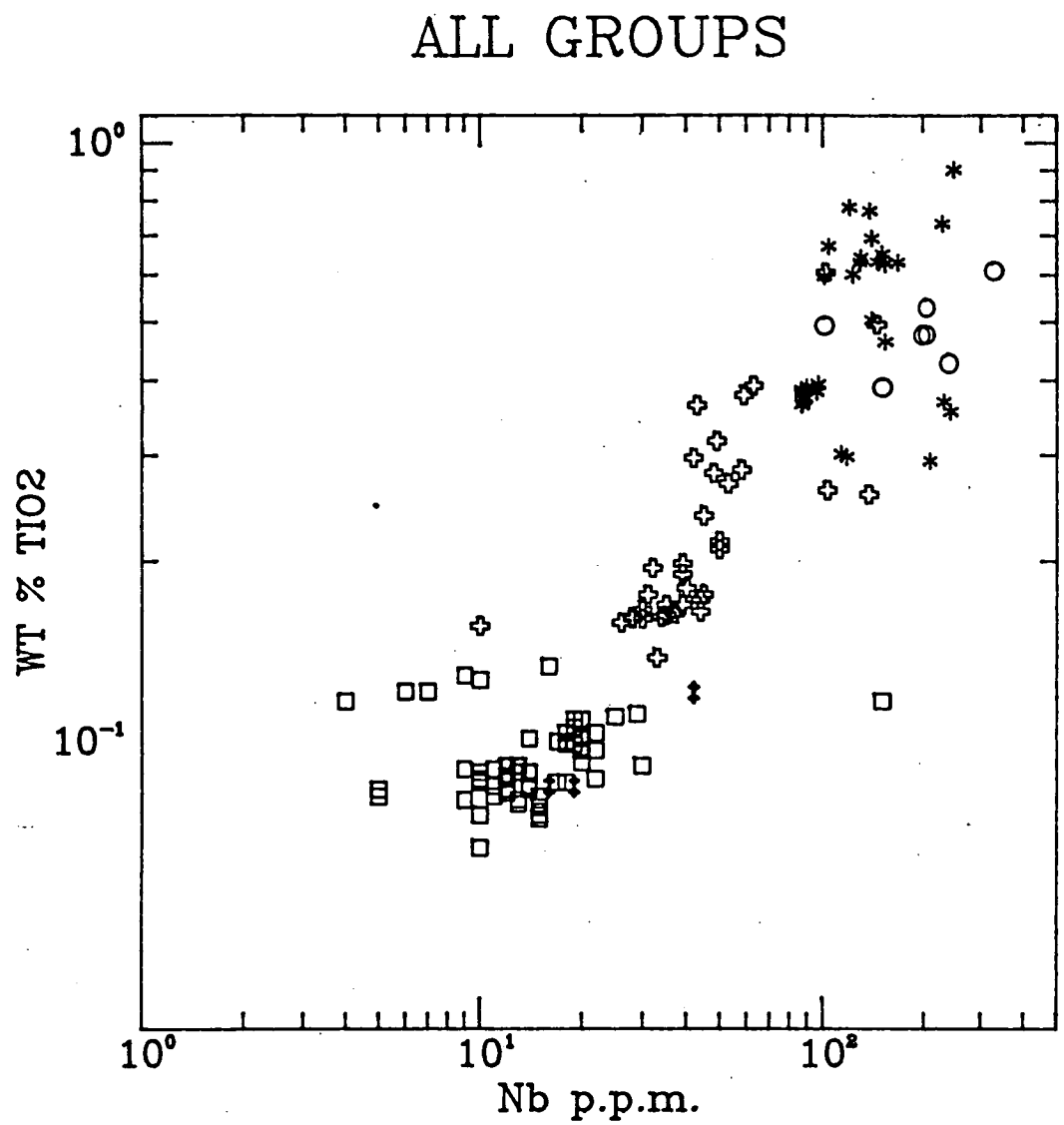

Figure 15

Ti vs Nb diagram for ultrapotassic rocks showing correlation of these two elements inferred to indicate control of both elements by residual phases. Asterisks = West Kimberley and Gaussberg; Circles = Group II except for San Venanzo & Cupaello; Crosses = non-standard group I; Double dagger = San Venanzo & Cupaello; Squares = Group III.

which may be indicating the involvement of different residual titanate phases.

Models for the origin of Italian group III rocks and also some group I rocks generally assume the involvement of subducted material by [i] generation of melts from the mantle wedge previously metasomatised by fluids from the slab [Dal Piaz et al. 1979; Venturelli et al. 1984a]; or [ii] continued release of fluid or melt from a seismically inactive fossil subduction zone [Kuehner 1980; Rowell and Edgar 1983]. There is no evidence for currently active subduction beneath the Recent ultrapotassic rocks of central Italy [Cundari 1980]. The possibility of K_2O derived from mantle metasomatism not related to subducted material is difficult to assess at present for the Italian volcanics because of the time interval between subduction and volcanism. The source regions of Italian group III lavas are believed to be characterised by $\delta^{18}O$ values >6, which is higher than most mantle rocks, and may indicate a subducted component [Hawkesworth and Vollmer 1979; Ferrara et al. 1985]. Hawkesworth and Vollmer [1979] argue against crustal contamination of the magma during ascent for the Roman region, but indicate that this may occur in the Tuscany lavas to the north (Group IV). The Nd and Sr isotopic systems are not considered reliable indicators of crustal involvement [Hawkesworth and Vollmer 1979].

The more unradiogenic Nd and radiogenic Sr compositions of Group I rocks relative to other groups can be explained just as readily by a mantle enrichment event as by crustal involvement. Crustal models generally suffer from a lack of definition of crustal composition, which can be very variable [Taylor and McClennan 1985 p.86-88; Collerson and McCulloch 1983]. Ancient enrichment events occurring at least as early as the mid Proterozoic would be required to produce the isotopic characteristics of lamproites, although more extreme enrichment would also assist [McCulloch et al. 1983; Nelson et al. 1986]. It is noteworthy that ultrapotassic rocks are primarily a Phanerozoic phenomenon, but the only Proterozoic occurrences are Group I rocks.

Discussion of differences between possible primordial fluids is limited by the lack of constraints on their origin. In the case of primordial fluids derived from the lower mantle [Bailey 1970, 1980] there will be a compositional dependence of solute content as discussed earlier. The involvement of 'megalith' material [Ringwood 1982] from long-term

recycling of subducted material could produce some of the isotopic enrichments seen in group I rocks (table 2; Nelson et al. 1986). Chemical characteristics would be controlled by similar considerations to material in more recent subduction zones, but with time-integrated isotopic signatures.

1.5.3.4 Variation at the magma generation stage

Factors affecting the composition of partial melts, other than those already discussed, can be split into three groups; the control of residual accessory phases, variations in the composition and abundance of volatiles, and variations in pressure and temperature of melting.

1.5.3.4.1 Accessory phases

Incompatible element concentrations in magmas may be controlled by accessory phases in the source region as discussed above for titanate minerals. Green and Pearson [1986] suggested that titanate saturation is unlikely in arc magma source regions due principally to the strong negative correlation of TiO_2 saturation level with SiO_2 content of melts. Residual titanate control appears more likely at the enrichment stage, although the effect of very high pressures is not yet known.

The lack of substantial positive or negative deviations from a smooth slope in the spidergrams (figures 8 and 9) for standard members of groups I and II suggests that $D_i^{ct/lq}$ for incompatible elements in different phases are not substantially different. Whilst element control by accessory phases is most likely in group III, some detailed characteristics of group I, such as the differing K*/Nb* between olivine lamproites and leucite lamproites, may be indicating differing accessory phase solubilities.

1.5.3.4.2 Volatile components

It is well documented that addition of H_2O to peridotitic compositions promotes stability of less polymerised phases resulting in the production of more silica-rich melts at considerably reduced temperatures relative to volatile-free systems. This depolymerisation occurs by breakage of bridging Si-O bonds resulting in splitting of the aluminosilicate network into smaller units [Mysen 1977; Stolper 1982]. CO_2 has the opposite effect of producing silica-poor melts at temperatures only slighty lower than in volatile-free conditions. In a mica-bearing mantle, the liquidus phase field of phlogopite is reduced at even moderate

$CO_2/(CO_2+H_2O)$ [Wendlandt and Eggler 1980c; Ryabchikov and Green 1978], but even in an H_2O-poor environment it will be promoted by the presence of fluorine [Part 3]. Recently, an increasing body of evidence, reviewed by Arculus [1985] and Taylor [1985], has led to arguments for more reduced mantle in which a vapour phase would consist dominantly of CH_4 and H_2O. Taylor [1985] has demonstrated that methane has a slight depolymerising effect, so that the degree of silica saturation of the melt produced will depend critically on the oxidation state of carbon as well on the C/H ratio.

In a study of the liquidus chrome-spinels of lamproites, Foley [Part 2] suggested that lamproitic magmas may be oxidised appreciably during emplacement, originating from a reduced environment at depth. In a reduced environment, H_2O, CH_4 and HF would all cause depolymerisation [Part 4] which could lead to silica-rich magmas similar to leucite lamproites, which are the most silica-rich ultrapotassic rocks which unequivocally represent primary mantle derived magmas.

The association of East African group II rocks with carbonatites argues for a CO_2-rich eruptive environment which is supported by the presence of CO_2-rich, H_2O-poor volcanic gases [Bailey 1980]. The enrichment in CaO and Sr characteristic of this group is explained readily by complexing with carbonate. This alone need not mean that the original mantle enrichment was also oxidised: Vollmer and Norry [1983] suggested that a Pb pseudoisochron age of 400-500 my for Group II rocks of the western rift may be due to a mantle enrichment event of that age. Oxidation of the mantle source could well have occurred in the intervening period, especially since the volcanism is associated with uplift [Bailey 1974], and oxidation may occur mostly at shallow depths [Mathez 1984; Part 4].
However, the metasomatising reactions seen in the nodules indicate introduction of Ca to form clinopyroxene [Lloyd 1981], so that the characteristic high Ca and Sr may have been introduced at the enrichment stage.

A CO_2-rich melting environment is also likely for other group II rocks which are mostly ultrabasic lamprophyres and melilitites [Rock 1986; Brey and Green 1975].

Group III rocks, and arc rocks in general, are charaterised by a greater amount of H_2O than CO_2 [Gill 1981]. However, the effects of

volatiles on group III trace element characteristics would be insignificant compared to those apparently due to residual accessory phases.

1.5.3.4.3 Pressure-temperature variations

In volatile-bearing systems, temperature of melting of a given source rock is essentially a function of the volatile composition. Pressure, however, has an appreciable effect on the composition of melts produced. Increasing pressure causes expansion of the stability fields of more silica-saturated phases such as enstatite relative to forsterite, so that melts produced are progressively less silica saturated [Green 1971; Kushiro 1972; Wendlandt and Eggler 1980c]. This pressure effect is apparently related to liquid structure, and is distinct from any effect which pressure and temperature variations may have on the stabilty of mantle phases. Foley et al. [Part 4] have suggested that the trend of decreasing silica content between primary leucite lamproites and olivine lamproites may be due to increasing pressure with largely similar source and volatile compositions. This suggestion is supported by liquidus experiments on olivine lamproite and leucite lamproite compositions [Part 5].
This mechanism has more potential for explaining group I standard members than other rocks because of their stable continental setting. Group II are associated with rift environments in areas of mantle upwelling so that a relatively shallow source is likely. Group III primary magmas have very similar silica contents (46-49 wt %) so that pressure variation is probably not important.

1.5.3.5. Some comments on Group IV rocks

Group IV is defined as a chemically transitional group on the basis of major elements, but in terms of petrogenesis these rocks may be transitional or quite distinct. Treatment of this group suffers from a lack of trace element data, which for many occurrences listed in table 1 is incomplete or non-existent. Primary magmas are usually difficult to define, particularly for those which may originate in the lower crust, but good evidence for a primary mantle origin exists for the mantle nodule-bearing Navajo and Sierra Nevada rocks.

The Sierra Nevada incompatible element patterns show weaker REE enrichment than all the major ultrapotassic rock groups. Apart from this

and the higher Sr, they are generally transitional between groups I and III. Van Kooten [1980] suggested they originate by partial melting of a mica-peridotite enriched in clinopyroxene by a distinct enrichment episode. This may explain the transitional chemistry and also the positive Sr spike, and may also indicate Ca and Sr introduction in a Group II-style enrichment episode. The Navajo rocks also contain garnet lherzolite xenoliths [Ehrenberg 1982] which may indicate a less depleted source than for group I rocks. They have incompatible elements generally intermediate between groups I and III with small negative deviations for Ba and Nb, but not for Ti. Titanclinohumite-bearing nodules are unique to this area [Smith 1979], which may indicate unusual conditions under which incompatible element contents of melts may be influenced by a different set of accessory minerals to those in most ultrapotassic rock source regions. It has been argued that alkaline volcanics and their inclusions in the western U.S.A. are related to a fossil shallow level subduction zone [Helmstaedt and Schulze 1979; Rowell and Edgar 1983], which may have produced unusual mantle mineralogy. The Highwood Mountains rocks further north have depletions for Ti and Nb, but not for Ba.

A number of group IV rocks such as vaugnerites and durbachites probably originate by melting of the lower crust. Evidence includes association with more common granitic rocks and abundant lower crustal nodules [Holub 1977; Sabatier 1980]. The origin of these may overlap with some minettes: Palm [1958] considered that they may represent mica-rich cumulate parts of granitic magmas, and some minettes also occur as marginal facies to granitic rocks [Guintrand et al. 1963]. Rock [1984] has reviewed occurrences and petrogenetic models for minettes, many of which invoke melting of, or interaction with, lower crustal material. More work, particularly isotopic, is needed to clarify these relationships.
The minettes are heterogeneous in terms of trace elements, which probably indicates considerable crystal accumulation or crustal interaction for some of them. Rock [1984] suggested that the most K-rich and mafic minettes may be due to crustal modification of lamproitic/leucititic magmas themselves derived from the mantle. Experimental evidence that the low Al lamproitic magmas readily gain alumina by reaction [Jaques and Foley 1985] indicates that this suggestion warrants further investigation.

1.6 SUMMARY AND SYNTHESIS

A chemical definition for ultrapotassic rocks is introduced using the whole-rock major element chemical delimiters $K_2O/Na_2O > 2$, $K_2O > 3$ wt% and $MgO > 3$ wt%. A literature survey using this definition amassed more than 800 analyses from 82 localities including olivine melilitites, ultrabasic and alkaline lamprophyres and K-Mg-rich dioritic rocks as well as most of the leucite-rich rocks usually considered in discussions of ultrapotassic rocks. These were divided into subgroups using a resemblance classification in which standard group members (or end members) are chosen, and abstracted qualities of the other rocks are compared to these. This has the advantage of by-passing the entrenched and confusing mineralogically-based nomenclature, and also allows the recognition of transitional features amongst rocks which may otherwise be part of one group.

Three end-member groups are recognised with a fourth transitional group including rocks which probably have a variety of origins. The groups, together with their chief characteristics, are:

GROUP I: Lamproites, characterised by low CaO, Al_2O_3 and Na_2O and variable SiO_2. West Kimberley and Gaussberg are chosen as standard members. Incompatible elements are most enriched in this group, with no marked deviation from a regular spidergram pattern. TiO_2 contents are variable, but generally distincive for a given locality. This reflects geological setting, with higher TiO_2 in rocks from continental anorogenic areas and lower TiO_2 together with variable P_2O_5 in rocks from orogenic areas. Mantle-derived nodules are dominated by depleted types such as harzburgites and dunites, with spinel- or garnet- lherzolites occurring only rarely. Isotopic compositions have strongly negative ε_{Nd} and high $^{87}Sr/^{86}Sr$, and standard members have distinctive Pb isotopes plotting to the left of the geochron [Nelson et al. 1986].

GROUP II: The Toro Ankole rocks, frequently referred to as kamafugites, are chosen as standard members. Group II rocks have low SiO_2 and Al_2O_3 and high CaO. Incompatible elements are less enriched than group I and have a positive Sr spike. With the exception of the rocks from San Venanzo and Cupaello, which are the only group II rocks emplaced in active orogenic

areas, K*/Nb* is less than one in common with low silica rocks from group I. Nodules in the Toro Ankole rocks are rich in mica and clinopyroxene and probably result from mantle metasomatism. Nodules in non-standard members include less metasomatised lherzolites. Isotopic data for group II are lacking, but related rocks fron East Africa show mild enrichment in radiogenic Nd and Sr. The rocks are mostly rift related, either in continental or incipient oceanic rift environments. The Italian group II rocks appear to be a special case since they have many features in common with group III Italian lavas.

GROUP III: These are distinguished by high Al_2O_3 and CaO, and have incompatible element patterns with characteristic negative spikes for Ba, Nb and Ti. They occur exclusively in orogenic environments and lack mantle-derived nodules not related to high-pressure crystallisation of magma. Isotopic characteristics are very variable for oxygen, and vary from similar to bulk earth to compositions more enriched in $^{87}Sr/^{86}Sr$ and depleted in $^{143}Nd/^{144}Nd$.

The classification provides a basis for the discussion of petrogenetic models, and the constraints introduced by the data and classification are discussed. The processes which lead to group characteristics are discussed without attempting specific detailed models for individual areas. The compositions of likely primary magmas are outlined, including a range of silica contents for lamproites. Petrogenetic models invoking partial melting of pre-enriched mantle sources are preferred for the explanation of most primary magmas. Previous models involving crustal contamination and assimilation, zone refining and high pressure crystallisation are discounted as major factors in the generation of primary magmas. Processes which may lead to chemical variations seen in the ultrapotassic rocks are divided into those predating mantle enrichment, the mantle enrichment processes themselves, and variations at the time of partial melting to produce magmas.

Pre-enrichment processes are substantial melting of the mantle leaving a refractory source composition depleted in Ca, Al and Na, and rich in Mg-number and Cr. Group I rocks are considered to originate from a depleted source indicated by their low Al, Na and Ca. Toro Ankole major element chemistry may indicate a depleted source subsequently enriched in Ca, or a partly depleted source with lowered Al and Na, but from which

clinopyroxene was not eliminated. High Ca and Al in Group III probably indicates a relatively fertile source.

Mantle enrichment processes may vary due to the nature, composition and origin of the 'metasomatising' agent or the stability of incompatible element-rich host phases in the enriched mantle. In a depleted mantle, the low Al and high Cr contents should allow stabilisation of rarer incompatible element-rich minerals such as priderite, wadeite and members of the crichtonite group [Haggerty 1983]. This would lead to a greater variety of mantle hosts for these elements which could explain the smoother spidergrams of group I, and maybe group II, although the degree of enrichment may also explain the overall abundances. The F-rich chemistry of ultrapotassic rocks. particularly lamproites, suggests stabilisation of mica and possibly amphibole by fluorine [Jaques et al. 1984a; Part 3].

Different enrichment chemistries can be expected where the enriching agent is a silicate melt, H_2O-rich or CO_2-rich oxidised fluid, or reduced H_2O-CH_4-rich fluid. Small silicate melt fractions and H_2O-rich fluids can be expected to introduce the greatest enrichment concentrations, but more experimental data is needed on reduced fluids to constrain variations introduced at this stage.

The chemical characteristics of ultrapotassic rocks from orogenic areas have been variously attributed to [i] contamination of the overlying mantle wedge by fluids derived from the subduction zone; [ii] release of fluids or melts from a fossil subduction zone; [iii] involvement of enrichment components similar to those inferred to occur in continental non-orogenic areas, but melted in a high-pressure, low temperature environment in the vicinity of the subduction zone. H_2O-rich fluids derived from the subducted slab should be rich in normative quartz and feldspar, and poor in TiO_2. The low Ti-group element contents in orogenic ultrapotassic rocks may also be explained by retention of these elements in accessory phases residual after melting at very high pressures. However, experimental data at very high pressures are needed to investigate this possibility. The high K_2O may originate from subducted crustal material or from mantle metasomatism; isotopic evidence indicates this may vary between regions of group III rocks.

Chemical variations developed during the partial melting event can

be caused by residual accessory phases, volatile mixtures and abundances, and pressure variations. Many of the chemical variations seen between the ultrapotassic rock groups can be explained by combinations of these three factors. Differing stabilities of residual phases which take in a limited set of elements plotted in the spidergrams can explain negative spikes in the patterns, provided that the partition coefficients ($D_i^{ct/lq}$) for these elements are very large. Residual accessory phase control is the best explanation for the low Ti, Ba and Nb contents of group III rocks because crystal sites are more element-specific than fluids or melts. The stabilities and partition coefficients for accessory minerals will be related to source chemistry and pressure-temperature conditions, which are a function of tectonic setting. More experimental data on distribution coefficients for incompatible elements and mineral stabilities is needed to develop and constrain such models.

The existence of a range of silica contents in primary lamproitic magmas can be explained by partial melting at variable pressures. Production of high silica (> 51 wt%) leucite lamproite melts would be favoured by H_2O- and HF rich, CO_2-poor and maybe reduced (CH_4-H_2O) conditions [Jaques et al. 1984a; Part 4]. Melts with similar volatiles under greater pressures may lead to olivine lamproites. The association of the low silica Toro Ankole rocks with carbonatites suggests a high CO_2 environment which is also indicated by low H_2O volcanic gases [Bailey 1980]. Complexing with CO_2 at the magmatic stage also explains high Ca and Sr characteristic of group II. This need not imply a CO_2-rich enrichment stage.

Group IV includes both rocks which are mantle-derived, such as the peridotite-bearing Navajo and Sierra Nevada examples, and rocks which probably originate in the lower crust. Most members of this group are transitional between groups I and III, which may indicate derivation from a relatively undepleted source for the mantle-derived ones. Many minettes and vaugneritic rocks may represent mica-rich accumulations from granodioritic magmas, whereas other minettes may be mantle-derived or originate by crustal modification of mantle-derived potassic magmas [Rock 1984].

PART II

THE OXIDATION STATE OF LAMPROITIC MAGMAS

An experimental study of liquidus phase compositions in the Gaussberg Olivine Leucitite with variable oxygen fugacity

1.1 INTRODUCTION AND RATIONALE

The ultrapotassic igneous rocks have attracted much attention due to their unusual chemistry. Classified on silica content they are ultrabasic to intermediate, generally have relatively high Ni, Cr and Mg-number characteristic of primitive magmas, and yet have exceptionally high alkalis and other incompatible elements normally characteristic of more differentiated rock types. The effect of this unusual chemistry is seen in the frequent occurrence of phlogopitic mica and leucite as phenocryst phases, together with crystallisation of rare minerals such as priderite, wadeite, potassic richterite and kalsilite in the groundmass.

The variety of ultrapotassic rocks apparently derived from the mantle must be due to variations in mantle composition and/or conditions of melting. Recent studies have shown that it is highly unlikely that ultrapotassic rocks can be derived by melting of a garnet or spinel-lherzolite mantle, but that some enrichment of the mantle by a component rich in potassium and other incompatible elements is a necessary precursor to the genesis of these rocks [e.g. Lloyd and Bailey 1975; Edgar et al. 1976]. Mixed volatile components and oxygen fugacity will play a major role in determining the type of melt produced in the mantle. Therefore, as a precursor to experimental studies, intrinsic evidence for factors such as volatile contents and oxygen fugacity must be sought amongst primitive representatives of the ultrapotassic rock groups.

The Gaussberg volcano consists of olivine leucitites which are primitive members of the lamproite group of ultrapotassic rocks (see Part 1). The Gaussberg rocks contain chrome spinels as liquidus phases which are rich in ferric iron relative to chrome spinels in most basaltic rocks. Liquidus chrome spinels in other ultrapotassic rocks have widely varying ferric iron contents, and the ferric iron content of leucites also

exhibits some variation. Because of these variations, it was decided that the initial step in an experimental investigation of lamproite petrogenesis should be to determine the fO_2 conditions of crystallisation of the phenocryst assemblage, i.e. the conditions at eruption of the olivine leucitite melt. This paper reports the results of investigation of the liquidus phases as a function of oxygen fugacity at atmospheric pressure.

2.2 GAUSSBERG OLIVINE LEUCITITE

The Gaussberg olivine leucitite is an ideal subject for experimental study of the lamproite rock group. It has all the chemical characteristics outlined in Part I for lamproites, including an Mg-number of 70, and is one of the most potassic igneous rocks known (K_2O = 11.6 wt%). Sheraton and Cundari [1980] described a spinel lherzolite included within the leucitite, and list mineral compositions from the xenolith. High Al_2O_3 contents of pyroxenes accompanied by low Cr/(Cr+Al) of spinel establish the xenolith as a typical medium pressure, high temperature lherzolite assemblage (in the range 8-20 kbar).

The olivine leucitite consists of olivine, leucite and clinopyroxene phenocrysts set in a brown glass with quench mica, leucite and clinopyroxene [figure 16]. Numerous melt inclusions occur in olivine and leucite and have compositions which are not significantly different from the analysed whole-rock composition. Thus the rock composition is arguably that of a mantle-derived liquid, with the exception of possible volatile exchange near the surface. Less rapidly quenched examples have a matrix of mica, clinopyroxene and leucite with minor ilmenite and partly devitrified glass. The mineralogy has been described by Sheraton and Cundari [1980] and so only additional features are noted here.

Phenocryst clinopyroxenes occasionally include corroded green salite cores which are compared with the typical diopsidic phenocryst compositions in table 4. Green salite cores have been reported from all three groups of ultrapotassic rocks [Kuehner 1980; Barton and van Bergen 1981; Holmes and Harwood 1932; Barton et al. 1982] and also from other potassic rocks such as shoshonites [Pe-Piper 1984]. Their simultaneous occurrence with Mg-rich phenocrysts is not yet adequately explored, but Barton et al. [1982] and Pe-Piper [1984] have suggested magma mixing for

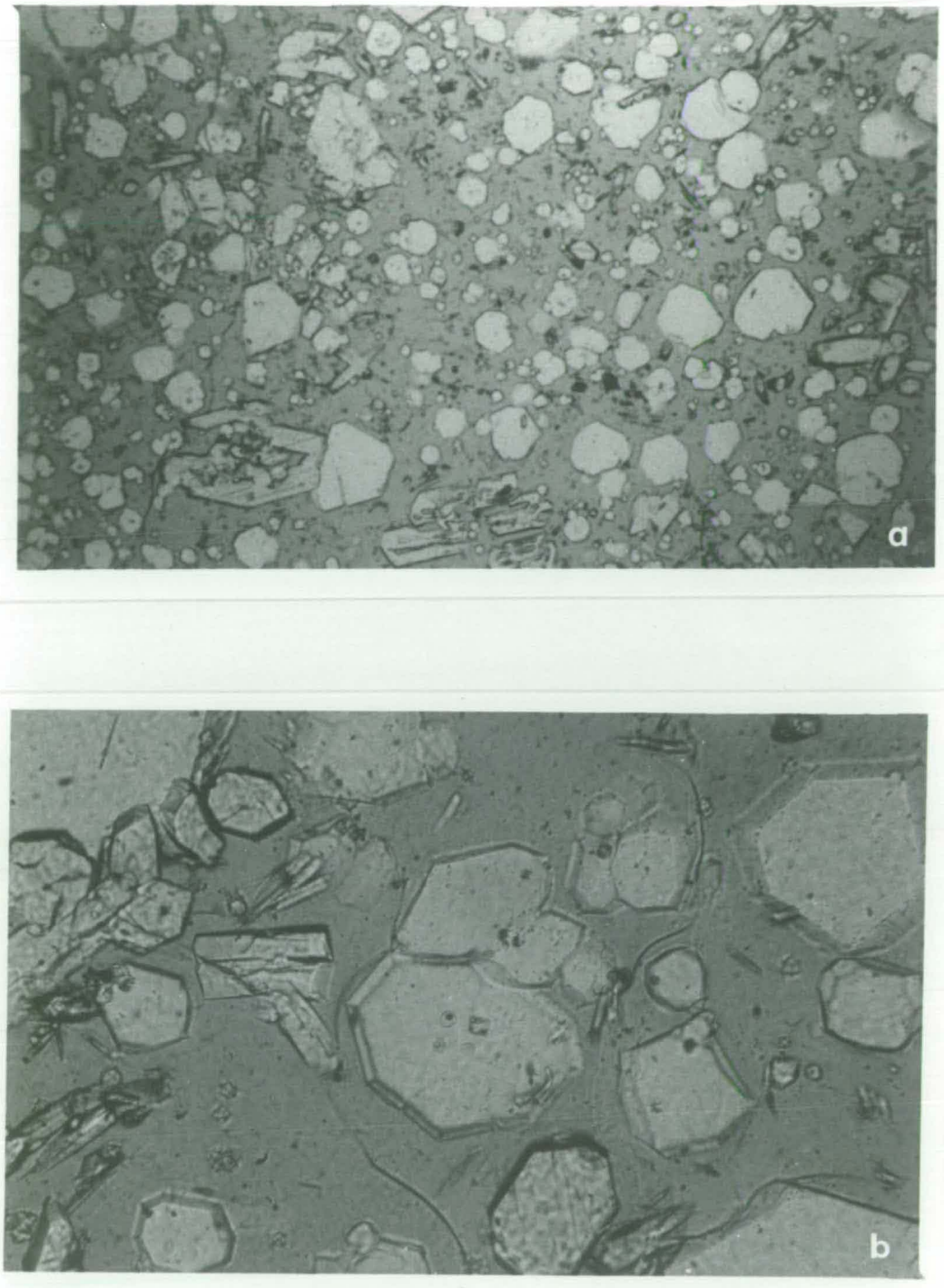

Figure 16

A glassy example of the Gaussberg olivine leucitite with

[a] phenocrysts of olivine, clinopyroxene and leucite (magnification x40)

[b] quench leucite and clinopyroxene, and melt inclusions in leucite (magnification x100).

TABLE 4

Compositional comparison of green salite cores to pyroxene phenocrysts (1-3) with diopside phenocrysts (4-6) from Gaussberg olivine leucitites. Mg = 100Mg/(Mg+Fe), FeO = total iron as FeO. Analyses normalised to 100% by EDAX microprobe system.

	1	2	3	4	5	6
SiO2	52.09	50.94	51.39	54.04	54.69	54.13
TiO2	0.29	0.21	--	1.01	0.74	0.90
Al2O3	2.49	1.99	1.79	0.63	0.53	0.56
Cr2O3	0.43	--	--	0.75	0.59	1.12
MnO	0.23	0.48	0.51	--	--	--
FeO	11.32	15.79	15.19	2.80	3.16	2.65
MgO	12.13	9.59	9.67	17.40	17.83	17.42
CaO	20.52	20.42	20.91	23.13	22.26	22.96
Na2O	0.49	0.57	0.51	0.24	0.26	0.25
Mg	65.6	52.0	53.2	91.7	91.0	92.2

TABLE 5

Analyses of leucites from Gaussberg olivine leucitite (1-4), Leucite Hills (5 - from Kuehner et al. 1981) and West Kimberley (6). 1 and 2 are early leucite cores; 3 and 4 are typical phenocryst leucites.

	1	2	3	4	5	6
SiO2	55.91	55.69	56.79	57.06	57.71	55.51
Al2O3	22.79	22.83	21.68	21.37	19.62	21.17
Fe2O3	0.27	0.29	1.04	1.30	2.03	0.65
K2O	20.68	20.66	20.40	20.64	20.77	20.11
Total	99.65	99.47	99.91	100.37	100.13	97.45
Cations per six oxygens:						
Si	2.027	2.023	2.056	2.062	2.145	2.058
Al	0.974	0.978	0.925	0.910	0.837	0.925
Fe	0.007	0.008	0.028	0.035	0.055	0.020
K	0.956	0.958	0.943	0.951	0.959	0.951

TABLE 6

Analyses of chrome spinel occurring as inclusions in olivine phenocrysts. G = Gaussberg olivine leucitite; WK = West Kimberley olivine leucitite [=leucite lamproite]; SP = inclusion in olivine from a Spanish fortunite [A.J.Crawford, unpublished]; LH = Cr-spinel in Leucite Hills wyomingite [Kuehner et al. 1981]. Iron cation ratio calculated assuming cation total = 3.000

Cr = $100Cr/(Cr+Al)$, Ferric = $100Fe^{3+}/(Fe^{3+}+Fe^{2+})$,
Mg = $100Mg/(Mg+Fe^{2+})$

	G1	G2	G3	G4	WK1	WK2	WK3	SP	LH
TiO2	4.3	4.7	4.3	4.2	4.6	4.8	3.9	1.3	0.7
Al2O3	3.8	3.8	4.0	3.7	2.0	2.1	3.0	2.1	6.7
Cr2O3	50.4	49.1	50.7	50.2	55.1	55.2	58.0	61.7	44.1
FeO	28.0	29.1	28.4	28.4	26.1	26.2	22.5	21.4	32.8
MgO	13.0	12.8	12.6	9.8	10.8	12.8	10.9	9.8	10.8
Total	99.7	99.5	100.0	99.8	99.1	99.5	100.0	96.3	95.1
Cations:									
Ti	0.107	0.116	0.108	0.105	0.119	0.124	0.099	0.033	0.018
Al	0.150	0.151	0.155	0.146	0.081	0.085	0.118	0.086	0.271
Cr	1.332	1.290	1.327	1.317	1.489	1.482	1.529	1.709	1.195
Fe3+	0.313	0.326	0.302	0.328	0.291	0.186	0.156	0.139	0.498
Fe2+	0.466	0.482	0.484	0.459	0.552	0.557	0.470	0.487	0.443
Mg	0.641	0.634	0.624	0.633	0.557	0.566	0.629	0.514	0.552
Mg	57.9	56.8	56.3	58.0	50.2	50.4	57.2	51.4	55.5
Cr	89.8	89.5	89.5	90.0	94.9	94.7	92.9	95.2	81.5
Ferric	40.2	40.3	38.5	41.7	25.8	25.0	24.9	22.2	53.0

the origin of Italian and Greek examples. The high Mg-number, Al_2O_3 and Na_2O contents, and low TiO_2 and Cr_2O_3 contents of the Gaussberg salites preclude them from a genetic relationship with the olivine leucitite liquid.

The olivine leucitite contains two generations of leucite (table 5). The first has a low ferric iron content and typically contains numerous melt inclusions; these early leucites typically have a rim of well-formed leucite crystals, as originally noted by Reinisch [1912]. The later leucites are richer in ferric iron and have higher excess silica (2.045-2.068 atoms per 6 oxygens as against 2.012-2.038 atoms for the first generation). The silica content of the second generation is typical of lamproitic leucites, contrasting with the view formed by Sheraton and Cundari [1980] from limited data.

Inclusions of chrome-rich spinels within olivine (Fo 89-90) apparently indicate quite a high oxidation state at an early stage of crystallisation (table 6). The spinels have a ferric value of 38-42, where ferric iron is calculated assuming stoichiometry, which suggests an oxygen fugacity higher than that of most basaltic compositions. New analyses of chrome spinel inclusions in olivine phenocrysts from a West Kimberley olivine leucitite and a Spanish fortunite are also presented in table 6.

2.3 EXPERIMENTAL METHODS

The starting material for the experiments was a synthetic glass, the composition of which is compared to natural Gaussberg rocks in table 7. A mixture of oxides, carbonates (for K, Na, Ba, Sr and part Ca) and $Ca_2P_2O_7$ was sintered at 1000°C prior to addition of fayalite. The mixture was then melted at 1320°C in an argon atmosphere and quenched to a glass.

The mix was loaded into iron-doped Pt capsules which were included in evacuated silica tubes above a separate Pt capsule containing the oxygen buffer. The buffers used were haematite-magnetite [HM], manganosite-haussmanite [MnH], nickel-nickel oxide [NNO] and magnetite-wustite [MW] (figure 18). Buffers were checked by XRD after each run. Experiments were run suspended by a Pt harness in a one inch diameter vertical furnace for 2.5 to 5 hours, and were quenched in distilled water. Temperatures were checked with a $Pt/Pt_{90}Rh_{10}$ thermocouple immediately

TABLE 7

Comparison of synthetic Gaussberg glass with natural compositions.

[1] Target composition: average of 11 olivine leucitite analyses recalculated volatile-free [Sheraton and Cundari 1980].

[2] Average microprobe analysis (area scans) of synthetic composition prepared for the experiments. FeO = wet chemical determination (analyst P.Robinson). Discrepancy in the total is due to minor elements not analysed for by microprobe.

[3] Glassy pillow rim 4870B [Sheraton 1981] used in Fe-doping runs, recalculated volatile-free.

	1	2	3
SiO2	51.45	52.38	51.19
TiO2	3.46	3.67	3.43
Al2O3	9.97	9.89	9.98
Fe2O3	2.49	3.3	2.45
FeO	3.82	2.8	3.93
MgO	8.04	8.02	8.08
CaO	4.68	4.57	4.81
Na2O	1.67	1.79	1.67
K2O	11.78	11.00	11.77
P2O5	1.50	1.52	1.49
MnO	0.09		
BaO	0.63		
SrO	0.23		1.21
ZrO2	0.14		
Cr2O3	0.045		
NiO	0.03		
Mg #	70.3	71.2	70.2

prior to each run and are accurate to ±1°C.

Hill and Roeder [1974] used alumina sample capsules for low fO_2 runs to overcome the problem of Fe-loss to Pt capsules and found only a small alumina gain in run products. A trial near-liquidus run using an alumina sample capsule proved unsatisfactory with the Gaussberg composition: the glass gained 4-7 wt% alumina, and pleonaste series spinels crystallised.

Therefore, Pt capsules were used, but an attempt to minimise iron loss was made by doping with iron. A preliminary doping run was made for each experiment with a mixture of a natural glassy pillow rim (4870B: see table 7) and wustite or iron metal powder. Capsules were then cleaned by heating in HF for 1-2 days. The doping runs were made with the appropriate buffer capsules for 4 hours at 1300°C. Doping mixtures found to give best results were as follows; 4870B + 3% wustite for HM and MnH, 4870B + 10% wustite for NNO and 4870B + 30% Fe for MW. Success of the doping procedure was variable as shown by the Mg-number of the glass in runs at 1250°C and above (tables 8 and 9). Some NNO runs lost iron (e.g. runs 117A and 141B) and some MW runs (e.g. 137) gained iron from the doped capsules. These effects were least in runs where the resulting glass Mg-number is closest to the starting mix Mg-number of 71.2

Microprobe analyses of both natural rocks and experimental products were made with a JEOL JXA-50A microprobe with EDAX attachment calibrated on pure Cu.

2.4 EXPERIMENTAL RESULTS

The experiments formed two groups: the composition noted in table 7 (with 0.045 wt% Cr_2O_3) was used for series I, whereas additional Cr_2O_3 to a total of 0.20wt% was added for series II in order to bring spinel group minerals to the liquidus in quantity and grain size sufficient for analysis.

2.4.1 SERIES I:

Results for series I experiments are listed in table 8 and summarised graphically in figure 17. Series I experiments were run for 2.5 hours at near-liquidus temperatures, and for 4-4.5 hours at lower temperatures to allow growth of larger crystals. Crystals were abundant

TABLE 8

Experimental data for Series I runs (0.045wt% Cr_2O_3).
OL = olivine; LC = leucite; CPX - clinopyroxene; SP = chrome spinel.
Figures in brackets are wt% Fe_2O_3 for leucite, and Mg# (total Fe) for glass.

Run#	Duration	Buffer	T°C	Run products
121	2.5	HM	1270	Glass [70.5]
119	2.5	HM	1260	OL + LC + Glass [69.7]
120	2.5	HM	1250	OL + LC [3.6] + Glass [68.7]
122C	4.0	HM	1200	OL + LC [3.8] + CPX + SP + Glass [66.6]
123C	4.5	HM	1150	OL + LC [3.6] + CPX + SP + Glass
117B	2.5	MnH	1270	Glass [71.6]
118B	2.5	MnH	1260	OL + LC [3.6] + Glass [69.8]
116B	2.5	MnH	1250	OL + LC [3.2] + Glass [71.3]
122B	4.0	MnH	1200	OL + LC [3.4] + CPX + SP + Glass [67.5]
123B	4.5	MnH	1150	OL + LC [2.9] + CPX + SP + Glass [66.1]
117A	2.5	NNO	1270	Glass [83.9]
118A	2.5	NNO	1260	OL + Glass [79.8]
116A	2.5	NNO	1250	OL + LC + Glass [75.1]
122A	4.0	NNO	1200	OL + LC [2.1] + CPX + Glass [75.9]
123A	4.5	NNO	1150	OL + LC [1.5] + CPX + SP + Glass [68.4]
137	2.5	MW	1250	OL + Glass [61.3]
140	2.5	MW	1230	OL + LC [0.9] + Glass [65.2]

TABLE 9

Experimental data for Series II runs (0.2wt% Cr_2O_3).
Abbreviations as for table 8 except figures in brackets are 100Mg/(Mg+Fe) where Fe = Fe^{2+} for olivine and Fe = total Fe as Fe^{2+} for glass.

Run#	Duration	Buffer	T°C	Run products
131C	5	HM	1280	SP + Glass [71.7]
128B	5	HM	1270	SP + Glass [70.7]
127B	5	HM	1260	SP + OL [98.5] + Glass [71.8]
126C	5	HM	1250	SP + OL [97.7] + LC + Glass [71.5]
131B	5	MnH	1280	SP + Glass [72.4]
128A	5	MnH	1270	SP + Glass [73.1]
127A	5	MnH	1260	SP + OL [97.7] + LC + Glass [71.7]
126B	5	MnH	1250	SP + OL [96.1] + LC + Glass [71.8]
131A	5	NNO	1280	SP + Glass [81.3]
141B	5	NNO	1270	SP + Glass [83.5]
129	5	NNO	1260	SP + OL [95.7] + LC + Glass [80.6]
126A	5	NNO	1250	SP + OL [92.7] + LC + Glass [71.5]
141A	5	MW	1270	SP + Glass [70.9]
134	5	MW	1260	SP + OL [90.2] + Glass [68.4]
135	5	MW	1250	SP + OL [87.8] + Glass [63.6]

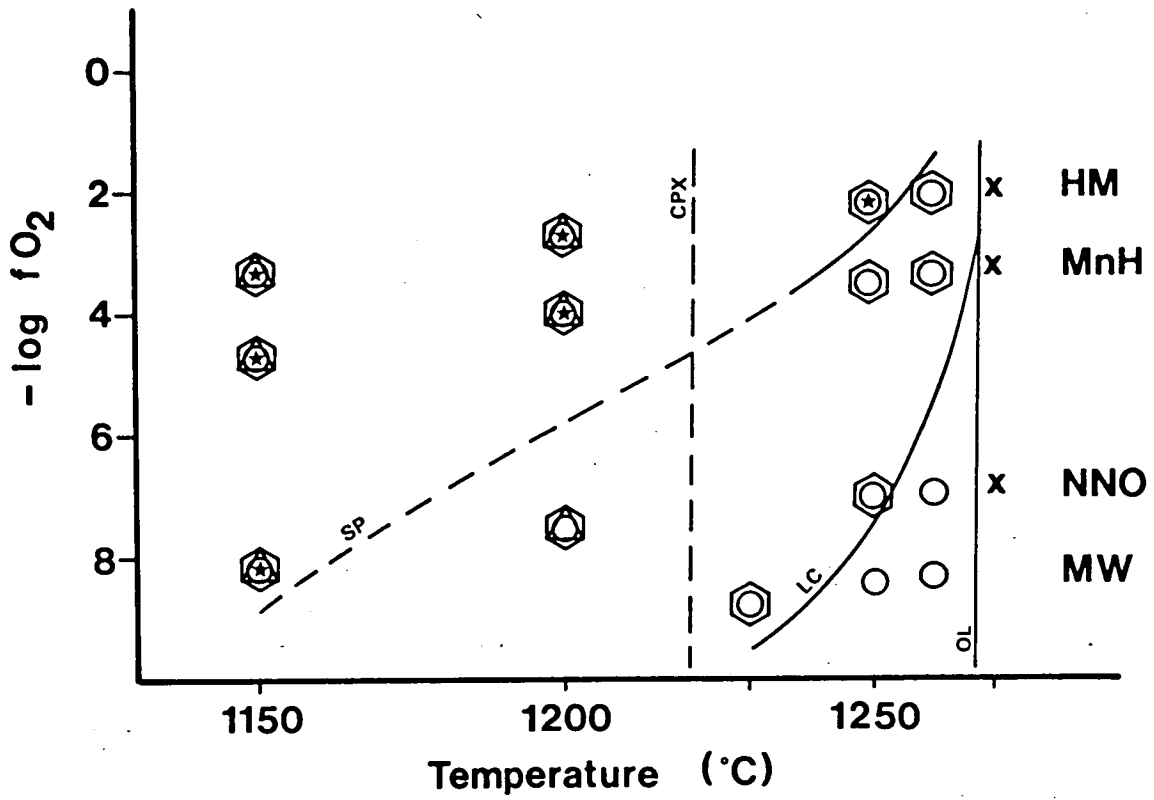

Figure 17

Summary of results from Series I experiments [Cr_2O_3 = 0.045 wt%]

- ○ = olivine
- ⬡ = leucite
- △ = clinopyroxene
- ★ = spinel
- × = liquid only

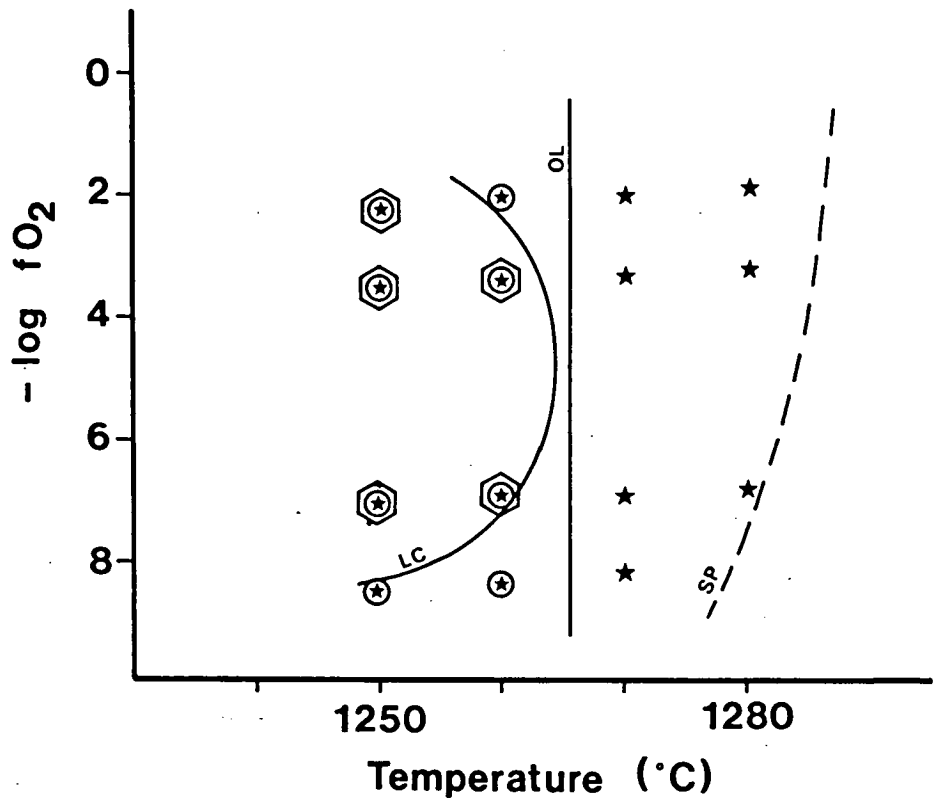

Figure 18

Summary of results from Series II experiments [Cr_2O_3 = 0.2 wt%]
Symbols as in figure 17.

but small, so that in many cases mineral+glass overlap analyses were taken from which an average glass composition was subtracted to obtain the mineral analysis.

Olivine is a liquidus phase at all oxygen fugacities studied, and varied in composition from Fo_{98} at HM to Fo_{89} at MW. Results were variable at NNO and MW due to differing amounts of iron loss/gain to/from the capsules. The range of Fo in olivines given above is from runs in which iron exchange was minimal. At the higher oxygen fugacities leucite stability is enhanced and leucite contains a greater amount of ferric iron. Ferric iron contents of leucites were obtained graphically from leucite+glass overlap analyses so that some of the microprobe precision is lost. The range in Fe_2O_3 contents from 0.9 wt% at MW to 3.6 wt% at HM is nevertheless realistic in comparison with natural leucites, and Fe_2O_3 values are consistent among runs at a given oxygen buffer (table 8).

Clinopyroxene did not crystallise within 50°C of the liquidus in these experiments but coprecipitates with olivine and leucite below ~1220°C. In the natural rock, somewhat ambiguous petrographic criteria indicate that a significant proportion of the clinopyroxene crystallised before much of the leucite. By analogy with Barton and Hamilton's [1978] experiments on orendite (similar to Gaussberg olivine leucitite), clinopyroxene is expected to crystallise before leucite at depths as little as 1km.

The appearance of spinels is strongly dependent on oxygen fugacity (figure 16) and spinels did not occur at the liquidus in any series I run. This contrasts with the natural rock where spinel occurs as inclusions in olivine phenocrysts. Very small spinels occurred only in runs with a high degree of crystallisation, precluding satisfactory analyses.

2.4.2 SERIES II:

For series II runs, Cr_2O_3 was added as it has been shown previously to stabilise spinels to higher temperatures [Hill and Roeder 1974]. Only near-liquidus temperature runs were repeated to enable spinel compositions to be compared with those naturally occurring as inclusions in olivine. Results from series II experiments are listed in table 9 and summarised in figure 18. Series II experiments were run for 5 hours to enable better mineral analyses to be obtained. Spinel occurs alone as the liquidus phase

at all oxygen fugacities studied. The liquidus temperature was not determined precisely, but few grains were present in the 1280°C runs (especially at NNO) indicating that the liquidus probably lies at around 1290°C.

The olivine out curve remains unaffected by the extra Cr_2O_3, and the change in the leucite-out curve is insignificant. Clinopyroxene did not appear at the temperatures studied. Olivine and glass Mg-numbers are given in table 9. Each glass analysis quoted is the average of a minimum of six microprobe area scans.

Leucite crystals frequently occur in aggregates and, in series II runs, also commonly contain Cr-free aluminous spinel inclusions. These aluminous spinels occur regardless of oxygen fugacity. Similar Cr-free Al-spinels in natural leucites are known from lamproites in the West Kimberley region. These spinels are described in more detail by Jaques and Foley [Appendix 4], who attribute their formation to exsolution following incorporation of Mg and Fe into leucite by a Tschermak substitution. Their appearance in series II runs only is interpreted to be a kinetic effect: Mg- and Fe-bearing leucites have had time to exsolve spinels given the longer run times of series II experiments [Jaques and Foley, Appendix 4]. The extremely large partition coefficient for Cr between spinel and liquid precludes crystallisation of Cr-free spinels from the melt.

Leucite compositions for series II are not listed because they are anomalously high in Mg and Al due to overlaps with the spinels contained within them.

Chrome-spinels occur as numerous but generally small crystals, especially at lower oxygen fugacities. Their colour varies from greenish brown at MW, through orange to deep red at HM. A single spinel analysis for each experiment (table 10) was obtained by linear regression of each oxide against silica for numerous spinel-glass overlap analyses of varying sizes. Ferric values were calculated assuming stoichiometry, and then other ratios involving iron were calculated from these.

The spinels are comparable to natural spinels from ultrapotassic rocks in high Cr and Fe^{3+} and low Al contents. Increasing oxygen fugacity causes an increase in the ferric values of the spinels and an increasing

TABLE 10

Analyses of synthetic spinels. Analyses produced by subtraction of glass analysis from spinel+glass overlap microprobe analyses.

Buffer	HM	HM	HM	HM	MnH	MnH	MnH	MnH	NNO	NNO	NNO	NNO	MW	MW	MW
T°C	1280	1270	1260	1250	1280	1270	1260	1250	1280	1270	1260	1250	1270	1260	1250
TiO2	2.0	2.5	2.3	2.2	2.3	1.9	2.2	2.5	2.9	2.3	2.8	2.7	3.0	3.5	3.7
Al2O3	5.1	6.0	5.8	4.3	5.5	4.6	3.5	3.9	6.2	5.6	5.3	4.0	5.3	5.3	4.9
Cr2O3	45.1	39.2	36.5	44.9	47.7	49.5	51.7	50.8	60.9	62.8	61.4	59.7	61.2	60.0	60.3
FeO	27.0	31.2	31.8	26.3	24.2	23.9	22.3	23.9	12.2	9.5	11.9	17.3	15.4	16.1	18.9
MgO	21.4	20.7	22.5	20.7	19.4	20.4	20.5	18.8	17.8	19.6	18.6	16.7	15.4	14.3	12.6
Total	100.7	99.5	98.8	98.4	98.8	100.2	100.2	99.8	100.0	99.7	100.0	100.4	100.3	99.3	100.5
Cations															
Ti	0.047	0.058	0.052	0.053	0.054	0.045	0.052	0.058	0.069	0.053	0.067	0.066	0.073	0.087	0.093
Al	0.184	0.218	0.211	0.159	0.203	0.168	0.127	0.146	0.232	0.208	0.198	0.150	0.202	0.207	0.191
Cr	1.096	0.960	0.887	1.120	1.192	1.219	1.280	1.274	1.531	1.565	1.540	1.519	1.565	1.561	1.574
Fe3+	0.627	0.706	0.798	0.614	0.498	0.524	0.489	0.463	0.099	0.120	0.128	0.199	0.086	0.058	0.050
Fe2+	0.068	0.101	0.021	0.078	0.141	0.098	0.095	0.170	0.226	0.131	0.187	0.265	0.330	0.384	0.471
Mg	0.979	0.957	1.031	0.975	0.913	0.946	0.957	0.889	0.844	0.922	0.880	0.801	0.743	0.703	0.621
Mg	93.5	90.5	98.0	92.6	86.6	90.6	91.0	84.0	78.9	87.6	82.5	75.1	69.2	64.6	56.9
Cr	85.6	81.5	80.8	87.5	65.4	87.9	91.0	89.7	86.8	88.3	88.6	91.0	88.6	88.3	89.2
Ferric	90.2	87.5	97.5	88.7	78.0	84.2	83.8	73.2	30.4	47.8	40.7	42.9	20.8	13.1	9.6

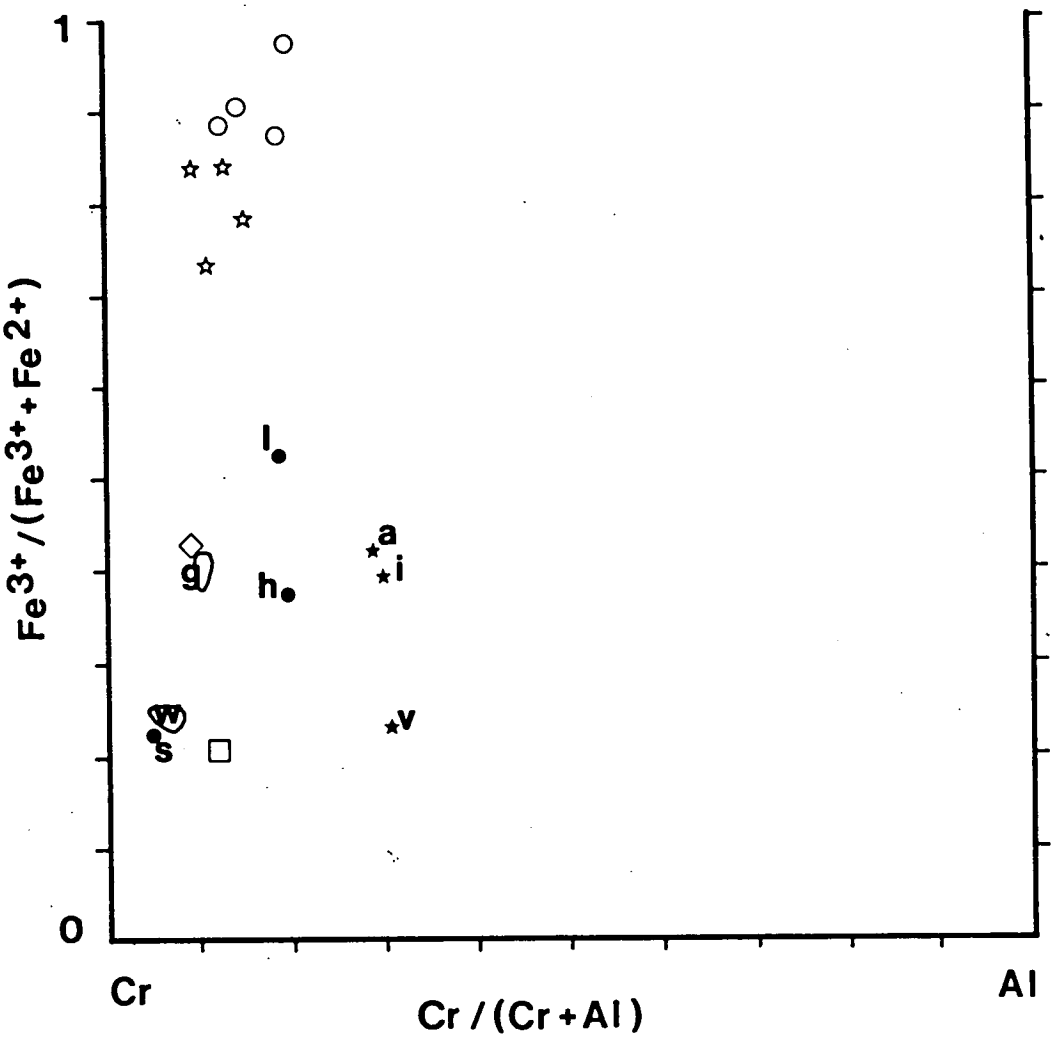

Figure 19

Ferric value vs. Cr/(Cr+Al) plot for synthetic and natural spinels. Bold type are natural spinels from lamproites (●) and group II and III ultrapotassic rocks (★). l = Leucite Hills [Kuehner et al. 1981]; g = Gaussberg (this study); h = Holsteinsborg, West Greenland [Scott 1981]; s = Spanish fortunites [A.J.Crawford, unpublished data]; i = Indonesia [Whitford 1975]; a = western rift valley of Africa [Edgar and Arima 1981]; v = San Venanzo, Italy [Gallo et al. 1984]; w = West Kimberley (this study)

magnesioferrite component. No significant change in $Al/(Al+Cr+Fe^{3+})$ ratio is seen; the trivalent substitution is $Cr = Fe^{3+}$. Titanium shows little change in the fO_2 range studied except for a slight increase at the MW buffer. At buffers (NNO and MW) where there is a spread of Mg-number due to iron loss or gain, analyses of glass and neighbouring phases were selected which show the least change in Mg-number from starting mix compositions.

These selected analyses are plotted in figure 19 along with all data for HM and MnH. Natural spinels from lamproites, mostly occurring as inclusions in olivine phenocrysts, are also plotted in figure 19.

Relative to the natural spinels from Gaussberg, the experimental spinels are richer in Cr and Mg, and poorer in total Fe. This discrepancy is attributed to the addition of Cr_2O_3 in excess of that of the primitive Gaussberg melt. The single element partition between spinel and liquid (D(sp-lq)) for Cr is much larger than D(sp-lq) for Fe^{3+}, so that the series II experimental studies contain less Fe^{3+} than they would in a less Cr-rich melt. Mg contents of the spinels are therefore correspondingly higher due to the fO_2 control of the Fe^{3+}/Fe^{2+} ratio.

The original Cr_2O_3 content of the Gaussberg olivine leucitite can be estimated as approximately 0.08-0.10 wt%. This estimate is made assuming a similar form of relationship in Cr_2O_3(sp) vs. Cr_2O_3(lq) to that indicated by the data of Maurel and Maurel [1982a] for olivine tholeiites.

The experimental data demonstrates that Fe is a sensitive indicator of fO_2 at crystallisation of the lamproite liquidus phases spinel, leucite and olivine. Comparison of natural and experimental spinels (figure 19) indicates that natural lamproite spinels began to crystallise at fO_2 ranging from values in excess of the NNO buffer to values as low as the MW buffer.

2.5 COMPARISON OF SPINELS BETWEEN BASALTIC AND ULTRAPOTASSIC ROCKS.

The compositional behaviour of spinel in these ultrapotassic melts has some significant differences from that in the more commonly studied basaltic compositions. Experimental spinel-liquid K_Ds indicate a preferential partitioning of Fe^{3+} relative to Al into the spinel, and a

high Fe^{3+}/Fe^{2+} ratio in the spinel. Spinel compositions in natural ultrapotassic rocks are all notably poor in alumina. Groundmass spinels may contain greater amounts of Ti and Fe, but never plot far from the $(MgFe)Cr_2O_4$-$(MgFe)Fe_2O_4$ face of the spinel prism. The most Al-rich Cr spinels from West Kimberley lamproites (titaniferous, magnesian aluminous chromites; Jaques et al. 1984a, p.241) have Cr/(Cr+Al) > 0.8. In contrast, basaltic spinels are usually Al-rich and relatively poor in ferric iron, and so are restricted to near the $(MgFe)Cr_2O_4$-$(MgFe)Al_2O_4$ base of the spinel prism [Haggerty 1976].

Maurel and Maurel [1982a,b,c] experimentally studied spinel compositions in tholeiites at 1 atm. They formulated the relationship

$$(Al_2O_3)_{sp} = 0.035\ (Al_2O_3)^{2.42} \qquad [1]$$

[Maurel and Maurel 1982b] from their own data and that of Fisk and Bence [1980]. This is plotted in figure 20 where it is compared to the experimental data for the Gaussberg study (series II). It can be seen that the partition coefficient D(sp-lq) for Al_2O_3 is significantly lower for the ultrapotassic composition. This is not due to the excess Cr_2O_3 added for the series II runs, since the composition used by Maurel and Maurel [1982b] contained 0.25 wt% Cr_2O_3.

The low alumina is a manifestation of the alkali-ferric iron effect [Carmichael and Nicholls 1967] whereby addition of K_2O to a silicate melt causes an increase in the Fe^{3+}/Fe^{2+} ratio of the liquid. This is thought to be due to the charge balancing of tetrahedral Fe^{3+} by K, which is accompanied by depolymerisation of the silicate network [Virgo et al. 1981; Dickenson and Hess 1981; Mysen et al. 1981, 1982]. Spinels crystallising in ultrapotassic liquids will have higher Fe^{3+}/Fe^{2+} ratios than those in tholeiitic basalts [Maurel and Maurel 1982c, 1984] which, together with the high Cr content, results in lower Al contents. Maurel and Maurel [1983] recognised that higher ferric iron contents in the liquid would result in higher Fe^{3+}/Fe^{2+} and lower Al_2O_3 in spinels, but did not study the effect of alkalis. The alkali-ferric iron effect is seen in the empirical equations of Sack et al. [1980] and Kilinc et al. [1983] (see below, equation 2) as large regression constants for the alkali oxides in the bulk composition term. Because of this, the simplified expression of Maurel and Maurel [1984, equation 6] must be used with care

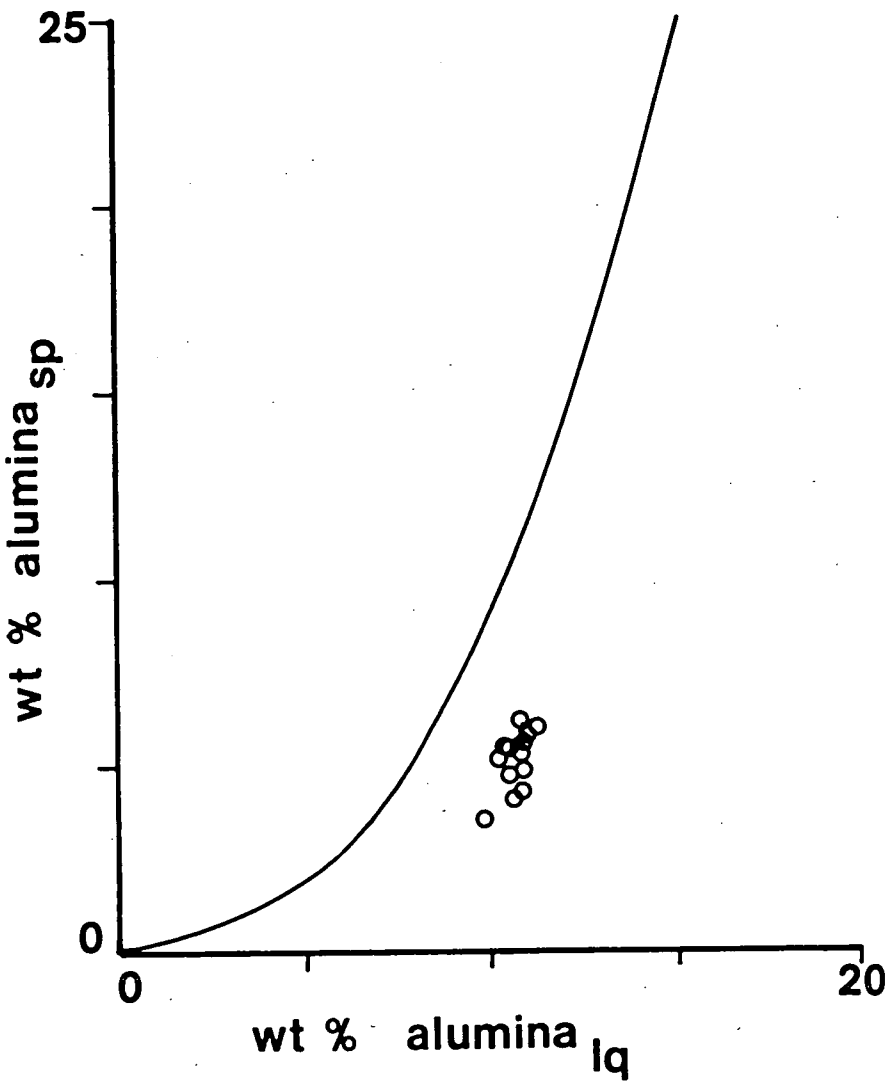

Figure 20

Comparison of synthetic spinels from this study (O) with the D^{Al2O3}_{sp-lq} variation described by Maurel and Maurel [1982b] for tholeiitic basalts.

for alkaline rocks, since it contains a bulk composition term (after Kilinc et al. 1983) which is generalised for non-alkaline rocks.

2.6 ELEMENT PARTITIONING

A number of mineral-liquid and mineral-mineral distribution coefficients were calculated from the experimental data, and these are listed in table 11. In order to calculate coefficients involving liquid, a ferric value for the liquid must be determined. There are currently two well documented empirically derived expressions relating the molar ratio Fe_2O_3/FeO of the liquid to oxygen fugacity and melt composition [Sack et al. 1980; Kilinc et al. 1983]. These use the same equation but with different regression constants, thus:

$$\ln (X^{Fe2O3}_{lq}/X^{FeO}_{lq}) = a \ln fO_2 + b/T + c + \Sigma d_i X_i \qquad [2]$$

where a,b and c are constants, d(i) are constants for individual oxide components in the melt, and X = mole fraction. The formulation by Kilinc et al. [1982] is slightly different and gives ferric values intermediate between these two for the Gaussberg composition. The ferric value predicted by these expressions for the Gaussberg composition are plotted in figure 21. A limited number of accurate (to within 4%) wet chemical determinations for FeO on 1 mg samples of run products are available, and these are also plotted in figure 21.

In calculation of distribution coefficients involving liquid, a combination of these methods was used as follows: Kilinc et al. [1983] for HM and MnH, Sack et al. [1980] for NNO and the wet chemical values for MW. The choice between values from the different equations was made because the former incorporated high oxygen fugacity experiments in their data base. Sack et al.'s [1980] was made from data restricted almost entirely to around the FMQ buffer, which is intermediate in fO_2 between the NNO and MW buffers. The wet chemical analysis was preferred for MW because it was determined on a run in which the final Fe content was very similar to that in the starting composition, indicating that the Fe-doping procedure had worked best in this run.

The wet chemical values for NNO were not used because the runs analysed had lost iron. These results show the effects of modification of

TABLE 11
Mineral-mineral and mineral-liquid distribution coefficients calculated from the experimental data.

Distribution coefficient	Value	Regression coefficient	Number of points
$K_D^{Fe2+-Mg}_{ol-lq}$	0.26	0.991	8
$K_D^{Fe2+-Mg}_{sp-ol}$	4.697	0.986	5
$K_D^{Al-Fe3+}_{sp-lq}$	0.125	0.989	10
$K_D^{Fe2+-Mg}_{sp-lq}$	1.184	0.962	10
$K_D^{Fe2+-Fe3+}_{sp-lq}$	0.643	0.998	10

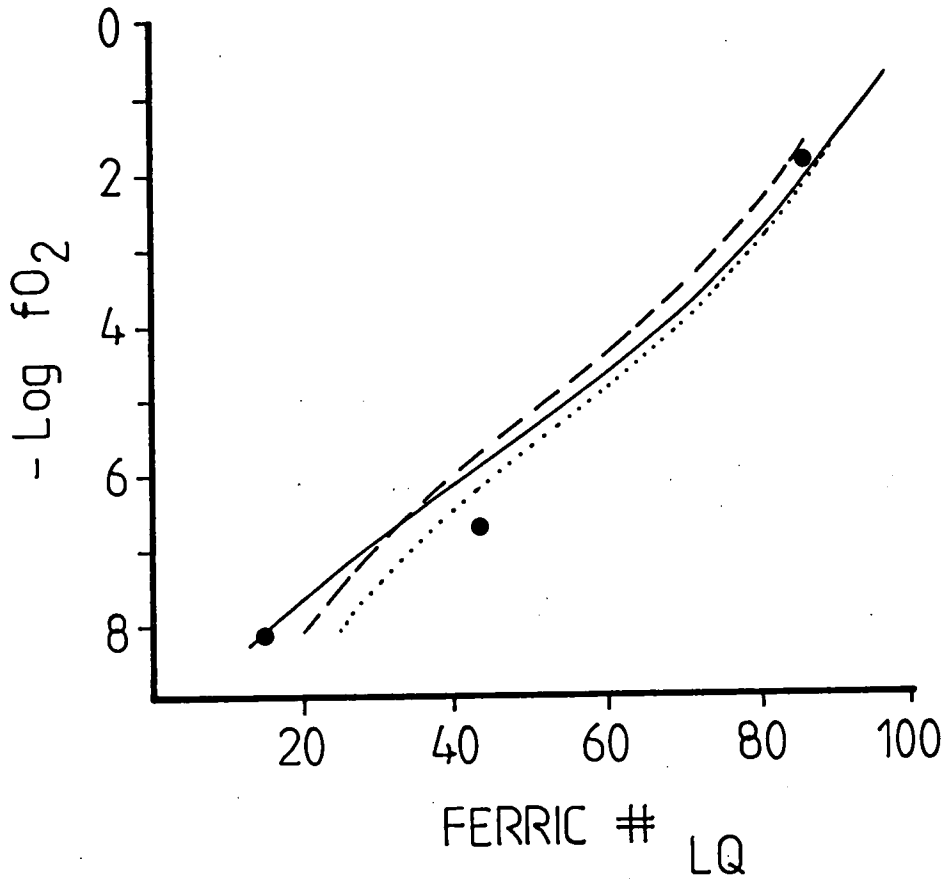

Figure 21

Comparison of liquid ferric values predicted by the equations of Sack et al. [1980] (----) and Kilinc et al. [1983] (....) to measured wet chemical values for run products (●). Solid curve shows values used in calculation of K_Ds.

the external buffer by the capsule/melt reaction

$$2\ FeO + 2\ Pt = 2\ FePt + O_2 \qquad [3]$$

Underdoping, i.e.loss of iron to the capsule, forces the equilibrium to the right and results in a higher fO_2 and higher ferric value. The HM wet chemical analysis supports the use of the Kilinc et al. values for the higher fO_2 buffers.

Despite the uncertainties discussed above concerning ferric value of the liquid, the resulting K_Ds have good correlation coefficients and are internally consistent: the $K_D^{Fe2+-Mg}_{sp-lq}$ with lowest r can be calculated independently by

$$K_D^{Fe2+-Mg}_{sp-lq} = K_D^{Fe2+-Mg}_{ol-lq} \cdot K_D^{Fe2+-Mg}_{sp-ol} = 1.221 \qquad [4]$$

which compares favourably with the value of 1.184 obtained by linear regression of the spinel + liquid compositional data.

The $K_D^{Fe2+-Mg}_{ol-lq}$ value of 0.26 is at the lower end of the range 0.25-0.38 found from experimental studies of varying composition [Ford et al. 1983]. Comparable values are found between olivines and Ti-rich lunar basaltic liquids [Longhi et al. 1978; Green et al. 1975]. The difference between 0.26 and the more typical basaltic K_D of 0.30 [Roeder and Emslie 1970] is considered to be real. It is too large to be explained by errors in measurement of the low levels of FeO, and is unlikely to be caused by a systematic underestimation of liquid ferric value by the Sack-Kilinc equations, because the wet chemical determination used for MW gives a lower ferric value than the calculated value. The high K_2O contents of the melt would be expected to promote crystallisation of olivine because of its depolymerising effect [Kushiro 1975; Fraser 1977], but the reason for crystallisation of a more forsteritic olivine in these conditions is uncertain.

$K_D^{Al-Fe3+}_{lc-lq}$ is estimated at 2.8, based on series I data. Series II leucites could not be used because of Al-spinel inclusions. A regression was not performed because of the scarcity of data.

2.7 APPLICATION TO ULTRAPOTASSIC ROCKS

Mineral compositions from these experiments clearly indicate that the Gaussberg olivine leucitite crystallised at oxygen fugacities less than 0.5 log units below that of the NNO buffer. Compositions of natural spinels (ferric value), leucite (Fe_2O_3 content) and olivine (Mg-number) compare well with values interpolated from experimental data. The agreement of all these values suggests that re-equilibration of spinels included in olivine as suggested by Thy [1983] has not occurred.

The expression of Sack et al. [1980] noted above (equation 2) can be rearranged to give an estimate of the intrinsic oxygen fugacity. Using the whole-rock chemical data for Fe_2O_3 and FeO, which is considered to be realistic in view of the extremely fresh glassy nature of the Gaussberg lava, log fO_2 is calculated at -6.7 at 1280°C; this is virtually identical to the NNO buffer (-6.65 from the equation of Schwab and Küstner 1981). This agreement emphasises the value of spinel, olivine and leucite as calibrated by the experimental data for estimates of oxygen fugacity. The use of Sack et al.'s [1980] equation for estimating fO_2 must be limited to exceptionally fresh rocks: application to a West Kimberley olivine leucitite gave an fO_2 4 log units higher than that deduced from the spinel ferric value data.

The experimental data for spinel ferric value (figure 19) indicate a wide range of fO_2s for lamproitic magmas. The high fO_2 indicated for the Leucite Hills spinel is supported by the occurrence of leucites containing in excess of 2wt% Fe_2O_3 [table 5; Kuehner et al. 1981]. Carmichael and Nicholls [1967] estimated that madupite crystallised at an fO_2 well above the NNO buffer by using forsterite + enstatite as a thermodynamic proxy for phlogopite. Their conclusion is supported by the present data. The Spanish and West Kimberley spinels have ferric values close to those of experiments at the MW buffer. The Spanish analysis is from an inclusion in an olivine phenocryst in a fortunite. The fortunites are the most primitive of the Spanish lamproites and carry lherzolite xenoliths [Venturelli et al. 1984b]. Spinels from other Spanish lamproite types have lower Mg-number and higher ferric values.

Chrome spinels are preserved in the Gaussberg olivine leucitite only

as inclusions in olivine. Whilst some fractionation of spinels is indicated by the neccessity of chrome addition to stabilise spinels at the liquidus, it is considered likely that a reaction between spinel and melt to produce Cr-bearing clinopyroxene, as described by Hill and Roeder [1974], has operated at Gaussberg: any spinels not armoured by olivine are thus considered to have reacted out.

Application of the experimental results to ultrapotassic rock groups II and III may be limited because of some significant compositional differences. The spinels from these rocks contain greater amounts of Al_2O_3 (figure 19) reflecting the higher alumina content of these rocks relative to lamproites. The calibration for Fe_2O_3 content of leucites must be restricted in use to rocks with low alumina because Fe^{3+} incorporation in leucite is a function of Fe^{3+} and Al content of the melt. The characteristically high Fe_2O_3 content of leucites from lamproites [Barton 1979] is as much a function of the low Al_2O_3 of lamproites as an oxidation effect. The low Mg-number of group III rocks may hinder application of the crystal-liquid K_Ds because of the uncertainty about the degree of crystallisation which has occurred. Cr-rich spinels are only rarely present in group II and III rocks.

The Gaussberg rocks contain large early-crystallised leucites with low Fe_2O_3 contents which are rimmed by leucites with the higher Fe_2O_3 typical of leucites in the rest of the rock (table 5). Application of the experimental calibration suggests that the low Fe_2O_3 cores crystallised at fO_2 below the MW buffer, and that the Gaussberg lava has oxidised during emplacement.

Variations in oxygen fugacity with depth will have an important bearing on the presence or absence of diamonds. If the diamonds in West Kimberley lamproites have a magmatic origin then diamond-bearing lamproite magmas must be reduced at depth. The oxidation state as measured by liquidus spinel ferric values may therefore indicate whether or not diamonds, if present at depth, are likely to have survived. The effect of pressure on spinel composition is uncertain: the low ferric values given by West Kimberley and Spanish lamproite spinels may be partly due to crystallisation at greater depth than spinels in other lamproites. Nevertheless, the spinels from the diamondiferous West Kimberley region give amongst the lowest fO_2 readings of all lamproites considered on the

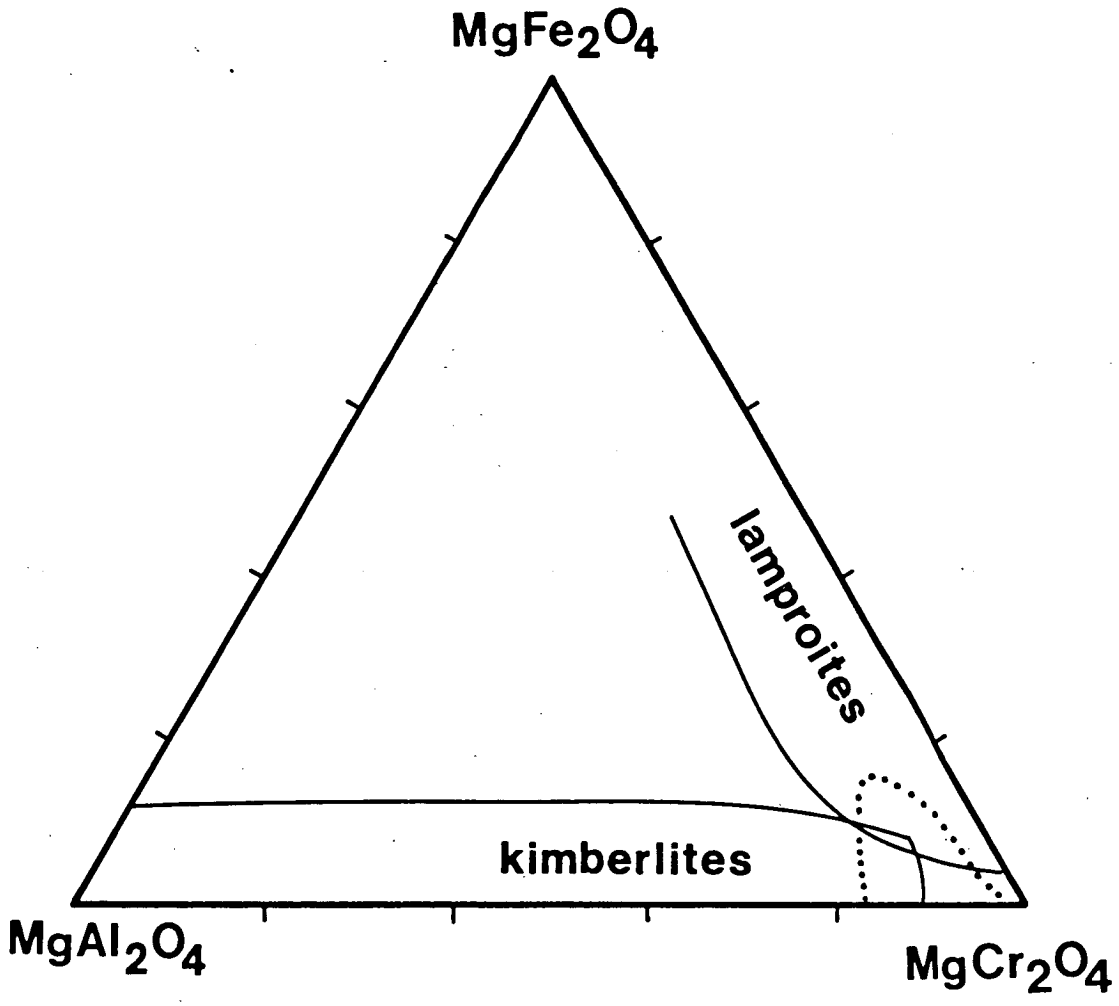

Figure 22

Natural lamproite spinel compositions compared to kimberlite spinels and spinels occurring within diamonds. Lamproite spinel field is from liquidus minerals as in figure 19 and table 6. Kimberlite spinel data from Sobolev [1977], Haggerty [1976] and Mitchell & Clarke [1976]. Data for spinels included in, or intergrown with diamonds (.....) from Meyer & Boyd [1972], Prinz et al. [1975], Tsai et al. [1979] and Sobolev [1977].

experimental calibration. In the West Kimberley area, diamonds are restricted to olivine-rich lamproites with high Cr_2O_3 contents [Atkinson et al. 1984; Jaques et al. 1984a].

Spinel inclusions in diamond [Meyer and Boyd 1972; Tsai et al. 1979; Prinz et al. 1975; Sobolev 1977] are chrome-rich, alumina- and ferric iron-poor, and plot close to the $MgCr_2O_4$-$FeCr_2O_4$ edge of the spinel prism (figure 22). The most oxidised of these inclusions, including a spinel-diamond intergrowth believed to indicate coprecipitation [Sobolev 1977, p.134], have ferric values comparable with the most Cr-rich and reduced of the West Kimberley and Spanish lamproites. The range of spinel compositions in the lamproite group as a whole approaches that of spinel inclusions in diamond chiefly by variation in ferric value, or down the front face of the spinel prism. Kimberlitic spinels, on the other hand, approach the range of diamond inclusions by variation in Cr/(Cr+Al), or along the base of the spinel prism [Haggerty 1976,1979].

It thus appears that the Fe^{3+} content of spinel may be a useful "diamond survival indicator" for application to lamproitic rocks. If diamonds existed at depth in lamproites which are now highly oxidised, they would be unlikely to survive the oxidation.

2.8 SUMMARY

Atmospheric pressure liquidus experiments were conducted on the Gaussberg olivine leucitite composition to study the effects of oxygen fugacity on phase compositions. Results show that olivine is the liquidus phase followed by leucite and clinopyroxene. Addition of Cr_2O_3 was required to crystallise chrome spinel at the liquidus, implying that fractionation of chrome spinel has occurred in the natural rock, causing some Cr-depletion. The added Cr_2O_3 did not affect the stability of other phases. Runs with extra Cr_2O_3 produced Cr- and Fe^{3+}-rich spinels which are comparable with natural examples once allowance is made for the excess Cr_2O_3. The ferric value of spinels is a good indicator of oxygen fugacity at the time of crystallisation.

Experimental data for spinels, olivine and leucite show conclusively that the bulk of the Gaussberg olivine leucitite phenocrysts began to crystallise at oxygen fugacities just below those of the NNO buffer. This

is in excellent agreement with an estimate from the empirical expression derived by Sack et al. [1980] based on the Fe_2O_3/FeO contents of the fresh, quenched glass. However, an earlier stage of crystallisation at lower fO_2 (below MW) is recorded by rare cores to leucite crystals with very low Fe_2O_3 contents. Other lamproites range in fO_2 at crystallisation from well above NNO down to MW. The more reduced examples include the West Kimberley leucite lamproites, and their spinels are similar to the most oxidised of spinel inclusions found in diamonds. Oxidation during emplacement, possibly by H_2-loss from the magma [Sato 1978], may be common in lamproitic magmas, and the ferric value of spinels may indicate whether or not any diamonds are likely to have survived the oxidation.

The range of lamproitic spinels approahes that of spinel inclusions in diamonds largely by variation in $(Fe^{3+}/(Fe^{3+}+Fe^{2+}))$, whereas kimberlitic spinels approach the field of spinel inclusions in diamond by variation in Cr/(Cr+Al).

A number of mineral-liquid and mineral-mineral distribution coefficients have been empirically derived from the experimental data. These may be an aid to estimating the conditions of origin of other ultrapotassic rocks.

PART III

THE EFFECT OF FLUORINE ON PHASE RELATIONSHIPS IN THE SYSTEM KAlSiO4 - Mg2SiO4 - SiO2 AT 28 KBAR AND THE SOLUTION MECHANISM OF FLUORINE IN SILICATE MELTS

3.1 INTRODUCTION

Fluorine has long been recognised as an important constituent of late-stage granitic melt-fluid systems where, along with other anionic elements, it exerts control on the distribution of economically important metals such as Sn. Experimental studies of the effect of HF on silicate melt equilibria have been restricted to silica-rich melts, where a large depression of the liquidus temperature and expansion of the quartz liquidus phase volume relative to feldspar has been found [Wyllie and Tuttle 1961; Manning et al. 1980].

The role of fluorine in basic melts has been neglected because of the generally low content of fluorine in common basaltic rocks; typically less than 500ppm [Aoki et al. 1981; Schilling et al. 1980]. However, fluorine is abundant in potassium-rich mafic rocks such as lamproites, and shows a positive correlation with potassium content [Aoki et al. 1981]. The probable importance of fluorine in lamproite petrogenesis has been emphasised recently by Jaques et al. [1984a], who predicted increased stability for fluormica over hydroxymica.

The system kalsilite-forsterite-quartz [Ks-Fo-Qz] was chosen for experimental studies of the fluorine effect on silicate melts because it is the potassic analogue of the base of the basalt tetrahedron of Yoder and Tilley [1962], and is thus relevant for ultrapotassic rocks. This paper reports experimental results and an investigation of the solution mechanism of fluorine in silicate melts: the implications for ultrapotassic rock genesis are discussed in a companion paper [Part 4].

Experiments were run at 28kbar to enable direct comparison with the studies of Gupta and Green [in prep.] on the system Ks-Fo-Qz in volatile-free conditions and with H_2O and CO_2. The rationale behind this choice is compatibility with the earlier studies in the system nepheline-forsterite-

quartz [Gupta, Green and Taylor 1986; Windom and Boettcher 1981]. The pressure of 28kb is taken to represent the approximate pressure at the top of the low velocity zone defined by the high pressure stability limit of pargasitic amphibole [Green and Liebermann 1976]. However, there are indications that in the presence of fluorine, the stability limit of pargasite will be expanded to higher temperatures and pressures [Holloway and Ford 1975].

3.2 EXPERIMENTAL METHODS

Experiments were run in solid media piston-cylinder apparatus with 0.5 inch furnace assemblies with talc/pyrex sleeves. A 10% pressure correction was used and pressures are accurate to within 0.5kbar. Temperatures were measured with a $Pt/Pt_{90}Rh_{10}$ thermocouple within 0.5mm above the sample capsule and are accurate to approximately $\pm 10^{o}C$. No correction was made for the effect of pressure on emf of the thermocouple.

Starting materials were synthetic kalsilite, Al_2O_3, MgO, SiO_2 and MgF_2. Kalsilite was prepared by sintering a mixture of K_2CO_3, Al_2O_3 and SiO_2 at $750^{o}C$ for 10 hours after slowly increasing the temperature from $500^{o}C$ over two days to minimise loss of K_2O. MgF_2 was prepared by heating analytical reagent grade MgO in an excess of 50% HF and evaporating to dryness. The MgF_2 was then heated at $450^{o}C$ for several hours to eliminate all traces of H_2O. Both kalsilite and MgF_2 were checked for purity by X ray diffraction. All starting materials were stored in a desiccator and dried thoroughly before use.

Fluorine was added as MgF_2 by direct substitution for MgO, i.e. by the exchange vector F_2O_{-1}. Most experiments were conducted with 4% F_2O_{-1}, meaning that 4 atom% of the oxygen in the starting composition was replaced by fluorine. This is approximately equal to 4 wt% F for the compositions used.

Minerals from Ks-Fo-Qz-F were analysed with a JEOL JXA 50A electron microprobe with integrated wavelength (F and Cl) and energy dispersive (all other elements) systems with operating conditions of 15kV and 5×10^{-8} A. F and Cl were calibrated on synthetic MgF_2 and natural scapolite standards respectively. The Ks-Fo-Qz-H_2O analyses were made at routine EDAX operating conditions (15kV, 7×10^{-10} A). Volatilisation of alkalis from fluormicas

at the higher current was checked by reanalysing at 7 x 10^{-10} A, and found to be minimal. Detection limits were approximately 0.20 wt % for fluorine and 0.04 wt % for chlorine.

3.3 RESULTS

3.3.1 PHASE RELATIONSHIPS:

Experimental results are listed in table 12. Phases encountered were forsterite, enstatite, phlogopite, kalsilite, sanidine and quartz, identified optically and by microprobe. Primary phlogopite was not difficult to identify: it occurred as large hexagonal plates (RI 1.54: Shell and Ivey 1969), usually with easily distinguishable thin feathery quench outgrowths. Quench crystals of phlogopite and enstatite occurred in the more Mg-rich compositions, but only phlogopite formed quench crystals from compositions outside its own primary phase field. Enstatite crystals occurred as stubby laths usually more elongate than olivines, although enstatite vs. olivine was always confirmed with the microprobe. Kalsilite, sanidine and quartz are reported only where confirmed by microprobe, since all these minerals formed lath-shaped crystals with refractive indices slightly greater than the glass. Residual MgF_2, easily recognised by its low RI (1.38), was found only in a premininary 1250°C run of short duration (composition 1 with 10%F_2O_{-1}; not listed in table 12). It was absent from all other runs, which are much closer to liquidus temperatures.

Figure 23 presents the results for 4%F_2O_{-1} projected onto the Ks-Fo-Qz face from the corresponding fluorine end-members $KAlSiF_8$-Mg_2SiF_8-SiF_4. It is thus a prismatic projection along the F_2O_{-1} exchange vector from a plane within the prism because of the addition of fluorine by direct substitution. It is not a saturation surface projected from the apex of a tetrahedron as in the H_2O and CO_2 systems, but the differences in projection angles are not large enabling reasonable comparisons to be made. Phase boundaries were located by optical estimates of relative abundances of phases present and, in more Mg-poor compositions, by probe analyses of glasses. Glass analyses could not be used in the Mg-rich compositions (1,2,3,4,7) due to modification by quench crystal formation.

In the dry system Ks-Fo-Qz at 28kbar MgO-rich liquids crystallise forsterite and enstatite and their compositions move towards a FO+EN+SAN+L

TABLE 12 : Experimental run data for Ks-Fo-Qz at 28kb pressure

Run No.	%F	Composition	Mix	Duration (mins)	Temp[°C]	Phases
1372	10	Ks44Fo39Qz17	1a	60	1350	Phl,L
1373	10	Ks44Fo39Qz17	1a	45	1450	Phl,L
1378	10	Ks44Fo39Qz17	1a	30	1480	Ol,Phl,2xL
1380	10	Ks44Fo39Qz17	1a	30	1510	Phl,2xL
1375	10	Ks44Fo39Qz17	1a	30	1550	L
1385	4	Ks44Fo39Qz17	1	30	1480	Ol,Phl,L
1387	4	Ks44Fo39Qz17	1	40	1500	Ol,Phl,L
1390	4	Ks44Fo39Qz17	1	25	1540	Ol,L
1391	4	Ks15Fo50Qz35	2	25	1540	En,L
1393	4	Ks15Fo50Qz35	2	40	1480	En,L
1395	4	Ks15Fo50Qz35	2	50	1430	En,Phl,L
1399	4	Ks33Fo45Qz22	3	45	1450	En,Phl,L
1400	4	Ks33Fo45Qz22	3	55	1480	En,Phl,Ol,L
1401	4	Ks33Fo45Qz22	3	50	1510	En,L
1404	4	Ks17Fo63Qz20	4	40	1530	En,Ol,L
1407	4	Ks17Fo63Qz20	4	30	1560	En,Ol,L
1408	4	Ks17Fo63Qz20	4	20	1590	En,L
1409	4	Ks50Fo15Qz35	5	45	1400	Phl,L
1412	4	Ks50Fo15Qz35	5	35	1450	Phl,L
1413	4	Ks50Fo15Qz35	5	30	1480	L
1419	4	Ks50Fo15Qz35	5	90	1340	Phl,San,L
1414	4	Ks78Fo15Qz7	6	40	1480	L
1417	4	Ks78Fo15Qz7	6	45	1420	Phl,Ks,L
1418	4	Ks78Fo15Qz7	6	60	1380	Phl,Ks,L
1421	4	Ks78Fo15Qz7	6	40	1450	Phl,L
1425	4	Ks42Fo25Qz33	7	40	1440	Phl,En,L
1427	4	Ks42Fo25Qz33	7	30	1470	Phl,En,L
1438	4	Ks48Fo8 Qz44	8	180	1300	Phl,L
1441	4	Ks48Fo8 Qz44	8	144	1340	Phl,L
1449	4	Ks48Fo8 Qz44	8	800	1240	Phl,San,L
1450	4	Ks48Fo8 Qz44	8	600	1270	Phl,L
1455	4	Ks39Fo18Qz43	9	200	1350	Phl,Qz,L
1457	4	Ks39Fo18Qz43	9	150	1410	Phl,L
1458	4	Ks39Fo18Qz43	9	60	1450	L
1459	4	Ks39Fo18Qz43	9	345	1290	Phl,Qz,L
1469	4	Ks36Fo10Qz54	10	200	1320	Phl,Qz,L
1473	4	Ks36Fo10Qz54	10	150	1380	Phl,Qz,L
1475	4	Ks36Fo10Qz54	10	180	1410	L

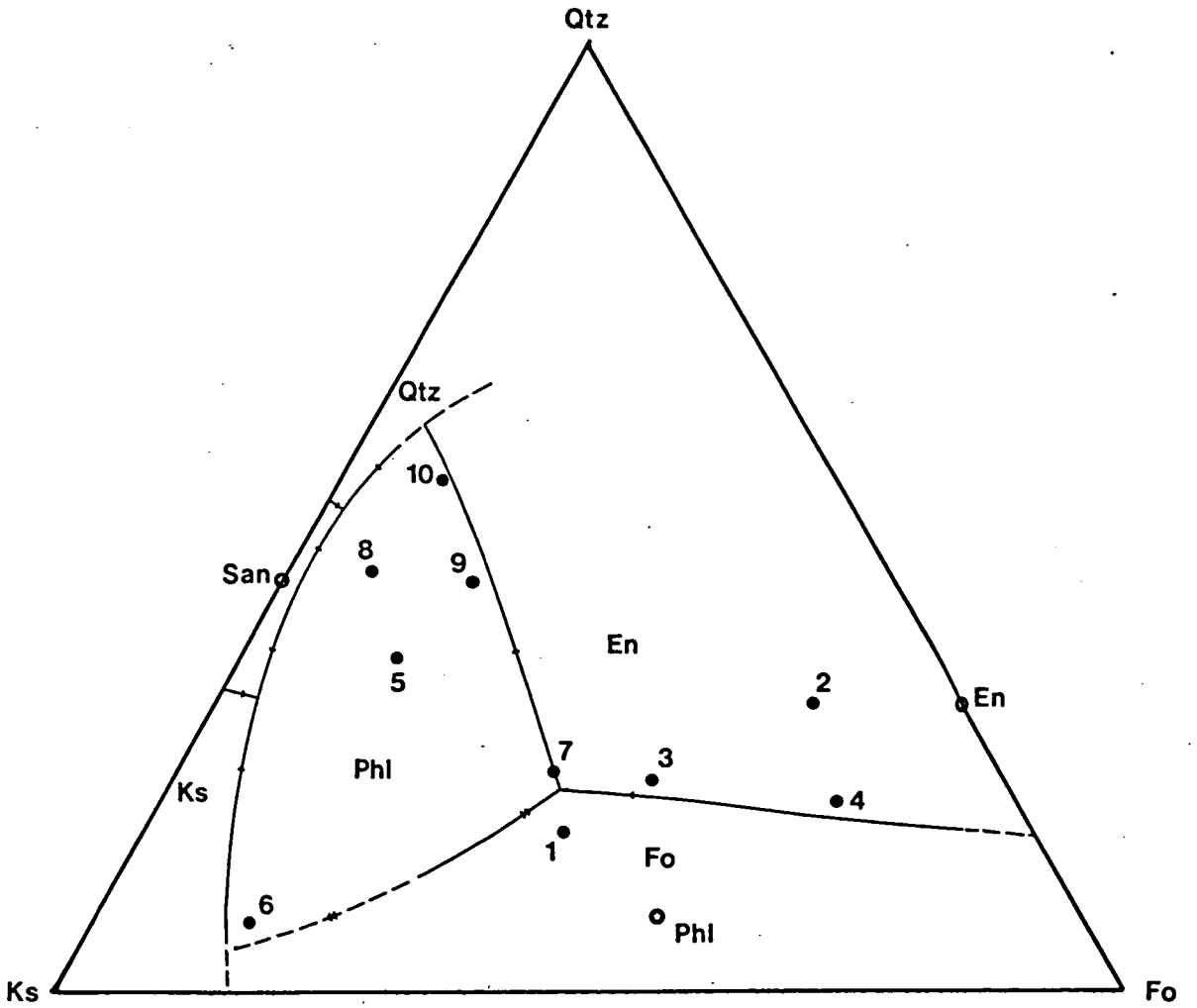

Figure 23: Liquidus phase fields at 28kb and 4% F_2O_{-1}. Numbers mark starting compositions as listed in table 13. ✪ = pure mineral composition.

peritectic, and from there to a PHL+SAN+KS+L eutectic in the case of silica-undersaturated compositions [figure 24]. Both these four-phase points lie in the silica-undersaturated region delimited by the FO-SAN join. Luth [1967] studied the water-saturated Ks-Fo-Qz system at pressures up to 3kbar. In comparison with the water-saturated system at 28kbar, crystallisation paths are similar except for the presence of leucite at low pressures. Compositions defined by EN-SAN-PHL crystallise through the QZ+PHL+EN+L peritectic at all pressures from 1 to 28kbar. The phlogopite phase volume expands greatly with increasing pressure, so that the EN+FO+PHL+L peritectic lies at much more Mg-rich compositions at mantle pressures than was estimated by Sekine and Wyllie [1982].

The phase diagram for $4\%F_2O_{-1}$ at 28kbar broadly resembles the water-saturated, fluorine-free system [figure 24] in having a large primary phase volume for phlogopite, plus primary phase volumes for the same six minerals [En, Fo, Phl, Ks, San and Qz]. However, the fluorine-bearing system differs in that the fluorphlogopite has a much greater thermal stablility (max. 1490-1500°C) than hydroxyphlogopite [<1200 °C: Gupta and Green in prep.]. This may be attributed to the lack of K-H repulsion in fluorphlogopite. This repulsion exists in hydroxyphlogopite due to orientation of the O-H bond directly away from neighbouring octahedral cations and towards the interlayer potassium cations [McCauley et al. 1973]. The EN+PHL phase boundary is not a peritectic reaction despite its extension apparently lying outside the join EN-PHL. This is an artifact of the projection due to Phl_{ss} and liquid compositions lying outside the plane of projection. As in the H_2O-saturated system, the intersection of the FO+PHL phase boundary with the extension of the FO-PHL join forms a thermal maximum. Liquids with compositions to the silica-rich side of this divide will fractionate either through the EN+FO+PHL+L peritectic point or across the phlogopite phase field to either the PHL+SAN+QZ or PHL+SAN+KS eutectics. Compositions to the silica-poor side of the PHL-FO join and its extension will fractionate through the KS+FO+PHL+L peritectic point or across the phlogopite phase field towards the KS+SAN+PHL eutectic.

In the fluorine-bearing system the primary phase field of enstatite relative to forsterite is enlarged compared to the volatile-free system, so that the EN+FO phase boundary is in a similar position to that in the CO_2-saturated system (figure 24). The position of this phase boundary

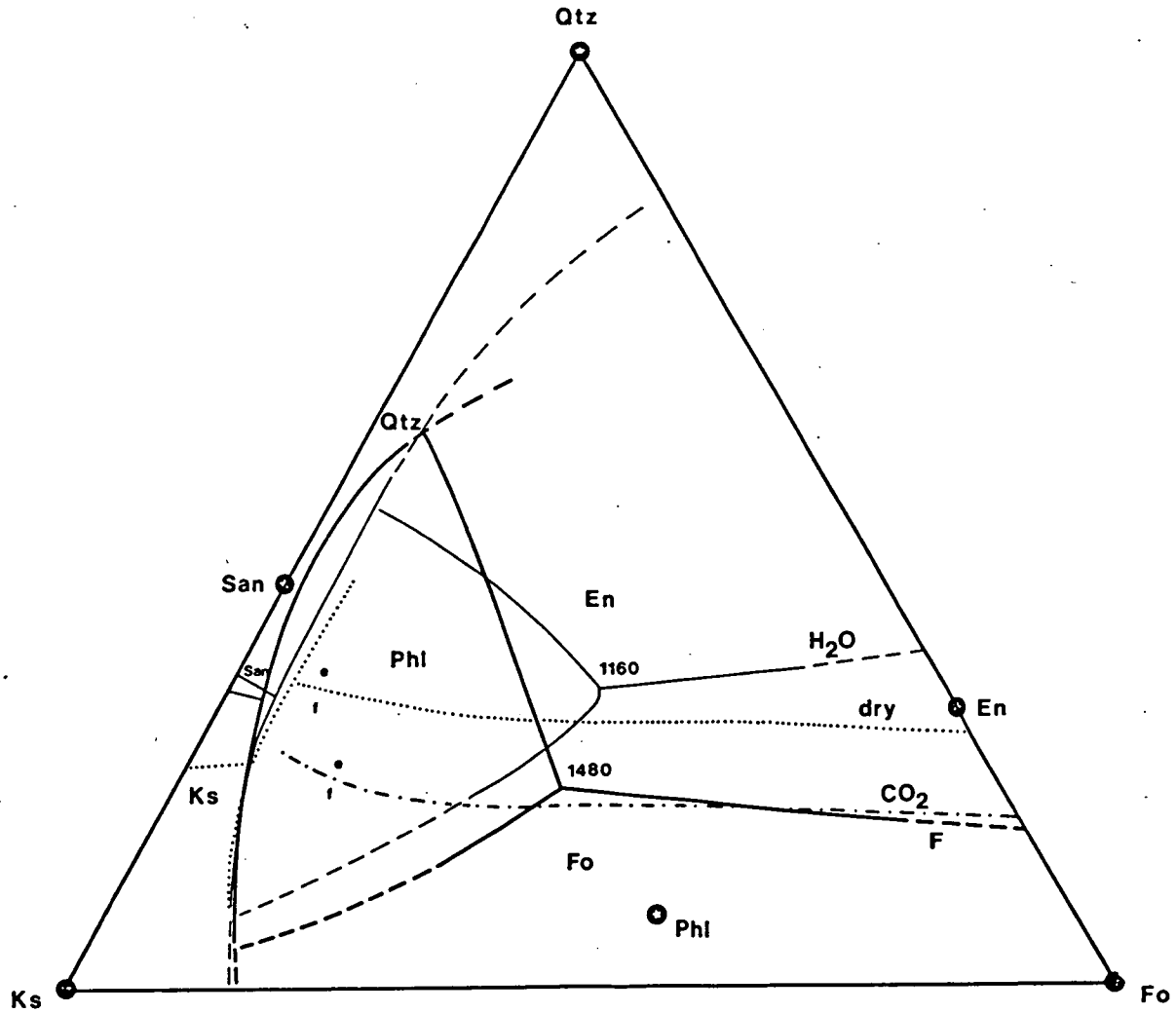

Figure 24: Comparison of data for Ks-Fo-Qz at 28kb with various volatiles. e/f marks enstatite-forsterite boundary in dry and CO_2-present systems where there is no phlogopite field. Phase fields for H_2O, CO_2 and volatile-free systems are from Gupta and Green [in prep.]

is frequently taken to indicate the degree of polymerisation of the melt [Eggler 1974; Kushiro 1975]. Expansion of the enstatite phase volume at the expense of forsterite with the addition of fluorine thus suggests that fluorine causes polymerisation of the melt.

The peritectic point PHL+EN+FO+L is a simple system analogue for a phlogopite harzburgite. The position of this point indicates that partial melting of a phlogopite harzburgite in H_2O-free conditions but in the presence of fluorine would produce a silica-undersaturated magma lying to the silica-poor side of the forsterite-sanidine join at 1480°C. In contrast, in the water saturated system, the first melt would be in the more silica saturated part of the system delineated by the joins between forsterite, enstatite and sanidine at 1160°C.

Several experiments were run with composition 1 with $10\%F_2O_{-1}$. Near-liquidus runs contained a very minor immiscible liquid phase rich in Mg and F. The immiscibility may extend above the liquidus, but this could not be ascertained because of the abundance of quench crystals in the above liquidus run. With $10\%F_2O_{-1}$, composition 1 lies just inside the primary phase volume of phlogopite, indicating expansion of the phlogopite phase volume with increasing fluorine. However, because of the apparent immiscibility which occurs at high fluorine contents, it is unlikely that phlogopite will melt congruently at any fluorine content.

3.3.2. MINERAL COMPOSITIONS:

Enstatites have alumina contents varying between 0.5 and 1.9 wt % (table 13) but with no strong correlation with temperature or accompanying phases. These alumina contents are mostly greater than those of enstatites in water-saturated runs at 28kbar [Gupta and Green in prep.]

Phlogopites show a large range in composition between the different mixes used (table 14). Phlogopites in the more magnesian mixes are closer to the ideal $K_2Mg_6Al_2Si_6O_{20}F_4$ than those in less magnesian mixes. Phlogopites in silica-rich compositions (10,9,8,5) have excess silica (>6 cations), less Mg and Al, and have a lower average octahedral occupancy. Micas from composition 6 are distinct in having high Al and no excess Si. Excess silicon correlates positively with fluorine in approximately 1:1 proportions. This and other correlations are illustrated in figures 25 and 26. Individual substitution mechanisms are difficult to isolate

TABLE 13: Representative compositions of enstatites from experimental products at 28kb and 4% F_2O_{-1}. [analyses normalised to 100%]

Mix No.	2	2	2	3	3	3	4
Temp[°C]	1430	1480	1540	1450	1480	1510	1530
Coexisting phases	Phl			Phl	Phl,Ol		ol
SiO2	59.56	59.64	59.52	58.92	59.27	58.74	59.11
Al2O3	0.54	0.70	0.77	1.69	0.99	1.86	1.41
MgO	39.90	39.66	39.71	39.40	39.73	39.39	39.48
Si	1.990	1.992	1.989	1.969	1.981	1.964	1.975
Al	0.021	0.028	0.030	0.066	0.039	0.073	0.056
Mg	1.987	1.974	1.977	1.962	1.979	1.963	1.966
Sum	3.999	3.994	3.996	3.998	4.000	4.000	3.997

TABLE 14 : Representative compositions of micas in experimental products: Mixes 1-10 have 4% F_2O_{-1}, mix 11 has 10% F_2O_{-1}

Mix No.	1	1	3	3	5	5	5
Temp[°C]	1480	1500	1480	1450	1340	1400	1450
Coexisting phases	ol	ol	ol,en	en	san		
SiO2	43.12	42.87	43.83	44.12	46.37	44.19	45.17
Al2O3	13.03	13.32	12.72	12.26	11.43	12.05	11.85
MgO	27.59	27.39	26.93	27.44	24.03	26.93	26.42
K2O	10.84	10.68	10.75	10.79	11.33	10.75	11.07
F	5.41	5.73	5.76	5.39	6.84	6.09	5.20
Si	6.030	6.011	6.137	6.156	6.539	6.206	6.318
Al	2.148	2.200	2.099	2.015	1.900	1.994	1.941
Mg	5.750	5.724	5.618	5.707	5.053	5.636	5.473
K	1.934	1.910	1.920	1.919	2.038	1.925	1.961
Sum	15.863	15.844	15.773	15.797	15.529	15.760	15.693
F	2.348	2.464	2.606	2.364	3.211	2.611	2.226

Mix No.	6	6	7	7	7	8	8
Temp[°C]	1380	1420	1440	1470	1490	1240	1270
Coexisting phases	ks	ks	en	en	en	san	
SiO2	41.73	41.39	44.53	44.04	43.40	46.52	45.89
Al2O3	14.76	15.75	11.82	12.75	12.41	11.55	10.96
MgO	26.41	26.03	26.64	26.77	27.26	24.05	25.39
K2O	11.31	10.90	10.91	10.90	10.89	11.01	10.98
F	5.78	5.93	6.10	5.54	6.04	6.88	6.78
Si	5.880	5.823	6.256	6.153	6.109	6.547	6.472
Al	2.451	2.613	1.956	2.098	2.058	1.915	1.821
Mg	5.546	5.458	5.577	5.575	5.718	5.045	5.338
K	2.034	1.957	1.956	1.944	1.955	1.976	1.975
Sum	15.911	15.849	15.745	15.770	15.840	15.483	15.605
F	2.620	2.671	2.721	2.504	2.649	3.123	3.037

[Table 14 continued]

Mix No.	8	8	9	9	9	10
Temp[°C]	1300	1340	1290	1350	1410	1380
Coexisting phases			qz	qz		qz
SiO2	47.33	45.36	48.89	46.95	45.99	47.83
Al2O3	11.77	11.54	10.33	10.29	10.45	9.79
MgO	23.36	25.57	23.64	25.21	26.42	25.15
K2O	11.08	10.97	11.03	10.94	10.94	10.62
F	6.45	6.56	6.10	6.60	6.20	6.62
Si	6.617	6.387	6.794	6.594	6.452	6.693
Al	1.939	1.916	1.693	1.703	1.728	1.615
Mg	4.869	5.367	4.896	5.278	5.526	5.245
K	1.976	1.970	1.955	1.960	1.958	1.896
Sum	15.401	15.640	15.338	15.535	15.663	15.448
F	2.871	3.046	2.713	2.923	2.842	2.845

Mix No	1a	1a	1a
Temp[°C]	1510	1480	1450
Coexisting phases		ol	ol
SiO2	42.26	43.25	42.46
Al2O3	11.45	11.33	11.17
MgO	26.96	26.32	26.84
K2O	12.05	11.61	12.37
F	7.09	7.49	7.16
Si	6.104	6.212	6.122
Al	1.939	1.918	1.899
Mg	5.778	5.636	5.769
K	2.210	2.128	2.275
Sum	16.031	15.962	16.065
F	3.239	3.429	3.275

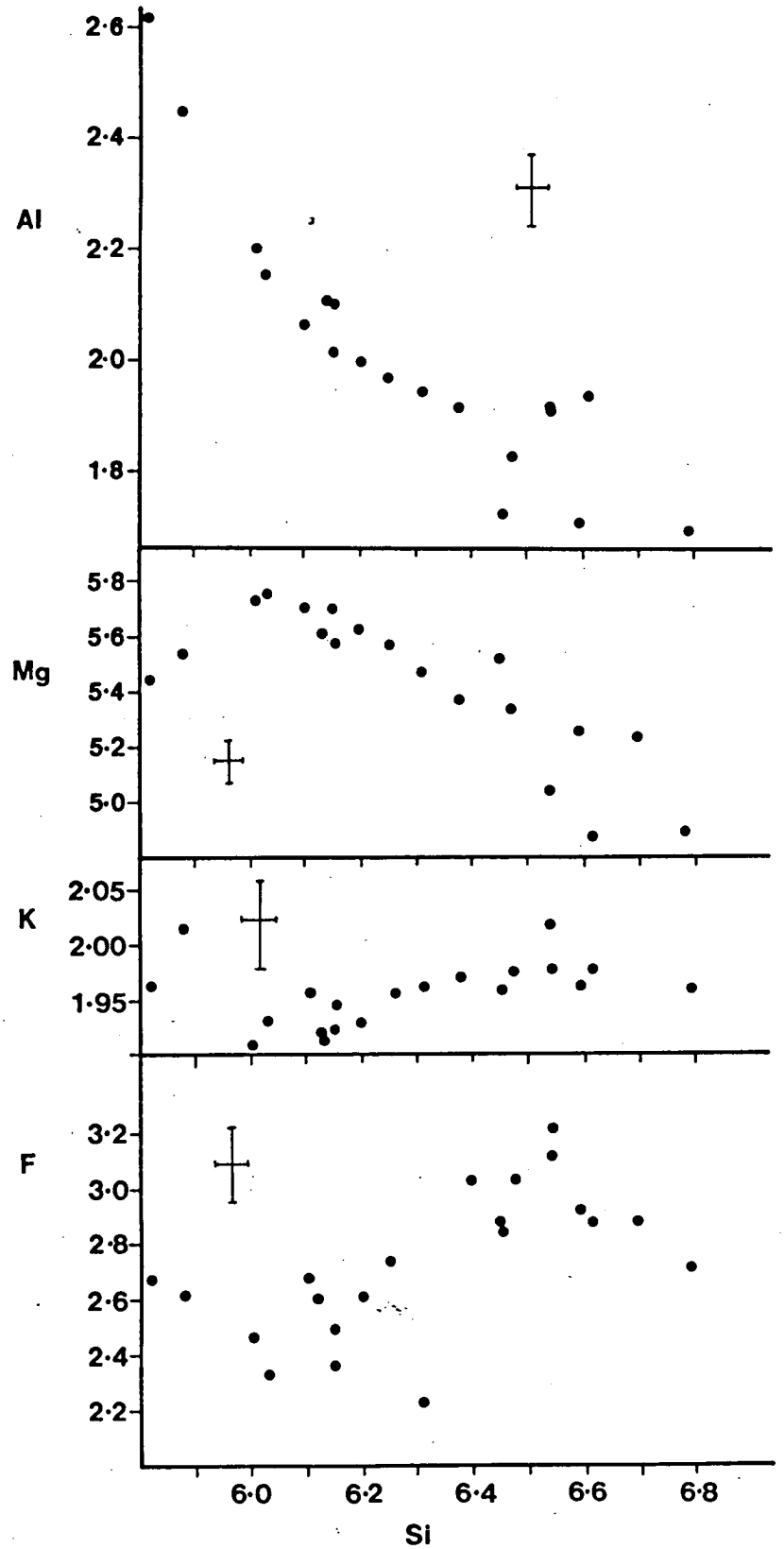

Figure 25: Compositional variation in phlogopites from 4% F_2O_{-1} runs. Ions are calculated on 44 cation valencies per formula unit. Cross hairs denote analytical uncertainty.

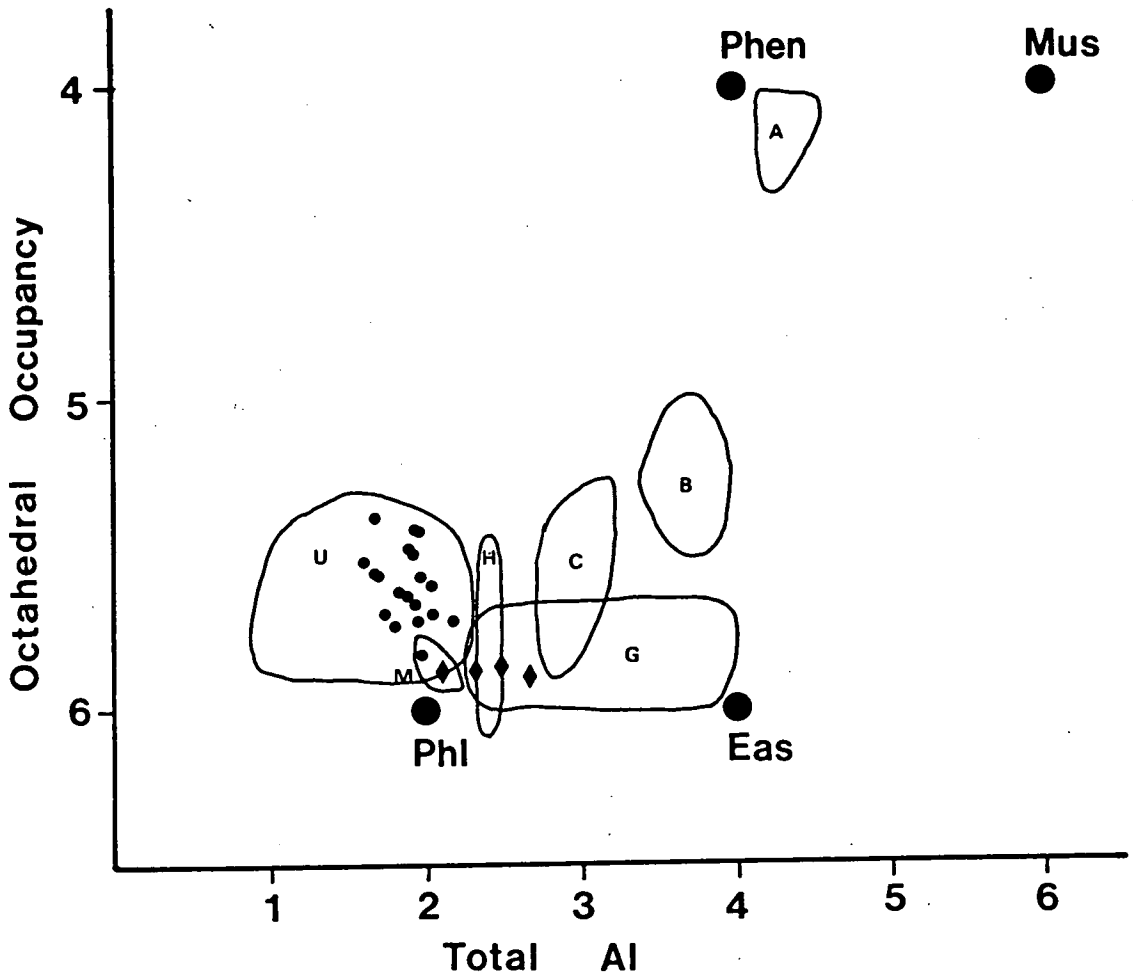

Figure 26: Plot of total Al vs. octahedral site occupancy for phlogopites for fluorine-present experimental runs: Field M = magnesian compositions [1,3,7]; ● = silicic compositions [10,9,8,5]; ♦ = comp.6; Other fields marked are U = natural lamproitic micas; H = micas from H_2O-saturated system [Gupta and Green ms]; G = granitic micas [Green 1981]. Fields A, B and C are synthetic intermediate micas of Green [1981]. Phl= phlogopite, Eas= eastonite, Phen= phengite, Mus= muscovite.

because of scatter in the data and also compositional dependence of substitutions, which is indicated by deviation of data from linearity in figure 25 (especially for the Al-rich micas of composition 6). The coupling of Si with F requires substitution for O^* as well as Mg and Al to charge balance (where O^* is oxygen on the OH site). Dependence of the F/O^* of mica on the F/O of bulk composition is to be expected, and is indicated by higher F contents of micas in the experiments with $10\%F_2O_{-1}$ on composition 1. These contain $F/(F+O^*)$ ratios of 0.81-0.86 (bulk composition ratio = 0.182) relative to 0.59-0.61 with $4\%F_2O_{-1}$ (bulk composition = 0.077). The micas in the 10% F_2O_{-1} runs have an excess of K over the ideal 2 cations per formula unit. This excess is significantly greater than analytical uncertainty. Excess alkalis have been described previously in Si-rich micas from a melilitic rock by Hazen et al [1981], who assigned Na to octahedral sites. However, octahedral K is difficult to envisage in view of its larger ionic radius (1.33Å vs. 0.97Å for Na): this problem cannot be resolved with the data available here.

The chemistry of the experimental micas in the fluorine-bearing system indicate substitution with a mica end-member intermediate between trioctahedral and dioctahedral micas. Where this end-member is present, octahedral site occupancies are lower than in pure trioctahedral micas (figure 26), which can be attributed to a higher average octahedral cation charge (increase in Al and decrease in Mg). In the tetrahedral sites, Si is present in excess of the six cations per formula unit of the pure phlogopite end-member (figure 25). The existence of such an intermediate end-member is suggested by the lack of any known micas with between 4.3 and 5 octahedral cations, which would be expected in the case of solid solution between trioctahedral and dioctahedral micas [Seifert and Schreyer 1971; Green 1981]. The experimental micas are compared to other known intermediate micas in figure 26. Amongst the natural micas, only those from ultrapotassic rocks show an excess of Si, a depletion in Al and a decrease in octahedral site occupancy similar to the fluormicas in the experiments. These include micas from silica-poor melilitic rocks [Velde 1979] which may be related to the lamproites [Gallo et al. 1984; Best et al. 1968].

Analyses of micas from the water-saturated Ks-Fo-Qz system [Gupta and Green in prep.] show less compositional variation than those in the F system. Some have excess Si but show no variation in Al (2.3-2.5 cations). Cation variation diagrams (figures 26 and 27) show that the substitutions here are

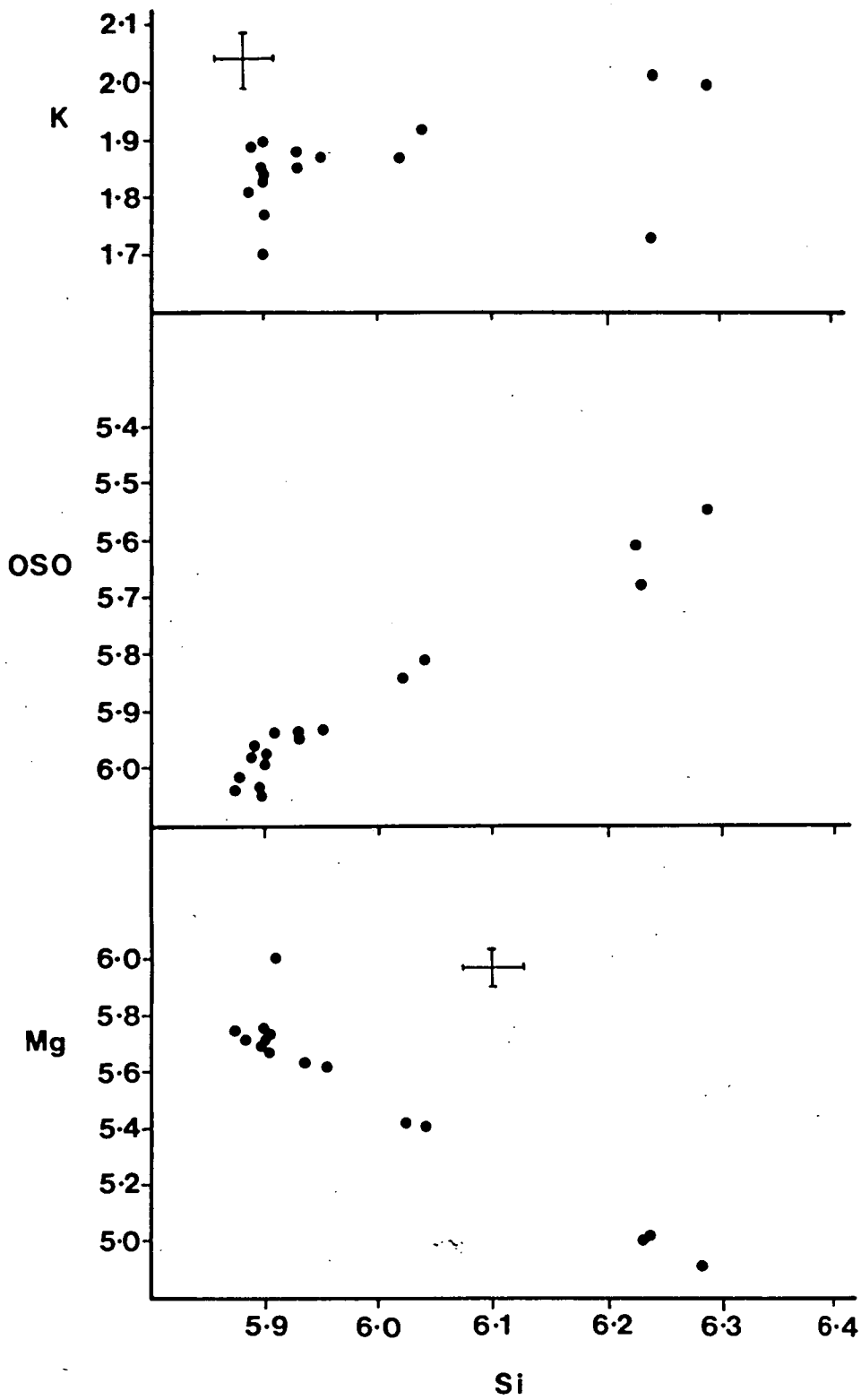

Figure 27: Compositional variation in phlogopites from the H_2O saturated Ks-Fo-Qz system of Gupta and Green [in prep.]. Cross hairs denote analytical uncertainty.

much simpler, and that excess Si is achieved by

$$2\ Mg^{VI} + Al^{IV} = Si^{IV} + Al^{VI} + []^{VI}$$

Mica substitution schemes can thus be expected to change with F/OH ratios with more variability occurring in F-rich than OH-rich micas.

3.4 THE DISSOLUTION MECHANISM OF FLUORINE IN SILICATE MELTS

As noted earlier, the movement of the FO + EN phase boundary towards more silica-undersaturated compositions with the addition of fluorine indicates polymerisation of the melt. The position of this phase boundary is similar to that in the CO_2 saturated system (figure 24) in which the melt is polymerised by complexing of carbonate ions with one or more cations [Brey and Green 1975; Eggler and Rosenhauer 1978; Taylor 1985].

The mechanism of melt polymerisation in the presence of fluorine was investigated by infrared spectroscopy. Composition 1 was chosen for infrared study because of its proximity to the PHL + EN + OL + L peritectic point. Glasses were prepared at 1 atm for infrared studies: high pressure experimental products could not be used due to the abundance of quench crystals in the above liquidus runs. Even a small amount of crystalline material results in sharp, intense peaks in the infrared spectra, which mask the broader absorptions of the glasses. The structure of glasses and liquids of the same composition are known to be similar [Seifert et al. 1981; Taylor et al. 1980; Mysen et al. 1982].

3.4.1 SPECTROSCOPIC METHODS:

Spectra were obtained using a DIGILAB FTS-20E Fourier Transform interferometric spectrometer in the regions 4000-400 cm^{-1} (mid-infrared) and 500-100 cm^{-1} (far-infrared). The use of these regions permits study of absorption bands characteristic of vibrations in the aluminosilicate network (mid-IR) and those of network modifying cations, especially uni- and divalent (far-IR). Crystal-free glasses of composition 1 were prepared with 0.9 wt%, 0.3 wt% and no fluorine at 1 atm. For mid-IR, 1.5 to 2 mg of glass were thoroughly dispersed in approximately 200mg KBr and then pressed into a disc. Samples for far-IR (2-3mg) were prepared by mixing with nujol and mounting the mixture between two high density polyethylene plates.

Absorption bands in the glasses caused by vibrations involving

fluorine atoms were characterised by comparing them with crystalline fluoride samples. This approach is justified by the existence of short-range order in silicate glasses [reviewed by Bottinga et al. 1981]: the structural sites remain comparable with crystalline material, but have a greater variability in bond angles as shown by NMR studies [Dupree and Pettifer 1984] resulting in broad absorption envelopes. The fluorides used were AlF_3, MgF_2, KF and K_2SiF_6. AlF_3, MgF_2 and KF were obtained as fluorides and heated to 450°C to eliminate H_2O, but since KF is strongly hygroscopic (prepared from $KF.2H_2O$) not all the H_2O could be removed. Synthetic cubic hieratite (K_2SiF_6;Palache et al. 1951) was used to characterise Si-F bond absorptions in octahedral co-ordination. There are no known minerals with tetrahedral Si-F bonds [Allmann 1971]. Hieratite was prepared by the reaction

$$K_2CO_3 + SiO_2 + 6\ HF = K_2SiF_6 + 3\ H_2O + CO_2$$

Reactants were mixed thoroughly and placed in a teflon beaker with H_2O added to make the reaction with HF less violent. After reaction the mixture was dried to a gel on a hotplate and then at room temperature to avoid loss of SiF_4 from K_2SiF_6 which occurs at above 427°C. All crystalline fluorides were checked by X-ray diffraction and stored in an oven at 110°C until used.

3.4.2 SPECTROSCOPIC RESULTS

3.4.2.1 BASIC MELTS:

The high frequency region of the mid infrared spectrum (1300-800 cm^{-1}) contains a broad envelope of absorption bands which are assigned to symmetric and asymmetric stretching vibrations of bridging (BO) and non-bridging (NBO) Si-O bonds. In simple binary metal oxide - silica glasses with high NBO/Si the bridging and non-bridging Si-O vibrations can be resolved into two distinct envelopes [Ferraro and Manghnani 1972], but this is not possible in more complex glasses. Lower frequency mid-IR absorptions are due to a mixture of Al-O stretching vibrations and rocking (O motion perpendicular to the Si-O-Si plane) and bending (O motion in the Si-O-Si plane) motions of bridging oxygen bonds [Laughlin and Joannopoulos 1977].

The spectra for the three compositions studied here are given in figure 28. These show little difference between 0 and 0.3 wt% F, but more difference with greater amounts of fluorine. The broad high frequency

envelope shows a shift to higher wavenumbers due to a larger component at approximately 1100 cm^{-1}. This is clearly seen in figure 29, which shows difference spectra generated by computer subtraction of the digital spectra: these highlight the structural changes resulting from substitution of fluorine for oxygen. Difference spectra for (0.9 - 0 wt%F) and (0.3 - 0 wt%F) are compared on the same vertical scale in figure 29. The change in the high frequency region is seen to be due to addition of at least two absorption bands at approximately 1100 and 1200 cm^{-1}, and removal of absorption near 950 cm^{-1}. Studies of simpler silicate and aluminosilicate glasses have demonstrated that a shift to higher frequencies may be due to an increase in the degree of polymerisation of the silicate anions or an increase in the Si/(Si+Al) ratio of the silicate network [Tarte 1967; Furukawa et al. 1981; White 1975; Seifert et al. 1982]. The new bands in the region 1100-1200 cm^{-1} cannot be assigned to specific anionic units as vibrations in more polymerised structures will be coupled through bridging bonds [Furukawa et al. 1981]. The calculated IR spectra of Furukawa et al. [1981] for sodium silicate melts predict the occurrence of absorption bands in the 750-800 cm^{-1} region for $(Si_2O_6)^{4-}$ chains and more polymerised units, but not for less polymerised units. The appearance of an absorption band at 780 cm^{-1} together with the shift to higher wavenumbers in the high frequency envelope for the fluorine-bearing glasses (figures 28 and 29) suggests that fluorine is causing polymerisation of the silicate network.

The far-IR region contains absorptions due to "cage-like" vibrations of cations of larger size and co-ordination number than the mid-IR region [Rao and Elliott 1981]. The precise frequencies are dependent on cation mass, co-ordination number, bond length and the nature of the network attachment and the effective charge of the co-ordinating anion. In general, an increase in size or co-ordination number of the cation leads to absorption at lower wavenumbers [Tarte 1965, 1967; Rao and Elliott 1981; Kovach et al. 1975]. The far-IR region thus contains information on the bonding characteristics of the network modifying cations (particularly K and Mg) in the Ks-Fo-Qz glasses.

The far-IR difference spectra in figure 30 correspond to the samples for which the mid IR difference spectra are given in figure 29. The effect of fluorine on the far-IR spectra is pronounced; bonding interactions with all network modifying cations are seen, and these are evident even at low

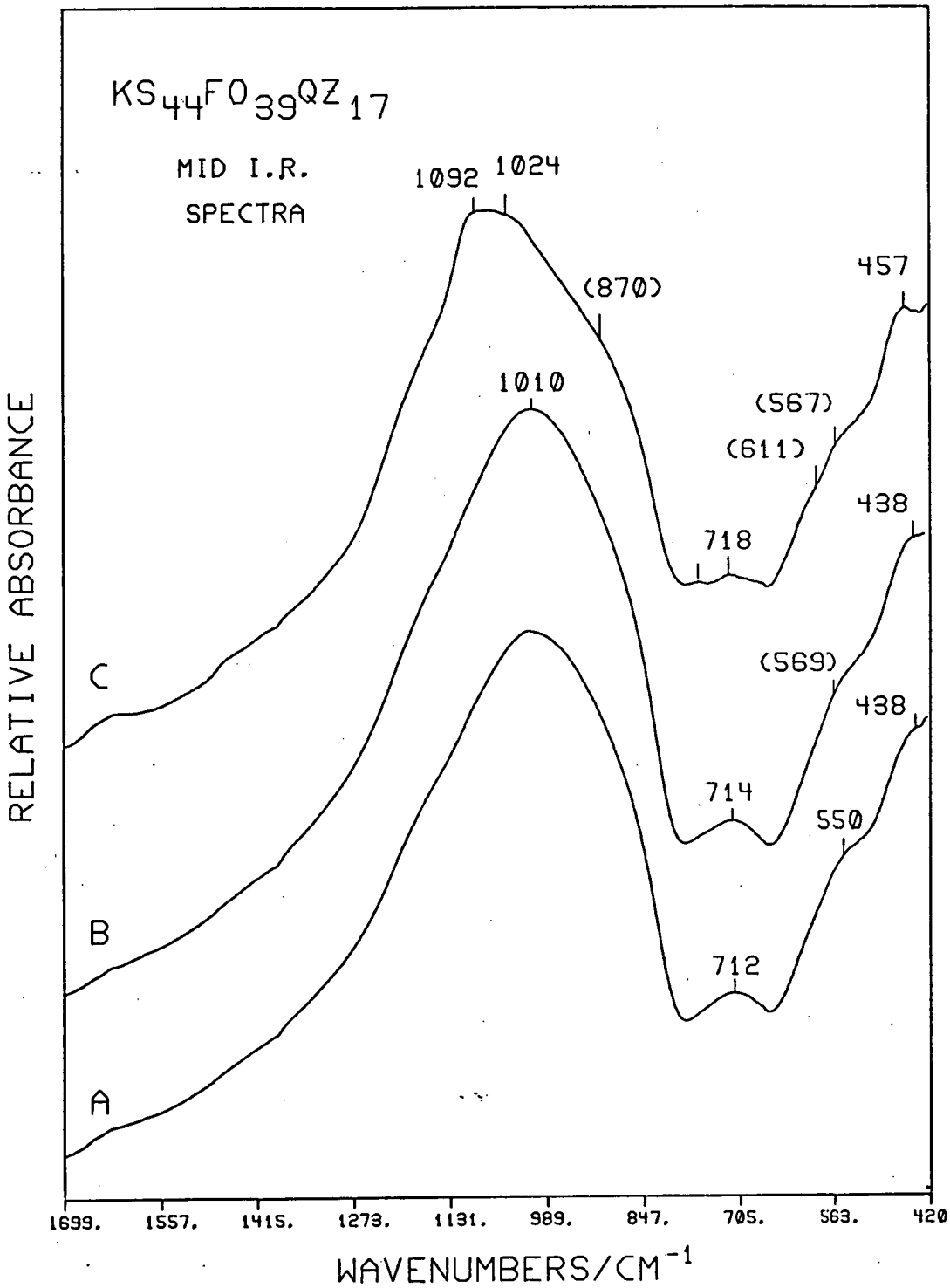

Figure 28: Mid infrared spectra of composition 1 glasses (1 atm) with no fluorine (A), 0.3 wt% F (B) and 0.9 wt% F (C).

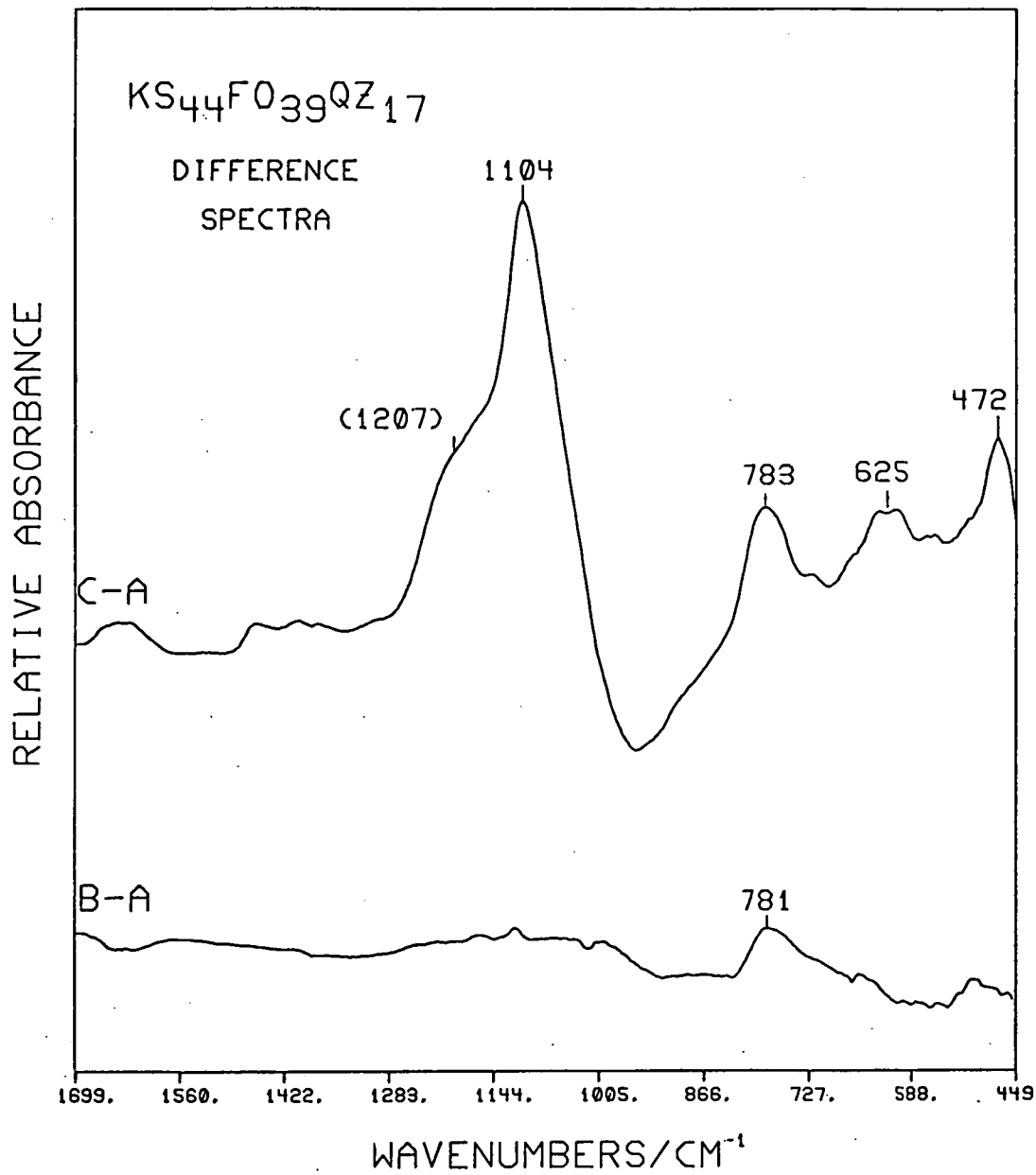

Figure 29: Mid infrared difference spectra. Fluorine-free glass (A in figure 28) subtracted to reveal the effect of fluorine on the silicate network. A,B and C as in figure 28. The shift of the silicate network stretching frequencies to higher wavenumbers (1100-1200 cm^{-1}) indicates polymerisation

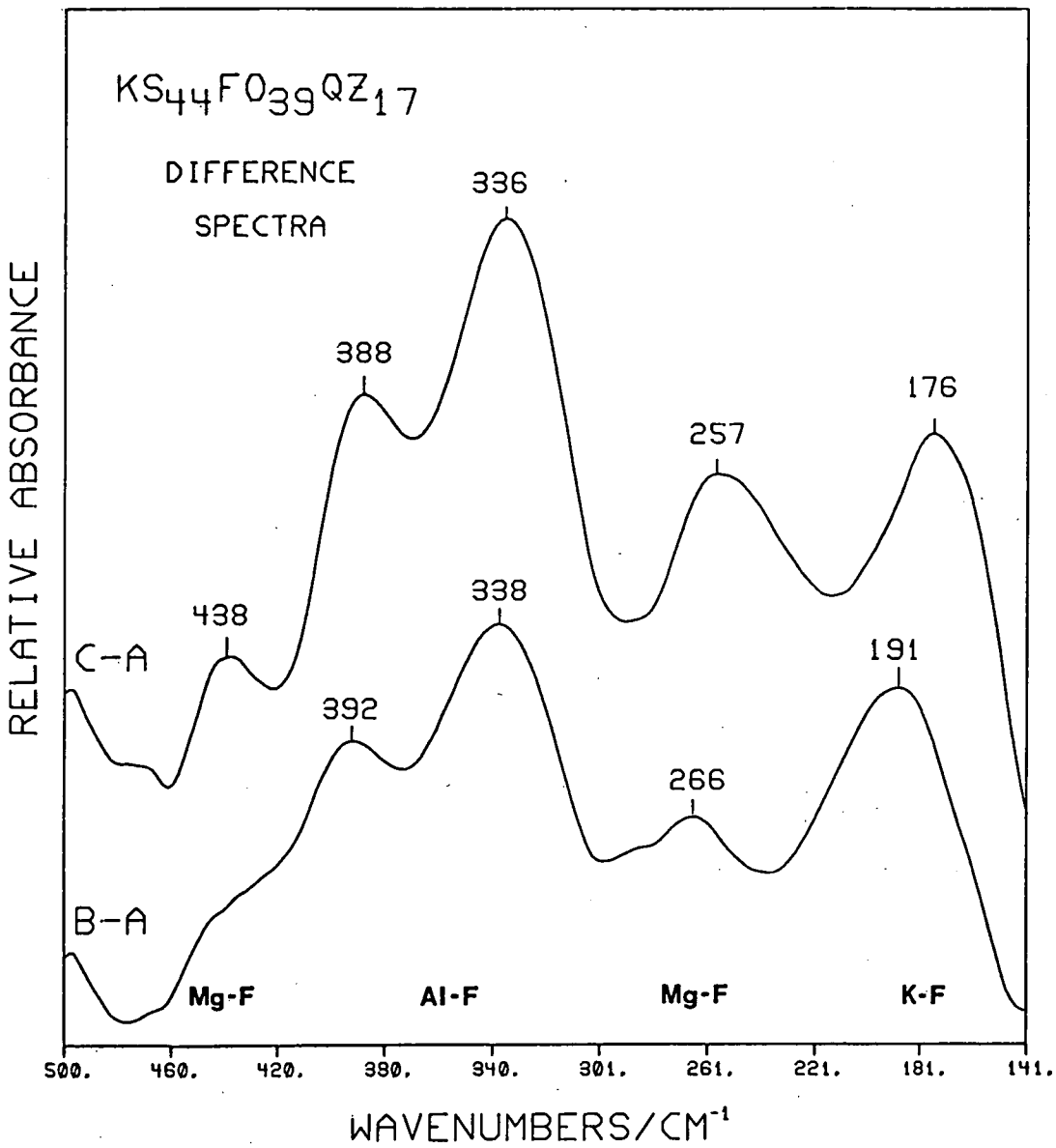

Figure 30: Far infrared difference spectra showing absorption bands characteristic of fluoride bonds with Al, Mg and K as defined by pure fluoride minerals. A, B and C as in figure 28.

fluorine contents where there is no corresponding effect in the mid-IR region. The far-IR absorption bands are assigned with reference to the simple fluoride mineral samples which have similar co-ordination environments to species in the melts.

The far-IR and mid-IR spectra can be explained by the following mechanism of fluorine dissolution. At low fluorine contents, fluorine initially forms bonds with network modifying cations without appreciably altering the aluminosilicate network. At higher fluorine contents, tetrahedral $KAl^{IV}O_2$ groups are complexed by fluorine and removed from the aluminosilicate network simultaneously polymerising and increasing the Si/(Si+Al) ratio of the network, resulting in the shift of the high frequency mid-IR absorption envelope to higher wavenumbers. This polymerising action of fluorine is in accord with calculations made by Tsunawaki et al. [1981] from Raman spectra of fluorine-bearing calcium silicate glasses. These authors observed polymerisation in glasses where fluorine was added by direct substitution, but not where CaF_2 was added to compositions with constant CaO/SiO_2. The fluorine in these melts lowers a_{CaO} by forming $Ca^{2+} - F^-$ complexes and raises a_{SiO2} in the network.

In natural silicate melts the solution mechanism will differ in detail due to the presence of water, the dominant fluorine species then being HF [Munoz and Eugster 1969]. In this case fluorine will behave in a similar manner, bonding with network modifiers, but the dissolution of HF will result in the release of water which will have a depolymerising effect. Examples of possible reactions showing the complexing of fluorine with network modifiers are:

$$(Mg_2SiO_4) + 2\ HF = (MgSiO_3) + (MgF_2) + H_2O \quad (5)$$

$$(KAl^{IV}O_2) + 4\ HF = (Al^{VI}F_3) + (KF) + 2\ H_2O \quad (6)$$

The effect on the silicate network is clearly seen by

$$2\ (KAl^{IV}Si_2O_6) + 4\ HF = (KAl^{IV}Si_3O_8.SiO_2) + (KF) + (Al^{VI}F_3) + 2\ H_2O \quad (7)$$

Water is known to dissolve in silicate melts both as hydroxyl groups and, particularly at higher total water contents, as molecular H_2O [Stolper 1982]. The formation of hydroxyl ions depolymerises the melt due to breakage of bridging bonds to form two non-bridging bonds. It is not certain whether this process is concentrated on Si-O-Si bonds [Burnham 1975, 1979a] or on Al-O-Si bonds [de Jong and Brown 1980; Taylor 1985], but this uncertainty does not have any bearing on the broad depolymerising effect discussed here. Evidence for depolymerisation is seen

in the expansion of the liquidus phase volumes of less polymerised minerals such as olivine relative to enstatite [Kushiro 1972; Mysen 1977]. The polymerising action of fluorine will thus be masked by the depolymerising action of the H_2O released by HF dissolution. In the presence of mixed H_2O-HF fluids, the forsterite-enstatite phase boundary in the system Ks-Fo-Qz can be expected to show overall depolymerisation.

3.4.2.2 **SILICIC MELTS:**

The solution mechanism for HF outlined above for basic melts contradicts the popular assumption that HF dissolves in granitic melts by Si-F bond formation. Consideration of the applicability of the HF solution mechanism for silicic melts is therefore necessary.

Many workers studying silicic melts have assumed that HF dissolves by a process analagous to H_2O in that Si-O-Si bridging bonds are broken resulting in tetrahedral Si-F bonds and a depolymerised melt [eg. Burnham 1979b; Bailey 1977; Collins et al. 1982]. This is based on the similarity of ionic radii of O (1.32 Å) and F (1.33 Å) [Buerger 1948] and the assignment of mid infrared absorption bands in alkali- and alkaline earth-silicate glasses to Si-F bonds [Kumar et al. 1961, 1965].

However, it has been shown above that the dissolution of HF, at least in basic melts, is a two-stage process in which the depolymerisation is due to H_2O released by HF dissolution, so that the assumption of Si-F bond formation as a major process is not justified. Manning [1981] also proposed a two-stage dissolution process for HF but with Si-F bonds as the intermediate stage occurring prior to hydrolysis: the infrared spectra of H_2O-free, fluorine-bearing glasses lead us to prefer the process rperesented by equations 5-7. A process similar to that in basic melts causing an increase in Si/(Si+Al) of the network is supported by the observed expansion of the quartz phase volume with respect to feldspars on addition of fluorine [Wyllie and Tuttle 1961; Kovalenko 1977; Manning et al. 1980].

A number of arguments have been put forward, particularly in the Russian literature, that despite an increase in the proportion of Si-F bonds in silicic relative to basic melts, the proportion of Si-F bonds will still be very minor [Kogarko and Krigman 1973; Kogarko et al. 1968; Kogarko and Ryabchikov 1978; Mitchell 1967]. Arguments include the absence

of minerals with tetrahedral Si-F bonds, immiscibility between silica-rich and alkali-fluoride-rich melts [Kogarko 1967], the predominance of alkali fluoride in vapours in equilibrium with silicic melts, and thermodynamic calculations. In addition, acid-base theory predicts that reactions will proceed in favour of the formation of bonds of maximum and minimum polarity [Ramberg 1952; Kogarko 1974]. Thus, reactions of the type

$$4\ MF + SiO_2 = SiF_4 + 2\ M_2O \qquad (8)$$

where M = any cation, will favour the left side due to the higher electronegativity of F relative to O and Si relative to all other common cations in silicate melts.

Attempts in this study to form tetrahedral Si-F bonds in glasses for infrared study failed, producing instead crystalline fluorosilicates containing octahedral [SiF_6] units. Crystallisation of fluorosilicates is common in pressurised experiments on fluorine-bearing compositions [Wyllie and Tuttle 1961; Glyuk and Anfilogov 1973; Manning et al. 1980]. The assignment of absorption bands to tetrahedral Si-F bonds by Kumar et al. [1961, 1965] is considered to be erroneous, as bands due to more polymerised silicate units will occur in the regions described by Kumar et al. [Ito et al. 1967; Mitchell 1967; Furukawa et al. 1981]. Reference to the fluorosilicate mineral spectra shows that any Si-F bonds in this region would be octahedral, probably due to octahedral [SiF_nO_{6-n}] units and not tetrahedral [SiF_nO_{4-n}] units.

Mysen and Virgo [1985] reported Raman spectra for glasses on the joins SiO_2-AlF_3 and SiO_2-NaF, and they suggested that tetrahedral Si-F bonds are important, particularly on the SiO_2-AlF_3 join. However, these results are inappropriate for extrapolation to complex natural silicate melts as they used fully polymerised SiO_2 melts as a starting point for fluorine addition. The compositions studied here in the system Ks-Fo-Qz contain an array of structural species which form a better analogy for natural silicate melts. Also, the addition of fluorine as fluorides is less suitable for studying the structural effect of fluorine than is direct substitution of fluorine for oxygen, because the effect due to fluorine cannot be isolated from the effect due to the accompanying cation. Tsunawaki et al. [1981] have demonstrated that addition of fluorine as fluoride does not cause polymerisation, whereas addition of the same amount of fluorine by direct substitution does.

The larger viscosity decrease in silicic melts on fluorine addition [Kozakevitch 1954; Kumar et al. 1961] has been used as evidence for melt depolymerisation and Si-F bond formation. Dingwell et al. [1985] and Dingwell and Mysen [1985] confirmed the large viscosity decrease due to fluorine in melts in the system SiO_2-Na_2O-Al_2O_3 where fluorine was added by direct substitution for oxygen. It is important to note that 'polymerisation' as used in this paper refers to the aluminosilicate network, whereas viscosity reflects the overall stucture of the melt. The polymerisation state of the aluminosilicate network, which can be represented by the EN+FO phase boundary, is more useful for considering the composition of partial melts produced in the mantle because the phase volumes of the silicate minerals reflect their relative stabilities as residual phases. The viscosity decrease in fluorine-bearing silicate melts relative to fluorine-free melts can be attributed to the formation of fluoride complexes incorporating cations which form part of the aluminosilicate network in fluorine-free melts (equations 5-7). We found no evidence in the present study to support the proposal of Dingwell et al. [1985] that the decrease in viscosity is due to tetrahedral Si-F bond formation.

3.5 SUMMARY

Phase relationships in the system kalsilite-forsterite-quartz with fluorine added by direct substitution for oxygen were examined at 28 kbar. A large liquidus field for fluorphlogopite exists with approx. 4 wt% F added to the system and the thermal stability of phlogopite is increased by ~300°C relative to the water saturated system. Fluorine expands the phase volume of enstatite relative to forsterite so that the peritectic point PHL+EN+FO+L, a model for melting of a phlogopite harzburgite, lies in the silica-undersaturated field. Experimental phlogopites have excess Si which correlates with F content and are Al-deficient. The high Si contents indicate solid solution with an end member intermediate between tri- and di-octahedral micas.

Glasses with compositions analogous to partial melts from phlogopite harzburgite were examined by infrared spectroscopy in the mid- and far-IR regions. Results show that fluorine polymerises the melt by bonding with all the network modifying cations K, Mg and Al. At higher F contents, but still less than 1 wt%, tetrahedral $KAlO_2$ groups are

complexed by fluorine and removed from the aluminosilicate network simultaneously polymerising and increasing the Si/(Si+Al) ratio of the network. However, when HF rather than F is present, the overall effect will be to depolymerise melts due to the effect of OH released by dissolution of HF. The presence of abundant Si-F bonds is considered unlikely even in silica-rich magmas: the viscosity decrease characteristic of fluorine-bearing melts can be attributed to the formation of fluoride complexes.

PART IV

THE ROLE OF FLUORINE AND OXYGEN FUGACITY IN THE GENESIS OF THE ULTRAPOTASSIC ROCKS

4.1 INTRODUCTION

The ultrapotassic rocks are a compositionally heterogeneous group of rocks in which volatile species (H_2O,CO_2,F,Cl, SO_2) are more abundant than in less alkaline rocks. Experimental studies on natural ultrapotassic rock compositions [eg. Edgar et al. 1976; Barton and Hamilton 1979, 1982; Ryabchikov and Green 1978; Arima and Edgar 1983a,b] and simple systems [eg. Wendlandt and Eggler 1980a,b; Gupta and Green in prep.] at high pressures have been limited to consideration of the effect of H_2O and CO_2 on phase relationships as a guide to petrogenesis. These studies have emphasised the stability of mica under H_2O-rich conditions, and the different roles of H_2O and CO_2 in stabilising more depolymerised and polymerised anhydrous silicate minerals respectively.

In this paper we extend the discussion of volatiles to include fluorine and methane. The effect of fluorine will be greater in ultrapotassic rocks than in other mafic rocks because fluorine correlates positively with K content [Aoki et al. 1981]. Jaques et al. [1984a] suggested that H_2O+HF-rich volatile mixtures are important in generating lamproite magmas and that F would increase the stability of mica. Our studies of the fluorine solution mechanism and phase relationships in the system kalsilite - forsterite - quartz [Ks-Fo-Qz; Part 3] provide more evidence for the role of fluorine in ultrapotassic rock genesis.

Methane has not been considered important in the past mainly due to models for the oxidation state of the upper mantle during magma genesis which presuppose stability of carbonates forming oxygen buffer reactions with fO_2 close to that of the FMQ and MW buffers [Eggler 1978; Wyllie 1978, 1979]. However, measurements of intrinsic oxygen fugacity and oxygen barometry on megacrysts and xenoliths believed to be derived from the mantle [eg. Arculus et al. 1984; Haggerty and Tompkins 1983] indicate that the oxidation state of the mantle is likely to be heterogeneous, including regions with fO_2 as low as that of the IW buffer. The relative importance

of reduced and oxidised environments in the mantle within the range noted above is currently the subject of much debate [see discussions by Ryabchikov et al. 1981, Eggler and Baker 1982, Arculus 1985, Taylor 1985, Woermann and Rosenhauer 1985]: we therefore consider variations in oxygen fugacity on ultrapotassic rock genesis, and develop a model for the production of lamproites in a F-rich, reduced environment.

4.2 FLUORINE IN ULTRAPOTASSIC MAGMAS

Fluorine is most abundant in Group I rocks, ranging up to 0.8 wt%. Examples of fluorine contents in lamproitic rocks are 0.20 to 0.54 wt% for West Kimberley, Australia [Jaques et al. 1984a], 0.59-0.76 wt% for the Leucite Hills, USA [Kuehner et al. 1981; Aoki et al. 1981] and 0.33 wt% for Gaussberg, Antarctica [Sheraton and Cundari 1980]. Group II rocks range up to 0.28 wt% in the katungites and melilitic rocks of the Toro Ankole field [Holmes 1937; Holmes and Harwood 1932; Edgar and Arima 1981] with generally lower values in the less potassic rock types to the south. Group III rocks contain the lowest amounts of fluorine amongst the ultrapotassic rocks, generally less than 0.2 wt% [Fornaseri et al. 1963; Iddings and Morley 1915] although data are sparse for this group. The understanding of the behaviour of fluorine in magmatic systems is therefore particularly important for elucidating the petrogenesis of the lamproites.

Fluorine contents in phlogopite phenocrysts/xenocrysts in lamproitic rocks are frequently high [see table 15]. Natural mica compositions from ultrapotassic rocks have been reviewed by Arima and Edgar [1981] and Bachinski and Simpson [1984], but their data lacked fluorine contents. Foley et al. [Part 3] showed that synthetic micas in the system Ks-Fo-Qz with fluorine have more complex compositional variations than micas in the same system under water-saturated, fluorine-free conditions, so that natural mica compositions can be expected to vary with F/OH ratios.

Micas crystallising from melts containing relatively small amounts of fluorine, such as ultrapotassic melts, can be expected to have high F/OH ratios since micas are very efficient at removing fluorine from a melt [Munoz and Eugster 1969]. Ion variation plots of natural micas (figure 31) show several broad trends amongst ultrapotassic rocks as a group, but these are not necessarily reproduced in rocks from a single area, especially where fluorine content is low. Si and F do show a positive

TABLE 15 : Fluorine contents of micas from natural lamproites and related rocks.

F wt%	F ions	Locality & description	Sample	Ref.	
2.46	1.069	Leucite Hills, wyomingite	B	1	*
2.38	1.029	Leucite Hills, orendite	SK36	2	
2.51	1.084	Leucite Hills, orendite	SK36	2	
4.11	1.784	Leucite Hills, orendite	SK36	2	
2.95	1.279	Leucite Hills, orendite	SK36	2	
4.52	1.996	Leucite Hills, wyomingite	SK9	2	
4.86	2.214	Leucite Hills, madupite	SK23	2	
0.84	0.362	Holsteinsborg, lamproite	5944	3	
0.74	0.319	Holsteinsborg, lamproite	5944	3	
0.24	0.104	Holsteinsborg, lamproite	5944	3	
0.87	0.391	Holsteinsborg, lamproite (core)	5622	3,4	
0.88	0.384	Holsteinsborg, lamproite (core)	5622	3,4	
nd	--	Holsteinsborg, lamproite (rim)	5622	3,4	
2.69	1.187	SE Spain, jumillite	SP059	5	
1.35	0.598	SE Spain, jumillite	SP059	5	
2.07	0.917	SE Spain, jumillite	SP059	5	
1.25	0.537	SE Spain, fortunite	SP081	5	
0.97	0.419	SE Spain, fortunite	SP081	5	
1.52	0.666	SE Spain, fortunite	SP081	5	
2.40	1.058	SE Spain, lamproite	2	6	*
1.4	0.621	Gaussberg, olivine leucitite	4755	7	*
1.42	0.638	Gaussberg, olivine leucitite (gd)	2780	-	
1.93	0.871	Gaussberg, olivine leucitite (gd)	4882	-	
1.95	0.883	Gaussberg, olivine leucitite (gd)	2780	-	
4.01	1.843	Priestley Peak, alkali melasyenite	3949C	8	
3.91	1.786	Priestley Peak, alkali melasyenite	3949C	8	
4.07	1.860	Priestley Peak, alkali melasyenite	3949C	8	
5.55	2.589	Prairie Creek,Ark, olivine lamproite	PK1/19	9	*
5.32	2.449	Prairie Creek,Ark, olivine lamproite	PK1/19	9	*
5.74	2.673	Prairie Creek,Ark, olviine lamproite	PK1/19	9	*
5.06	2.343	Utah, melilite peridotite	Y127	10	*
3.76	1.681	Sierra Nevada, high-K basanite	MP410	11	*
2.91	1.314	Sierra Nevada, high-K basanite	MP410	11	*
3.56	1.579	Sierra Nevada, high-K basanite	B5	11	*
3.69	1.701	Sierra Nevada, high-K basanite	M74B	11	*
2.88	1.284	Sierra Nevada, high-K basanite	M74B	11	*

New analyses unless denoted (*). (gd)=groundmass.
New analyses by JEOL JXA 50A microprobe (wavelength dispersive system) with topaz and synthetic MgF_2 standards.

References: [1] Carmichael 1967; [2] Kuehner et al. 1981; [3] Scott 1977; [4] Scott 1981; [5] Venturelli et al. 1984; [6] Fuster et al. 1967; [7] Sheraton and Cundari 1980; [8] Sheraton and England 1980; [9] Scott-Smith and Skinner 1984; [10] Velde 1979; [11] Van Kooten 1980.
Chlorine (detection limit <0.05 wt %) was not detected in any of the new analyses

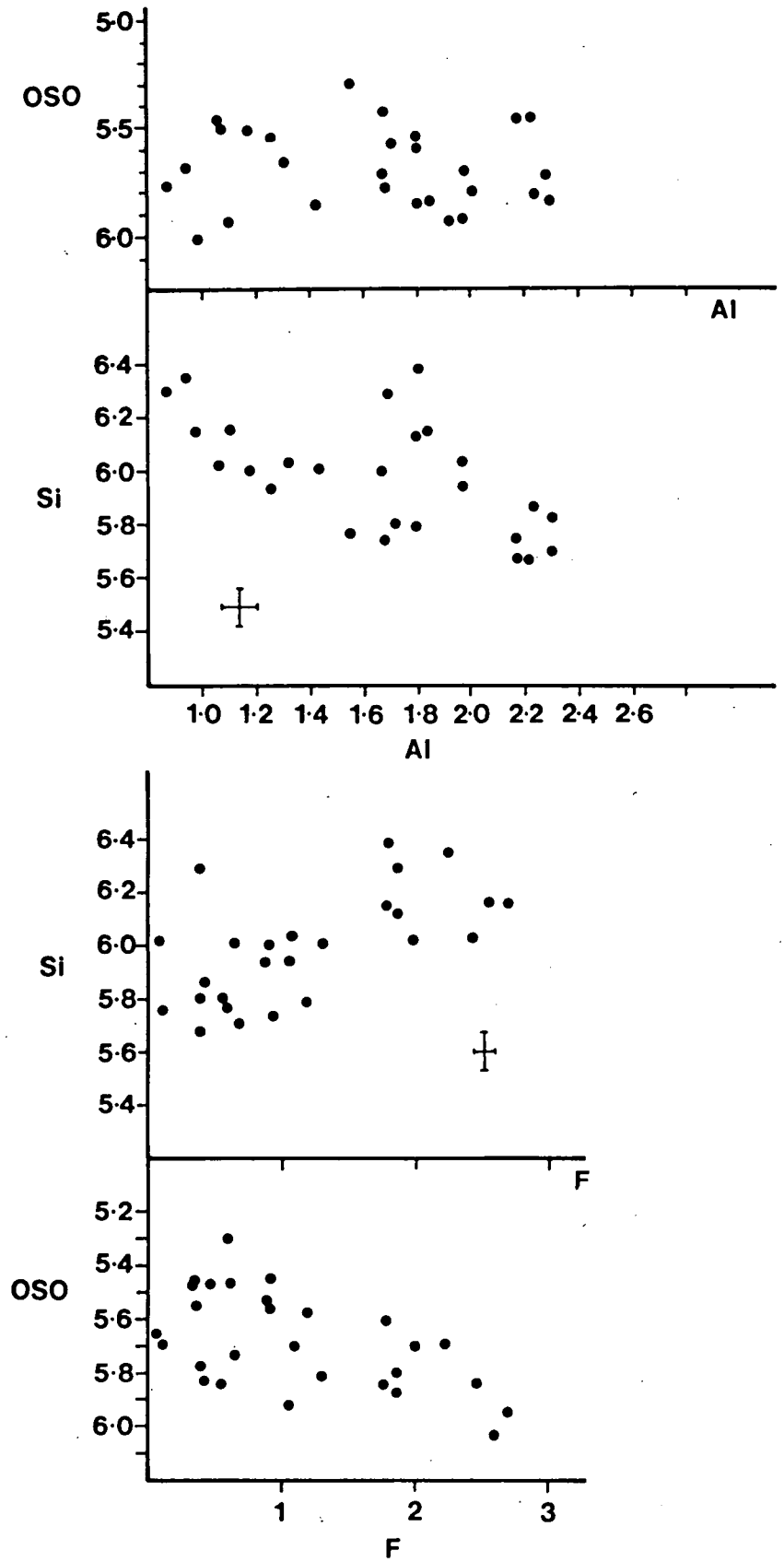

Figure 31: Compositional variation in natural ultrapotassic micas from Leucite Hills, Gaussberg, Holsteinsborg, Southeastern Spain and Priestley Peak (Antarctica). OSO = Octahedral site occupancy.

correlation, but the ratio is nearer 1:2 than the 1:1 in the experimental micas, indicating more complex substitution relationships. No simple correlation of fluorine with any other cation is seen, although this may be partly due to scatter between ultrapotassic rock localities.

The alumina contents of many ultrapotassic rock micas are much lower than any of the experimental micas. This is probably a consequence of the peralkaline and, in the case of lamproites, often perpotassic, nature of the melts. The experiments are restricted to K=Al, whereas K is frequently in excess of Al in lamproitic rocks. The dominant Al substitution in the natural micas appears to be a Tschermak-type substitution indicated by the Si = 2 Al slope and large variation in Al relative to octahedral occupancy (figure 31). The low Al-content of natural ultrapotassic rock micas will reflect both the low Al content of the melt and the F/OH ratio. For a constant K/Al, Si in micas is likely to increase with F towards more silica-rich whole-rock compositions. The substitution mechanisms cannot be formulated in detail as they are complicated by other cations, particularly Ti and Fe (see discussion by Arima and Edgar 1981), which are not present in the Ks-Fo-Qz system. The difference between fluormicas and hydroxymicas in the system Ks-Fo-Qz indicates that coupled substitutions of specific cations with F, O and OH on the (OH) site, as discussed by Bohlen et al. [1980], are probably important. As an example, the Fe^{2+}-F avoidance principle [Rosenberg and Foit 1977; Sanz and Stone 1979] should cause coupling of F with cations other than Fe^{2+}.

The effect of fluorine on the compositions of melts generated in the mantle is best represented by the polymerisation state of the aluminosilicate network. The most convenient simple system indicator for this in Ks-Fo-Qz is the movement of the forsterite-enstatite phase boundary (figure 32) since these two minerals are likely to be major components of the mantle residuum. The phase equilibrium and spectroscopic data for the Ks-Fo-Qz system [Part 3] indicate that fluorine polymerises the aluminosilicate network. However, in most geological conditions H_2O will be present in excess of fluorine, so that HF will be the dominant fluorine species. HF will dissolve by a reaction in which the polymerising effect of F is counterbalanced by the depolymerising effect of H_2O released by HF dissolution [Part 3]. Under these conditions the overall effect will be an increase in the liquidus phase volume of the most depolymerised phase, resulting in the production of

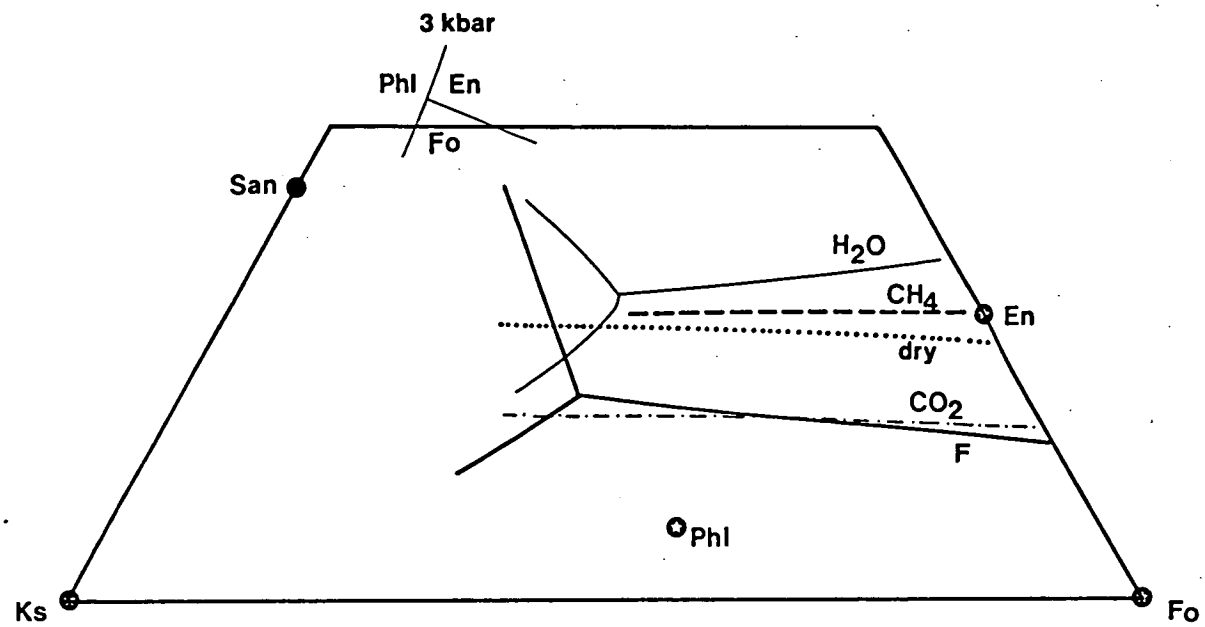

Figure 32: Part of the system Ks-Fo-Qz showing the relative positions of the enstatite - forsterite phase boundary in the presence of various volatile species discussed in the text. The boundary for CH_4 is estimated from its position in the Ne-Fo-Qz system, taken from Gupta et al. [in prep.]. The position with HF is uncertain, but can be expected to be close to the CH_4 position. The data for the water-saturated Ks-Fo-Qz system at 3 kbar are taken from Luth [1967].

more silica-rich melts (ol, en, san normative). In the event of H_2O-poor but F-rich conditions, melts generated in the mantle will be silica-undersaturated (ol, san, lc normative) as modelled by the PHL+EN+FO+L peritectic point (figure 32).

4.3 OXYGEN FUGACITY AND ULTRAPOTASSIC MAGMAS

Oxygen fugacity will also be an important controlling factor of melt polymerisation, particularly affecting the behaviour of carbon. CO_2 has been found to polymerise silicate melts by forming carbonate complexes with network-modifying cations. This causes expansion of the phase volume of enstatite relative to that of forsterite (figure 32) so that lower silica partial melts result [Brey and Green 1975; Eggler 1974, 1978; Ryabchikov and Green 1978]. Experiments investigating the solution of CO_2 in silicate melts of the same composition at widely differing fO_2 have shown that the amount of carbonate dissolved in the melt, and thus the polymerisation, increases with increasing fO_2 [Brey and Green 1976].

At low fO_2 methane will be the dominant carbon species. Recent studies by Taylor [1985] have shown that the solubility of reduced carbon in simple system silicate melts is limited to 1000-2000 ppm before saturation and crystallisation of graphite occurs. This small amount of carbon is probably contained as atomic carbon on cation vacancies and defect sites as envisaged by Freund et al. [1980, 1983] for silicate minerals. Methane dissolution is accompanied by reduction in the stoichiometry of the silicate network (ie. O/Si < 2) [Taylor 1985]. The enstatite-forsterite phase boundary in the methane-saturated system Ne-Fo-Qz (fO_2 < IW buffer) is to the silica-rich side of its position in the volatile-free system. Thus, in a very reduced environment with H_2O, CH_4 and HF, depolymerisation will be at a maximum, and melts produced will be more silica-rich than those in source regions containing H_2O, CO_2 and HF. In a reduced C-O-H fluid at mantle pressures (fO_2 between the iron-wustite buffer and ~2 log units above IW) the H_2O/CH_4 ratio will vary greatly with fO_2, temperature and pressure, but there will always be a significant amount of H_2O [Taylor 1985].

Intrinsic fO_2 measurements on mantle derived xenoliths and xenocrysts indicate two distinct oxygen fugacities may be prevalent in the upper mantle; one reduced near the IW buffer and the other oxidised near QFM

[Arculus and Delano 1981; Arculus et al. 1984]. However, this data is sparse at present and these may represent extremes of a continuum of oxygen fugacities in the mantle, with the majority of measurements clustering around the MW buffer [O'Neill and Wall 1982, Arculus 1985].

What evidence then, is there of the oxygen fugacity in ultrapotassic magma source regions? CO_2 contents are variable between ultrapotassic rock groups: Group II rocks are rich in CO_2, frequently with carbonates present in the groundmass, whereas Group I rocks, in most cases, have very low CO_2 contents. However, the source regions of CO_2-poor rocks need not have been poor in carbon if oxygen fugacity was low.

Foley [Part 2] studied early crystallising chrome-spinels which form inclusions in olivine phenocrysts in lamproites, and experimentally calibrated the ferric number $[100Fe^{3+}/(Fe^{3+}+Fe^{2+})]$ of spinel as an oxygen fugacity sensor. Spinels from various lamproites show a wide range in oxygen fugacities for different lamproitic rocks, and these differences are also seen in the Fe_2O_3 content of leucites. There may be a large disparity (up to 4 log units) between the fO_2 indicated by the spinel (more reduced) and the fO_2 given by the whole rock analysis by the equation

$$\ln fO_2 = \left[\ln(X_{melt}^{Fe_2O_3}/X_{melt}^{FeO}) - (\frac{b}{T} + c + \Sigma K_i X_i)\right] \cdot \frac{1}{a} \qquad (9)$$

which is rearranged from Kilinc et al [1983]. In equation 9, a,b,c and d are constants, X = mole fraction, and K_i are empirical constants for each oxide component i. Ultrapotassic rocks may therefore have experienced oxidation during emplacement, and this effect must be allowed for in deducing source conditions.

Diffusion of H_2 out of an ascending magma into the surrounding rock has been proposed by Sato [1978] as a possible oxidation mechanism. H_2 can originate by dissociation of water represented by the equilibrium

$$H_2O = H_2 + 1/2\ O_2 \qquad (10)$$

which will be driven to the right by diffusive H_2 loss. Arculus and Delano [1981] reserved judgement on this model, noting that a spread of oxidation states would be expected in resulting melts due to differing degrees of H_2O dissociation: this is precisely what is seen in the lamproite spinels [Part 2].

In considering oxidation during magma ascent, we have to assume an oxygen fugacity for the source mantle. In H_2O-rich, CO_2-poor conditions suggested by analyses of lamproites, the fO_2 is best represented by the 'CW buffer' (carbon-water) which is the locus of points on the carbon saturation surface where X_{H2O} is a maximum. This lies roughly midway between the IW and WM buffers at temperatures and pressures likely to represent diamond stability in the mantle [Taylor 1985]. There is no direct evidence for the oxygen fugacity of lamproite magmas in the mantle: it is also possible that melt generation is triggered by the introduction of a water-rich volatile phase. This may be more oxidised than CW if not constrained by carbon saturation. In this case the survival of diamonds in lamproites could be attributed to sluggish diamond breakdown reactions.

However, for the following discussion we will assume a starting fO_2 equivalent to the CW buffer in order to assess [a] the oxidation model given by reaction (10), and [b] the relevance of reduced fluids to lamproite petrogenesis. As shown in the following sections, many of the features of lamproites can be explained by a model of a reduced source with oxidation during emplacement. Under these conditions diamonds may be stable in the lamproite source region. This model is limited to the lamproites as CO_2 may be important for Group II rocks, and the applicability of the spinel fO_2 sensor [Part 2] is limited by compositional differences. Whilst this discussion contrasts the extremes of oxidation, a continuum between the two is most realistic for application to natural magmas.

4.4 A MODEL FOR THE Fe2O3/FeO RATIO OF AN ASCENDING LAMPROITIC MAGMA

The following thermodynamic model estimates the amount of H_2O dissociation which would be required to cause an increase in Fe_2O_3/FeO of the order inferred from compositions of phenocrysts [Part 2] which crystallised during emplacement of a lamproitic magma.

Whilst non-volatile components of the liquid and solid phases of a magma are likely to remain relatively constant during ascent, those of the fluid or vapour phase, particularly H_2, are likely to be lost more readily via diffusion and outgassing. The amount of H_2O dissociation which can occur must be affected by the magma ascent rate. The survival of mantle-derived ultramafic nodules and diamonds in some lamproites indicates

that eruption times must be relatively short. The approximation used here that exchange with the surroundings is limited to hydrogen only is more realistic under these conditions because of the fast diffusion rate of H_2. The calculation which follows contains much thermodynamic idealisation, but it is only intended to give an approximate value for H_2O dissociation. It is sufficient to demonstrate that the resulting wt % H_2O dissociated is not unreasonably high and that this mechanism may be realistic for the oxidation of magmas during ascent.

Mo et al. [1982] have determined the partial molar volumes of FeO and $FeO_{1.5}$ in silicate liquids as a function of temperature. Since $\bar{V}_{FeO}$ is less than $\bar{V}_{FeO1.5}$ and noting the relation

$$\left(\frac{\partial \mu_i}{\partial P}\right)_T = \bar{V}_i \qquad (11)$$

FeO will have the lowest chemical potential (μ) at high pressures, and should be favoured over $FeO_{1.5}$ in silicate melts at depth. It is assumed that $\bar{V}_i$ is independent of pressure (ie no compressibility terms).

A melt containing a variable ratio of $FeO_{1.5}/FeO$ is not an oxygen buffer but responds to changes in the intensive parameters P, T, fO_2 etc [Carmichael and Nicholls 1967]. When a magma ascends rapidly from depth two extreme forms of behaviour can be considered, i.e. closed system and open system behaviour. The model presented here considers a limited open system case in which escape of H_2 is the only exchange with the surroundings. In the closed system case, μO_2 of the system will change because of the equilibrium

$$FeO + \tfrac{1}{2}O_2 \rightleftarrows FeO_{1.5} \qquad (12)$$

so that

$$\mu O_2 = 2\mu_{FeO_{1.5}} - 2\mu_{FeO} \qquad (13)$$

The closed system case was considered by Mo et al. [1982] from which they proposed that the oxygen fugacity in the source regions of basic magmas is greater than that at the surface. Calculations from their equations give fO_2 conditions at high pressures several orders of magnitude higher than the MW buffer, which are geologically unreasonable. The implied reduction during transport to the surface is also the opposite of observed crystallisation sequences in spinel and leucite.

In the "limited open system " case considered further here, the intrinsic fO_2 of the system is assumed to be maintained (ie. μO_2 constant) during ascent due to diffusive H_2 loss via the reaction

$$FeO + 1/2\ H_2O = 1/2\ H_2\uparrow + FeO_{1.5} \qquad (14)$$

The closed and open system emplacement paths are contrasted in figure 33a.

A magma originating at depth may have its fO_2 determined by an oxygen buffer reaction in the source region [Ryabchikov et al. 1981, Eggler 1983] such as

$$\underset{\text{olivine}}{6\ Fe_2SiO_4} + O_2 = \underset{\text{spinel}}{2\ Fe_3O_4} + \underset{\text{opx}}{6\ FeSiO_3}$$

or possibly a vapour phase reaction involving graphite (or diamond) plus C-O-H-S vapour [Eggler and Baker 1982, Woermann and Rosenhauer 1985]. During ascent, however, the magma will not be buffered (unless it contains an abundant phenocryst assemblage capable of acting as a buffer; Carmichael and Nicholls 1967) and hence the Fe^{3+}/Fe^{2+} ratio of the melt may change.

In our model system $FeO-FeO_{1.5}-H_2O$ we consider the case of isothermal ascent in which the oxygen potential of the system remains constant. O_2 is gained from the dissociation of H_2O in order to maintain μO_2. Differentiating equation (13) with respect to pressure at constant temperature we get

$$0 = \left(\frac{\partial \mu_{O_2}}{\partial P}\right)_T = \left[\frac{\partial \mu_{FeO_{1.5}}}{\partial P} - \frac{\partial \mu_{FeO}}{\partial P}\right] \qquad (15)$$

Using the standard relation

$$\mu_i = \mu^\circ_i + RT\ln a_i \ , \qquad (16)$$

noting

$$\left(\frac{\partial \ln a_i}{\partial P}\right)_T = V^\circ_i \ , \qquad (17)$$

rearranging and integrating over pressure, we get

$$\ln\left(\frac{a_{FeO}}{a_{FeO_{1.5}}}\right)^{P\ bar} - \ln\left(\frac{a_{FeO}}{aFeO_{1.5}}\right)^{1\ bar} = \frac{V^\circ_{FeO_{1.5}} - V^\circ_{FeO}}{RT}(P-1) \qquad (18)$$

but

$$\ln(\gamma^P_{FeO}/\gamma^1_{FeO}) = \frac{\overline{V}_{FeO} - \overline{V}^\circ_{FeO}}{RT}(P-1) \qquad (19)$$

and similarly for $FeO_{1.5}$ (where γ_i is the activity coefficient of i).

Therefore

$$\left(\frac{X_{FeO}}{X_{FeO_{1.5}}}\right)^{P} = \left(\frac{X_{FeO}}{X_{FeO_{1.5}}}\right)^{1} \cdot \exp\left[\frac{(\overline{V}_{FeO_{1.5}} - \overline{V}_{FeO})}{RT}(P-1)\right] \quad (20)$$

For the calculation X^1_{FeO} and $X^1_{FeO1.5}$ are known, let $X^1_{H2O} = 0$ and applying the mass balance constraint

$$X^P_{FeO} + X^P_{FeO_{1.5}} + X^P_{H_2O} = 1 \quad (21)$$

X^P_{H2O} can be calculated from equation 21 where

$$X^P_{FeO} = \left[\exp\left(\frac{(\overline{V}_{FeO_{1.5}} - \overline{V}_{FeO})}{RT}(P-1)\right) \cdot \left(\frac{X^1_{FeO}}{X^1_{FeO_{1.5}}}\right)\right] \cdot X^P_{FeO_{1.5}} \quad (22a)$$

and

$$X^P_{FeO_{1.5}} = \frac{1 + \frac{1}{2}X^1_{FeO}}{\left[1.5\left(\exp\left(\frac{(\overline{V}_{FeO_{1.5}} - \overline{V}_{FeO})}{RT}(P-1)\right) \cdot \left(\frac{X^1_{FeO}}{X^1_{FeO_{1.5}}}\right)\right) + 1\right]} \quad (22b)$$

The calculation based on the simple FeO-$FeO_{1.5}$-H_2O system may be extended to natural compositions assuming an ideal solution of liquid components so that the activities of FeO, $FeO_{1.5}$ and H_2O may be represented by their mole fractions. In this model H_2O is assumed to act as an "inert dilutant" and does not affect $(\overline{V}_{FeO1.5} - \overline{V}_{FeO})$ of the liquid. The assumption of ideal solution of H_2O rather than setting activity as a function of X^2_{H2O} [cf. Burnham 1979a; Nicholls 1980] is insignificant considering the approximate nature of this calculation, making a difference of only 0.01 wt% H_2O to the result noted below. The emplacement path chosen for a model lamproitic magma (A→B in figure 33b) is from a relatively reduced source. The source condition (A in figure 33b) is at the intersection of CW with the diamond-graphite transition boundary [Kennedy and Kennedy 1976]. For the end-point (B in figure 33b) the oxidation state at near-surface conditions of a melt yielding the glassy olivine leucitite of Gaussberg, Antarctica is chosen, since this is a pristine example of a lamproitic volcanic rock [Part 2]. The Gaussberg composition has a median value for primary lamproite magmas for both surface oxidation state [Part 2] and for wt% FeO, which is the only compositional parameter of

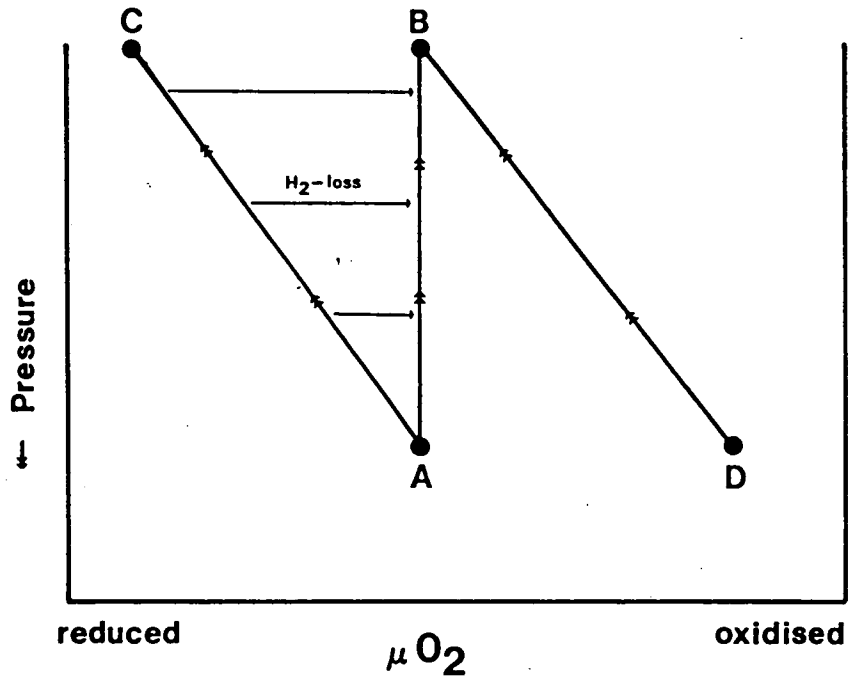
C
B
H_2-loss
← Pressure
A
D
reduced
oxidised
μO_2

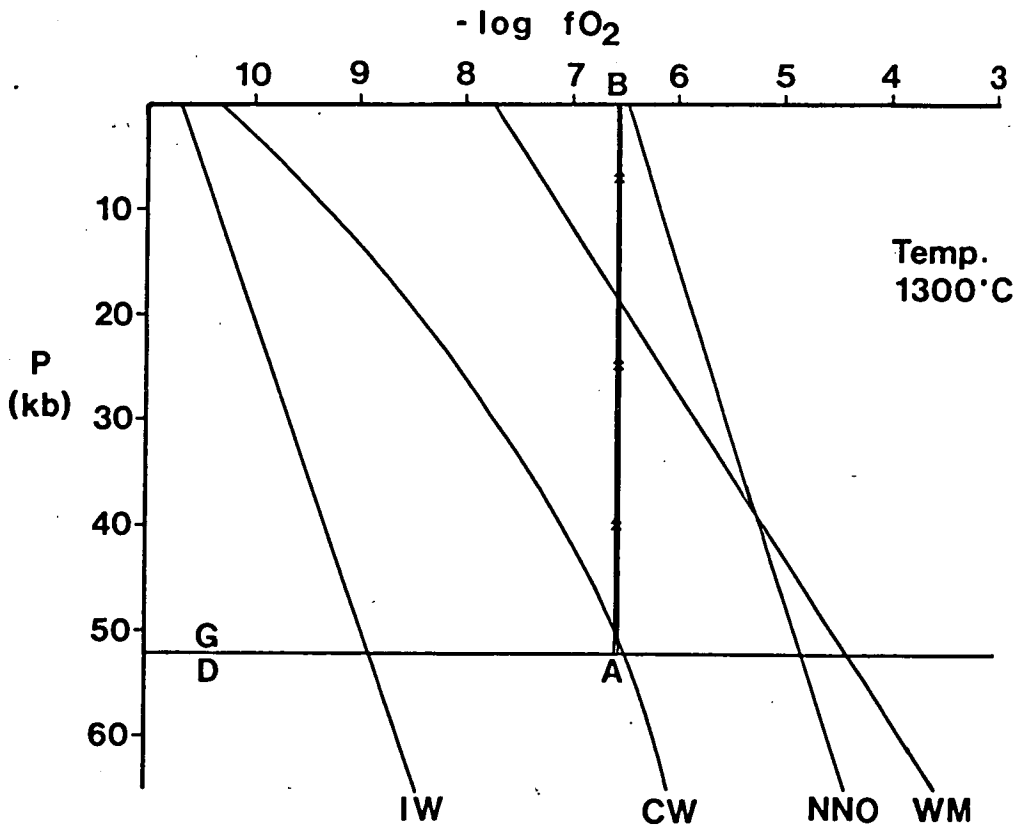
- log fO_2
10
9
8
7
B
6
5
4
3
10
20
30
40
50
60
P
(kb)
Temp.
1300°C
G
D
A
IW
CW
NNO
WM

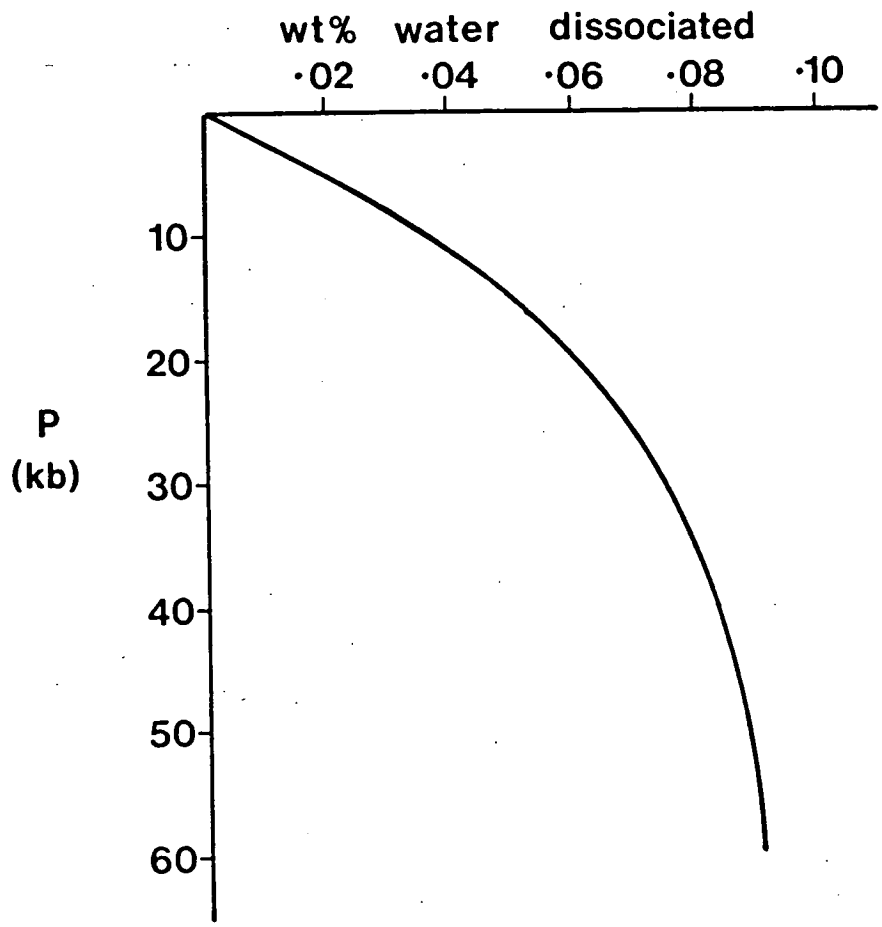

Figure 34: Curve showing the amount of water dissociation required to maintain constant oxygen fugacity with depth. Calculation is made from variation of partial molar volumes of FeO and Fe_2O_3 with pressure in the system $FeO-FeO_{1.5}-H_2O$.

the rock which affects this calculation (total Fe as FeO in Gaussberg = 6% compared to a range of 4-8% for primary lamproites; Barton and Hamilton 1978; Jaques et al. 1984a; Part 1). This is not intended to imply that the Gaussberg magma originated at 52 kbar, indeed it is argued in the next section that the more silicic lamproite magmas originate at much shallower levels. By the above calculation, 0.09 wt% H_2O must dissociate between A (52kbar) and the surface to maintain the fO_2 of the system at 1300°C. The form of the curve in figure 34 indicates that the rate of increase of $FeO_{1.5}/FeO$ will increase towards the surface, with half of the water dissociation occurring in the uppermost 15 kbar. Dissociation of water in the order of 0.1 wt % water does not appear unreasonably high, and is consistent with the 0.07 wt% calculated by Mathez [1984] for oxidation between the iron-wustite and quartz-fayalite-magnetite buffers. This small amount of dissociation will be lessened if the near-surface oxidation by degassing of carbon species proposed by Mathez [1984] also operates.

4.5 GENESIS OF ULTRAPOTASSIC ROCKS WITH A RANGE OF SILICA CONTENTS

The fluorine rich lamproites range in silica content from 40 to 60wt% and, whilst accumulation of olivine and crystal fractionation is important [Jaques et al. 1984a], a range in primary magma silica contents seems likely. West Australian lamproite compositions considered to be primary range in silica content from approximately 40 to 52 wt% [Atkinson et al. 1984; Jaques et al. 1984a]. Primary lamproite magmas from other regions may have even higher silica contents: a Leucite Hills orendite with 55 wt% silica has been found to crystallise olivine, orthopyroxene, clinopyroxene and garnet at its liquidus at 27 kbar, indicating that it may represent a primary melt from the mantle [Barton and Hamilton 1982].

Experimental work on dry compositions and with mixed H_2O+CO_2 volatiles indicates that for the more silicic magmas to be primary, the H_2O/CO_2 ratio would have to be extremely high because of the polymerising effect of CO_2 leading to lower silica partial melts. The presence of HF will assist the formation of silica-rich melts by the process outlined previously, so that the effect of any CO_2 present will be lessened. If conditions are sufficiently reduced for CH_4 to be important rather than CO_2, then this will further assist the production of silica-rich melts.

Compositions with lower silica contents are represented among

Group I and Group II ultrapotassic rocks. Referring to the Ks-Fo-Qz system, there are two ways by which melting of the model phlogopite harzburgite may give rise to silica-undersaturated melts: (i) by increasing CO_2/H_2O, demonstrated by movement of the FO+EN phase boundary (figure 32) or (ii) by increasing pressure. It has been shown in both Ne-Fo-Qz and Ks-Fo-Qz systems that the FO+EN phase boundary moves to more silica-poor compositions with increasing pressure [Kushiro 1968,1980], and that in Mg-poor compositions the phase volume of sanidine also expands [Wendlandt and Eggler 1980a]. Figure 35 illustrates, from the data of Kushiro [1972] and Gupta and Green [in prep.] in the Ne-Fo-Qz system, that this holds for water saturated systems. The same source giving rise to silicic leucite lamproites may therefore produce more silica-undersaturated melts at higher pressures without any difference in volatile composition, i.e. in a CO_2-free mantle. It is not necessary to appeal to widely differing volatile compositions to explain the silica variation in likely primary magmas within a given locality, for example, the West Kimberley lamproite suite. A greater depth of origin for primary olivine lamproite compositions from West Kimberley in a reduced environment is in accord with the occurrence of diamonds being commonest in the Mg-rich, Si-poor lamproites [Atkinson et al. 1984; Jaques et al. 1984a].

The position of the PHL+EN+FO+L peritectic point will depend critically on the stability of phlogopite. Since there can be no phlogopite field in fluorine-free conditions with CO_2 as the only volatile, the composition of the first melt from a model (phlogopite) harzburgite will vary greatly in both SiO_2 content and Ks/Fo ratio with $H_2O/(H_2O+CO_2)$. The liquidus phase field for phlogopite is reduced at moderate $CO_2/(CO_2+H_2O)$ ratios [Ryabchikov and Green 1978; Wendlandt and Eggler 1980c; Arima and Edgar 1983a]. The position for PHL+EN+FO+L under H_2O-saturated conditions given by Sekine and Wyllie [1982] is considered to be erroneous (too low Fo) due to an extensive extrapolation from the low pressure data of Luth [1967]. The data of Gupta and Green [in prep.] at 28 kbar indicate that the phlogopite phase field will be much larger (see figure 32). The large difference in the position of the PHL+FO+EN+L peritectic point at 3 kbar and 28 kbar (figure 32) indicates that the Ks/Fo ratio of melts must be strongly dependent on pressure, but compositions at intermediate pressures can only be estimated due to the lack of data. The argument put forward above that more silica-rich lamproites may originate at shallower depths corresponds to this expected variation in Ks/Fo ratio

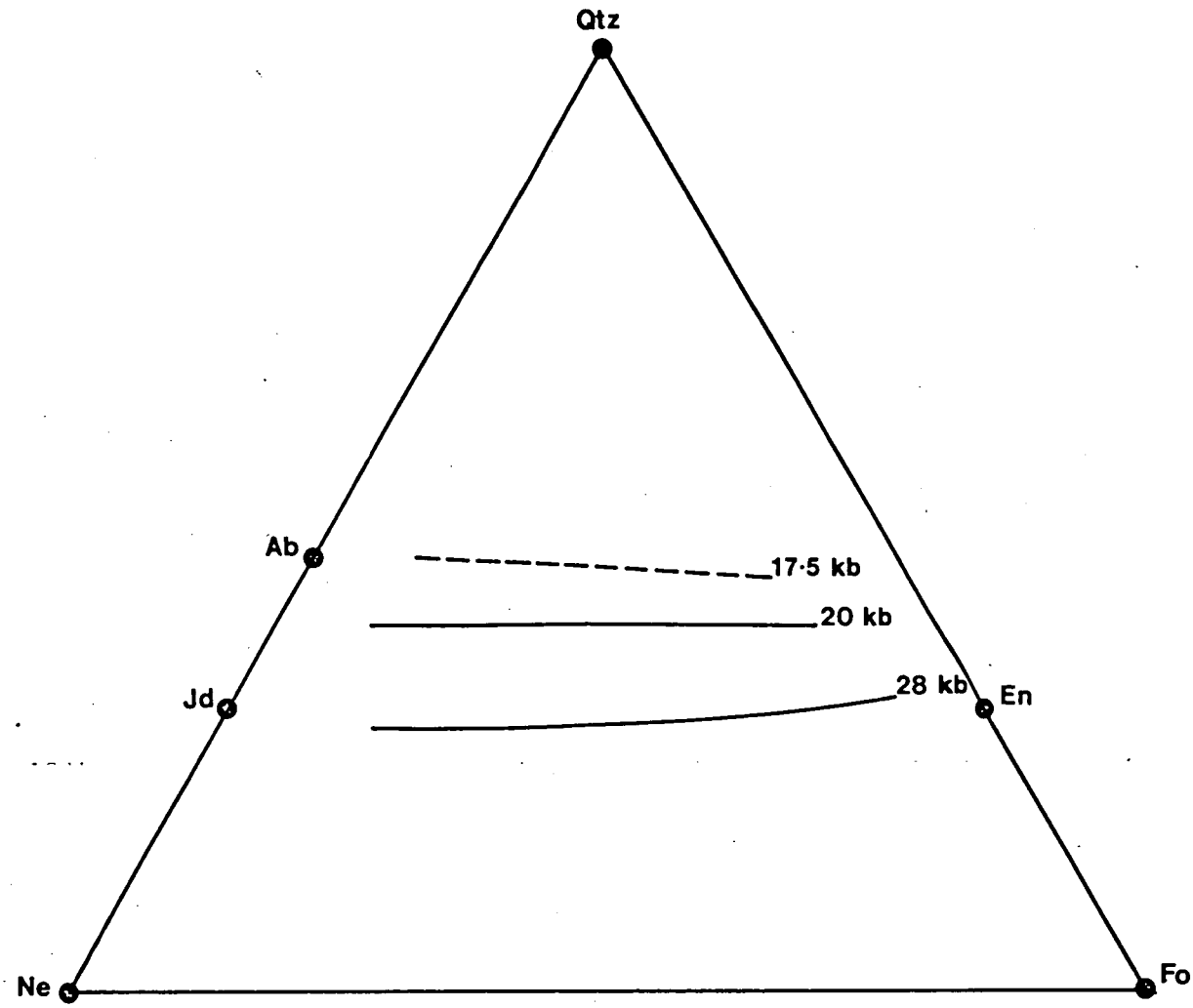

Figure 35: The effect of pressure on the forsterite-enstatite phase boundary in the water-saturated Ne-Fo-Qz system showing shift to more silica-undersaturated compositions at higher pressures. Positions taken from Kushiro [1972: 17.5 and 20 kbar] and Gupta and Green [in prep.: 28 kbar].

with pressure: the Gaussberg olivine leucitite (51 wt% SiO_2) has an MgO content of 8 wt% and K_2O in excess of 11 wt%, whereas typical West Kimberley olivine lamproites (40-43 wt% SiO_2) have MgO in excess of 20 wt% and K_2O of 4-5 wt%, and yet both these lamproite types have high Mg-number and carry mantle-derived nodules. The addition of fluorine to a mixed volatile system will greatly enlarge the phase volume of phlogopite, increasing the Fo/Ks ratio and leading to more magnesian melts regardless of silica content.

These arguments for a reduced source may be more applicable in some regions of lamproite magmatism than others, because lamproites from different localities differ both in their range of probable primary magma compositions and in their oxidation state at near-surface conditions as measured by spinel phenocryst compositions. The variation in spinel phenocryst compositions does not correlate with silica content of the rock in different lamproite regions, indicating that the effectiveness of oxidation during emplacement may differ greatly.

4.6 APPLICATION TO OTHER ULTRAPOTASSIC ROCK GROUPS

The source region for Group II rocks of the Toro Ankole volcanic field was probably poor in H_2O. This is indicated by low H_2O contents of volcanic gases in African Rift volcanoes [Bailey 1978,1980], and by the occurrence of carbonatites in the Toro Ankole field. The Ks-Fo-Qz analogue of a source poor in H_2O and with lower F than Group I rocks (though still F-rich relative to most basaltic rocks) would move initial melts to more Si-poor, K-rich compositions, possibly giving rise to rocks akin to katungite. The oxidation state in the source regions of Western Rift rocks is poorly known, though volcanic gases [Bailey 1978] and dissolved methane of possible volcanic origin in Lake Kivu to the south of the Virunga field (Burke 1963, discussed by Gerlach 1980) may indicate a reduced environment at depth. However, in a reduced environment, carbon saturation should occur at low concentrations so that transportation of carbon in the melt will be limited: a much greater amount of carbon would dissolve in a melt (as carbonate) in a more oxidised environment. A reduced source should therefore result in carbon-poor volcanics regardless of the oxidation state at the surface, unless emplacement takes place as a melt+fluid system, and oxidation of the fluid occurs preferentially. If the source is oxidised, the presence of fluorine will maintain a phlogopite phase field so that melts

will still have an appreciable MgO content.

The above discussion covers, in general terms, the effect of mixed C-H-O-F volatiles on ultrapotassic rock genesis, but does not address differences in source composition, and so cannot hope to explain the origin of the entire spectrum of potassic rocks. A number of experimental studies on ultrapotassic rocks [Arima and Edgar 1983a,b; Ryabchikov and Green 1978; Edgar et al. 1976; Barton and Hamilton 1979] indicate that discussion of a phlogopite harzburgite may be inappropriate for some compositions. This is backed up by studies of ultramafic xenoliths [Lloyd and Bailey 1975; Lloyd 1981] which show that the 'fluid' which supplies K-enrichment to the mantle is reacting with the mantle rocks causing progressive elimination of orthopyroxene and even olivine in favour of mica and clinopyroxene. The observed northward increase in K and decrease in Si of the western rift lavas [Pouclet 1980b] may be related to a northward increase in the 'fluid' component of the mantle source. Studies of such xenoliths provide insight into the K-enrichment processes, and may provide evidence of the nature and oxidation state of volatile mixtures at depth.

4.7 SUMMARY

The effects of H_2O, CO_2, CH_4 and HF on partial melting of a model phlogopite harzburgite mantle have been considered with regard to the production of ultrapotassic magmas. The arguments developed above from evidence in the system Ks-Fo-Qz with added fluorine support the suggestion of Jaques et al. [1984a] that fluorine is an important controlling factor in lamproite petrogenesis. Fluorine has a polymerising effect in H_2O-poor conditions, but in the presence of abundant H_2O where HF than F is dominant, the overall effect is depolymerisation. Methane also dissolves by forming $(OH)^-$ groups, and so has a depolymerising effect.

Group I ultrapotassic rocks (lamproites) probably originate from primary magmas with SiO_2 contents ranging from around 40 wt% to at least 52 wt%. This range can be explained by differing depths of origin from a similar source with a similar reduced H_2O-CH_4-HF volatile mixture, with more silica-poor melts originating at greater depths. The formation of silica-rich initial melts from a model phlogopite harzbugite is assisted by the presence of CH_4 and HF. Dissociation of less than 0.1 wt% H_2O, driven by H_2 loss, is sufficient to cause oxidation during

emplacement to observed oxidation states. Silica-poor ultrapotassic rocks could be produced at higher pressures in a reduced environment, or in an oxidised environment with high $CO_2/(CO_2+H_2O)$ ratios. Group II (African Rift) potassic rocks may originate in H_2O-poor conditions in which fluorine will maintain a large phlogopite phase field, so that initial melts will be magnesian and silica-undersaturated.

The effects of F, C/H ratio and fO_2 on a phlogopite harzburgite analogue as a source for ultrapotassic rocks can be tested by high-pressure experiments on natural ultrapotassic rock compositions with variations in these parameters. Individual areas of ultrapotassic volcanism can then be examined in the light of these experimental studies, combined with information gathered from the rocks themselves on fluid phase composition, oxidation state and pressure-temperature crystallisation path.

PART V

THE GENESIS OF LAMPROITIC MAGMAS IN A REDUCED, FLUORINE-RICH MANTLE

5.1 INTRODUCTION

Lamproites include a range of compositions which have high Mg-number, Ni and Cr contents, and carry mantle-derived ultramafic nodules, and thus appear to represent little-modified mantle-derived liquids. The term lamproite is used here in the sense of Foley et al. [Part 1] as a chemically characterised ultrapotassic rock group with low Ca, Al and Na contents. Primary lamproitic magmas range in silica content from about 40 wt% to at least 51 wt%, and experimental work on a Leucite Hills orendite indicates that leucite lamproites as silica-rich as 55 wt% could be in equilibrium with an olivine-orthopyroxene-clinopyroxene-garnet assemblage at mantle pressures [Barton and Hamilton 1982]. Petrogenetic models must account for this range of apparently primary magma compositions, which may be greater than 10 wt% in a single volcanic field, such as the West Kimberley region of Western Australia [Jaques et al. 1984a].

Previous experimental studies on a variety of alkaline rock compositions, including kimberlites and lamproites, have emphasised the importance of volatile constituents in their genesis. These have shown that a range of SiO_2 contents may be attributed to variation in the H_2O/CO_2 ratio. Experimental studies of both liquidus phase relationships of alkaline rocks and melting of proposed mantle source compositions have shown that H_2O greatly depresses the melting temperature and promotes stability of less polymerised silicate minerals such as olivine relative to orthopyroxene in the mantle residue, leading to more silicic melt compositions [Kushiro 1972; Green 1973a; Nicholls and Ringwood 1973]. The effect of CO_2 is limited at pressures less than ~20 kbar due to its low solubility in silicate melts [Wyllie and Huang 1976], but at higher pressures it has the opposite effect to H_2O of promoting stability of more polymerised silicate phases, leading to lower silica partial melts [Eggler 1974; Brey and Green 1975]. It has been argued from the experimental data that low silica compositions such as olivine melilitites and kimberlites require the presence of CO_2 and carbonates in the source [Green 1976; Eggler 1978; Brey 1978; Wyllie 1978].

However, most lamproites, both silica-rich and silica-poor, have high H_2O, but very low CO_2 contents, so that the H_2O/CO_2 ratio does not appear to be the controlling factor of the composition of most lamproite suites. A number of studies specifically considering the genesis of lamproitic magmas have emphasised the need for high H_2O/CO_2 in the source [Barton and Hamilton 1978,1982; Jaques et al. 1984a]. This contrasts with studies of low-silica ultrapotassic rocks from Uganda (Group II of Part 1) which suggest low or intermediate H_2O/CO_2 [Ryabchikov and Green 1978; Edgar et al. 1980]. Jaques et al. [1984a] and Venturelli et al. [1984] noted the high levels of fluorine in lamproites, and suggested that this may be important in their genesis.

The oxidation state of the mantle has recently been debated widely due to apparently conflicting evidence for either oxidised (~EMOD/EMOG or FMQ) or reduced (~IW to IW+2 log units fO_2) conditions from a variety of sources including intrinsic oxygen fugacity measurements of mantle-derived xenoliths and minerals, volcanic gas compositions in both continental and submarine environments, internal oxygen buffers of proposed mantle mineral assemblages, and studies of inclusions in diamonds [see reviews by Woermann and Rosenhauer 1985; Arculus 1985]. This presents the possibility that some alkaline rocks may originate in a reduced source where C-O-H fluids will consist of CH_4+H_2O mixtures rather than H_2O+CO_2 [Holloway 1981; Taylor 1986a]: a reduced source has been proposed specifically for lamproites by Foley et al. [Part 4]. The possibility of a reduced mantle source has not been treated in experimental work, which has generally had no direct control of fO_2, or has buffered fO_2 indirectly by fH_2 control through noble metal capsules (the "double capsule" method), mostly using the hematite-magnetite buffer.

This paper reports the results of liquidus experiments on two lamproite compositions, one silica-rich and one silica-poor. The starting compositions include fluorine, and the experiments were run in reduced conditions with a C-O-H fluid in order to assess the hypothesis outlined in Part 4 that lamproitic magmas originate by melting of mica-harzburgite in reduced conditions.

5.2 THE REDUCED MANTLE ORIGIN HYPOTHESIS FOR LAMPROITES

Olivine lamproites in Western Australia contain diamonds with a mineral inclusions suite indicating that the diamonds are unrelated to the host lamproite (L.Jaques, D.Ryan, pers. comm.), and showing that diamonds are likely to be stable in the mantle source regions of the lamproites at pressures >45 kbar. For a water-bearing mantle, the maximum fO_2 stability of diamonds can be modelled by CW (carbon-water), which lies midway between IW and EMOD/EMOG at temperatures and pressures likely to exist in the mantle [Taylor and Green 1986a]. Fluid compositions at CW are dominated by H_2O (85-95 mol%), and CH_4/H_2O increases with decreasing fO_2 towards IW, where theoretical and experimental studies show that $CH_4>H_2O$ [Taylor 1986a; Appendix III].

Foley et al. [Part 4] developed the hypothesis that the range of lamproite primary magma compositions can be explained by pressure variation in melting of a reduced mica-harzburgite mantle source in the fO_2 range IW to IW+2 log units due to the effects of the major volatile components H_2O, CH_4 and HF. Methane and HF have similar effects to H_2O on melt structure due to depolymerisation of the aluminosilicate network by OH groups involved in the solution mechanisms of CH_4 and HF [Taylor and Green 1986b; Part 3]. In a system rich in H_2O, CH_4 and HF with no CO_2 to cause competing polymerisation reactions, the production of silica-rich melts such as leucite lamproites is promoted. The range in silica contents of primary lamproite magmas down to those typical of olivine lamproites (40-43 wt%) may correspond to increasing pressure, which is known to cause generation of melts with lower silica contents even in H_2O-rich conditions [Eggler and Wendlandt 1979; Kushiro 1980]. A greater depth of origin for olivine lamproites relative to leucite lamproites is compatible with the commoner occurrence of diamonds in the olivine lamproites.

In simple system experimental studies, fluorine has been shown to increase the stability of mica so that melt compositions saturated in phlogopite, olivine and orthopyroxene, and thus with high K_2O and MgO, may exist at higher temperatures and pressures than in water-rich, fluorine-free conditions [Part 3].

The oxygen fugacity of lamproitic magmas at the time of phenocryst

crystallisation can be estimated from the compositions of chrome-spinels occurring as inclusions in olivine phenocrysts, thereby avoiding any weathering effect on measured whole-rock oxidation state. Estimates of fO_2 by this method range from MW to above NNO for different lamproites Part 2]. The proposition of a reduced source thus requires oxidation during magma ascent: some evidence for this is seen in the Gaussberg leucite lamproite which has leucites with relict cores lower in Fe_2O_3 content than the main leucite phenocryst population. [Part 2]. Foley et al. [Part 4] estimated that dissociation of 0.1 wt% H_2O, driven by diffusive loss of H_2 from the magma, could account for oxidation from fO_2=CW in the magma source region to NNO at the surface. This amount of dissociation would be lower still if carbon species are involved in the oxidation.

5.3 EXPERIMENTAL METHODS

5.3.1 TECHNIQUES:

Experiments were performed in a 0.5 inch (1.27cm) piston-cylinder apparatus using standard techniques and talc or, more rarely, NaCl assemblies. Capsules consisted of a 3mm i.d. Pt or $Ag_{50}Pd_{50}$ outer capsule with two graphite inner capsules (2-2.3mm i.d.) containing sample and iron-wustite mixture respectively. Equilibrium C-O-H fluids (denoted 'CWI' for carbon-water-iron, as they lie between CW and the intersection of the carbon saturation surface with the Fe-FeO buffer) were attained by interaction between [i] CH_4-H_2O fluids produced from a solid source of Al_4C_3+$Al(OH)_3$, leaving residual Al_2O_3, [ii] distilled H_2O (~12% of sample weight) added by microsyringe to the sample capsule, and [iii] the graphite capsules, which also served to prevent loss of Fe to the noble metal outer capsules. Excess carbon is geologically reasonable in reduced conditions since the solubility of reduced carbon in silicate melts is limited to 1000-2000 p.p.m. [Taylor and Green 1986b]. The added water ensured fO_2 conditions close to CW, and the inclusion of the Fe-FeO mixture prevented oxidation beyond CW, but did <u>not</u> buffer oxygen fugacity at Fe-FeO [Appendix III]. Thus the fluid composition, rather than the fO_2, was controlled with the result that fO_2 was bracketed within a narrow range. Fluid compositions lie at the H_2O-rich end of the region where the carbon saturation surface turns towards more methane-rich compositions with a large range in X_{H2O} of the fluid over a limited fO_2 range (figure 36).

The change in shape of the carbon saturation surface with pressure

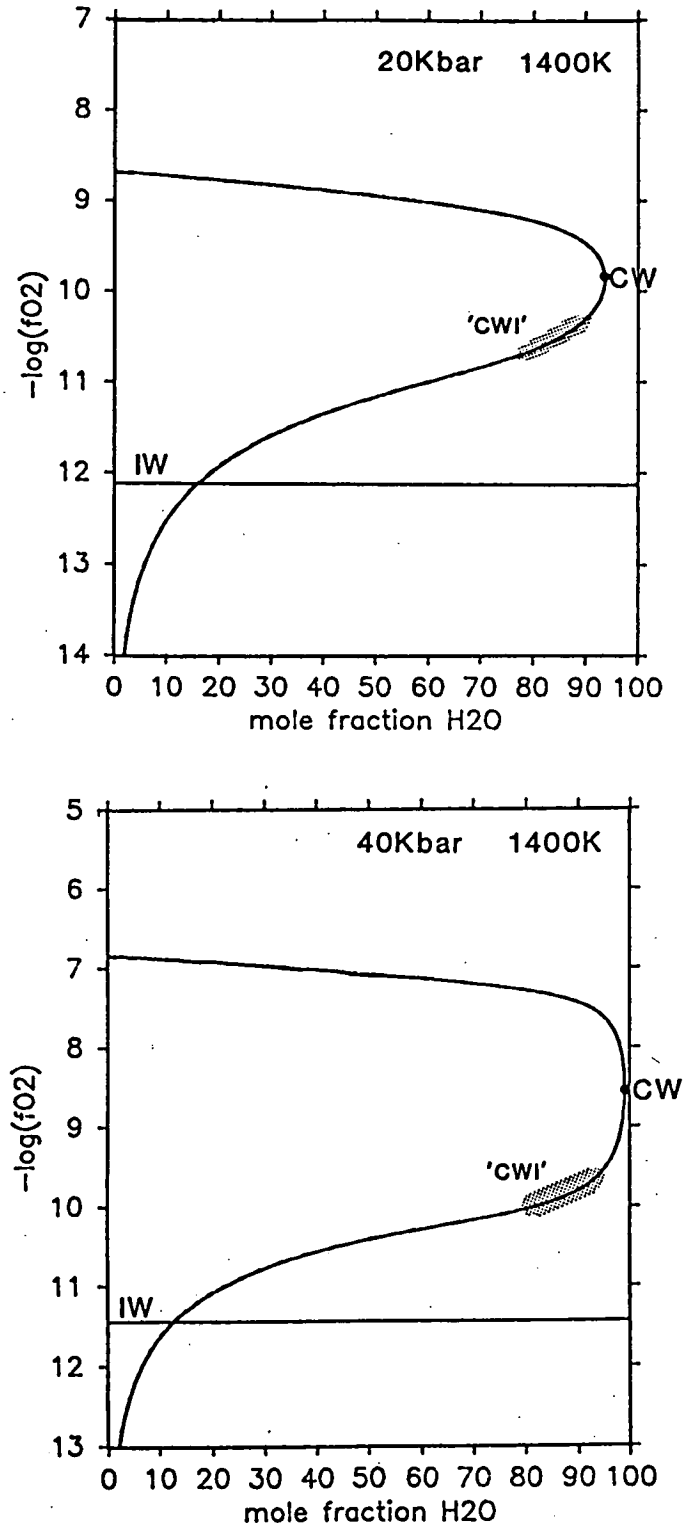

Figure 36

Plot showing the change in X_{H2O} of the fluid phase with oxygen fugacity from calculations in the system C-O-H [Taylor 1986]. Other major fluid constituents are CH_4 at low fO_2 and CO_2 at high fO_2. 'CWI' experiments lie at H_2O-rich fluid conditions at lower fO_2 than the X_{H2O}-maximum (CW), and so are closely bracketed in fO_2. IW = Fe-FeO in text

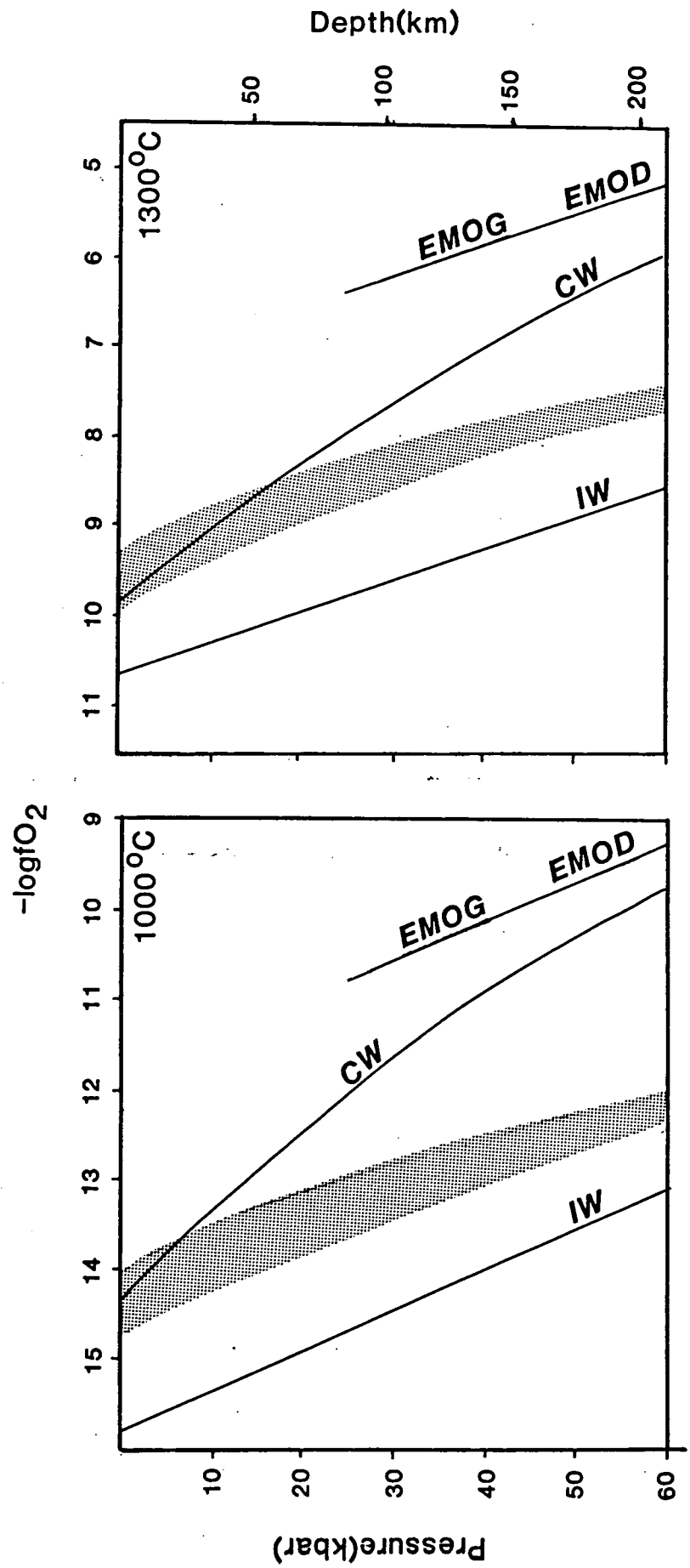

Figure 37

The shaded region indicates the fO_2 region of 'CWI' experiments with respect to common reference buffers and CW. The divergence between the experiments and CW at high pressure is due to increased width of the H_2O-maximum. IW = Fe-FeO in text

and temperature means that the uncertainty in fO_2 of these 'CWI' experiments is less at low temperatures and high pressures where there is a more rapid change in CH_4/H_2O with fO_2. The region of fO_2 in 'CWI' experiments is represented by the shaded region in figure 37, where it is compared to the Fe-FeO and EMOD/EMOG buffers.

Fluid compositions were measured by piercing capsules under vacuum and passing quenched fluids directly into a mass spectrometer. Spectra were collected and integrated over a 35-55 minute period. Measured fluid compositions for 'CWI' experiments were dominated by H_2O (>80 mol%) with minor CH_4 and a trace of CO_2. Details of the experimental and mass spectrometry techniques, plus a discussion of equilibration in experimental systems with C-O-H fluids, are given in Appendix III.

Results of several experiments with a variety of fluid compsitions are included for comparison of phase assemblages with those at 'CWI'. Runs with higher CH_4/H_2O used the same experimental design except that H_2O was not added to the sample capsule. Runs with CO_2+H_2O fluids had oxidised beyond CW due to omission of the second graphite capsule containing the Fe-FeO mixture.

5.3.2 ROCK COMPOSITIONS:

Table 16 lists starting compositions of olivine lamproite and leucite lamproite used in the experiments. The olivine lamproite is a likely primary magma composition for the West Kimberley region estimated by A.L.Jaques after an extensive study of these rocks. The leucite lamproite is from Gaussberg, Antarctica, and is the same composition used in 1 atm. experiments under varying fO_2 conditions apart from a higher Cr_2O_3 content believed to be representative of the primary magma [Part 2]. The Gaussberg composition is similar to many leucite lamproites of the West Kimberley region. The compositions used therefore come from the localities and composition range used by Foley et al. [Part 1] as standard members of the lamproite group.

The compositions were synthesised from oxides (Ti, Al, Mn, Zr, Cr, Ni and part Si and Mg), carbonates (Na, K, Ba, Sr and part Ca), and synthetic $Ca_2P_2O_7$, Fe_2SiO_4 and MgF_2. Components were mixed thoroughly and sintered at 900°C prior to addition of fayalite to ensure all Fe remained as Fe^{2+} for these reduced experiments. Fluorine was added to the rock

Table 16 : Starting compositions of lamproites used in the experiments [normalised to 100%]

	Olivine Lamproite	Leucite Lamproite
SiO2	43.78	51.37
TiO2	3.86	3.45
Al2O3	4.49	9.95
FeO	8.67	6.05
MnO	0.17	0.09
MgO	23.79	8.03
CaO	5.08	4.67
Na2O	0.58	1.67
K2O	5.08	11.76
P2O5	1.64	1.50
BaO	1.75	0.63
SrO	0.15	0.23
ZrO2	0.15	0.14
Cr2O3	0.17	0.10
NiO	0.13	0.03
F	0.53	0.33
Normative compositions:		
Qz	--	--
Or	24.5	54.3
Ns	1.1	3.3
Ks	1.5	4.2
Cpx	11.5	10.7
Opx	7.2	4.7
Ol	40.2	11.3
Ilm	7.3	6.6
Ap	3.9	3.6

composition (as MgF_2 substituted for MgO) rather than to the fluid source because it is known to be strongly partitioned into the melt phase [Wyllie and Tuttle 1964; Koster van Groos and Wyllie 1968; Ishikawa et al. 1980]. No relict MgF_2 was found in any run product, indicating that complete solution had occurred.

5.3.3 MINERAL COMPOSITIONS:

Minerals were analysed using a JEOL JXA 50A electron microprobe fitted with EDAX energy dispersive analyser with operating conditions of 15kV and $7x10^{-10}$A, and calibrated on pure Cu. Fluorine in micas was analysed by crystal spectrometer in an integrated wavelength/energy dispersive system at $5x10^{-8}$A sample current on the same machine using 100sec count time (detection limit 0.15-0.20 wt%) and synthetic sellaite standard.

5.4 EXPERIMENTAL RESULTS

Results described in the following two sections on olivine lamproite and leucite lamproite are from 'CWI' experiments with fO_2 corresponding to the region shown in figure 37. For experiments in this series at pressures at and above 15 kbar measured fluid compositions had H_2O >> CH_4 > CO_2. Lower pressure runs on leucite lamproite are included despite higher CH_4/H_2O and CO/CO_2 contents since X_{H2O} is predicted to decline at lower pressures by the thermodynamic calculations [Taylor 1986]. Figure 38 shows the calculated C-O-H species distributions for CW and C-IW separately; the 'CWI' conditions of the experiments lie between these limits, but are closer to CW at low pressures (see figure 37). 'CWI' fluids at 5 and 10 kbar should therefore be similar to CW but with higher CH_4. Figure 39 illustrates mass spectrometry results for Run 1934 at 5kbar and 1100°C. H_2O/CH_4 was 1.4 in this run, and was measured at 1.7 in Run 1951 at 5 kbar and 1050°C. Higher pressure runs typically have H_2O/CH_4 of between 6 and 10. Figure 39b is a single mass spectrum at the peak of methane release with background N_2 and O_2 stripped to reveal the CO peak at mass 28, which is about three times the intensity of CO_2 (mass 44 plus part 28). In Run 1940 at 10 kbar/1100°C, CO/CO_2 ~0.3, and at higher pressures CO decreases markedly, and CO_2 is also frequently below threshold (see figure 55 in Appendix III), although CO_2 level varies within the range of 'CWI' experiments, with higher values at fO_2 closer to CW.

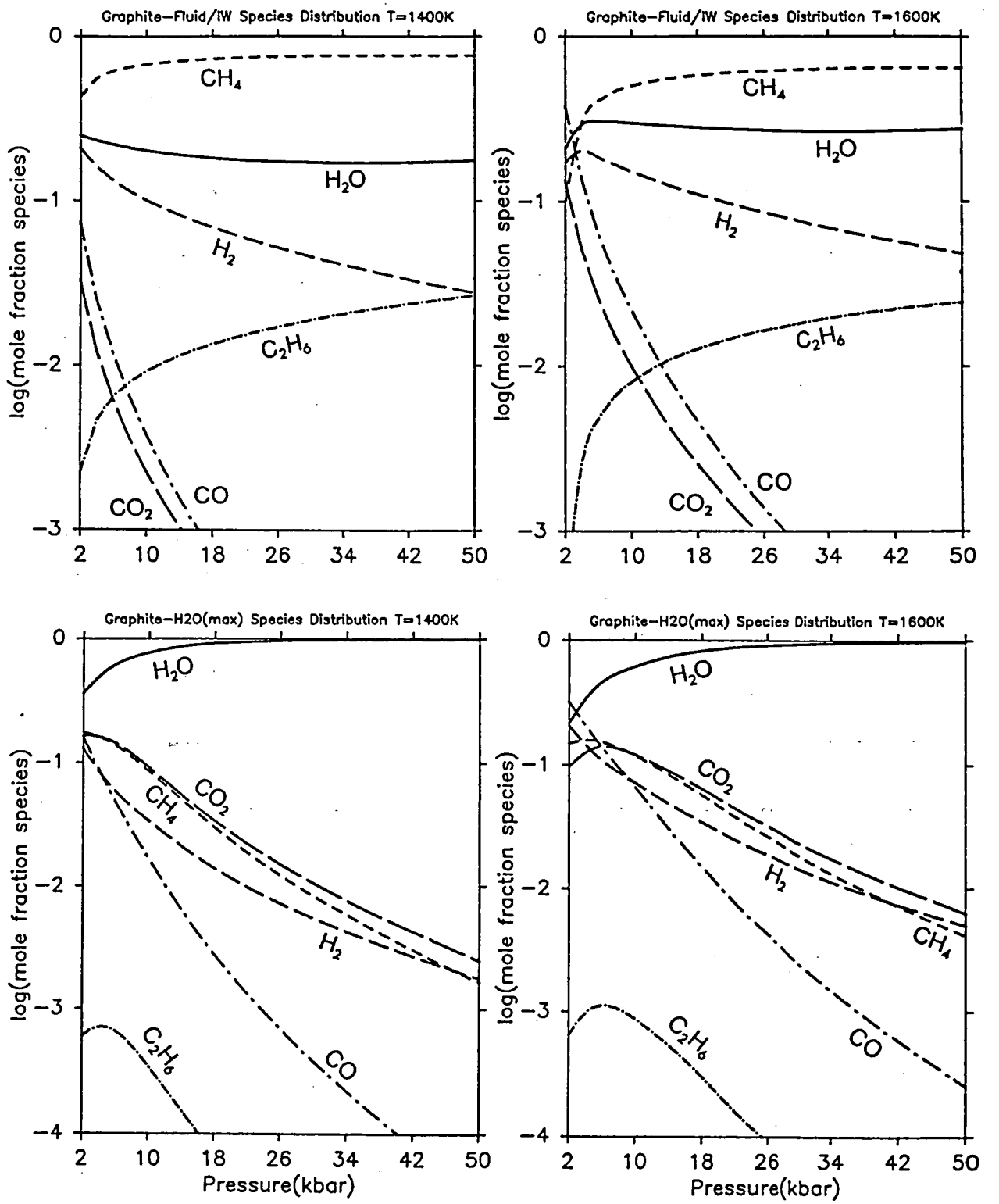

Figure 38

Calculated fluid species distribution in the C-O-H system at IW and CW, showing the large change in species abundance, particularly CH_4 and H_2O, in this fO_2 region. The decrease in X_{H2O} at low pressures at CW is seen as increasing CH_4/H_2O and CO and CO_2 in the experiments.

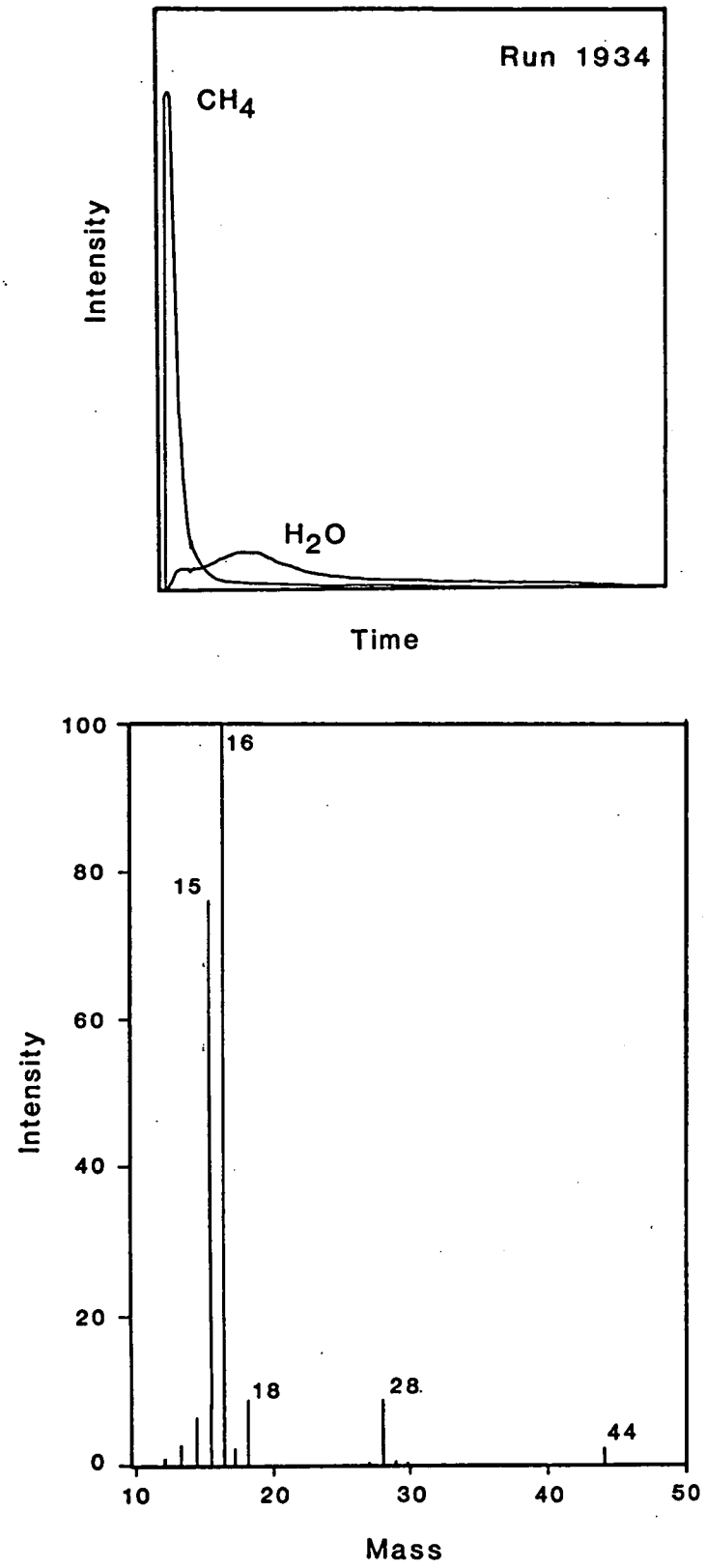

Figure 39

Mass spectra of collected fluid from Run 1934 at 5 kbar/1100°C with leucite lamproite sample. [a] Integrated spectra for H_2O and CH_4 giving H_2O/CH_4=1.4. [b] Single spectrum taken at the peak of CH_4 release: background N_2 and O_2 are stripped to reveal CO>CO_2 (peaks 28 and 44). Note that H_2O (peaks 17 and 18) release is minor at this early stage.

5.4.1 OLIVINE LAMPROITE

Experiments on the olivine lamproite composition were run in the pressure range 20-40 kbar, and results are listed in table 17 and illustrated on a pressure-temperature grid in figure 40. Olivine is the liquidus phase throughout the pressure range studied. It is joined below the liquidus by mica at low pressures, but reacts out to an orthopyroxene+ mica assemblage ~50°C below the liquidus at pressures above 30 kbar. At 20 kbar olivine and mica coexist with liquid for a temperature interval greater than 100°C, below which clinopyroxene, orthopyroxene and magnesian ilmenite appear within 50°C of each other: the order of appearance of these three minerals and their reaction relationships are not known. At higher pressures, chromian rutile replaces magnesian ilmenite as the titanate phase, and has a greater thermal stability. Representative analyses of orthopyroxene, magnesian ilmenite and chromian rutile are given in table 18.

With reference to melting of mica-harzburgite, there is no evidence for such an origin for the olivine lamproite under these experimental conditions at the pressures studied. However, the increasing stability of mica and orthopyroxene with increasing pressure suggests that these minerals may occur at the liquidus at higher pressures, beyond the range of the apparatus used. Figure 41a shows a schematic theoretical liquidus diagram for a partial melt of a mica harzburgite constructed from experimental phase relationships in the system $KAlSiO_4$ - Mg_2SiO_4 - SiO_2 with H_2O or F [Gupta and Green 1987; Part 3]. Consider a partial melt produced at pressure b at the peritectic point X (FO+PHL+EN+L) in figure 41b. This point is a unique pressure-temperature point at which mica, olivine and orthopyroxene occur together at the liquidus. The topologies for lower and higher pressures (a and c) are estimated from the known pressure effect in this system [Part 4]. For pressure a, composition X lies in the olivine liquidus phase field (figure 41b) and thus olivine will be the liquidus phase (figure 41a). Similarly, orthopyroxene will be the liquidus phase at pressure c.

The occurrence of olivine as the liquidus phase of olivine lamproite is therefore consistent with an origin by melting of a mica-harzburgite at higher pressures: the 40 kbar data of figure 40 can be represented by pressure a in figure 41a. The mica+olivine+orthopyroxene liquidus assemblage is interpreted to lie at between 45 and 55 kbar, which is

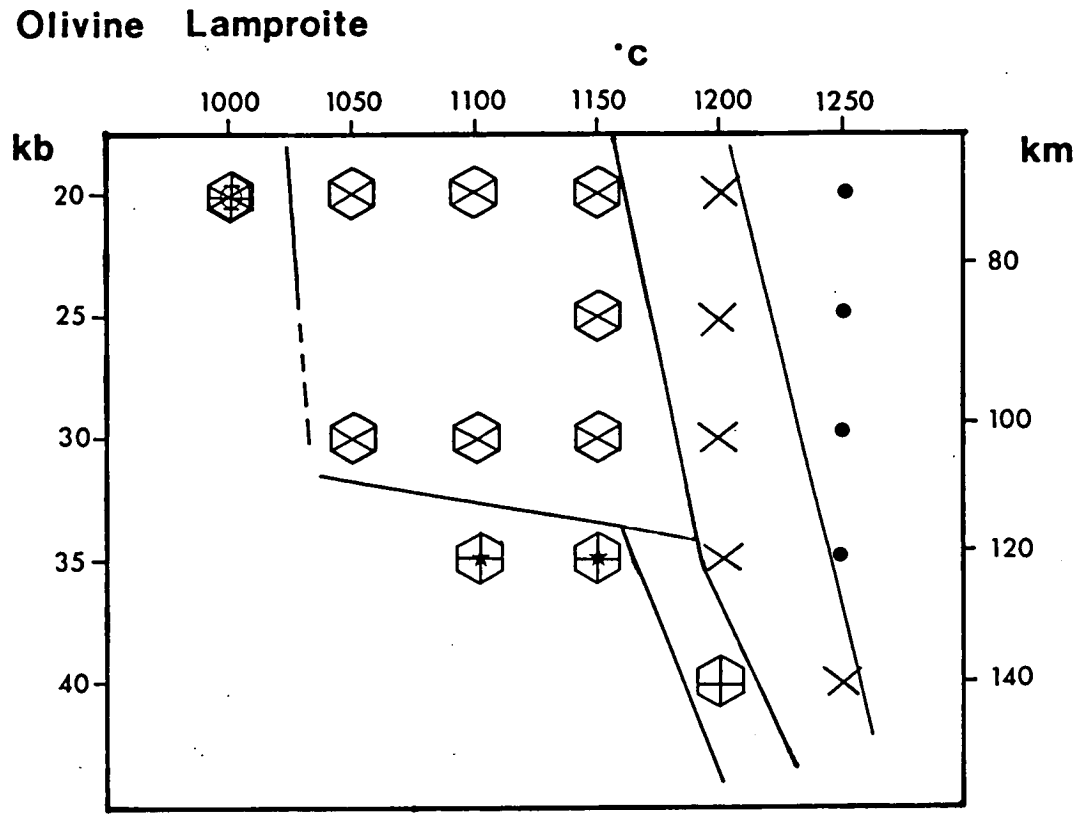

Figure 40

Pressure-temperature grid of olivine lamproite experimental results. ● = liquid only; x = olivine; + = orthopyroxene; ⬡ = mica; * = rutile; I = magnesian ilmenite; o = clinopyroxene.

Table 17 : Experimental run data for Olivine Lamproite at 'CWI'
H_2O/CH_4 is measured ratio in the quenched fluid by mass spectrometry. Experiments marked [*] have no quantitative measurement of H_2O/CH_4 as they were run during development of the fluid measuring technique. CH_4 was detected and the experiments were run with the same capsule assembly and starting materials, and so these are comparable to experiments with measured H_2O/CH_4.

Run	Capsule	Pressure [kbar]	Temp. [°C]	Duration [hr]	H_2O/CH_4	Run products
1891	AgPd	40	1200	2	5	Opx + Mica + L
1892	AgPd	40	1250	2	*	Ol + L
1885	AgPd	35	1100	3.5	6	Opx + Mica + rut + L
1888	AgPd	35	1150	2.5	6	Opx + Mica + rut + L
1679	Pt	35	1200	2	*	Ol + L
1681	Pt	35	1250	2	*	L
1645	Pt	30	1150	2	*	Ol + Mica + L
1906	AgPd	30	1050	10	5	Ol + Mica + L
1677	Pt	30	1250	2	*	L
1791	Pt	30	1200	22	9	Ol + L
1695	Pt	30	1100	2	*	Ol + Mica + L
1653	Pt	25	1150	2	*	Ol + Mica + L
1655	Pt	25	1200	2	*	Ol + L
1676	Pt	25	1250	2	*	L
1659	Pt	20	1200	2	*	Ol + L
1663	Pt	20	1150	2	*	Ol + Mica + L
1670	Pt	20	1250	2	*	L
1711	Pt	20	1100	2	*	Ol + Mica + L
1835	AgPd	20	1050	10	10	Ol + Mica + L
1846	AgPd	20	1000	20	8	Ol+Mica+Opx+Cpx+Ilm+L

Table 18 : Representative compositions of magnesian ilmenite, chromian rutile and orthopyroxene from olivine lamproite experiments.

Mineral	opx	opx	rutile	rutile	ilm	ilm
Run	1891	1891	1885	1885	1846	1846
Press [kb]	40	40	35	35	20	20
Temp.[°C]	1200	1200	1100	1100	1000	1000
SiO2	57.52	57.50	--	--	--	--
TiO2	--	--	91.31	91.29	55.13	55.58
Al2O3	1.61	1.27	1.31	1.46	--	--
Cr2O3	--	--	2.80	2.29	0.84	0.91
Fe2O3	--	--	--	--	3.72	3.28
FeO	5.83	6.36	1.54	1.46	26.74	27.49
MgO	34.42	34.19	0.41	0.40	12.52	12.45
CaO	0.53	0.68	--	--	--	--
MnO	--	--	--	--	0.27	0.29
Mg-number	91.3	90.6				

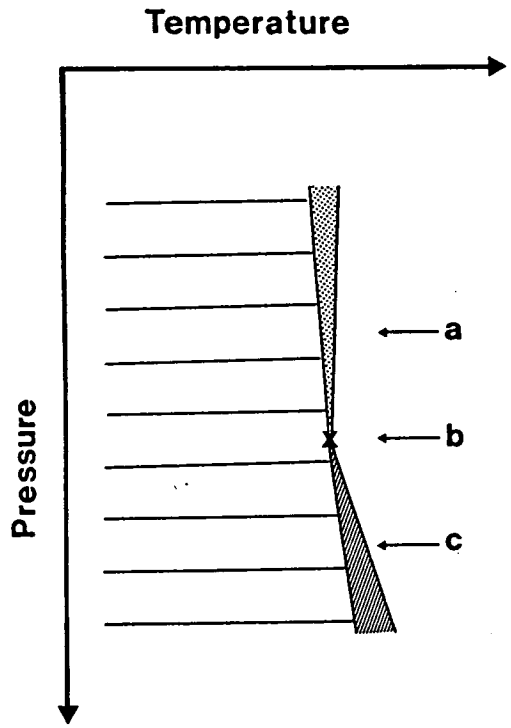
Temperature
Pressure
a
b
c

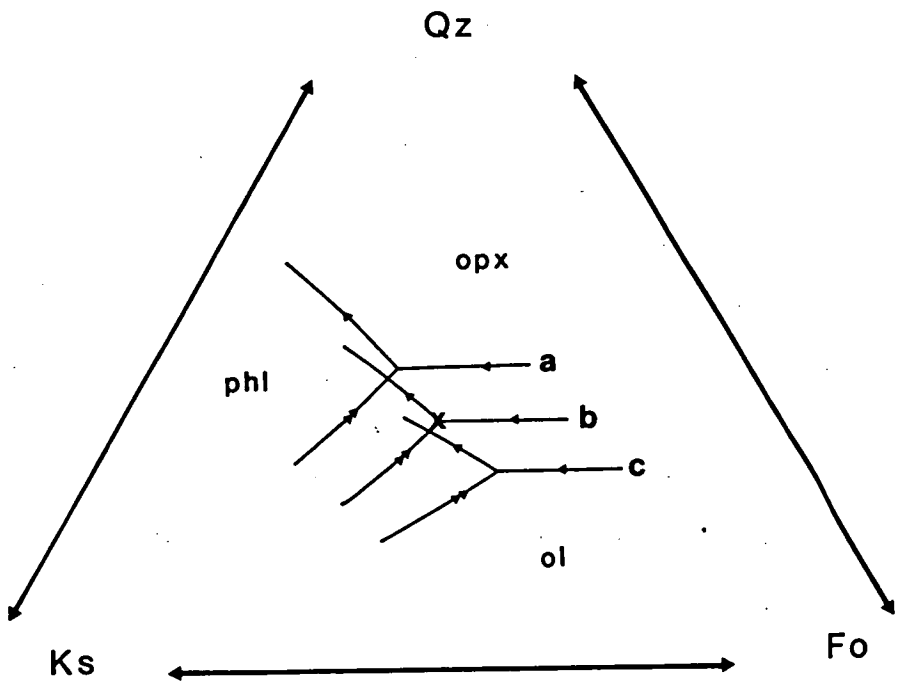
Qz
opx
phl
a
b
c
ol
Ks
Fo

consistent with the occurrence of diamonds in olivine lamproites, as the graphite-diamond transition boudary lies at 51-52 kbar at 1250-1300°C [Kennedy and Kennedy 1976].

5.4.2 LEUCITE LAMPROITE

Experiments on the leucite lamproite composition were run between 5 and 35 kbar, and results are given in table 19 and illustrated in figure 42. Three individual liquidus minerals appear in this range: olivine, mica and orthopyroxene with increasing pressure, but no point with the three together at the liquidus is seen. Clinopyroxene occurs in only one experiment at 5 kbar/1050°C; the extrapolation towards latm is only approximate as it is based on the experiments of Part 2, which were anhydrous. The dotted line marks the approximate leucite-out curve with a similar extrapolation using the results of Part 2. Barton and Hamilton [1978] discovered that leucite stability is restricted to <0.5 kbar in a Leucite Hills orendite in water-saturated conditions. The high pressure stability limit may be slightly greater under 'CWI' conditions as X_{H2O} is slightly lower, and leucite pressure stability is strongly dependent on H_2O content [Gupta and Yagi 1980], although the low fO_2 will not favour leucite [Part 2].

Rutile is the only titanate phase occurring in the leucite lamproite experiments and is restricted to high pressures in the temperature range studied. A large increase in the thermal stability of rutile occurs between 30 and 35 kbar, which is the same pressure interval as in the olivine lamproite. The appearance of rutile in the leucite lamproite is not correlated with the disappearance of olivine as in the olivine lamproite. However, magnesian ilmenite is the only titanate coexisting with olivine in any of the lamproite experiments [cf. Green and Ringwood 1967, p.800]. Representative analyses of orthopyroxene and rutile are listed in table 20.

Although there is no point at the liquidus where olivine, orthopyroxene and mica coexist for the leucite lamproite composition, the phase relationships can be interpreted to indicate an origin by melting of mica-harzburgite if allowances are made for minor fractional crystallisation or conditions of melting. Once again, there should theoretically be a unique pressure for a primary magma, at which the three mica-harzburgite phases coexist at the liquidus as in figure 41. It is not

Leucite Lamproite

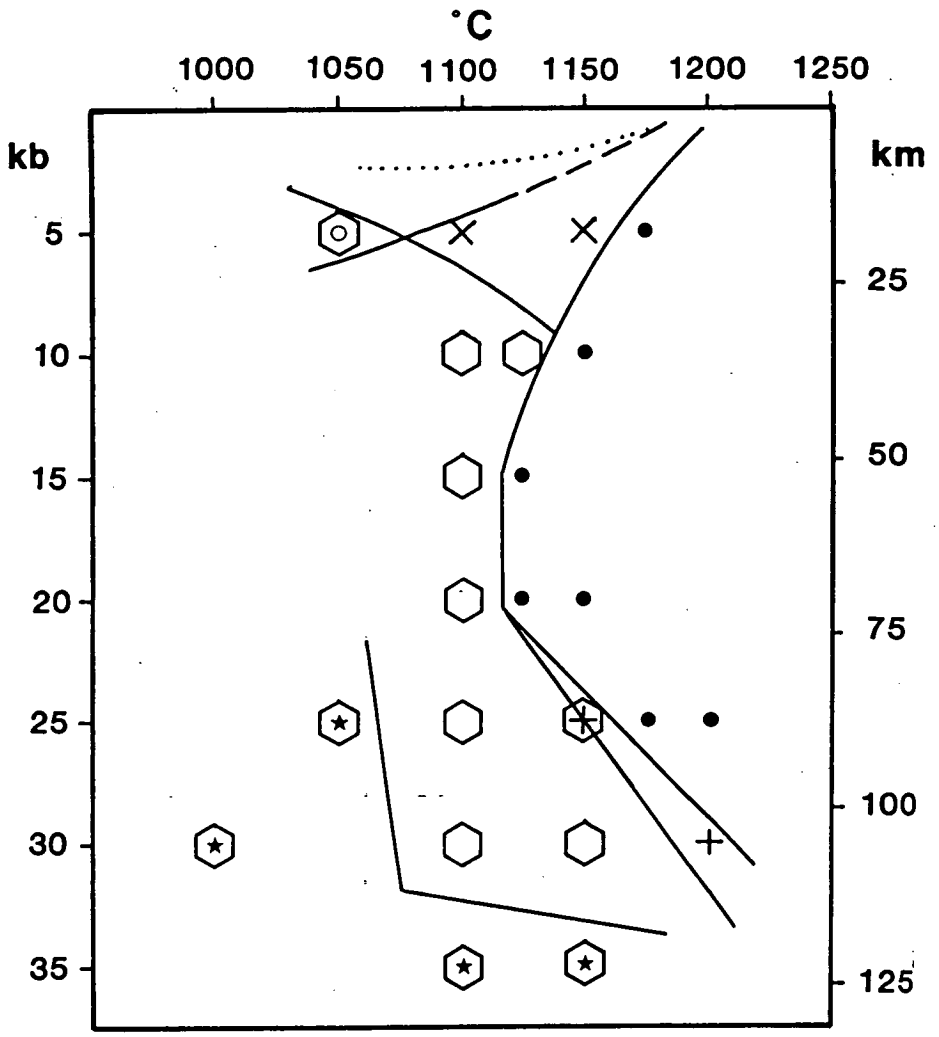

Figure 42

Pressure-temperature grid of experimental results on leucite lamproite. ⬡ = mica; x = olivine; + = orthopyroxene; * = rutile; o = clinopyroxene; ● = liquid only. Dotted line marks approximate position of the leucite-out curve.

Table 19 : Experimental run data for Leucite Lamproite at 'CWI'
* = qualitative fluid determination only [see table 17]

Run	Capsule	Pressure [kbar]	Temp. [°C]	Duration [hr]	H_2O/CH_4	Run products
1866	AgPd	35	1150	3.5	7	Mica + rut + L
1870	AgPd	35	1100	3.5	*	Mica + rut + L
1715	Pt	30	1150	2	*	Mica + L
1716	Pt	30	1100	2	*	Mica + L
1877	AgPd	30	1200	2.5	6	Opx + L
1879	AgPd	30	1000	6.5	10	Mica + rut + L
1738	Pt	25	1100	2	4	Mica + L
1863	AgPd	25	1150	2.7	8	Mica + Opx + L
1869	AgPd	25	1050	5	7	Mica + rut + L
1898	AgPd	25	1175	2	5	L
1909	AgPd	20	1150	2	9	L
1913	AgPd	20	1125	2.5	6	L
1731	Pt	20	1100	2	7	Mica + L
1918	AgPd	15	1100	2	4	Mica + L
1921	AgPd	15	1125	2	7	L
1940	AgPd	10	1100	2	9	Mica + L
1947	AgPd	10	1125	2	8	Mica + L
1950	AgPd	10	1150	2	7	L
1934	AgPd	5	1100	2	1.4	Ol + L
1936	AgPd	5	1150	2	*	Ol + L
1946	AgPd	5	1175	2	2	L
1951	AgPd	5	1050	3.5	1.7	Ol + Cpx + Mica + L

Table 20 : Representative analyses of orthopyroxene and rutile from leucite lamproite experiments

Mineral	opx	opx	rutile	rutile
Run	1877	1877	1879	1879
Press [kb]	35	35	30	30
Temp [°C]	1100	1100	1000	1000
SiO2	56.96	56.81	--	--
TiO2	--	0.31	91.61	91.50
Al2O3	1.45	1.41	1.60	1.57
Cr2O3	0.52	0.38	2.59	2.85
FeO	7.95	8.01	1.17	1.36
MgO	31.86	31.48	--	--
CaO	1.26	1.59	0.15	--
Mg-number	87.7	87.5		

reasonable to propose that the olivine liquidus field remains narrower than 25°C for >10 kbar, which is required for it to fall between the points determined. The appearance of mica alone at the liquidus over this pressure range can be reconciled with the mica-harzburgite melting model by either of the following scenarios:

[1] The composition is not primary, but has crystallised, and subsequently lost, a small amount of olivine at high pressures. This explanation is illustrated in figure 43, and requires removal of melt from the source and emplacement through some pressure interval (b-->a) without substantial cooling. This causes olivine to crystallise from the original composition, followed by mica crystallisation and olivine resorption (figure 43b). The liquid composition will then leave the PHL+EN+L phase boundary and pass onto the mica liquidus surface either by fractional crystallisation of olivine or by complete resorption of olivine. The latter is more likely the smaller the interval between pressures a and b, since a smaller amount of olivine will need to be resorbed. It is not possible to determine whether or not olivine fractionation must occur, since this depends on the precise direction of movement of the peritectic point with pressure. However, if this movement causes virtually no difference in silica saturation (i.e. it approximately parallels the SAN-FO join), then olivine fractionation becomes necessary.

[2] The experiments may contain more water than natural melting conditions. If the excess of H_2O has the effect of expanding the liquidus phase volume of phlogopite, then the leucite lamproite may represent a primary liquid but will fall in the phlogopite liquidus phase field (figure 44) due to inappropriate experimental conditions.

In either of the above scenarios, the pressure at which multiple saturation in mica, orthopyroxene and olivine occurs cannot be much greater than 20 kbar as constrained by the kink in the liquidus in figure 42, and the difference between the true primary and experimental compositions is very small or none.

A major difference between the leucite lamproite and olivine lamproite P,T diagrams is the presence of a subliquidus field of mica in the leucite lamproite with no coexisting crystalline phases at pressures where the liquidus field is olivine, mica or orthopyroxene. This can be

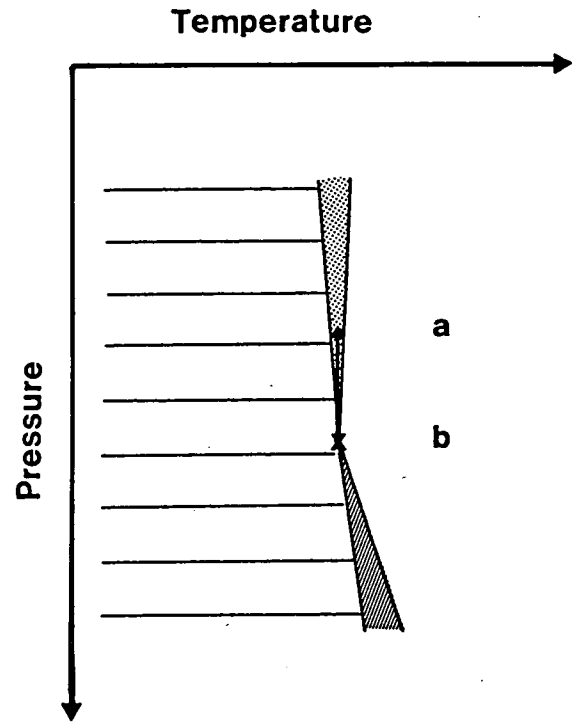
Temperature
Pressure
a
b

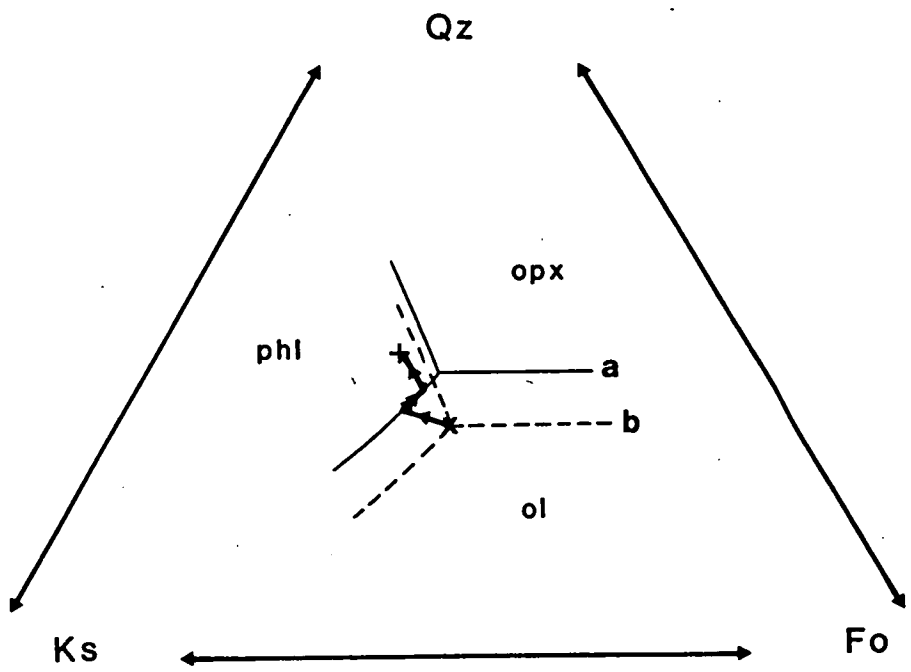
Qz
opx
phl
a
b
ol
Ks
Fo

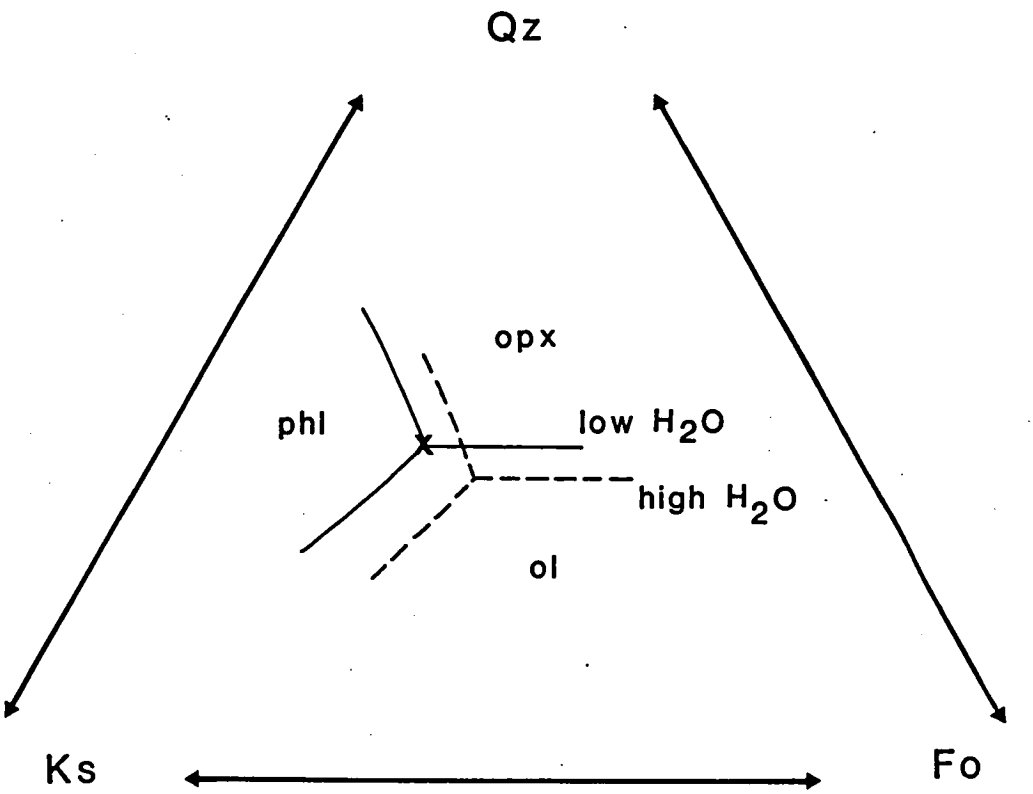

Figure 44

An alternative explanation for the mica liquidus phase field in figure 42. If the experiments contain more water ("high H_2O") than the original source ("low H_2O"), and if the excess water causes expansion of the phlogopite phase volume, then the bulk composition (X) will lie in the phlogopite liquidus phase field at the pressure of origin.

explained with reference to the Ks-Fo-Qz system in figure 45, into which the experimentally determined positions for the PHL+FO+EN+L peritectic point in water saturated conditions at 3 kbar [Luth 1967] and 28 kbar [Gupta and Green 1987] are plotted. The approximate positions for recast normative compositions of the experimental leucite lamproite and olivine lamproite compositions are also plotted, and marked as ~20 kbar and ~50 kbar "water-rich" (i.e. 'CWI') positions. The positions of the natural rock and simple system compositions are not directly comparable since the entire analyses of the rock compositions have not been recast (e.g. 10-11% normative ilmenite+apatite), but are intended to show the effect of pressure on the movement of the peritectic point. Both natural rock and simple system compositions show that increasing pressure strongly affects the Mg-content of melts at the peritectic point, but does not greatly modify the degree of silica saturation for pressures of 20 kbar and above. Taking the positions plotted as a guide, and once again considering theoretical melting of mica-harzburgite, the occurrence of mica alone or mica + orthopyroxene at subliquidus temperatures in the liquidus phase diagram of the resulting melt depends on the orientation of the phlogopite+enstatite phase boundary with respect to the phlogopite-enstatite join. For olivine lamproite [~50 kbar "water-rich"], the tangent to the PHL+EN boundary cuts the PHL-EN join and thus mica and orthopyroxene will both crystallise. In the case of leucite lamproite [~20 kbar "water-rich"], the tangent cuts the extension of the PHL-EN join at point b, indicating peritectic crystallisation of mica and dissolution of enstatite [Morse 1980], leading to the appearance of a mica+liquid field at subliquidus temperatures.

The results of these experiments can be taken to support the hypothesis of Foley et al. [Part 4] that the two lamproite compositions, representing the range of primary lamproite compositions, may be derived by melting of mica-harzburgite in reduced conditions with pressure as the major control on melt composition. The results suggest a range in pressure of 20 kbar for leucite lamproites to 50 kbar or more for olivine lamproites. Olivine lamproites with lower normative olivine contents than the experimental composition may therefore originate by melting at intermediate pressures.

5.4.3 EXPERIMENTS WITH VARIABLE FLUID COMPOSITIONS

Several experiments had fluid compositions which deviated from the H_2O-rich 'CWI' conditions, and thus give some indications as to how the

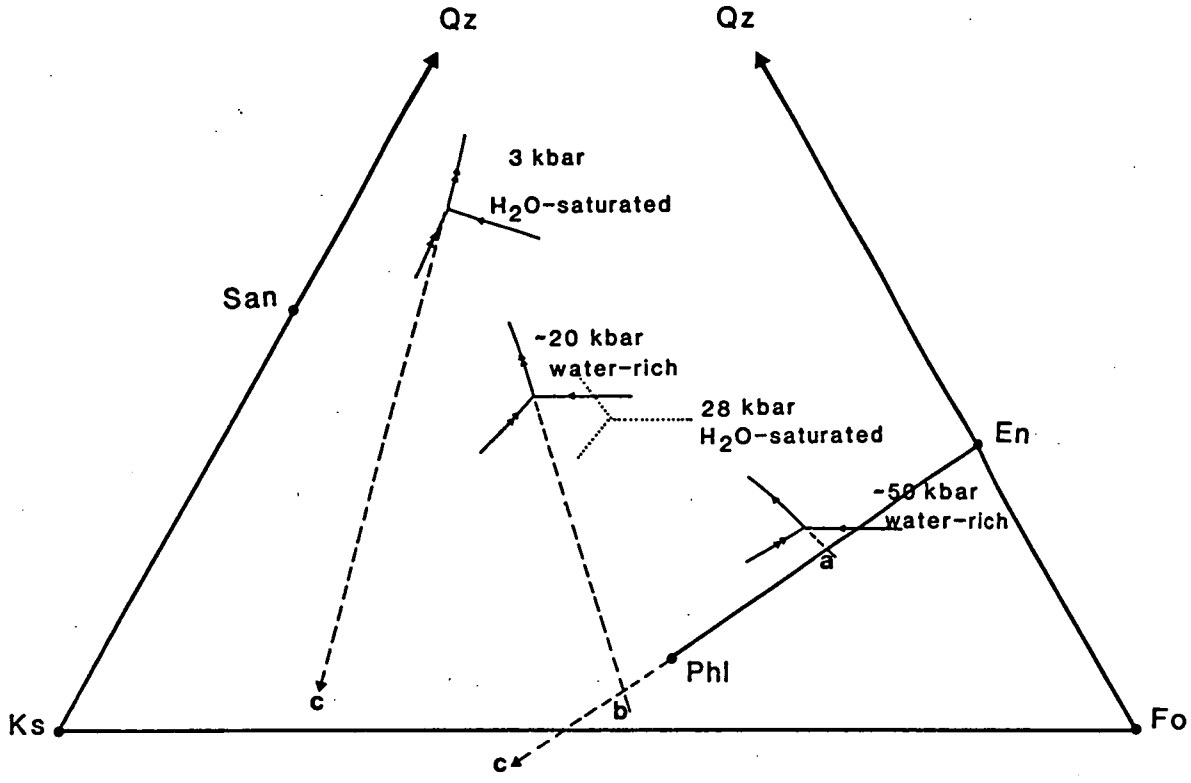

Figure 45

Schematic diagram illustrating the difference in subliquidus phase assemblages between the two lamproite compositions. Positions for the peritectic points Fo+En+Phl+L at 3 kbar and 28 kbar are from the experimental results of Luth [1967] and Gupta and Green [1987]. Approximate positions for recast normative compositions of leucite lamproite and olivine lamproite are shown as "~20 kbar" and "~50 kbar" respectively. The tangent to the En+Phl phase boundary cuts the En-Phl join for olivine lamproite (a), indicating crystallisation of both En and Phl below the liquidus at the pressure of melting. The tangent for the leucite lamproite composition cuts the extension of the En-Phl join, explaining the presence of a field of Phl+L at subliquidus temperatures in figure 42.

phase relationships of the lamproites vary with fluid composition. Results are listed in table 21 together with 'CWI' results at the same pressure-temperature conditions for comparison. These experiments include both fluids with higher CH_4/H_2O (fO_2 lower than 'CWI') and H_2O+CO_2 mixtures in which CH_4 is absent or present in very low abundances (higher fO_2). In the latter case, the CO_2/H_2O ratio is listed in the fluid composition column of table 21, and marked with an asterisk.

The effect of variable CH_4/H_2O on phase relationships follows the behaviour expected from variation in X_{H2O}. In runs at 20 kbar/1050°C, an increase in CH_4/H_2O causes an increase in thermal stability of the five-phase mineral assemblage seen at 1000°C in H_2O-rich conditions. At higher pressures, the liquidus temperature is seen to be very sensitive to CH_4/H_2O of the fluid: Run 1807, with CH_4/H_2O=0.3 compared to the more usual 0.1-0.15 of 'CWI' runs, crystallised olivine at 30 kbar/1300°C, an increase of >50°C in the liquidus temperature.

The greatest range in CH_4/H_2O of experiments at a single pressure and temperature has been obtained for 30 kbar/1200°C, for which phase assemblages are pictured as back-scattered electron images in figure 46. The large olivine plus quench mica assemblage pictured in figure 46a is typical of the olivine liquidus phase field in olivine lamproite. With an increase in CH_4/H_2O the assemblage changes through olivine+mica+quench (figure 46b) to the five phase assemblage seen only at temperatures lower by 200°C in water-rich runs. The high degree of crystallinity and small grain size show the CH_4-rich run to be well below the liquidus. In this run, mica is still present despite the low H_2O content due to the presence of fluorine. The CH_4/H_2O ratio of Run 1799 (figure 46c) indicated fO_2=IW [Appendix III].

Partial analyses of micas from the CH_4-rich (1799) and H_2O-rich (1795) runs are compared in table 22. Fluorine contents are higher in the methane-rich run but are still quite low due to the abundance of fluid relative to the fixed fluorine content of the starting composition. The correlation of decreasing Al with increasing F is also seen in simple system experiments with fluorine and water [Part 3], and is particularly important for melting of mica-bearing mantle to produce lamproites. The fluorine-rich micas are perpotassic (K>Al), unlike the fluorine-poor micas, suggesting that melting of a fluorine-rich source will give rise

Table 21 : Experimental results indicating variation in phase relationships with fluid composition
OL = Olivine lamproite; LL = Leucite lamproite

Run	Comp.	Pressure [kbar]	Temp. [°C]	Duration [hr,min]	Fluid CH_4/H_2O (CO_2/H_2O)"	Run products
1835	OL	20	1050	10	0.1	Ol + Mica + L
1832	OL	20	1050	10	0.42	Ol + Mica + L
1821	OL	20	1050	10	1.8	Ol+Mica+Opx+Cpx+Ilm+L
1750	OL	30	1150	24	1.0	Opx + Mica + L
1645	OL	30	1150	2	0.2	Ol + Mica + L
1799	OL	30	1200	6	2.7	Ol+Mica+Opx+Cpx+Ilm+L
1795	OL	30	1200	6	0.5	Ol + Mica + L
1791	OL	30	1200	22	0.2	Ol + L
1876	OL	30	1200	2	0.35 "	Ol + Opx + L
1807	OL	30	1300	3	0.3	Ol + L
1857	LL	20	1150	2	6 "	Mica + Opx + Cpx + L
1860	LL	20	1150	2	0.16(CO_2>CH_4)	Mica + Cpx + L
1909	LL	20	1150	2	0.14(CH_4>CO_2)	L

Table 22 : Partial analyses of micas from experiments at the same temperature and pressure but with differing fluid composition.
[c] = cations per 22 oxygen

Run	1799	1799	1795	1795
Press [kb]	30	30	30	30
Temp [°C]	1200	1200	1200	1200
CH_4/H_2O [fluid]	2.7	2.7	0.5	0.5
SiO2	40.17	40.29	42.18	42.04
Al2O3	10.46	10.11	13.10	12.96
F	1.12	1.22	0.73	0.73
Mg-number	86.4	87.3	89.0	89.4
Si [c]	5.85	5.81	5.90	5.90
Al [c]	1.80	1.72	2.16	2.14

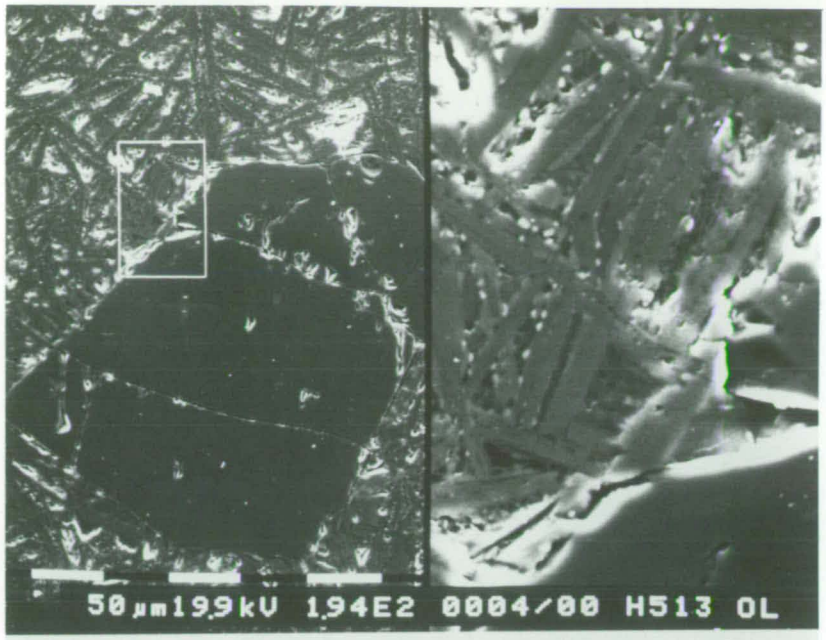
50µm19.9kV 1.94E2 0004/00 H513 OL


0.1mm19.9kV 8.45E2 0001/00 T-1795

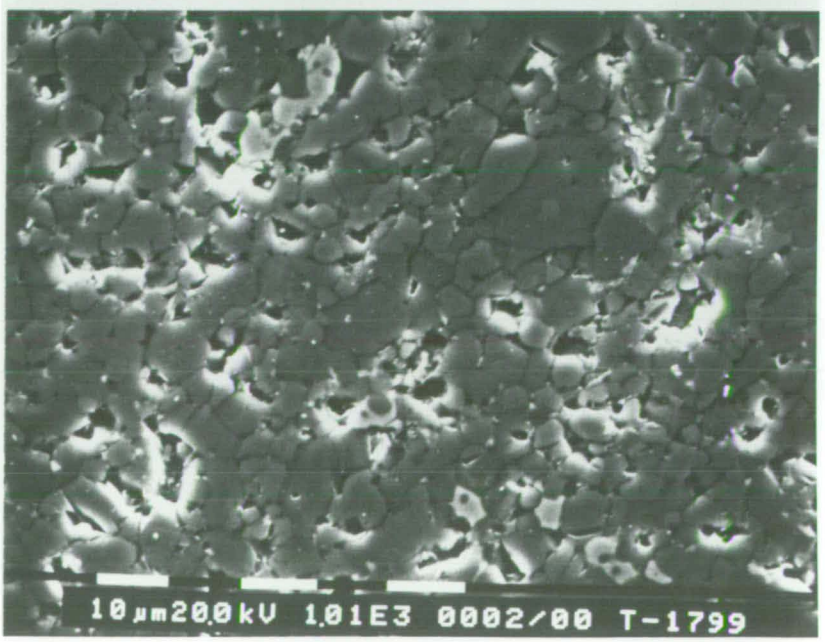
10µm20.0kV 1.01E3 0002/00 T-1799

to perpotassic melts. The Al_2O_3-content of orthopyroxenes present in the source during melting, or possibly produced by incongruent melting of phlogopite, are very low (see tables 18 and 20), but will nevertheless serve to enhance the peralkalinity of partial melts. The presence of fluorine may therefore be essential to the production of lamproites, many of which are perpotassic [Part 1].

In the leucite lamproite runs with CO_2, comparison of runs 1860 and 1909 suggests that a small amount of CO_2 may have an enormous influence on the appearance of clinopyroxene. Both these runs are H_2O-rich, but differ in having CO_2 or CH_4 as the second most abundant fluid component. Whilst this effect must be viewed with caution since it is based on only one experiment, in the more CO_2-rich run (CO_2/H_2O=6; Run 1857) clinopyroxene is accompanied by orthopyroxene and mica. The coexistence of mica with a CO_2-rich fluid in Run 1857 is interpreted to indicate buffering of the fluid phase by mica in an analogous manner to CO_2-rich fluids in equilibrium with amphibole-peridotite [Wyllie 1977; Eggler 1978; Olafsson and Eggler 1983]. This run, and run 1876 with an olivine lamproite sample, had no iron-wustite mixture to prevent oxidation, which has proceeded beyond CW, supporting the assertion of Woermann and Rosenhauer [1985] that graphite+H_2O has little buffering capacity. However, in Run 1876 mica does not occur and the fluid has much lower CO_2/H_2O. This may be due to the lower K_2O content of the olivine lamproite causing mica to be exhausted before CO_2-rich fluid compositions were attained.

5.5 DISCUSSION

5.5.1 APPLICABILITY OF THE EXPERIMENTS TO LAMPROITE PETROGENESIS

The model for the origin of lamproites by partial melting of mica-harzburgite in reduced conditions explains many of the features of standard lamproites, including the observed H_2O-rich volatile compositions, those aspects of the geochemistry which indicate a chemically depleted and re-enriched source [Part 1], and the predominance of depleted nodule types [Atkinson et al. 1984; Jaques et al. 1984a].

When applied to non-standard lamproites, particularly those bearing characteristics transitional towards the low-silica Group II

ultrapotassic rocks [Part 1], the model is less suitable, and needs to take into account factors such as the presence of clinopyroxene, garnet or spinel in the source, and the presence of other volatile species such as CO_2. Examples of these rocks include the clinopyroxene-rich madupites which are related to more typical lamproites in the Leucite Hills [Kuehner et al. 1981], and the West Greenland lamproites which contain considerable CO_2 as carbonate [Scott 1979]. Primary magmas giving rise to these compositions may be derived from melting of a clinopyroxene- and mica-rich source, possibly with a mixed CO_2-H_2O volatile phase [Barton and Hamilton 1979]. The experiment described above with high CO_2 shows that CO_2 may be very important in stabilising clinopyroxene in geochemically depleted compositions, but further studies are needed to investigate this link of CO_2 with "madupitic" lamproites.

Barton and Hamilton [1982] performed melting experiments at high pressures on a Leucite Hills orendite with 55 wt% SiO_2 to which no volatiles were added, but including minor H_2O (1.23 wt%) and CO_2 (0.2 wt%) which were present in the rock. They reported the occurrence of coexisting olivine, orthopyroxene, clinopyroxene and garnet at the liquidus at 27 kbar, and concluded that silica-rich orendites may originate by melting of garnet lherzolite at about that pressure. Phlogopite appeared >100°C below the liquidus in the orendite experiments, which Barton and Hamilton argued was due to a lower water content in the experiments than in the mantle source, believing that the high K_2O content of the rock (11.8 wt%) requires buffering by residual phlogopite. This discrepancy in phlogopite stability is unlikely to be due to fluorine as a natural rock starting composition was used, although no fluorine analysis was given.

Barton and Hamilton [1982] noted uncertainty in their identification of olivine in high pressure runs due to the very small crystal size: these were too small for confirmation by microprobe analysis in runs above 5 kbar. In the current experiments on the Gaussberg composition, olivine did not occur at pressures higher than 5 kbar. Acceptance of the high pressure crystals in the orendite experiments as primary olivines would cause irreconcilable discrepancies between the orendite and Gaussberg experiments: the higher H_2O in the Gaussberg runs should promote the stability of olivine, as should the lower silica composition (11 % normative olivine versus 2% normative quartz for the

orendite). Thus, it may be that the multiphase saturation seen in the orendite is in two pyroxenes and garnet, but not olivine. Other differences between the experimental results may be largely due to oxygen fugacity: fO_2 was not controlled in the orendite experiments, but the high Fe_2O_3/FeO indicates a high intrinsic oxygen fugacity of the sample which may have persisted throughout the runs.

5.5.2 MELTING OF MANTLE WITH INPUT OF REDUCED FLUIDS

Taylor and Green [1986a] and Green et al. [1986] suggested that water released by the interaction of upwelling CH_4-rich volatiles derived from the deep mantle with relatively oxidised lithosphere would cause a zone of "redox melting". If this process is considered to operate in the source regions of ultrapotassic magmas, then the type of melt produced will depend on the the manner of fluid input, i.e. episodic or continuous volatile addition, and on the initial oxidation state of the mantle into which the fluids are introduced.

[i] Episodic fluid supply: The redox behaviour of mantle interacting with reduced fluids can be demonstrated with reference to figure 47. An initially oxidised mantle with fO_2 around MW or FMQ in fluid-saturated conditions would lie in the field HPer+V or HCPer+V and would be forced towards the carbon saturation surface (CSS) by interaction with reduced fluids. Fluid compositions would proceed along the CSS towards the left of the diagram until melting commenced at B. Fluids at this point are H_2O+CO_2 mixtures and so melts are likely to be relatively silica-poor, possibly kimberlitic or "madupitic". Fluids introduced as a single pulse will become completely assimilated by the oxidised environment so that melting will be restricted to CO_2-bearing conditions.

The fields in figure 47 refer to fluid-saturated conditions, in which melt must exist in the mantle with compositions towards the top left of the diagram. However, if the mantle is fluid-undersaturated, mantle compositions very close to the H_2O-maximum on the CSS may exist in subsolidus conditions prior to addition of the reduced fluids. In this case melting will start with H_2O-rich, CO_2-poor fluids present and the initial melt compositions will resemble more typical lamproites. These mantle compositions lying close to the H_2O-maximum are more reduced than the compositions in the HPer+V or HCPer+V fields, and could be produced by successive episodes of melting of the more oxidised compositions.

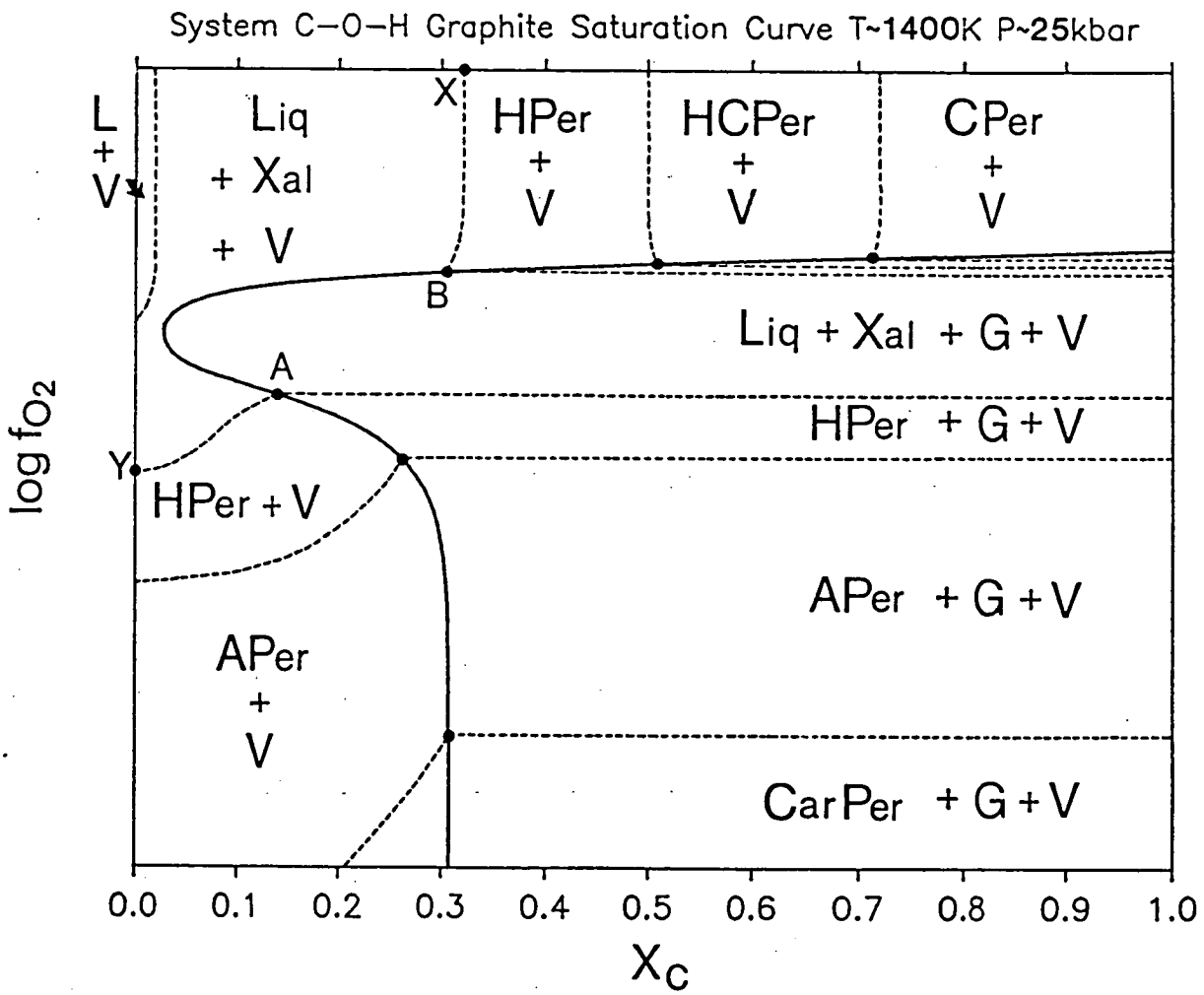

Figure 47

Schematic diagram illustrating possible phase relationships in Fe-free peridotite with excess C-O-H fluid phase (after Taylor and Green 1986a). This assumes the stability limit of hydrous phases coincides with the solidus (Y-A and X-B)(Green 1973a).

Abbreviations: CPer = carbonated peridotite, HCPer = hydrated, carbonated peridotite, HPer = hydrated peridotite, Liq (or L) = liquid, V = volatile phase, Xal = anhydrous crystals, G = graphite, APer = anhydrous peridotite, CarPer = carbide-bearing peridotite.

[2] Continuous fluid supply: Continuous supply of reduced fluids to an oxidised mantle would result initially in production of silica-poor melt compositions as descibed above, followed by silica-rich melts as fluid compositions pass around the H_2O-maximum, and finally production of melts in the presence of a fluid phase whose composition is buffered by the incoming fluid species. In this case relatively large volumes of lamproitic melt may be produced in the reduced, buffered environment. It is considered likely that fO_2 in a reduced mantle below CW will be controlled by carbon reactions and thus the supply of C-O-H fluids, because the buffering capacity of Fe-bearing minerals will be extremely low due to their low Fe^{3+} contents [Woermann and Rosenhauer 1985; Kadik and Lukanin 1985a]. Continuous supply of fluids to an initially reduced mantle would produce much the same results, except that the initial stage of silica-poor melt production would not occur.

Either of the above models for episodic or continuous supply of reduced fluids to a more oxidised mantle produces a dynamic explanation for the correlation of lamproitic magmas with geochemically depleted mantle. Progressive redox melting produces a geochemically depleted residue which could be the source for lamproitic magmas as deduced from lamproite chemistry and ultramafic nodule compositions. By this process reduction accompanies geochemical depletion, which is compatible with the H_2O-rich volatile compositions of most lamproites. However, the time scale for this process must be very large in most cases, since an enrichment event introducing incompatible elements must occur between the depletion event and melting to produce lamproites, and isotopic studies indicate that these enrichment events are generally Proterozoic events in sources for Tertiary lamproites [Fraser et al. 1985; Nelson et al. 1986]. If the mantle source remains reduced between the early redox melting depletion event and melting to produce lamproites, this implies that the enrichment event may also occur in a reduced environment, involving reduced melt or fluids.

It is suggested that the occurrence of low-silica madupites coexisting with higher silica orendites and wyomingites in the Leucite Hills region may be due to melting of a more oxidised pocket of mantle material in the presence of CO_2-bearing fluids. It is interesting to note that madupites in the Leucite Hills contain rare ferridiopsides as

inclusions in clinopyroxene phenocrysts [S.M.Kuehner pers. comm.] indicating contact with, or derivation from, extremely oxidised materials, although their relationship with the madupites is uncertain.

5.5.3 SURVIVAL OF DIAMONDS AND LAMPROITE-KIMBERLITE COMPARISONS

Inclusions in diamonds in the West Kimberley olivine lamproites show that the diamonds are not of magmatic origin, but are accidental inclusions in the lamproites. The abundance of diamonds must therefore be a function of their survival in the lamproite during ascent. If the model for the origin of lamproites in a reduced mantle is correct, diamonds will not be out of equilibrium in the source of the olivine lamproites prior to or during melting, and will only be removed from equilibrium after ascent through the diamond-graphite transition pressure. The kinetics of diamond breakdown during emplacment are not well understood, but their survival must depend on pressure-temperature paths and oxidation paths which prevent attainment of the activation energy for diamond-graphite transition. Simple models of the oxidation of reduced magmas during ascent suggest that the greater part of the oxidation occurs in the uppermost 15 kbar, and carbon saturation may persist to 5 kbar or less [Part 4; Kadik and Lukanin 1985b]. This oxidation path may lessen the potential for diamond breakdown, but this and other factors affecting diamond breakdown require further assessment.

The occurrence of diamonds, although rare, in some leucite lamproites in the West Kimberley region indicates that although some leucite lamproites may be primary magmas, others must be the products of crystal fractionation from olivine lamproites: according to the experiments, only olivine lamproites have a deep enough origin to contain diamonds. This conclusion is supported by geochemical modelling [Jaques et al. 1984a, 1986].

If the reduced mantle origin model for lamproites is correct, the major difference between lamproites and kimberlites may be in the oxidation state of the mantle source. The large amounts of carbonate present in many kimberlites, if primary [e.g. Dawson and Hawthorne 1973; Mitchell 1979], precludes a reduced source for kimberlites followed by oxidation during emplacement because of the low solubility of reduced carbon in silicate melts [Taylor and Green 1986b]. However, kimberlites may

originate by interaction of oxidised mantle with reduced fluids at high pressures as discussed in the preceding section. Alternatively, oxidised fluids, possibly from recycled subducted material, may be involved in kimberlite genesis.

The progressive redox melting model may be applicable to the East Kimberley region of Western Australia where olivine lamproites and kimberlites occur in close proximity. It is possible that the kimberlites are derived from melting of oxidised and more fertile pockets of mantle, and the olivine lamproites from more reduced and depleted areas.

APPENDICES

APPENDIX I

ULTRAPOTASSIC ROCK DATABASE

This appendix contains the database used in the review and classification of ultrapotassic rocks (Part I). Analyses include major elements in wt%, volatiles where available (wt%), and a standard set of 13 trace elements (p.p.m.). Source references are coded as shown by the list below, and full references are given in the integrated list at the back of the thesis together with references cited in the text.

Number	Reference	Number	Reference
1	L.-Ruiz and R.-Badiola [1980]	30	Bolivar and Brookins [1979]
2	Fuster et al. [1967]	31	Scott-Smith and Skinner [1984b]
3	Nixon et al. [1980]	32	Atkinson et al. [1984]
4	Borley [1967]	33	Jaques et al. [1984a]
5	Fuster and Pedro [1953]	34	Prider [1982]
6	Venturelli et al. [1984a]	35	Wade and Prider [1940]
7	Venturelli et al. [unpubl.]	36	Prider [1960]
8	Hall [1982]	37	Sheraton and Cundari [1980]
9	Velde [1967]	38	Sheraton [1981]
10	Dal Piaz et al. [1979]	39	Foley [unpubl. - appendix 2]
11	Venturelli et al. [1984b]	40	Sheraton and England [1980]
12	Vila et al. [1974]	41	Mittempergher [1965]
13	Scott [1977]	42	Sahama [1974]
14	Scott [1979]	43	Gallo et al. [1984]
15	Scott [1981]	44	Holm et al. [1982]
16	Velde [1975]	45	Gragnani [1972]
17	Kuehner et al. [1981]	46	Carstens [1962]
18	Schultze and Cross [1912]	47	Griffin and Taylor [1975]
19	Cross [1897]	48	Kresten and Edelman [1975]
20	Ogden [1979]	49	Vartiainen et al. [1978]
21	Smithson [1959]	50	Denaeyer et al. [1965]
22	Johnston [1959]	51	Holmes and Hecht [1936]
23	Barton and Hamilton [1978]	52	Holmes [1937]
24	Yagi and Matsumoto [1966]	53	Holmes and Harwood [1937]
25	Barton and van Bergen [1981]	54	Combe and Holmes [1945]
26	Carmichael [1967]	55	Higazy [1954]
27	Best et al. [1968]	56	Holmes [1950]
28	Merrill et al. [1977]	57	Holmes [1942]
29	Cullers et al. [1985]	58	Sahama [1954]

59 Bell and Powell [1969]
60 Mitchell and Bell [1976]
61 Holmes [1945]
62 Holmes and Harwood [1932]
63 Holmes [1952]
64 Holmes [1956]
65 Edgar and Arima [1981]
66 El-Hinnawi [1965]
67 Bailey [1984]
68 McIver [1981]
69 McIver and Ferguson [1979]
70 Kranck [1928]
71 Ukhanov [1963]
72 Gupta et al. [1983]
73 He Guan-Zhi [1984]
74 Brooks et al. [1981]
75 Gold [1970]
76 Kemp [1891]
77 Ravich et al. [1978]
78 Grikurov et al. [1980]
79 Poli et al. [1984]
80 van Bergen et al. [1983]
81 Thompson [1977]
82 Barton et al. [1982]
83 Schneider [1965]
84 Giammetti and Beccaluva [1968]
85 Varekamp [1979]
86 Trigila [1966]
87 Trigila [1969]
88 Rogers et al. [1985]
89 Puxeddu [1972]
90 Cundari and Matthias [1974]
91 Amendolagine et al. [1962]
92 Cundari [1979]
93 Fornaseri et al. [1963]
94 Peccerillo et al. [1984]
95 Civetta et al. [1981]
96 Angelluci [1974]
97 Appleton [1972]
98 Appleton [1970]
99 Arevalo et al. [1962]
100 Savelli [1967]
101 Grubb [1965]
102 Ferrara et al. [1981]
103 Foden [1979]
104 Foden and Varne [1980]
105 Van Padang [1951]
106 Wheller [1986]
107 Perchuk [1965]
108 Miller [1972]
109 Cosgrove [1972]
110 Lees [1974]
111 Velde [1971a]
112 Barberi and Innocenti [1967]
113 Wimmenauer [1973]
114 Guintrand et al. [1963]
115 Van Moort [1966]
116 Velde [1971b]
117 Sabatier [1980]
118 Holub [1977]
119 Palivcova et al. [1968]
120 Kramer [1976]
121 Nemec [1973]
122 Nemec [1970]
123 Nemec [1974]
124 Stefanova [1966]
125 LaCroix [1926]
126 Lepvrier and Velde [1976]
127 Keller [1983]
128 Maksimov and Ugryumov [1971]
129 Vitterbo and Zanettin [1959]
130 Chao Tsung-pu [1960]
131 Pirsson [1905]
132 Iddings and Morley [1915]
133 Daly [1912]
134 Knopf [1936]
135 Larsen [1941]
136 Schmidt et al. [1961]
137 Nash and Wilkinson [1970]
138 Nash and Wilkinson [1971]
139 Witkind [1973]
140 Buie [1941]

141 Burgess [1941]
142 Joplin [1966]
143 Nicholls and Carmichael [1967]
144 Kirchner [1979]
145 Johnson [1968]
146 Johnson [1964]
147 Roden and Smith [1979]
148 Roden [1981]
149 Ehrenberg [1982]
150 Nicholls [1969]
151 Rogers et al. [1982]
152 Williams [1936]
153 Roden et al. [1979]
154 Van Kooten [1980]
155 Dodge and Moore [1981]
156 Cundari [1973]
157 Langworthy and Black [1978]
158 Solomon [1964]
159 Sutherland and Corbett [1974]
160 De Marco [1958]
161 Dawson [1972]

Group I : Page 1

Locality	SE Spain	SE Spain	SE Spain	SE Spain	SE Spain	SE Spain	SE Spain	SE Spain	SE Spain	SE Spain
Rock	Jumillite	Cancalite	Fortunite	Verite	Fortunite	Fortunite	Cancalite	Cancalite	Jumillite	Fortunite
Reference	1	1	1	1	3	3	3	3	3	3
SiO2	47.72	55.05	56.05	61.22	57.90	54.90	56.80	57.40	46.30	58.20
TiO2	1.43	1.76	1.35	1.23	1.49	1.40	1.58	1.62	1.55	1.45
Al2O3	7.72	9.31	11.43	12.21	10.90	10.30	9.42	9.28	8.54	12.00
Fe2O3	3.01	2.14	2.23	2.06	5.51	5.21	5.23	5.42	7.96	5.01
FeO	3.40	3.07	3.31	1.96	0.00	0.00	0.00	0.00	0.00	0.00
MnO	0.10	0.08	0.08	0.04	0.06	0.10	0.06	0.08	0.13	0.04
MgO	16.27	12.18	9.27	4.57	6.59	6.87	12.20	11.50	13.90	7.67
CaO	7.11	3.75	4.21	2.72	3.11	6.66	2.80	3.54	9.97	2.71
Na2O	1.71	1.40	2.10	1.96	1.30	1.16	0.54	1.09	1.13	1.06
K2O	4.99	8.67	6.14	5.71	7.71	7.22	9.38	9.18	4.30	8.43
P2O5	1.68	0.99	0.81	0.77	0.50	0.49	0.67	0.76	1.18	0.71
H2O+	3.48	1.43	2.91	4.88	2.13	1.94	1.20	0.55	3.15	1.58
H2O-	--	--	--	--	1.85	1.34	0.84	0.49	0.90	1.21
CO2	0.44	0.07	0.06	0.21	0.38	3.20	--	--	0.1	--
Ba	4568	0	1164	1343	--	--	--	--	--	--
Rb	147	597	489	232	--	--	--	--	--	--
Sr	1499	902	507	596	--	--	--	--	--	--
Zr	748	776	541	378	920	821	903	857	66	735
Nb	--	--	--	--	30	10	31	40	44	28
Y	--	--	--	--	--	--	--	--	--	--
La	--	--	--	--	87	80	91	109	165	72
Ce	--	--	--	--	241	239	262	301	422	216
Nd	--	--	--	--	150	138	169	184	239	136
Sc	--	--	--	--	17	15	15	15	24	16
V	--	--	--	--	100	90	91	92	135	106
Ni	796	590	428	236	--	--	--	--	--	--
Cr	668	617	531	395	--	--	--	--	--	--

Group I : Page 2

Locality	SE Spain	SE Spain	SE Spain	SE Spain	SE Spain	SE Spain	SE Spain	SE Spain	SE Spain	SE Spain
Rock	Fortunite	Fortunite	Jumillite	Jumillite	Jumillite	Jumillite	Jumillite	Jumillite	Jumillite	Jumillite
Reference	3	3	2	2	2	2	2	2	2	2
SiO2	57.50	56.30	46.43	46.23	48.81	47.03	45.75	51.25	47.07	45.64
TiO2	1.42	1.44	1.52	1.50	1.34	1.32	1.29	1.37	1.32	1.51
Al2O3	12.00	11.40	7.20	7.74	8.17	7.20	7.26	9.10	7.20	8.20
Fe2O3	5.09	5.72	2.97	2.65	3.46	2.87	2.92	1.45	3.03	3.44
FeO	--	--	3.36	3.09	3.22	3.33	3.02	4.21	3.19	3.83
MnO	0.04	0.08	0.10	0.14	0.00	0.08	0.15	0.07	0.10	0.12
MgO	7.66	9.55	16.72	18.04	14.84	17.37	17.84	15.79	16.88	14.65
CaO	2.51	2.32	7.45	7.43	7.06	6.77	7.43	4.25	7.90	8.95
Na2O	1.14	1.00	1.40	1.64	1.71	1.40	1.43	2.20	1.40	1.60
K2O	8.72	8.31	5.20	4.24	5.73	4.70	4.24	6.40	5.00	3.80
P2O5	0.65	0.57	1.73	2.17	1.39	1.45	1.94	1.16	1.78	2.04
H2O+	1.80	2.10	3.10	4.37	3.46	3.80	4.19	0.80	2.90	3.60
H2O-	1.39	1.47	0.74	--	--	1.22	--	0.37	0.52	0.66
CO2	--	0.1	0.90	--	0.81	0.10	--	0.60	1.20	0.80
Ba	--	--								
Rb	--	--								
Sr	--	--								
Zr	689	692								
Nb	26	28								
Y	--	--								
La	72	64								
Ce	215	180								
Nd	134	116								
Sc	24	16								
V	103	109								
Ni	--	--								
Cr	--	--								

Group I : Page 3

Locality	SE Spain	SE Spain	SE Spain	SE Spain	SE Spain	SE Spain	SE Spain	SE Spain	SE Spain	SE Spain
Rock	Jumillite	Jumillite	Jumillite	Jumillite	Cancalite	Cancalite	Cancalite	Cancalite	Cancalite	Cancalite
Reference	2	2	2	2	2	2	2	2	2	2
SiO2	46.96	45.53	51.52	50.78	53.39	54.10	55.55	55.15	54.65	55.35
TiO2	1.66	1.57	1.42	1.28	1.76	1.43	1.52	1.62	1.68	1.70
Al2O3	6.40	8.50	8.60	9.05	10.83	10.40	9.94	9.62	8.35	9.51
Fe2O3	3.90	2.93	2.58	2.96	2.11	1.93	1.67	1.94	2.04	1.05
FeO	2.64	4.31	3.28	3.64	2.77	3.16	2.87	3.07	3.63	3.23
MnO	0.11	0.11	0.09	0.09	0.04	0.15	0.04	0.07	0.08	0.08
MgO	16.80	14.86	15.55	14.29	12.79	12.09	11.37	13.09	15.54	12.39
CaO	7.77	9.06	4.14	5.29	5.00	5.61	4.20	4.20	3.22	4.06
Na2O	1.50	1.50	2.00	1.05	1.49	1.40	1.38	1.18	1.18	1.38
K2O	5.10	3.60	6.80	7.39	8.53	8.40	8.76	9.36	8.20	8.72
P2O5	1.90	1.82	1.25	1.31	0.63	0.90	1.05	1.20	1.18	1.25
H2O+	3.10	4.10	0.80	2.53	0.68	0.57	0.82	0.48	0.81	0.44
H2O-	0.77	1.13	0.40	--	0.45	--	--	--	--	--
CO2	0.80	0.60	0.80	0.46	--	--	--	--	--	--
Ba										
Rb										
Sr										
Zr										
Nb										
Y										
La										
Ce										
Nd										
Sc										
V										
Ni										
Cr										

Group I : Page 4

Locality	SE Spain	SE Spain	SE Spain	SE Spain	SE Spain	SE Spain	SE Spain	SE Spain	SE Spain	SE Spain
Rock	Cancalite	Cancalite	Cancalite	Cancalite	Cancalite	Cancalite	Cancalite	Cancalite	Cancalite	Fortunite
Reference	2	2	2	2	2	2	2	2	2	2
SiO2	55.00	55.60	55.35	55.90	56.01	55.19	52.80	53.92	53.90	55.79
TiO2	1.79	1.68	1.62	1.66	2.03	1.89	1.51	1.70	2.26	1.56
Al2O3	8.48	8.35	9.32	8.76	9.23	8.15	9.18	9.94	8.88	10.39
Fe2O3	1.74	1.82	1.68	2.16	2.31	4.04	1.27	0.83	1.78	1.39
FeO	3.69	3.39	2.95	2.96	2.87	2.36	3.79	3.81	4.16	4.17
MnO	0.08	0.07	0.09	0.07	0.07	0.07	0.01	0.09	0.13	0.02
MgO	13.75	13.23	12.39	12.02	12.03	10.36	12.98	12.49	13.24	9.98
CaO	3.69	3.92	3.50	4.06	2.50	2.62	4.14	3.92	3.76	2.00
Na2O	1.18	1.20	1.80	1.20	1.42	3.08	1.00	0.80	1.17	4.07
K2O	8.56	8.78	8.60	9.10	8.62	8.52	8.30	8.72	7.56	8.11
P2O5	1.12	1.22	1.23	1.20	0.84	0.86	1.05	1.05	0.65	0.61
H2O+	0.82	1.13	0.63	0.97	0.92	1.67	2.97	1.87	1.23	1.80
H2O-	--	--	--	--	0.28	1.20	--	--	1.01	0.33
CO2	--	--	--	--	0.59	0.13	--	--	0.47	--
Ba										
Rb										
Sr										
Zr										
Nb										
Y										
La										
Ce										
Nd										
Sc										
V										
Ni										
Cr										

Group I : Page 5

Locality	SE Spain	SE Spain	SE Spain	SE Spain	SE Spain	SE Spain Barqueros	SE Spain Barqueros	SE Spain Barqueros	SE Spain Puebla de Mula	SE Spain
Rock	Fortunite	Fortunite	Fortunite	Fortunite	Fortunite					Jumillite
Reference	2	2	2	2	2	2	2	2	2	4
SiO2	56.68	57.13	57.51	56.25	56.72	55.56	54.70	56.60	53.43	45.53
TiO2	1.50	1.60	1.24	1.17	1.37	1.38	1.21	1.58	1.21	1.57
Al2O3	10.73	10.28	10.57	11.85	11.05	11.60	12.38	12.49	10.87	8.50
Fe2O3	2.81	1.90	0.93	1.54	2.53	0.72	1.42	0.77	1.35	2.93
FeO	4.28	4.11	4.62	3.74	3.59	4.82	4.09	4.53	2.03	4.31
MnO	0.01	0.09	0.08	0.01	0.00	0.12	0.12	0.10	0.06	0.11
MgO	11.50	9.73	10.12	9.77	9.91	10.68	9.27	9.47	11.81	14.86
CaO	1.41	3.37	3.44	3.22	2.90	3.08	3.64	3.36	3.82	9.06
Na2O	1.71	2.56	1.54	1.58	1.43	1.48	1.38	1.52	1.38	1.50
K2O	7.62	6.07	7.02	5.94	6.62	6.80	6.50	6.54	6.94	3.60
P2O5	0.50	0.82	0.76	0.71	0.95	0.41	0.62	0.75	1.57	1.82
H2O+	1.00	2.55	2.22	3.44	2.76	2.44	4.53	1.86	2.08	4.10
H2O-	0.15	--	--	--	--	--	--	--	2.44	1.13
CO2	--	0.07	--	--	--	--	--	--	0.70	0.6
Ba										3700
Rb										--
Sr										1900
Zr										1000
Nb										--
Y										--
La										--
Ce										--
Nd										--
Sc										--
V										--
Ni										--
Cr										--

Group I : Page 6

Locality	SE Spain	SE Spain	SE Spain	SE Spain	SE Spain	SE Spain	SE Spain	SE Spain	SE Spain	SE Spain
Rock	Jumillite	Jumillite	Jumillite	Jumillite	Jumillite	Jumillite	Jumillite	Verite	Verite	Verite
Reference	4	4	4	4	4	4	4	5	5	5
SiO2	45.64	51.25	51.52	47.07	46.96	46.43	47.03	58.08	56.24	61.88
TiO2	1.51	1.37	1.42	1.66	1.66	1.52	1.32	1.05	1.32	1.43
Al2O3	8.20	9.10	8.60	7.20	6.40	7.20	7.20	9.25	10.17	11.34
Fe2O3	3.44	1.45	2.58	3.03	3.90	2.97	2.87	2.93	0.84	2.38
FeO	3.83	4.21	3.28	3.19	2.64	3.36	3.33	1.42	1.96	1.55
MnO	0.12	0.07	0.09	0.10	0.08	0.10	0.08	0.00	0.04	0.05
MgO	14.65	15.79	15.55	16.88	16.80	16.72	17.37	2.64	5.31	5.50
CaO	8.95	4.25	4.14	7.90	7.77	7.45	6.77	5.13	6.47	3.92
Na2O	1.60	2.20	2.00	1.40	1.50	1.40	1.40	3.71	1.86	1.02
K2O	3.80	6.40	6.80	5.00	5.10	5.20	4.70	7.71	7.00	5.57
P2O5	2.04	1.16	1.25	1.78	1.90	1.73	1.45	1.20	1.55	0.88
H2O+	3.60	0.80	0.80	2.90	3.10	3.10	3.80	3.24	4.85	2.65
H2O-	0.66	0.37	0.40	0.52	0.77	0.74	1.22	0.80	1.50	1.09
CO2	0.8	0.6	0.8	1.2	0.8	0.9	0.1	2.35	0.85	0.26
Ba	3700	3600	3500	4400	4900	5800	5500			
Rb	--	--	--	--	--	--	--			
Sr	2200	1100	1150	1650	1500	1500	1250			
Zr	850	250	600	700	600	700	750			
Nb	--	--	--	--	--	--	--			
Y	--	--	--	--	--	--	--			
La	--	--	--	--	--	--	--			
Ce	--	--	--	--	--	--	--			
Nd	--	--	--	--	--	--	--			
Sc	--	--	--	--	--	--	--			
V	--	--	--	--	--	--	--			
Ni	--	--	--	--	--	--	--			
Cr	--	--	--	--	--	--	--			

Group I : Page 7

Locality	SE Spain	SE Spain	SE Spain	SE Spain	SE Spain	SE Spain	SE Spain	SE Spain	SE Spain	SE Spain
Rock	Verite	Verite								
Reference	5	5	6	6	6	6	6	6	6	6
SiO2	61.15	68.49	58.90	57.40	57.50	53.40	48.90	57.20	55.80	56.90
TiO2	1.44	1.30	1.24	1.46	1.45	1.44	1.48	1.78	1.52	1.88
Al2O3	13.33	10.42	12.30	12.00	11.80	9.88	9.35	8.98	10.00	9.27
Fe2O3	4.39	2.62	5.80	5.85	5.89	6.01	6.71	5.89	5.37	5.69
FeO	0.96	1.30	--	--	--	--	--	--	--	--
MnO	0.04	0.04	0.07	0.07	0.07	0.07	0.08	0.06	0.07	0.06
MgO	3.14	3.60	5.29	9.27	9.15	12.80	15.70	7.99	12.30	11.20
CaO	1.82	1.88	4.50	2.87	2.93	4.86	5.71	3.66	3.41	2.72
Na2O	1.61	1.18	1.48	1.36	1.14	1.90	1.83	1.22	1.18	1.75
K2O	7.75	7.21	7.88	6.84	6.84	6.54	5.10	8.72	8.78	8.75
P2O5	1.11	1.05	0.94	0.75	0.79	0.98	1.53	0.83	0.98	0.88
H2O+	2.62	0.62	--	--	--	--	--	--	--	--
H2O-	--	0.49	--	--	--	--	--	--	--	--
CO2	0.16	0.07	--	--	--	--	--	--	--	--
L.O.I.	--	--	1.50	1.86	2.28	2.05	3.40	3.45	0.28	0.83
Ba			2075	1615	1450	2450	3140	1965	1695	1980
Rb			426	496	495	238	153	472	539	503
Sr			616	528	514	709	1032	772	828	608
Zr			540	630	620	575	675	800	700	980
Nb			33	35	34	30	44	39	39	50
Y			28	32	30	26	32	30	28	30
La			--	--	--	--	--	--	--	--
Ce			--	--	--	--	--	--	--	--
Nd			--	--	--	--	--	--	--	--
Sc			20	14	14	15	14	13	14	15
V			107	100	97	96	102	88	80	96
Ni			324	379	416	669	724	490	600	540
Cr			794	614	624	827	925	465	816	641

Group I : Page 8

Locality	SE Spain	SE Spain	SE Spain	SE Spain	SE Spain	SE Spain	SE Spain	SE Spain	SE Spain	SE Spain
Reference	6	6	6	6	6	6	7	7	7	7
SiO2	57.30	54.60	53.60	57.80	56.80	59.50	55.70	56.70	57.20	56.40
TiO2	1.94	1.75	1.71	1.52	1.52	1.47	0.98	1.59	1.53	1.77
Al2O3	9.60	9.52	9.41	12.10	11.80	11.90	12.50	10.30	10.80	9.51
Fe2O3	5.54	5.66	5.74	6.36	5.89	5.55	5.47	6.36	5.64	5.25
FeO	--	--	--	--	--	--	--	--	--	--
MnO	0.05	0.07	0.07	0.06	0.07	0.07	0.08	0.07	0.07	0.06
MgO	7.45	13.30	14.60	3.24	8.99	8.59	9.21	9.12	8.81	11.60
CaO	3.65	2.87	2.90	3.54	3.34	2.26	5.27	2.83	2.57	3.29
Na2O	1.57	0.69	0.64	1.66	1.40	1.23	1.43	1.04	1.11	0.80
K2O	8.49	8.86	8.58	8.34	7.18	8.28	6.40	8.12	8.15	8.32
P2O5	0.91	0.95	1.13	1.34	0.66	0.56	0.78	0.75	0.79	0.88
H2O+	--	--	--	--	--	--	--	--	--	--
H2O-	--	--	--	--	--	--	--	--	--	--
CO2	--	--	--	--	--	--	--	--	--	--
L.O.I.	3.35	1.60	1.62	4.00	2.28	0.53	--	--	--	--
Ba	2800	2050	2040	2590	1350	1610	1880	1550	1695	2120
Rb	465	541	603	451	523	569	365	644	658	582
Sr	654	526	558	898	500	426	562	521	484	743
Zr	1030	680	795	550	705	790	440	560	635	795
Nb	50	32	39	39	35	37	29	30	35	39
Y	29	24	31	35	35	32	26	28	27	33
La	--	--	--	--	--	--	--	--	--	--
Ce	--	--	--	--	--	--	--	--	--	--
Nd	--	--	--	--	--	--	--	--	--	--
Sc	14	14	13	--	14	14	18	15	14	13
V	87	91	89	115	91	88	106	115	122	94
Ni	399	657	719	178	363	439	421	410	446	554
Cr	633	638	679	718	642	550	658	574	637	615

Locality	SE Spain	SE Spain	SE Spain	SE Spain	SE Spain	SE Spain	SE Spain	England Pendennis Minette	Corsica Sisco Minette	Corsica Sisco Minette
Rock Reference	7	7	7	7	7	7	7	8	9	9
SiO2	56.30	56.50	56.50	57.30	55.10	57.60	57.50	50.69	56.23	57.06
TiO2	1.70	1.89	1.86	1.94	1.82	1.73	1.53	1.58	1.14	1.36
Al2O3	9.68	9.80	9.42	9.60	9.88	11.70	11.40	9.71	12.06	11.07
Fe2O3	5.39	5.75	5.23	5.54	5.55	5.93	5.75	3.06	1.91	1.96
FeO	--	--	--	--	--	--	--	3.37	2.91	2.99
MnO	0.06	0.07	0.05	0.05	0.06	0.07	0.08	0.13	0.07	0.00
MgO	11.60	10.20	9.52	7.45	12.40	5.87	9.98	6.07	6.90	6.48
CaO	3.21	2.78	3.62	3.65	2.83	3.54	2.57	5.28	3.48	4.52
Na2O	0.83	1.88	1.41	1.57	0.71	1.33	1.31	0.47	1.03	1.45
K2O	8.37	9.34	8.08	8.49	9.08	8.13	7.75	9.22	10.00	9.60
P2O5	0.82	0.76	0.72	0.91	1.12	0.54	0.61	1.73	0.79	0.41
H2O+	--	--	--	--	--	--	--	0.82	1.56	0.81
H2O-	--	--	--	--	--	--	--	--	1.58	0.55
CO2	--	--	--	--	--	--	--	6.91	0.41	2.11
L.O.I.	--	--	--	--	--	--	--	--	--	--
Ba	2095	2030	3055	2800	1900	1545	1200	6306		
Rb	587	537	466	465	556	556	643	--		
Sr	738	655	730	654	555	405	384	2345		
Zr	760	1010	1010	1030	750	895	750	1984		
Nb	39	51	50	50	37	40	37	45		
Y	28	32	31	29	28	31	30	36		
La	--	--	--	--	--	--	--	274		
Ce	--	--	--	--	--	--	--	616		
Nd	--	--	--	--	--	--	--	264		
Sc	13	14	14	14	14	14	18	18		
V	89	91	81	87	93	87	94	128		
Ni	549	491	470	399	567	250	455	122		
Cr	--	665	612	633	675	399	706	262		

Group I : Page 10

Locality	NW Alps	NW Alps	NW Alps	NW Alps	NW Alps	Algeria Koudiat	Algeria Koudiat	West Greenland	West Greenland	West Greenland
Sample								5611	5612	5616
Reference	10,11	10,11	10,11	10,11	10,11	12	12	13,14	13	13
SiO2	56.00	54.85	49.33	50.22	56.03	56.18	56.56	38.28	38.29	48.99
TiO2	1.40	1.50	1.05	1.06	1.24	1.43	1.45	2.24	2.34	3.81
Al2O3	8.90	8.87	11.28	10.76	10.98	12.80	13.15	5.60	5.73	8.45
Fe2O3	2.00	2.05	1.63	1.81	2.21	1.80	1.70	2.33	2.22	2.30
FeO	3.30	3.76	4.60	5.23	2.65	3.32	2.87	4.83	4.93	3.95
MnO	0.11	0.18	0.10	0.11	0.09	0.08	0.08	0.09	0.09	0.07
MgO	9.40	9.54	13.61	12.87	9.27	8.83	8.24	15.30	14.89	6.72
CaO	4.20	4.33	7.65	6.43	4.11	3.16	3.42	8.99	8.40	5.60
Na2O	1.90	1.78	1.60	0.85	1.29	1.61	1.21	1.60	1.52	1.92
K2O	9.60	9.40	5.94	6.72	9.07	6.56	8.33	6.27	6.44	9.31
P2O5	1.20	1.40	1.10	1.19	1.09	0.30	0.32	0.76	0.83	1.85
H2O+	--	--	--	--	--	2.99	1.51	3.30	2.75	1.18
H2O-	--	--	--	--	--	0.62	0.83	--	--	--
CO2	--	--	--	--	--	--	--	9.00	9.04	2.74
L.O.I.	1.60	2.05	2.34	2.46	1.78	--	--	--	--	--
Ba	--	--	--	--	--			1730	1767	2560
Rb	371	400	245	325	496			144	149	141
Sr	580	1030	690	625	440			1385	1394	2842
Zr	730	854	375	450	592			557	557	724
Nb	40	54	26	28	30			--	--	--
Y	52	68	36	46	47			17	18	25
La	164	--	--	--	--			221	206	518
Ce	357	--	213	265	258			284	293	642
Nd	227	--	140	173	175			--	--	--
Sc	--	--	--	--	--			--	--	--
V	110	80	125	125	95			219	228	309
Ni	315	364	395	460	396			557	541	19
Cr	586	660	802	839	600			755	703	178

Locality	West Greenland	West Greenland	West Greenland	West Greenland	West Greenland	West Greenland	West Greenland	West Greenland	West Greenland	West Greenland
Sample	5620	5621	5622	5622A	5623	5624	5625	5625A	5625B	5628
Reference	13	13	13,15	13,14	13,14	13	13	13	13	13
SiO2	45.95	47.30	39.29	39.21	41.58	40.63	39.98	40.79	38.23	40.52
TiO2	3.62	3.88	2.17	2.24	3.46	3.44	2.96	3.23	2.33	3.06
Al2O3	8.19	8.36	4.90	5.01	7.11	6.66	6.47	7.07	5.14	6.60
Fe2O3	3.52	2.92	1.35	1.49	1.28	1.51	0.88	1.24	0.70	0.96
FeO	3.31	3.77	6.25	6.14	6.19	6.38	6.54	6.14	6.68	6.55
MnO	0.09	0.07	0.10	0.10	0.09	0.11	0.10	0.11	0.10	0.11
MgO	8.37	6.81	22.55	21.61	12.02	11.32	14.17	11.17	17.27	12.52
CaO	5.34	5.64	4.73	5.02	7.40	7.05	6.92	7.34	6.12	7.00
Na2O	1.32	1.91	1.00	1.13	1.59	1.46	1.38	1.54	0.34	1.42
K2O	9.51	9.45	6.16	6.25	7.54	7.93	7.29	7.76	6.43	7.71
P2O5	2.18	1.75	0.94	0.94	1.60	1.45	1.23	1.32	0.95	1.57
H2O+	2.11	1.42	2.82	3.36	2.25	2.56	2.26	2.47	3.37	2.31
H2O-	--	--	--	--	--	--	--	--	--	--
CO2	3.40	3.67	5.14	5.94	5.33	5.94	6.99	7.33	7.26	6.65
Ba	7721	6271	3227	2838	6405	4966	5571	5261	3850	4966
Rb	232	164	168	162	180	173	168	163	153	165
Sr	3458	2477	2563	2549	1582	2260	2089	2060	2374	2456
Zr	1051	1217	490	505	730	861	686	716	546	717
Nb	--	--	--	--	--	--	--	--	--	--
Y	30	30	20	19	27	22	25	32	19	25
La	633	610	262	322	395	459	397	432	341	412
Ce	770	722	345	384	487	515	475	517	400	478
Nd	--	--	--	--	--	--	--	--	--	--
Sc	--	--	--	--	--	--	--	--	--	--
V	378	375	220	236	364	350	320	347	259	319
Ni	94	50	856	782	250	226	392	207	650	291
Cr	280	211	756	744	509	518	546	492	623	547

Group I : Page 12

Locality	West Greenland	West Greenland	West Greenland	West Greenland	West Greenland	West Greenland	West Greenland	West Greenland	West Greenland	West Greenland
Rock	5625A	5630	5632	5634	5635	5636	5637	5641	5643	5645
Reference	13,14	13,14	13,15	13,14	13	13	13,14	13	13,15	13
SiO2	40.22	41.37	42.75	41.92	42.38	44.16	41.91	42.66	46.48	47.17
TiO2	3.11	4.00	3.18	3.15	2.34	3.66	2.65	3.08	3.38	3.62
Al2O3	6.47	7.44	8.47	7.01	7.51	7.55	5.94	7.31	7.66	8.21
Fe2O3	0.12	1.31	1.74	2.46	1.54	0.81	0.97	0.70	3.14	0.92
FeO	7.41	7.86	5.01	5.27	5.10	6.07	6.93	4.91	4.09	5.99
MnO	0.09	0.10	0.09	0.10	0.09	0.09	0.10	0.14	0.07	0.07
MgO	13.44	8.75	12.16	11.17	11.89	11.30	18.95	10.10	10.74	8.08
CaO	7.37	9.69	7.38	6.65	6.39	5.66	5.22	8.91	5.54	5.30
Na2O	1.55	1.14	0.96	1.95	1.80	1.62	1.16	1.18	1.37	1.58
K2O	7.36	6.81	7.99	7.54	7.89	8.42	6.10	7.38	8.14	8.85
P2O5	1.39	1.65	0.73	1.31	0.86	1.40	0.88	1.30	1.43	1.24
H2O+	2.96	2.84	2.65	2.43	2.34	2.03	2.36	1.22	2.92	1.93
H2O-	--	--	--	--	--	--	--	--	--	--
CO2	6.29	4.45	4.96	6.68	7.62	4.29	4.73	8.49	3.05	3.21
Ba	7002	2764	4224	3149	2909	2073	6379	1607	1524	1385
Rb	133	180	242	159	159	202	175	154	171	174
Sr	1940	857	1621	2174	1738	2142	1578	2287	1467	1395
Zr	759	714	279	844	560	953	516	887	1078	1259
Nb	--	--	--	--	--	--	--	--	--	--
Y	21	30	16	25	16	28	19	18	24	26
La	486	390	209	351	208	340	206	302	393	377
Ce	598	477	287	441	270	455	298	417	478	463
Nd	--	--	--	--	--	--	--	--	--	--
Sc	--	--	--	--	--	--	--	--	--	--
V	352	407	320	318	222	348	288	261	291	330
Ni	294	94	378	291	296	259	728	284	332	150
Cr	536	285	174	393	514	408	657	465	331	286

Group I : Page 13

Locality	West Greenland	West Greenland	West Greenland	West Greenland	West Greenland	West Greenland	West Greenland	West Greenland	West Greenland	West Greenland
Sample	5646	5647	5651	5652	5653	5655	5658	5659	5663	5664
Reference	13	13	13	13,14	13,14	13	13	13	13	13,14
SiO2	42.37	42.11	46.51	49.60	40.13	38.73	43.68	39.55	40.03	41.39
TiO2	2.82	3.15	3.75	4.15	2.88	2.77	3.07	3.05	2.62	2.84
Al2O3	6.98	6.95	8.23	8.64	6.59	6.50	8.15	6.41	6.72	6.54
Fe2O3	1.27	1.38	1.39	2.21	1.36	2.31	0.81	0.72	3.10	0.98
FeO	5.38	5.26	5.39	4.75	5.97	5.96	6.30	7.23	4.29	6.09
MnO	0.09	0.07	0.08	0.07	0.10	0.10	0.10	0.09	0.10	0.09
MgO	12.32	10.00	8.20	6.32	12.53	13.38	10.39	14.41	12.32	17.38
CaO	7.29	7.37	4.77	4.32	7.47	7.37	6.46	5.45	7.00	5.37
Na2O	1.29	1.70	1.59	1.60	1.54	1.27	1.38	1.66	1.29	1.49
K2O	7.22	7.69	9.40	10.03	7.25	6.38	8.27	7.11	6.64	7.09
P2O5	1.14	1.34	1.25	1.26	1.05	0.89	1.05	1.33	1.06	0.65
H2O+	2.89	2.37	1.23	1.12	2.27	3.14	2.20	3.22	2.77	3.17
H2O-	--	--	--	--	--	--	--	--	--	--
CO2	6.92	7.40	4.60	2.93	8.81	8.09	6.51	5.58	8.38	7.24
Ba	2790	2118	4457	2590	3017	3489	2097	2539	4461	2622
Rb	164	151	192	216	170	140	138	163	139	138
Sr	2320	2645	2367	2365	1994	1635	2488	1669	1998	1619
Zr	888	1061	1211	1648	586	531	720	637	722	495
Nb	--	--	--	--	--	--	--	--	--	--
Y	22	27	22	19	20	19	25	23	18	16
La	346	388	366	341	235	217	313	367	266	215
Ce	413	483	463	423	364	321	412	474	381	312
Nd	--	--	--	--	--	--	--	--	--	--
Sc	--	--	--	--	--	--	--	--	--	--
V	267	304	372	359	300	299	299	319	293	253
Ni	412	294	163	54	342	293	123	293	303	505
Cr	553	409	198	164	486	519	334	647	469	627

Group I : Page 14

Locality	West Greenland	West Greenland	West Greenland	West Greenland	West Greenland	West Greenland	West Greenland	West Greenland	West Greenland	West Greenland
Rock	5665	5692	5890	5891	5934	5935	5937	5938	5940	5940
Reference	13	13,14	13	13	13	13	13	13	13,15	13,14
SiO2	38.37	43.79	43.94	40.79	43.66	42.31	39.38	38.93	38.29	49.06
TiO2	2.34	2.67	3.25	4.59	2.89	3.07	4.55	3.31	3.31	4.05
Al2O3	5.99	7.04	7.71	7.54	7.88	7.93	7.76	7.90	7.29	9.26
Fe2O3	0.59	1.35	3.30	2.01	2.88	1.47	2.87	2.35	2.81	1.41
FeO	6.48	5.73	4.88	6.40	4.74	5.90	5.87	5.04	5.15	5.65
MnO	0.10	0.09	0.10	0.10	0.09	0.09	0.11	0.08	0.12	0.08
MgO	15.00	15.59	12.02	10.91	12.06	8.48	7.52	8.70	10.01	7.32
CaO	6.94	5.21	7.16	8.16	6.98	8.71	10.07	10.90	12.24	4.98
Na2O	1.36	1.30	1.01	1.56	1.23	1.47	1.38	1.37	1.16	1.56
K2O	6.25	7.06	7.53	7.77	7.66	7.70	7.45	6.77	5.67	9.19
P2O5	0.80	1.16	1.04	1.19	1.18	1.11	1.85	1.46	1.00	1.30
H2O+	2.35	3.19	2.19	2.41	2.77	2.17	2.17	2.54	2.91	1.86
H2O-	--	--	--	--	--	--	--	--	--	--
CO2	6.08	2.94	2.18	4.39	4.11	6.50	4.81	5.87	8.97	1.98
Ba	3971	6200	4677	4139	4548	3887	4725	4600	5758	3883
Rb	189	189	245	213	199	179	184	184	152	176
Sr	1683	2190	1710	1163	1209	1069	1283	872	1052	2419
Zr	562	789	659	866	493	588	1033	584	561	894
Nb	--	--	--	--	--	--	--	--	--	--
Y	16	22	27	25	25	17	31	22	28	25
La	228	373	340	284	254	322	363	293	367	421
Ce	286	447	398	365	368	409	537	394	439	523
Nd	--	--	--	--	--	--	--	--	--	--
Sc	--	--	--	--	--	--	--	--	--	--
V	291	278	342	472	303	332	462	346	362	400
Ni	549	518	243	131	250	115	--	82	151	89
Cr	731	533	357	257	334	258	120	255	351	208

Locality	West Greenland	West Greenland	West Greenland	West Greenland	West Greenland	West Greenland	Smoky Butte	Smoky Butte	Smoky Butte	Leucite Hills
Sample	5943	5944	5945	E12	E14	5638	Lamproite	Lamproite	Lamproite	U.S.A.
Reference	13,15	13	13,14	13	13	13	16	16	16	17
SiO2	41.20	43.41	41.63	39.17	41.34	44.15	52.19	53.53	51.89	51.03
TiO2	2.50	3.86	3.11	2.28	3.06	2.34	4.96	5.23	5.17	2.67
Al2O3	8.43	7.33	7.70	5.80	7.72	6.02	9.04	9.08	9.05	9.81
Fe2O3	2.38	1.37	1.28	2.39	1.56	2.85	5.02	4.39	3.86	3.67
FeO	3.85	6.16	6.14	4.84	6.00	3.21	3.50	1.02	1.31	0.65
MnO	0.09	0.09	0.10	0.08	0.10	0.09	0.00	0.08	0.00	0.07
MgO	12.30	7.26	9.88	15.42	10.33	9.72	7.98	7.78	7.90	7.24
CaO	9.68	7.89	10.14	8.38	10.93	13.95	4.90	4.43	4.44	5.37
Na2O	1.11	1.88	1.34	1.57	1.35	1.82	1.14	1.93	1.97	1.03
K2O	7.38	8.42	6.89	6.40	6.58	5.78	7.85	7.85	7.63	10.61
P2O5	0.46	1.25	1.26	0.85	1.18	0.87	0.22	0.22	0.25	1.71
H2O+	2.70	2.01	2.71	2.34	6.58	1.80	0.95	2.69	4.05	2.91
H2O-	--	--	--	--	--	--	0.54	1.72	1.27	--
CO2	6.90	4.90	7.10	9.06	7.05	5.56	--	--	--	0.52
									SO3	1.00
									F	0.69
									Cl	0.02
Ba	4075	3166	2738	2240	2778	4277	--	--	--	
Rb	218	187	160	161	161	163	--	--	--	
Sr	642	872	1114	1438	1184	1609	2700	2790	2950	
Zr	346	1181	648	583	593	451	--	--	--	
Nb	--	--	--	--	--	--	--	--	--	
Y	20	14	20	17	16	23	--	--	--	
La	174	242	308	201	210	307	--	--	--	
Ce	256	356	413	253	314	378	--	--	--	
Nd	--	--	--	--	--	--	--	--	--	
Sc	--	--	--	--	--	--	--	--	--	
V	250	396	298	228	274	251	--	--	--	
Ni	286	--	98	550	157	35	600	415	405	
Cr	399	200	257	752	342	1919	--	--	--	

Group I : Page 16

Locality	Leucite Hills U.S.A.	Leucite Hills U.S.A.	Leucite Hills U.S.A.	Leucite Hills U.S.A.	Leucite Hills U.S.A.	Leucite Hills U.S.A.	Leucite Hills U.S.A.	Leucite Hills U.S.A.	Leucite Hills U.S.A.	Leucite Hills U.S.A.
Reference	17	17	17	17	17	18	19	19	19	19
SiO2	52.98	51.57	54.86	53.45	43.10	51.07	50.23	53.70	54.08	54.17
TiO2	2.55	2.42	2.52	2.14	2.32	2.13	2.27	1.92	2.08	2.67
Al2O3	10.49	10.10	10.80	10.27	8.58	9.93	11.22	11.16	9.49	10.16
Fe2O3	2.64	2.85	3.00	3.60	5.34	2.72	3.34	3.10	3.19	3.34
FeO	1.94	1.63	0.96	1.00	0.80	1.19	1.84	1.21	1.03	0.65
MnO	0.07	0.08	0.05	0.08	0.13	0.00	0.05	0.04	0.05	0.06
MgO	7.23	7.78	6.56	9.61	11.60	10.31	7.09	6.44	6.74	6.62
CaO	4.31	5.03	3,57	4.21	10.71	4.87	5.99	3.46	3.55	4.19
Na2O	1.29	1.31	1.24	1.26	0.93	0.82	1.37	1.67	1.39	1.21
K2O	11.15	11.32	10.70	10.62	8.53	9.92	9.81	11.16	11.76	11.91
P2O5	1.37	1.61	1.32	1.28	2.13	1.53	1.89	1.75	1.35	1.59
H2O+	--	--	--	1.15	3.87	4.23	1.72	2.61	2.71	1.01
H2O-	--	--	--	--	--	--	0.93	0.80	0.79	0.52
CO2	--	--	--	0.57	0.48	--	--	--	--	0.49
L.O.I.	2.86	2.79	3.24	--	--	--	--	--	--	--
SO3	--	--	--	--	0.50	0.33	0.74	0.06	0.29	0.16
F	--	--	--	0.06	0.71	--	0.50	0.44	0.49	0.36
Cl	--	--	--	0.03	--	--	0.03	0.03	0.04	0.06
Ba	5408	6561	4621	3065	4319		10000	5500	5200	5000
Rb	249	246	259	246	195		--	--	--	--
Sr	1840	2179	1652	1674	3196		2000	1700	1750	1600
Zr	1250	1256	1298	1283	1232		--	--	--	--
Nb	58	53	48	45	137		--	--	--	--
Y	16	17	16	14	27		--	--	--	--
La	--	--	--	--	--		--	--	--	--
Ce	--	--	--	--	--		--	--	--	--
Nd	--	--	--	--	--		--	--	--	--
Sc	--	--	--	--	--		--	--	--	--
V	--	--	--	--	--		--	--	--	--
Ni	274	267	309	428	162		--	--	--	--
Cr	417	565	402	565	607		--	--	--	--

Locality	Leucite Hills U.S.A.	Leucite Hills U.S.A.	Leucite Hills U.S.A.	Leucite Hills U.S.A.	Leucite Hills U.S.A.	Leucite Hills U.S.A.	Leucite Hills U.S.A.	Leucite Hills U.S.A.	Leucite Hills U.S.A.	Leucite Hills U.S.A.
Reference	19	20	20	20	20	20	20	20	21	22
SiO2	42.65	53.40	53.10	51.20	52.70	55.00	55.80	53.60	42.83	47.54
TiO2	1.64	2.40	2.40	2.40	2.60	2.60	2.60	2.30	2.39	2.60
Al2O3	9.14	10.30	8.90	10.00	9.20	10.30	10.80	10.40	8.14	11.28
Fe2O3	5.13	3.80	4.70	5.40	4.70	3.90	4.00	4.80	5.89	4.96
FeO	1.07	--	--	--	--	--	--	--	0.70	0.96
MnO	0.12	0.05	0.06	0.08	0.06	0.05	0.05	0.07	0.14	0.03
MgO	10.89	6.50	7.70	7.40	10.00	5.60	5.70	6.00	10.83	7.84
CaO	12.36	4.50	4.20	7.20	4.00	2.50	2.70	4.10	12.42	9.31
Na2O	0.90	1.70	1.40	2.00	1.10	1.20	0.80	1.30	0.54	0.81
K2O	7.99	12.70	12.40	10.50	10.00	12.00	12.00	12.10	6.56	9.08
P2O5	1.52	1.70	1.50	1.90	2.50	2.10	2.00	3.00	1.39	0.72
H2O+	2.18	0.80	1.80	1.20	1.50	3.10	3.20	1.40	3.00	3.78
H2O-	2.04	--	--	--	--	--	--	--	--	--
CO2	--	--	--	--	--	--	--	--	--	--
SO3	0.58	--	--	--	--	--	--	--	--	--
F	0.47	--	--	--	--	--	--	--	0.60	--
Cl	0.03	--	--	--	--	--	--	--	--	--
Ba	8000								9000	5000
Rb	--								--	--
Sr	3000								--	--
Zr	--								--	--
Nb	--								--	--
Y	--								--	--
La	--								--	--
Ce	--								--	--
Nd	--								--	--
Sc	--								--	--
V	--								--	--
Ni	--								--	--
Cr	--								--	--

Locality	Leucite Hills U.S.A.	Leucite Hills U.S.A.	Leucite Hills U.S.A.	Leucite Hills U.S.A.	Leucite Hills U.S.A.	Leucite Hills U.S.A.	Leucite Hills U.S.A.	Leucite Hills U.S.A.	Leucite Hills U.S.A.	Northeast Utah U.S.A.
Reference	23	24	24	25	26	26	26	26	26	27
SiO2	50.20	48.94	52.64	46.50	50.23	55.43	53.07	55.14	43.56	50.46
TiO2	2.30	1.76	1.72	2.30	2.30	2.64	2.41	2.58	2.31	2.12
Al2O3	11.39	12.44	13.38	11.50	10.15	9.73	8.96	10.35	7.85	11.73
Fe2O3	4.23	4.28	5.19	5.30	3.65	2.12	3.86	3.27	5.57	3.11
FeO	0.57	3.71	1.63	0.14	1.21	1.48	0.91	0.62	0.85	1.84
MnO	0.07	0.10	0.09	0.09	0.09	0.08	0.08	0.06	0.15	0.09
MgO	7.23	5.84	4.40	8.06	7.48	6.11	11.17	6.41	11.03	10.78
CaO	6.00	4.77	3.16	7.83	6.12	2.69	3.56	3.45	11.89	4.62
Na2O	0.86	2.17	2.22	2.88	1.29	0.94	1.15	1.21	0.74	1.02
K2O	10.19	11.01	11.96	10.40	10.48	12.66	10.72	11.77	7.19	9.53
P2O5	--	0.47	0.44	1.81	1.81	1.52	1.24	1.40	1.50	1.67
H2O+	3.54	1.43	1.87	--	2.34	2.07	1.16	1.23	2.89	1.67
H2O-	--	0.54	0.44	--	1.09	0.61	0.40	0.61	2.09	0.21
CO2	--	--	--	--	--	--	--	--	--	--
L.O.I.	--	--	--	2.80	--	--	--	--	--	--
SO3	--	0.44	0.09	--	0.35	0.46	0.16	0.40	0.52	--
F	--	0.71	0.53	--	--	--	--	--	--	--
Cl	--	0.05	0.03	--	--	--	--	--	--	--
Ba		7200	3200	5700	5500	5800	3000	4700	6000	7400
Rb		--	--	--	--	330	290	310	205	--
Sr		3200	1800	3600	2800	2300	2300	2200	3500	1100
Zr		--	--	1600	2100	2300	2200	2300	2300	--
Nb		--	--	--	--	--	--	--	--	--
Y		--	--	--	--	25	25	20	25	--
La		--	--	--	--	260	200	130	360	--
Ce		--	--	--	--	--	--	--	--	--
Nd		--	--	--	--	--	--	--	--	--
Sc		--	--	--	--	--	--	--	--	--
V		--	--	--	--	--	--	--	--	--
Ni		--	--	--	--	--	--	--	--	--
Cr		--	--	--	--	--	--	--	--	--

Locality	Northeast Utah U.S.A.	Kansas Hills Pond	Kansas Hills Pond	Kansas Hills Pond	Kansas Hills Pond	Kansas Hills Pond	Kansas Hills Pond	Kansas Hills Pond	Kansas Hills Pond	Arkansas Prairie Creek
Reference	27	28	28	28	29	29	29	29	29	30
SiO2	55.73	44.62	45.55	47.34	42.70	41.60	42.70	45.80	49.80	44.32
TiO2	2.82	2.68	2.85	2.97	1.90	2.20	2.53	2.80	2.95	2.22
Al2O3	10.72	5.00	4.96	5.06	4.00	4.40	3.90	4.30	4.50	3.80
Fe2O3	3.73	--	--	--	7.68	7.83	7.99	8.20	7.00	5.95
FeO	0.95	6.82	6.74	6.78	--	--	--	--	--	1.15
MnO	0.08	0.10	0.14	0.16	0.09	0.09	0.09	0.10	0.09	0.11
MgO	6.96	20.40	18.65	17.29	22.50	22.50	20.80	18.50	16.70	20.00
CaO	3.85	3.51	3.67	2.88	3.03	3.70	3.90	2.70	1.55	4.15
Na2O	1.21	0.34	0.49	0.66	0.34	0.31	0.42	0.58	0.99	0.50
K2O	10.49	4.31	5.18	5.71	6.33	6.17	6.79	8.40	9.46	3.07
P2O5	1.13	0.72	0.78	1.00	--	--	--	--	--	--
H2O+	1.14	--	--	--	--	--	--	--	--	0.30
H2O-	0.89	--	--	--	--	--	--	--	--	3.62
CO2	--	--	--	--	--	--	--	--	--	8.85
L.O.I.	--	--	--	--	10.90	10.20	10.30	8.00	7.40	--
S	--	0.31	0.24	0.10	--	--	--	--	--	--
Ba	3000	--	--	--	4450	5200	6440	8200	10030	
Rb	--	--	--	--	227	204	193	217	156	
Sr	500	--	--	--	--	--	--	--	--	
Zr	--	--	--	--	--	--	--	--	--	
Nb	--	--	--	--	--	--	--	--	--	
Y	--	--	--	--	--	--	--	--	--	
La	--	167	172	184	139	142	157	195	199	
Ce	--	341	356	374	260	262	290	354	396	
Nd	--	--	--	--	--	--	--	--	--	
Sc	--	12	14	13	11	12	13	15	13	
V	--	--	--	--	--	--	--	--	--	
Ni	--	870	770	730	--	--	--	--	--	
Cr	--	1290	1260	1170	2600	1540	1440	1190	1040	

Locality	Prairie Creek U.S.A.	Prairie Creek U.S.A.	East Kimberley Australia	West Kimberley Australia	West Kimberley Australia	West Kimberley Australia	West Kimberley Australia	West Kimberley Australia	West Kimberley Australia	West Kimberley Australia
Reference	30	31	32	32	33	33	33	33	33	33
SiO2	42.90	38.40	45.00	37.40	41.52	40.10	42.80	42.61	40.71	42.43
TiO2	2.48	2.36	3.32	3.30	2.68	2.64	2.71	3.19	3.31	5.77
Al2O3	3.75	3.47	4.84	3.36	3.54	3.50	3.30	4.40	4.51	4.44
Fe2O3	3.48	8.65	3.00	6.93	4.57	3.80	4.90	4.52	4.58	4.94
FeO	4.25	--	4.66	1.55	3.90	4.98	3.52	4.26	4.28	2.37
MnO	0.12	0.13	0.12	0.12	0.13	0.14	0.12	0.14	0.14	0.11
MgO	27.50	26.31	21.20	25.50	26.90	26.10	24.90	22.33	22.20	19.04
CaO	4.20	4.60	4.88	4.24	4.38	5.61	4.30	5.21	5.37	4.06
Na2O	0.28	0.73	0.46	0.16	0.36	0.45	0.51	0.47	0.37	0.63
K2O	4.00	3.07	5.50	3.28	4.10	3.46	4.23	4.03	4.51	5.11
P2O5	1.01	0.81	1.58	1.62	0.62	1.17	0.60	0.78	1.48	0.80
H2O+	0.54	8.10	3.01	6.73	4.13	3.55	3.74	4.45	4.74	4.93
H2O-	0.48	--	0.67	3.72	1.60	1.93	1.74	1.71	0.95	2.32
CO2	5.00	0.18	0.50	0.55	0.19	0.12	0.10	0.17	0.21	0.70
S	0.09	--	--	--	0.01	0.07	0.01	--	0.01	--
F	--	--	--	--	0.20	0.47	0.26	--	0.54	--
Ba		2540	800	4342	10093	8966	6976	10106	18281	3867
Rb		211	--	--	386	556	376	611	486	300
Sr		1284	600	1250	959	1245	986	1098	1172	1150
Zr		704	400	200	564	683	603	841	796	1215
Nb		103	100	60	118	211	113	244	233	130
Y		13	10	10	16	19	17	10	20	12
La		--	150	300	185	344	232	237	412	158
Ce		--	--	300	261	415	270	346	673	210
Nd		--	--	--	--	--	--	--	--	--
Sc		14	--	--	18	22	17	--	21	9
V		27	--	--	20	73	83	97	19	142
Ni		--	400	400	1500	960	1120	792	1100	673
Cr		1417	600	300	1250	1396	1703	932	947	528

Group I : Page 21

Locality	West Kimberley Australia	West Kimberley Australia	West Kimberley Australia	West Kimberley Australia	West Kimberley Australia	West Kimberley Australia	West Kimberley Australia	West Kimberley Australia	West Kimberley Australia	West Kimberley Australia
Reference	33	33	33	33	33	33	33	33	33	33
SiO2	46.04	48.12	50.47	49.26	52.59	49.69	51.84	52.50	52.36	50.31
TiO2	6.59	8.12	5.67	5.41	5.37	6.92	6.03	6.22	7.01	5.77
Al2O3	6.85	5.97	7.38	5.41	8.28	8.62	8.33	7.47	8.55	9.12
Fe2O3	7.12	5.99	5.72	7.27	5.05	6.75	5.20	5.86	5.79	6.16
FeO	0.88	1.50	1.62	1.92	1.69	0.88	1.60	1.45	1.58	1.33
MnO	0.10	0.09	0.09	0.10	0.08	0.09	0.07	0.09	0.08	0.05
MgO	10.74	10.74	9.12	8.29	7.28	7.03	6.85	6.84	6.36	6.35
CaO	3.89	2.80	4.15	2.56	3.53	2.64	3.10	3.97	2.23	2.06
Na2O	0.45	0.49	0.44	0.45	1.01	0.44	0.65	0.72	0.50	0.17
K2O	9.67	9.56	8.80	7.74	9.72	10.15	10.06	9.44	10.47	10.56
P2O5	1.68	1.05	0.75	0.64	0.50	1.07	0.69	0.97	0.48	1.33
H2O+	2.20	2.65	2.64	5.29	1.79	2.06	1.73	1.46	2.03	2.84
H2O-	0.11	0.42	0.41	2.97	0.56	0.81	0.86	0.35	0.54	1.65
CO2	0.23	0.25	0.75	0.30	0.76	0.23	0.21	0.15	0.36	0.15
S	--	--	0.19	0.08	--	--	--	--	0.14	--
F	--	--	0.40	0.32	--	--	--	--	0.30	--
Ba	18993	10337	11253	31446	9810	12209	13939	12463	9322	8155
Rb	656	667	341	1448	199	429	292	319	353	302
Sr	1620	1990	777	1070	1176	1070	985	1288	887	1097
Zr	1651	1914	1225	1238	1057	1428	1164	1296	1302	1321
Nb	231	250	166	123	101	138	104	140	120	130
Y	13	15	15	20	17	23	15	11	14	11
La	436	519	245	301	189	317	259	242	269	270
Ce	619	788	355	382	286	459	361	377	387	415
Nd	--	--	--	--	--	--	--	--	--	--
Sc	--	--	--	18	--	--	--	--	--	--
V	109	215	204	151	162	169	215	228	216	224
Ni	235	312	235	390	363	407	383	83	259	297
Cr	440	389	490	317	267	278	205	209	204	297

Locality	West Kimberley Australia	West Kimberley Australia	West Kimberley Australia	West Kimberley Australia	West Kimberley Australia	West Kimberley Australia	West Kimberley Australia	West Kimberley Australia	West Kimberley Australia	West Kimberley Australia
Reference	33	33	33	33	34	35	35	35	35	35
SiO2	59.01	53.61	54.67	58.75	51.39	36.02	45.82	46.56	51.19	52.45
TiO2	5.68	5.66	5.86	5.64	4.47	5.31	7.34	6.86	4.89	5.85
Al2O3	7.02	9.85	7.90	7.29	8.55	5.32	6.86	6.88	8.53	8.64
Fe2O3	6.02	5.66	7.39	6.02	4.75	5.37	6.07	6.94	6.12	5.48
FeO	1.02	1.22	0.72	0.87	1.80	0.89	1.98	1.15	1.38	0.94
MnO	0.08	0.11	0.07	0.07	0.07	0.04	0.10	0.05	0.06	0.13
MgO	5.31	4.99	4.86	4.47	6.30	7.79	10.90	10.07	7.15	6.42
CaO	2.51	2.13	2.38	2.07	3.15	15.12	4.70	3.36	5.82	2.01
Na2O	0.69	0.67	0.34	0.38	0.25	0.16	0.84	0.21	0.58	0.38
K2O	8.67	11.22	9.10	8.64	7.62	7.25	8.82	9.37	9.02	10.42
P2O5	0.65	0.72	1.18	1.06	0.98	1.15	1.83	1.49	0.79	1.58
H2O+	1.42	1.53	2.12	1.75	5.31	1.92	0.75	2.48	1.99	1.99
H2O-	0.62	0.48	1.07	0.97	2.80	0.90	2.40	1.16	1.26	2.89
CO2	0.18	0.30	0.35	0.22	<0.05	9.84	0.08	--	--	--
S	--	--	0.13	--	--	SO3 0.27	--	0.35	0.11	--
F	--	--	0.25	--	--	0.17	--	0.22	--	--
Ba	5734	10105	13293	9338	--	14000	1100	18000	5300	10500
Rb	260	322	356	333	3100	--	--	--	--	--
Sr	805	1033	1005	1042	1093	1800	--	2500	--	--
Zr	1220	1215	1267	1278	1132	1600	--	2100	--	--
Nb	145	129	150	153	--	--	--	--	--	--
Y	14	18	15	12	32	--	--	--	--	--
La	227	409	263	230	--	--	--	--	--	--
Ce	347	552	387	358	--	--	--	--	--	--
Nd	--	--	--	--	--	--	--	--	--	--
Sc	--	--	--	--	--	--	--	--	--	--
V	216	282	208	183	--	--	--	--	--	--
Ni	77	263	342	248	310	--	--	--	--	--
Cr	201	296	356	345	698	--	--	--	--	--

Group I : Page 23

Locality	West Kimberley Australia	West Kimberley Australia	West Kimberley Australia	West Kimberley Australia	West Kimberley Australia	West Kimberley Australia	West Kimberley Australia	West Kimberley Australia	West Kimberley Australia	West Kimberley Australia
Reference	35	35	36	36	36	36	36	3	3	3
SiO2	54.09	54.48	51.98	44.02	51.22	52.37	52.79	52.60	49.30	54.20
TiO2	4.08	5.57	4.96	6.57	4.00	4.82	5.00	5.34	4.54	6.04
Al2O3	11.67	9.87	7.97	6.30	10.59	9.86	11.37	7.08	7.05	8.70
Fe2O3	4.91	4.89	3.93	5.98	6.91	6.15	5.41	6.59	7.18	7.26
FeO	2.14	1.70	1.34	2.01	1.33	1.48	1.83	--	--	--
MnO	0.03	0.09	0.04	0.06	0.05	0.07	0.07	0.06	0.09	0.07
MgO	4.76	5.35	9.41	11.98	6.67	5.90	4.84	8.54	12.10	5.38
CaO	1.91	1.89	3.18	4.61	2.34	3.32	2.21	3.83	4.63	2.17
Na2O	0.10	0.88	0.36	0.28	0.07	0.24	0.45	0.45	0.52	0.19
K2O	12.60	11.06	9.61	6.59	11.90	10.35	11.40	8.28	7.67	10.70
P2O5	0.26	0.40	1.36	1.55	1.33	0.91	1.03	1.19	0.73	1.71
H2O+	2.30	1.36	2.36	3.83	2.04	1.94	1.49	--	--	--
H2O-	0.73	0.89	2.87	3.42	1.04	1.52	1.04	--	--	--
CO2	--	--	--	--	--	--	--	--	--	--
L.O.I.	--	--	--	--	--	--	--	5.03	5.39	2.70
SO3	--	0.10	--	--	--	--	--	--	--	--
F	--	0.09	--	--	--	--	--	--	--	--
Ba	6500	5300						11000	5200	2700
Rb	--	--						368	204	238
Sr	--	1300						1100	1000	1150
Zr	--	--						1202	879	1081
Nb	--	--						179	140	163
Y	--	--						13	16	22
La	--	--						--	--	--
Ce	--	--						--	--	--
Nd	--	--						--	--	--
Sc	--	--						17	16	16
V	--	--						--	--	--
Ni	--	--						450	650	220
Cr	--	--						1100	2600	650

Locality	West Kimberley Australia	West Kimberley Australia	West Kimberley Australia	West Kimberley Australia	West Kimberley Australia	Gaussberg Antarctica	Gaussberg Antarctica	Gaussberg Antarctica	Gaussberg Antarctica	Gaussberg Antarctica
Reference	3	3	3	3	3	37-39	37-39	37-39	37-39	37-39
SiO2	59.00	51.10	50.90	59.30	52.60	50.80	50.20	50.70	50.50	50.10
TiO2	4.17	5.12	5.38	5.44	5.20	3.43	3.36	3.34	3.28	3.34
Al2O3	6.26	7.23	7.76	8.21	8.13	9.95	9.79	9.95	10.04	9.92
Fe2O3	6.11	6.78	6.39	6.49	7.12	2.47	2.40	2.32	2.77	3.12
FeO	--	--	--	--	--	3.76	3.85	3.84	3.39	3.14
MnO	0.09	0.08	0.08	0.05	0.09	0.09	0.09	0.09	0.09	0.09
MgO	6.17	9.25	9.19	4.24	7.21	8.09	7.92	8.34	8.19	8.21
CaO	5.85	4.60	3.94	1.08	3.49	4.78	4.72	4.76	4.84	4.91
Na2O	0.55	0.49	0.85	0.30	1.21	1.78	1.64	1.70	1.53	1.17
K2O	7.49	8.94	8.74	10.10	9.68	11.49	11.54	11.54	11.30	10.97
P2O5	0.81	0.61	0.42	0.50	0.46	1.46	1.46	1.44	1.46	1.46
H2O+	3.04	4.53	4.93	3.58	3.06	1.24	1.03	1.09	1.13	2.72
H2O-	--	--	--	--	--	0.07	0.07	0.06	0.03	0.04
CO2	--	--	--	--	--	0.09	0.07	0.03	0.02	<0.01
Ba	4500	7000	8300	3300	9000	5550	5440	5620	5850	5970
Rb	186	170	237	289	193	309	305	311	311	313
Sr	950	830	950	750	1100	1870	1890	1830	1860	1940
Zr	929	1114	1114	1243	1040	903	915	901	890	893
Nb	153	131	118	160	125	88	89	88	87	88
Y	17	17	14	17	15	19	19	18	18	18
La	155	--	--	--	--	214	207	211	213	215
Ce	279	--	--	--	--	348	334	339	341	338
Nd	93	--	--	--	--	130	129	131	130	--
Sc	15	16	16	18	17	--	--	--	--	--
V	--	--	--	--	--	112	108	110	108	107
Ni	140	500	450	300	380	223	231	234	243	234
Cr	650	900	850	800	950	308	333	311	324	338

Locality	Gaussberg Antarctica	Gaussberg Antarctica	Gaussberg Antarctica	Gaussberg Antarctica	Gaussberg Antarctica	Gaussberg Antarctica	Mount Bayliss Antarctic	Mount Bayliss Antarctic	Priestly Peak Antarctic	Priestly Peak Antarctic
Reference	37-39	37-39	37-39	37-39	37-39	37-39	39-40	39-40	39-40	39-40
SiO2	51.60	51.60	51.00	51.20	51.50	51.00	52.90	50.30	52.60	49.60
TiO2	3.47	3.50	3.50	3.44	3.54	3.42	4.45	5.45	3.40	3.27
Al2O3	10.00	10.05	9.98	9.42	9.49	9.89	8.92	8.90	8.67	9.10
Fe2O3	2.33	2.12	2.48	2.54	2.31	2.15	2.64	2.72	2.03	2.45
FeO	3.84	4.00	3.83	3.86	4.12	3.94	5.30	6.00	4.12	4.06
MnO	0.08	0.08	0.09	0.09	0.09	0.08	0.11	0.11	0.09	0.08
MgO	7.53	7.50	7.81	8.19	7.95	7.76	5.95	5.56	7.43	8.77
CaO	4.48	4.50	4.81	4.35	4.38	4.37	4.00	5.06	4.97	5.32
Na2O	2.19	1.85	1.55	1.53	1.65	1.53	2.05	1.75	0.73	0.89
K2O	11.50	11.87	11.68	11.73	12.16	11.89	9.35	8.90	8.32	9.83
P2O5	1.49	1.48	1.50	1.48	1.53	1.50	1.75	1.85	3.05	3.28
H2O+	0.84	0.65	1.14	1.17	0.92	0.96	0.89	1.06	0.77	0.84
H2O-	0.05	0.03	0.04	0.06	0.07	0.08	0.31	0.29	0.05	0.06
CO2	0.13	0.02	0.04	0.03	0.02	0.05	0.25	1.45	0.16	0.02
SO3	--	--	--	--	--	--	0.09	0.10	0.84	0.53
F	--	--	--	--	--	--	0.28	0.33	0.96	1.03
Cl	--	--	--	--	--	--	0.01	0.03	0.03	0.02
Ba	5640	5640	5380	5450	5340	5320	412	1320	15100	9700
Rb	315	316	307	336	330	313	210	149	252	314
Sr	1740	1760	1840	1710	1720	1720	1780	1260	2910	2590
Zr	957	972	943	1350	1360	955	1580	1240	1770	1420
Nb	87	90	93	96	97	87	145	102	59	43
Y	19	19	18	18	19	18	32	37	32	36
La	212	206	204	211	211	204	162	156	172	138
Ce	335	331	321	343	343	334	276	270	294	268
Nd	128	127	127	131	134	123	116	118	133	150
Sc	--	--	--	--	--	--	--	--	--	--
V	107	104	107	100	101	107	94	133	168	143
Ni	231	249	226	240	223	228	131	128	243	298
Cr	303	272	315	287	284	288	215	180	274	348

Group I : Page 26

Locality	Priestly Peak Antarctic	Priestly Peak Antarctic	NW Alps	NW Alps	NW Alps	NW Alps	NW Alps
Reference	39-40	39-40	160	160	160	160	160
SiO2	50.40	52.00	52.48	49.88	50.82	52.16	55.34
TiO2	3.52	2.85	0.97	1.29	1.21	0.95	1.18
Al2O3	8.95	8.74	10.74	9.93	11.24	12.66	10.10
Fe2O3	1.97	3.19	7.34	6.84	6.60	6.91	5.12
FeO	4.63	3.39	--	--	--	--	--
MnO	0.10	0.11	0.11	0.10	0.11	0.11	0.11
MgO	8.55	7.29	8.29	11.13	11.79	8.47	9.18
CaO	5.47	4.54	7.94	5.90	6.60	5.88	3.84
Na2O	0.85	1.90	1.39	0.67	2.50	2.51	2.01
K2O	8.49	8.34	7.20	8.41	6.65	7.56	9.57
P2O5	3.32	2.76	1.44	1.26	1.29	1.20	1.42
H2O+	0.86	0.88	--	--	--	--	--
H2O-	0.02	0.04	--	--	--	--	--
CO2	0.02	0.06	--	--	--	--	--
SO3	0.30	0.74	1.44	4.52	0.83	1.56	1.15
F	1.40	1.07					
Cl	0.02	0.09					
Ba	10100	13600					
Rb	284	186					
Sr	2950	2350					
Zr	1780	1690					
Nb	63	49					
Y	39	29					
La	173	153					
Ce	335	273					
Nd	164	--					
Sc	--	--					
V	152	170					
Ni	300	220					
Cr	362	249					

Group II : Page 1

Locality	San Venanzo	San Venanzo	San Venanzo	Cupaello	Cupaello	Cupaello	Fen Norway	Aland Is. Finland	Sokli Finland	Toro Ankole
Rock							Damkjernite			
Reference	41,42	43	44	43	45	41,42	46,47	48	49	50-56
SiO2	40.52	41.00	42.33	42.60	41.74	41.45	39.31	30.40	21.80	35.37
TiO2	0.74	0.76	0.76	1.09	1.24	1.20	3.25	2.90	3.50	3.87
Al2O3	10.43	11.30	10.67	7.71	7.36	7.56	15.68	8.60	2.40	6.50
Fe2O3	4.66	2.60	2.82	4.90	4.56	4.41	6.38	7.90	7.00	7.23
FeO	2.92	4.23	4.01	2.64	2.77	2.96	8.55	6.30	7.40	5.00
MnO	0.11	0.12	0.08	0.11	0.10	0.14	0.21	0.28	0.29	0.24
MgO	12.65	13.00	13.24	10.60	11.12	11.20	8.21	13.70	17.60	14.08
CaO	16.23	14.80	15.41	14.10	15.71	15.99	12.50	15.80	13.80	16.79
Na2O	1.11	1.09	0.95	0.39	0.38	0.55	0.35	0.40	1.20	1.32
K2O	7.41	7.76	7.60	8.45	5.45	5.33	4.93	3.50	3.60	4.09
P2O5	0.32	0.33	0.30	1.18	1.10	1.21	0.52	2.10	1.06	0.74
H2O+	--	--	--	--	--	--	1.65	2.60	1.90	2.78
H2O-	--	--	--	--	--	--	0.13	0.70	0.50	1.15
CO2	--	--	--	--	--	--	1.20	3.85	17.60	0.09
L.O.I.	--	2.97	1.32	6.30	3.83	--	--	--	--	--
S							0.20	0.68	0.12	0.35
F							--	0.40	0.58	0.16
Cl							--	0.01	--	0.02
Ba		779	718	3570					880	2900
Rb		404	445	432					100	200
Sr		1591	1729	3987					900	4500
Zr		330	337	662					345	1200
Nb		16	19	42					150	--
Y		36	31	44					--	--
La		--	81	--					93	40
Ce		--	156	--					150	--
Nd		--	94	--					--	--
Sc		23	37	14					21	--
V		129	140	70					--	250
Ni		136	125	69					350	270
Cr		832	880	55					--	900

Group II : Page 2

Locality	Toro Ankole	Toro Ankole	Toro Ankole	Toro Ankole	Toro Ankole	Toro Ankole	Toro Ankole	Toro Ankole	Toro Ankole	Toro Ankole
Reference	50,55,56	50,54-57	50,55-57	50,54-56	50,54,55, 57,58	50,58	50,57, 59,60	50,54,57	50,54,57	50,57,61
SiO2	33.89	33.22	33.52	34.23	39.06	40.65	39.28	37.05	40.00	38.62
TiO2	4.43	6.08	6.04	4.56	4.36	2.40	4.29	4.09	4.75	4.44
Al2O3	8.27	9.71	8.04	8.02	8.18	8.44	7.90	7.82	7.68	6.34
Fe2O3	7.03	6.68	5.88	6.62	4.61	4.71	4.88	5.11	5.38	4.60
FeO	5.21	5.30	5.50	5.34	4.98	5.49	5.23	5.23	4.77	6.00
MnO	0.26	0.52	0.15	0.22	0.26	0.16	0.27	0.25	0.15	0.09
MgO	10.93	12.12	13.54	9.22	17.66	17.06	17.58	14.76	15.46	20.06
CaO	16.98	15.64	15.22	16.54	10.40	11.03	11.03	14.28	9.79	10.45
Na2O	1.42	1.51	1.42	1.20	0.32	0.89	1.05	1.27	0.65	1.27
K2O	3.65	3.54	4.26	3.39	6.98	6.79	4.98	5.39	7.04	3.66
P2O5	0.97	1.12	0.82	0.96	0.61	0.57	0.36	0.76	0.42	0.45
H2O+	2.08	3.28	2.34	2.80	1.42	1.12	2.36	2.29	1.66	2.52
H2O-	1.19	0.80	1.68	1.72	0.50	0.50	0.40	0.71	0.97	1.08
CO2	3.27	0.42	0.96	4.02	tr	0.10	0.14	0.58	0.34	tr
S	0.14	--	--	0.12	0.13	--	0.12	0.16	0.09	0.18
F	0.18	0.08	--	0.14	0.13	--	0.09	0.12	0.18	0.10
Cl	--	--	--	--	--	--	--	--	tr	--
Ba	7000	1800	4500	2000	7500		--			
Rb	240	150	380	220	450		167			
Sr	--	4000	9500	7500	7000		2004			
Zr	1100	1200	800	850	900		613			
Nb	--	--	--	--	--		205			
Y	--	--	--	--	--		--			
La	100	30	70	50	80		155			
Ce	--	--	--	--	--		328			
Nd	--	--	--	--	--		--			
Sc	--	--	--	--	--		22			
V	170	350	210	260	220		--			
Ni	100	160	180	200	300		--			
Cr	290	500	1200	650	1300		--			

Group II : Page 3

Locality	Toro Ankole	Toro Ankole	Toro Ankole	Toro Ankole	Toro Ankole	Toro Ankole	Toro Ankole	Toro Ankole	Toro Ankole	Toro Ankole
Reference	50,55,57, 61,62	50,61	50,54, 59-61	50,54	50,54	50,54	50,52-56	50,55,56	50,62	50,63
SiO2	40.47	41.36	36.22	35.58	37.28	38.37	35.51	38.94	46.17	38.97
TiO2	3.52	3.68	4.76	5.07	4.97	4.54	4.88	3.88	2.24	4.66
Al2O3	5.38	5.47	8.21	7.97	7.55	8.73	6.83	6.92	13.03	8.92
Fe2O3	4.03	5.04	7.58	7.40	7.13	7.99	9.68	5.27	6.77	11.93
FeO	6.47	5.58	4.55	5.23	4.52	3.71	2.70	5.09	2.50	0.99
MnO	0.23	0.12	0.18	0.19	0.21	0.20	0.22	0.23	0.20	0.33
MgO	24.84	24.28	9.76	10.25	10.13	9.58	11.67	11.58	3.56	10.46
CaO	8.06	7.91	13.98	14.21	13.91	14.23	16.00	15.95	8.67	14.72
Na2O	0.68	0.91	1.28	1.27	1.39	1.20	1.56	1.01	1.29	1.68
K2O	3.46	3.19	7.29	6.21	5.64	5.98	3.30	3.96	4.61	4.36
P2O5	0.29	0.09	1.09	1.27	1.03	0.87	1.18	0.91	0.97	0.79
H2O+	1.11	1.87	1.55	2.09	1.74	1.39	3.11	2.26	6.13	1.24
H2O-	0.57	0.21	1.03	1.44	1.93	1.86	1.31	1.20	3.23	1.22
CO2	0.36	0.38	1.52	0.93	1.65	0.48	1.47	2.12	0.62	--
S	0.04	--	0.31	0.38	0.40	0.26	0.13	0.14	--	--
F	0.10	--	0.14	0.11	0.15	0.23	0.27	0.13	--	--
Cl	0.01	--	--	--	tr	0.01	tr	--	--	--
Ba	2000		--				2800	1700		
Rb	450		156				200	100		
Sr	1800		2531				7500	2500		
Zr	300		605				800	1200		
Nb	--		205				--	--		
Y	--		-				--	--		
La	35		197				30	20		
Ce	--		404				--	--		
Nd	--		--				--	--		
Sc	--		25				--	--		
V	110		--				320	320		
Ni	900		--				230	250		
Cr	1200		--				700	550		

Group II : Page 4

Locality	Toro Ankole	Toro Ankole	Toro Ankole	Toro Ankole	Virunga	Virunga	Virunga	Virunga	South Africa	South Africa
Reference	50,64	65	66	67	59	59	50,62,53	50,53	68	68
SiO2	40.19	38.05	36.20	35.90	43.37	45.23	39.98	46.59	32.93	33.28
TiO2	4.75	3.84	4.84	5.49	4.44	4.28	5.42	3.60	6.51	2.30
Al2O3	8.20	7.54	5.63	6.09	10.34	16.33	12.47	15.57	7.06	18.51
Fe2O3	5.13	8.41	8.33	5.50	4.02	3.33	7.06	2.51	13.15	8.22
FeO	7.18	2.80	5.46	6.55	5.54	5.98	6.43	8.81	6.21	8.69
MnO	0.17	0.21	0.22	0.21	0.17	0.17	0.00	0.20	0.27	0.11
MgO	11.60	13.55	13.82	10.38	11.60	4.28	6.59	4.66	8.82	6.02
CaO	12.51	13.90	15.21	14.97	14.16	7.81	11.85	8.58	11.25	12.03
Na2O	1.86	1.31	1.74	2.74	1.77	3.21	1.70	2.37	1.52	0.55
K2O	4.08	3.02	4.02	6.98	3.55	7.89	3.80	5.68	3.66	3.02
P2O5	0.52	0.95	0.88	1.46	0.58	0.90	0.73	0.74	1.54	--
H2O+	2.14	2.27	2.99	1.31	0.43	0.05	3.71	0.40	--	--
H2O-	0.95	3.00	0.84	--	0.13	0.12	--	0.10	--	--
CO2	0.21	0.53	0.10	0.50	--	--	--	0.02	--	--
L.O.I.	--	--	--	--	--	--	--	--	7.11	6.64
S	0.06	--	--	--	--	--	0.14	--	--	--
F	0.19	0.27	--	--	--	--	--	0.06	--	--
Cl	0.01	0.02	--	--	--	--	--	0.02	--	--
Ba		2251		2400	--	--				
Rb		114		120	175	242				
Sr		2935		2848	824	1488				
Zr		580		464	276	479				
Nb		241		328	101	198				
Y		16		29	--	--				
La		--		270	--	--				
Ce		--		480	--	--				
Nd		--		--	--	--				
Sc		--		--	--	--				
V		--		--	--	--				
Ni		253		118	--	--				
Cr		799		321	--	--				

Group II : Page 5

Locality	South Africa	Kola	Bergyda-malakh	Damodar Valley	Damodar Valley	Damodar Valley	Damodar Valley	Boshan China	Batbjerg Greenland	Batbjerg Greenland
Rock		Turjaite								
Reference	69	70	71	72	72	72	72	73	74	74
SiO2	37.24	37.31	34.02	32.37	35.29	35.70	34.11	22.49	40.55	44.56
TiO2	1.35	3.33	5.52	9.32	4.25	5.94	6.56	0.67	1.31	1.02
Al2O3	6.63	8.81	5.98	9.84	5.54	5.99	9.08	6.04	6.66	7.00
Fe2O3	1.43	8.42	5.47	8.68	11.20	11.22	10.44	4.26	8.41	7.67
FeO	6.93	2.60	8.48	--	--	--	--	3.73	6.74	5.44
MnO	0.28	0.19	0.23	0.12	0.29	0.14	0.15	0.20	0.20	0.22
MO	13.58	11.02	20.15	8.09	8.31	10.05	6.10	5.53	11.07	11.93
CaO	11.83	16.23	12.82	8.26	7.18	5.85	11.55	26.86	14.46	13.58
Na2O	1.33	1.66	1.00	0.13	0.11	0.08	0.21	0.45	0.95	1.92
K2O	3.22	4,46	3.08	7.09	3.42	4.69	4.90	3.47	3.90	3.92
P2O5	0.63	1.33	0.66	2.93	6.32	2.42	5.18	4.80	2.67	1.17
H2O+	--	2.17	--	--	--	--	--	--	1.24	0.55
H2O-	0.16	0.10	--	--	--	--	--	--	--	--
CO2	9.23	2.36	--	--	--	--	--	--	--	--
L.O.I.	4.46	--	2.54	11.78	14.77	15.61	8.75	21.07	--	--
Ba										
Rb										
Sr										
Zr										
Nb										
Y										
La										
Ce										
Nd										
Sc										
V										
Ni										
Cr										

Locality	Batbjerg Greenland	Oka Canada	N.E.Utah	Arkansas Magnet Cove	Beaver Lake Antarctica	Beaver Lake Antarctica	Boshof South Africa
Reference	74	75	27	76,70	77-78	77-78	161
SiO2	45.13	30.37	37.68	36.40	33.97	34.77	36.12
TiO2	1.12	2.39	0.64	0.42	2.43	2.48	1.45
Al2O3	7.35	9.20	7.33	12.94	8.96	9.97	4.38
Fe2O3	8.74	5.55	3.99	8.27	4.74	3.12	6.80
FeO	5.27	6.02	5.36	4.59	6.08	7.50	2.68
MnO	0.19	0.35	0.19	0.00	0.21	0.23	0.22
MgO	9.62	10.70	20.61	11.44	14.30	14.40	22.82
CaO	14.39	15.31	12.15	14.46	16.96	17.03	8.33
Na2O	1.46	1.54	0.71	0.97	1.41	1.51	0.29
K2O	4.67	3.79	5.33	3.01	3.00	3.12	5.04
P2O5	0.60	0.87	0.78	1.04	0.50	0.56	1.46
H2O+	0.71	1.96	3.44	2.36	--	--	4.89
H2O-	--	0.36	1.24	--	--	--	1.28
CO2	--	9.88	--	--	--	--	3.80
L.O.I.	--	--	--	--	7.83	5.89	--
F	--	0.40	--	--	--	--	0.29
						S	0.02
Ba		3900	350				
Rb		--	--				
Sr		3200	2600				
Zr		225	--				
Nb		--	--				
Y		36	--				
La		110	--				
Ce		140	--				
Nd		--	--				
Sc		13	--				
V		790	--				
Ni		130	--				
Cr		210	--				

Group III : Page 1

Locality	Mt.Amiata Italy	Mt.Amiata Italy	Mt.Amiata Italy	Mt.Amiata Italy	Mt.Amiata Italy	Mt.Amiata Italy	Mt.Amiata Italy	Mt.Amiata Italy	Mt.Amiata Italy	Mt.Amiata Italy
Reference	79	79	80	80	80	80	80	80	80	80
SiO2	60.68	62.05	48.99	49.49	49.57	51.02	51.19	51.27	51.57	52.27
TiO2	0.96	0.63	0.73	0.83	0.75	0.80	0.82	0.75	0.79	0.78
Al2O3	16.21	16.43	14.71	16.77	13.97	16.40	17.29	15.69	17.42	17.04
Fe2O3	2.27	4.65	5.57	4.74	5.78	3.67	3.54	3.40	4.46	3.22
FeO	1.75	--	1.69	2.40	1.47	2.88	3.54	3.11	2.18	3.18
MnO	0.07	0.08	0.12	0.11	0.12	0.12	0.12	0.12	0.12	0.12
MgO	3.46	3.36	7.20	5.54	7.09	5.01	4.98	5.28	4.32	4.64
CaO	4.03	4.46	11.06	8.61	10.05	9.22	8.09	8.40	8.59	8.06
Na2O	1.99	1.92	1.00	1.63	1.17	1.84	1.77	1.42	1.94	1.49
K2O	5.36	5.70	4.90	5.70	5.12	5.61	5.77	5.42	5.85	5.33
P2O5	0.27	0.24	0.39	0.38	0.39	0.38	0.40	0.36	0.40	0.39
H2O+	--	--	2.29	2.59	2.46	1.83	1.62	2.29	1.97	2.29
H2O-	0.75	--	0.54	0.61	0.68	0.30	0.49	0.64	0.35	0.69
L.O.I.	2.03	0.48	--	--	--	--	--	--	--	--
Ba	743	681	1100	1035	1110	930	960	1055	920	990
Rb	320	333	302	337	313	378	362	297	373	283
Sr	593	581	995	730	632	760	750	627	795	712
Zr	206	279	245	230	180	255	210	222	255	205
Nb	--	--	11	15	17	14	13	13	19	12
Y	--	--	20	25	30	17	17	22	20	31
La	72	73	78	78	81	66	70	71	70	75
Ce	155	156	139	147	124	129	136	133	122	137
Nd	69	68	--	--	--	--	--	--	--	--
Sc	16	16	--	--	--	--	--	--	--	--
V	102	112	--	--	--	--	--	--	--	--
Ni	22	24	--	--	--	--	--	--	--	--
Cr	94	87	--	--	--	--	--	--	--	--

Group III : Page 2

Locality	Mt.Amiata Italy	Mt.Amiata Ialy	Mt.Amiata Italy	Mt.Amiata Italy	Mt.Amiata Italy	Mt.Amiata Italy	Mt.Amiata Italy	Mt.Amiata Italy	Mt.Amiata Italy	Mt.Amiata Italy
Reference	80	80	80	80	80	80	80	80	80	80
SiO2	52.45	52.72	52.82	52.89	53.14	53.29	53.38	53.39	53.42	53.86
TiO2	0.77	0.77	0.81	0.78	0.79	0.75	0.77	0.80	0.76	0.69
Al2O3	17.24	17.47	16.49	17.41	17.29	17.37	16.76	17.11	17.25	15.29
Fe2O3	2.82	5.14	3.03	3.87	3.10	2.74	1.80	2.41	3.86	4.96
FeO	3.30	1.26	3.40	2.52	3.46	3.42	4.40	3.90	2.89	1.29
MnO	0.11	0.11	0.12	0.12	0.12	0.11	0.12	0.12	0.12	0.12
MgO	6.14	3.74	6.04	3.47	4.24	4.29	5.67	4.85	4.33	5.06
CaO	7.30	8.41	7.79	8.39	7.50	7.41	7.74	7.56	8.14	8.05
Na2O	2.03	1.71	1.65	1.68	1.67	1.65	1.67	1.71	1.66	1.58
K2O	5.38	5.65	5.28	5.57	5.41	5.33	5.68	5.53	5.34	5.41
P2O5	0.35	0.38	0.39	0.34	0.35	0.33	0.37	0.36	0.28	0.36
H2O+	1.51	2.33	1.58	2.16	2.05	2.31	1.32	1.50	1.63	3.01
H2O-	0.60	0.60	0.60	0.64	0.55	0.69	0.32	0.76	0.25	0.49
CO2	--	--	--	--	--	--	--	--	--	--
Ba	940	855	960	820	1005	945	935	920	1000	895
Rb	389	348	356	353	346	313	380	304	340	335
Sr	825	645	810	615	690	670	712	647	832	640
Zr	242	225	180	225	220	230	232	185	207	198
Nb	11	18	9	11	16	20	7	14	14	22
Y	16	34	17	15	31	23	15	19	20	31
La	71	67	65	65	75	78	74	69	71	71
Ce	129	129	130	125	129	144	157	124	140	135
Nd	--	--	--	--	--	--	--	--	--	--
Sc	--	--	--	--	--	--	--	--	--	--
V	--	--	--	--	--	--	--	--	--	--
Ni	--	--	--	--	--	--	--	--	--	--
Cr	--	--	--	--	--	--	--	--	--	--

Group III : Page 3

Locality	Mt.Amiata Italy	Mt.Amiata Italy	Mt.Amiata Italy	Mt.Amiata Italy	Mt.Amiata Italy	Mt.Amiata Italy	Mt.Amiata Italy	Mt.Amiata Italy	Mt.Amiata Italy	Mt.Amiata Italy
Reference	80	80	80	80	80	80	80	80	80	80
SiO2	54.88	55.54	55.61	55.68	55.95	56.26	56.49	56.59	57.02	57.20
TiO2	0.70	0.83	0.81	0.75	0.82	0.80	0.76	0.72	0.79	0.71
Al2O3	15.95	16.37	17.70	17.07	17.52	16.68	16.85	16.65	17.21	17.14
Fe2O3	5.47	2.34	1.05	2.51	2.20	3.80	2.48	4.43	1.82	3.20
FeO	0.79	4.30	4.50	3.36	3.02	2.05	2.87	1.30	3.75	2.01
MnO	0.11	0.13	0.11	0.11	0.11	0.11	0.10	0.11	0.11	0.10
MgO	4.51	3.38	4.37	4.05	4.36	4.13	4.96	3.22	3.81	4.20
CaO	7.86	8.45	5.76	6.49	5.67	7.01	5.50	5.54	4.97	5.15
Na2O	1.73	1.17	2.09	1.96	1.70	1.87	1.96	1.72	1.80	1.96
K2O	5.28	5.80	5.46	5.77	5.63	5.65	5.22	5.87	5.55	5.51
P2O5	0.34	0.37	0.31	0.32	0.34	0.31	0.30	0.28	0.29	0.28
H2O+	1.64	1.01	1.65	1.89	1.88	0.76	1.80	1.71	1.88	1.64
H2O-	0.39	0.31	0.58	0.45	0.80	0.57	0.71	0.50	1.00	0.90
CO2	--	--	--	--	--	--	--	--	--	--
Ba	875	935	835	810	875	780	850	825	985	870
Rb	348	346	337	324	324	356	324	389	318	281
Sr	695	830	770	600	605	740	610	580	487	525
Zr	207	232	250	230	240	220	222	207	267	230
Nb	15	14	13	14	13	12	12	15	12	13
Y	16	20	20	14	30	21	21	27	40	30
La	66	71	69	64	72	90	70	132	78	73
Ce	134	128	136	129	95	136	137	136	146	140
Nd	--	--	--	--	--	--	--	--	--	--
Sc	--	--	--	--	--	--	--	--	--	--
V	--	--	--	--	--	--	--	--	--	--
Ni	--	--	--	--	--	--	--	--	--	--
Cr	--	--	--	--	--	--	--	--	--	--

Group III : Page 4

Locality	Mt.Amiata Italy	Mt.Amiata Italy	Mt.Amiata Italy	Mt.Amiata Italy	Mt.Amiata Italy	Mt.Amiata Italy	Mt.Amiata Italy	Mt.Amiata Italy	Radicofani Italy	Radicofani Italy
Reference	80	80	80	80	80	80	80	80	79	79
SiO2	57.63	58.24	58.44	58.72	58.82	59.90	60.81	61.64	52.95	54.10
TiO2	0.72	0.75	0.78	0.70	0.75	0.70	0.64	0.62	1.28	1.35
Al2O3	16.79	17.63	16.94	16.81	16.81	16.59	16.08	16.22	15.45	14.34
Fe2O3	1.36	3.26	3.39	1.74	3.75	0.89	1.00	1.17	2.58	2.76
FeO	3.83	2.00	2.16	3.10	1.65	4.03	3.69	3.32	3.85	3.46
MnO	0.10	0.10	0.10	0.09	0.10	0.09	0.09	0.08	0.10	0.09
MgO	3.95	3.30	3.11	3.30	3.44	3.13	3.30	3.35	9.13	9.07
CaO	5.91	5.30	5.91	5.73	5.21	5.39	5.25	4.53	7.15	6.52
Na2O	2.27	2.18	2.09	2.20	2.14	1.72	2.01	1.92	1.71	1.64
K2O	5.62	5.36	5.66	5.68	5.71	5.35	5.62	5.66	4.21	5.43
P2O5	0.30	0.30	0.30	0.27	0.28	0.24	0.24	0.23	0.47	0.47
H2O+	0.90	1.17	0.86	1.12	0.86	1.45	0.96	0.85	0.45	0.65
H2O-	0.62	0.41	0.26	0.54	0.48	0.52	0.30	0.40	0.18	0.20
CO2	--	--	--	--	--	--	--	--	--	--
Ba	835	785	805	785	820	730	730	705	669	
Rb	353	297	418	324	380	362	378	394	264	
Sr	690	560	732	605	775	585	725	630	346	
Zr	240	225	217	250	205	225	195	230	269	
Nb	13	12	11	17	19	15	15	18	--	
Y	24	19	29	18	22	17	15	20	--	
La	83	82	102	70	88	67	64	70	53	
Ce	134	136	137	127	128	136	132	139	146	
Nd	--	--	--	--	--	--	--	--	67	
Sc	--	--	--	--	--	--	--	--	25	
V	--	--	--	--	--	--	--	--	177	
Ni	--	--	--	--	--	--	--	--	171	
Cr	--	--	--	--	--	--	--	--	585	

Group III : Page 5

Locality	Radicofani Italy	Vulsini Italy	Vulsini Italy	Vulsini Italy	Vulsini Italy	Vulsini Italy	Vulsini Italy	Vulsini Italy	Vulsini Italy	Vulsini Italy
Reference	79	81	81	44	44	44	82	82	83	83
SiO2	54.15	46.85	48.29	47.16	47.55	48.64	46.82	46.34	46.60	49.90
TiO2	1.40	3.25	0.95	0.74	0.77	0.78	0.74	0.76	1.00	0.60
Al2O3	15.74	15.30	15.67	12.46	14.15	17.34	16.21	18.06	19.80	18.90
Fe2O3	6.68	4.40	3.94	3.60	3.94	4.29	5.54	3.80	4.50	4.05
FeO	0.40	3.52	3.32	3.89	3.78	3.08	2.34	4.06	3.70	3.40
MnO	0.09	0.17	0.18	0.11	0.14	0.15	0.15	0.17	0.09	0.15
MgO	7.05	3.42	5.26	9.22	7.09	4.05	5.35	3.38	5.10	3.10
CaO	7.01	9.23	10.73	15.41	14.01	10.04	11.19	9.66	9.80	8.10
Na2O	1.82	2.97	1.87	0.68	1.06	1.66	1.85	2.40	1.50	1.80
K2O	4.81	9.26	7.93	4.67	5.88	7.46	7.23	8.44	5.00	7.60
P2O5	0.40	0.65	0.56	0.22	0.32	0.41	0.46	0.50	0.43	0.48
H2O+	0.47	0.81	1.77	--	--	--	--	--	--	--
H2O-	0.11	--	--	--	--	--	--	--	--	--
CO2	--	--	--	--	--	--	--	--	--	--
L.O.I.	--	--	--	1.46	1.48	1.30	2.25	1.32	2.20	1.70
Ba	668			853	1113	1368				
Rb	334			356	474	530				
Sr	378			784	1077	1471				
Zr	386			187	284	308				
Nb	--			12	17	22				
Y	--			23	35	34				
La	52			62	92	108				
Ce	160			112	158	182				
Nd	79			60	83	90				
Sc	25			46	32	20				
V	166			225	239	225				
Ni	100			116	80	46				
Cr	479			295	125	96				

Group III : Page 6

Locality	Vulsini Italy	Vulsini Italy	Vulsini Italy	Vulsini Italy	Vulsini Italy	Vulsini Italy	Vulsini Italy	Vulsini Italy	Vulsini Italy	Vulsini Italy
Reference	83	83	84	84	84	84	84	84	84	84
SiO2	48.60	52.10	47.49	50.90	50.58	46.67	49.74	45.62	50.69	47.93
TiO2	0.70	0.70	1.09	0.61	0.73	0.14	0.86	0.80	0.13	0.81
Al2O3	16.40	17.50	16.82	19.44	17.93	13.21	15.40	13.43	18.52	18.60
Fe2O3	3.30	3.00	6.44	4.20	4.14	2.98	5.18	6.46	5.27	6.44
FeO	4.90	3.30	1.06	1.25	3.10	4.93	2.49	2.18	1.90	1.85
MnO	0.14	0.12	0.13	0.12	0.15	0.15	0.13	0.12	0.17	0.15
MgO	5.80	5.60	5.09	3.83	3.28	8.72	6.11	7.80	3.84	3.98
CaO	11.60	7.00	9.35	7.88	7.92	13.75	10.98	14.04	9.15	9.32
Na2O	1.60	2.00	1.73	2.69	2.22	1.63	1.67	1.72	2.17	2.07
K2O	5.10	4.40	8.44	7.39	8.04	5.57	5.96	4.95	6.25	7.10
P2O5	0.42	0.27	0.41	0.27	0.37	0.24	0.34	0.36	0.25	0.32
H2O+	--	--	--	--	--	--	--	--	--	--
H2O-	--	--	--	--	--	--	--	--	--	--
CO2	--	--	--	--	--	--	--	--	--	--
L.O.I.	1.00	3.70	1.55	1.61	1.36	1.76	1.42	2.06	1.43	1.20
Ba										
Rb										
Sr										
Zr										
Nb										
Y										
La										
Ce										
Nd										
Sc										
V										
Ni										
Cr										

Group III : Page 7

Locality	Vulsini Italy	Vulsini Italy	Vulsini Italy	Vulsini Italy	Vulsini Italy	Vulsini Italy	Vulsini Italy	Vulsini Italy	Vulsini Italy	Vulsini Italy
Reference	84	84	84	85	85	85	85	85	85	85
SiO2	46.57	47.85	48.51	49.40	56.20	55.60	46.60	47.50	48.90	47.30
TiO2	0.77	0.11	0.76	1.00	1.30	1.30	0.90	0.90	0.80	0.80
Al2O3	13.04	12.69	15.41	18.20	17.00	14.00	15.60	17.80	16.40	16.20
Fe2O3	4.66	3.69	4.42	4.50	3.50	4.40	5.70	5.60	6.70	5.90
FeO	3.22	4.07	3.04	4.00	3.30	2.20	2.50	3.00	1.50	2.00
MnO	0.13	0.16	0.12	--	--	--	--	--	--	--
MgO	8.01	8.10	8.21	3.30	6.50	7.20	4.40	5.20	5.00	5.20
CaO	13.46	14.04	11.89	7.90	4.50	5.30	9.60	10.00	10.90	10.80
Na2O	1.22	1.53	1.39	3.10	2.00	2.70	2.30	1.60	2.20	2.30
K2O	6.89	5.22	5.15	6.80	4.70	6.60	8.80	6.10	6.40	6.40
P2O5	0.40	0.41	0.29	0.40	0.30	0.30	0.50	0.50	0.40	0.30
H2O+	--	--	--	--	--	--	--	--	--	--
H2O-	--	--	--	--	--	--	--	--	--	--
CO2	--	--	--	--	--	--	--	--	--	--
L.O.I.	1.34	1.81	0.72	--	--	--	--	--	--	--
Ba										
Rb										
Sr										
Zr										
Nb										
Y										
La										
Ce										
Nd										
Sc										
V										
Ni										
Cr										

Group III : Page 8

Locality	Vulsini Italy	Vulsini Italy	Vulsini Italy	Vulsini Italy	Vulsini Italy	Vulsini Italy	Vulsini Italy	Vulsini Italy	Vulsini Italy	Vulsini Italy
Reference	85	86	86	87	87	88	88	88	88	88
SiO2	47.10	53.70	53.80	48.10	47.60	47.12	47.88	47.90	47.25	46.74
TiO2	0.80	0.95	0.95	0.95	0.92	0.64	0.66	0.68	0.74	0.75
Al2O3	18.00	16.50	16.20	15.60	16.10	11.84	12.13	12.55	12.15	12.30
Fe2O3	4.90	4.83	4.82	3.92	3.02	3.26	2.78	4.86	3.08	3.30
FeO	2.80	3.95	4.49	3.31	4.52	4.16	4.51	2.45	4.54	4.59
MnO	--	0.13	0.14	0.18	0.21	0.15	0.14	0.14	0.17	0.19
MgO	3.20	3.01	3.16	5.24	4.36	12.84	12.20	11.17	9.26	8.96
CaO	7.70	6.38	6.35	10.70	10.10	13.88	14.05	14.37	15.61	15.35
Na2O	3.10	2.16	1.94	1.86	2.80	1.42	1.24	1.42	1.10	0.81
K2O	7.50	5.95	6.27	7.89	8.01	3.29	3.18	3.35	4.49	4.59
P2O5	0.30	0.34	0.38	0.56	0.58	0.30	0.29	0.29	0.35	0.34
H2O+	--	--	--	--	--	--	--	--	--	--
H2O-	--	--	--	--	--	0.12	0.05	0.01	0.19	0.22
CO2	--	--	--	--	--	--	--	--	--	--
L.O.I.	--	1.23	1.15	1.76	1.68	0.65	0.51	0.50	0.93	1.08
Ba						620	561	530	754	738
Rb						253	242	228	368	396
Sr						769	724	714	799	791
Zr						128	122	122	179	182
Nb						8	5	6	6	7
Y						24	24	24	28	28
La						40	42	39	--	52
Ce						92	87	87	--	124
Nd						42	43	42	--	56
Sc						--	--	--	--	--
V						186	177	203	218	212
Ni						261	224	189	114	109
Cr						911	782	750	223	230

Group III : Page 9

Locality	Vulsini Italy	Vulsini Italy	Vulsini Italy	Vulsini Italy	Cimini Italy	Cimini Italy	Cimini Italy	Cimini Italy	Cimini Italy	Cimini Italy
Reference	88	88	88	88	79	79	89	89	89	89
SiO2	47.52	47.10	44.70	48.30	57.43	60.25	60.08	59.50	59.04	58.69
TiO2	0.87	0.81	0.85	0.80	0.85	0.75	0.82	0.87	0.97	0.94
Al2O3	14.52	15.56	16.71	17.84	15.99	15.80	15.16	15.94	15.23	15.30
Fe2O3	4.95	3.16	5.27	3.58	1.22	1.62	2.34	1.29	1.53	1.50
FeO	3.49	4.58	3.44	3.72	3.66	3.16	2.51	3.11	2.16	3.12
MnO	0.14	0.15	0.15	0.15	0.09	0.09	0.11	0.10	0.10	0.12
MgO	7.38	6.04	5.55	4.84	6.30	4.50	3.00	3.07	3.61	4.37
CaO	13.15	12.67	13.11	10.39	6.82	5.44	5.59	5.26	6.00	6.65
Na2O	0.96	1.50	1.56	2.43	1.81	2.14	2.29	2.17	1.91	2.08
K2O	5.14	6.54	6.49	6.19	5.01	5.36	5.92	5.88	5.92	5.76
P2O5	0.33	0.45	0.44	0.38	0.31	0.31	0.36	0.31	0.33	0.35
H2O+	--	--	--	--	--	--	--	--	--	--
H2O-	0.05	0.21	0.13	0.28	--	--	--	--	--	--
CO2	--	--	--	--	--	--	--	--	--	--
L.O.I.	0.40	1.01	0.94	0.94	0.51	0.59	1.11	1.63	1.34	0.62
Ba	592	1161	1032	1158	1061	883				
Rb	425	558	436	431	336	353				
Sr	1122	1278	1094	1586	688	613				
Zr	180	308	219	304	366	362				
Nb	6	16	14	23	--	--				
Y	26	42	37	31	--	--				
La	56	77	73	82	94	91				
Ce	127	163	154	169	196	196				
Nd	64	69	71	61	85	82				
Sc	--	--	--	--	21	18				
V	243	18	245	173	137	117				
Ni	61	64	42	48	108	59				
Cr	138	22	19	23	302	204				

Group III : Page 10

Locality	Cimini Italy	Cimini Italy	Cimini Italy	Cimini Italy	Cimini Italy	Cimini Italy	Cimini Italy	Cimini Italy	Cimini Italy	Vico Italy
Reference	89	89	89	89	89	89	89	89	89	90
SiO2	58.66	58.56	58.30	57.99	57.95	56.44	54.78	54.63	52.45	55.00
TiO2	0.94	0.98	0.90	1.13	0.98	0.93	1.05	1.02	1.16	0.59
Al2O3	14.93	14.86	14.63	15.37	15.30	14.37	14.04	14.18	14.19	16.80
Fe2O3	2.07	1.75	1.60	1.65	1.86	2.32	1.58	2.66	2.78	2.60
FeO	2.96	3.31	3.24	3.16	3.15	3.11	3.60	2.93	2.92	3.00
MnO	0.12	0.11	0.10	0.10	0.10	0.10	0.13	0.09	0.13	0.13
MgO	4.45	4.64	4.38	4.62	4.29	6.34	7.56	7.73	8.48	3.60
CaO	6.25	6.45	6.67	6.45	6.57	6.73	7.36	6.45	6.45	6.20
Na2O	1.98	2.00	2.03	2.01	2.06	1.55	1.79	1.45	1.42	1.50
K2O	5.50	5.79	6.01	5.88	5.96	5.88	6.02	6.12	6.26	8.40
P2O5	0.33	0.38	0.41	0.35	0.35	0.31	0.44	0.34	0.27	0.45
H2O+	--	--	--	--	--	--	--	--	--	1.48
H2O-	--	--	--	--	--	--	--	--	--	--
CO2	--	--	--	--	--	--	--	--	--	0.12
L.O.I.	1.06	0.97	1.06	0.95	1.18	1.14	1.08	1.38	2.17	--
Ba										2047
Rb										539
Sr										1401
Zr										396
Nb										--
Y										--
La										--
Ce										--
Nd										--
Sc										--
V										--
Ni										--
Cr										--

Group III : Page 11

Locality	Vico Italy	Vico Italy	Vico Italy	Vico Italy	Vico Italy	Vico Italy	Vico Italy	Vico Italy	Vico Italy	Vico Italy
Reference	90	90	90	90	90	90	90	90	90	91
SiO2	51.60	53.10	52.60	52.20	51.70	51.90	51.80	49.70	49.30	52.20
TiO2	0.86	0.70	0.75	0.76	0.82	0.78	0.80	0.90	0.80	1.24
Al2O3	15.90	17.90	15.80	16.00	18.00	17.20	17.40	16.40	18.30	17.00
Fe2O3	3.30	3.60	2.20	2.40	2.50	3.20	2.20	4.00	3.60	1.67
FeO	3.90	2.80	4.60	4.50	4.50	3.50	4.80	3.70	3.40	3.98
MnO	0.13	0.13	0.14	0.14	0.16	0.14	0.15	0.15	0.15	--
MgO	5.10	3.30	5.10	5.10	3.80	3.80	3.60	5.20	3.50	5.56
CaO	8.30	6.10	8.20	8.50	7.60	7.20	7.00	9.00	8.30	9.31
Na2O	1.10	2.40	1.80	1.80	1.90	1.70	1.80	1.60	1.30	2.22
K2O	7.00	6.60	6.80	6.90	7.30	8.10	8.10	7.40	8.80	4.82
P2O5	0.64	0.48	0.50	0.49	0.53	0.50	0.58	0.57	0.60	0.42
H2O+	1.78	2.10	1.28	1.14	1.16	1.10	1.22	0.94	1.56	1.40
H2O-	--	--	--	--	--	--	--	--	--	--
CO2	0.02	0.02	0.16	0.06	--	0.10	--	0.08	0.22	--
L.O.I.	--	--	--	--	--	--	--	--	--	1.40
Ba	1983	1165	2020	1975	2077	2208	1765	2342	3659	
Rb	552	584	458	425	430	586	733	435	627	
Sr	1155	1205	1325	1292	1394	1463	1541	1479	2590	
Zr	359	469	373	372	428	391	490	377	551	
Nb	--	--	--	--	--	--	--	--	--	
Y	--	--	--	--	--	--	--	--	--	
La	--	--	--	--	--	--	--	--	--	
Ce	--	--	--	--	--	--	--	--	--	
Nd	--	--	--	--	--	--	--	--	--	
Sc	--	--	--	--	--	--	--	--	--	
V	--	--	--	--	--	--	--	--	--	
Ni	--	--	--	--	--	--	--	--	--	
Cr	--	--	--	--	--	--	--	--	--	

Locality	Vico Italy	Vico Italy	Vico Italy	Vico Italy	Vico Italy	Vico Italy	Vico Italy	Vico Italy	Vico Italy	Vico Italy
Reference	91	90	90	90	90	90	90	90	90	90
SiO2	52.40	55.60	54.60	55.00	55.30	52.30	52.30	52.00	51.80	52.10
TiO2	1.51	0.60	0.62	0.65	0.63	0.76	0.68	0.67	0.80	0.74
Al2O3	14.90	15.10	18.40	17.40	17.30	15.40	16.90	16.50	17.10	16.70
Fe2O3	3.05	2.20	2.60	2.20	2.00	4.20	2.20	2.30	2.30	2.50
FeO	3.64	3.50	3.00	3.60	3.60	2.60	4.10	3.90	4.80	4.20
MnO	--	0.13	0.14	0.12	0.13	0.12	0.14	0.15	0.15	0.15
MgO	5.66	3.90	3.20	3.40	3.00	5.20	5.50	5.30	3.70	4.80
CaO	7.69	6.80	5.60	5.90	5.60	8.60	7.70	7.80	7.20	7.80
Na2O	2.09	1.80	2.50	2.20	2.40	1.70	2.10	2.20	1.80	1.90
K2O	4.82	8.20	7.00	7.60	7.70	6.70	6.40	6.30	8.40	7.00
P2O5	0.50	0.45	0.40	0.40	0.48	0.50	0.38	0.73	0.63	0.52
H2O+	--	1.24	1.44	1.12	1.04	1.72	1.40	1.26	1.10	1.22
H2O-	--	--	--	--	--	--	--	--	--	--
CO2	--	--	0.08	0.12	0.08	0.04	0.06	0.04	0.06	0.07
L.O.I.	2.02	--	--	--	--	--	--	--	--	--
Ba		1964	1629	1679	1614	1378	1531	1493	1801	1884
Rb		571	739	515	509	774	483	416	602	466
Sr		1346	1225	1147	1145	1267	1090	1096	1525	1277
Zr		420	496	477	496	383	396	365	475	388
Nb		--	--	--	--	--	--	--	--	--
Y		--	--	--	--	--	--	--	--	--
La		--	--	--	--	--	--	--	--	--
Ce		--	--	--	--	--	--	--	--	--
Nd		--	--	--	--	--	--	--	--	--
Sc		--	--	--	--	--	--	--	--	--
V		--	--	--	--	--	--	--	--	--
Ni		--	--	--	--	--	--	--	--	--
Cr		--	--	--	--	--	--	--	--	--

Group III : Page 13

Locality	Vico Italy	Vico Italy	Sabatini Italy	Sabatini Italy	Sabatini Italy	Sabatini Italy	Sabatini Italy	Sabatini Italy	Sabatini Italy	Sabatini Italy
Reference	90	90	92	92	92	92	92	92	92	92
SiO2	55.10	55.20	48.50	47.90	48.70	47.20	48.10	46.70	47.40	46.70
TiO2	0.60	0.64	0.89	0.89	0.84	0.79	0.72	0.90	0.79	0.82
Al2O3	16.80	17.40	17.70	16.80	17.40	17.40	14.30	16.20	13.20	15.60
Fe2O3	2.50	2.10	4.60	3.30	6.00	3.50	3.70	3.50	3.70	5.80
FeO	3.20	3.60	2.50	3.70	1.70	4.00	4.00	5.20	4.50	2.60
MnO	0.13	0.13	0.16	0.13	0.13	0.17	0.15	0.16	0.14	0.15
MgO	3.60	3.20	3.50	5.20	4.90	3.80	7.10	5.80	7.40	5.40
CaO	6.20	5.80	9.70	10.60	9.60	9.50	11.40	11.40	12.40	11.00
Na2O	1.90	2.30	1.70	1.30	1.80	1.70	1.20	0.87	1.10	1.10
K2O	7.90	7.70	7.60	7.00	6.40	8.50	7.20	7.00	7.60	8.00
P2O5	0.43	0.44	0.65	0.64	0.63	0.54	0.49	0.66	0.58	0.61
H2O+	1.39	1.08	0.86	1.14	0.43	1.10	0.51	0.81	0.40	0.72
H2O-	--	--	--	--	--	--	--	--	--	--
CO2	0.07	0.10	0.43	0.15	0.09	0.10	0.09	0.00	0.05	0.08
SO3	--	--	0.18	0.18	0.18	0.18	0.18	0.17	0.19	0.18
Ba	1880	1647	2060	2020	1540	2100	990	1510	1320	1280
Rb	616	512	456	450	462	372	456	476	384	669
Sr	1324	1146	1684	1726	1537	2203	1574	1607	1401	1574
Zr	437	487	350	373	266	430	271	300	281	302
Nb	--	--	--	--	--	--	--	--	--	--
Y	--	--	31	32	29	35	29	34	28	35
La	--	--	--	--	--	--	--	--	--	--
Ce	--	--	--	--	--	--	--	--	--	--
Nd	--	--	--	--	--	--	--	--	--	--
Sc	--	--	--	--	--	--	--	--	--	--
V	--	--	--	--	--	--	--	--	--	--
Ni	--	--	--	--	--	--	--	--	--	--
Cr	--	--	118	185	150	101	320	109	230	132

Group III : Page 14

Locality	Sabatini Italy	Alban Hills Italy	Alban Hills Italy	Alban Hills Italy	Alban Hills Italy	Alban Hills Italy	Alban Hills Italy	Alban Hills Italy	Alban Hills Italy	Alban Hills Italy
Reference	92	93,94	93,94	93,94	93,94	93,94	93,94	93,94	93	93
SiO2	47.70	42.84	45.74	42.36	52.63	43.28	44.67	43.93	47.03	45.84
TiO2	0.78	1.22	0.92	1.36	0.52	0.55	1.12	1.18	0.88	0.08
Al2O3	13.40	13.79	17.52	15.37	17.57	15.78	14.46	15.17	15.23	18.41
Fe2O3	3.20	4.47	3.90	3.94	2.47	6.17	6.04	6.43	5.29	--
FeO	4.60	5.02	3.51	6.22	6.36	3.63	3.09	3.94	4.15	9.45
MnO	0.14	0.11	0.10	0.16	0.08	0.13	0.16	0.28	0.10	0.91
MgO	7.30	6.30	3.54	3.98	4.24	4.07	4.71	4.63	4.56	4.13
CaO	13.00	9.93	11.60	11.91	11.82	9.67	11.20	10.25	11.00	10.65
Na2O	0.82	1.38	1.73	2.52	2.11	1.64	0.80	1.34	1.30	3.02
K2O	7.00	6.74	8.83	8.05	7.77	8.01	7.43	8.61	7.84	7.41
P2O5	0.56	0.70	0.43	0.49	0.64	0.64	0.82	0.85	0.54	--
H2O+	0.37	4.89	1.06	2.26	1.87	2.11	1.88	1.40	1.62	0.51
H2O-	--	0.12	0.49	0.47	0.71	1.40	2.68	1.58	0.47	--
CO2	0.07	2.30	0.19	1.15	0.76	2.29	0.65	0.85	0.15	--
SO3	0.19	--	--	--	--	--	--	--	--	--
Ba	1260	--	--	--	--	--	--	--		
Rb	398	390	540	140	290	330	380	380		
Sr	1321	1290	1450	2300	4600	1680	1090	1460		
Zr	287	--	--	--	--	--	--	--		
Nb	--	--	--	--	--	--	--	--		
Y	29	--	--	--	--	--	--	--		
La	--	159	111	194	201	178	143	148		
Ce	--	352	271	426	435	371	360	340		
Nd	--	--	--	--	--	--	--	--		
Sc	--	14	17	10	10	16	23	21		
V	--	--	--	--	--	--	--	--		
Ni	--	47	41	33	56	51	51	57		
Cr	--	18	19	9	12	16	32	14		

Locality	Alban Hills Italy	Alban Hills Italy	Alban Hills Italy	Alban Hills Italy	Alban Hills Italy	Alban Hills Italy	Alban Hills Italy	Alban Hills Italy	Alban Hills Italy	Alban Hills Italy
Reference	93	93,94	93	93,94	93	93	93,94	93	93,94	93,94
SiO2	45.99	46.10	45.75	48.58	48.36	46.66	48.18	45.54	46.43	47.37
TiO2	0.37	1.20	1.11	0.99	1.31	0.36	1.09	0.71	0.96	1.10
Al2O3	16.56	14.90	17.06	14.90	15.01	18.20	14.85	18.69	16.86	20.13
Fe2O3	4.13	4.90	6.12	1.96	3.54	4.32	2.51	4.38	3.02	0.62
FeO	5.38	3.70	3.20	5.08	5.22	4.93	4.79	2.01	4.55	4.32
MnO	--	0.30	0.09	0.12	0.12	0.09	0.08	0.11	0.17	0.10
MgO	5.30	4.80	4.00	6.44	4.89	3.13	7.37	4.68	4.44	5.21
CaO	10.47	10.50	9.68	1.263	10.32	10.12	11.81	10.44	10.36	9.86
Na2O	2.18	1.80	2.30	2.71	2.21	2.20	1.20	2.60	2.53	3.40
K2O	8.97	8.80	9.35	5.59	8.04	8.65	6.18	7.92	9.05	6.89
P2O5	0.56	0.70	0.63	0.53	0.35	0.53	0.48	0.59	0.26	0.34
H2O+	0.45	1.50	0.72	0.60	0.85	0.77	0.88	1.19	0.55	0.60
H2O-	--	0.60	0.10	0.24	0.29	0.13	0.17	0.49	0.75	0.10
CO2		0.30								
SO3		0.02								
F		0.09								
Cl		0.01								
Ba		--		--			--		--	--
Rb		550		440			360		400	410
Sr		1440		1600			1450		2000	2450
Zr		--		--			--		--	--
Nb		--		--			--		--	--
Y		--		--			--		--	--
La		115		93			97		123	125
Ce		258		211			218		267	267
Nd		--		--			--		--	--
Sc		18		35			33		18	6
V		--		--			--		--	--
Ni		46		93			73		39	0
Cr		16		359			366		30	5

Group III : Page 16

Locality	Alban Hills Italy	Alban Hills Italy	Alban Hills Italy	Alban Hills Italy	Alban Hills Italy	Alban Hills Italy	Alban Hills Italy	Alban Hills Italy	Alban Hills Italy	Alban Hills Italy
Reference	93,94	93	93	93	93	93	93	93	93	93
SiO2	48.48	48.71	45.82	44.32	43.90	43.02	44.44	44.69	47.03	48.16
TiO2	0.84	0.82	0.99	0.96	0.96	0.80	0.81	1.03	0.50	0.86
Al2O3	17.72	18.06	16.42	12.98	15.80	15.76	15.06	14.57	18.82	12.98
Fe2O3	4.44	3.80	6.33	6.45	3.65	4.98	3.30	5.56	4.19	2.92
FeO	2.92	2.93	2.43	5.06	5.20	4.31	4.67	3.69	4.20	4.55
MnO	0.17	0.19	0.23	0.20	0.16	0.20	0.15	0.15	0.15	0.16
MgO	3.54	3.20	4.01	5.63	5.02	7.20	6.35	5.83	4.00	9.02
CaO	7.72	8.20	10.70	13.30	12.43	10.13	10.13	11.68	10.39	12.50
Na2O	2.99	2.92	1.50	1.74	1.82	1.46	2.15	2.37	2.58	1.30
K2O	8.99	8.33	8.31	8.29	8.41	7.98	8.11	8.62	6.18	6.54
P2O5	0.39	0.39	0.67	0.63	0.60	0.65	0.75	1.16	0.41	0.43
H2O+	1.39	1.35	1.30	0.60	0.71	2.04	1.10	0.60	1.34	0.84
H2O-	0.57	0.48	0.64	0.01	0.68	1.73	1.33	0.11	0.46	0.26
CO2				0.20	--	0.20	1.17		--	
SO3				0.05	0.02	--	0.08		0.04	
F				--	--	--	--		0.07	
Cl				0.03	0.01	--	0.01		--	
Ba	--									
Rb	470									
Sr	2700									
Zr	--									
Nb	--									
Y	--									
La	132									
Ce	277									
Nd	--									
Sc	6									
V	--									
Ni	--									
Cr	5									

Locality	Alban Hills Italy	Alban Hills Italy	Alban Hills Italy	Alban Hills Italy	Alban Hills Italy	Alban Hills Italy	Alban Hills Italy	Alban Hills Italy	Ernici Italy	Ernici Italy
Reference	93,94	93,94	93,94	93	93	93,94	93,94	93	95	95
SiO2	47.26	44.90	46.50	47.20	49.10	43.79	46.52	47.03	45.81	46.46
TiO2	0.99	0.99	0.98	1.19	1.20	1.02	0.95	0.50	0.86	0.82
Al2O3	12.74	15.92	13.74	17.66	9.49	16.23	16.40	18.82	17.02	16.62
Fe2O3	5.95	5.77	4.95	3.51	3.17	9.30	5.83	4.19	4.53	5.86
FeO	3.72	3.08	2.87	4.50	4.70	1.14	2.18	4.20	3.32	1.77
MnO	0.17	0.17	0.17	--	--	0.18	0.18	0.15	0.16	0.15
MgO	6.46	6.49	7.13	4.20	10.31	4.88	5.04	4.00	5.81	6.04
CaO	12.66	9.85	11.73	9.52	14.48	12.05	11.05	10.39	12.07	10.87
Na2O	1.84	1.68	1.84	2.25	0.95	1.10	1.83	2.58	1.97	2.60
K2O	7.03	8.04	7.02	7.63	5.50	6.46	8.80	6.18	7.24	6.94
P2O5	0.53	0.55	0.51	0.58	0.38	0.65	0.53	0.41	0.44	0.45
H2O+	0.83	1.67	1.57	0.72	0.51	2.47	0.66	1.34	--	--
H2O-	0.29	1.07	1.32	0.57	0.11	2.27	0.37	0.46	--	--
CO2	--	--	--	--	--	0.07	0.17	--	--	--
L.O.I.								--	0.76	1.56
SO3								0.04		
F								--		
Cl								0.07		
Ba	--	--	--			--	--		1594	1213
Rb	365	510	350			460	480		366	421
Sr	1550	1500	1750			1800	1550		1845	1666
Zr	--	--	--			--	--		218	227
Nb	--	--	--			--	--		13	12
Y	--	--	--			--	--		--	32
La	104	109	108			125	99		96	93
Ce	239	250	247			280	232		205	173
Nd	--	--	--			--	--		91	87
Sc	34	22	23			20	24		21	24
V	--	--	--			--	--		217	241
Ni	52	--	34			47	42		39	63
Cr	192	24	47			14	78		100	146

Locality	Ernici Italy	Ernici Italy	Ernici Italy	Ernici Italy	Ernici Italy	Ernici Italy	Ernici Italy	Ernici Italy	Ernici Italy	Ernici Italy
Reference	95	95	95	95	95	95	95	95	95	95
SiO2	46.64	46.67	46.67	46.86	47.03	47.27	47.38	47.39	47.43	46.13
TiO2	0.82	0.80	0.80	0.79	0.81	0.76	0.77	0.72	0.75	1.00
Al2O3	17.62	17.10	17.96	18.14	17.62	17.91	17.89	17.85	18.21	16.92
Fe2O3	3.11	3.85	2.70	3.35	3.44	2.34	4.68	1.76	3.47	4.28
FeO	3.47	3.65	3.71	2.91	3.36	4.67	2.52	4.27	3.61	2.64
MnO	0.14	0.15	0.14	0.14	0.14	0.14	0.14	0.13	0.14	0.14
MgO	5.50	6.13	5.50	5.10	6.13	5.40	6.10	6.36	5.07	4.80
CaO	10.96	11.15	10.66	10.51	10.62	10.29	10.06	10.53	9.88	9.67
Na2O	2.75	2.55	2.71	2.46	2.58	2.42	2.33	2.51	2.79	2.60
K2O	7.31	6.52	7.88	8.06	6.83	7.32	6.78	7.36	7.34	8.85
P2O5	0.47	0.38	0.46	0.54	0.44	0.58	0.42	0.54	0.55	1.14
H2O+	--	--	--	--	--	--	--	--	--	--
H2O-	--	--	--	--	--	--	--	--	--	--
CO2	--	--	--	--	--	--	--	--	--	--
L.O.I.	1.21	1.05	0.80	1.14	0.99	0.92	0.94	0.57	0.76	1.83
Ba	1664	1229	1675	1592	832	913	877	892	945	4057
Rb	358	413	335	341	339	356	379	335	355	451
Sr	1864	1655	1909	1932	1523	1538	1491	1412	1554	1815
Zr	217	207	218	219	228	237	226	218	240	443
Nb	13	13	12	12	11	11	12	9	12	29
Y	32	31	--	32	32	33	--	31	30	44
La	98	93	--	94	80	83	83	83	93	257
Ce	212	180	--	204	170	178	183	177	193	398
Nd	95	84	--	80	83	62	81	81	82	166
Sc	22	26	--	21	24	25	25	27	22	23
V	220	214	236	228	256	240	215	233	244	242
Ni	38	50	47	37	55	52	51	58	52	30
Cr	87	138	90	66	134	108	108	151	109	11

Group III : Page 19

Locality	Ernici Italy	Ernici Italy	Ernici Italy	Ernici Italy	Ernici Italy	Ernici Italy	Ernici Italy	Ernici Italy	Ernici Italy	Ernici Italy
Reference	96	96	96	96	96	96	96	96	96	96
SiO2	46.78	47.23	47.67	48.07	47.37	48.05	46.96	46.83	47.15	47.88
TiO2	0.77	0.75	0.77	0.73	0.78	0.74	0.77	0.80	0.78	0.72
Al2O3	15.69	15.52	15.90	15.52	15.81	15.69	15.66	15.81	15.79	15.58
Fe2O3	1.72	3.81	2.86	2.63	3.33	1.90	4.62	4.97	5.35	2.15
FeO	5.45	3.36	4.14	4.07	3.90	4.94	2.52	2.74	2.25	4.83
MnO	0.14	0.14	0.14	0.12	0.14	0.13	0.14	0.15	0.14	0.14
MgO	6.96	6.99	6.34	7.21	6.87	6.98	6.24	6.30	6.28	6.52
CaO	11.44	11.18	11.39	10.72	11.34	10.91	11.03	11.42	11.03	10.61
Na2O	2.05	2.18	1.93	1.99	2.26	2.33	2.51	2.22	2.05	1.99
K2O	5.96	6.48	6.90	6.47	6.70	6.51	6.00	6.68	6.61	6.81
P2O5	0.43	0.41	0.41	0.41	0.53	0.41	0.49	0.52	0.47	0.41
H2O+	--	--	--	--	--	--	--	--	--	--
H2O-	--	--	--	--	--	--	--	--	--	--
CO2	--	--	--	--	--	--	--	--	--	--
L.O.I.	1.91	1.27	1.02	1.17	0.99	0.82	2.20	0.92	1.29	1.18
Ba										
Rb										
Sr										
Zr										
Nb										
Y										
La										
Ce										
Nd										
Sc										
V										
Ni										
Cr										

Locality	Ernici Italy	Ernici Italy	Ernici Italy	Ernici Italy	Ernici Italy	Ernici Italy	Ernici Italy	Ernici Italy	Ernici Italy	Ernici Italy
Reference	96	96	96	96	96	96	96	96	96	96
SiO2	47.53	47.17	47.86	47.95	47.93	47.86	47.78	47.58	48.02	47.57
TiO2	0.77	0.78	0.77	0.73	0.73	0.75	0.74	0.76	0.75	0.77
Al2O3	15.47	15.81	16.06	15.50	16.06	15.49	15.93	15.47	15.61	15.69
Fe2O3	3.40	3.69	3.48	2.24	2.89	2.99	3.23	3.45	2.16	3.43
FeO	3.74	3.51	3.37	4.81	4.00	4.16	3.93	3.65	4.98	3.61
MnO	0.14	0.14	0.14	0.14	0.13	0.15	0.14	0.14	0.14	0.14
MgO	6.48	5.95	5.85	6.44	5.87	6.57	6.00	6.37	6.36	5.91
CaO	11.44	11.35	10.81	10.83	10.53	11.16	10.73	11.24	10.79	11.19
Na2O	2.29	2.00	1.93	2.33	1.83	2.16	1.82	2.33	2.30	2.37
K2O	6.80	7.05	6.63	6.58	6.75	7.04	7.03	6.95	6.94	7.17
P2O5	0.44	0.50	0.38	0.42	0.43	0.41	0.43	0.41	0.46	0.50
H2O+	--	--	--	--	--	--	--	--	--	--
H2O-	--	--	--	--	--	--	--	--	--	--
CO2	--	--	--	--	--	--	--	--	--	--
L.O.I.	1.01	1.07	1.48	1.27	1.43	0.81	1.35	0.96	0.70	0.89
Ba										
Rb										
Sr										
Zr										
Nb										
Y										
La										
Ce										
Nd										
Sc										
V										
Ni										
Cr										

Locality	Ernici Italy	Ernici Italy	Ernici Italy	Ernici Italy	Rocca-monfina Italy	Rocca-monfina Italy	Rocca-monfina Italy	Rocca-monfina Italy	Rocca-monfina Italy	Rocca-monfina Italy
Reference	96	96	96	96	97	98	98	98	98	98
SiO2	47.99	48.07	47.91	46.95	46.40	46.61	47.40	48.93	49.32	48.85
TiO2	0.73	0.74	0.75	0.95	0.94	1.02	0.97	0.80	0.81	0.84
Al2O3	16.31	16.10	16.18	15.02	15.70	16.77	17.58	18.48	18.39	17.94
Fe2O3	4.17	2.10	3.79	5.02	5.30	2.63	4.83	1.68	1.56	2.80
FeO	2.96	4.92	3.02	2.76	3.40	6.00	4.59	5.66	5.67	5.05
MnO	0.14	0.14	0.14	0.14	0.15	0.15	0.16	0.15	0.14	0.16
MgO	5.94	6.13	5.63	5.20	6.00	5.49	4.97	3.93	3.87	4.08
CaO	10.56	10.43	10.67	9.53	11.60	11.35	10.37	8.21	8.28	9.19
Na2O	2.33	2.67	2.22	2.00	1.60	1.47	1.74	2.21	2.29	2.50
K2O	6.86	7.06	7.41	9.00	6.60	5.99	5.40	6.55	6.61	5.97
P2O5	0.43	0.45	0.48	1.08	0.58	0.53	0.43	0.36	0.36	0.39
H2O+	--	--	--	--	0.94	--	--	--	--	--
H2O-	--	--	--	--	--	--	--	--	--	--
CO2	--	--	--	--	--	--	--	--	--	--
L.O.I.	0.94	0.70	1.05	1.12	--	1.25	0.44	0.73	0.55	0.97
Ba					1509					
Rb					497					
Sr					1607					
Zr					285					
Nb					--					
Y					50					
La					--					
Ce					160					
Nd					--					
Sc					--					
V					--					
Ni					--					
Cr					--					

Group III : Page 22

Locality	Rocca-monfina Italy	Rocca-monfina Italy	Somma Italy	Somma Italy	Somma Italy	Somma Italy	Somma Italy	Somma Italy	Somma Italy	Somma Italy
Reference	98	99	100	100	100	100	100	100	100	100
SiO2	45.84	45.80	49.90	50.30	50.10	48.50	52.10	52.20	50.10	51.20
TiO2	0.94	0.87	0.99	0.73	0.68	0.87	0.87	0.82	0.92	0.68
Al2O3	14.66	16.80	16.10	18.60	16.90	15.80	19.30	19.20	18.50	18.60
Fe2O3	4.02	5.25	5.50	2.90	3.10	2.50	2.90	4.50	2.80	4.60
FeO	4.66	4.20	3.20	3.90	4.40	5.80	4.50	3.50	4.30	3.30
MnO	0.16	0.16	0.14	0.12	0.11	0.11	0.09	0.12	0.11	0.11
MgO	6.72	6.10	5.10	4.90	5.90	6.20	3.30	3.20	4.10	4.70
CaO	12.41	11.80	10.40	8.90	9.60	11.80	8.10	7.30	8.80	7.30
Na2O	1.56	1.70	2.10	2.20	2.20	2.00	2.50	2.80	2.40	2.30
K2O	6.85	6.20	5.80	5.60	5.50	5.30	5.80	6.00	6.20	5.50
P2O5	0.69	0.57	0.66	0.63	0.65	0.88	0.45	0.54	0.60	0.62
H2O+	--	--	0.58	0.29	0.39	0.64	0.16	0.70	0.74	0.53
H2O-	--	--	0.14	0.45	0.07	0.04	0.28	0.30	0.48	0.41
CO2	--	--	--	--	--	--	--	--	--	--
L.O.I.	0.49	0.90	--	--	--	--	--	--	--	--
F			0.08	0.10	0.16	0.08	0.10	0.17	0.06	0.06
Cl			0.01	0.01	0.03	0.04	--	0.02	--	--
Ba			1700	1800	1300	1400	1800	2000	2400	1900
Rb			220	310	230	190	230	210	270	250
Sr			910	680	610	820	660	800	820	800
Zr			370	250	220	280	310	300	270	290
Nb			25	15	10	20	20	30	20	--
Y			--	--	--	--	--	--	--	--
La			--	--	--	--	--	--	--	--
Ce			--	--	--	--	--	--	--	--
Nd			--	--	--	--	--	--	--	--
Sc			--	--	--	--	--	--	--	--
V			--	--	--	--	--	--	--	--
Ni			--	--	--	--	--	--	--	--
Cr			--	--	--	--	--	--	--	--

Locality	Vesuvius Italy	Vesuvius Italy	Vesuvius Italy	Vesuvius Italy	Vesuvius Italy	Vesuvius Italy	Vesuvius Italy	Vesuvius Italy	Vesuvius Italy	Vesuvius Italy
Reference	100	100	100	100	100	100	100	100	100	100
SiO2	48.60	48.50	48.80	47.50	48.10	48.40	46.20	48.40	47.70	48.60
TiO2	0.72	0.68	0.83	0.72	0.82	0.83	0.82	0.72	0.83	0.60
Al2O3	18.20	18.50	19.70	16.60	16.40	17.90	20.50	18.10	18.80	18.90
Fe2O3	1.20	5.10	3.20	3.30	2.90	5.90	6.30	2.80	3.40	3.50
FeO	6.40	3.20	5.40	4.80	5.80	3.20	2.70	5.10	4.70	5.00
MnO	0.13	0.13	0.14	0.11	0.14	0.14	0.15	0.12	0.13	0.13
MgO	4.30	4.20	3.10	5.40	4.80	3.30	3.00	4.30	3.40	3.20
CaO	10.20	9.80	8.70	11.60	8.30	8.60	7.60	9.00	9.20	8.60
Na2O	2.70	2.80	2.90	2.30	2.40	2.70	3.10	3.10	3.10	2.80
K2O	6.80	6.50	6.70	6.70	7.00	7.30	8.20	6.80	6.50	7.50
P2O5	0.66	0.66	0.65	0.79	0.60	0.57	0.60	0.68	0.66	0.50
H2O+	0.45	0.65	0.40	0.36	0.47	0.36	0.22	0.32	0.39	0.72
H2O-	0.25	0.15	0.20	0.32	0.23	0.14	0.28	0.20	0.19	0.18
CO2	--	--	--	--	--	--	--	--	--	--
F	0.19	0.21	0.16	0.06	0.15	0.12	0.16	0.15	0.14	0.15
Cl	0.27	0.39	0.57	0.55	0.16	0.27	0.33	0.73	0.56	0.19
Ba	1950	2350	2400	2000	2400	2300	2500	1500	2000	2200
Rb	250	250	240	250	220	300	320	280	260	300
Sr	810	860	1030	810	840	970	1030	910	960	1000
Zr	210	290	280	230	250	310	360	300	360	270
Nb	--	15	--	--	--	--	--	--	20	10
Y	--	--	--	--	--	--	--	--	--	--
La	--	--	--	--	--	--	--	--	--	--
Ce	--	--	--	--	--	--	--	--	--	--
Nd	--	--	--	--	--	--	--	--	--	--
Sc	--	--	--	--	--	--	--	--	--	--
V	--	--	--	--	--	--	--	--	--	--
Ni	--	--	--	--	--	--	--	--	--	--
Cr	--	--	--	--	--	--	--	--	--	--

Group III : Page 24

Locality	Vesuvius Italy	Vesuvius Italy	Vesuvius Italy	Vesuvius Italy	Vesuvius Italy	Vesuvius Italy	Vesuvius Italy	Vesuvius Italy	Segamat Malaysia	Segamat Malaysia
Reference	100	100	100	100	100	100	100	100	101	101
SiO2	47.50	47.80	47.50	48.70	48.00	47.80	47.40	48.20	47.74	49.28
TiO2	0.88	0.80	0.73	0.77	0.68	0.67	0.75	0.78	0.97	0.95
Al2O3	18.40	18.40	18.60	18.70	16.40	18.10	17.10	16.50	8.98	15.79
Fe2O3	2.30	2.50	4.10	2.90	3.60	2.70	2.30	5.30	5.56	6.37
FeO	5.40	6.10	4.30	5.30	4.30	5.10	6.00	2.90	5.48	4.37
MnO	0.10	0.14	0.14	0.13	0.12	0.12	0.13	0.13	0.18	--
MgO	3.70	3.50	3.20	3.90	5.90	4.20	4.40	5.80	10.59	8.56
CaO	9.10	9.20	9.80	8.40	10.50	9.70	9.40	12.50	11.96	4.70
Na2O	2.80	3.00	2.70	3.10	2.40	2.60	2.40	2.40	1.31	2.68
K2O	7.20	7.20	7.60	6.60	6.80	6.50	7.10	5.60	3.78	6.12
P2O5	0.68	0.64	0.60	0.68	0.84	0.68	0.57	0.82	0.44	--
H2O+	0.36	0.90	0.51	0.41	0.10	0.50	0.50	0.46	2.38	1.64
H2O-	0.16	0.10	0.11	0.21	0.10	0.10	0.20	0.10	0.76	0.59
CO2	--	--	--	--	--	--	--	--	--	--
F	0.15	0.29	0.17	0.13	0.13	0.15	0.13	0.12	--	--
Cl	0.19	0.35	0.62	0.48	0.35	0.35	0.14	0.08	--	--
Ba	2450	2100	2300	2000	1700	3100	2150	1650		
Rb	260	240	340	270	200	260	210	210		
Sr	960	960	980	860	720	850	780	800		
Zr	230	340	370	300	260	260	250	270		
Nb	--	10	5	10	10	15	5	10		
Y	--	--	--	--	--	--	--	--		
La	--	--	--	--	--	--	--	--		
Ce	--	--	--	--	--	--	--	--		
Nd	--	--	--	--	--	--	--	--		
Sc	--	--	--	--	--	--	--	--		
V	--	--	--	--	--	--	--	--		
Ni	--	--	--	--	--	--	--	--		
Cr	--	--	--	--	--	--	--	--		

Locality	Segamat Malaysia	Muriah Java Indonesia	Sangenges Sumbawa Indonesia	Sangenges Sumbawa Indonesia	Sangenges Sumbawa Indonesia	Batu Tara Indonesia	Batu Tara Indonesia	Batu Tara Indonesia	Batu Tara Indonesia	Batu Tara Indonesia
Reference	101	102	103	103	103,104	105	105	105	106	106
SiO2	49.13	45.47	43.86	45.38	44.71	48.01	47.95	45.38	49.74	47.81
TiO2	1.05	1.05	1.09	1.05	1.09	0.92	0.87	1.17	0.78	0.92
Al2O3	18.30	17.03	11.09	12.79	13.20	15.23	13.81	18.51	15.68	13.64
Fe2O3	4.68	9.95	2.04	1.92	1.96	3.19	3.96	5.96	8.61	9.13
FeO	4.42	--	10.38	9.78	9.99	5.50	4.76	4.24	--	--
MnO	--	0.17	0.20	0.18	0.18	0.17	0.16	0.18	0.17	0.17
MgO	4.31	5.61	9.00	8.29	7.77	7.18	8.21	4.79	6.40	8.19
CaO	7.15	10.73	15.16	14.38	13.88	11.75	12.19	11.73	10.28	12.12
Na2O	2.79	2.50	2.03	1.73	2.07	1.97	1.65	1.79	2.24	1.84
K2O	6.26	5.25	4.34	3.81	4.42	5.12	5.03	3.81	4.97	4.76
P2O5	--	1.06	0.81	0.69	0.74	0.84	1.00	0.96	0.78	0.90
H2O+	3.00	1.19	1.40	1.75	1.34	0.29	0.48	1.05	0.04	0.01
H2O-	0.46	--	--	--	--	0.09	0.15	0.60	0.10	0.10
CO2	--	--	--	--	--	--	--	--	--	--
Ba		2830	--	--	--				1057	1159
Rb		500	191	246	319				206	196
Sr		1562	753	849	836				940	856
Zr		187	187	122	139				218	210
Nb		150	7	4	6				12	20
Y		30	38	20	25				39	29
La		221	--	--	37				76	49
Ce		282	--	--	--				148	106
Nd		--	--	--	--				65	48
Sc		--	51	53	49				32	38
V		277	--	--	--				278	292
Ni		26	42	35	30				51	79
Cr		83	200	129	70				194	267

Group III : Page 26

Locality	Batu Tara Inodonesia	Batu Tara Indonesia	Batu Tara Indonesia	Batu Tara Indonesia	Batu Tara Indonesia	Batu Tara Indonesia	Batu Tara Indonesia	Batu Tara Indonesia	Batu Tara Indonesia	Batu Tara Indonesia
Reference	106	106	106	106	106	106	106	106	106	106
SiO2	47.76	47.71	47.85	48.08	47.62	47.61	47.70	48.01	47.96	46.53
TiO2	0.90	0.89	0.91	0.90	0.89	0.91	0.95	0.98	0.98	1.16
Al2O3	13.48	13.60	14.07	13.83	13.72	14.15	14.13	14.79	14.84	16.07
Fe2O3	9.12	9.03	9.29	9.15	9.04	9.35	9.26	9.21	9.25	9.84
FeO	--	--	--	--	--	--	--	--	--	--
MnO	0.17	0.17	0.17	0.17	0.17	0.18	0.17	0.17	0.17	0.17
MgO	8.38	8.24	7.94	8.28	8.33	7.39	7.56	7.14	7.11	6.35
CaO	12.24	11.92	11.52	11.94	11.80	11.83	12.00	11.63	11.76	11.97
Na2O	1.48	1.91	2.14	2.07	2.12	1.97	1.97	1.98	2.05	1.80
K2O	4.69	4.60	4.82	4.53	4.40	4.88	4.92	4.90	4.86	4.18
P2O5	0.87	0.87	0.91	0.85	0.87	0.90	0.87	0.85	0.85	0.82
H2O+	0.11	0.14	0.08	0.03	0.19	0.00	0.00	0.00	0.00	0.38
H2O-	0.07	0.12	0.12	0.15	0.18	0.14	0.13	0.10	0.10	0.39
CO2	--	--	--	--	--	--	--	--	--	--
Ba	1128	1038	1167	1049	1055	1178	1189	1221	1275	1177
Rb	196	196	199	193	192	207	194	205	198	215
Sr	819	809	900	820	810	924	888	896	883	937
Zr	206	212	216	215	213	215	216	210	217	134
Nb	17	18	20	18	19	14	19	19	20	9
Y	30	29	30	31	29	34	31	30	31	26
La	51	50	53	52	53	62	57	52	53	41
Ce	104	105	104	106	106	134	104	109	106	81
Nd	48	46	48	50	48	59	47	48	48	40
Sc	36	39	35	38	36	36	36	34	36	35
V	276	296	300	287	298	300	311	304	310	338
Ni	81	85	78	89	86	57	62	55	56	32
Cr	287	287	240	282	278	198	208	171	168	98

Locality	Batu Tara Indonesia	Batu Tara Indonesia	Batu Tara Indonesia	Batu Tara Indonesia	Batu Tara Indonesia	Batu Tara Indonesia	Dezhnev Soviet Union	Dezhnev Soviet Union	Dezhnev Soviet Union	West Alaska
Reference	106	106	106	106	106	106	107	107	107	108
SiO2	47.14	48.77	47.92	47.28	48.71	46.83	59.44	58.48	54.23	44.50
TiO2	0.93	0.82	0.93	1.14	0.87	1.20	0.65	0.84	1.25	2.00
Al2O3	13.76	12.17	14.56	16.15	14.50	17.74	14.60	16.68	14.35	11.00
Fe2O3	9.16	2.40	2.86	2.98	4.09	4.59	1.81	1.57	2.94	4.30
FeO	--	5.81	5.82	6.47	5.07	5.37	3.23	2.61	5.25	7.70
MnO	0.17	0.16	0.16	0.18	0.19	0.20	0.10	0.10	0.07	0.21
MgO	7.68	9.53	7.18	6.16	5.94	4.32	3.79	3.30	4.10	9.10
CaO	12.05	11.65	11.38	11.85	10.05	10.04	4.71	4.83	5.78	12.60
Na2O	1.87	1.72	2.01	1.79	1.98	2.03	2.48	2.55	3.58	1.10
K2O	4.51	5.09	5.12	4.45	6.71	5.35	8.01	8.29	7.66	4.40
P2O5	0.85	0.95	0.79	0.78	0.94	1.04	--	--	--	1.20
H2O+	0.24	--	--	--	--	--	0.43	0.64	0.22	1.50
H2O-	0.19	--	--	--	--	--	--	--	--	0.29
CO2	--	--	--	--	--	--	--	--	--	<0.05
S										0.00
F										0.34
Cl										0.00
Ba	1072	926	1114	1125	1256	1623				
Rb	192	266	197	215	288	189				
Sr	847	793	870	901	1040	1130				
Zr	212	183	212	128	312	189				
Nb	18	13	22	10	22	16				
Y	30	25	29	26	42	29				
La	51	--	--	--	--	--				
Ce	100	86	99	79	171	105				
Nd	47	44	46	39	85	45				
Sc	42	36	36	37	30	20				
V	307	268	295	327	282	331				
Ni	68	105	56	34	43	23				
Cr	244	461	176	93	120	23				

Locality	West Alaska	West Alaska	West Alaska	West Alaska	West Alaska	West Alaska
Reference	108	108	108	108	108	108
SiO2	48.90	50.30	51.40	52.20	54.30	55.80
TiO2	1.60	1.20	1.20	1.20	0.71	0.96
Al2O3	12.10	15.00	12.20	15.20	17.20	15.20
Fe2O3	2.60	3.40	6.20	2.80	2.70	2.30
FeO	5.20	4.00	2.70	4.20	2.40	3.80
MnO	0.17	0.17	0.17	0.15	0.15	0.17
MgO	8.70	5.40	6.40	4.60	3.20	3.20
CaO	11.20	9.10	10.10	7.50	4.40	6.70
Na2O	0.91	2.40	2.20	2.80	3.50	3.20
K2O	6.10	6.30	5.00	7.30	7.20	7.00
P2O5	0.69	0.71	0.86	0.67	0.71	0.39
H2O+	1.40	1.60	1.10	1.20	3.10	1.00
H2O-	0.49	0.24	0.30	0.19	0.68	0.26
CO2	<0.05	<0.05	<0.05	<0.05	0.08	<0.05
S	<0.05	0.00	0.00	0.00	<0.05	0.00
F	0.33	0.25	0.20	0.18	0.15	0.20
Cl	0.00	0.00	0.01	0.00	0.00	0.00
Ba						
Rb						
Sr						
Zr						
Nb						
Y						
La						
Ce						
Nd						
Sc						
V						
Ni						
Cr						

Group IV : Page 1

Locality	Devon Egnland	Devon England	Devon England	Devon England	Devon England	Devon England	Devon England	Devon England	Devon England	Jersey Channel Isles
Reference	109	109	109	109	109	109	109	109	109	110
SiO2	48.93	50.08	47.73	57.33	46.80	49.51	49.22	43.35	46.13	52.84
TiO2	1.24	2.03	1.65	2.17	1.95	1.66	1.77	1.59	2.39	1.10
Al2O3	13.78	14.82	13.42	14.42	18.48	17.71	16.98	14.55	15.06	12.30
Fe2O3	7.05	11.61	8.85	3.72	13.87	12.23	12.06	12.57	9.30	3.01
FeO	--	--	--	--	--	--	--	--	--	3.80
MnO	0.07	0.13	0.13	0.02	0.15	0.21	0.19	0.13	--	0.14
MgO	5.72	3.02	10.71	5.39	3.27	3.64	3.95	4.10	7.79	8.20
CaO	7.52	3.93	5.52	3.18	0.43	1.93	1.06	7.70	3.92	7.08
Na2O	1.74	1.23	2.63	2.31	0.26	2.56	2.28	1.12	0.35	1.61
K2O	7.72	9.49	5.37	8.85	9.24	5.21	7.76	8.14	7.10	6.82
P2O5	0.16	0.47	0.33	0.39	0.05	0.05	0.05	0.05	0.80	1.47
H2O+	1.82	1.60	2.81	1.13	3.63	3.71	3.24	2.56	3.56	1.64
H2O-	--	--	--	--	--	--	--	--	--	--
CO2	4.43	0.42	0.14	0.37	0.07	0.33	0.16	6.99	0.09	3.91
Ba	3625	5146	3748	3627	545	559	703	509	4183	6027
Rb	112	268	417	950	67	54	53	71	598	287
Sr	2508	1079	978	889	55	107	32	45	786	2034
Zr	412	872	650	876	151	141	160	127	1645	647
Nb	8	30	28	31	17	15	16	13	30	21
Y	21	39	42	54	24	26	26	17	75	93
La	166	97	87	84	25	26	24	16	112	316
Ce	280	198	160	151	33	40	39	52	245	45
Nd	116	58	62	59	15	--	11	--	130	196
Sc	--	--	--	--	--	--	--	--	--	19
V	91	69	79	89	195	250	161	172	167	140
Ni	162	333	384	300	179	146	220	189	549	414
Cr	--	--	--	--	--	--	--	--	--	574

Group IV : Page 2

Locality	Jersey Channel Isles	Jersey Channel Isles	Jersey Channel Isles	Guernsey Channel Isles	Tuscany Italy	Tuscany Italy	Tuscany Italy	Tuscany Italy	Fenster-tollen Germany	St. Bresson France
Reference	111	111	111	111	112	112	112	112	113	114
SiO2	47.56	46.97	61.73	47.91	52.90	56.10	56.60	55.30	50.70	64.30
TiO2	1.74	1.00	1.14	1.28	1.45	1.50	1.33	1.80	1.21	0.80
Al2O3	15.04	15.08	13.33	12.46	13.06	12.61	11.72	11.98	14.08	12.63
Fe2O3	2.30	3.34	2.44	5.21	4.76	2.08	3.81	3.42	0.79	1.03
FeO	4.68	6.10	2.58	3.25	2.02	2.78	1.35	2.60	5.21	2.65
MnO	0.20	0.01	0.07	0.00	0.06	0.08	0.17	0.09	0.09	0.13
MgO	8.06	8.95	5.28	12.46	8.01	7.56	9.12	8.35	6.00	3.36
CaO	6.28	3.81	1.86	5.48	4.28	4.07	4.41	4.28	5.90	2.45
Na2O	2.24	1.28	1.40	0.91	1.34	1.61	1.67	1.25	1.16	2.72
K2O	6.89	7.42	6.98	6.29	7.23	7.23	7.57	8.11	5.84	6.56
P2O5	0.28	0.22	0.18	0.14	1.27	1.14	0.62	0.62	0.91	0.70
H2O+	2.41	3.67	0.24	2.98	--	--	--	--	3.82	1.58
H2O-	2.08	0.27	0.61	1.61	--	--	--	--	0.19	0.34
CO2	--	--	--	0.31	--	--	--	--	3.25	0.27
Ba										
Rb										
Sr										
Zr										
Nb										
Y										
La										
Ce										
Nd										
Sc										
V										
Ni										
Cr										

Group IV : Page 3

Locality	Dommartin France	Col-des Croix France	Schirmeck France	Albbruck-Teifenstein Germany	Pont de Montvert France	Limousin France	Limousin France	Limousin France	Limousin France	Vaugnerite France
Reference	111	111	111	111	115	116	116	116	116	116
SiO2	64.24	57.40	42.64	58.07	55.50	57.30	55.21	59.36	54.33	48.55
TiO2	1.28	1.58	1.45	1.06	1.50	1.15	1.05	1.10	0.00	0.72
Al2O3	14.04	12.65	10.30	14.24	13.00	15.64	14.77	15.48	16.00	19.59
Fe2O3	1.66	1.53	2.71	2.05	2.00	3.60	1.85	2.68	4.51	2.20
FeO	2.44	3.58	5.13	4.42	5.40	2.83	4.77	2.99	3.44	7.15
MnO	0.01	0.14	0.95	0.01	0.15	0.07	0.15	0.05	0.02	0.05
MgO	4.45	6.20	11.60	5.80	5.10	5.65	6.99	4.47	5.45	6.74
CaO	1.07	3.50	8.98	2.12	3.20	2.93	4.96	2.50	5.96	9.38
Na2O	1.73	2.06	1.37	2.33	0.50	2.10	2.22	1.79	2.11	1.45
K2O	6.72	5.86	6.05	4.68	3.50	5.92	5.02	5.22	5.62	3.19
P2O5	0.82	1.14	0.61	0.79	0.00	0.65	1.15	0.52	0.03	0.51
H2O+	1.45	3.02	5.56	3.34	0.22	1.92	2.34	2.76	1.50	0.75
H2O-	0.60	0.65	0.32	0.50	6.00	0.48	0.35	0.96	0.20	0.23
CO2	--	0.58	2.78	--	--	0.09	--	--	--	--
Ba										
Rb										
Sr										
Zr										
Nb										
Y										
La										
Ce										
Nd										
Sc										
V										
Ni										
Cr										

Group IV : Page 4

Locality	Vaugnerite France	Vaugnerite France	Vaugnerite France	Durbach Czechos-lovakia	Durbach Czechos-lovakia	Durbach Czechos-lovakia	Durbach Czechos-lovakia	Durbach Czechos-lovakia	Durbach Czechos-lovakia	Durbach Czechos-lovakia
Reference	117	117	117	118	118	118	118	118	117,119	119
SiO2	46.73	58.35	63.20	59.68	53.95	57.19	63.92	63.12	62.10	58.41
TiO2	1.74	1.06	0.80	0.77	0.84	0.97	0.67	0.83	0.60	0.86
Al2O3	17.38	15.70	14.20	13.25	13.92	13.86	13.37	13.50	13.21	13.29
Fe2O3	0.90	0.70	0.60	1.08	1.21	1.82	0.29	0.42	1.45	0.60
FeO	6.36	4.31	3.70	3.71	5.70	4.50	3.14	3.13	3.13	4.60
MnO	0.10	0.06	0.07	0.08	0.10	0.08	0.06	0.06	0.08	0.15
MgO	9.25	3.71	4.30	6.00	9.94	7.76	4.26	4.32	4.00	6.73
CaO	8.42	4.73	3.55	2.97	5.04	3.48	2.88	2.12	2.77	3.75
Na2O	1.28	2.60	2.30	1.97	1.69	2.11	2.46	2.31	2.91	1.98
K2O	4.51	5.31	6.10	7.34	6.73	5.63	6.22	6.79	6.72	6.71
P2O5	0.94	0.65	0.60	0.80	0.66	0.75	0.51	0.47	0.65	0.97
H2O+	--	1.63	1.10	1.65	0.17	0.73	1.28	1.47	1.64	0.55
H2O-	--	0.20	--	0.22	0.01	0.22	0.04	0.02	0.42	0.24
CO2	--	--	--	--	--	--	--	--	--	--
S				0.01				0.05		
Ba										
Rb										
Sr										
Zr										
Nb										
Y										
La										
Ce										
Nd										
Sc										
V										
Ni										
Cr										

Locality	Durbach Czechos-lovakia	Durbach Czechos-lovakia	Erzgebirge	Erzgebirge	Erzgebirge	Erzgebirge	Erzgebirge	Erzgebirge	Erzgebirge	Erzgebirge
			D.D.R.	D.D.R.	D.D.R.	D.D.R.	D.D.R.	D.D.R.	D.D.R.	D.D.R.
Reference	119	119	120	120	120	120	120	120	120	120
SiO2	39.07	56.58	49.80	48.30	52.60	42.10	50.30	53.20	49.00	47.20
TiO2	1.83	1.19	1.30	1.40	1.40	1.10	2.80	1.50	1.20	1.30
Al2O3	10.98	14.78	15.50	14.90	12.50	13.40	18.10	13.70	12.80	9.50
Fe2O3	1.60	1.08	1.70	1.50	1.60	2.10	2.50	2.60	1.20	1.90
FeO	10.23	6.13	3.10	6.80	3.60	5.20	8.40	8.00	5.90	6.10
MnO	0.30	0.19	0.11	0.48	0.10	0.37	0.90	0.08	0.16	0.14
MgO	14.02	6.32	5.20	9.90	7.20	7.70	4.10	8.80	12.70	17.80
CaO	8.70	4.62	6.70	3.90	5.10	8.60	1.40	1.40	8.20	7.50
Na2O	0.50	2.09	0.80	2.00	1.90	1.60	0.07	0.05	1.60	0.95
K2O	6.60	4.95	6.00	5.00	5.70	3.80	4.30	6.50	4.23	4.50
P2O5	1.98	1.36	0.76	0.81	0.76	0.83	0.52	0.64	0.76	0.81
H2O+	2.97	0.70	2.70	3.40	2.50	2.90	4.70	2.40	0.70	1.00
H2O-	0.40	0.06	0.50	0.40	0.30	0.50	0.30	0.40	0.30	0.30
CO2	--	--	7.00	--	4.60	8.90	--	0.50	0.10	--
F			--	0.115	0.19	--	0.475	0.57	0.135	0.185
Ba			2700	1800	3700	888	90	280	1500	5500
Rb			200	240	175	170	60	820	300	230
Sr			--	--	--	--	--	--	--	--
Zr			630	340	530	240	40	270	270	330
Nb			--	--	--	--	--	--	--	--
Y			--	--	--	--	--	--	--	--
La			--	--	--	--	--	--	--	--
Ce			--	--	--	--	--	--	--	--
Nd			--	--	--	--	--	--	--	--
Sc			--	--	--	--	--	--	--	--
V			110	170	95	240	--	100	180	180
Ni			110	280	155	85	--	175	260	500
Cr			260	670	330	330	135	370	750	1450

Group IV : Page 6

Locality	Erzgebirge	Erzgebirge	Erzgebirge	Erzgebirge	Erzgebirge	Erzgebirge	Erzgebirge	Waldviertel	Waldviertel	Waldviertel
	D.D.R.	D.D.R.	D.D.R.	D.D.R.	D.D.R.	D.D.R.	D.D.R.	Austria	Austria	Austria
Reference	120	120	120	120	120	120	120	121	121	121
SiO2	57.50	49.50	52.00	53.10	47.70	50.70	47.80	64.15	59.46	58.78
TiO2	9.00	1.40	1.30	1.60	1.60	2.10	1.50	1.54	0.97	0.88
Al2O3	14.60	13.80	13.30	14.20	12.00	12.80	11.80	10.69	12.54	14.37
Fe2O3	2.40	4.70	0.50	1.00	0.40	1.70	3.60	2.87	2.30	2.35
FeO	4.10	2.80	5.60	5.80	6.00	4.90	2.90	1.26	1.88	1.87
MnO	0.14	0.10	0.13	0.10	0.12	0.07	0.21	--	--	0.04
MgO	7.50	8.70	8.20	3.90	10.70	10.10	9.20	3.45	5.18	4.89
CaO	4.50	6.80	6.00	5.60	6.80	5.10	7.80	1.90	4.70	4.54
Na2O	1.50	1.50	1.00	1.00	1.10	0.65	2.00	1.81	2.95	2.61
K2O	3.10	3.40	5.90	5.40	5.20	6.80	4.50	9.68	7.36	7.88
P2O5	--	--	0.27	0.12	0.24	1.00	0.98	0.90	1.18	0.86
H2O+	1.30	2.40	1.90	2.80	2.00	3.30	2.10	--	--	0.88
H2O-	0.30	0.60	0.30	0.50	0.30	1.50	0.70	--	--	0.52
CO2	1.00	3.10	3.70	4.80	4.00	--	--	--	--	--
S	--	--	0.27	0.117	0.239	--	--	--	--	--
Ba	400	1650	3450	1550	1310	830	2100			
Rb	360	190	330	30	300	260	200			
Sr	--	--	--	7	--	--	--			
Zr	170	260	700	40	530	900	830			
Nb	--	--	--	--	--	--	--			
Y	--	--	--	--	--	--	--			
La	--	--	--	--	--	--	--			
Ce	--	--	--	--	--	--	--			
Nd	--	--	--	--	--	--	--			
Sc	--	--	--	--	--	--	--			
V	75	115	110	--	70	160	250			
Ni	60	80	240	--	95	230	180			
Cr	260	300	690	140	205	540	520			

Locality	Waldviertel	Waldviertel	Waldviertel	Bohemia	Bohemia	Bohemia	Bohemia	Bohemia	Bohemia	Bohemia
		Waldviertel		Czechos-	Czechos-	Czechos-	Czechos-	Czechos-	Czechos-	Czechos-
	Austria	Austria	Austria	lovakia	lovakia	lovakia	lovakia	lovakia	lovakia	lovakia
Reference	121	121	121	122	122	122	122	122	122	122
SiO2	58.66	58.94	49.68	52.00	51.76	47.81	61.49	67.25	60.16	58.78
TiO2	1.28	0.95	1.16	1.46	1.21	1.65	2.11	2.19	2.27	0.88
Al2O3	12.11	13.30	9.85	13.28	15.01	13.14	8.30	9.59	9.20	13.47
Fe2O3	1.86	1.89	1.38	4.19	1.73	2.47	3.27	2.75	3.68	2.35
FeO	1.88	1.85	5.33	5.02	6.21	5.06	1.30	1.34	2.80	1.87
MnO	0.06	--	0.10	0.40	0.78	0.11	0.07	0.02	0.03	0.04
MgO	4.98	3.81	10.57	5.33	6.36	8.40	6.14	3.13	3.78	4.89
CaO	5.11	5.79	7.87	6.49	3.71	8.96	2.56	1.20	3.00	4.54
Na2O	1.96	2.49	1.02	2.88	2.06	1.60	1.80	1.76	2.22	2.61
K2O	8.24	7.02	7.10	6.06	4.24	3.54	9.50	8.71	9.66	7.88
P2O5	1.48	1.34	1.45	0.19	0.39	0.84	1.39	0.36	1.12	0.86
H2O+	0.57	--	2.29	2.55	3.69	3.26	0.97	1.27	0.53	0.88
H2O-	0.20	0.27	0.23	0.32	0.31	0.52	0.30	0.41	0.26	0.52
CO2	--	--	2.07	--	3.46	2.58	0.15	0.06	0.29	0.06
S	--	--	--	0.12	0.06	--	--	--	--	--
Ba										
Rb										
Sr										
Zr										
Nb										
Y										
La										
Ce										
Nd										
Sc										
V										
Ni										
Cr										

Group IV : Page 8

Locality	Central Bohemia	Central Bohemia	Central Bohemia	Central Bohemia	Central Bohemia	Central Bohemia	Central Bohemia	Central Bohemia	Central Bohemia	Central Bohemia
Reference	123	123	123	123	123	123	123	123	123	123
SiO2	64.88	66.73	58.16	62.55	62.86	61.50	60.97	62.94	61.89	54.30
TiO2	0.79	0.60	1.05	0.86	1.10	0.63	0.66	0.79	0.71	0.64
Al2O3	15.27	14.50	12.57	13.93	14.36	13.70	13.78	14.44	15.07	12.74
Fe2O3	0.41	0.73	1.66	1.55	0.54	1.48	1.22	0.93	0.28	1.40
FeO	2.48	2.40	3.55	2.79	3.32	2.92	3.08	3.35	4.30	5.46
MnO	0.04	0.04	0.09	0.05	0.06	0.07	0.07	0.05	0.09	0.16
MgO	3.06	3.19	8.26	4.61	3.73	5.38	4.83	5.23	3.45	6.38
CaO	1.91	2.42	2.96	3.14	2.75	2.43	2.69	2.39	2.54	6.38
Na2O	2.00	2.40	2.00	2.50	2.22	2.20	2.21	2.15	2.30	1.56
K2O	6.25	5.65	5.26	6.32	5.55	6.16	5.72	5.05	4.94	5.04
P2O5	0.39	0.50	0.75	0.87	0.54	0.54	0.49	0.56	0.33	0.42
H2O+	1.54	1.13	2.31	0.47	2.18	1.86	2.57	1.75	2.93	3.02
H2O-	0.20	0.26	0.61	0.15	0.15	0.10	0.09	0.36	0.26	0.10
CO2	--	--	0.17	--	0.96	0.16	0.77	--	0.15	2.05
S	--	--	0.02	--	--	0.01	0.07	--	0.13	0.18
Ba										
Rb										
Sr										
Zr										
Nb										
Y										
La										
Ce										
Nd										
Sc										
V										
Ni										
Cr										

Locality	Central Bohemia	Central Bohemia	Central Bohemia	Central Bohemia	Bohemia Bohemia	Central Bohemia	Central Bohemia	Central Bohemia	Central Bohemia	Central Bohemia
Reference	123	123	123	123	123	123	123	123	123	123
SiO2	53.81	55.14	58.20	57.27	58.75	59.41	57.30	55.35	60.17	61.59
TiO2	0.91	1.07	1.16	1.28	1.13	1.10	1.33	1.47	0.95	0.65
Al2O3	13.56	13.23	12.88	13.54	12.35	12.63	12.99	12.48	14.02	13.16
Fe2O3	1.51	0.31	0.27	2.30	1.73	1.73	1.51	1.64	2.23	1.55
FeO	5.00	5.58	5.07	3.67	3.76	3.46	3.95	4.28	2.90	2.87
MnO	0.09	0.10	0.09	0.08	0.09	0.09	0.10	0.10	0.06	0.05
MgO	8.52	7.56	6.19	6.00	6.03	5.52	7.02	7.63	5.21	5.60
CaO	5.16	5.71	4.10	3.72	3.76	4.00	3.81	5.23	3.94	3.63
Na2O	1.61	1.61	1.91	1.89	1.72	1.82	1.95	1.25	2.17	2.08
K2O	4.87	6.02	6.50	6.66	7.05	6.93	6.00	6.30	6.36	5.20
P2O5	0.81	0.83	1.00	0.81	1.16	1.37	0.91	1.07	1.16	0.80
H2O+	2.74	1.43	1.32	1.75	1.30	1.49	1.99	1.95	0.93	2.21
H2O-	0.40	0.23	0.49	0.61	0.35	0.41	0.28	0.37	0.32	0.74
CO2	0.23	--	0.13	0.06	--	--	0.73	--	--	--
S	--	--	--	--	--	--	0.01	--	--	--
Ba										
Rb										
Sr										
Zr										
Nb										
Y										
La										
Ce										
Nd										
Sc										
V										
Ni										
Cr										

Group IV : Page 10

Locality	Central Bohemia	Central Bohemia	Central Bohemia	Central Bohemia	Central Bohemia	Central Bohemia	Svidnya Bulgaria	Svidnya Bulgaria	Svidnya Bulgaria	Svidnya Bulgaria
Reference	123	123	123	123	121	121	124	124	124	124
SiO2	57.19	58.68	55.23	56.94	57.32	59.96	46.38	48.63	49.53	50.72
TiO2	1.08	1.38	1.41	1.44	1.15	1.55	1.65	0.65	0.61	0.49
Al2O3	14.24	12.02	10.81	10.81	12.89	10.61	10.33	11.13	10.13	13.11
Fe2O3	1.48	2.41	2.37	2.46	1.47	2.02	2.59	3.81	4.31	2.71
FeO	3.66	3.06	2.73	2.48	4.23	2.44	7.88	5.37	5.20	5.76
MnO	0.08	0.07	0.06	--	--	--	0.07	0.18	0.27	0.26
MgO	6.03	6.48	7.84	7.52	6.60	6.09	9.11	8.57	8.18	6.83
CaO	3.73	3.70	3.97	3.75	4.59	3.33	7.96	8.17	7.13	6.92
Na2O	2.61	1.44	1.01	1.17	1.72	1.75	1.72	1.38	1.83	1.93
K2O	5.27	8.03	8.22	8.47	6.58	8.16	7.39	7.50	7.89	8.41
P2O5	0.65	1.45	2.38	1.89	1.06	1.56	2.07	1.99	1.75	1.43
H2O+	2.57	1.09	1.89	--	--	--	--	--	--	--
H2O-	0.23	0.21	2.01	--	--	--	0.34	0.26	0.24	0.12
CO2	0.63	--	--	--	--	--	--	--	--	--
L.O.I.	--	--	--	--	--	--	1.94	1.87	2.44	0.93
S	0.09	--	--	--	--	--	--	--	--	--
Ba										
Rb										
Sr										
Zr										
Nb										
Y										
La										
Ce										
Nd										
Sc										
V										
Ni										
Cr										

Locality	Svidnya Bulgaria	Svidnya Bulgaria	Svidnya Bulgaria	Svidnya Bulgaria	Svidnya Bulgaria	Svidnya Bulgaria	Svidnya Bulgaria	Svidnya Bulgaria	Svidnya Bulgaria	Svidnya Bulgaria
Reference	124	124	124	124	124	124	124	124	124	124
SiO2	51.29	51.42	51.51	51.88	52.75	53.30	53.56	53.88	54.04	54.35
TiO2	0.51	1.55	1.28	1.36	0.52	1.50	1.40	1.38	1.43	1.35
Al2O3	12.08	11.29	10.97	10.26	12.00	12.00	11.16	10.84	12.51	12.12
Fe2O3	2.97	4.13	3.15	6.16	3.59	4.48	3.97	3.03	3.06	4.19
FeO	5.30	3.18	4.36	5.11	4.30	6.08	3.05	4.52	5.07	3.92
MnO	0.18	0.13	0.14	0.14	0.19	0.09	0.07	0.19	0.13	0.11
MgO	6.20	7.22	6.91	6.23	7.39	6.06	6.32	5.65	5.59	5.60
CaO	5.97	6.71	6.51	6.24	5.87	4.15	5.88	5.74	5.25	5.53
Na2O	2.52	1.83	2.31	2.63	2.33	2.72	2.34	2.66	2.26	2.42
K2O	8.00	7.66	8.66	7.28	8.01	6.52	9.01	9.12	8.29	7.96
P2O5	1.54	1.75	1.63	1.10	1.64	0.76	1.77	1.30	0.90	0.77
H2O+	--	--	--	0.88	--	1.73	--	--	0.90	1.20
H2O-	0.52	0.28	0.20	0.11	0.20	0.13	0.22	0.39	0.27	0.13
CO2	--	--	--	--	--	0.41	--	--	--	--
L.O.I.	2.41	2.25	2.06	--	0.96	--	1.00	0.99	--	--
Ba										
Rb										
Sr										
Zr										
Nb										
Y										
La										
Ce										
Nd										
Sc										
V										
Ni										
Cr										

Locality	Svidnya Bulgaria	Svidnya Bulgaria	Svidnya Bulgaria	Svidnya Bulgaria	Svidnya Bulgaria	Svidnya Bulgaria	Svidnya Bulgaria	Svidnya Bulgaria	Svidnya Bulgaria	Serbia Yugoslavia
Reference	124	124	124	124	124	124	124	124	124	125
SiO2	54.43	54.80	56.47	57.01	50.80	59.02	60.75	56.13	62.16	47.82
TiO2	1.13	1.21	1.18	1.40	1.09	0.63	1.00	1.00	1.07	1.44
Al2O3	11.16	9.85	11.13	12.40	13.41	13.57	10.81	9.05	10.12	13.43
Fe2O3	3.83	4.28	3.64	2.02	1.60	4.50	6.27	6.12	7.07	4.47
FeO	3.10	2.48	2.45	6.27	7.10	2.70	2.72	0.70	1.16	3.04
MnO	0.10	0.14	0.10	0.15	0.23	0.14	0.12	0.11	0.11	0.12
MgO	5.80	6.14	5.41	4.10	7.70	3.30	3.29	6.03	3.17	9.81
CaO	5.50	5.06	4.43	4.05	8.40	2.30	2.39	4.84	1.31	7.64
Na2O	2.29	2.50	2.68	3.04	1.44	3.12	3.44	3.74	3.45	2.77
K2O	8.70	9.00	9.64	6.36	6.42	9.97	8.19	8.64	9.27	5.97
P2O5	1.40	1.30	1.05	1.13	1.30	0.75	0.50	1.80	0.54	1.46
H2O+	--	--	--	0.81	--	--	0.85	--	0.51	1.05
H2O-	0.26	0.10	0.15	0.11	0.20	0.10	0.11	0.24	0.08	0.59
CO2	--	--	--	0.72	--	--	--	--	--	--
L.O.I.	1.16	2.56	1.17	--	1.05	0.30	--	1.08	--	--
Cl										0.07
Ba										
Rb										
Sr										
Zr										
Nb										
Y										
La										
Ce										
Nd										
Sc										
V										
Ni										
Cr										

Locality	Serbia Yugoslavia	North Algeria (Micromz)	North Algeria (Micromz)	North Algeria (Micromz)	Afyon Turkey	Afyon Turkey	Afyon Turkey	Aldan Soviet Union	Aldan Soviet Union	Aldan Soviet Union
Reference	125	126	126	126	127	127	127	128	128	128
SiO2	49.12	54.92	54.35	51.30	53.00	52.25	57.65	43.53	44.00	48.80
TiO2	1.42	0.93	1.29	1.12	1.44	1.61	1.17	0.65	1.90	0.97
Al2O3	12.61	12.52	14.11	11.50	11.94	10.81	13.73	6.45	8.76	9.99
Fe2O3	2.60	1.67	2.18	2.82	1.58	1.75	3.51	3.10	2.86	5.78
FeO	4.57	5.17	3.99	4.14	4.63	3.71	1.60	7.17	7.59	1.58
MnO	0.15	0.21	0.06	0.08	0.10	0.01	0.10	0.14	0.14	0.17
MgO	9.84	7.56	6.41	10.32	8.67	7.97	5.67	24.14	15.11	8.67
CaO	8.36	7.91	6.45	7.60	5.54	4.80	5.01	7.59	9.27	8.10
Na2O	2.76	1.31	1.97	1.34	1.92	1.26	1.94	0.54	0.73	2.86
K2O	6.22	6.14	6.98	5.78	5.90	7.30	6.27	3.48	6.33	6.70
P2O5	1.24	0.40	0.44	0.51	1.03	0.68	0.56	0.38	2.38	0.67
H2O+	0.49	0.99	1.87	2.38	0.60	1.67	1.20	0.13	0.14	0.26
H2O-	0.33	0.24	0.20	1.18	--	--	--	--	--	--
CO2	--	--	--	--	2.94	5.35	0.11	--	--	--
L.O.I.	--	--	--	--	--	--	--	2.10	0.13	1.31
SO3	0.04	--	--	--	--	--	--	0.01	0.80	0.05
Cl	0.17	--	--	--	--	--	--	--	--	--
Ba					1688	601	1207			
Rb					189	294	239			
Sr					737	618	783			
Zr					618	827	552			
Nb					--	--	--			
Y					--	--	--			
La					--	--	--			
Ce					--	--	--			
Nd					--	--	--			
Sc					--	--	--			
V					--	--	--			
Ni					270	315	139			
Cr					511	475	268			

Locality	Aldan Soviet Union	Aldan Soviet Union	Aldan Soviet Union	Baltoro Karakorum Pakistan	Baltoro Karakorum Pakistan	Tsao-Li Taiwan	Kajan Kalimantan Indonesia	Pic de Maros Indonesia	Pic de Maros Indonesia	Pic de Maros Indonesia
Reference	128	128	128	129	129	130	125	131	131	132
SiO2	51.61	53.32	51.73	53.69	47.05	46.82	46.04	52.80	48.05	46.08
TiO2	0.98	0.99	0.85	1.64	2.26	0.35	2.20	1.00	1.10	1.39
Al2O3	14.51	11.74	12.15	11.18	6.90	12.64	12.40	19.99	13.94	20.40
Fe2O3	5.27	1.51	5.22	2.16	1.81	3.67	3.54	3.63	2.67	2.12
FeO	1.73	1.44	1.86	2.43	3.56	4.72	5.58	3.40	5.98	3.27
MnO	0.15	0.45	0.15	0.09	0.10	0.18	--	--	--	0.19
MgO	3.77	6.28	6.12	6.32	11.53	15.42	12.60	3.20	7.81	6.30
CaO	6.90	8.82	8.13	5.88	7.95	7.06	8.38	4.22	7.25	8.48
Na2O	3.32	2.69	2.62	1.82	2.28	1.64	1.62	3.10	2.72	2.07
K2O	7.20	5.78	5.64	10.13	5.82	4.00	4.87	7.74	6.56	6.72
P2O5	--	0.37	0.95	0.92	1.32	--	--	0.70	1.15	1.19
H2O+	0.88	0.37	0.19	--	--	2.72	3.55	1.18	1.66	1.70
H2O-	--	--	--	--	--	--	--	--	--	0.06
CO2	--	--	--	1.32	3.54	--	--	--	--	--
L.O.I.	--	0.52	1.01	1.83	5.08	--	--	--	--	--
SO3	--	0.01	--	--	--	--	--	--	--	S 0.06
F										0.09
Cl										0.10
Ba										
Rb										
Sr										
Zr										
Nb										
Y										
La										
Ce										
Nd										
Sc										
V										
Ni										
Cr										

Locality	Pic de Maros Indonesia	British Columbia Canada	British Columbia Canada	Little Belt Mts U.S.A.	Bearpaw Mts U.S.A.	Bearpaw Mts U.S.A.	Bearpaw Mts U.S.A.	Bearpaw Mts U.S.A.	Highwood Mts U.S.A.	Highwood Mts U.S.A.
Reference	132	133	133	134	134	135	136	136	137,138	137,138
SiO2	43.98	48.33	53.32	47.63	50.00	46.51	50.34	50.38	47.00	46.47
TiO2	2.24	0.81	0.90	2.22	0.73	0.83	0.76	0.58	0.80	0.74
Al2O3	12.28	12.56	14.16	12.01	9.87	11.86	10.32	10.20	12.91	11.50
Fe2O3	3.49	1.87	2.15	4.20	3.46	7.59	3.04	1.90	1.30	0.60
FeO	7.70	5.26	5.08	4.99	5.01	4.39	5.90	6.28	7.20	7.20
MnO	0.51	0.13	0.10	0.17	--	0.22	0.09	0.09	0.15	0.15
MgO	8.00	9.07	7.90	8.31	11.92	4.73	12.58	14.78	7.75	7.98
CaO	11.19	8.94	7.12	7.28	8.30	7.41	7.40	7.28	9.70	13.64
Na2O	1.33	1.81	2.39	1.98	2.41	2.39	2.16	2.20	1.85	0.71
K2O	5.06	4.67	4.80	5.40	5.02	8.71	4.47	4.57	6.45	5.15
P2O5	1.81	0.78	0.66	1.08	0.81	0.80	0.78	0.61	0.91	1.00
H2O+	1.61	2.63	1.24	1.83	1.16	2.45	1.85	0.93	1.74	2.41
H2O-	0.12	0.97	0.26	0.94	0.17	1.10	--	--	0.40	0.39
CO2	--	2.64	--	0.74	--	0.31	0.07	--	1.01	0.81
L.O.I.	--	--	--	--	--	--	--	--	--	--
S	0.10	--	--	SO3 0.19	--	0.02	--	--	S 0.06	0.21
F	0.15	--	--	--	--	--	--	--	--	--
Cl	0.12	--	--	--	--	0.08	0.11	--	--	--
Ba									6410	4730
Rb									200	165
Sr									2195	1435
Zr									190	170
Nb									15	5
Y									30	25
La									80	55
Ce									155	130
Nd									55	50
Sc									--	--
V									--	--
Ni									65	70
Cr									170	85

Locality	Highwood Mts U.S.A.	Highwood Mts U.S.A.	Highwood Mts U.S.A.	Highwood Mts U.S.A.	Highwood Mts U.S.A.	Highwood Mts U.S.A.	Highwood Mts U.S.A.	Highwood Mts U.S.A.	Highwood Mts U.S.A.	Highwood Mts U.S.A.
Reference	137,138	139	139	139	134	135	140	140	141	141
SiO2	49.90	48.30	50.00	49.20	46.04	46.62	49.26	51.94	46.06	48.18
TiO2	0.81	0.75	1.40	1.30	0.64	0.76	1.11	0.39	0.73	0.55
Al2O3	18.02	10.40	13.20	12.90	12.23	12.48	13.64	15.78	10.01	11.28
Fe2O3	2.92	2.00	4.20	3.90	3.86	4.78	1.72	4.07	3.17	3.29
FeO	4.07	7.70	2.90	3.10	4.60	4.44	7.76	3.17	5.61	3.84
MnO	0.12	0.16	0.08	0.10	--	0.09	0.12	--	--	0.05
MgO	3.11	16.00	6.80	6.90	10.38	8.90	8.31	3.48	14.74	12.89
CaO	5.43	6.80	8.90	9.40	8.97	11.94	8.42	6.04	10.55	9.22
Na2O	3.75	1.40	2.40	2.10	2.42	1.97	1.90	3.44	1.31	1.94
K2O	7.75	3.60	4.90	4.60	5.77	4.42	5.02	7.69	5.14	6.57
P2O5	0.72	0.65	1.30	1.60	1.14	0.18	0.75	0.59	0.21	0.53
H2O+	2.47	1.70	2.20	1.40	2.87	2.83	1.21	2.17	1.44	1.55
H2O-	0.44	0.31	1.30	1.60	--	--	0.32	--	--	--
CO2	--	0.08	0.43	1.30	--	--	--	--	--	--
S	0.02	--	--	--	--	0.05	0.02	SO3 0.29	0.05	S 0.03
								Cl 0.08	0.03	--
Ba	7540									
Rb	245									
Sr	1800									
Zr	195									
Nb	25									
Y	20									
La	65									
Ce	130									
Nd	50									
Sc	--									
V	--									
Ni	20									
Cr	35									

Locality	Highwood Mts	Highwood Mts	Highwood Mts	Yogo Peak	Absaroka	Yellow-stone	Yellow-stone	Black Hills	Spanish Peaks	Spanish Peaks
	U.S.A.	U.S.A.	U.S.A.	Montana U.S.A.	Wyoming U.S.A.	U.S.A.	U.S.A.	U.S.A.	U.S.A.	U.S.A.
Reference	141	131	131	131	131	142	143	144	145	145
SiO2	51.75	53.47	46.73	48.98	48.36	51.62	49.71	46.69	47.90	46.90
TiO2	0.23	1.19	0.78	1.44	0.78	0.78	1.57	1.02	2.00	2.50
Al2O3	14.52	12.43	10.05	12.29	12.42	12.56	13.30	10.51	11.40	11.10
Fe2O3	5.08	6.19	3.53	2.88	5.25	3.39	4.41	4.97	7.70	7.90
FeO	3.58	3.73	8.20	5.77	2.48	4.61	3.37	2.54	2.60	3.10
MnO	--	--	--	--	--	0.16	--	0.21	0.13	0.09
MgO	4.55	3.07	9.27	9.19	9.36	7.69	7.96	6.58	6.90	6.30
CaO	7.04	7.23	13.22	9.65	8.65	7.37	8.03	7.17	9.00	10.60
Na2O	2.93	3.40	1.81	2.22	1.46	2.26	1.49	2.17	2.20	2.10
K2O	7.61	7.59	3.76	4.96	3.97	5.10	4.81	7.95	4.80	4.50
P2O5	0.18	0.84	1.51	0.98	1.51	0.60	0.66	0.65	1.80	2.10
H2O+	2.25	--	1.24	0.56	5.54	--	--	0.41	2.00	1.40
H2O-	--	--	--	--	--	--	--	--	1.40	0.37
CO2	--	0.40	--	--	--	--	--	3.76	<0.05	<0.05
L.O.I.	--	--	--	--	--	--	--	--	--	--
SO3	--	0.62	--	--	--	--	--	--	--	--
Cl	--	--	0.18	--	--	--	--	--	--	--
Ba										
Rb										
Sr										
Zr										
Nb										
Y										
La										
Ce										
Nd										
Sc										
V										
Ni										
Cr										

Locality	Spanish Peaks U.S.A.	Spanish Peaks U.S.A.	Spanish Peaks U.S.A.	Navajo U.S.A.	Navajo U.S.A.	Navajo U.S.A.	Navajo U.S.A.	Navajo U.S.A.	Navajo U.S.A.	Navajo U.S.A.
Reference	145	145	146	147	147,148	147	147,148	147	147,148	149
SiO2	46.00	45.10	46.70	49.13	48.94	55.46	56.23	58.88	59.50	48.80
TiO2	1.10	1.80	2.00	2.02	2.03	0.91	1.08	0.87	0.89	2.44
Al2O3	11.10	11.40	10.90	10.51	10.11	10.65	12.14	13.38	12.93	8.60
Fe2O3	4.50	7.50	9.50	3.82	4.47	3.68	4.38	3.77	3.02	3.89
FeO	1.30	2.40	1.80	4.30	3.60	1.08	1.36	1.17	1.46	3.85
MnO	0.28	0.19	0.16	0.12	0.12	0.05	0.08	0.06	0.06	0.16
MgO	4.10	8.00	6.80	9.87	10.03	9.17	6.63	4.31	4.90	12.30
CaO	10.80	9.30	8.60	9.06	8.98	4.34	6.37	6.12	5.30	8.81
Na2O	1.10	1.20	2.10	2.06	1.28	1.42	2.60	2.87	2.53	1.74
K2O	6.60	4.70	4.60	4.86	5.22	6.98	6.76	7.20	7.21	4.72
P2O5	0.44	1.60	1.60	0.97	1.08	0.63	0.77	0.74	0.64	1.08
H2O+	1.80	2.70	2.80	2.38	2.92	2.09	0.84	0.36	0.54	--
H2O-	2.90	1.40	2.00	0.38	0.80	2.71	0.36	0.08	0.60	--
CO2	7.80	2.00	<0.05	0.00	0.01	0.00	0.02	0.06	0.10	--
L.O.I.	--	--	--	--	--	--	--	--	--	2.46
Ba					--		--		--	
Rb					--		--		--	
Sr					--		--		--	
Zr					--		--		--	
Nb					74		74		26	
Y					--		--		--	
La					116		123		109	
Ce					238		243		211	
Nd					99		99		83	
Sc					--		--		--	
V					195		132		100	
Ni					--		--		--	
Cr					338		176		123	

Locality	Navajo U.S.A.	Navajo U.S.A.	Navajo U.S.A.	Navajo U.S.A.	Navajo U.S.A.	Navajo U.S.A.	Navajo U.S.A.	Navajo U.S.A.	Navajo U.S.A.	Navajo U.S.A.
Reference	149	149	150	150	150	151	151	151	151	151
SiO2	58.40	53.20	50.95	52.79	58.00	49.10	48.30	51.00	5.450	56.70
TiO2	0.93	1.89	1.98	1.93	1.02	2.05	1.84	1.63	1.81	1.20
Al2O3	11.90	10.70	10.09	10.74	11.06	10.10	10.60	10.60	11.60	12.10
Fe2O3	--	--	3.93	3.49	2.64	4.46	3.63	3.99	3.21	3.14
FeO	4.55	6.30	3.43	3.62	2.22	3.10	4.74	2.55	3.57	2.26
MnO	0.07	0.09	0.16	0.16	0.14	0.12	0.14	0.11	0.11	0.08
MgO	5.04	8.56	9.60	7.62	6.73	10.77	10.14	8.14	7.52	6.23
CaO	6.12	6.98	8.27	7.73	6.79	8.66	9.99	9.48	7.09	6.24
Na2O	2.30	1.84	2.42	2.44	2.08	0.80	1.80	1.50	1.90	1.94
K2O	7.11	5.56	5.27	6.38	6.72	5.35	4.57	5.92	6.76	6.93
P2O5	0.83	0.86	0.91	0.77	0.52	0.94	1.04	0.93	0.83	0.72
H2O+	--	--	1.22	0.88	0.69	2.83	1.97	1.12	0.94	0.71
H2O-	--	--	0.65	0.39	0.39	1.47	0.75	1.23	0.62	0.92
CO2	--	--	--	--	--	0.11	0.11	2.17	0.11	0.58
L.O.I.	1.12	1.90	--	--	--	--	--	--	--	--
S	--	--	0.04	0.01	0.01	--	--	--	--	--
Cl	--	--	0.02	0.01	0.02	--	--	--	--	--
Ba	3197	1503	2780	2810	2310	--	--	--	--	--
Rb	246	137	160	190	200	--	--	--	--	--
Sr	1141	1078	1100	1190	890	--	--	--	--	--
Zr	--	--	320	410	310	--	--	--	--	--
Nb	--	--	30	30	--	--	--	--	--	--
Y	--	--	10	20	20	--	--	--	--	--
La	162	96	140	150	90	133	156	179	228	152
Ce	311	153	240	250	170	266	359	388	331	317
Nd	--	--	100	110	70	118	148	166	141	137
Sc	12	11	--	--	--	16	20	16	17	19
V	--	--	150	270	170	--	--	--	--	--
Ni	163	267	290	270	270	--	--	--	--	--
Cr	153	326	400	300	370	492	552	354	360	439

Locality	Navajo U.S.A.	Navajo U.S.A.	Navajo U.S.A.	Navajo U.S.A.	Navajo U.S.A.	Navajo U.S.A.	Sullivan Butte U.S.A.	Sierra Nevada U.S.A.	Sierra Nevada U.S.A.	Sierra Nevada U.S.A.
Reference	152	152	152	152	152	152	153	154	154	154
SiO2	49.05	51.50	51.60	51.80	55.10	58.75	58.58	51.70	53.50	51.00
TiO2	1.70	1.85	2.30	1.80	1.55	0.80	0.78	1.80	1.57	1.50
Al2O3	10.65	11.55	10.54	11.10	13.85	12.70	14.47	12.70	12.30	11.60
Fe2O3	4.80	2.38	3.30	3.55	1.53	1.80	--	3.70	3.82	4.60
FeO	3.00	4.72	3.66	3.42	2.02	2.44	5.21	2.80	2.20	2.80
MnO	0.08	0.10	0.08	--	0.08	0.08	0.09	0.13	0.10	0.16
MgO	9.45	7.90	9.30	8.15	6.65	6.40	3.59	5.70	7.36	9.20
CaO	10.30	9.10	8.70	7.95	7.45	5.50	4.62	6.40	4.65	7.40
Na2O	1.92	2.55	1.87	2.25	2.54	2.22	2.57	2.00	2.16	2.00
K2O	5.00	5.65	5.76	5.97	5.93	6.44	5.15	8.40	8.22	7.00
P2O5	0.94	0.96	0.73	0.95	0.82	0.58	0.36	1.50	1.56	1.60
H2O+	2.15	1.10	1.30	1.90	1.25	1.15	1.46	1.80	0.26	0.67
H2O-	1.15	0.45	0.90	1.00	1.10	1.10	1.66	0.89	0.26	0.24
CO2	0.20	--	--	--	--	--	--	0.05	0.05	0.05
Ba								5094	4541	4740
Rb								640	68	92
Sr								2375	2005	2475
Zr								652	803	575
Nb								--	--	--
Y								105	31	25
La								43	30	46
Ce								82	50	91
Nd								43	25	48
Sc								15	15	18
V								--	--	--
Ni								280	235	185
Cr								164	626	353

Locality	Sierra Nevada U.S.A.	Sierra Nevada U.S.A.	Sierra Nevada U.S.A.	Sierra Nevada U.S.A.	Sierra Nevada U.S.A.	Sierra Nevada U.S.A.	Sierra Nevada U.S.A.	Sierra Nevada U.S.A.	Sierra Nevada U.S.A.	Sierra Nevada U.S.A.
Reference	155	155	155	155	155	155	155	155	155	155
SiO2	45.27	45.69	46.69	55.53	50.73	49.28	51.00	51.70	53.10	53.70
TiO2	1.85	1.78	1.72	1.57	2.02	1.52	1.50	1.80	1.90	1.20
Al2O3	11.61	11.64	12/00	12.33	13.88	11.30	11.60	12.70	13.00	13.90
Fe2O3	2.71	2.65	3.17	3.82	5.27	4.46	4.60	3.70	3.70	5.70
FeO	6.73	6.45	5.81	2.20	3.54	2.36	2.80	2.80	2.80	1.40
MnO	0.16	0.15	0.15	0.10	0.12	0.10	0.16	0.13	0.08	0.15
MgO	12.70	12.38	11.70	7.36	6.39	11.51	9.20	5.70	5.60	6.40
CaO	8.38	8.24	8.11	4.65	6.80	8.34	7.40	6.40	5.80	6.80
Na2O	1.88	1.88	2.29	2.16	2.63	2.18	2.00	2.00	1.70	2.70
K2O	5.34	5.20	5.07	8.22	5.71	5.50	7.00	8.40	7.70	6.00
P2O5	1.16	1.10	1.08	1.56	1.23	1.60	1.60	1.50	1.50	1.40
H2O+	0.60	0.64	0.43	0.26	0.71	0.64	0.67	1.80	1.40	0.49
H2O-	0.42	0.28	0.17	0.26	0.21	0.37	0.24	0.89	0.82	0.10
CO2	0.06	0.07	0.09	0.05	0.03	0.03	<0.05	<0.05	0.02	<0.05
Ba	4200	4550	4350	4435	3650	3700				
Rb	116	113	111	--	38	280				
Sr	920	960	980	--	1700	2200				
Zr	--	--	--	--	--	510				
Nb	--	--	--	--	--	--				
Y	24	33	22	--	7	51				
La	--	--	--	--	--	--				
Ce	--	--	--	--	--	--				
Nd	--	--	--	--	--	--				
Sc	23	22	20	--	22	21				
V	265	245	250	--	295	130				
Ni	335	320	300	241	128	--				
Cr	570	550	520	410	--	410				

Locality	New South Wales Australia	New South Wales Australia	New South Wales Australia	New South Wales Australia	New South Wales Australia	New South Wales Australia	New South Wales Australia	New South Wales Australia	New South Wales Australia	New South Wales Australia
Reference	156	156	156	156	156	156	156	156	156	156
SiO2	42.94	44.92	46.93	41.91	41.82	45.90	44.97	44.37	43.73	44.45
TiO2	5.51	5.12	3.22	5.40	5.46	5.26	4.68	3.74	4.05	4.44
Al2O3	8.72	8.84	8.08	7.58	7.54	8.95	8.60	8.22	7.91	8.47
Fe2O3	4.98	6.12	5.68	7.07	6.55	5.09	3.02	4.87	5.92	5.45
FeO	6.31	4.99	1.88	4.24	4.52	5.56	6.67	5.70	4.97	5.85
MnO	0.15	0.15	0.12	0.15	0.15	0.13	0.12	0.17	0.17	0.17
MgO	12.17	9.44	8.54	13.31	13.15	9.71	13.64	14.43	15.16	11.88
CaO	9.30	8.30	8.84	9.09	9.27	7.86	7.89	9.01	8.60	8.57
Na2O	0.74	1.28	1.08	0.92	0.66	1.21	0.88	1.94	1.35	1.82
K2O	5.14	6.82	4.16	5.44	5.92	7.24	7.09	5.11	5.20	6.34
P2O5	0.87	0.91	2.88	1.19	1.34	0.67	0.87	1.02	0.86	1.53
H2O+	2.60	1.80	6.14	2.36	2.60	1.32	0.86	0.88	1.40	0.86
H2O-	--	--	--	--	--	--	--	--	--	--
CO2	--	0.16	0.20	--	0.26	--	--	--	0.10	--
Ba	2950	1500	9616	6800	4950	1350	1100	1420	1390	1440
Rb	157	212	14	293	355	299	218	112	108	114
Sr	2100	1680	3039	2190	2200	830	940	1300	1330	1510
Zr	657	600	988	740	755	700	515	570	635	650
Nb	--	--	--	--	--	--	--	--	--	--
Y	--	--	--	--	--	--	--	--	--	--
La	--	--	--	--	--	--	--	--	--	--
Ce	--	--	--	--	--	--	--	--	--	--
Nd	--	--	--	--	--	--	--	--	--	--
Sc	--	--	--	--	--	--	--	--	--	--
V	--	--	--	--	--	--	--	--	--	--
Ni	290	266	108	424	367	351	437	425	520	392
Cr	212	213	58	317	296	266	330	573	546	367

Locality	New South Wales Australia	New South Wales Australia	New South Wales Australia	New South Wales Australia	New South Wales Australia	New South Wales Australia	New South Wales Australia	New South Wales Australia	New South Wales Australia	New South Wales Australia
Reference	156	156	156	156	156	156	156	156	156	156
SiO2	45.77	43.39	44.18	44.75	44.83	47.99	43.49	43.30	47.30	44.45
TiO2	4.30	4.07	4.14	3.71	4.22	3.87	4.35	3.70	3.99	3.93
Al2O3	8.60	8.61	8.03	8.49	8.01	8.38	8.81	8.30	11.60	9.34
Fe2O3	5.13	3.26	4.44	4.55	5.08	6.48	5.01	5.20	3.46	5.90
FeO	5.70	7.64	6.64	5.92	5.46	3.70	5.74	5.74	5.28	4.71
MnO	0.16	0.17	0.17	0.17	0.16	0.14	0.16	0.17	0.15	0.16
MgO	10.76	14.58	12.66	13.66	13.53	10.02	12.29	14.50	7.13	10.70
CaO	8.01	9.36	7.92	9.06	8.27	6.96	8.96	9.57	9.89	10.47
Na2O	1.79	1.93	1.69	2.13	1.62	1.55	1.66	1.55	2.43	2.09
K2O	6.97	4.13	6.40	5.40	6.09	7.32	5.29	4.60	6.07	4.71
P2O5	1.05	1.08	1.39	1.10	1.28	1.21	1.32	0.80	1.07	1.08
H2O+	1.00	0.66	1.26	0.56	1.06	1.38	1.78	1.60	1.34	1.38
H2O-	--	--	--	--	--	--	--	--	--	--
CO2	--	--	0.04	0.08	--	--	0.04	--	--	0.16
Ba	750	1150	2260	1100	1700	1000	1500	1900	1420	1390
Rb	149	108	109	87	119	162	137	154	192	216
Sr	1400	1070	1440	1160	1500	1290	1550	1390	1900	1370
Zr	725	405	635	540	685	720	640	510	570	490
Nb	--	--	--	--	--	--	--	--	--	--
Y	--	--	--	--	--	--	--	--	--	--
La	--	--	--	--	--	--	--	--	--	--
Ce	--	--	--	--	--	--	--	--	--	--
Nd	--	--	--	--	--	--	--	--	--	--
Sc	--	--	--	--	--	--	--	--	--	--
V	--	--	--	--	--	--	--	--	--	--
Ni	275	466	362	567	398	448	367	438	102	267
Cr	316	519	378	480	413	394	391	543	189	347

Locality	New South Wales Australia	New South Wales Australia	Mordor Australia	Mordor Australia	West Tasmania Australia	West Tasmania Australia	West Tasmania Australia
Reference	156	156	157	157	158	158	159
SiO2	44.70	46.51	42.73	48.12	47.06	44.81	54.60
TiO2	3.89	3.40	0.89	1.20	0.90	1.32	0.07
Al2O3	8.82	8.68	6.20	12.11	11.22	11.44	15.20
Fe2O3	4.41	4.15	1.87	2.65	3.75	4.11	6.30
FeO	6.19	6.08	10.25	8.39	4.61	5.58	6.30
MnO	0.16	0.15	0.17	0.13	0.20	0.28	--
MgO	13.12	12.92	22.44	10.52	12.36	11.80	3.30
CaO	8.96	8.08	5.94	8.05	7.26	9.16	2.70
Na2O	2.09	2.04	0.56	1.15	0.94	1.02	1.20
K2O	4.63	5.05	3.07	4.31	3.10	3.27	8.20
P2O5	1.16	1.10	0.84	1.25	0.48	0.85	--
H2O+	1.72	0.72	--	--	3.06	3.21	--
H2O-	--	--	--	--	2.26	0.86	--
CO2	--	--	0.85	0.50	1.99	2.10	--
L.O.I.	--	--	2.37	0.85	--	--	--
SO3	--	--	0.39	--	--	--	--
Ba	1470	1290	6130	--			
Rb	111	172	172	240			
Sr	1330	1230	780	1192			
Zr	635	550	95	--			
Nb	--	--	--	--			
Y	--	--	--	--			
La	--	--	100	--			
Ce	--	--	--	--			
Nd	--	--	--	--			
Sc	--	--	--	--			
V	--	--	--	--			
Ni	359	412	570	--			
Cr	412	483	2550	--			

APPENDIX II

Rare Earth Elements in Antarctic Lamproites

Rare earth element analyses are given here (in parts per million) for rocks from Gaussberg, Mount Bayliss and Priestly Peak. The samples are the same as those analysed for major and trace elements by Sheraton and Cundari [1980] and Sheraton and England [1980], and are included in the ultrapotassic rock database in Appendix I.

Analyses were taken by XRF from papers prepared by an ion-exchange technique modified after Fryer [1977]. BCR-1 and TASGRAN were used as standards: values are given by Robinson et al [1986].

	La	Ce	Nd	Sm	Eu	Gd	Dy	Er	Yb
Priestly Peak									
3950	167	358	164	15.7	3.9	12.9	6.7	12.9	4.5
3951C	153	273	-	35.5	9.0	27.2	13.2	25.0	11.2
3949D	151	327	150	30.8	7.9	24.4	13.0	23.3	12.2
3949C	163	316	133	26.6	7.1	21.5	11.1	23.3	9.8
Mount Bayliss									
11370	144	304	118	19.9	5.5	14.2	10.4	22.7	13.8
1545	158	314	116	16.5	4.7	12.9	8.7	21.1	14.6
Gaussberg									
4870A	209	392	130	16.9	4.5	12.7	7.2	16.4	8.4
4870B	201	368	129	15.0	3.3	9.9	6.9	18.0	12.6
4872	210	382	131	15.6	3.9	10.6	6.6	13.3	7.7
4875	216	390	130	16.0	4.6	11.0	6.6	13.7	6.3
4887	218	379	128	15.5	3.9	10.9	7.0	14.6	9.8
4888	204	374	127	15.4	3.7	11.3	7.1	15.7	9.4
4889	205	381	127	15.6	3.9	11.2	6.9	14.1	10.2
4893A	214	388	131	16.6	4.2	11.2	6.9	14.6	8.9
4893B	212	394	134	15.3	3.4	10.7	7.1	15.8	10.9
4894	195	360	123	16.4	4.2	11.7	6.7	15.4	11.3

APPENDIX III

EXPERIMENTAL TECHNIQUES FOR MELTING STUDIES ON ROCK COMPOSITIONS IN THE PRESENCE OF REDUCED C-O-H FLUIDS

ABSTRACT

Experimental techniques have been developed for melting experiments on rock compositions with controlled CH_4-H_2O fluids for comparison with H_2O- and CO_2-bearing experiments. Sample capsules consist of an outer noble metal capsule with two inner graphite capsules containing oxygen buffer and sample. A solid source for CH_4 and H_2O (Al_4C_3 + $Al(OH)_3$) is packed between the graphite capsules. Quenched fluid compositions were analysed by passing fluids directly from the pierced capsule into a mass spectrometer. The ideally preferred technique of fixing fO_2 and fluid composition at the intersection of the IW buffer and the carbon saturation surface was successful in sample-absent fluid test experiments, but proved unreliable with sample present.

A technique is described in which fO_2 is closely bracketed at the low fO_2 end of the X_{H2O}-maximum on the carbon saturation surface where fluids consist of H_2O >> CH_4 > CO_2. This was achieved by addition of H_2O to the sample capsule and inclusion of an IW buffer to prevent oxidation to H_2O+CO_2 fluids. Oxygen fugacity is therefore not fixed, but fluid compositions, and thus fO_2, are monitored by the capsule piercing technique.

The fluid test results at IW indicate that CH_4/H_2O in the fluid is a stronger function of temperature than predicted by thermodynamic calculations. A rapid increase in CH_4/H_2O with decreasing temperature would cause partial melts ascending through the mantle to freeze or experience significant crystal fractionation if fO_2 ~ IW is maintained.

A3.1 INTRODUCTION

The oxidation state of the mantle in source regions of basic magmas has recently been debated widely [see reviews by Woermann and Rosenhauer 1985; Arculus 1985] with suggested fO_2 values ranging from those of the IW

buffer (IW) to near quartz-fayalite-magnetite (QFM). An increasing body of evidence, principally from intrinsic oxygen fugacity measurements of mantle-derived minerals and rocks [Arculus et al. 1984], the identification of primordial methane outgassing at mid-ocean ridges [Welhan and Craig 1983; Kim 1983], and studies of fluid inclusions in diamonds [Taylor 1986b], favours the interpretation that large areas of the upper mantle have oxidation states towards the reduced end of this range. This challenges popular models for a more oxidised mantle in which C-O-H fluids, if present, would be H_2O+CO_2 mixtures, and would coexist with carbonate minerals [Wyllie 1978; Eggler 1978] and probably graphite, resulting in control of fO_2 by the EMOD/EMOG buffer [Eggler and Baker 1982]. C-O-H fluids in the fO_2 range IW to IW+2 log units would consist of H_2O+CH_4 mixtures with minimal CO_2.

Experimental studies of melting of peridotites and of liquidus phase assemblages of basic magmas have reflected the prevailing oxidised mantle model by considering the effects of adding varying amounts of H_2O and CO_2 compared to volatile-free experiments. These experiments have generally not had oxygen fugacity control, but results indicate that H_2O and CO_2 remained the dominant fluid species present. In some cases, indirect fO_2 control by an external HM buffer depending on fH_2 control through a noble metal capsule has been used to prevent reduction of CO_2 to graphite: in these experiments fO_2 varied between fairly broad limits (~NNO to HM; Brey and Green 1977; Ryabchikov and Green 1978]. The analyses of ilmenites reported by Green and Sobolev [1975] from a number of experiments on peridotite and basanite compositions with added H_2O, but without fO_2 control [Green 1973a,b] show low Fe_2O_3 contents indicative of low fO_2. It appears likely that these "furnace-buffered" experiments [Brey and Green 1975] had fO_2 close to IW+2 log units, rather than close to MW and NNO as suggested at the time. This may be due to the influence of graphite + H_2O in the assembly (see below for fO_2 characteristics) on fH_2 and thus indirectly on fO_2, particularly for experiments with large amounts of water in unsealed graphite capsules [Green 1973b]. Ilmenites from experiments with known low fO_2 using the technique described here have similar or slightly lower Fe_2O_3 contents than those of Green and Sobolev [1975] (Part 5).

This paper reports techniques for experiments in reduced conditions with H_2O+CH_4 fluids. Preliminary results using lamproite rock compositions

show that fO_2 conditions can be controlled quite closely by bracketing between limits at IW and CW (see below). Oxygen fugacity and fluid compositions are not fixed, but can be monitored by analysis of the fluid phase by mass spectrometry.

A3.2 THEORETICAL C-O-H FLUID COMPOSITIONS IN A REDUCED MANTLE

Taylor [1985, 1986a] has calculated C-O-H fluid compositions in equilibrium with graphite or diamond using a modified Redlich-Kwong equation of state. The assumption that excess carbon may exist in the mantle during melting is reasonable as the solubility of reduced carbon in silicate melts is limited to 1000-2000 p.p.m. [Taylor and Green 1986b]. Calculated fluid compositions can be represented on a plot of fO_2 against X_C [$C/(C+H_2)$ of the fluid phase; Taylor 1986a], in which fluids in equilibrium with carbon are confined to the carbon saturation surface (figure 48). Fluids have fixed compositions at the intersection of oxygen buffers with the carbon saturation surface, and consist of CH_4>H_2O mixtures at C-IW (the intersection of IW with the carbon saturation surface).

About midway between fO_2 corresponding to IW (CH_4>H_2O fluids) and EMOD/EMOG (H_2O+CO_2 fluids), fluid compositions pass through a X_{H2O}-maximum at which fluids consist of 85-95 mol% H_2O at >15kbar. The locus of points in pressure-temperature space corresponding to maximum H_2O content in the fluid phase is referred to here as CW (carbon-water). The oxygen fugacity of CW varies with pressure and temperature as shown in figure 49, from which it can be seen that fO_2 defined by CW is less certain at high pressures and low temperatures due to increased width of the "nose" in the carbon saturation surface, e.g. X_{H2O} is close to the maximum value over >3 log units fO_2 at 55 kbar and 1400K (figure 49a), whereas it is more sharply defined (~1 log unit fO_2) at 30 kbar and 1600K (figure 49b).

A3.3 EXPERIMENTAL PROCEDURES FOR REDUCED FLUID EXPERIMENTS

The ideal situation in experiments using reduced C-O-H fluids would be to make use of the invariant nature of fluids during experiments at fixed pressure and temperature at the intersection of an oxygen buffer with the carbon saturation surface (e.g. C-IW). Two experimental designs were considered: [a] C-IW experiments which would have the advantage of

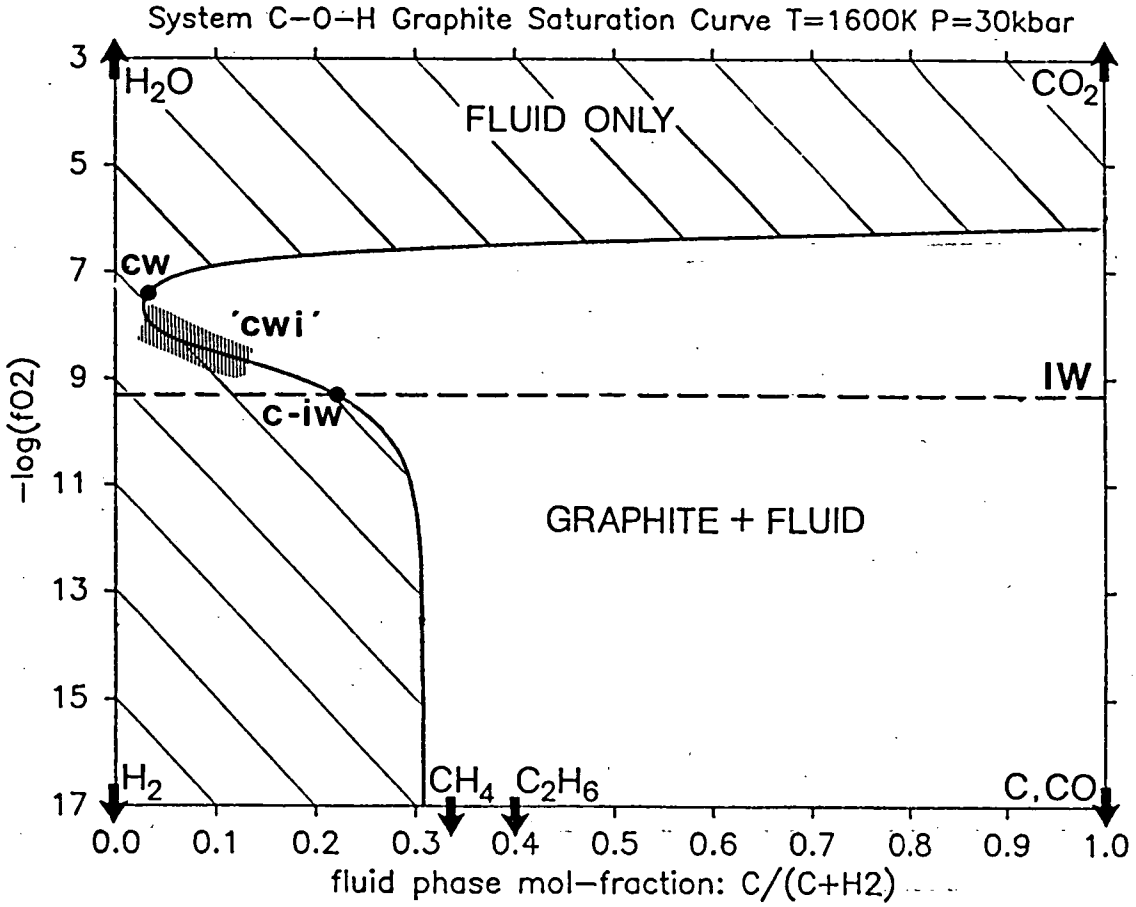

Figure 48

Variation in composition of C-O-H fluids with oxygen fugacity. Fluids in equilibrium with solid carbon lie on the carbon saturation surface. The region of interest for mantle oxidation states lies between IW and EMOD/EMOG. The labels CW, 'CWI' and C-IW denote fO_2 and composition of fluids in the techniques described in this paper.

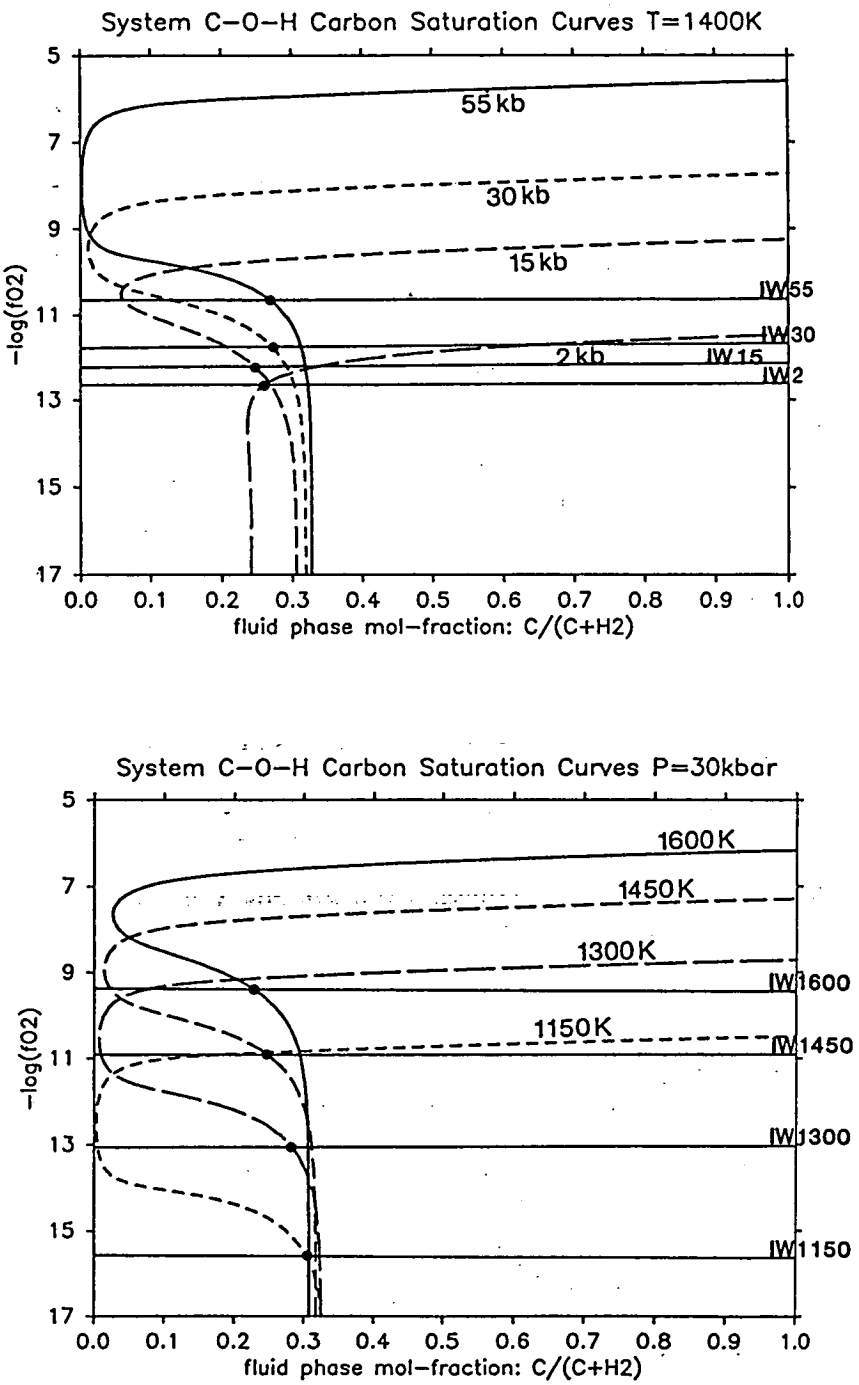

Figure 49

The effect of [a] pressure and [b] temperature on the position of the carbon saturation surface. Note that fluids are close to X_{H2O}-maximum over a wider range of fO_2 at higher pressures and lower temperatures.

fixed fluid composition, and lie at the reduced end of the spectrum of envisaged mantle oxidation states; and [b] CW experiments, which lack the invariant fluid composition and fixed fO_2, but lie between the fO_2 of IW and EMOD/EMOG, a region in which there is a lack of suitable metal-oxide solid-gas oxygen buffers. A capsule piercing technique was used to directly measure fluid compositions by mass spectrometry so that checks could be made on the attainment of equilibrium, the correspondence of calculated and experimental fluid compositions, and the fO_2 of CW experiments. The experiments did not behave as expected, but the results of the exploratory experiments described below permitted development of a dependable experimental technique for rock liquidus studies which was used in a study of olivine lamproite and leucite lamproite compositions described elsewhere [Part 5].

To summarise, three categories of experiments were attempted:
[1] **C-IW experiments without rock sample [fluid test experiments].** These permitted a check of fluid equilibration at C-IW and comparison with compositions calculated by Taylor [1986a]. Results were very close to calculations at 1050°C, but calculated fluid compositions give systematically higher CH_4/H_2O for higher temperatures (1200-1300°C).
[2] **C-IW experiments with rock sample.** These experiments proved unreliable as fluids consisted of H_2O in excess of CH_4 which is inconsistent with both calculations and the fluid test experiments. Fluid compositions were not reproducible in different runs at the same pressure and temperature. The inconsistencies are believed to arise from kinetic problems in attainment of equilibrium between the iron-wustite buffer and fluid in the presence of the rock sample.
[3] **'CWI' experiments with rock sample.** Fluid composition measurements indicate that the fO_2 of these experiments can be controlled within narrow limits at the lower end of the X_{H2O}-maximum where fluids consist of $H_2O >> CH_4 > CO_2$. Oxidation to the high fO_2 side of CW is prevented by the presence of an iron-wustite mixture.

A3.3.1 Experimental details

Experiments were performed in a 0.5 inch [1.27cm] piston-cylinder apparatus using techniques similar to those described by Green and Ringwood [1967b]. Temperatures were recorded by $Pt/Pt_{90}Rh_{10}$ thermocouples sited within 0.5mm of the sample capsule, and were controlled

automatically to within 6°C of the nominated temperature. No pressure correction on emf was applied. No deterioration of Pt thermocouples occurred at the temperatures required (<1300°C), so that experiments up to 30 hours duration were run at nearly constant current. Experiments were carried out using the "piston-in" technique, using assemblies consisting of either talc (run with -10% pressure correction; Green et al. 1966) or NaCl (no pressure correction).

A3.3.2 CAPSULE PIERCING TECHNIQUE FOR MASS SPECTROMETRIC FLUID ANALYSIS

The capsule piercing device used for fluid analysis is a modified Whitey (#SS-1VS6) regulating valve with its stem redesigned as a hardened needle tip. (figure 50). The capsule is inserted into a removable cradle with optional metal washers serving as additional confining rings for longer capsules (>9mm). The piercer was loaded into the oven of a PYE UNICAM 204 Gas Chromatograph connected to the ion-source of a VG-micromass 7070F double-focussing mass spectrometer. The loaded piercer was evacuated to 10^{-6} to 10^{-7} torr and heated to 150°C to eliminate adsorbed water from the metal surfaces (15-25 minutes). After the sample capsule was pierced, the piercer was returned to 150°C and mass spectra were acquired by multiple scans of ~2sec duration over the mass range 10-100. Methane and CO_2 were released quickly so that in methane-rich runs a needle valve was used to regulate flow into the mass spectrometer. Water was released only slowly, presumably due to absorption in the graphite inner capsules or internal metal surfaces, so that mass spectra had to be collected for 35-55 minutes until the H_2O level (gauged by the m/z 18 peak returned to the background levels obtained immediately before piercing (m/z 14>18; see figure 51).

Gas analyses were obtained by integrating over time for mass 17+18 for H_2O, 13+15+16 for CH_4, and 44 for CO_2. Other peaks in the spectra for these gases were not included due to [a] overlapping with other background gases (e.g. mass 14 in CH_4 and N_2), or [b] low levels close to threshold leading to discontinuous collection. These were corrected for by multiplying by standard factors after integration. Ionisation cross-section characteristics of the machine were corrected for by reference to standard gases (CO_2+CO+N_2; and CH_4+H_2O produced from pyrolysis of hexacosane, stearic acid and lignoceric acid). An approximate measure of CO could be obtained by subtraction on a single spectrum at the peak of CH_4

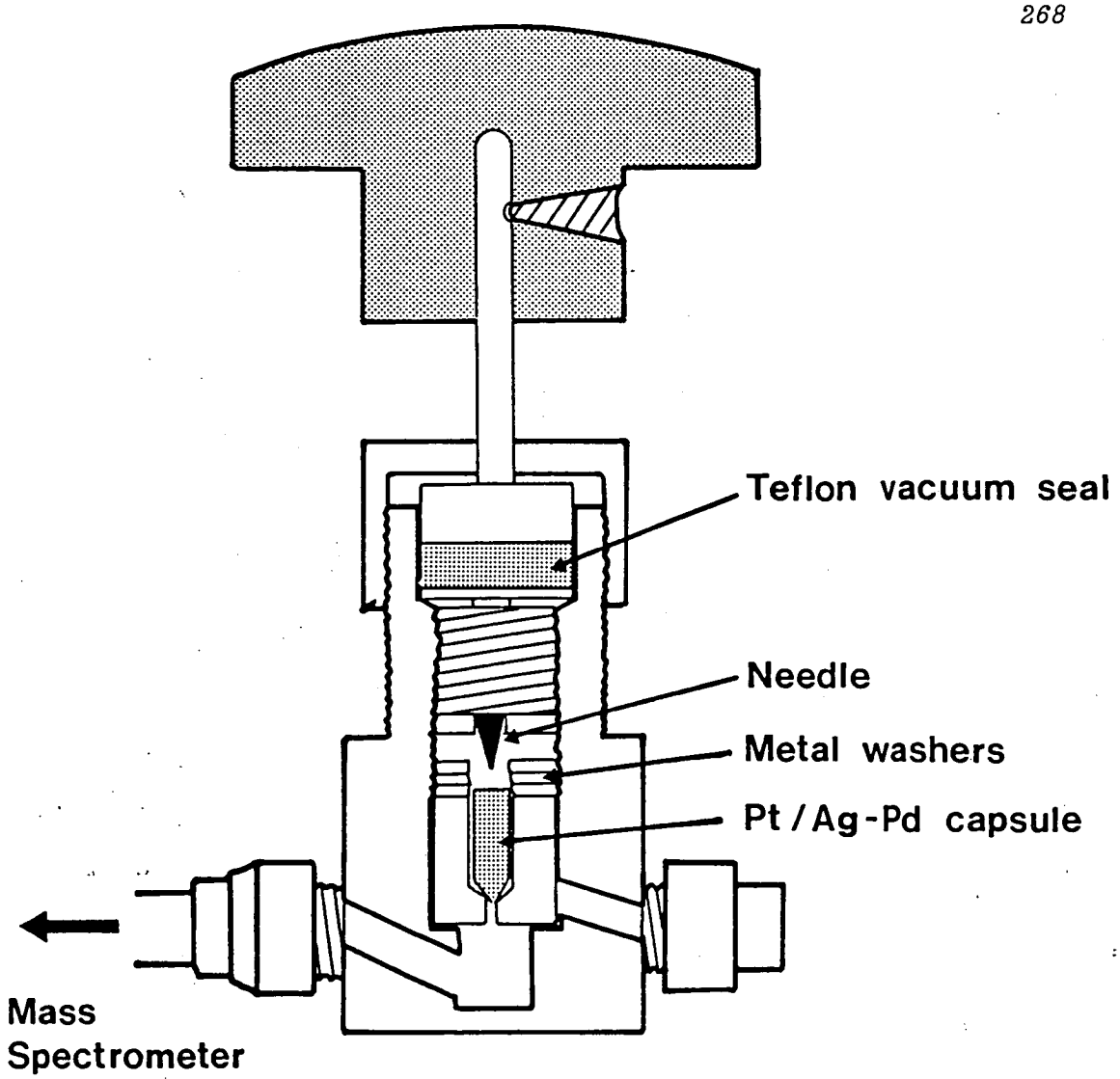

Figure 50

Diagram of the capsule piercing device used for mass spectrometric fluid analysis.

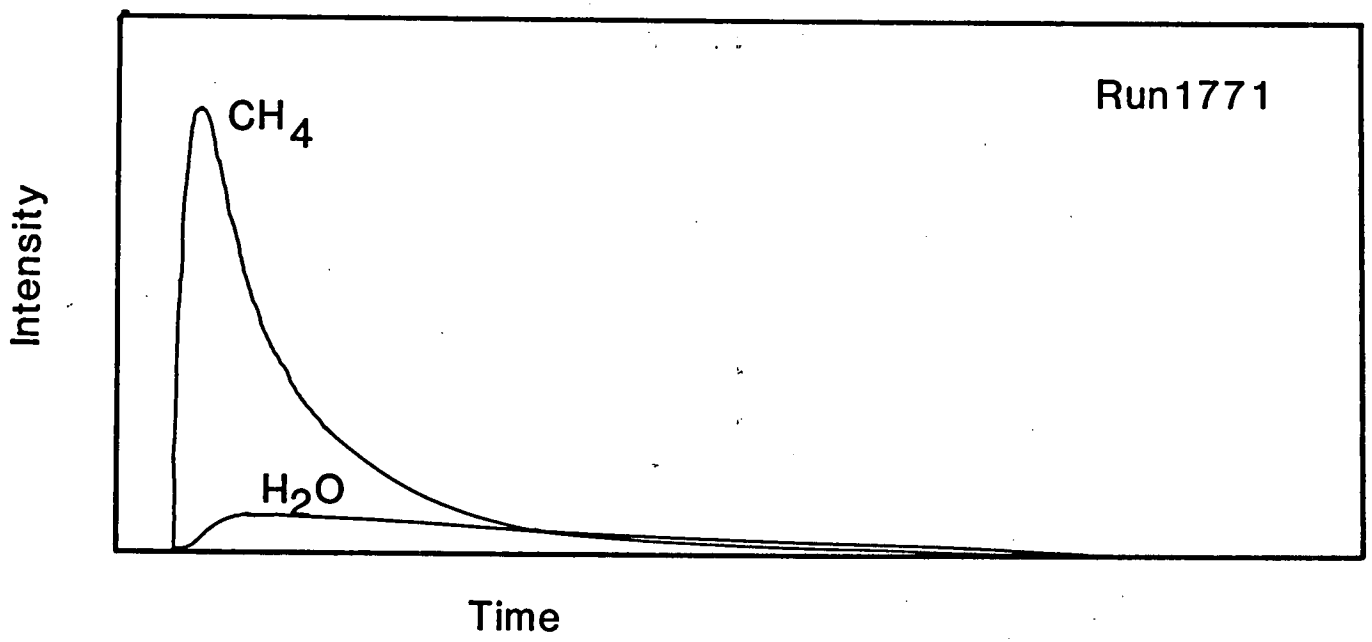

Figure 51

Mass spectra intensity vs. time traces for C-IW fluid test experiment 1771 at 20kbar/1200°C. Methane release is initially rapid whereas water release is gradual after heating to 150°C.

and CO_2 release assuming a constant 28/32 intensity in the background and correcting for CO^+ fragments derived from CO_2. Hydrogen spectra could not be collected by the data acquisition system used, but the presence of both H_2 and H^+ fragments was confirmed by oscillograph traces. Minor ethane (corrected from mass 27+29+30), the presence of which is predicted by the thermodynamic calculations, was seen in CH_4-rich experiments.

A3.3.3 C-IW FLUID TEST EXPERIMENTS

All experiments described in this paper used a sealed 3mm i.d. Pt or $Ag_{50}Pd_{50}$ capsule containing two inner graphite capsules of 2-2.3mm i.d. (figure 53). For C-IW fluid test experiments both buffer and sample capsules were filled with IW buffer (1:1 mix of Fe and FeO). The methane+water fluid was generated from a solid source mixture of Al_4C_3 and $Al(OH)_3$ by the rapid action of water on Al_4C_3 to produce methane [Wade and Bannister 1973]. Water is released by thermal decomposition of $Al(OH)_3$ in two steps at ~250°C and ~550°C [Kennedy 1959], thus lessening the risk of capsule rupture relative to fluid generation at a single P,T point. The overall reaction can be expressed by the equation

$$Al_4C_3 + 2\ Al(OH)_3 \quad \text{--->} \quad 3\ Al_2O_3 + 3\ CH_4 \ (+\ C_2H_6 + H_2) \qquad [1]$$

Generation of CH_4-rich fluids by this mechanism rather than by decomposition of more complex hydrocarbons has the advantages of [i] rapid equilibration to CH_4-rich fluids for experiments of short duration [Taylor 1985; Taylor and Green 1986b], and [ii] fluids with different CH_4/H_2O ratios can be generated by addition of the appropriate amount of excess $Al(OH)_3$, so that high pressure equilibrium CH_4/H_2O can be mimicked by generated fluids to achieve short equilibration times. For C-IW fluid tests, a mixture of Al_4C_3 + $Al(OH)_3$ which should produce a CH_4/H_2O ratio of 5 was used. All mixtures containing Al_4C_3 were stored under vacuum desiccation to prevent reaction with atmospheric moisture.

C-IW equilibrium should be achieved at high pressure and temperature by reaction of CH_4 and H_2O from the fluid source with graphite capsules and the IW buffer by the equilibrium

$$CH_4 + O_2 \quad \rightleftharpoons \quad 2\ H_2O + C \qquad [2]$$

Table 23 lists experimental details and CH_4/H_2O ratios measured by the capsule piercing technique. H_2 and C_2H_6 were detected in these fluid test experiments, but H_2O and CH_4 are the dominant species (>90mol%), so that the CH_4/H_2O ratio gives a simple and useful indication of fluid composition. C_2H_6 is present in much lower abundances than in the experiments of Taylor and Green [1986b] which were at fO_2 ~4 log units below IW.

Several experiments were conducted at 30 kbar and 1200°C with varying run duration (2 hr 15 min to 25 hr) to test the rate of equilibration, precision of the MS technique, and buffering capacity of the IW mixture. The measured CH_4/H_2O of 30kbar/1200°C experiments ranged from 2.2 to 3.1 and showed no systematic trend with time. This indicates that equilibrium can be reached with graphite capsules and IW buffer inside 2hr 15min, and that H_2-loss by diffusion out of the capsule is insufficient to exhaust the buffer after 25hr. IW buffers were checked after each run both optically and by XRD, and had frequently developed a ring of Fe metal, but had iron+wustite still present in each case. Although there are insufficient experiments for a meaningful statistical analysis of precision, the measurements fall within 0.5 of a 2.6 ratio for CH_4/H_2O.

The rest of the experiments listed in table 23 permit comparison of measured CH_4/H_2O with thermodynamically calculated values over a pressure-temperature range relevant to mantle-melting studies. The CH_4/H_2O measurements are superimposed in figure 52 on a P,T grid contoured in CH_4/H_2O predicted by the thermodynamic calculations of Taylor [1985; 1986a]. It can be seen that agreement at 1050°C is extremely good, whereas at higher temperatures the calculations predict systematically higher CH_4/H_2O than the measured values.

The experimental data confirm that CH_4/H_2O of the fluid is essentially a function of temperature, with pressure having negligible effect in the pressure-temperature range of interest. Run 1771 at 20kbar/1200°C (CH_4/H_2O=2.6) matches the average for the 30kbar/1200°C runs described above. Agreement between the 1050°C runs is good despite the different assemblies used. This confirms that H_2-loss from the capsules is not a problem at fO_2=IW even given the low external fH_2 of NaCl sleeves. Taylor and Green [1986b] used talc exclusively for their lower fO_2 runs in

Table 23 : Experimental run data for fluid test experiments at C-IW

Run	Pressure [kbar]	Temp. [°C]	Duration [hr]	Assembly	Vapour CH_4/H_2O
1768	30	1200	2.25	Talc	3.5
1756	30	1200	6.1	Talc	2.2
1764	30	1200	16	Talc	3
1767	30	1200	25	Talc	2.2
1777	20	1050	6.1	Talc	5.2
1725	20	1150	2	Talc	3.8
1771	20	1200	7.5	Talc	2.6
1772	30	1050	7	NaCl	5.5
1812	30	1300	6	Talc	1.8

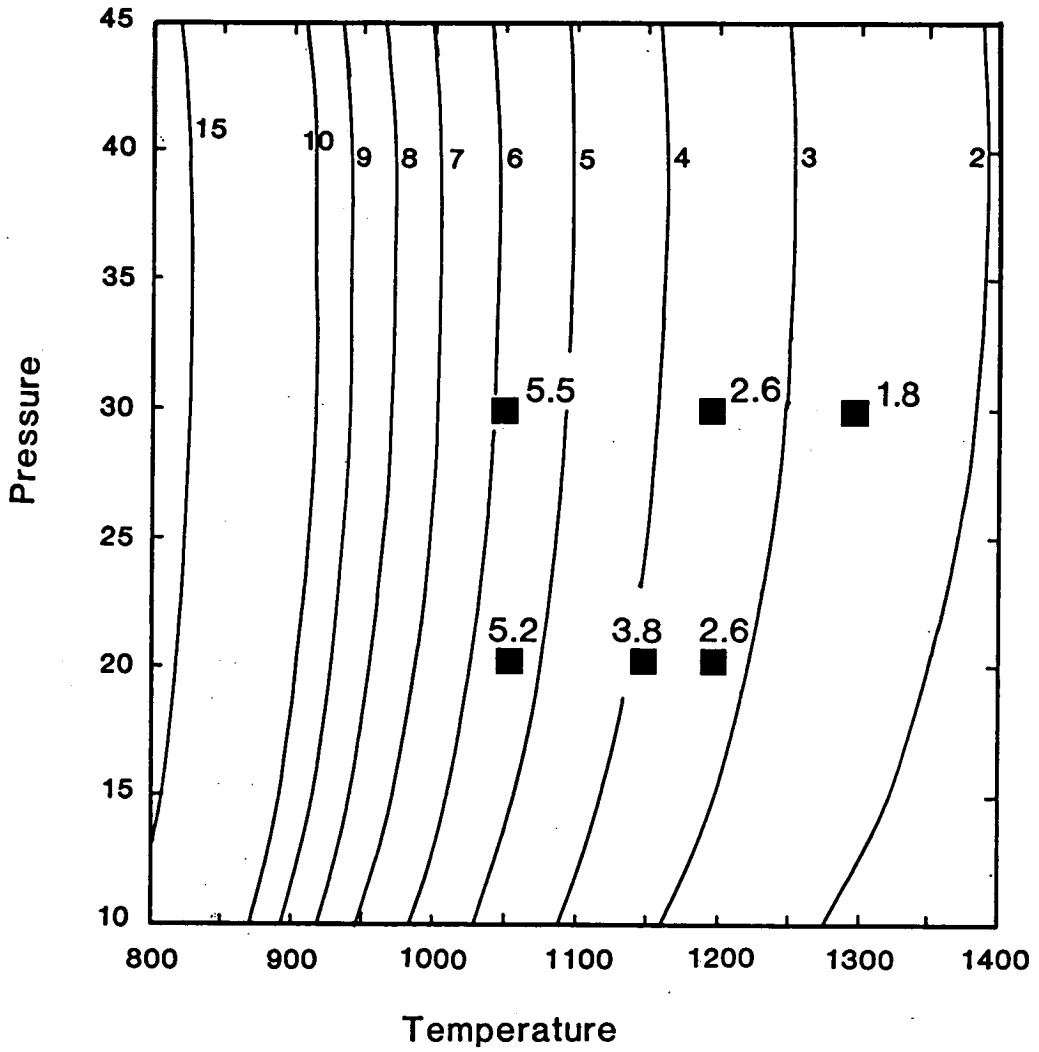

Figure 52

Comparison of C-IW fluid test CH_4/H_2O ratios measured by mass spectrometer (points) with thermodynamically calculated values of Taylor [1986a] (contoured).

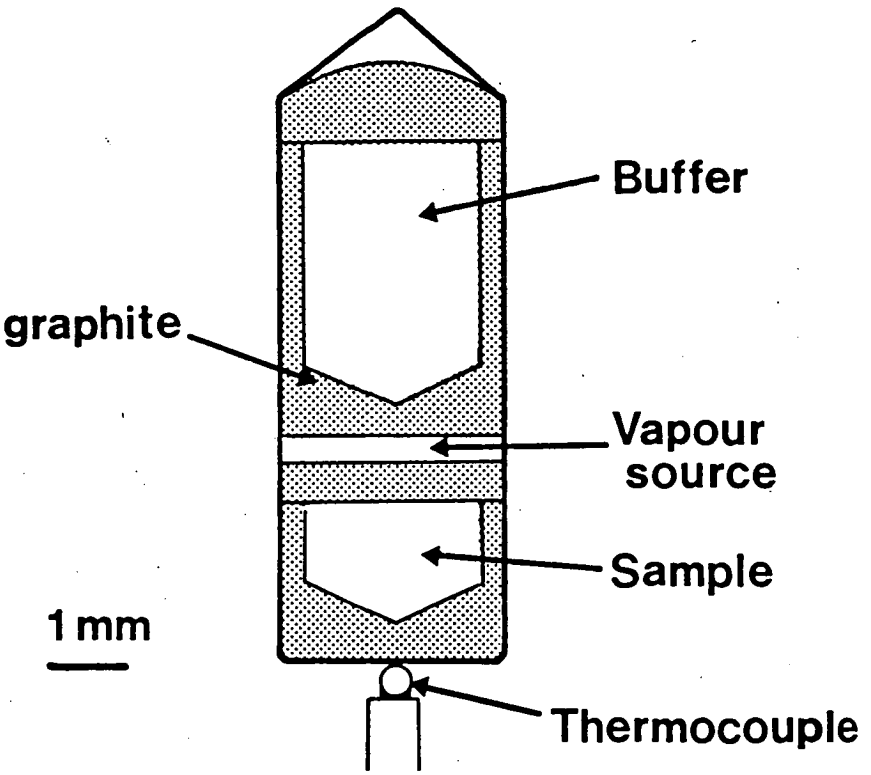

Figure 53

Capsule configuration used in most C-IW and 'CWI' experiments. The outer capsule is Pt or $Ag_{50}Pd_{50}$ alloy. Stipple denotes graphite.

which H_2 was a more prominent component of the fluid phase.

The results of these fluid tests have important implications for melt generation in the mantle at fO_2~IW, and these are discussed in the final section.

A3.3.4 C-IW EXPERIMENTS WITH SAMPLE

The rock sample added for these experiments was prepared from analytical grade oxides and carbonates, plus synthetic $Ca_2P_2O_7$, MgF_2 and Fe_2SiO_4. All iron was added as fayalite to avoid problems in attaining low oxygen fugacities caused by the presence of ferric iron in the sample. Components were mixed thoroughly in an agate mortar and sintered at 900°C prior to the addition of fayalite to avoid oxidation of FeO. The composition used in these experiments was a high MgO (~23wt%), low SiO_2 (~43wt%) olivine lamproite; full details of the composition are given by in Part 5. The capsule configuration depicted in figure 53 was used in these experiments, initially with the same 1:1 IW buffer and Al_4C_3 + $Al(OH)_3$ mixtures as in the C-IW fluid tests experiments.

Several attempts were made to achieve the equilibrium fluid compositions predicted by the thermodynamic calculations and characterised by the fluid tests, but these all proved unsuccessful. Measured CH_4/H_2O, using the same capsule piercing technique, was variable but usually around 0.2-0.5, i.e. with a very much lower CH_4 content than the fluid tests. Assuming the fluids lie on or near the graphite saturation surface, these CH_4/H_2O ratios indicate oxygen fugacity well above IW, but below CW. Examination of the IW buffers showed that they were <u>not</u> exhausted, but apparently lack the ability to buffer fluid compositions in this system. Charges contained abundant mica and a significant amount of glass, even at 1050°C. Melting in the presence of CH_4+H_2O fluids can be expected to be largely a function of X_{H2O}, since the solubility of methane in melts is low [Taylor and Green 1986a,b]. In an MgO-rich composition such as olivine lamproite in an anhydrous or low-H_2O environment, the degree of melting at 1050°C would be very small. Therefore, the presence of a significant amount of melt, together with the close agreement of calculations and C-IW fluid tests, indicates that the low CH_4/H_2O measurements are real, and not due to either analytical error in the capsule piercing technique or to buffering of fluid compositions to high X_{H2O} where the system as a whole

is less water-rich.

It is concluded that C-IW experiments on rock compositions, whilst theoretically more attractive in that fO_2 and fluid compositions should be fixed, are unreliable, and that this is probably due to kinetic interference by the sample in the attainment of equilibrium with the IW buffer. Calculations discounted the possibility of increased fO_2 due to excess O_2 from [i] trapped O_2 in the sample, [ii] assumed oxidation of FeO in the sample, and [iii] H_2-loss by diffusion out of the capsule.

Further experiments with variation in Fe/FeO of the buffer, the amount of IW buffer (up to 55mg compared to 6-8mg sample), $Al_4C_3/Al(OH)_3$ of the fluid source, run duration (up to 30hr), and the P,T-path followed during heating and compression to run conditions, were performed in an attempt to isolate the cause of the disagreement between sample-present and sample-absent runs. The runs with larger buffer capacity had buffer present in excess of that which would be required to completely reduce the fluid and sample, further indicating that the lack of equilibration was due to buffer kinetics rather than capacity.

It is considered likely that some decomposition of the Al_4C_3 had occurred by reaction with atmospheric moisture prior to the experiments, although products of decomposition did not register on XRD. The initial fluid produced may therefore have had a much lower CH_4/H_2O than the intended ratio of five. In this case, the initial presence of large amounts of H_2O may have caused melting of the sample and dissolution of much larger amounts of H_2O than at the C-IW equilibrium conditions. This presents the possibility that fluid-liquid equilibrium interferes in C-O-H fluid equilibrium by buffering the concentration of a fluid component at a rate-limiting step. This explanation is necessarily conjectural, since no data are available on the kinetics or mechanisms at such high pressures. However, experiments at 850-900°C and 10-20kbar of 20hr duration produced similar low CH_4/H_2O fluids. Under these conditions the fluid composition should be extremely methane-rich (see figure 52) and the sample should be subsolidus, so that fluid-liquid interaction slowing the attainment of equilibrium can be discounted unless the lack of equilibrium at 850-900°C is simply due to the effect of temperature. C-IW fluid tests equilibrated at 1050°C in less than 6 hours, but reactions may slow drastically between 1050°C and 900°C.

The main reason for choosing the carbide source for methane generation was the need for rapid equilibration for runs of short duration (20 minutes and less) without graphite inner capsules [Taylor 1985; Taylor and Green 1986b]. Given the requirement in the present experiments for equilibration of the fluid with graphite capsules, this kinetic consideration may be unnecessary, and long-chain aliphatic hydrocarbons may be more reliable sources. The possibility cannot be ruled out that the equilibration problem of C-IW + sample experiments is specific to formation of CH_4 from H_2O-rich fluids, and that if CH_4/H_2O is initially higher than equilibrium values, then equilibrium may be achieved. However, we consider it more likely that the iron-wustite buffer is unable to buffer fluid compositions in the system described. Consequently, attempts to control experiments with reduced fluids must look to either another fO_2 buffer, or to monitoring fluid compositions which are only approximately controlled in fO_2. The latter option was chosen in this study by way of graphite-water [CW] experiments.

A3.3.5 'CWI' EXPERIMENTS WITH SAMPLE

The 'CWI' technique described here was used for a liquidus study of olivine lamproite and leucite lamproite compositions [Part 5] and found to be dependable.

The X_{H2O}-maximum in fluids on the carbon saturation surface (CW) has the advantage of lying in the fO_2 region of interest for a reduced mantle, in which there is a lack of suitable metal-metal oxide solid-gas oxygen buffers for the control of fO_2 in experiments. Measurements of fluid composition by the capsule piercing technique enable monitoring of the fO_2 of each experiment.

The first experiments attempting to fix fO_2 at CW used only one graphite inner capsule containing ~18mg sample with 12.5wt% H_2O added as distilled water to the sample capsule by microsyringe. A carbide-hydroxide source was added below the sample capsule to produce a 1:1 CH_4/H_2O fluid to ensure that CW was approached from the low fO_2 side. However, results of these experiments with both olivine lamproite and leucite lamproite produced CO_2-rich fluids with no CH_4, indicating oxidation beyond fO_2=CW. The experiment with leucite lamproite (containing >11wt% K_2O) had CO_2/H_2O

=6, and yet contained mica in the sample. This is interpreted to indicate buffering of the fluid phase composition by minerals in the sample in an analogous manner to CO_2-rich fluids in equilibrium with amphibole-peridotite [Wyllie 1977; Eggler 1978; Olafsson and Eggler 1983]. Two methods were considered to overcome this; [i] increasing the amount of H_2O added to the sample to increase the buffering capacity at CW, and [ii] including the IW buffer capsule to prevent oxidation to CO_2-rich compositions. The latter was preferred, since adding excessive amounts of H_2O at high pressures and temperatures would result in high levels of solution of sample components in the fluid, effectively changing the composition of the experimental charge.

The second option was found to give satisfactory results and bracketed fO_2 between narrow limits, giving fluid compositions of H_2O(>80mol%) >> CH_4 > CO_2 at high pressures. The caspule configuration was that of figure 53, and 12.5wt% H_2O was added to the sample capsule to ensure high X_{H2O} was achieved. The IW buffer did not control fO_2 at IW as described above, but did hold fO_2 to the lower side of the X_{H2O}-maximum, hence the notation 'CWI' (carbon-water-iron). Fluid compositions therefore lie in the region where the carbon saturation surface turns from the X_{H2O}-maximum towards more methane-rich compositions (i.e. higher $C/(C+H_2)$). Figure 54 gives an indication of the fO_2 range of these experiments with pressure: the uncertainty in fO_2 is less at higher pressures where there is a more rapid change in CH_4/H_2O with fO_2. Under these conditions, the X_{H2O}-maximum is wider, which explains the widening of the gap between experimental fO_2 range and CW with increasing pressure in figure 54, because the CW curve represents the middle of the wider X_{H2O}-maximum (see figure 49a).

Figure 55 illustrates a typical result from capsule piercing of an lamproite run at 'CWI' (run 1921: 15kbar/1125°C). Water is released more gradually than methane after piercing as the system is reheated to 150°C to drive water out of the graphite capsules. The spectra in figures 55b and 55c are from the peaks of CH_4 and H_2O release respectively. At the peak of CH_4 release, water release has hardly begun as can be guaged by reference to the background mass 28 (N_2) and 32 (O_2) peaks, which remain roughly constant. C_2H_6 (mass 25-30) and CO_2 (mass 44) are barely above threshold in this example.

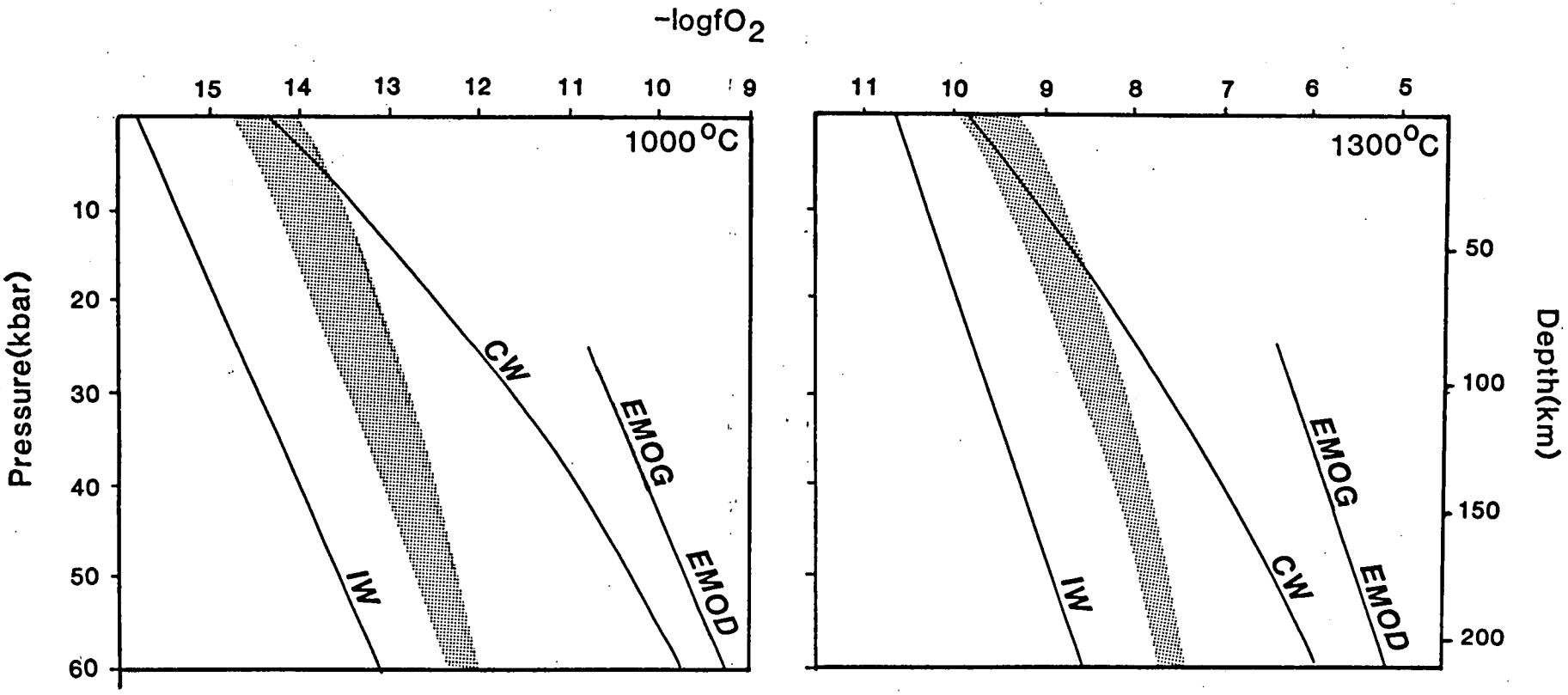

Figure 54

Pressure vs. fO_2 plot showing the approximate fO_2 range of 'CWI' experiments (shaded) relative to common reference buffers. The line marked CW is the X_{H2O}-maximum on the graphite saturation surface.

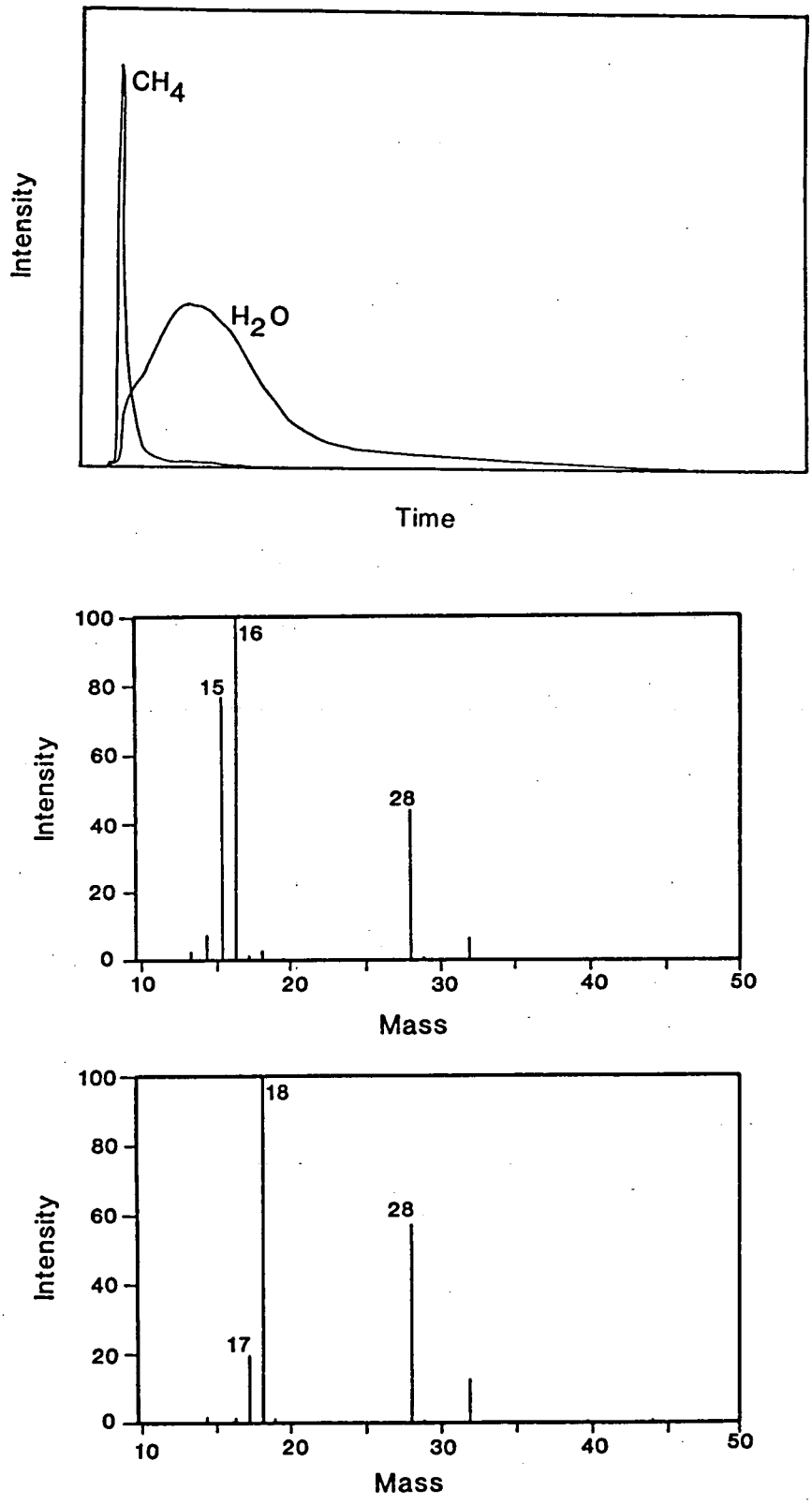

Figure 55

Intensity vs. time trace [a] and mass spectra at the peaks of CH_4 [b] and H_2O [c] release for a typical 'CWI' experiment with leucite lamproite sample (15kbar/1125°C). Note very low values close to threshold for ethane and CO_2.

Experiments occasionally contained higher CH_4/H_2O fluids, or had $CO_2>CH_4$ (with >80 mol%H_2O) showing that the preferred fluid composition of $H_2O>>CH_4>CO_2$ cannot be assumed, and that monitoring of fluid composition by capsule piercing is necessary. Repetitions of these experiments generally produced the desired $CH_4>CO_2$ fluid at the first attempt.

A3.4 IMPLICATIONS OF THE C-IW FLUID TESTS FOR MELTING IN THE MANTLE

The results of the C-IW fluid test experiments have important implications for melting of mantle material at fO_2~IW. The solubility of CH_4 in silicate melts, and therefore the depression of the liquidus temperature due to CH_4, is low [Taylor and Green 1986b], meaning that melting in the presence of CH_4+H_2O fluid mixtures is essentially a function of X_{H2O}. The thermodynamic calculations of Taylor [1985,1986b] predict that contours of X_{H2O} and CH_4/H_2O in the fluid will be strongly temperature dependent, with pressure important only below 10kbar. The results of the fluid test experiments, superimposed on the calculated values in figure 52, show that the CH_4/H_2O contours are even more closely spaced than the calculations predict at temperatures above 1050°C. Since increased H_2O-content and temperature both promote melting, the degree of melting in reduced, carbon-saturated systems will increase much more rapidly over a short temperature interval than seen in experimental studies with only a single volatile species. The effect of temperature on degree of melting or crystallinity will probably be greater in the region 1000-1250°C than at higher temperatures, as the calculations predict closer spacing of CH_4/H_2O contours at lower temperatures. Therefore, changes in temperature may be more important to the crystallisation of melts escaping from the mantle source than in the melting interval of peridotite: an experiment on olivine lamproite with high CH_4/H_2O, and thus fO_2~IW [Part 5] has five phases plus liquid and a high degree of crystallisation at 30kbar/1200°C, implying that the peridotite solidus lies above 1300°C. However, any melts produced at 1200-1300°C, presumably at lower pressures and having lower MgO and higher SiO_2 compositions than olivine lamproite, will be much more likely to freeze or experience significant crystal fractionation if fO_2 remains at IW, than melts at higher fO_2 where changes in CH_4/H_2O with temperature are less important. A rise in fO_2 from C-IW during ascent of melts or fluids will promote melting at higher levels; these processes are considered by Taylor and Green [1986a] and Green et al. [1986].

REFERENCES

ALLMANN R [1971] Fluorine. In: [ed. KH Wedepohl] Handbook of Geochemistry Section 9A, 6pp

ALLSOPP HL, NICHOLAYSEN LO, HAHN-WEINHEIMER P [1969] Rb/K ratios and Sr-isotopic compositions of minerals in eclogitic and peridotitic rocks. Earth Planet Sci Lett 5:231-244

AMENDOLAGINE M, DELL'ANNA L, MATTIAS P [1962] Lave dell'apparato vicano: zona orientale-Soriano-Canepina-Vignanello-Fabrica. Periodico Miner (Rome) 32: 197-249

ANGELUCCI A, BROTZU P, CIVITELLI G, MORBIDELLI L, TRAVERSA G [1974] Il vulcanismo pleistocenico della Media Valle Latina (Lazio). Caratteristiche petrografiche e geologiche dei principali affioramenti lavici. Geol Romana 13:83-123

AOKI K, ISHIKAWA K, KANISAWA S [1981] Fluorine geochemistry of basaltic rocks from continental and oceanic regions and petrogenetic application. Contrib Mineral Petrol 76:53-59

APPLETON JD [1970] The petrology of the potassium-rich lavas of the Roccamonfina volcano, Italy. PhD thesis, Edinburgh University

APPLETON JD [1972] Petrogenesis of potassium-rich lavas from the Roccamonfina volcano, Roman region, Italy. J Petrol 13:425-456

ARCULUS RJ [1985] Oxidation status of the mantle: past and present. Ann Rev Earth Planet Sci 13:75-95

ARCULUS RJ, DELANO JW [1981] Intrinsic oxygen fugacity measurements: techniques and results for spinels from upper mantle peridotites and megacryst assemblages. Geochim Cosmochim Acta 45:899-913

ARCULUS RJ, DAWSON JB, MITCHELL RH, GUST DA, HOLMES RD [1984] Oxidation states of the upper mantle recorded by megacryst ilmenite in kimberlite and type A and B spinel lherzolites. Contrib Mineral Petrol 85:85-94

AREVALO PC, BURRI C, WEIBEL M [1962] Zur Petrochemie des Roccamonfina-Vulkans (Prov. Caserta, Italien) Schweiz Min Pet Mitt 42: 237-268

ARIMA M, EDGAR AD [1980] Stability of wadeite ($Zr_2K_4Si_6O_{18}$) under upper mantle conditions: petrological implications. Contrib Mineral Petrol 72:191-195

ARIMA M, EDGAR AD [1981] Substitution mechanisms and solubility of titanium in phlogopites from rocks of probable mantle origin. Contrib Mineral Petrol 77:288-295

ARIMA M, EDGAR AD [1983a] High pressure experimental studies on a katungite and their bearing on the genesis of some potassium-rich magmas of the west branch of the African Rift. J Petrol 24:166-187

ARIMA M, EDGAR AD [1983b] A high pressure experimental study on a

magnesian-rich leucite lamproite from the West Kimberley area, Australia: petrogenetic implications. Contrib Mineral Petrol 84:228-234

ATKINSON WJ, HUGHES FE, SMITH CB [1984] A review of the kimberlitic rocks of western Australia. In: J.Kornprobst (editor), Kimberlites I: Kimberlites and related rocks. p195-224 Elsevier

BACHINSKI SW, SIMPSON EL [1984] Ti-phlogopites of the Shaw's Cove minette: a comparison with micas of other lamprophyres, potassic rocks, kimberlites and mantle xenoliths. Am Mineral 69:41-56

BAILEY DK [1970] Volatile flux, heat-focussing and the generation of magma. In: G.Newall and N.Rast (editors), Mechanisms of Igneous intrusion p 177-186. Geol Soc London Special Publication

BAILEY DK [1974] Continental rifting and alkaline magmatism. In: H.Sorensen (editor), The alkaline rocks. p148-159 Wiley.

BAILEY DK [1978] Continental rifting and mantle degassing. In: [ed ER Neumann & IB Ramberg] Petrology and Geochemistry of continental rifts, p.1-13. D Riedel.

BAILEY DK [1980] Volcanism, Earth degassing and replenished lithosphere mantle. Phil Trans Roy Soc London A 297:309-322

BAILEY DK [1984] Kimberlite: "The mantle sample" formed by ultrametasomatism. In: J.Kornprobst (editor), Kimberlites I: Kimberlites and related rocks. p323-333 Elsevier

BAILEY JC [1977] Fluorine in granitic rocks and melts: a review. Chem Geol 19:1-42

BAKER PE, GASS IG, HARRIS PG, LE MAITRE RW [1964] The volcanological report of the Royal Society expedition to Tristan da Cunha. Phil Trans Roy Soc London A 256: 439-578

BARBERI F, INNOCENTI F [1967] Le rocce selagitiche di Orciatico e Monticatini in Val di Cecina. Atti Soc Toscana Sc Nat Serie A 74:139-186

BARTH TFW, RAMBERG I [1966] The Fen circular complex. In: O.F.Tuttle and J.Gittins (editors), Carbonatites. p 225-257 Interscience

BARTON M [1979] A comparative study of some minerals occurring in the potassium-rich alkaline rocks of the Leucite Hills, Wyoming, the Vico volcano, western Italy, and the Toro Ankole region, Uganda. Neues Jb Min Abh 137:113-134

BARTON M, HAMILTON DL [1978] Water saturated melting relations to 5kb of three leucite lavas. Contrib Mineral Petrol 66:41-49

BARTON M, HAMILTON DL [1979] The melting relationships of a madupite from the Leucite Hills, Wyoming, to 30 kb. Contrib Mineral Petrol 69:133-142

BARTON M, HAMILTON DL [1982] Water-undersaturated melting experiments bearing upon the origin of potassium-rich magmas. Mineral Mag 45:267-278

BARTON M, VAN BERGEN MJ [1981] Green clinopyroxenes and associated phases in a potassium-rich lava from the Leucite Hills, Wyoming. Contrib Mineral Petrol 77:101-114

BARTON M, VAREKAMP JC, VAN BERGEN MJ [1982] Complex zoning of clinopyroxenes in the lavas of Vulsini, Latium, Italy: evidence for magma mixing. J Volc Geotherm Res 14:361-388

BELKIN HE, DE VIVO B, ROEDDER E, CORTINI M [1985] Fluid inclusion geobarometry from ejected Mt. Somma-Vesuvius nodules. Amer Mineral 70: 288-303

BELL K, POWELL JD [1969] Strontium isotopic studies of alkalic rocks: the potassium-rich lavas of the Birunga and Toro-Ankole regions, east and central equatorial Africa. J Petrol 10:536-572

BELLON H, LEPVRIER C, MAGNE J, RAYMOND D [1975] L'activité eruptive dans l'Algerois: nouvelles données géochronologiques. Rev Geol Medit- Annales Univ Provence 4:291-299

BERGMAN SC [1986] Lamproites and other potassium-rich igneous rocks: a review of their occurrence, mineralogy and geochemistry. Geol Soc London Special Paper [in press]

BESANG C, ECKHARDT FJ, HARRE W, KREUZER H, MULLER P [1977] Radiometrische alterbestimmungen an neogenen Eruptivgesteinen der Turkei. Geol Jahrb, Riehe B 25:3-36

BEST MJ, HENAGE LF, ADAMS JAS [1968] Mica peridotite, wyomingite, and associated potassic igneous rocks in northeastern Utah. Am Mineral 53:1041-1048

BOCTOR NZ, MEYER HOA [1979] Oxide and sulfide minerals in kimberlite from Green Mountain, Colorado. In: F.R.Boyd and H.O.A.Meyer (editors), Kimberlites, diatremes and diamonds: their petrology, mineralogy and geochemistry. p.217-228. American Geophysical Union.

BOHLEN SR, PEACOR DR, ESSENE EJ [1980] Crystal chemistry of a metamorphic biotite and its significance in water barometry. Am Mineral 65:55-62

BOLIVAR SL, BROOKINS DG [1979] Geophysical and Rb-Sr study of the Prairie Creek, AK kimberlite. In: F.R.Boyd and H.O.A.Meyer (editors), Kimberlites, diatremes and diamonds: their geology, petrology and geochemistry. p289-299. American Geophysical Union.

BORLEY GD [1967] Potassium-rich volcanic rocks from southern Spain. Mineral Mag 36:364-379

BOTTINGA Y, WEILL DF, RICHET P [1981] Thermodynamic modeling of silicate melts. In: [RC Newton, A Navrotsky, BJ Wood eds] Thermodynamics of minerals and melts: Adv Phys Geochem 1:207-245.

BREY GP [1978] Origin of olivine melilitites - chemical and experimental constraints. J Volcanol Geotherm Res 3:61-88

BREY G, GREEN DH [1975] The role of CO_2 in the genesis of olivine melilitite. Contrib Mineral Petrol 49:93-103

BREY GP, GREEN DH [1976] Solubility of CO_2 in olivine melilitite at high pressures and role of CO_2 in the earth's upper mantle. Contrib Mineral Petrol 55:217-230

BREY GP, GREEN DH [1977] Systematic study of liquidus phase relations in olivine melilitite + H_2O + CO_2 at high pressures and petrogenesis of an olivine melilitite magma. Contrib Mineral Petrol 61:141-162

BROOKS CK, FAWCETT JJ, GITTINS J [1976] Caledonian magmatic activity in south-eastern Greenland. Nature 260:694-696

BROOKS CK, FAWCETT JJ, GITTINS J, RUCKLIDGE JC [1981] The Batbjerg complex, east Greenland: a unique ultrapotassic Caledonian intrusion. Can J Earth Sci 18:274-285

BUERGER MJ [1948] The structural nature of the mineraliser action of fluorine and hydroxyl. Am Mineral 33:744-746

BUIE BF [1941] Igneous rocks of the Highwood Mountains, Montana. Part III. Dikes and related intrusives. Geol Soc Am Bull 52:1753-1808

BURGESS CH [1941] Igneous rocks of the Highwood Mountains, Montana. Part IV. The stocks. Geol Soc Am Bull 52:1809-1828

BURKE K [1963] Dissolved gases in East African Lakes. Nature 198:568-569

BURNHAM CW [1975] Water and magmas: a mixing model. Geochim Cosmochim Acta 39:1077-1084

BURNHAM CW [1979a] The importance of volatile constituents. In: [HS Yoder, ed] The Evolution of the Igneous Rocks: Fiftieth Anniversary perspectives. pp 439-482. Princeton.

BURNHAM CW [1979b] Magmas and hydrothermal fluids. In: [ed. HL Barnes] Geochemistry of hydrothermal ore deposits. pp71-136 Wiley.

CARMICHAEL ISE [1967] The mineralogy and petrology of the volcanic rocks from the Leucite Hills, Wyoming. Contrib Mineral Petrol 15:24-66

CARMICHAEL ISE, NICHOLLS JW [1967] Iron-titanium oxides and oxygen fugacities in volcanic rocks. J Geophys Res 72:4665-4687

CARMICHAEL ISE, TURNER FJ, VERHOOGEN J [1974] Igneous Petrology. McGraw-Hill

CARSTENS H [1962] A post-Caledonian ultrabasic biotite lamprophyre dyke of the Isnad Ytteroy in the Trondheimsfjord. Norsk Geol Unders 215:10-21

CARTER JL [1970] Mineralogy and chemistry of the Earth's upper mantle based on the partial fusion-partial crystallisation model. Bull Geol Soc America 81:2021-2034

CHADWICK RA [1970] Belts of eruptive centers in the Absaroka - Gallutin

volcanic province, Wyoming - Montana. Geol Soc Am Bull 81:267-274

CHAO TSUNG-PU [1960] Petrochemical study of the Cenozoic basaltic rocks in Eastern China (Pts 1 & 2) Int Geol Rev 2: 196-217 & 2:273-297

CIVETTA L, ORSI G, SCANDONE P [1978] Eastwards migration of the Tuscan anatectic magmatism due to anticlockwise rotation of the Apennines. Nature 276:604

CIVETTA L, INNOCENTI F, MANETTI P, PECCERILLO A, POLI G [1981] Geochemical characteristics of potassic volcanics from Mts Ernici (Southern Latium, Italy). Contrib Mineral Petrol 78:37-47

COLLERSON KD, McCULLOCH MT [1983] Nd and Sr isotope geochemistry of leucite-bearing lavas from Gaussberg, East Antarctica. In: R.L.Oliver, P.R.James and J.B.Jago (editors), Antarctic Earth Science p.676-680

COLLINS WJ, BEAMS SD, WHITE AJR, CHAPPELL BW [1982] Nature and origin of A-type granites with particular reference to southeastern Australia. Contrib Mineral Petrol 80:189-200

COMBE AD, HOLMES A [1945] The kalsilite-bearing lavas of Kabirenge and Lyakauli, South-West Uganda. Trans Roy Soc Edin 61:359-379

COPI M [1978] Introduction to logic. MacMillan, New York.

CORTINI M, HERMES OD [1981] Sr isotope evidence for a multi-source origin of the potassic magmas in the Neapolitan area (S.Italy). Contrib Mineral Petrol 77:47-55

COSGROVE ME [1972] The geochemistry of the potassium-rich Permian volcanic rocks of Devonshire, England. Contrib Mineral Petrol 36:155-170

COX KG, HAWKESWORTH CJ, O'NIONS RK, APPLETON JD [1976] Isotopic evidence for the derivation of some Roman region volcanics from anomalously enriched mantle. Contrib Mineral Petrol 56:173-180

CROSS W [1897] Igneous rocks of the Leucite Hills and Pilot Butte, Wyoming. Am J Sci 14:115-141

CULLERS RL, RAMAKRISHNAN S, BERENDSEN P, GRIFFIN T [1985] Geochemistry and petrogenesis of lamproites, late Cretaceous age, Woodson County, Kansas, U.S.A. Geochim Cosmochim Acta 49:1383-1402

CUNDARI A [1973] Petrology of the leucite-bearing lavas in New South Wales. J Geol Soc Aus 20:465-492

CUNDARI A [1979] Petrogenesis of the leucite-bearing lavas in the Roman volcanic region, Italy. The Sabatini Lavas. Contrib Mineral Petrol 70:9-21

CUNDARI A [1980] Role of subduction in the genesis of leucite-bearing rocks: facts or fashion? Contrib Mineral Petrol 73:432-434

CUNDARI A [1982] Petrology of clinopyroxenite ejecta from Somma-Vesuvius and their genetic implications. Tschermaks Min Petr Mitt 30:17-35

CUNDARI A, FERGUSON AK [1982] Significance of the pyroxene chemistry from leucite-bearing and related assemblages. Tschermaks Min Petr Mitt 30:189-204

CUNDARI A, LE MAITRE RW [1970] On the petrogeny of leucite-bearing rocks of the Roman and Birunga volcanic regions. J Petrol 11:33-47

CUNDARI A, MATTIAS PP [1974] Evolution of the Vico lavas, Roman volcanic region, Italy. Bull Volc 38:98-114

CUNDARI A, RENARD JGR, GLEADOW AJW [1978] Uranium - potassium relationship and apatite fission-track ages for a differentiated leucitite suite from New South Wales. Chem Geol 22:11-20

DAL PIAZ GV, VENTURELLI G, SCOLARI A [1979] Calc-alkaline to ultrapotassic postcollisional volcanic activity in the internal northwestern Alps. Mem Sci Geol 32:1-16

DALY RA [1912] Geology of the North American Corillera at the forty-ninth parallel. Geol Surv Canada Mem 38 Pt 1, 546pp

DAWSON JB [1971] Advances in kimberlite geology. Earth Sci Rev 7:187-214

DAWSON JB [1972] Kimberlites and their relation to the mantle. Phil Trans Roy Soc London, Series A 271:297-311

DAWSON JB [1980] Kimberlites and their xenoliths. Springer-Verlag, 250pp.

DAWSON JB, HAWTHORNE JB [1973] Magmatic sedimentation and carbonatitic differentiation in kimberlite sills at Benfontein, South Africa. J Geol Soc London 129:61-85

DAWSON JB, POWELL DG [1969] Mica in the upper mantle. Contrib Mineral Petrol 22:233-237

DE JONG BHWS, BROWN GE [1980] Polymerisation of silicate and aluminate tetrahedra in glasses, melts, and aqueous solutions - I. Electronic structure of $H_6Si_2O_7$, $H_6SiAlO_7^-$, and $H_6Al_2O_7^{2-}$. Geochim Cosmochim Acta 44:491-511

DE MARCO L [1958] Su alcuni filoni radioattivi del complesso Sesia-Lanzo. Studi i Ric Div Geomineraina I, 30pp.

DENAEYER M, SCHELLINCK F, COPPEZ A [1965] Recueil d'analyses des laves du Fossé tectonique de l'Afrique centrale. Mus Roy Afr Centr 49:234pp Tervuren.

DESIO A [1979] Geologic evolution of the Karakorum. In: A.Farah and K.A. de Jong (editors), Geodynamics of Pakistan p.111-124 Geol Survey Pakistan.

DICKENSON MP, HESS PC [1981] Redox equilibria and the structural role of iron in alumino-silicate melts. Contrib Mineral Petrol 78:352-357

DINGWELL DB, MYSEN BO [1985] The effect of water and fluorine on the viscosity of albite melt at high pressure: a preliminary investigation.

Earth Planet Sci Lett 74:266-274

DINGWELL DB, SCARFE CM, CRONIN DJ [1985] The effect of fluorine on viscosities in the system Na_2O-Al_2O_3-SiO_2: implications for phonolites, trachytes and rhyolites. Am Mineral 70:80-87

DODGE FCW, MOORE JG [1981] Late Cenozoic volcanic rocks of the southern Sierra Nevada, California: II Geochemistry. Bull Geol Soc Am 92:1670-1761

DOIG R [1970] An alkaline province linking Europe and North America. Can J Earth Sci 7:22-28

DUBEAU MI, EDGAR AD [1985] Priderite stability in the system $K_2MgTi_7O_{16}$ - $BaMgTi_7O_{16}$. Mineral Mag 49:603-606

DUDA A, SCHMINCKE HU [1978] Petrology and chemistry of potassic rocks from the Laacher See area. Neues Jb Min Abh 132:1-33

DUPREE E, PETTIFER RF [1984] Determination of the Si-O-Si bond angle distribution in vitreous silica by magic angle spinning NMR. Nature 308: 523-525

EBY GN [1984] Geochronology of the Monteregian Hills alkaline igneous province, Quebec. Geology 12:468-470

EDGAR AD, ARIMA M [1981] Geochemistry of three potassium-rich ultrabasic lavas from the west branch of the African rift: inferences on their geneses. Neues Jb Miner Mh 12:539-552

EDGAR AD, GREEN DH, HIBBERSON WO [1976] Experimental petrology of a highly potassic magma. J Petrol 17:339-356

EDGAR AD, CONDLIFFE E, BARNETT RL, SHIRRAN RJ [1980] An experimental study of an olivine ugandite magma and mechanisms for the formation of its K-enriched derivatives. J Petrol 21:475-497

EGGLER DH (1974) Effect of CO_2 on the melting of peridotite. Carn Inst Wash Yb 73:215-224

EGGLER DH [1978] The effect of CO_2 upon melting in the system Na_2O - CaO - Al_2O_3 - SiO_2 - CO_2 to 35 kb, with an analysis of melting in a peridotite - H_2O - CO_2 system. Am J Science 278:305-343

EGGLER DH [1983] Upper mantle oxidation state: evidence from olivine-orthopyroxene-ilmenite assemblages. Geophys Res Lett 10:365-368

EGGLER DH, BAKER DR [1982] Reduced volatiles in the system C-O-H: implications to mantle melting, fluid formation, and diamond genesis. In: High pressure research in geophysics [ed. S Akimoto and M Manghnani] 237-250. Center for Academic Publications, Tokyo.

EGGLER DH, ROSENHAUER M [1978] Carbon dioxide in silicate melts,II, Solubilities of CO_2 and H_2O in $CaMgSi_2O_6$ (diopside) liquids and vapors at pressures to 40kb. Am J Science 278:64-94

EGGLER DH, WENDLANDT RF [1979] Experimental studies on the relationship between kimberlite magmas and partial melting of peridotite. In: FR Boyd & HOA Meyer (editors), Kimberlites, diatremes and diamonds: their geology, petrology and geochemistry. p.330-338. American Geophysical Union

EHRENBERG SN [1979] Garnetiferous ultramafic inclusions in minette from the Navajo volcanic field. In: F.R.Boyd and H.O.A.Meyer (editors), The mantle sample: inlcusions in kimberlites and other volcanics p.330-344. American Geophysical Union

EHRENBERG SN [1982] Rare earth element geochemistry of garnet lherzolite and megacrystalline nodules from minette of the Colorado Plateau province. Earth Planet Sci Lett 57:191-210

EL-HINNAWI EE [1965] Petrochemical characters of African volcanic rocks. Part III. Central Africa. Neues Jb Miner Abh 103:126-146

ERLANK AJ [1973] Kimberlite potassic richterite and the distribution of potassium in the upper mantle. First Internat Kim Conf Ext Abs:103-106

ERLANK AJ, FINGER LW [1970] The occurrence of potassic richterite in a mica nodule from the Wesselton kimberlite, South Africa. Carn Inst Wash Yearb 68:442-443

FERGUSON AK, CUNDARI A [1975] Petrological aspects and evolution of the leucite-bearing lavas from Bufumbira, South West Uganda. Contrib Mineral Petrol 50:25-46

FERRARA G, LUCCHINI F, ROSSI PL, TONARINI S [1981] Dati geologici, petrochimici e isotopici sul vulcano Muria (central Java, Indonesia). Rend Soc Geol It 4:289-299

FERRARA G, LAURENZI MA, TAYLOR HP, TONARINI S, TURI B [1985] Oxygen and strontium isotope studies of K-rich volcanic rocks from the Alban Hills, Italy. Earth Planet Sci Lett 75:13-28

FERRARO JR, MANGHNANI MH [1972] Infrared absorption spectra of sodium silicate glasses at high pressures. J Appl Phys 43:4595-4599

FISK AR, BENCE AE [1980] Experimental crystallisation of chrome spinels in FAMOUS basalt 527-1-1. Earth Planet Sci Lett 48:111-123

FODEN JD [1979] The petrology of some young volcanic rocks from Lombok and Sumbawa, Lesser Sunda Islands. Ph.D thesis, Univeristy of Tasmania.

FODEN JD, VARNE R [1980] The petrology and tectonic setting of Quaternary-Recent volcanic centres of Lombok and Sumbawa, Sunda Arc. Chem Geol 30:201-226

FORD CE, RUSSELL DG, CRAVEN JA, FISK MR [1983] Olivine-liquid equilibria: temperature, pressure and composition dependence of the crystal/liquid partition coefficients for Mg, Fe^{2+}, Ca and Mn. J Petrol 24:256-265

FORNASERI M, TURI B [1969] Carbon and oxygen isotopic composition of carbonates in lavas and ejectites from the Alban Hills, Italy. Contrib

Mineral Petrol 23:244-256

FORNASERI M, SCHERILLO A, VENTRIGLIA U [1963] La regione vulcanica dei Colli Albani, Vulcano Laziale. [Consiglio Nazionale delle Richerche] Roma, 561 pp.

FRASER DG [1977] Thermodynamic properties of silicate melts. In: Thermodynamics in Geology [ed. DG Fraser] 301-325 D.Reidel.

FRASER KJ, HAWKESWORTH CJ, ERLANK AJ, MITCHELL RH, SCOTT-SMITH BH [1985] Sr, Nd and Pb isotope and minor element geochemistry of lamproites and kimberlites. Earth Planet Sci Lett 76:57-70

FREUND F, KATHREIN H, WENGELER H, KNOBEL R, HEINEN HJ [1980] Carbon in solid solution in forsterite - a key to the untractable nature of reduced carbon in terrestrial and cosmogenic rocks. Geochim Cosmochim Acta 44:1319-1333

FREUND F, WENGELER H, KATHREIN H, KNOBEL R, OBERHEUSER G, MAITI GC, REIL D, KOTZ J [1983] Hydrogen and carbon derived from dissolved H_2O and CO_2 in minerals and melts. Bull Mineral 106:185-200

FREY FA, GREEN DH [1974] The mineralogy, geochemistry and origin of lherzolite inclusions in Victorian basanites. Geochim Cosmochim Acta 38: 1023-1059

FREY FA, GREEN DH, ROY SD [1978] Integrated models of basalt petrogenesis: a study of quartz tholeiites to olivine melilitites from South Eastern Australia utilising geochemical and experimental petrological data. J Petrol 19:463-513

FROST BR [1979] Mineral equilibria involving mixed volatiles in a C-O-H fluid phase: the stabilities of graphite and siderite. Am J Science 279: 1035-1059

FRYER BJ [1977] Rare earth evidence in iron formation for changing oxidation states. Geochim Cosmochim Acta 41:361-367

FURUKAWA T, FOX KE, WHITE WB [1981] Raman spectroscopic investigation of the structure of silicate glasses. III.Raman intensities and structural units in sodium silicate glasses. J Chem Phys 75:3226-3237

FUSTER JM, DE PEDRO F [1953] Estudio petrologico de las rocas lamproiticas de Cabezo Maria (Almeria). Estud Geol 9:477-508

FUSTER JM, GASTESI P, SAGREDO J, FERMOSO ML [1967] Las rocas lamproiticas del SE de Espana. Estud Geol 23:35-69

FYFE WS, McBIRNEY AR [1975] Subduction and the structure of andesite volcanic belts. Amer J Sci 275A:285-297

GALLO F, GIAMMETTI F, VENTURELLI G, VERNIA L [1984] The kamafugitic rocks of San Venanzo and Cupaello, central Italy. Neues Jb Min Mh 5:198-210

GAST PW [1968] Trace element fractionation and the origin of tholeiitic and alkaline magma types. Geochim Cosmochim Acta 32:1057-1086

GERASIMOVSKIY VI, VOLKOV VP, KOGARKO LN, POLYAKOV AI [1974] Alkaline Provinces 2. Kola Peninsula. In: H.Sorensen (editor), The alkaline rocks p.206-221 Wiley

GERLACH TM [1980] Chemical characteristics of the volcanic gases from Nyiragongo lava lake and the generation of CH_4-rich fluid inclusions in alkaline rocks. J Volcanol Geotherm Res 8:177-189

GIAMMETTI F, BECCALUVA L [1968] Carta geologica delle lave affioranti nei dintorni di Bagnoregio. L'Ateneo Parmense, Acta Nat (Parme) 4:164-220

GIANNETTI B [1982] Cumulate inclusions from K-rich magmas, Roccamonfina volcano, Italy. Earth Planet Sci Lett 57:313-335

GILL JB [1981] Orogenic andesites and plate tectonics. Springer-Verlag 390pp.

GLYUK DS, ANFILOGOV VN [1973] Phase equilibria in the system granite-H_2O-HF at a pressure of 1000kg/cm^2. Geochem Int 10:321-325

GOGINENI SV, MELTON CE, GIARDINI AA [1978] Some petrological aspects of the Prairie Creek diamond-bearing kimberlite diatreme, Arkansas. Contrib Mineral Petrol 66:251-261

GOLD DP [1970] The Oka carbonatite and alkaline complex. In: G.Pouliot (editor), Geology of the Monteregian Hills p.43-62 Geological Association of Canada.

GRAGNANI R [1972] Le vulcaniti melilitiche di Cupaello (Rieti). Rend SIMP 28:165-189

GREEN DH [1970] The origin of basaltic and nephelinitic magmas. Trans Leicester Lit Phil Soc 64:28-54

GREEN DH [1971] Composition of basaltic magmas as indicators of conditions of origin: application to oceanic volcanism. Phil Trans Roy Soc London A 268:707-725

GREEN DH [1973a] Experimental melting studies on a model upper mantle composition at high pressure under water-saturated and water-undersaturated conditions. Earth Planet Sci Lett 19:37-53

GREEN DH [1973b] Conditions of melting of basanite magma from garnet peridotite. Earth Planet Sci Lett 17:456-465

GREEN DH [1976] Experimental petrology in Australia - a review. Earth Sci Rev 12:99-138

GREEN DH, LIEBERMANN RC [1976] Phase equilibria and elastic properties of a pyrolite model for the oceanic upper mantle. Tectonophysics 32:61-92

GREEN DH, RINGWOOD AE [1963] Mineral assemblages in a model mantle composition. J Geophys Res 68:937-945

GREEN DH, RINGWOOD AE [1967a] The genesis of basaltic magmas. Contrib

Mineral Petrol 15:103-190

GREEN DH, RINGWOOD AE [1967b] An experimental investigation of the gabbro to eclogite transformation and its petrological applications. Geochim Cosmochim Acta 31:767-833

GREEN DH, SOBOLEV NV [1975] Coexisting garnets and ilmenites synthesized at high pressures from pyrolite and olivine basanite and their significance for kimberlitic assemblages. Contrib Mineral Petrol 50:217-229

GREEN DH, RINGWOOD AE, HIBBERSON WO, WARE NG [1975] Experimental petrology of Apollo 17 mare basalts. Proc 6th Lunar Sci Conf, 871-893

GREEN DH, TAYLOR WR, FOLEY SF [1986] The Earth's upper mantle as a source for volatiles. Geol Soc Australia Spec Publ 12 [submitted]

GREEN TH [1980] Island arc and continent-building magmatism - a review of petrogenetic models based on experimental petrology and geochemistry. Tectonophysics 63:367-385

GREEN TH (1981) Synthetic high-pressure micas compositionally intermediate between the dioctahedral and trioctahedral mica series. Contrib Mineral Petrol 78:452-458

GREEN TH, PEARSON NJ [1986] Ti-rich accessory phase saturation in hydrous mafic-felsic compositions at high P,T. Chem Geol 54:185-201

GREEN TH, RINGWOOD AE, MAJOR A [1966] Friction effects and pressure calibration in a piston-cylinder apparatus at high pressure and temperature. J Geophys Res 71:3589-3595

GRIFFIN WL [1973] Lherzolite nodules from the Fen alkaline complex. Contrib Mineral Petrol 38:135-146

GRIFFIN WL, TAYLOR PN [1975] The Fen Damkjernite: petrology of a "central-complex kimberlite". Phys Chem Earth 9:163-177

GRIKUROV GE, ORLENKO EM, FEDOROV LV [1980] Alkaline-ultrabasic rocks of the Beaver Lake region, eastern Antarctica. Trudi Sovietskoy Antarcticheskoy Expeditsiy 70:87-99 [Russian]

GRUBB PLC [1965] Undersaturated potassic lavas and hypabyssal intrusives in North Jahore. Geol Mag 102:338-346

GUINTRAND Y, METAIS D, THIERAUT J [1963] Sur un roche de nature lamprophyrique dans la région de Saint-Bresson (Haute-Saône). Bull Soc Geol France 5:16-19

GUPTA AK, GREEN DH [in prep] Phase equilibria study of the system kalsilite - forsterite - SiO_2 under 28kb with or without volatiles (H_2O or CO_2) and its implications.

GUPTA AK, YAGI K [1980] Petrology and genesis of the leucite-bearing rocks. Spinger-Verlag 252pp.

GUPTA AK, GREEN DH, TAYLOR WR [1985] Experimental study of the system forsterite-nepheline-jadeite at variable temperature under 28kb. Amer J Sci [submitted]

GUPTA AK, LEMAITRE RW, HAUKKA MT, YAGI K [1983] Geochemical studies on the carbonated apatite glimmerites from Damodar Valley, India. Proc Jap Acad B. 59:113-116

HAGGERTY SE [1976] Opaque oxide minerals in terrestrial rocks. In: Oxide minerals. Reviews in Mineralogy 3:101-300 Min Soc America

HAGGERTY SE [1979] Spinels in high pressure regimes. In: The mantle sample: inclusions in kimberlites and other volcanics [ed. FR Boyd and HOA Meyer] 183-196

HAGGERTY SE [1983] The mineral chemistry of new titanates from the Jagersfontein kimberlite, South Africa: implications for metasomatism in the upper mantle. Geochim Cosmochim Acta 47:1833-1854

HAGGERTY SE, TOMPKINS LA [1983] Redox state of Earth's upper mantle from kimberlitic ilmenites. Nature 303:295-300

HAGGERTY SE, SMYTH JR, ERLANK AJ, RICKARD RS, DANCHIN RV [1983] Lindsleyite (Ba) and Mathiasite (K): two new chromium-titanates in the crichtonite series from the upper mantle. Amer Mineral 68:494-505

HALL A [1982] The Pendennis peralkaline minette. Min Mag 45:257-266

HARRIS PG [1957] Zone refining and the origin of potassic basalts. Geochim Cosmochim Acta 12:195-208

HARRIS PG, MIDDLEMOST EAK [1969] The evolution of kimberlites. Lithos 3:77-88

HARTE B [1983] Mantle peridotites and processes - the kimberlite sample. In: C.J.Hawkesworth and M.J.Norry (editors), Continental basalts and mantle xenoliths p.46-91. Shiva, Nantwich.

HARTE B, COX KG, GURNEY JJ [1975] Petrography and geological history of upper mantle xenoliths from the Matsoku Kimberlite pipe. Phys Chem Earth 9:477-506

HARUMOTO A [1970] Volcanic rocks and associated rocks of Utsuryo Island (Japan Sea). Nippon Publ. Co. Osaka. 39pp.

HATHERTON T, DICKINSON WR [1969] The relationship between andesitic volcanism and seismicity in Indonesia, the Lesser Antilles and other island arcs. J Geophys Res 74:5301-5310

HAWKESWORTH CJ, VOLLMER R [1979] Crustal contamination versus enriched mantle: $^{143}Nd/^{144}Nd$ and $^{87}Sr/^{86}Sr$ evidence from the Italian volcanics. Contrib Mineral Petrol 69:151-165

HAZEN RM, FINGER LW, VELDE D (1981) Crystal structure of a silica- and alkali-rich trioctahedral mica. Am Mineral 66:586-591

HE GUAN-ZHI [1984] Kimberlites in China and their major components: a discussion on the physico-chemical properties of the upper mantle. In: J.Kornprobst (editor), Kimberlites I: kimberlites and related rocks p181-194. Elsevier

HEISENBERG W [1958] Physics and philosophy: the revolution in modern science. George Allen & Unwin, 176pp.

HELMSTAEDT H, SCHULZE DJ [1979] Garnet clinopyroxenite - chlorite eclogite transition in a xenolith from Moses Rock: further evidence for metamorphosed ophiolites under the Colorado Plateau. In: F.R.Boyd and H.O.A Meyer (editors) The mantle sample: inclusions in kimberlites and other volcanics. p.357-365. American Geophysical Union

HERMES OD, CORNELL WC [1983] The significance of mafic nodules in the ultrapotassic rocks from central Italy - discussion. J Volcanol Geotherm Res 16:166-172

HICKEY RL, FREY FA [1982] Geochemical characteristics of boninite series volcanics: implications for their source. Geochim Cosmochim Acta 46: 2099-2115

HIGAZY R [1954] Trace elements of volcanic ultrabasic potassic rocks of southwestern Uganda and adjoining part of the Belgian Congo. Bull Geol Soc Am 66:39-70

HILL R, ROEDER PL [1974] The crystallisation of spinel from basaltic liquid as a function of oxygen fugacity. J Geol 709-729

HOLLOWAY JR [1981] Volatile interactions in magmas. Adv Phys Geochem 1:273-293

HOLLOWAY JR, FORD CE [1975] Fluid absent melting of the fluor-hydroxy amphibole pargasite to 35 kilobars. Earth Planet Sci Lett 25:44-48

HOLM PM, MUNKSGAARD NC [1982] Evidence for mantle metasomatism: an oxygen and strontium isotope stduy of the Vulsinian District, central Italy. Earth Planet Sci Lett 60:376-388

HOLM PM, LOU S, NIELSEN A [1982] The geochemistry and petrogenesis of the lavas of the Vulsinian district, Roman province, central Italy. Contrib Mineral Petrol 80:367-378

HOLMES A [1937] The petrology of katungite. Geol Mag 74:200-219

HOLMES A [1942] A suite of volcanic rocks from South-West Uganda containing kalsilite (a polymorph of $KAlSiO_4$). Min Mag 26:197-217

HOLMES A [1945] Leucitized granite xenoliths from potash-rich lavas of Bunyaruguru, South-West Uganda. Am J Sci 243A:313-332

HOLMES A [1950] Petrogenesis of katungite and its associates. Am Mineral 35:772-792

HOLMES A [1952] The potash ankaratrite-melaleucitite lavas of Nabugando and Mbuga craters (south-west Uganda). Trans Edin Geol Soc 15:187-213

HOLMES A [1956] The ejectamenta of Katwe crater, South-West Uganda. [in Denaeyer et al 1965]

HOLMES A, HARWOOD HF [1932] Petrology of the volcanic fields East and Southeast of Ruwenzori, Uganda. Quart J Geol Soc London 88:370-442

HOLMES A, HARWOOD HF [1937] The volcanic area of Bufumbira (Part II). Geol Survey Uganda Mem 3, 300pp

HOLMES A, HECHT F [1936] Transfusion of quartz xenoliths in alkali basic and ultrabasic lavas. Min Mag 24:408-421

HOLUB FV [1977] Petrology of inclusions as a key to petrogenesis of the durbachitic rocks from Czechoslovakia. Tschermaks Min Petr Mitt 24:133-150

HUEBNER JS, SATO M [1970] The oxygen fugacity - temperature relationships of manganese oxide and nickel oxide buffers. Amer Mineral 55:934-952

IDDINGS JP, MORLEY EW [1915] Contributions to the petrography of Java and Celebes. J Geol 23:231-245

IRVING AJ [1978] A review of experimental studies of crystal/liquid trace element partitioning. Geochim Cosmochim Acta 42:743-770

ISHIKAWA K, KANISAWA S, AOKI K [1980] Content and behaviour of fluorine in Japanese Quaternary volcanic rocks and petrogenetic application. J Volcanol Geotherm Res 8:161-175

ITO H, YANAGASE T, SUGINOHARA Y, MIYAZAKI N [1967] Studies on the structure of molten fluoride-silicate systems by infrared absorption spectra. Chem Abs 67:68972g from Nippon Kinzoku Gakkaishi 31:290-295

JAQUES AL, GREEN DH [1979] Anhydrous melting of peridotite at 0-15 kb pressure and the genesis of tholeiitic basalts. Contrib Mineral Petrol 73:287-310

JAQUES AL, LEWIS JD, SMITH CB, GREGORY GP, FERGUSON J, CHAPPELL BW, McCULLOCH MT [1984a] The diamond-bearing ultrapotassic (lamproitic) rocks of the West Kimberley region, Western Australia. In: J.Kornprobst (editor), Kimberlites I: kimberlites and related rocks p.225-254. Elsevier.

JAQUES AL, WEBB AW, FANNING CM, BLACK LP, PIDGEON RT, FERGUSON J, SMITH CB, GREGORY GP [1984b] The age of the diamond-bearing pipes and associated leucite lamproites of the West Kimberley region, Western Australia. BMR J Geol Geophys 9:1-7

JAQUES AL, CHAPPELL BW, SUN S-S, LEWIS JD, SMITH CB [1986] The West Kimberley lamproites: intraplate volcanism of extreme character. I.A.V.C.E.I. Abstract, Auckland.

JOHNSON RM [1964] Walsen composite dyke near Walsenburg, Colorado. US Geol Surv Prof Paper 501B:69-73

JOHNSON RM [1968] Geology of the igneous rocks of the Spanish Peaks

region, Colorado. US Geol Surv Prof Paper 549G: 1-47

JOHNSTON RH [1959] Geology of the northern Leucite Hills, Sweetwater County, Wyoming. MA thesis, University of Wyoming

JONES AP, WYLLIE PJ [1984] Minor elements in perovskite from kimberlites and distribution of rare earth elements: an electron probe study. Earth Planet Sci Lett 69:128-140

JONES AP, SMITH JV, DAWSON JB [1982] Mantle metasomatism in 14 veined peridotites from the Bultfontein mine, South Africa. J Geol 90:435-453

JOPLIN GA [1966] On lamprophyres. J Proc Roy Soc New South Wales 99:37-44

KADIK AA, LUKANIN OA [1985a] Paths of mantle outgassing during melting: the role of partial melting of upper mantle rocks in the evolution of fluid composition and redox regime. Internat Geol Rev 27:563-572

KADIK AA, LUKANIN OA [1985b] Paths for mantle outgassing during melting: changes in fluid composition and conditions in basaltic magmas during migration to the surface. Internat Geol Rev 27:573-586

KAY RW, GAST PW [1973] Rare earth content and origin of alkali-rich basalts. J Geol 81:653-682

KELLER J [1983] Potassic lavas in the orogenic volcanism of the Mediterranean area. J Volc Geotherm Res 18:321-335

KEMP JF [1891] The basic dykes occurring outside of the syenite areas of Arkansas. Ann Report Geol Surv Arkansas (1890) 2:392-406

KENNEDY CS, KENNEDY GC [1976] The equilibrium boundary between graphite and diamond. J Geophys Res 81:2467-2470

KENNEDY GC [1959] Phase relations in the system Al_2O_3-H_2O at high temperatures and pressures. Amer J Sci 257:563-573

KILINC AI, CARMICHAEL ISE, SACK RO, RIVERS ML [1982] Fe^{3+}/Fe^{2+} ratio in silicate melts as a function of T, fO_2 and bulk composition. Geol Soc America Abs Prog 14:420

KILINC AI, CARMICHAEL ISE, RIVERS ML, SACK RO [1983] The ferric-ferrous ration of natural silicate liquids equilibrated in air. Contrib Mineral Petrol 83:136-140

KIM K-R [1983] Methane and radioactive isotopes in submarine hydrothermal systems. Ph.D. thesis, Scripps Institute of Oceanography, University of California, San Diego, 206pp.

KIRCHNER JG [1979] Petrographic significance of a carbonate-rich lamprophyre from Squaw Creek, northern Black Hills, South Dakota. Am Mineral 64:986-992

KNOPF A [1936] Igneous geology of the Spanish Peaks region. Bull Geol Soc Am 47:1727-1784

KOGARKO LN [1967] Lamination area in melts of the system Si,Al,Na//O,F. Dokl Akad Nauk Earth Sci Sec 176:203-205

KOGARKO LN [1974] Role of volatiles. In: [ed. H Sorensen] The alkaline rocks. pp 474-487 Wiley

KOGARKO LN, KRIGMAN LD [1973] Structural position of fluorine in silicate melts (according to melting curves). Geochem Int 10:34-40

KOGARKO LN, RYABCHIKOV ID [1978] Volatile components in magmatic processes. Geochem Int 15:9-32

KOGARKO LN, KRIGMAN LD, SHARUDILO NS [1968] Experimental investigations of the effect of alkalinity of silicate melts on the separation of fluorine into the gas phase. Geochem Int 5:782-790

KÖRNER S [1966] Experience and theory: an essay in the philosophy of science. Routledge & Keegan Paul. London.

KOSTER VAN GROOS AF, WYLLIE PJ [1968] Melting relationships in the system $NaAlSi_3O_8$-NaF-H_2O to 4 kilobars pressure. J Geol 76:50-70

KOVACH JJ, HISER AL, KARR C [1975] Far-infrared spectroscopy of minerals In: [C.Karr, ed.] Infrared and Raman spectroscopy of lunar and terrestrial minerals. p. 231-254. Academic Press New York

KOVALENKO NI [1977] The reactions between granite and aqueous hydrofluoric acid in relation to the origin of fluorine-bearing granites. Geochem Int 14:108-118

KOZAKEVITCH P [1954] Viscosity of blast furnace slags. Revue Metall Mem Scient 51:569-587

KRAMER W [1976] Genese der lamprophyre im Bereich der Fichtelgebirgisch - Erzgebirgischen Antiklinalzone. Chem Erde 35:1-49

KRANCK EH [1928] On turjaite and the ijolite stem of Turja, Kola. Fennia 51:1-109

KRESTEN P, EDELMAN N [1975] A boulder of ouachitite from Inderskar, Aland Islands, Finland. Bull Geol Soc Finland 47:167-169

KUEHNER SM [1980] Petrogenesis of ultrapotassic rocks, Leucite Hills, Wyoming. M.Sc. thesis, University of Western Ontario, 200pp.

KUEHNER SM, EDGAR AD, ARIMA M [1981] Petrogenesis of the ultrapotassic rocks from the Leucite Hills, Wyoming. Am Mineral 66:663-677

KUMAR D, WARD RG, WILLIAMS DJ [1961] Effect of fluorides on silicates and phosphates. Disc Faraday Soc 32:147-154

KUMAR D, WARD RG, WILLIAMS DJ [1965] Infrared absorption of some solid silicates and phosphates with and without fluoride additions. Trans Faraday Soc 61:1850-1857

KURAT G, PALME H, SPETTEL B, BADDENHAUSEN H, HOFMEISTER H, PALME C, WÄNKE

H [1980] Geochemistry of ultramafic xenoliths from Kapfenstein, Austria: evidence for a variety of upper mantle processes. Geochim Cosmochim Acta 44:45-60

KUSHIRO I [1968] Compositions of magmas formed by partial zone melting of the earth's upper mantle. J Geophys Res 73:619-637

KUSHIRO I [1972] Effect of water on the compositions of magmas formed at high pressures. J Petrol 13:311-334

KUSHIRO I [1975] On the nature of silicate melt and its significance in magma genesis: regularities in the shift of the liquidus boundaries involving olivine, pyroxene and silica minerals. Am J Sci 275:411-431

KUSHIRO I [1980] Changes with pressure of degree of partial melting and K_2O content of liquids in the system Mg_2SiO_4-$KAlSiO_4$-SiO_2. Carn Inst Wash Yb 79:267-271

KUSHIRO I, ERLANK AJ [1970] Stability of potassic richterite. Carn Inst Wash Yb 68:231-233

KUSHIRO I, SYONO Y, AKIMOTO S [1967] Stability of phlogopite at high pressures and possible presence of phlogopite in the Earth's upper mantle. Earth Planet Sci Lett 3:197-203

LACROIX A [1926] La systématique des roches leucitiques; les types de la famille syénitique. C R Acad Sci Paris 182:597-601

LACROIX A [1933] Les roches éruptives potassiques, leucitiques ou non, du Tonkin occidental. C R Acad Sci Paris 197:625-627

LANGWORTHY AP, BLACK LP [1978] The Mordor Complex: a highly differentiated potassic intrusion with kimberlitic affinities in central Australia. Contrib Mineral Petrol 67:51-62

LARSEN ES [1941] Igneous rocks of the Highwood Mountains, Montana. Bull Geol Soc Am 52:1733-1752

LAUGHLIN RB, JOANNOPOULOS JD [1977] Phonons in amorphous silica. Phys Rev B 16:2942-2952

LEES GJ [1974] Petrochemistry of the mica lamprophyres (minettes) of Jersey. Proc Ussher Soc 3:149-155

LEPVRIER C, VELDE D [1976] A propos des intrusions tertiaires de la marge nord-africaine entre Cherchel et Tenes (Algérie). Bull Soc Geol France 18:991-998

LINDSLEY DH, KESSON SE, HARTZMAN MJ, CUSHMAN MK [1974] The stability of armalcolite: experimental stduies in the system MgO-Fe-Ti-O. Proc Lunar Sci Conf 5:521-534

LLOYD FE [1981] Upper mantle metasomatism beneath a continental rift: clinopyroxenes in alkali mafic lavas and nodules from South West Uganda. Mineral Mag 44:315-323

LLOYD FE [1983] Extreme mantle metasomatism beneath continental rifts: evidence from ultra akaline lavas and nodules of South West Uganda. Abstract for: Mantle metasomatism and the origin of ultrapotassic and related rocks. London, Ontario

LLOYD FE, BAILEY DK [1975] Light element metasomatism of the continental mantle: the evidence and the consequences. Phys Chem Earth 9:389-416

LLOYD FE, ARIMA M, EDGAR AD [1985] Partial melting of a phlogopite clinopyroxenite nodule from south-west Uganda: an experimental study bearing on the origin of highly potassic continental rift volcanics. Contrib Mineral Petrol 91:321-329

LOCARDI E [1981] La provincia comagmatica romana e l´evoluzione geodinimica dell´area tirrenica. Comitato Nazionale Energia Nucleare, Casaccia, 72 pp.

LOPEZ-RUIZ J, RODRIGUEZ-BADIOLA E [1980] La region volcanica neogena del sureste de Espana. Estud Geol 36:5-63

LONGHI J, WALKER D, HAYS JF [1978] The distribution of Fe and Mg between olivine and lunar basaltic liquids. Geochim Cosmochim Acta 42:1545-1558

LUTH WC [1967] Studies in the system $KAlSiO_4$-Mg_2SiO_4-SiO_2-H_2O: I, Inferred phase relations and petrologic apllications. J Petrol 8:372-416

MAKSIMOV EP, UGRYUMOV AN [1971] Mesozoic magmatic formations of the Aldan Shield. Sov Geol 7:107-119 [Russian]

MANNING DAC [1981] The effect of fluorine on liquidus phase relationships in the system Qz-Ab-Or with excess water at 1 kb. Contrib Mineral Petrol 76:206-215

MANNING DAC, HAMILTON DL, HENDERSON CMB, Dempsey MJ (1980) The probable occurrence of interstitial Al in hydrous, F-bearing and F-free aluminosilicate melts. Contrib Mineral Petrol 75:257-262

MARINELLI G [1975] Magma evolution in Italy. In: C.H.Squyres (editor), Geology of Italy p165-219 Earth Sci Soc Libyan Arab Repl, Tripoli

MATHEZ EA [1984] Influence of degassing on oxidation states of basaltic magmas. Nature 310:371-375

MAUREL C, MAUREL P [1982a] Détermination Expérimentale de la solubilité du chrome dans les bains silicatés basiques et spinelle chromifère. C R Acad Sci Paris Série II 295:371-373

MAUREL C, MAUREL P [1982b] Étude expérimentale a la distribution de l´aluminium entre bain silicaté basique et spinelle chromifère. Implications petrogénétiques: teneur en chrome des spinelles. Bull Mineral 105:197-202

MAUREL C, MAUREL P [1982c] Étude expérimentale de l´equilibre Fe^{2+}-Fe^{3+} dans les spinelles chromifères et les liquides silicatés basiques coexistants, à 1 atm. C R Acad Sci Paris Série II 295:209-212

MAUREL C, MAUREL P [1983] Influence du fer ferrique sur la distribution de l'aluminium entre bain silicaté basique et spinelle chromifère. Bull Mineral 106:623-624

MAUREL C, MAUREL P [1984] Étude expérimentale de la distribution du fer ferrique entre spinelle chromifère et bain silicaté basique. Bull Mineral 107:25-33

McCAULEY JW, NEWNHAM RE, GIBBS GV (1973) Crystal structure analysis of synthetic fluorphlogopite. Am Mineral 58:249-254

McCULLOCH MT, JAQUES AL, NELSON DR, LEWIS JD [1983] Nd and Sr isotopes in kimberlites and lamproites from Western Australia: an enriched mantle origin. Nature 302:400-403

McIVER JR [1981] Apsects of ultrabasic and basic alkaline intrusive rocks from Bitterfontein, South Africa. Contrib Mineral Petrol 78:1-11

McIVER JR, FERGUSON J [1979] Kimberlitic, melilititic,trachytic and carbonatite eruptives at Salpetre Kop, Sutherland, South Africa. In: F.R.Boyd and H.O.A.Meyer (editors), Kimberlites, diatremes and diamonds: their geology, petrology and geochemistry p111-128. American Geophysical Union.

MENZIES M [1983] Mantle ultramafic xenoliths in alkaline magmas: evidence for mantle heterogeneity modified by magmatic activity. In: C.J.Hawkesworth and M.J.Norry (editors), Continental basalts and mantle xenoliths p.92-110 Shiva, Nantwich.

MERRILL RB, BICKFORD ME, IRVING AJ [1977] The Hills Pond peridotite, Woodson County, Kansas: a richterite-bearing Cretaceous intrusive with kimberlitic affinities. Second Int Kim Conf Ext Abs 232-234

MEYER HOA, BOYD FR [1972] Composition and origin of crystalline inclusions in natural diamond. Geochim Cosmochim Acta 36:1255-1273

MILLER TP [1972] Potassium-rich alkaline intrusive rocks of Western Alaska. Bull Geol Soc Am 83:2111-2128

MITCHELL A [1967] Reactions of calcium silicates in solution in liquid calcium fluoride. Trans Faraday Soc 63:1408-1417

MITCHELL RH [1979] The alleged kimberlite-carbonatite relationship: additional contrary mineralogical evidence. Amer J Sci 279:570-589

MITCHELL RH [1986] A review of the mineralogy of lamproites. Trans Geol Soc South Africa (in press)

MITCHELL RH, BELL K [1976] Rare earth element geochemistry of potassic lavas from the Birunga and Toro-Ankole regions of Uganda, Africa. Contrib Mineral Petrol 58:293-303

MITCHELL RH, BRUNFELT AO [1975] Rare earth element geochemistry of kimberlite. Phys Chem Earth 9:671-686

MITCHELL RH, CLARKE DB [1976] Oxide and sulphide mineralogy of the Peyeuk

kimberlite, Somerset Island, N.W.T., Canada. Contrib Mineral Petrol 56:157-172

MITCHELL RH, CROCKETT JH [1972] Isotopic composition of strontium in rocks of the Fen complex, South Norway. J Petrol 13:83-98

MITCHELL RH, LEWIS RD [1983] Priderite-bearing xenoliths from the Prairie Creek mica peridotite, Arkansas. Can Mineral 21:59-64

MITTEMPERGHER M [1965] Vulcanismo e petrogenesi nella zona di San Venanzo (Umbria). Atti Soc Toscana Sci Nat Serie A 72:437-479

MO X, CARMICHAEL ISE, RIVERS ML, STEBBINS JB [1982] The partial molar volume of Fe_2O_3 in multicomponent silicate liquids and the pressure dependence of oxygen fugacity in magmas. Mineral Mag 45:237-245

MODRESKI PJ, BOETTCHER AL [1972] The stability of phlogopite + enstatite at high pressures: a model for micas in the interior of the Earth. Amer J Sci 272:852-869

MORSE SA [1980] Basalts and phase diagrams. An introduction to the quantitative use of phase diagrams in igneous petrology. Spinger-Verlag, New York. 493pp.

MUNOZ JL, EUGSTER HP (1969) Experimental control of fluorine reactions in hydrothermal systems. Am Mineral 54:943-959

MYSEN BO [1977] The solubility of H_2O and CO_2 under predicted magma genesis conditions and some petrological and geophysical implications. Rev Geophys Space Phys 15:351-361

MYSEN BO, VIRGO D [1985] Interaction between fluorine and silica in quenched melts on the joins SiO_2-AlF_3 and SiO_2-NaF determined by Raman spectroscopy. Phys Chem Minerals 12:77-85

MYSEN BO, VIRGO D, SEIFERT F [1981] Ferric iron as a network former and as a network modifier in melts relevant to petrological processes. Carn Inst Wash Yearb 80:311-313

MYSEN BO, VIRGO D, SEIFERT FA [1982] The structure of silicate melts: implications for chemical and physical properties of natural magmas. Rev Geophys Space Phys 20:353-383

NASH WP, WILKINSON JFG [1970] Shonkin Sag laccolith, Montana I. Mafic minerals and estimates of temperature, pressure, oxygen fugacity and silica activity. Contrib Mineral Petrol 25:241-269

NASH WP, WILKINSON JFG [1971] Shonkin Sag Laccolith, Montana II. Bulk rock geochemistry. Contrib Mineral Petrol 33:162-170

NELSON DR, McCULLOCH MT, SUN SS [1986] The origins of ultrapotassic rocks as inferred from Sr, Nd and Pb isotopes. Geochim Cosmochim Acta 50:231-245

NEMEC D [1970] Lamprophyrische und lamproide Ganggesteine im Sudteil der bohmisch-mahrischen Anhohe. Tsch Min Pet Mitt 14:235-284

NEMEC D [1973] Paragenetische Analyse der Ganggesteine der Minettengruppe. Chem Erde 32:80-97

NEMEC D [1974] Petrochemistry of the dyke rocks of the Central Bohemian pluton. Neues Jb Min Mh 193-206

NICHOLLS IA, RINGWOOD AE [1974] Effect of water on olivine stability in tholeiites and the production of silica-saturated magmas in island arc environments. J Geol 81:285-300

NICHOLLS J [1969] Studies of the volcanic petrology of the Navajo-Hopi area, Arizona. Ph.D. thesis, University of California, Berkeley, 107pp.

NICHOLLS JW [1980] A simple thermodynamic model for estimating the solubility of H_2O in magmas. Contrib Mineral Petrol 74:211-220

NICHOLLS J, CARMICHAEL ISE [1969] A commentary on the absarokite - shoshonite - banakite series of Wyoming, USA. Schweiz Min Pet Mitt 49:47-64

NINKOVICH D, HAYS JD [1972] Mediterranean island arcs and origin of high potash volcanoes. Earth Planet Sci Lett 16:331-345

NIXON PH, BOYD FR [1973] The discrete nodule association in kimberlites from northern Lesotho. In P.H.Nixon (editor), Lesotho Kimberlites. p.67-75 Maseru.

NIXON PH, BOYD FR [1979] Garnet bearing lherzolites and discrete nodule suites from the Mailaita alnoite, Solomon islands, S.W. Pacific, and their bearing on oceanic mantle composition and geotherm. In: F.R.Boyd and H.O.A.Meyer (editors), The Mantle Sample: inclusions in kimberlites and other volcanics p.400-423 American Geophysical Union

NIXON PH, HORNUNG G [1973] The carbonatite lavas and tuffs near Fort Portal, western Uganda. Inst Geol Sci Overseas Geol Min Res 41:168-179

NIXON PH, THIRLWALL MF, BUCKLEY F, Davies CJ [1984] Spanish and Western Australian lamproites: aspects of whole rock geochemistry. In: J.Kornprobst (editor), Kimberlites I: kimberlites and related rocks p285-296 Elsevier.

OGDEN PR [1979] The geology, major element geochemistry, and petrogenesis of the Leucite Hills volcanic rocks, Wyoming. Ph.D.thesis, University of Wyoming, Laramie.

O'HARA MJ, YODER HS [1967] Formation and fractionation of basic magmas at high pressures. Scottish J Geol 3:67-117

OHTANI E [1984] Generation of komatiitic magma and gravitational differentiation in the deep upper mantle. Earth Planet Sci Lett 67: 261-272

OLAFSSON M, EGGLER DH [1983] Phase relations of amphibole, amphibole-carbonate, and phlogopite-carbonate peridotite: petrologic constraints on the asthenosphere. Earth Planet Sci Lett 64:305-315

O'NEILL HS, WALL VJ [1982] Oxygen fugacities from the assemblage olivine-orthopyroxene-spinel. Research School Earth Sciences, Australian National Univeristy, Annual Report 177-179

PALACHE C, BERMAN H, FRONDEL C [1951] Dana's system of mineralogy II pp 103-104 Wiley

PALIVCOVA M, BENES K, ZOUBEK V [1968] Genesis of granitoids in the Bohemian Massif. Int Geol Congress 23, Excursion Guide 29A, 42pp

PALM QA [1958] Les roches cristallines des Cévennes médianes à hauteur de Largentière, Ardèche, France. Geol Ultraectina, No.3

PECCERILLO A [1985] Roman comagmatic province (central Italy): evidence for subduction-related magma genesis. Geology 13:103-106

PECCERILLO A, POLI G, TOLOMEO L [1984] Genesis, evolution and tectonic significance of K-rich volcanics from the Alban Hills (Roman comagmatic region) as inferred from trace element geochemistry. Contrib Mineral Petrol 86:230-240

PE-PIPER G [1984] Zoned pyroxenes from shoshonite lavas of Lesbos, Greece: inferences concerning shoshonite petrogenesis. J Petrol 25:453-472

PERCHUK LL [1965] Magmatic replacement of carbonate bodies involving formation of nepheline syenites and other alkalic rocks, with example of Cape Dezhnev massif. Int Geol Rev 7:280-296

PIRSSON LV [1905] Petrography and geology of the igneous rocks of the Highwood Mountains, Montana. US Geol Surv Bull 237

POLI G, FREY FA, FERRARA G [1984] Geochemical characteristics of the South Tuscany (Italy) volcanic province: constraints on lava petrogenesis. Chem Geol 43:203-221

POUCLET A [1980a] Les laves du rift de l'Afrique centrale;revue des données pétrographiques et chimiques. Essai de magmatologie. Rapp Ann Mus Roy Afr Centr 1979:81-128

POUCLET A [1980] Contribution à la systématique des laves alcalines, les laves du rift de l'Afrique Centrale (Zaïre-Uganda). Bull Volcanol 43: 527-540

POUCLET A, MENOT R-P, PIBOULE M [1981] Classement par l'analyse factorielle discriminante des laves du rift de l'Afrique Centrale (Zaïre, Rwanda, Uganda). C R Acad Sci Paris 292:679-684

POUCLET A, MENOT R-P, PIBOULE M [1984] Differenciation des laves de l'Afrique Centrale (Rift Ouest). Contribution de l'analyse statistique multivariée. Neues Jb Min Abh 149:283-308

POWELL JL, BELL K [1970] Strontium isotopic studies of alkalic rocks: localities from Australia, Spain and Western United States. Contrib Mineral Petrol 17:1-10

PRIDER RT [1960] The leucite lamproites of the Fitzroy Basin, Western

Australia. J Geol Soc Aus 6:71-118

PRIDER RT [1982] A glassy lamproite from the West Kimberley area. Min Mag 45:279-282

PRINZ M, MANSON DV, HLAVA PF, KEIL K [1975] Inclusions in diamonds: garnet lherzolite and eclogite assemblages. Phys Chem Earth 9:797-815

PUXEDDU M [1972] Studio chimico - petrografio delle vulcaniti del Monte Cimino (Viterbo). Atti Soc Toscana Sci Nat Pisa Mem, P.V., Ser A 78:329-394

RAMBERG H [1952] Chemical bonds and distribution of cations in silicates. J Geol 60:331-355

RAO KJ, ELLIOTT SR [1981] Characteristic vibrations of cations in glasses. J Non-Cryst Solids 46:371-378

RAVICH MG, SOLOVEV DS, FEDOROV LV [1978] Geological structure of MacRobertson Land (East Antarctica). p206-214 Gidrometeoizdat, Leningrad [Russian]

REINISCH R [1912] Petrographische beschreibung der Gaussberg-gesteine. Geographie und Geologie 2:74-89

RIGDEN SM, AHRENS TJ, STOLPER EM [1984] Densities of liquid silicates at high pressures. Science 226:1071-1074

RINGWOOD AE [1974] Petrological evolution of island arc systems. J Geol Soc London 130:183-204

RINGWOOD AE [1982] Phase transformations and differentiation in subducted lithosphere: implications for mantle dynamics, basalt petrogenesis, and crustal evolution. J Geol 90:611-643

RITTMAN A [1933] Die geologisch bedingte Evolution und Differentiation des Somma-Vesuv-magma. Z Vulk 15:8-94

ROBINSON P, HIGGINS NC, JENNER GA [1986] Determination of rare-earth elements, yttrium and scandium in rocks by an ion-exchange x-ray fluorescence technique. Chem Geol 55:121-137

ROCK NMS [1980] Rare-earth and other trace element contents and the origin of minettes. A critical comment on a paper by Bachinski and Scott. Geochim Cosmochim Acta 44:1385-1388

ROCK NMS [1984] Nature and origin of calc-alkaline lamprophyres: minettes, vogesites, kersantites and spessartites. Trans Roy Soc Edinburgh, Earth Sciences 74:193-227

ROCK NMS [1986] The nature and origin of lamprophyres: alnoites and allied rocks (ultramafic lamprophyres). J Petrol 27:155-196

RODEN MF [1981] Origin of coexisting minette and ultramafic breccia, Navajo volcanic field. Contrib Mineral Petrol 77:195-206

RODEN MF, SMITH D [1979] Field geology, chemistry and petrology of Buell Park minette diatreme, Apache County, Arizona. In: F.R.Boyd and H.O.A.Meyer (editors), Kimberlites, diatremes and diamonds: their geology, petrology and geochemistry. p 364-381 American Geophysical Union.

RODEN MF, SMITH D, MCDOWELL FW [1979] Age and extent of potassic volcanism on the Colorado plateau. Earth Planet Sci Lett 43:279-284

ROEDER PL, EMSLIE RF [1970] Olivine-liquid equilibrium. Contrib Mineral Petrol 29:275-289

ROGERS NW, BACHINSKI SW, HENDERSON P, PARRY SJ [1982] Origin of potash-rich basic lamprophyres: trace element data from Arizona minettes. Earth Planet Sci Lett 57:305-312

ROGERS NW, HAWKESWORTH CJ, PARKER RJ, MARSH JS [1985] The geochemistry of potassic lavas from Vulsini, central Italy and implications for mantle enrichment processes beneath the Roman region. Contrib Mineral Petrol 90:244-257

ROSENBERG PE, FOIT FF (1977) Fe^{2+} - F avoidance in silicates. Geochim Cosmochim Acta 41:345-346

ROWELL WF, EDGAR AD [1983] Cenozoic potassium-rich mafic volcanism in the western USA: its relationship to deep subduction. J Geol 91:338-341

RYABCHIKOV ID, GREEN DH [1978] The role of carbon dioxide in the petrogenesis of highly potassic magmas. In: Problems of petrology of the Earth's crust and upper mantle. Trudy Inst Geol Geofiz, Nauka Novosibirsk 403:49-64 [Russian]

RYABCHIKOV ID, GREEN DH, WALL VJ, BREY GP [1981] The oxidation state of carbon in the reduced-velocity zone. Geokhimiya 2:221-232

SABATIER H [1980] Vaugnérites et granites: une association particulière de roches grenues acides et basiques. Bull Mineral 103:507-522

SACK RO, CARMICHAEL ISE, RIVERS ML, GHIORSO MS [1980] Ferric-ferrous equilibria in natural silicate liquids at 1 bar. Contrib Mineral Petrol 75:369-376

SAHAMA TG [1954] Mineralogy of mafurite. C R Soc Geol Finlande 27:21-28

SAHAMA TG [1974] Potassium-rich alkaline rocks. In: H.Sorensen (editors), The alkaline rocks. p.96-109 Wiley

SANZ J, STONE WEE [1979] NMR study of micas, II. Distribution of Fe^{2+}, F^-, and OH^- in the octahedral sheet of phlogopites. Am Mineral. 64:119-126

SATO M [1978] Oxygen fugacity of basaltic magmas and the role of gas-forming elements. Geophys Res Lett 5:447-449

SAVELLI C [1967] The problem of rock assimilation by Somma-Vesuvius magma I.Composition of Somma and Vesuvius lavas. Contrib Mineral Petrol

16:328-353

SCHILLING J-G, BERGERON MB, EVANS R (1980) Halogens in the mantle beneath the North Atlantic. Phil Trans Roy Soc Lond A 297:147-178

SCHMIDT RG, PECORA WT, BRYANT B, ERNST WG [1961] Geology of the Lloyd Quadrangle, Bearpaw Mountains, Blaine County, Montana. US Geol Survey Bull 1081-E: 159-188

SCHNEIDER H [1965] Petrographie des Lateravulkans und die Magmanantwicklung der Monti Volsini. Schweiz Min Pet Mitt 45:331-455

SCHNEIDER ME, EGGLER DH [1984] Compositions of fluids in equilibrium with peridotite: implications for alkaline magmatism-metasomatism. In: J.Kornprobst (editor), Kimberlites I: kimberlites and related rocks p.383-394 Elsevier, Amsterdam

SCHULTZ AR, CROSS W [1912] Potash-bearing rocks of the Leucite Hills, Sweetwater County, Wyoming. US Geol Surv Bull 512

SCHWAB RG, KUSTNER D [1981] Die gleichgewichtsfugazitäten technologisch und petrologisch wichtiger Sauerstoffpuffer. Neues Jb Miner Abh 140:111-142

SCOTT BH [1977] Petrogenesis of kimberlites and associated potassic lamprophyres from central West Greenland. PhD thesis, Edinburgh University

SCOTT BH [1979] Petrogenesis of kimberlites and associated potassic lamprophyres from central West Greenland. In: F.R.Boyd and H.O.A.Meyer (editors), Kimberlites, diatremes and diamonds: their geology, petrology and geochemistry p.190-205

SCOTT BH [1981] Kimberlite and lamproite dykes from Holsteinsborg, West Greenland. Meddelelser om Gronland Geosci 4:1-24

SCOTT-SMITH BH, Skinner EMW [1984a] Diamondiferous lamproites. J Geol 92: 433-438

SCOTT-SMITH BH, Skinner EMW [1984b] A new look at Prairie Creek, Arkansas. In: J.Kornprobst (editor), Kimberlites I: kimberlites and related rocks p.255-283 Elsevier

SEIFERT F, SCHREYER W [1971] Synthesis and stability of micas in the system K_2O - MgO - SiO_2 - H_2O and their relations to phlogopite. Contrib Mineral Petrol 30:196-215

SEIFERT F, MYSEN BO, VIRGO D [1981] Structural similarity of glasses and melts relevant to petrological processes. Geochim Cosmochim Acta 45: 1879-1884

SEIFERT F, MYSEN BO, VIRGO D [1982] Three-dimensional network melt structure in the systems SiO_2-$NaAlO_2$, SiO_2-$CaAl_2O_4$ and SiO_2-$MgAl_2O_4$. Am Mineral 67:696-717

SEKINE T, WYLLIE PJ [1982] Phase relationships in the system

$KAlSiO_4$-Mg_2SiO_4-SiO_2-H_2O as a model for hybridisation between hydrous siliceous melts and peridotite. Contrib Mineral Petrol 79:368-374

SHAFILQULLAH M, TUPPER WM, COLE TJS [1970] K-Ar age of the carbonatite complex, Oka, Quebec. Can Mineral 10:541-552

SHELL HR, IVEY KH (1969) Fluorine micas. US Bur Mines Bull 647:291pp

SHERATON JW [1981] Chemical analyses of rocks from East Antarctica. Bur Mineral Resources Record 1981/14:67-68

SHERATON JW, CUNDARI A [1980] Leucitites from Gaussberg, Antarctica. Contrib Mineral Petrol 71:417-427

SHERATON JW, ENGLAND RN [1980] Highly potassic dykes from Antarctica. J Geol Soc Aus 27:129-135

SMITH D [1979] Hydrous minerals and carbonates in peridotite inclusions from the Green Knobs and Buell Park kimberlitic diatremes on the Colorado Plateau. In: F.R.Boyd and H.O.A.Meyer (editors), The mantle sample: inclusions in kimberlites and other volcanics. p.345-356 American Geophysical Union.

SMITHSON SB [1959] The geology of the Southeastern Leucite Hills, Sweetwater County, Wyoming. MA thesis, Univeristy of Wyoming.

SOBOLEV NV [1975] Deep seated inclusions in kimberlites and the problem of the composition of the upper mantle. Amer Geophys Union, 279pp.

SOLOMON M [1964] The spilite-keratophyre association of west Tasmania and the ore deposits at Mt Lyell, Roseberry and Hercules. PhD thesis, University of Tasmania 419pp

STEFANOVA M [1966] Petrochemical peculiarities of the Svidnya potassium alkaline rocks. Bulg Acad Sci Bull 40:191-203 [Bulgarian]

STOLPER EM [1982] The speciation of water in silicate melts. Geochim Cosmochim Acta 46:2609-2620

STORMER JC [1972] Ages and nature of volcanic activity on the southern high plains, New Mexico and Colorado. Geol Soc Am Bull 83:2443-2448

SUN SS [1980] Lead isotopic study of young volcanic rocks from mid-ocean ridges, ocean islands and island arcs. Phil Trans Roy Soc London A 297: 409-445

SUN SS, HANSON GN [1975] Origin of Ross Island basanitoids and limitations upon the heterogeneity of mantle sources for alkali basalts and nephelinites. Contrib Mineral Petrol 52:77-106

SUTHERLAND FL, CORBETT EB [1974] The extent of upper Mesozoic igneous activity in relation to lamprophyric intrusions in Tasmania. Pap Proc Roy Soc Tasmania 107:175-190

TAKAHASHI E, SCARFE CM [1985] Melting of peridotite to 14GPa and the genesis of komatiite. Nature 315:566-568

TARTE P [1965] The determination of cation co-ordination in glasses by infra-red spectroscopy. In: [ed. JA Prins] Physics of non-crystalline solids. pp 549-565 Wiley

TARTE P [1967] Infra-red spectra of inorganic aluminates and characteristic vibrational frequencies of AlO_4 tetrahedra and AlO_6 octahedra. Spectrochim Acta 23A:2127-2143

TAYLOR HP, TURI B, CUNDARI A [1984] $^{18}O/^{16}O$ and chemical relationships in K-rich volcanic rocks from Australia, East Africa, Antarctica and San Venanzo-Cupaello, Italy. Earth Planet Sci Lett 69:263-276

TAYLOR M, BROWN GE, FENN PM [1980] Structure of silicate mineral glasses III, $NaAlSi_3O_8$ supercooled liquid at 805°C and the effects of thermal history. Geochim Cosmochim Acta 44:109-119

TAYLOR SR, McCLENNAN SM [1985] The Continental crust: its composition and evolution. Blackwell 312pp.

TAYLOR WR [1985] The role of C-O-H fluids in upper mantle processes: a theoretical, experimental and spectroscopic study. Ph.D. thesis, University of Tasmania, Hobart. 358pp.

TAYLOR WR [1986a] A 5-parameter modified Redlich-Kwong equation of state for C-O-H fluids at upper mantle pressure and temperature. In prep. for J Geophys Res

TAYLOR WR [1986b] A reappraisal of the nature of fluids included in diamond: a window to deep-seated mantle fluids and redox conditions. Geol Soc Australia Spec Publ. 12 [in press]

TAYLOR WR, GREEN DH [1986a] Mantle methane and the role of reduced volatiles in 'redox melting' of the mantle. Fourth Internat Kim Conf Ext Abstract

TAYLOR WR, GREEN DH [1986b] The petrogenetic role of methane: effect on liquidus phase relations and the solubility mechanism of reduced C-H volatiles. Geochemical Society Special Volume [submitted]

THOMPSON RN [1977] Primary Basalts and magma genesis III. Alban Hills, Roman comagmatic province, Central Italy. Contrib Mineral Petrol 60:91-108

THOMPSON RN [1982] Magmatism of the British Tertiary Volcanic province. Scottish J Geol 18:49-107

THOMPSON RN, MORRISON MA, DICKIN AP, HENDRY GL [1983] Continental flood basalts... arachnids rule OK? In: C.J.Hawkesworth and M.J.Norry (editors), Continental basalts and mantle xenoliths p.158-185 Shiva, Nantwich.

THY P [1983] Spinel minerals in transitional and alkali basaltic glasses from Iceland. Contrib Mineral Petrol 83:141-149

TINGEY RJ, McDOUGALL I, GLEADOW AJW [1983] The age and mode of formation

of Gaussberg, Antarctica. J Geol Soc Aus 30:241-246

TOMITA T [1970] Volcanic geology of the Cenozoic alkaline petrographic province of eastern Asia. In: T.Ogura (editor), Geology and Mineral Resources of the Far East 1:139-202 Tokyo Univ Press

TREIMAN AH, ESSENE EJ [1985] The Oka carbonatite complex, Quebec: geology and evidence for silicate-carbonate liquid immiscibility. Am Mineral 70:1101-1113

TRIGILA R [1966] Studio geopetrografico dell'edificio vulcanico di M.Calvo (Farnese, Viterbo). Periodico Miner (Rome) 35:1023-1095

TRIGILA R [1969] Studio geopetrografico del complesso vulcanico di Latera (Vulcani Vulsini) - Nota I. Periodico Miner (Rome) 38:155-220

TSAI HM, MEYER HOA, MOREAU J, MILLEDGE HJ [1979] Mineral inclusions in diamond: Premier, Jagersfontein and Finsch kimberlites, South Africa, and Williamson Mine, Tanzania. In: Kimberlites, diatremes and diamonds: their geology, petrology and geochemistry [ed. FR Boyd and HOA Meyer] 16-26

TSUNAWAKI Y, IWAMOTO N, HATTORI T, MITSUISHI A [1981] Analysis of $CaO-SiO_2$ and $CaO-SiO_2-CaF_2$ glasses by Raman spectroscopy. J Non-Cryst Solids 44:369-378

TURI B, TAYLOR HP [1976] Oxygen isotope studies of potassic volcanic rocks of the Roman Province, central Italy. Contrib Mineral Petrol 55:1-31

UKHANOV AV [1963] Olivine melilitite from the diamond-bearing diatremes on Anabar. Dokl Akad Nauk Earth Sci Secy 153:176-178

VAN BERGEN MJ, GHEZZO C, RICCI CA [1983] Minette inclusions in the rhyodacitic lavas of Mt Amiata (central Italy): mineralogical and chemical evidence of mixing between Tuscan and Roman type magmas. J Volc Geotherm Res 19:1-35

VAN BREEMEN O, AFTALION M, BOWES DR, DUDEK A, MISAR Z, POVONDRA P, VRANA S [1982] Geochronological studies of the Bohemian Massif, Czechoslovakia, and their significance in the evolution of central Europe. Trans Roy Soc Edinburgh , Earth Sciences 73: 89-108

VAN KOOTEN GK [1980] Mineralogy, petrology and geochemistry of an ultrapotassic bsaltic suite, central Sierra Nevada, California, USA. J Petrol 21:651-684

VAN KOOTEN GK [1981] Pb and Sr systematics of ultrapotassic and basaltic rocks from the central Sierra Nevada, California. Contrib Mineral Petrol 76:378-385

VAN MOORT JC [1966] Les roches cristallophylliennes des Cévennes et les roches plutoniques du Mont Lozère. Ann Fac Sci Univ Clermont No.31 272pp

VAN PADANG MN [1951] Catalogue of the active volcanoes of the world including solfatara fields. Part 1. Indonesia. Int. Volcanol. Assn.

VAREKAMP JC [1979] Geology and petrology of the Vulsinian volcanic area (Latium, Italy). Ph.D. dissertation, State University of Utrecht, Utrecht. 384pp.

VAREKAMP JC [1983] The significance of mafic nodules in the ultrapotassic rocks from central Italy - discusssion. J Volcanol Geotherm Res 16:161-165

VARNE R [1985] Ancient subcontinental mantle: a source for K-rich orogenic volcanics. Geology 13:405-408

VARNE R, GRAHAM AL [1971] Rare earth abundances in hornblende and clinopyroxene of a hornblende lherzolite xenolith: implications for upper mantle fractionation processes. Earth Planet Sci Lett 13:11-18

VARTIAINEN H, WOOLLEY AR [1974] The age of the Sokli carbonatite, Finland, and some relationships of the North Atlantic alkaline igneous province. Bull Geol Soc Finland 6:81-91

VARTIAINEN H, KRESTEN P, KAFKAS Y [1978] Alkaline lamprophyres from the Sokli complex, northern Finland. Bull Geol Soc Finland 50:59-68

VELDE D [1967] Sur un lamprophyre hyperalcalin potassique: la minette de Sisco (île de Corse). Bull Soc Fr Mineral Crist 90:214-223

VELDE D [1971a] Les lamprophyres à feldspath alcalin et biotite: minettes et roches voisines. Contrib Mineral Petrol 30:216-239

VELDE D [1971b] Les kersantites: étude des lamprohyres à plagioclase et biotite. Bull Soc Fr Min Crist 94:411-426

VELDE D [1975] Armalcolite - Ti-phlogopite - diopside - analcite - bearing lamproites from Smoky Butte, Garfield County, Montana. Am Mineral 60:566-573

VELDE D [1979] Trioctahedral micas in melilite-bearing eruptive rocks. Carn Inst Wash Yb 78:468-475

VENTURELLI G, DI BATTISTINI G [1980] Alcuni caratteri chimici delle rocce altamente potassiche: distribuzione di fosforo e titanio. In: Volume dedicato a Sergio Venzo. Grafiche STEP, Parma p.191-194

VENTURELLI G, CAPEDRI S, DI BATTISTINI G, CRAWFORD AJ, KOGARKO LN, CELESTINI S [1984a] The ultrapotassic rocks from southeastern Spain. Lithos 17:37-54

VENTURELLI G, THORPE RS, DAL PIAZ GV, DEL MORO A, POTTS PJ [1984b] Petrogenesis of calc-alkaline, shoshonitic and associated ultrapotassic Oligocene volcanic rocks from the northwestern Alps, Italy. Contrib Mineral Petrol 86:209-220

VILA JM, HERNANDEZ J, VELDE D [1974] Sur la presence d'un filon de roche lamproïtique (trachyte potassique à olivine) recoupant le flysch de type Guerrouch entre Azzaba (ex-Jemmapes) et Hammam-Meskoutine, dans l'Est du Constantinois (Algérie). C R Acad Sci Paris Serie D 278:2589-2592

VIRGO D, MYSEN BO, SEIFERT F [1981] Relationship between the oxidation state of iron and the structure of silicate melts. Carn Inst Wash Yearb 80:308-311

VITERBO C, ZANETTIN B [1959] I filoni lamprofirici dell'alto Baltoro, (Karakorum). Mem Acc Patavina Sc Lett Arti 71:1-39

VOLLMER R [1976] Rb-Sr and U-Th-Pb systematics of alkaline rocks; the alkaline rocks from Italy. Geochim Cosmochim Acta 40:283-295

VOLLMER R, NORRY MJ [1983] Unusual isotopic variations in Nyirangongo nephelinites. Nature 301:141-143

VOLLMER R, OGDEN P, SCHILLING J-G, KINGSLEY RH, WAGGONER DG [1984] Nd and Sr isotopes in ultrapotassic volcanic rocks from the Leucite Hills, Wyoming. Contrib Mineral Petrol 87:359-368

VON KNORRING O, DU BOIS CGB [1961] Carbonatitic lava from Fort Portal area in Western Uganda. Nature 192:1064-1065

VYALOV OS, SOBOLEV VS [1959] Gaussberg, Antarctica. Int Geol Rev 1:30-40

WADE A, PRIDER RT [1940] The leucite-bearing rocks of the West Kimberley area, Western Australia. Quart J Geol Soc London 98:39-98

WADE K, BANNISTER AJ [1973] The chemistry of aluminium, gallium, indium and thallium. In: Comprehensive Inorganic Chemistry Vol.12. Pergamon

WALKER KR, MOND A [1971] Mica lamprophyre (alnoite) from Radok Lake, Prince Charles Mountains, Antarctica. Record BMR Geol Geophys [unpubl.] 6pp

WELHAN JA, CRAIG H [1983] Methane, hydrogen and helium in hydrothermal fluids at 21°N on the East Pacific Rise. In: PA Rona, K Bostrom, L Laubier & KL Smith (editors), Hydrothermal processes at seafloor spreading centers, p.391-409, Plenum Press, New York

WENDLANDT RF, EGGLER DH [1980a] The origins of potassic magmas: 1. Melting relations in the systems $KAlSiO_4$-Mg_2SiO_4-SiO_2 and $KAlSiO_4$-MgO-SiO_2-CO_2 to 30 kilobars. Am J Science 280:385-420

WENDLANDT RF, EGGLER DH [1980b] Stability of sanidine+forsterite and its bearing on the genesis of potassic magmas and the distribution of potassium in the upper mantle. Earth Planet Sci Lett 51:215-220

WENDLANDT RF, EGGLER DH [1980c] The origins of potassic magmas: 2. Stability of phlogopite in natural spinel lherzolite and in the system $KAlSiO_4$-MgO-SiO_2-H_2O-CO_2 at high pressures and high temperatures. Amer J Science 280:421-458

WHELLER GE [1986] Petrogenetic studies of basalt-andesite-dacite volcanism at Batur volcano, Bali, and the causes of K-variation in Sunda-Banda Arc basalts. Ph.D. thesis, University of Tasmania, Hobart

WHELLER GE, VARNE R, FODEN JD, ABBOTT MJ [1986] Geochemistry of Quaternary volcanism in the Sunda-Banda Arc, Indonesia, and three component genesis

of island arc basaltic magmas. J Volc Geotherm Res, special issue [in press].

WHITE WB [1975] Structural interpretation of lunar and terrestrial minerals by Raman spectroscopy. In: [C Karr ed.] Infrared and Raman spectroscopy of lunar and terrestrial minerals. p.325-358 Academic Press, New York

WHITFORD DJ [1975] Geochemistry and petrology of volcanic rocks from the Sunda arc, Indonesia, and their petrogenetic implications. Ph.D. thesis, Australian National University, Canberra

WHITFORD DJ, FODEN J, VARNE R [1978] Sr isotope geochemistry of calcalkaline and alkaline lavas from the Sunda arc in Lombok and Sumbawa, Indonesia. Carn Inst Wash Yb 77:613-620

WHITFORD DJ, WHITE WM, JEZEK PA [1981] Neodymium isotopic composition of Quaternary island arc lavas from Indonesia. Geochim Cosmochim Acta 45: 989-995

WILLIAMS H [1936] Pliocene volcanoes of the Navajo-Hopi country. Bull Geol Soc Am 47:111-172

WIMMENAUER W [1973] Lamprophyre, semilamprophyre und anchibasaltische Ganggesteine. Fotschr Mineral 51:3-67

WINDOM KE, BOETTCHER AL (1981) Phase relations for the joins jadeite-enstatite and jadeite-forsterite at 28kb and their bearing on basalt genesis. Am J Sci 281:335-351

WITKIND IJ [1973] Igneous rocks and related mineral deposits of the Barker Quadrangle, Little Belt Mountains, Montana. US Geol Surv Prof Paper 752:1-58

WOERMANN E, ROSENHAUER M [1985] Fluid phases and the redox state of the Earth's mantle: extrapolations based on experimental, phase-theoretical and petrological data. Fortschr Mineral 63:263-349

WYLLIE PJ [1977] Mantle fluid compositions buffered by carbonates in peridotite - CO_2 - H_2O. J Geol 85:187-207

WYLLIE PJ [1978] Mantle fluid compositions buffered in peridotite-CO_2-H_2O by carbonates, amphibole, and phlogopite. J Geol 86:687-713

WYLLIE PJ [1979] Magmas and volatile components. Amer Mineral 64:469-500

WYLLIE PJ [1980] The origin of kimberlite. J Geophys Res 85:6902-6910

WYLLIE PJ, HUANG WL [1976] High CO_2 solubilities in mantle magmas. Geology 4:21-24

WYLLIE PJ, SEKINE T [1982] The formation of mantle phlogopite in subduction zone hybridization. Contrib Mineral Petrol 79:375-380

WYLLIE PJ, TUTTLE OF [1961] Experimental investigation of silicate systems containing two volatile components. Part II. The effects of NH_3 and HF

in addition to H_2O on the melting temperatures of albite and granite. Am J Sci 259:128-143

WYLLIE PJ, TUTTLE OF [1964] Experimental investigation of silicate systems containing two volatile components. Part III: The effects of SO_3, P_2O_5, HCl and Li_2O in addition to H_2O on the melting temperatures of albite and granite. Amer J Sci 262:930-939

YAGI K, MATSUMOTO H [1966] Note on the leucite-bearing rocks from Leucite Hills, Wyo., USA. J Fac Sci Hokkaido Univ IV (Geology & Mineralogy) 13:301-312

YODER HS, TILLEY CE (1962) Origin of basalt magmas: an experimental study of natural and synthetic rock systems. J Petrol 3:342-532

ZARTMAN RE, BROCK MR, HEYL AV, THOMAS HH [1967] K-Ar and Rb-Sr ages of some alkalic intrusive rocks from central and eastern United States. Am J Sci 265:848-870

ZINGG A, HUNZIKER JC, FREY M, AHRENDT H [1976] Age and degree of metamorphism of the Canavese Zone and the sedimentary cover of the Sesia Zone. Schweiz Min Pet Mitt 56:361-375

American Mineralogist, Volume 70, pages 1143–1150, 1985

The origin of Al-rich spinel inclusions in leucite from the leucite lamproites of Western Australia

A. L. JAQUES

Bureau of Mineral Resources
GPO Box 378, Canberra, ACT, Australia

AND S. F. FOLEY

Geology Department, University of Tasmania
GPO Box 252C, Hobart, Tasmania, Australia

Abstract

Aluminous spinels (pleonaste-hercynite) occur as tiny (mostly <20 μm) inclusions in leucite phenocrysts (and pseudomorphs) in leucite lamproites from the West Kimberley region, Western Australia. These spinels differ markedly from the "co-existing" groundmass titaniferous magnesiochromites which, like the other ferromagnesian phases in the rock, are poor in alumina. Similar Al-spinel inclusions in leucites were found in experiments at atmospheric pressure on another lamproite, the Gaussberg olivine leucitite. Based on mineralogical and experimental evidence the formation of the aluminous spinel inclusions in leucite in these peralkaline volcanics is attributed to exsolution under conditions of supersaturation from non-stoichiometric leucites originally incorporating Mg, Al and Fe^{2+} in solid solution.

Introduction

Spinels belonging to the $MgAl_2O_4$–$FeAl_2O_4$ series are uncommon in volcanic rocks; most spinels in basic to intermediate magmas show extensive solid solution towards (Mg, Fe)Cr_2O_4, Fe_3O_4 and, to a lesser extent, Fe_2TiO_4 (e.g., Haggerty, 1976). Aluminous spinels, commonly intergrown with silicates or in some cases other oxides (e.g., titanomagnetite), are well documented in plutonic and metamorphosed igneous rocks where they are inferred to result from sub-solidus reactions and re-equilibration, and/or oxidation. However, a number of occurrences of unusual, essentially Cr-free Al-spinel have been reported from basic to ultrabasic alkalic volcanics. Arculus (1978) described Fe-pleonaste rimmed by chromite enclosed in augite which was in turn enclosed by phenocrystal olivine in a basanitoid from Grenada. Fe-pleonaste has also been reported from ultrapotassic lavas (lamproites) from Leucite Hills (Kuehner et al., 1981) and southeastern Spain (Venturelli et al., 1984). Both Arculus (1978) and Kuehner et al. (1981) suggested that the Fe-pleonaste was of xenocrystal origin derived from disaggregated granulite or ultramafic nodules whereas Venturelli et al. (1984) suggested that the tiny Al-spinel inclusions in biotite phenocrysts (xenocrysts?) resulted in part from the breakdown of the host mica. In addition to these occurrences Mg-rich pleonaste rims on groundmass chromite/titanomagnetite have been described from several kimberlites (Haggerty, 1975; Pasteris, 1983).

This paper describes the occurrence of aluminous spinel inclusions in leucite phenocrysts in lamproites from the West Kimberley region of Western Australia observed in the course of detailed petrologic and geochemical study of the lamproite suite. Although previously unreported, the aluminous spinel inclusions are comparatively widespread, occurring in a wide range of lamproite types within the West Kimberley suite, all of which contain mica, alumina-deficient pyroxene, and amphibole and, commonly, alumina-free alkali-rich accessory phases. A similar occurrence of aluminous spinel inclusions in leucite was found independently by the second author during experimental studies of another lamproitic rock, the olivine leucitite of Gaussberg volcano, Antarctica.

Mineralogical, petrographic and experimental evidence are presented to explain the origin of the aluminous spinels in leucite in these ultrapotassic rocks. It is suggested that under appropriate conditions similar inclusions might occur in strongly leucite-phyric volcanics elsewhere.

Occurrence

Natural rocks

The Miocene leucite lamproites of the Fitzroy area of the West Kimberley region of Western Australia have been described by Wade and Prider (1940), Prider (1960, 1982), Derrick and Gellatly (1972) and, more recently, by Jaques et al. (1984). Petrological and geochemical studies indicate a continuum from the leucite-rich lamproites described by the earlier workers which contain phlogopite, diopside, or titanian potassium richterite as the major mafic phases, through lamproite with abundant olivine and leucite to the newly-discovered olivine lamproites (leucite-poor) some of which contain diamond (Atkinson et al., 1984; Jaques et al., 1984).

0003–004X/85/1112–1143$02.00

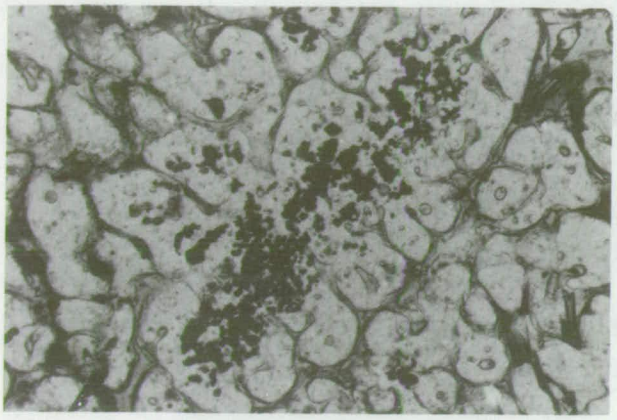

Fig. 1. Photomicrograph of Al-spinel (pleonaste-ferrian pleonaste) inclusions in leucite, glassy leucite lamproite, sample 71160408, Oscar Plug. Note irregular shape of aggregated leucite phenocrysts. Width of field is 0.55 mm.

The aluminous spinels occur exclusively as small—mostly less than 20 μm, rarely more than 40 μm—inclusions in aggregated leucite phenocrysts in fine grained to glassy, strongly leucite-phyric lamproites. The inclusions are more readily recognized in the rare rocks containing fresh leucite but can also be distinguished in lamproites where the leucite is replaced, generally pseudomorphed, by mixtures of K-feldspar, zeolite, chalcedony, opaline silica or clay (Prider and Cole, 1942). Fine grained inclusions of Fe oxide, particularly hematite are also common inclusions in altered leucite.

The leucite phenocrysts are typically euhedral and, where unaltered, weakly birefringent, twinned, and commonly contain inclusions of glass arranged in concentric zones. Many phenocrysts in the more glassy rocks are strongly resorbed and embayed. The leucite phenocrysts containing the aluminous spinel inclusions occur as amoeboid-shaped to strongly rounded, embayed, coalesced aggegates with numerous melt inclusions (Fig. 1). The aggregates range in size up to 5 mm and are irregularly distributed in the rock, apart from being more common in the finer-grained marginal phases of intrusives. No aluminous spinels have been observed in single, discrete leucite phenocrysts nor in any other phase; all are entirely contained in leucite.

Rock types containing the aluminous spinel inclusions include most of the types described by Wade and Prider (1940), and Prider (1960, 1982) except for the coarser grained lamproites of Rice (formerly Moulamen) Hill and Walgidee (formerly Wolgidee) Hills. The majority of the rocks containing aluminous spinel inclusions have phenocrysts of Al-poor diopside, phlogopite and/or olivine in addition to the leucite; potassic richterite is generally restricted to the groundmass. Alumina-free, alkali-rich accessory minerals (typically priderite, less commonly wadeite) are generally present in the groundmass as small prisms, and apatite is also invariably present. Most of the lamproites also contain a chrome-rich spinel which is present as tiny (<10 μm) inclusions in olivine and as small (mostly 50 μm or less) euhedra in the groundmass. The chromian spinels are mostly titaniferous magnesiochromites rich in Cr and Ti (50–65% Cr_2O_3, 3–6% TiO_2) and poor in Al but also include titaniferous chromian magnetites (see below). Ilmenite is comparatively rare occurring in the groundmass of only a few lamproites.

Experimental studies

The olivine leucitites of Gaussberg volcano in Wilhelm II Land, eastern Antarctica (Sheraton and Cundari, 1980), are closely comparable in composition to the mid-range (in terms of silica content) of the West Kimberley lamproites. The composition studied in the experiments is typical of the suite and is a good candidate for being a primary liquid; it is a fresh, glass-rich lava with phenocrysts of olivine, leucite and clinopyroxene, and carries mantle-derived spinel lherzolite xenoliths.

Two series of near-liquidus atmospheric pressure experiments have been conducted on the Gaussberg composition with controlled oxygen fugacities. Experiments were carried out in a one inch diameter vertical furnace using iron-doped Pt capsules included in evacuated silica tubes above a separate Pt capsule containing the oxygen buffer. The buffers used were hematite–magnetite, manganosite–haussmanite, nickel–nickel oxide, and magnetite–wüstite. Details of the composition and experiments are given elsewhere (Foley, 1985). The two series of experiments were conducted under similar conditions but with slightly different starting compositions. The first series involved an average Gaussberg composition, whereas the second series had additional Cr_2O_3 (0.2 wt.% cf. 0.045% in the first series) in order to ensure crystallization of chrome-spinel. The aluminous spinel inclusions in leucites occurred only in the second series runs. Apart from the slight difference in Cr_2O_3 content, the only other difference between the two series was run duration. The first series experiments were run for 2.5 hours, whereas the second were run for 5 hours to allow time for growth of chrome-spinel crystals to a size more easily analyzed. Both series of experiments were run under varying oxygen fugacity ranging between that controlled by magnetite-wüstite (MW) and the hematite–magnetite (HM) buffer reactions.

Aluminous spinel inclusions occurred exclusively in aggregated leucites in the second series runs. Groups of leucites also occurred in the first series runs but did not contain spinels. Although initially difficult to observe owing to their transparency in plane polarized light and isotropy under crossed polarizers, the spinels were identified in all of the second series runs containing leucites. The Al-spinels never occurred in direct contact with the glass.

Analytical method

Electron probe analyses of the spinels in the natural rocks were mostly obtained by wave-length dispersive methods using a Camebax (CAMECA) Microbeam fully automated EPMA employing an accelerating voltage of 15 kV, a beam current of 30 nA, a beam diameter of less than 1 micron, and full ZAF corrections. The

majority of the leucite analyses were made by energy-dispersive probe employing an accelerating voltage of 15 kV, a beam current of 3 nA, and a beam diameter of about 1 micron following the method of Reed and Ware (1975) and Ware (1980). Under these conditions leucite suffered little volatilization.

Analyses of experimental products were obtained using a JEOL JXA 50A microprobe fitted with an EDAX energy-dispersive analyzer calibrated on Cu. Owing to the small size of many crystals, compositions were frequently calculated by subtraction of average glass analyses from crystal/glass overlap analyses. Chrome-spinel compositions were obtained by linear regression for each oxide from several area scans of crystal plus glass overlap of varying sizes.

Compositions of the aluminous spinel inclusions

West Kimberley lamproites

The aluminous spinels occur mainly as either irregular clusters of discrete euhedra, mostly of green pleonaste, or elongate trains and clusters or aggregates of green to greenish brown euhedral to subhedral grains of pleonaste-ferrian pleonaste composition some of which are clustered in schlieren-like aggregates of leucite (Fig. 1). In addition one lamproite contained very rare coalesced aggregates of brownish black subhedra of hercynite included within aggregated leucite phenocrysts (Fig. 2).

A crude correlation exists between spinel composition and crystal form and size. The larger discrete green spinels are the most magnesian and are highly aluminous ($X_{Al} > 0.9$ where $X_{Al} = Al/(Al + Cr + Fe^{3+})$ and contain only minor magnetite in solid solution (Table 1; Fig. 3). The greenish brown to brown pleonaste-ferrian pleonaste grains are less magnesian, have higher magnetite contents (Fig. 3), and are commonly richer in TiO_2 than the green pleonaste grains although compositions overlap. The brownish ferrian pleonaste grains have the lowest Mg and highest magnetite contents. There is a correlation between Mg and X_{Al} (Fig. 3) and to a lesser extent between Mg and $X_{Fe^{3+}}$. The brownish black hercynite inclusions of sample 71449A are compositionally distinct from the other inclusions being much richer in Fe (Fig. 3). Like the discrete green pleonastes they have very low magnetite contents ($X_{Fe^{3+}} < 0.1$).

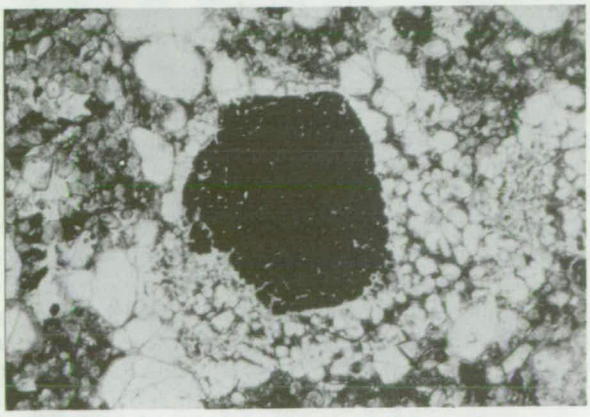

Fig. 2. Photomicrograph of aggregated hercynite inclusions in clustered leucite phenocrysts, olivine–diopside–leucite lamproite, sample 71449A, Ellendale No. 7. Width of field is 1.5 mm.

A feature of the spinel inclusions is their uniformly low Cr contents (<0.2%, commonly <0.1% Cr_2O_3). These contrast sharply with the high Cr contents of the groundmass titanium magnesiochromites (Table 1; Fig. 3). Other differences between the two generations of spinels are the much higher Ti and Mn, much lower Al contents, and generally higher Fe^{3+} and lower $Mg/(Mg + Fe^{2+})$ ratios of the groundmass spinels.

Experimental

The aluminous spinels in the Gaussberg experiments occur as tiny transparent single or, occasionally, grouped crystals. They contain negligible TiO_2 and Cr_2O_3, and have much higher Mg/(Mg + Fe) ratios than those in the West Kimberley rocks. They are also slightly more magnesian than coexisting Cr-rich spinels (Table 2). The Fe oxidation state in the spinels corresponds qualitatively to the oxygen buffer used, but the variable Fe^{3+}/Fe^{2+} indicates that f_{O_2} equilibrium was probably not fully reached for the Al-spinel inclusions.

Compositions of the leucites

Previous studies of leucite have shown that significant substitution of monovalent and trivalent cations into $KAlSi_2O_6$ may occur. End-members of the heavier alkalis (e.g., Rb, Cs) can be synthesized (Henderson and Taylor, 1969), but Na is the only important alkali substitution in natural leucites. Fudali (1963) showed that up to 28 wt.% $NaAlSi_2O_6$ may be incorporated in leucite at 1 kbar P_{H_2O} and 800°C on the join $KAlSi_2O_6$–$NaAlSi_2O_6$, but natural leucites are not known to incorporate more than 10 wt.% $NaAlSi_2O_6$. The Na contents of leucites in lamproitic rocks are very low, in accord with their ultrapotassic chemistry.

Leucites from areas of ultrapotassic volcanism such as the Leucite Hills commonly show an excess of silica and alkalis over alumina and ferric iron (e.g. Carmichael, 1967; Cundari, 1975; Barton, 1979). Experimental studies have shown that leucite may incorporate up to 8 wt.% $KAlSi_3O_8$ at 1 kbar and 800°C (Fudali, 1963) and less than 5 wt.% $NaAlSi_3O_8$ at 1 atmosphere and 800°C (Gupta and Edgar, 1975). Ferric iron forms the dominant substitution on the smaller Al site: Gupta and Yagi (1980, p. 142–146) suggested that solid solution between $KAlSi_2O_6$ and $KFe^{3+}Si_2O_6$ is limited to less than 6 wt.% $KFe^{3+}Si_2O_6$ at atmospheric pressure but increases with $P_{H_2O_2}$ to 7.7 wt.% at 2 kbar $P_{H_2O_2}$.

Incorporation of divalent cations is much rarer, although leucites of CaO contents in excess of 1 wt.% have been reported from potassic volcanics of the East African rift valley (Deer et al., 1963). Schairer (1948) observed the coupled substitution of Mg into leucite by the mechanism MgSi = AlAl, but did not state the extent of this substitution. The large W site favors cations of large ionic radius, and hence the solubility of Mg in leucite can be expected to be small, as is typically observed in natural leucites. How-

Table 1. Representative microprobe analyses of spinels in West Kimberley leucite lamproites

	Al-spinel inclusions					Groundmass		
	1	2	3	4	5	6	7	8
SiO_2	0.12	0.05	0.06	0.06	0.03	0.05	0.05	0.05
TiO_2	0.21	0.24	0.62	0.96	0.38	4.33	4.35	3.95
Al_2O_3	64.87	63.60	59.62	50.91	57.66	2.16	1.51	1.67
Cr_2O_3	0.23	0.16	n.d.	n.d.	0.02	55.20	57.15	58.98
FeO	13.23	21.86	20.74	28.37	34.02	29.68	27.25	24.21
MnO	0.05	0.09	0.12	0.19	0.16	0.93	0.31	0.48
MgO	21.77	14.59	18.88	18.18	7.46	7.15	8.95	10.47
CaO	0.02	0.02	n.d.	n.d.	0.02	n.d.	0.03	n.d.
Total	100.49	100.61	100.04	98.67	99.75	99.50	99.60	99.81
Fe_2O_3	3.72	1.82	8.64	17.07	4.67	5.80	5.57	5.35
FeO	9.88	20.22	12.96	13.01	29.82	24.46	22.24	19.40
Total	100.86	100.79	100.90	100.38	100.22	100.08	100.16	100.35
				O = 4				
Si	0.003	0.001	0.001	0.002	0.001	0.002	0.002	0.002
Ti	0.004	0.005	0.012	0.019	0.008	0.114	0.113	0.101
Al	1.905	1.950	1.812	1.611	1.886	0.089	0.062	0.067
Cr	0.006	0.003	-	-	0.001	1.526	1.563	1.591
Fe^{3+}	0.070	0.036	0.167	0.345	0.097	0.153	0.145	0.137
Fe^{2+}	0.206	0.439	0.279	0.292	0.692	0.716	0.644	0.554
Mn	0.001	0.002	0.003	0.005	0.004	0.027	0.009	0.014
Mg	0.808	0.564	0.725	0.727	0.308	0.373	0.462	0.533
Ca	0.001	0.001	-	-	0.001	-	0.001	-
XAl	0.962	0.981	0.915	0.824	0.950	0.050	0.035	0.037
XFe^{3+}	0.035	0.018	0.085	0.176	0.049	0.087	0.082	0.076
XCr	0.005	0.001	-	-	0.001	0.863	0.883	0.887
Mg#	0.797	0.562	0.722	0.713	0.308	0.343	0.418	0.490

Fe determined as FeO; Fe_2O_3 calculated from AB_2O_4 stoichiometry
n.d. = not detected (detection limit 0.02%)
XAl, etc. = Al/(Al+Cr+Fe^{3+}) etc; $Mg^{\#}$ = Mg/(Mg+Fe^{2+})

1. Pleonaste, 20 μm inclusion in leucite, 81210125.
2. Pleonaste, 20 μm inclusion in leucite, 71160408.
3. Pleonaste, 30 μm inclusion in leucite pseudomorph, 68165028.
4. Pleonaste, 15 μm inclusion in leucite pseudomorph, 68165028.
5. Hercynite, aggregate in leucite, 71449A.
6. Titaniferous magnesiochromite, 10 μm euhedra, 81210125.
7. Titaniferous magnesiochromite, 20 μm euhedra, 71160408.
8. Titaniferous magnesiochromite, 40 μm euhedra, 71449A.

ever, the coupled nature of the substitution leads to relationships more complex than this. For example, Henderson (1965) showed that Sr may be favored over Ba in leucites despite its smaller ionic radius.

West Kimberley lamproites

Analyses obtained for both inclusion-bearing and inclusion-free leucites from the same sample as well as bulk analyses of Al-spinel inclusion plus host leucite from the West Kimberley lamproites are given in Table 3 and projected into the system $KAlSiO_4$–$KFe^{3+}SiO_4$–SiO_2 (Fig. 4) following the method of Carmichael (1967). Both the leucite phenocrysts with Al-spinel inclusions and those without inclusions are of similar near-stoichiometric composition (Fig. 4) as previously found for West Kimberley leucites (Carmichael, 1967; Prider, 1982; Jaques et al., 1984). In general Fe, Ca and Na contents are low. Leucite cores and rims appear to show little difference in composition apart from slightly higher Fe at the rim.

Bulk analyses obtained with a defocussed beam or by scanning with a 40 to 50 μm raster of leucite host plus Al-spinel inclusion show an excess of Al and Fe over Si and alkalies (Table 3). These analyses, which deviate from stoichiometry, also have much higher Fe and Mg contents, and appear to exhibit limited solid solution towards $KFe^{3+}Si_2O_6$ (Fig. 4). Tie lines between the bulk analyses

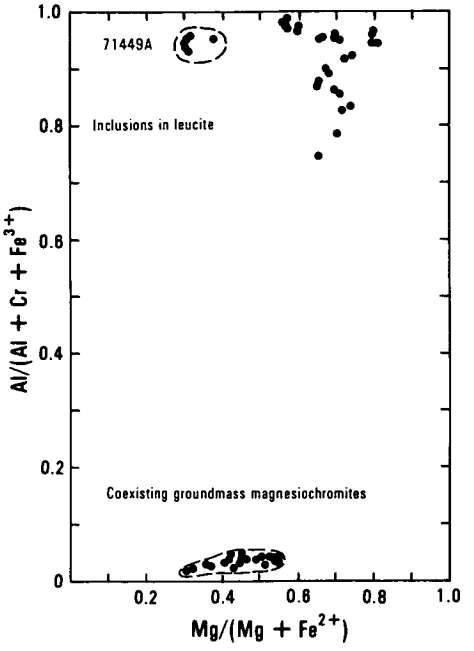

Fig. 3. Compositions of aluminous spinel inclusions in leucite in West Kimberley leucite lamproites contrasted with groundmass titanian magnesiochromites in terms of $Al/(Al + Cr + Fe^{3+})$ versus $Mg/(Mg + Fe^{2+})$.

and those of the leucite hosts (excluding spinel) show a trend towards the ideal leucite composition.

Gaussberg experiments

Compositions of leucites from both series of experiments are pertinent here and are listed in Table 4. The second series leucites containing Al-spinel inclusions were so small that clean (spinel-free) leucite analyses could not be obtained; these compositions are thus analogous to the bulk scan analyses in the West Kimberley rocks. The first series analyses listed in Table 4 are from run AT-116 ($MnO–Mn_3O_4$ buffer) which contains unusually large leucites which permitted direct analysis without the need to subtract included glass. Since the first series leucites contain no inclusions, the Mg and Fe reported in the analyses are considered to be incorporated in solid solution. Foley (1985) has shown that ferric iron contents in leucite increase with increasing oxygen fugacity, in agreement with the conclusions of Gupta and Yagi (1980) that increased $P_{H_2O_2}$ promoted solubility of Fe^{3+} in leucite. The first series experimental leucites have excess Si, indicating that Mg (and possibly some Fe) forms a coupled substitution MgSi–AlAl as originally proposed by Schairer (1948).

The second series leucite plus spinel overlap analyses form a range broadly similar to the West Kimberley leucites but displaced towards SiO_2 (Fig. 4), as a consequence of excess Si in their structural formulae (Table 4). The silica-poor nature of the West Kimberley bulk (spinel plus

Table 3. Representative microprobe analyses of leucite, West Kimberley leucite lamproites

	1	2	3	4	5
SiO_2	55.33	55.56	55.90	49.40	55.98**
TiO_2	0.17	0.16	0.11	0.35	0.06
Al_2O_3	21.03	20.85	21.12	25.57	20.86
Cr_2O_3	n.d.	n.d.	n.d.	0.07	n.d.
Fe_2O_3	1.08	1.11	0.56	3.36*	0.96
MnO	n.d.	0.03	n.d.	0.02	0.02
MgO	0.46	0.70	0.26	1.83	0.14
CaO	n.d.	n.d.	n.d.	0.08	0.12
Na_2O	0.09	0.02	0.10	0.09	0.09
K_2O	21.25	21.27	21.34	16.91	21.50
Total	99.41	99.70	99.39	97.66	99.75
		0 = 6			
Si	2.029	2.031	2.045	1.840	2.046
Ti	0.005	0.004	0.003	0.010	0.002
Al	0.909	0.899	0.911	1.122	0.899
Cr	-	-	-	0.002	-
Fe^{3+}	0.030	0.031	0.015	0.105*	0.026
Mn	-	0.001	-	0.001	0.001
Mg	0.025	0.038	0.014	0.102	0.008
Ca	-	-	-	0.003	0.005
Na	0.006	0.001	0.007	0.007	0.006
K	0.995	0.992	0.996	0.803	1.002
Total	3.999	3.997	3.991	3.993	3.994

Fe determined as FeO, recalculated to Fe_2O_3 except for 4;
* = Fe as FeO, ** BaO = 0.04%. n.d. = not detected (detection limit 0.02%)

1. Leucite host to Al-spinel, 81210125
2. Leucite host to Al-spinel, 71449A
3. Leucite host to Al-spinel, 71160408
4. Bulk analysis of leucite host plus inclusions (60 um scan), 71160408
5. Leucite phenocryst, 71160408

Table 2. Compositions of aluminous spinel inclusions in leucite [1–4] and coexisting chromian spinels from experiment AT-126 [5–6]

	1	2	3	4	5	6
Buffer	HM	HM	NNO	NNO	HM	NNO
TiO_2	-	-	-	-	2.27	2.71
Al_2O_3	66.3	68.2	69.6	69.9	4.36	3.78
Cr_2O_3	-	-	-	-	45.6	59.6
FeO*	6.9	4.86	6.10	5.84	26.7	17.2
MgO	28.8	27.0	24.3	24.3	21.1	16.7
		0 = 4				
Ti	-	-	-	-	0.053	0.066
Al	1.918	1.951	1.996	2.001	0.159	0.150
Cr	-	-	-	-	1.120	1.519
Fe	0.142	0.099	0.124	0.119	0.692	0.464
Mg	0.981	0.975	0.880	0.877	0.975	0.801
Total	3.041	3.025	3.000	2.999	2.999	3.000
Mg**	0.874	0.908	0.876	0.881	0.926	0.751

* Fe as FeO
** Mg = Mg/(Mg+Fe)

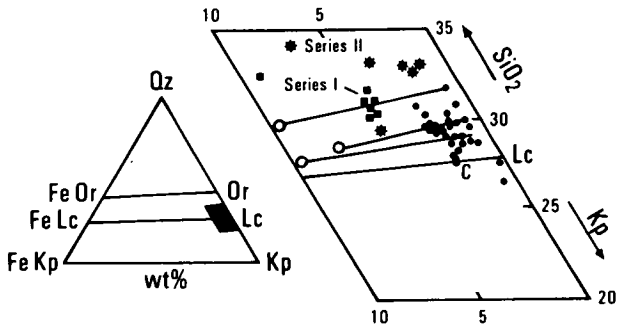

Fig. 4. Compositions of leucites in the West Kimberley lamproites (dots) compared with experimental leucite compositions in the system SiO_2–$KFe^{3+}SiO_4$–$KAlSiO_4$ (after Carmichael, 1967). Squares = first series experiments; crosses = second series experiments; open circles = bulk scans of Al-spinel plus leucite host in West Kimberley lamproites.

leucite host) analyses may be due to the predominance of Fe over Mg which causes a trend toward $KFe^{3+}SiO_4$. Alternatively, it might result from an excessive proportion of spinel in the rastered area of the analysis.

Origin of the Al-spinel inclusions

Several factors both preclude an origin for the Al-spinel inclusions in leucite by direct equilibrium crystallization from the host lamproite melt and strongly indicate an origin related to the crystallization of the leucite. (1) Al-spinel inclusions are restricted to leucite, particularly to poorly crystallized leucite aggregates. (2) Chrome-rich spinel coexists in the groundmass of the lamproite. Crystallization of two coexisting spinels one Al-rich with no Cr and the other Cr-rich, from the lamproite is highly unlikely since there is complete solid solution between $MgAl_2O_4$ and $MgCr_2O_4$ (e.g., Muan et al., 1972). (3) Equilibrium crystallization of Al-rich spinel containing negligible Cr (<0.2 wt.%) from a melt containing more than 250 ppm Cr is most unlikely under any conditions in view of the very high partition coefficient between chromite and liquid (e.g., Irving, 1978; and others).

Table 4. Representative compositions of leucite from first series [1–3] and second series (leucite + spinel overlap) experiments [4–6]

	1	2	3	4	5	6
SiO_2	56.11	56.19	56.34	57.3	57.9	54.7
Al_2O_3	20.76	20.88	21.04	22.0	21.7	22.7
FeO*	1.86	1.98	1.87	0.74	0.85	1.83
MgO	0.81	0.28	0.33	0.58	0.19	0.97
K_2O	20.22	20.43	20.40	19.4	19.4	19.8
Total	99.76	99.76	99.98	100.0	100.0	100.0
		O = 6				
Si	2.044	2.049	2.050	2.053	2.074	1.987
Al	0.891	0.898	0.902	0.931	0.915	0.971
Fe	0.057	0.060	0.057	0.022	0.025	0.056
Mg	0.044	0.015	0.018	0.031	0.010	0.052
K	0.940	0.950	0.946	0.887	0.890	0.920
Total	3.976	3.972	3.973	3.924	3.914	3.986

* Fe as FeO

Two possible explanations for the origin of the Al-spinel inclusions are considered: (1) crystallization during unmixing or "exsolution" of non-stoichiometric leucite, (2) crystallization from melt included within the leucite phenocrysts.

Evidence in favor of the first explanation includes the poorly crystallized, often aggregated, nature of the West Kimberley leucite hosts which suggests very rapid crystallization of the leucite as a consequence of supersaturation of the melt in leucite. Although solid solution between leucite and kaliophilite is apparently very limited under any conditions (Barton, 1979) and solid solution between leucite and $KFe^{3+}Si_2O_6$ is restricted, the substitution MgSi–AlAl is known to occur (Schairer, 1948). Formation of non-stoichiometric leucite would be promoted under conditions of supersaturation where crystallization would be rapid.

It is proposed that during crystallization of the leucite to a more ordered structure, excess Mg, Al and Fe were exsolved and recrystallized as spinel. The incorporation of Mg in leucite is proven by the first series of experiments. Furthermore, an indication of the kinetics of unmixing can be obtained by comparing the first series Mg-bearing leucites with the second series leucites in which unmixing has taken place. The first series near-liquidus experiments were run for 2.5 hours, whereas the second ran for 5 hours. The only other difference between the two series was the Cr_2O_3 content which could not have caused crystallization of Cr-free spinels. The experiments provide further indications of the conditions under which the natural spinels might have formed. The unmixing between 2.5 and 5 hours occurred at all oxygen fugacities studied (equivalent to $\log f_{O_2}$ of -8 to -2), demonstrating that f_{O_2} has minimal effect. In addition, the fact that the experiments were anhydrous shows that elevated P_{H_2O} is not necessary for incorporation of Mg and Fe into leucite.

The very low Fe^{3+} content of Al-spinels in the West Kimberley rocks indicates that much of the iron originally in the non-stoichiometric leucite was present in the divalent state. This view is supported by the Gaussberg experiments (Foley, 1985) which suggest an initially reducing environment for many lamproitic magmas. The Gaussberg olivine leucitites contain poorly-crystallized, inclusion-filled aggregates of leucite similar to the West Kimberley examples but to date no Al-spinels have been found in these. The Gaussberg leucites formed early in the crystallization sequence, are poor in Fe^{3+}, and have low excess Si relative to later phenocrystal leucites.

The second possible explanation for the Al-spinel inclusions, crystallization of the spinel from melt included within leucite, appears to require local super-saturation of the melt in alumina. Experimental support for the operation of this mechanism was serendipitously provided by

an initial attempt to run the Gaussberg experiments in alumina sample capsules. This was attempted in order to eliminate the problem of iron loss to noble metal capsules because experiments by Hill and Roeder (1974) showed that alumina contamination of basaltic samples run in alumina capsules was minimal. However, because of the alumina-undersaturated nature of the Gaussberg composition reaction with the capsule was much greater: the melt gained appreciable Al_2O_3, and aluminous spinels together with leucite crystallized near the liquidus. The spinels are remarkably similar to those occurring as inclusions in leucite in second series experiments (Table 5). Alumina addition to this experiment may be analogous to melt inclusions gaining alumina from surrounding leucites or, possibly, by localized incorporation of Al-rich (pelitic) country rock. There is no evidence of widespread assimilation in the West Kimberley lamproites but country rock inclusions are locally evident.

Both of the above mechanisms are suggested as viable mechanisms for the formation of Al-spinel in leucite. The key to operation of the first mechanism, which seems the more likely for the bulk of the spinel inclusions, may be the degree of supersaturation of the melt in leucite. The experimental method of rapidly heating a mixture of oxides to the run conditions means that the melt formed will be strongly supersaturated in all phases initially crystallizing. In natural rocks a high degree of supersaturation may be necessary to initially incorporate appreciable Mg and Fe^{2+} in leucites, which may account for the apparent rarity of these inclusions; supersaturation may have led to the rapid crystallization of leucites with numerous melt inclusions. Some of the spinels might have crystallized in melt inclusions by the second mechanism, or alternatively, the melt inclusions may have acted as nucleation sites for spinels which then grew by exsolution from the non-stoichiometric leucites. The large size of the hercynite inclusions compared to the enclosing leucites in sample 71449A suggests local supersaturation in alumina.

Although solid inclusions are common in leucite (Gupta and Yagi, 1980, p. 19) Al-spinel has not, to the best of our knowledge, been reported as inclusions from leucites in other ultrapotassic suites. The closest analogues appear to be the inclusions of magnetite (and augite) in leucite from Utsuryo Island, Japan (cited by Gupta and Yagi, 1980, p. 19) and the occurrence of Fe-pleonaste inclusions in biotite of presumed xenocrystal origin in the Spanish lamproites. The latter inclusions were attributed by Venturelli et al. (1984) to breakdown of biotite due to a near isothermal decrease in pressure at constant or increasing f_{O_2}. The Fe-pleonastes and associated salitic pyroxenes in some of the Leucite Hills rocks (wyomingites) have been interpreted as xenocrysts. Most of the pleonastes are included within mica although some occur as large, irregular, discrete grains. These probably formed in the upper mantle as a result of local metasomatism or by crystallization of previous unrelated magmas (Barton and van Bergen, 1981; Kuehner et al., 1981).

Table 5. Compositions of Al-spinels produced by addition of alumina to experiment on Gaussberg leucitite

	1	2	3
SiO_2	0.36	0.38	1.45
Al_2O_3	69.80	69.58	69.19
FeO*	9.35	9.36	9.14
MgO	20.27	20.43	19.58
Total	99.78	99.75	99.36
Mg**	0.795	0.795	0.792

* Fe as FeO
** Mg = Mg/(Mg+Fe)

The Mg-pleonaste rims on groundmass chromite and titanomagnetite in the Kao (Haggerty, 1975) and De Beers kimberlite (Pasteris, 1983) pipes differ from the pleonastes reported here in having significantly lower Al and higher Ti, Cr and Fe^{3+} contents. Pasteris (1983) suggested that the Mg–Al spinel rims in the De Beers kimberlite resulted from increased Mg and Al in the magma, probably as a consequence of temporary cessation of phlogopite crystallization by reactions such as:

$$4KMg_3AlSi_3O_{10}(OH)_2 \rightarrow \underset{\text{forsterite}}{5Mg_2SiO_4} + \underset{\text{spinel}}{2MgAl_2O_4} + \underset{\text{melt}}{(2K_2O + 4H_2O + 7SiO_2)}$$
phlogopite

Such a mechanism is unlikely to have resulted in the formation of the Al-spinel inclusions in leucite since: (1) the evolutionary trend of the groundmass spinels is to lower Al compositions (titaniferous magnesian aluminous chromite–titaniferous magnesian chromite–titaniferous chromian magnetite; Jaques et al., 1984); (2) there is no compelling evidence of a cessation or hiatus of phlogopite crystallization in the inclusion-bearing rocks; and (3) the evolutionary trend of the groundmass (commonly glassy) compositions is to higher K_2O and SiO_2 contents which would tend to stabilize phlogopite.

Therefore, with the possible exception of the magnetite inclusions in leucite from Utsuryo Island the mechanism proposed for the origin of the Al-rich spinel in leucite in the West Kimberley lamproites does not appear applicable to these other occurrences of Al-rich spinels. However, we suggest that under appropriate conditions aluminous spinels could form inclusions in leucite in other ultrapotassic suites. In the case of the West Kimberley leucite lamproites, the textural evidence from the leucites and their inclusions indicates rapid, near-surface (sub-volcanic) crystallization from magmas supersaturated in leucite. Low pressure fractionation resulted in silica-saturated residual liquids. Crystallization of olivine + leucite is restricted to less than 1.2 kbar under water-saturated conditions (Luth, 1967) but under water-undersaturated conditions olivine and leucite can coexist up to 4 kbar (Barton and Hamilton, 1982).

Acknowledgments

ALJ acknowledges CRAE Pty Ltd and J. D. Lewis (Geological Survey of Western Australia) for provision of one of the samples used. M. B. Duggan, J. W. Sheraton, and R. Wendlandt are thanked for reviews of the draft manuscript. SFF thanks K. L. Harris for technical assistance with the experiments, and D. J. Ellis, D. H. Green and S. M. Kuehner for helpful discussions and comments. SFF acknowledges a University of Tasmania postgraduate award. ALJ publishes with the permission of the Director, Bureau of Mineral Resources.

References

Arculus, R. J. (1978) Mineralogy and petrology of Grenada, Lesser Antilles island arc. Contributions to Mineralogy and Petrology, 65, 413–424.

Atkinson, W. J., Hughes, F. E., and Smith, C. B. (1984) A review of the kimberlitic rocks of Western Australia. In J. Kornprobst, Ed., Kimberlites. 1: Kimberlites and related rocks, p. 195–225. Developments in Petrology, 11A, Elsevier, Amsterdam.

Barton, M. (1979) A comparative study of some minerals occurring in the potassium-rich alkaline rocks of the Leucite Hills, Wyoming, the Vico Volcano, Western Italy, and the Toro-Ankole region, Uganda. Neues Jarhbuch für Mineralogie Abhandlungen, 137, 113–134.

Barton, M., and van Bergen, M. J. (1981) Green clinopyroxenes and associated phases in a potassium-rich lava from the Leucite Hills, Wyoming. Contributions to Mineralogy and Petrology, 77, 101–114.

Barton, M. and Hamilton, D. L. (1982) Water-undersaturated melting experiments bearing upon the origin of potassium-rich magmas. Mineralogical Magazine, 45, 267–278.

Carmichael, I. S. E. (1967) The mineralogy and petrology of the volcanic rocks from the Leucite Hills, Wyoming. Contributions to Mineralogy and Petrology, 15, 24–66.

Cundari, A. (1975) Mineral chemistry and petrogenetic aspects of the Vico lavas, Roman Volcanic Region, Italy. Contributions to Mineralogy and Petrology, 53, 129–144.

Deer, W. A., Howie, R. A., and Zussman, J. (1963) Rock-Forming Minerals, Volume 1V, p. 276–288. Longmans, London.

Derrick, G. M., and Gellatly, D. C. (1972) New leucite lamproites from the West Kimberley, Western Australia. Bureau of Mineral Resources, Australia Bulletin, 125, 103–119.

Foley, S. F. (1985) The oxidation state of lamproitic magmas. Tschermaks Mineralogische und Petrographische Mitteilungen, in press.

Fudali, R. F. (1963) Experimental studies on the origin of pseudoleucite and associated problems of alkalic rock systems. Geological Society of America Bulletin, 74, 1101–1126.

Gupta, A. K. and Edgar, A. D. (1975) Leucite–Na-feldspar incompatibility: an experimental study. Mineralogical Magazine, 40, 377–384.

Gupta, A. K. and Yagi, K. (1980) Petrology and Petrogenesis of Leucite-bearing Rocks. Springer-Verlag, Berlin.

Haggerty, S. E. (1975) The chemistry and genesis of opaque minerals in kimberlites. Physics and Chemistry of the Earth, 9, 295–307.

Haggerty, S. E. (1976) Opaque mineral oxides in terrestrial igneous rocks. In D. Rumble III, Ed., Reviews in Mineralogy, Volume 3, Oxide Minerals. Mineralogical Society of America, Washington, D. C.

Henderson, C. M. B. (1965) Minor element chemistry of leucite and pseudoleucite. Mineralogical Magazine, 35, 596–603.

Henderson, C. M. B. and Taylor, D. (1969) An experimental study of leucite and analcime mineral groups. In Progress in Experimental Petrology, first report, p. 45–50. Natural Environment Research Council, Manchester.

Hill, R. and Roeder, P. L. (1974) The crystallisation of spinel from basaltic liquid as a function of oxygen fugacity. Journal of Geology, 82, 709–729.

Jaques, A. L., Lewis, J. D., Smith, C. B., Gregory, G. P., Ferguson, J., Chappell, B. W., and McCulloch, M. T. (1984) The diamond-bearing ultrapotassic (lamproitic) rocks of the West Kimberley region, Western Australia. In J. Kornprobst, Ed., Kimberlites. 1: Kimberlites and related rocks, p. 225–254. Developments in Petrology, 11A. Elsevier, Amsterdam.

Kuehner, S. M., Edgar, A. D., and Arima, M. (1981) Petrogenesis of the ultrapotassic rocks from the Leucite Hills, Wyoming. American Mineralogist, 66, 663–677.

Luth, W. C. (1967) Studies in the system $KAlSiO_4$–Mg_2SiO_4–SiO_2–H_2O: 1, inferred phase relations and petrologic applications. Journal of Petrology, 8, 372–416.

Muan, A., Hauck, J., and Lofall, T. (1972) Equilibrium studies with a bearing on lunar rocks. Proceedings of the Third Lunar Science Conference, 185–196.

Pasteris, J. D. (1983) Spinel zonation in the De Beers kimberlite, South Africa: possible role of phlogopite. Canadian Mineralogist, 21, 41–58.

Prider, R. T. (1960) The leucite lamproites of the Fitzroy basin, Western Australia. Journal of the Geological Society of Australia, 6, 71–118.

Prider, R. T. (1982) A glassy lamproite from the West Kimberley area. Mineralogical Magazine, 45, 279–282.

Prider, R. T. and Cole, W. F. (1942) The alteration products of olivine and leucite in the leucite lamproites from the West Kimberley area, Western Australia. American Mineralogist, 27, 373–384.

Schairer, J. F. (1948) Phase equilibrium relations in the quaternary system K_2O–MgO–Al_2O_3–SiO_2 (preliminary report). Geological Society of America Bulletin, 59, 1349.

Sheraton, J. W. and Cundari, A. (1980) Leucitites from Gaussberg, Antarctica. Contributions to Mineralogy and Petrology, 71, 417–427.

Venturelli, G., Capedri, S., Di Battistini, G., Crawford, A., Kogarko, L. N. and Celestini, S. (1984) The ultrapotassic rocks from southeastern Spain. Lithos, 17, 37–54.

Wade, A. and Prider, R. T. (1940) The leucite-bearing rocks of the West Kimberley area, Western Australia. Quarterly Journal of the Geological Society of London, 98, 39–98.

Manuscript received, December 14, 1984;
accepted for publication, June 18, 1985.